THE JOURNAL
OF
CHEMICAL PHYSICS

VOLUME 20, NUMBER 9 SEPTEMBER, 1952

The Vibrational Spectra of Molecules and Complex Ions in Crystals. VI. Carbon Dioxide*

W. E. OSBERG† AND D. F. HORNIG
Metcalf Chemical Laboratories, Brown University, Providence, Rhode Island

(Received April 14, 1952)

A previously reported discrepancy between the predicted and observed infrared spectrum of crystalline carbon dioxide is shown to arise from the presence of two peaks due to $C^{13}O_2$, a combination band involving a lattice frequency near 110 cm^{-1} and two reflection peaks. The infrared spectrum was studied at −190°C and aside from the previous features shows one component from ν_3 and two from ν_2, shifted very little from the gas frequencies. The difficulties encountered in interpreting the spectrum of this simple crystal occur quite generally in the spectra of more complicated substances.

INTRODUCTION

IT has been pointed out that the reported infrared spectrum of crystalline carbon dioxide is incompatible with the structure determined by x-ray diffraction studies.[1] Such a discrepancy in so simple a molecular crystal seemed worthy of further investigation.

According to the x-ray structure determinations, carbon dioxide forms a face-centered cubic lattice of symmetry T_h[6] with four molecules per unit cell.[2–4]

The molecules all lie on sites of symmetry $C_{3i}(\equiv S_6)$. This site symmetry alone is sufficient to establish that the exclusion rule between infrared and Raman spectra should hold, as indeed it does. Only the Fermi doublet arising from the symmetric stretching vibration (ν_1) has been observed in the Raman spectrum,[5] while the antisymmetric stretching vibration (ν_3) and the bending vibration (ν_2) were found only in the infrared spectrum.[6]

The relation between the vibrations of the isolated molecule and of the active vibrations arising from the coupled motions of the molecules in the crystal is just the relation between the site symmetry and the space group.[7]

This relation is illustrated for the present case in Fig. 1. It is seen that ν_1 should give rise to two components in the crystal. They may both be Raman active. In fact this vibration is split by Fermi resonance with $2\nu_2$, just as in the gas, and no further splitting has been observed. The antisymmetric vibration ν_3 should give rise to two components (species A_u and F_u of T_h) of which only the second should be infrared active in the crystal. However, two peaks have been reported by Dahlke.[6] Finally, the bending vibration ν_2 should yield three components in the crystal, one of species E_u and two of species F_u. Only the latter pair should be active, but three peaks were observed. Consequently, we have reinvestigated the infrared spectrum of crystalline carbon dioxide in order to determine the origin of these differences.

EXPERIMENTAL RESULTS

Commercial carbon dioxide‡ whose purity was stated to be 99.5 percent was used for the work. The maximum amounts of impurity were stated to be 0.34 percent nitrogen, 0.09 percent oxygen, and 0.07 percent water vapor. The infrared spectrum of the gas disclosed no impurity which might affect the results of this investigation.

The films were prepared by subliming the CO_2, which had previously been condensed in a cold trap,

* Based on a thesis presented by W. E. Osberg in partial fulfillment of the requirements for the degree of Doctor of Philosophy, Brown University, 1951. This work was supported by the ONR.

† Present address: Hercules Powder Company, Wilmington, Delaware.

[1] D. F. Hornig, Disc. Faraday Soc. No. **9**, 115 (1950).

[2] J. de Smedt and W. H. Keesom, Proc. Amsterdam Acad. **27**, 839 (1924); Z. Krist. **62**, 312 (1926).

[3] H. Mark and E. Pohland, Z. Krist. **61**, 293 (1925); **64**, 113 (1926).

[4] J. C. McLennan and J. O. Wilhelm, Trans. Roy. Soc. Can. Sec. III (3) **19**, 51 (1925).

[5] J. C. McLennan and H. D. Smith, Can. J. Research **7**, 551 (1932).

[6] W. Dahlke, Z. Physik **102**, 360 (1936).

[7] D. F. Hornig, J. Chem. Phys. **16**, 1063 (1948).

‡ Pure Carbonic Company, Boston, Massachusetts.

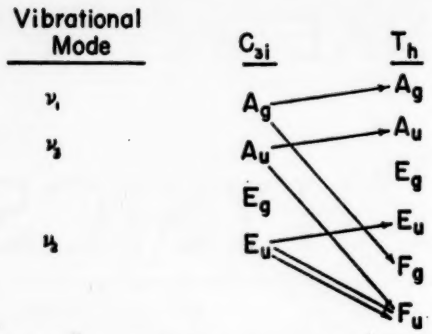

FIG. 1. Relation between the local symmetry of CO_2 in the crystal and the symmetry of the unit cell containing 4 molecules.

onto an NaCl backing plate which was mounted in a low temperature transmission type cell maintained at a temperature of −190°C. The resulting films were quite transparent to the eye, except for the thickest ones, and showed little scattering in the infrared region.

The spectra were obtained at −190°C on a double-beam infrared spectrophotometer,[8] using CaF_2, NaCl, and KBr prisms. They are shown in Figs. 2 to 5 and the results tabulated in Table I. The frequencies given are believed to be accurate to ±5 cm^{-1} at 3700 cm^{-1}, ±3 cm^{-1} at 2350 cm^{-1}, and ±1 cm^{-1} at 650 cm^{-1}. The spectrum of crystalline carbon dioxide obtained in the present work agrees well with that of Dahlke in the vicinity of 650 cm^{-1} and 3600 cm^{-1}. However, it is quite different in the neighborhood of 2300 cm^{-1}, and the absorption maximum which was reported at 2288 cm^{-1} actually occurs at 2344 cm^{-1}. Since the spectrometer was calibrated on the atmospheric carbon dioxide band at 2349 cm^{-1} before and after each run, it does not seem possible that the present results are in error. In addition, the study of a thick film revealed an absorption band at 637 cm^{-1} which had not been reported previously.

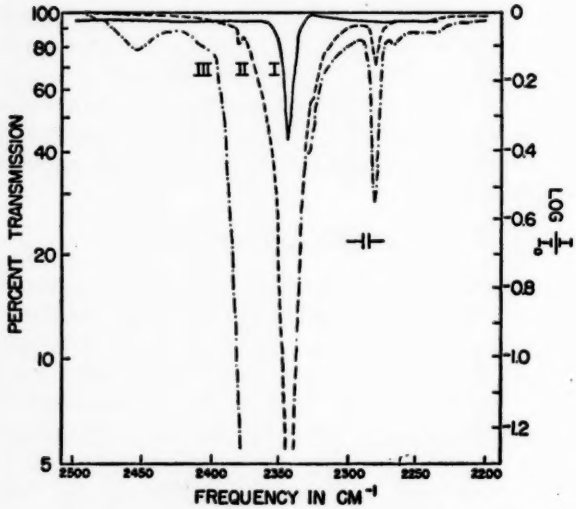

FIG. 2. The infrared spectrum of crystalline CO_2 at −190°C in the region of the fundamental ν_3.

[8] Hornig, Hyde, and Adcock, J. Opt. Soc. Am. 40, 497 (1950).

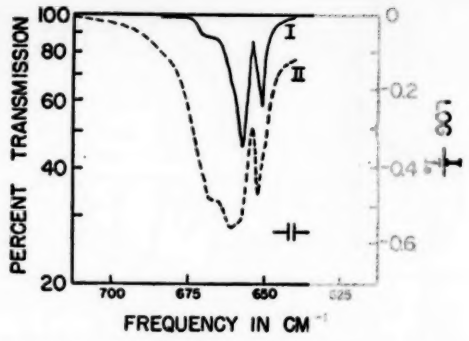

FIG. 3. The infrared spectrum of crystalline CO_2 at −190°C in the region of the fundamental ν_2 taken with NaCl prism.

DISCUSSION

It is to be expected that at this low temperature (−190°C) all of the fundamental vibrations should yield sharp lines in the infrared spectrum.[7] If all of the sharp lines in the spectrum of the thin film are assigned to the fundamentals, the pattern of lines coincides exactly with that expected theoretically. Only one line which can be ascribed to the asymmetric stretching vibration ν_3 is observed (Fig. 2), and in contrast to the earlier work this line has a frequency only 5 cm^{-1} different from that found in the gas. Similarly, two sharp lines due to the bending vibration ν_2 are observed. The mean observed width of these three lines at half the maximum absorption coefficient is only 5 cm^{-1}; most of the width of ν_3 and of the less intense component of ν_2 certainly originates in the finite resolution of the spectrometer, but the more intense component of ν_2 appears to have a natural width of approximately 3 cm^{-1}. Consequently, there appears to be no genuine discrepancy.

In addition to these three lines there are two sharp but weak bands which can be ascribed unambiguously to $C^{13}O_2$. Since the vibration frequencies of the $C^{13}O_2$ molecule differ from those of the surrounding molecules, the $C^{13}O_2$ spectrum should be simple, showing no structure caused by intermolecular coupling. This is indeed the case and only one peak due to ν_2 is found in $C^{13}O_2$ in contrast to $C^{12}O_2$ which shows two. This effect has

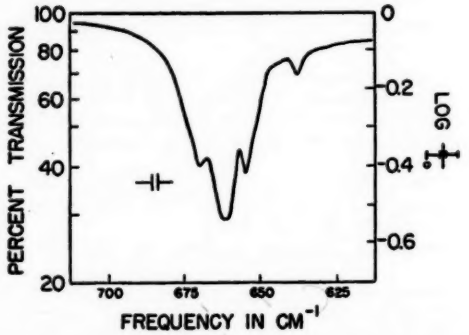

FIG. 4. The infrared spectrum of crystalline CO_2 at −190°C in the region of the fundamental ν_2 taken with a KBr prism.

been observed previously in solid solutions of HCl in DCl[9] and of naphthalene in anthracene.[10]

Aside from the peaks near 3600 cm^{-1} which are readily interpreted in terms of the large number of components of the two combinations lying in this vicinity (all of which may resonate) and those at 667 cm^{-1} and 2379 cm^{-1} which we believe are caused by reflection, all that remains is the relatively broad peak at 2454 cm^{-1} and a region of extremely weak absorption, scarcely above the noise level in the thickest film, between 2235 and 2270 cm^{-1}. It seems highly probable that the former arises from a combination of ν_3 with the torsional oscillation frequencies of the molecules in the lattice with a maximum density of frequencies near 110 cm^{-1}. It is not impossible, however, that the combination involves translational lattice frequencies since the $u-g$ selection rule applies only to limiting modes[11] but the selection rules for limiting modes appear to be valid empirically, no definite violations having yet been found. The absorption near 2260 cm^{-1} may arise from the corresponding difference bands.

TABLE I. Infrared absorption frequencies of crystalline carbon dioxide at −190°C.

Gas (cm^{-1})	Crystal (cm^{-1})	$\Delta\nu$ (cm^{-1})	Line width (cm^{-1})	Assignment
	3748[a]		...	
3716	3712	−4	27	$\nu_1+\nu_3$ and $2\nu_2+\nu_3$
	3639[a]		...	
3609	3610	+1	26	
	2454		35	$\nu_3+\nu$ Torsion
	2379[a]		...	Reflection
2349	2344	−5	7	ν_3
2284	2280	−4	7	ν_3 ($C^{13}O_2$)
	667	...	...	Reflection
667	660	−10	7	ν_2
	653		4	
642[b]	637	...	6	ν_2 ($C^{13}O_2$)

[a] Shoulder.
[b] Calculated.

THE EFFECT OF REFLECTION

The effect of reflection from the vacuum-sample and sample-backing interfaces, plus the reflection from the same interfaces traversed in the opposite direction,

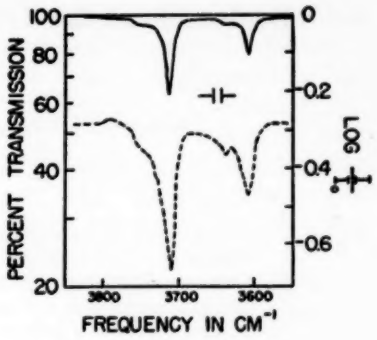

FIG. 5. The infrared spectrum of crystalline CO_2 at −190°C in the vicinity of $\nu_1+\nu_3$ and $2\nu_2+\nu_3$.

appear in the spectra of crystals as spurious absorption. Because of the rapid variation of the index of refraction near an absorption band the reflectivity of each interface varies widely in the neighborhood of an absorption band and may shift the apparent peak position or produce a spurious peak nearby, usually on the high frequency side. In a recent investigation of the reflection spectra of the ammonium salts, Bovey found reflection peaks shifted as much as 30 cm^{-1} to the high frequency side of the absorption maximum.[12]

However, they have also been observed shifted to low frequencies.[13]

A very characteristic feature of reflection maxima which frequently is sufficient to identify them is their very great intensity increase when the thickness of thin films is increased. This effect arises because the destructive interference of the beams reflected from the front and back surfaces of a vanishingly thin film changes to constructive interference when the film thickness is $\lambda/4$.

Such behavior is clearly apparent in the peaks at 667 cm^{-1} and 2379 cm^{-1}, both of which occur on the high frequency shoulders of the true absorption and both of which increase in intensity much more rapidly than the true absorption, as is evident from a comparison of the spectra of thin and thick films (Figs. 2 and 3).

CONCLUSIONS

The spectrum of crystalline carbon dioxide agrees with the theoretical expectations. It is complicated by the presence of peaks due to $C^{13}O_2$, reflection and combination between internal and lattice vibrations. These complications are of very general occurrence and may lead to difficulties in the interpretation of the infrared spectra of crystals of more complicated molecules.

[9] D. F. Hornig and G. L. Hiebert, J. Chem. Phys. **20**, 918 (1952).
[10] G. C. Pimentel, J. Chem. Phys. **19**, 1536 (1951).
[11] H. Winston and R. S. Halford, J. Chem. Phys. **17**, 607 (1949).
[12] L. F. Bovey, J. Chem. Phys. **18**, 1684 (1950).
[13] C. Schaeffer, Z. Physik **75**, 687 (1932).

Evaluation of the Zeta-Sums for Rotation-Vibration Interaction in Axially Symmetrical Molecules

R. C. LORD AND R. E. MERRIFIELD
Spectroscopy Laboratory and Department of Chemistry, Massachusetts Institute of Technology, Cambridge 39, Massachusetts

(Received March 31, 1952)

It is shown that the contribution of a set of equivalent nuclei to the zeta-sum for the fundamental vibrations of any symmetry species in a molecule possessing only one multiple axis of symmetry is zero unless the nuclei are situated on the axis. In the latter case the contribution of the set of equivalent nuclei to the zeta-sum in any species is one unit for every degree of freedom the set contributes to that species. With the help of these theorems a table is worked out from which the zeta-sums can be determined immediately for any axially symmetrical molecule of known structure. Use of the table is illustrated with several simple examples.

TELLER[1] showed in 1934 that the angular momentum of degenerate molecular vibrations can interact with angular momentum of molecular rotation so as to affect the rotational energy levels of the molecule. The vibrational angular momentum is $\zeta_i h/2\pi$, where ζ_i, the zeta-constant, is characteristic of the individual vibration i but is restricted to the range -1 to $+1$. The physical meaning of the minus sign is that the angular momentum of vibration is so related to that of the rotation as to produce an *increased* angular velocity of rotation of the vibrating molecular dipole moment about the molecular axis. The plus sign means that the velocity of rotation of the vibrating dipole moment is *less* than it would be if no angular momentum of vibration were present.

Teller[1] and Dennison and Johnston[2] also demonstrated that for harmonic vibrations the sum of the zetas of the vibrations in a given degenerate species is independent of the particular force system of the molecule. The latter authors[3] have applied the "limiting force field" reasoning of Dennison to the evaluation of the zeta-sums in several molecules.

Although it is clearly implicit in the expositions of Teller[1] and Dennison and Johnston[2] that the zeta-sums can be worked out on general grounds (i.e., with no knowledge about the force system other than that it is harmonic), there appears to be an impression in the literature[4] that it is still necessary to go through the limiting-force-field reasoning (or some similar process) for each molecule as a particular case. In fact this is no more necessary than it is to go through the group-theoretical reasoning for the determination of the number of vibrational frequencies belonging to the various symmetry species for each molecule separately. The latter quantities have been generalized in the form of tables for many years.[5] As has been pointed out earlier,[6] the preparation of analogous tables for the zeta-sums is entirely feasible.

It is the purpose of the present paper to report such a table for molecules with one symmetry axis of threefold or higher multiplicity. In such molecules the sets of equivalent nuclei[7] are of two kinds, those that lie on the symmetry axis and those that do not. The contributions of these two kinds to the zeta-sums are distinctly different.

A set of equivalent nuclei lying on the symmetry axis will consist of either one atom or two atoms, depending on whether certain additional symmetry (for example, a center of symmetry) is present. In either event the atoms can vibrate in only two ways, along the symmetry axis or within a plane perpendicular to it. Vibration along the axis is nondegenerate and produces no angular momentum and hence has a zero zeta-value, as do all nondegenerate vibrations. On the other hand, each vibration perpendicular to the axis (when excited to the first vibrational level above the zero level) can be shown to have $h/2\pi$ units of angular momentum and hence to contribute one unit to the zeta-sum. This result can be summarized by the following.

THEOREM I

A set of equivalent nuclei lying on the symmetry axis will contribute to the zeta-sum of a given degenerate symmetry species one unit for each vibration the set contributes to the species.

In the noncubic crystallographic point groups a set of equivalent nuclei not lying on the symmetry axis will consist of np identical atoms, where p is the multiplicity of the axis (three or more) and n is 1, 2, or 4. The value of n for a given set of equivalent nuclei depends on the symmetry elements present in addition to the p-fold

[1] E. Teller, Hand- und Jahrbuch der chem. Physik **IX**, 2, p. 125 (1934).
[2] D. M. Dennison and M. Johnston, Phys. Rev. **47**, 93; 868 (1935).
[3] See also D. M. Dennison and G. B. Hansen, J. Chem. Phys. **20**, 313 (1952).
[4] See, for example, the discussion of the zeta-sums in Herzberg, *Infrared and Raman Spectra* (D. Van Nostrand Company, Inc. New York, 1945), pp. 404–405; J. B. Howard, J. Chem. Phys. **5**, 451 (1937); R. D. Cowan, J. Chem. Phys. **18**, 1101 (1950).
[5] K. W. F. Kohlrausch, *Der Smekal-Raman Effekt* (Julius Springer, Berlin), Ergänzungs-band 1931–37, 1938, Tables 1–28; Herzberg, reference 4, Tables 34–36.
[6] R. C. Lord and P. Venkateswarlu, J. Chem. Phys. **20**, 1237 (1952).
[7] For definition of this term and a general discussion of the applications of symmetry to problems of molecular vibration and rotation see Herzberg, reference 4.

axis and on the location of the nuclei with respect to these elements.

The np nuclei of a set may be regarded as n independent subsets of p nuclei. The modes of vibration of one subset will be identical with those of the other subsets but can be coupled in n independent ways with them in accordance with the requirements imposed by symmetry operations which carry one subset of p equivalent nuclei into another. Since the coupling of the independent vibrations of the n subsets can be regarded as of arbitrary magnitude (so long as the coupling forces are harmonic), the contribution of the vibrations of each subset of p nuclei to the zeta-sum for any symmetry species can also be regarded as independent of the vibrations of the other subsets. Hence the contribution of n subsets to the zeta-sums will be n times that of one subset.

It is therefore necessary to consider what will be the contribution to the zeta-sum for each symmetry species by a set of p equivalent nuclei. Each such set will have $3p$ degrees of freedom, of which three will correspond to nondegenerate vibrations symmetrical to the p-fold axis. If p is even, three more vibrations will be nondegenerate but antisymmetric to the axis. The remaining degrees of freedom, which will be $3p-3$ in number if p is odd and $3p-6$ if p is even, will give rise, respectively, to $(3p-3)/2$ or $(3p-6)/2$ pairs of orthogonal doubly-degenerate vibrations. Such pairs of vibrations transform, on rotation about the p-fold axis, into equivalent pairs (i.e., sets of nuclear displacements corresponding to the same vibrational frequency) in accordance with the well-known transformation equation[8]

$$\begin{aligned} \xi_1' &= +\xi_1 \cos\phi + \xi_2 \sin\phi, \\ \xi_2' &= -\xi_1 \sin\phi + \xi_2 \cos\phi, \end{aligned} \tag{1}$$

where ξ_1, ξ_2 are a pair of orthogonal doubly-degenerate sets of nuclear displacements, $\xi_1'\xi_2'$ are a transformed pair, and ϕ is the angle of rotation about the p-fold axis.

The angle ϕ is restricted to the values $\pm l2\pi/p$, where $l=1, 2\cdots(p-1)/2$ for p odd, and $1, 2\cdots p/2$ for p even. In the latter case when $l=p/2$, the transformation Eqs. (1) give $\xi_1'=-\xi_1$, $\xi_2'=-\xi_2$, which is just the antisymmetric nondegenerate set of vibrations referred to above. The values of l applicable to the transformation of degenerate vibrations when p is even are therefore $1, 2\cdots(p-2)/2$.

The $(3p-3)/2$ pairs of degenerate vibrations for odd values of p consist of three pairs that transform with $l=1$, three with $l=2$, and so on up to $l=(p-1)/2$. Similarly the $(3p-6)/2$ pairs for even p consists of three with $l=1\cdots$, three with $l=(p-2)/2$. The three pairs of vibrations in every case are made up of two degrees of freedom each in the x, y, and z directions, the last named being taken as the direction of the p-fold axis. Vibrational degrees of freedom in the z direction may or may not be separated from the x and y degrees of freedom by the presence of additional symmetry, but the x degrees of freedom will never be separated from the y degrees of freedom since the p-fold axis carries one into the other (except for $l=p/2$, which is a nondegenerate case). In any event the z coordinates contribute zero to the angular momentum about the p-fold axis and thus cannot contribute to the zeta-sums.

For each symmetry species, then, corresponding to a particular value of ϕ, there will be two sets of double (x, y) degrees of freedom that contribute to the vibrational angular momentum. If nuclear displacements for one of these sets is constructed with the help of the transformation equations (1), they can be shown to have a zeta equal, say, to $+1$. If, then, the nuclear displacements are constructed for the other set by replacing ϕ by $-\phi$, the zeta so obtained is -1, and the sum of the two is a net zero.

From the result of the preceding paragraph and the earlier remarks about the independence of the subsets of p nuclei in a set of np equivalent nuclei, there follows the general Theorem II which holds irrespective of the presence of other symmetry in addition to the p-fold axis.

THEOREM II

A set of equivalent nuclei not lying on the figure axis will contribute a net zero to the zeta-sum for the vibrations of every symmetry species.

With the help of Theorems I and II the general expressions for the zeta-sums for the various degenerate species of all point groups of axial symmetry can be written down at once. Before these can be used for the zeta-sums for pure vibrations, however, the contributions of translation and rotation must be deducted. The doubly degenerate translations in the x, y directions contribute $+1$ to the zeta-sum and the rotations about the x, y axes contribute the quantity $1-I_A/2I_B$, where I_A = moment of inertia about the z axis and I_B = moment of inertia about the x, y axes.[9] Hence, the zeta-sum of the pure vibrations is less by unity than the general sum if there is a translation present in the species and less by $1-I_A/2I_B$ if a rotation is present.

The zeta-sums for the pure vibrations in different symmetry species of axially symmetrical molecules are listed in Table I. The notation of Herzberg[5] is used. The symbols m mean the number of sets of equivalent nuclei of different sorts present in the molecule (not, of course, the number of nuclei in each set), and the subscripts designate the kind of set: m_0 = number of sets lying on all elements of symmetry, m_p = number of sets lying on a p-fold axis of symmetry but not on all elements.

In conclusion, the use of Table I will be illustrated by

[8] See Herzberg, reference 4, p. 94.

[9] Translation in the z direction and rotation about the z axis contribute only to nondegenerate species.

TABLE I. Zeta-sum values for fundamental vibrations of axially symmetrical molecules.

Point groups	Species	$\Sigma\zeta_{vib}$	Point groups	Species	$\Sigma\zeta_{vib}$
C_3, C_4, C_{3v}, C_{4v}	E	$m_0-2+I_A/2I_B$	C_{3h}, D_{3h}	E'	m_p+m_0-1
				E''	$m_p-1+I_A/2I_B$
C_5, C_6, C_{5v}, C_{6v}	E_1	$m_0-2+I_A/2I_B$			
	E_2	0	C_{4h}, D_{4h}	E_g	$m_p-1+I_A/2I_B$
				E_u	m_p+m_0-1
D_3, D_{2d}, S_4, D_4	E	$2m_p+m_0-2+I_A/2I_B$			
			C_{5h}, D_{5h}	E_1'	m_p+m_0-1
D_5, D_6	E_1	$2m_p+m_0-2+I_A/2I_B$		E_1''	$m_p-1+I_A/2I_B$
	E_2	0		E_2'	0
				E_2''	0
D_{3d}, S_6	E_g	$m_p-1+I_A/2I_B$			
	E_u	m_p+m_0-1	C_{6h}, D_{6h}	E_{1g}	$m_p-1+I_A/2I_B$
				E_{1u}	m_p+m_0-1
D_{4d}	E_1	m_p+m_0-1		E_{2g}	0
	E_2	0		E_{2u}	0
	E_3	$m_p-1+I_A/2I_B$			

several simple examples, some by way of comparison with results previously reported.

C_{3v} Molecules

This symmetry group has only planes of symmetry passing through a threefold axis and hence only one degenerate species of vibrations. The simplest C_{3v} molecule is nonplanar YZ_3 (for instance ammonia), and the Y atom is the only "set of equivalent nuclei" situated on the threefold axis. Therefore $m_0=1$ and $\Sigma\zeta_{vib}=I_A/2I_B-1$. For molecules XYZ_3 in which both atoms X and Y are placed on the threefold axis (e.g., the methyl halides), $m_0=2$ and $\Sigma\zeta_{vib}=I_A/2I_B$. Both these results were obtained earlier by Dennison and Johnston.[2] For $WXYZ_3$, $m_0=3$ and $\Sigma\zeta_{vib}=1+I_A/2I_B$, as shown by Cowan[4] for BH_3CO. For $VWXYZ_3$ (e.g., methyl acetylene) $m_0=4$ and the sum is $2+I_A/2I_B$.

D_{3h} Molecules

If a plane of symmetry perpendicular to the threefold axis is added to C_{3v}, D_{3h} symmetry is obtained, which has two degenerate species, E' and E''. The simplest such molecule is symmetrical X_3 (no known example) for which the E' zeta-sum is zero, since there are no nuclei on the threefold axis. X_3 has no E'' vibrations. Planar XY_3 has the E' sum equal to zero, since $m_3=0$ and $m_0=1$. It is stated by Herzberg[4] that the E' sum for planar XY_3 is zero because $I_A=2I_B$ for planar molecules. It is clear from Table I that the ratio of I_A to I_B has no bearing on the E' sum, since rotation about the x, y axes belongs to the E'' species. There are no E'' vibrations in planar XY_3.

For the D_{3h} structure X_2Y_6, $m_3=1$ and therefore the sum for E' is zero and for E'', $I_A/2I_B$. The sums for ethane (C_2H_6) are reported by Herzberg[10] to be zero for both species E' and E'' in the D_{3h} structure, as well as for the analogous species E_u and E_g in the D_{3d} structure. These values are ascribed to Howard[4] who, however, gives only the correct value for E_u. The value for E_g is given by Hansen and Dennison[3] as $I_A/2I_B$.

C_{4v} Molecules

XYZ_4 molecules (a probable example is IF_5) have $m_0=2$, and hence for the only degenerate species E $\Sigma\zeta_{vib}=I_A/2I_B$.

D_{4h} Molecules

XY_2Z_4 molecules (a possible example is the appropriate isomer of SF_4Cl_2) have $m_0=1$ (the X-atom) and $m_4=1$ (the Y-atoms). Therefore the sum for species E_g is $I_A/2I_B$ and for E_u is 1.

D_{5h} Molecules

Molecules of the general formula XY_2Z_5 can have D_{5h} structure, a possible example being IF_7. In this molecule the iodine atom is at the center of a plane pentagon of fluorine atoms (therefore $m_0=1$), and the remaining two fluorine atoms are located on the fivefold axis above and below the plane (therefore $m_5=1$). From Table I the sums are: for E_1', -1; E_1'', $I_A/2I_B$; E_2', 0; E_2'', 0.

D_{6h} Molecules

Y_6Z_6 molecules such as C_6H_6 and C_6Cl_6 can have planar hexagonal (i.e., D_{6h}) structure. Since there are no nuclei located on the sixfold axis, m_0 and m_6 are both zero. Therefore, the sums are: for E_{1g}, $-1+I_A/2I_B$; E_{1u}, -1; E_{2g}, 0; E_{2u}, 0.

[10] Herzberg, reference 4, p. 49, Eq. IV.

Dipoles on a Lattice*: the Spherical Model†

MELVIN LAX
Department of Physics, Syracuse University, Syracuse, New York
(Received April 2, 1952)

The statistical treatment of a lattice of classical dipoles, electric or magnetic, has been intractable because of the "strong" condition that all dipoles have a fixed length. The spherical model consists in replacing the above strong condition by the weaker condition that the sum of the squares of the dipole vectors have the correct value, thus permitting some, but not much, fluctuation from the true situation.

The previous work of Berlin and Thomsen using the spherical model and nearest neighbor interactions is generalized to include a mixture of long and short range interactions. The evaluation of the partition sum in the presence of long-range forces requires care because some of the eigenvalues depend on specimen shape. A formula has been derived for the susceptibility, however, in which the shape dependence is explicitly shown to cancel. In fact, it is proven that in the spherical model a permanent dipole lattice is equivalent to an induced dipole lattice with a certain effective polarizability. Expansion of this polarizability in inverse powers of the temperature shows precise agreement to terms of order $(1/T)^3$ with an exact evaluation of the corresponding expansion coefficients.

All qualitative results are in agreement with those of Berlin and Thomsen. One- and two-dimensional lattices show no transition. A simple cubic lattice (the case they treat) shows an antiferroelectric transition bounded by a critical field curve $E=E_c[1-(T/T_c)]^{\frac{1}{2}}$.

The effective field and its application to an elementary quantum mechanical treatment of the ferromagnetic problem are described.

1. INTRODUCTION

IN this paper the interaction of permanent dipoles on a lattice is treated using sphericalization, a "relaxation" technique recently developed for treating problems of statistical mechanics that possess constraints.[1] Primary emphasis will be placed on the classical dipole-dipole interaction of a pair of electric (or magnetic) dipoles, including the long-range effects of such interactions. But the notation will be sufficiently general to include short-range forces of the exchange type, or a mixture of long- and short-range forces.

The interaction of induced dipoles on a lattice was treated exactly by Lorentz.[2] Important contributions to the permanent dipole problem have been made by a group of able physicists and chemists.[3–12]. An adequate statistical treatment of the dipole lattice problem that takes into account the directional properties of dipole-dipole forces and their long-range nature is still needed—particularly one that will be valid at both low and high temperatures.

Berlin and Thomsen[13] have considered the interaction of dipoles in simple lattices using the correct directional properties of dipole-dipole forces, but assuming only nearest neighbor forces. The completion of their analysis is made possible by the use of the sphericalization technique.[1] They do not regard their model as realistic from a quantitative point of view, but they hope it will shed light on transition phenomena—precisely the point at which previous calculations are weak. We shall see that their hope was justified.

The author was inspired by the work of Berlin and Thomsen to attempt an application of the sphericalization technique to the dipole lattice when long-range interactions are included. Our results may be summarized most briefly as follows: All qualitative conclusions of Berlin and Thomsen are verified when long-range interactions are included. For example, one- and two-dimensional lattices show no transition and three-dimensional simple cubic lattices show an antiferroelectric transition bounded by a critical field curve. The chief effect of including long-range interactions is to modify the critical temperature and critical field. All of Berlin and Thomsen's equations, when expressed in units of the critical temperature and field, are in fact still true when long-range interactions are included.

The procedure adopted in this paper is not, however, a straightforward generalization of the Berlin-Thomsen procedure. They factor the partition integral into a factor that involves only x components of the dipole vectors, a second that involves only y components, and a third that involves only z components. The quadratic forms in each of these integrals are then separately diagonalized. This factorization procedure is possible for nearest neighbor interactions in simple cubic crystals because no cross terms of the form $\mu_{ix}\mu_{jy}$ in the dipole com-

* This work forms part of a series on the multiple scattering of waves, i.e., the interaction of a field with a system of particles. For earlier work see M. Lax, Revs. Modern Phys. **23**, 287 (1951); Phys. Rev. **85**, 621 (1952).

† This work was supported in part by the ONR.

[1] E. W. Montroll, Nuovo cimento **6** (Suppl. No. 2) 265, (1949); T. H. Berlin, and M. Kac "The spherical model of a ferromagnet" Phys. Rev. (to be published).

[2] H. A. Lorentz, *Theory of Electrons* (B. G. Teubner, Leipzig, 1916), Second Edition, Note 54.

[3] P. Debye, *Polar Molecules* (Dover Publications, New York, 1945).

[4] P. Langevin, J. Phys. (U.S.S.R.) (4) **4**, 678 (1905); Ann. Chem. Phys. (8) **5**, 70 (1905).

[5] P. Debye, Physik. Z. **36**, 100, 193 (1935); Chem. Revs. **19**, 171 (1936).

[6] L. Onsager, J. Am. Chem. Soc. **58**, 1486 (1936).

[7] J. G. Kirkwood, J. Chem. Phys. **7**, 911 (1939).

[8] J. H. Van Vleck, J. Chem. Phys. **9**, 85 (1941).

[9] J. H. Van Vleck, J. Chem. Phys. **5**, 320, 556 (1937).

[10] J. A. Sauer, Phys. Rev. **57**, 142 (1940).

[11] J. M. Luttinger and L. Tisza, Phys. Rev. **70**, 954 (1946).

[12] J. A. Sauer and H. N. V. Temperley, Proc. Roy. Soc. (London) **176A**, 203 (1940).

[13] T. H. Berlin and J. S. Thomsen, J. Chem. Phys. (to be published). The author is indebted to Dr. Elliott Montroll for calling his attention in July 1951 to the work of Berlin and Thomsen, available as an ONR report.

ponents appear. For long-range interactions in simple cubic crystals, or nearest neighbor interactions in more complicated crystals, such cross terms appear and the factorization procedure breaks down.

The diagonalization procedure employed by Berlin and Thomsen is based on the cyclic nature of the quadratic forms describing the potential energy. This cyclic nature can be arranged simply only by using a dielectric specimen of rectangular shape. For short range forces, the results are not influenced by the shape, and this choice is permissible. The dipole-dipole interaction is long range, however. It is well known that the electric field within a specimen (compared to the external field) will be shape dependent. In fact, it is necessary to choose an ellipsoidal shape in order that the internal field be uniform. But if the specimen is ellipsoidal, how can cyclic boundary conditions be introduced?

It may be well to indicate here how the factorization and cyclic difficulties are overcome before entering upon the mathematical details. The general problem is to diagonalize a matrix of the form $G_{ij}{}^{xy}$ both with respect to its space indices x, y, z and its particle indices i, $j=1, 2, \cdots N$. The Berlin-Thomsen procedure is to make use of a property of $G_{ij}{}^{xy}$ special to simple cubic lattices and nearest neighbor interactions, namely, that G can be written as a sum of three terms each of which is already diagonalized with respect to its space indices. Since this procedure is not generally applicable, we reverse the order and diagonalize first with respect to the particle indices. In fact, the space diagonalization is not needed except for the final stages of numerical work. It is convenient, therefore, to suppress space indices altogether and use a dyadic notation $\mathbf{G}_{ij}$. The eigenvalues $\lambda(\mathbf{p})$ of $\mathbf{G}_{ij}$ will then be dyadics, i.e., three by three matrices whose diagonalization, when needed, can be performed by elementary methods.

The difficulties associated with shape dependence express themselves in the fact that such sums as $\sum_j \mathbf{G}_{ij}$ are conditionally convergent. In other words, for an infinite specimen the results will depend on the order in which the terms are added—in spherical layers, ellipsoidal layers, etc. If we wish to deal with a specimen of given shape (say an ellipsoid with principal axes a, b, c) we could modify the interaction matrix $\mathbf{G}_{ij}$ by a factor

$$f(\mathbf{r}_{ij})=\exp[-(x_{ij}/a)^2-(y_{ij}/b)^2-(z_{ij}/c)^2]. \quad (1.1)$$

An even simpler factor would be $f(\mathbf{r}_{ij})=1$ within the ellipsoid of principal axes a, b, c and $f(\mathbf{r}_{ij})=0$ outside. Such factors merely insure that the terms in the series are added up in the proper order. *The shape of the specimen is now contained in the convergence factor.*

With this convergence factor the sum over j can be carried over in *infinite* lattice, and the terms can be added in any order.[14] It is now convenient to forget the original purpose of the convergence factor and pretend that the modified interaction dyadic actually describes a true interaction energy. Sums over an infinite lattice can now be replaced by sums over any finite lattice all of whose dimensions are large compared to a, b, c. With respect to this fictitious finite specimen, the modified interaction energy can be regarded as a short range interaction. Shape and surface effects are unimportant, and it is possible to introduce a large fictitious specimen of rectangular shape to which cyclic boundary conditions can be applied. The modified matrix $\mathbf{G}_{ij}$ will now be cyclic. Its dyadic eigenvalues $\lambda(\mathbf{p})$ can be computed. And they will be characteristic of a *real* specimen of ellipsoidal shape and principle axes a, b, c.

In this way, the difficulties encountered in a straightforward generalization of the Berlin-Thomsen paper are overcome. No specific use is made of the tensor charactor of $\mathbf{G}_{ij}$ so that forces of exchange type can also be treated. No use is made of the specific lattice structure so that crystals of noncubic type are included in the analysis. The major achievement, however, is the inclusion of long-range interactions of dipole-dipole type.

2. FORMULATION

The energy U of a set of dipoles $\mu\boldsymbol{\varepsilon}_j$ situated at the lattice point j can be written in the form

$$-U=\tfrac{1}{2}n\mu^2\textstyle\sum_{i,j}\boldsymbol{\varepsilon}_i\cdot\mathbf{G}_{ij}\cdot\boldsymbol{\varepsilon}_j+\mu(\sum\boldsymbol{\varepsilon}_j)\cdot\mathbf{E}_0, \quad (2.1)$$

where $\mathbf{E}_0$ is the applied field external to the specimen, μ is the dipole strength, the $\boldsymbol{\varepsilon}_j$ are unit vectors, and n is the number of dipoles per unit volume. The interaction dyadic contains a long-range dipole-dipole term and a short-range dyadic $\mathbf{J}_{ij}$:

$$\begin{aligned}&\mathbf{G}_{ij}=f(\mathbf{r}_{ij})r_{ij}{}^{-5}[3\mathbf{r}_{ij}\mathbf{r}_{ij}-r_{ij}{}^2\mathbf{1}]+\mathbf{J}_{ij},\\&\mathbf{G}_{ii}=0,\end{aligned} \quad (2.2)$$

where $f(\mathbf{r}_{ij})$ is the convergence factor (1.1), and $\mathbf{J}_{ij}$ for isotropic exchange forces reduces to $J_{ij}\,\mathbf{1}$ where $\mathbf{1}$ is the unit dyadic. The vector distance between dipoles $\mathbf{r}_{ij}$ is measured in units of $n^{-\frac{1}{3}}$.

The partition function Q aside from a normalization factor is given by the integral

$$Q=\int\exp(-U/kT)d\boldsymbol{\varepsilon}, \quad (2.3)$$

where $d\boldsymbol{\varepsilon}$ is an abbreviation for $d\boldsymbol{\varepsilon}_1$, $d\boldsymbol{\varepsilon}_2$, $\cdots d\boldsymbol{\varepsilon}_N$. The mean value of any observable quantity $H(\boldsymbol{\varepsilon})=H(\boldsymbol{\varepsilon}_1, \boldsymbol{\varepsilon}_2, \cdots\boldsymbol{\varepsilon}_N)$ is given by

$$\langle H\rangle=Q^{-1}\int H(\boldsymbol{\varepsilon})\exp(-U/kT)d\boldsymbol{\varepsilon}. \quad (2.4)$$

Thus, $\langle H\rangle$ is independent of normalization constants as

[14] This procedure is equivalent to treating each dipole as if it were at the center of the ellipsoid, so that the effective field $\Sigma_j\mathbf{G}_{ij}$ is automatically independent of i. But the average field and the effective field in an ellipsoid are known to be independent of position by Lorentz's semimacroscopic calculation. Thus, no important change is made in the eigenvalues of the interaction matrix $\mathbf{G}_{ij}$, and the problem is made truly cyclic in that all dipoles play an equivalent role.

long as the numerator and denominator of (2.4) are treated in the same way. We shall find it convenient, therefore, to omit all normalization constants that appear in the subsequent calculations. The integrations (2.3) and (2.4) are to be carried out subject to the restrictions

$$\boldsymbol{\varepsilon}_j^2=1, \quad j=1, 2, \cdots N. \tag{2.5}$$

The corresponding calculation for induced dipoles may be performed by omitting these restrictions (2.5) and setting

$$\mathbf{G}_{ii}=-\mathbf{1}/(n\alpha) \text{ induced dipoles}, \tag{2.6}$$

where α is the polarizability of a single dipole.

The integrals (2.3) and (2.4) will not show a discontinuity characteristic of a phase transition except in the limit $N\to\infty$. We shall therefore introduce the partition function "per particle" Z and the free energy per particle ψ:

$$Z=\lim_{N\to\infty} Q^{1/N}; \quad \psi=-kT \ln Z. \tag{2.7}$$

Most physical observables $H(\boldsymbol{\varepsilon})$ can be inserted beneath the integral (2.4) by differentiation with respect to a parameter. In this way, we recover the usual formulas for internal energy per particle u, specific heat per particle C and polarization P:

$$u=kT^2 d(\ln Z)/dT, \tag{2.8}$$

$$C=du/dT, \tag{2.9}$$

$$P=nkT\partial(\ln Z)/\partial E_0. \tag{2.10}$$

The dielectric constant ϵ and electric susceptibility χ are defined by[15]

$$P=\chi E=(\epsilon-1)E/(4\pi), \tag{2.11}$$

where E is the macroscopic average electric field within the specimen. Since the ratio of E_0 to E depends on the shape of the specimen, it remains to be demonstrated that the dielectric constant calculated from (2.10) and (2.11) is independent of specimen shape.

3. THE SPHERICAL MODEL

The spherical model consists in relaxing the constraint (2.5) that all dipoles have unit length and replacing it by the weaker constraint:

$$\sum_j \boldsymbol{\varepsilon}_j^2=N. \tag{3.1}$$

The weaker constraint retains the correct average value $\langle\boldsymbol{\varepsilon}_j^2\rangle=1$ and prevents large fluctuations ($\boldsymbol{\varepsilon}_j^2$ of the order of N). However, it does permit appreciable fluctuations from the original constraints since $\langle\boldsymbol{\varepsilon}_j^4\rangle=5/3$ above the critical temperature. Admitting this important weakness, we shall nevertheless retain the spherical model because of its primary advantage: it permits an exact evaluation of the 10^{23} integrals required for the determination of the partition function Q.

The spherical restraint (3.1) may be taken into account in the integrals (2.3) and (2.4) by inserting a Dirac delta-function $\delta(N-\sum\boldsymbol{\varepsilon}_j^2)$. Aside from a normalization constant this delta-function can be given the integral representation

$$\delta(N-\textstyle\sum\boldsymbol{\varepsilon}_j^2)\propto\displaystyle\int_{\sigma-i\infty}^{\sigma+i\infty}\exp[Kt(N-\textstyle\sum\boldsymbol{\varepsilon}_j^2)]dt, \tag{3.2}$$

$$K=(n\mu^2)/(2kT). \tag{3.3}$$

Comparison with (2.1) and (2.3) indicates that we have in effect inserted into the negative energy $-U$ diagonal terms of the form $-\frac{1}{2}n\mu^2 t\boldsymbol{\varepsilon}_j^2$; in other words, $\mathbf{G}_{ii}=-t\mathbf{1}$. Further comparison with (2.6) indicates that (for a given value of t) we are dealing with an induced dipole lattice whose polarizability α is determined by

$$n\alpha=1/t. \tag{3.4}$$

The resulting integration over t then describes a superposition of induced dipole lattices with varying polarizabilities. The partition function (2.3) can be written in the form

$$Q=\int\exp(NKt)dtQ(t), \tag{3.5}$$

where $Q(t)$ is the corresponding partition function for an induced dipole lattice satisfying (2.6) and (3.4), i.e., using $\mathbf{G}_{ii}=-t\mathbf{1}$:

$$Q(t)=\int\exp[-U(t)/kT]d\boldsymbol{\varepsilon}. \tag{3.6}$$

In the limit of large N, we can, in analogy to (2.7), replace $Q(t)$ by

$$Q(t)\to[Z(t)]^N=\exp[N\ln Z(t)], \tag{3.7}$$

where $Z(t)$ is independent of N. If we define $H(t)$ to be the mean value of $H(\boldsymbol{\varepsilon})$ for an induced dipole lattice

$$Q(t)H(t)=\int H(\boldsymbol{\varepsilon})\exp[-U(t)/kT]d\boldsymbol{\varepsilon}, \tag{3.8}$$

the corresponding average for the permanent dipole case is

$$\langle H\rangle=\frac{\displaystyle\int H(t)\exp[NKt+N\ln Z(t)]dt}{\displaystyle\int\exp[NKt+N\ln Z(t)]dt}. \tag{3.9}$$

Because of the enormous size of N, a steepest descent procedure may be applied to (3.9). The major contribution to both numerator and denominator integrals will come from the saddle point t_s (when such a saddle point

[15] This definition differs from the more conventional one $\chi=\partial P/\partial E$ only when the susceptibility is field dependent.

exists). Thus,

$$\langle H\rangle = H(t_s). \tag{3.10}$$

In other words, mean values of all observables can be related to their corresponding values for an induced dipole lattice with effective polarizability α_s:

$$\alpha_s = (nt_s)^{-1}. \tag{3.11}$$

But an induced dipole lattice with depolarization constant L has an average field E and effective field E_e given by:

$$\begin{aligned} E &= E_0 - 4\pi LP, \\ E_e &= E + 4\pi L'P, \end{aligned} \tag{3.12}$$

where L' is structure dependent (and reduces to $L'=1/3$ for simple cubic lattices if only dipole-dipole interactions are present). Therefore, the electric susceptibility of a permanent dipole lattice of the same shape will be given by

$$\chi = n\alpha_s E_e/E = n\alpha_s/(1-4\pi L' n\alpha_s), \tag{3.13}$$

where $\alpha_s=(nt_s)^{-1}$, the effective polarizability, is an as yet unknown function of the temperature. The fact that the susceptibility is independent of shape, i.e., of L will be demonstrated explicitly as a check on the accuracy of our procedure.

In this section, therefore, we have broken the calculation of any observable $\langle H(\varepsilon)\rangle$ into two parts: (1) the calculation of its mean value $H(t)$ for an induced dipole lattice, (2) the determination of the partition function $Z(t)$ for the induced case and the saddle point t_s.

We may anticipate future results by remarking that a saddle point will exist only for temperatures T above a certain "Curie" temperature T_c. Below this temperature, long-range order will appear. Thus, the existence of transition phenomena will be represented in the theory by the disappearance of a normal saddle point.

4. DIAGONALIZATION OF THE INTERACTION ENERGY

The calculation of the partition function $Q(t)$ for an induced dipole lattice requires the evaluation of a multiple integral (3.6) of an exponential whose argument is a quadratic form. Aside from a normalization constant, the value of such an integral is simply one over the square root of the determinant of the quadratic form. The only practical way to evaluate this determinant, however, is to use the theorem that it is equal to the product of the eigenvalues. Thus we must diagonalize the interaction energy and find its eigenvalues. (Once the form is diagonalized the multiple integral factors into single integrals, each of which yields one over the square root of the corresponding eigenvalue, thus verifying the above statements in a trivial way.) We are, therefore, interested in the solution of the set of linear equations

$$\sum_j \mathbf{G}_{ij}\cdot\boldsymbol{\varepsilon}_j = \boldsymbol{\lambda}\cdot\boldsymbol{\varepsilon}_i, \tag{4.1}$$

whose eigenvalue $\boldsymbol{\lambda}$ is a dyadic. For simplicity, let us assume that we are dealing with a monatomic lattice so that the indices i, j refer to the unit cells rather than the particles. (For polyatomic lattices, the particles within a cell can be labeled with indices β, γ so that we must diagonalize $\mathbf{G}_{ij}{}^{\beta\gamma}$. For fixed β, γ the eigenvalue will be $\boldsymbol{\lambda}^{\beta\gamma}$. The individual eigenvalues must then be obtained by diagonalizing $\boldsymbol{\lambda}^{\beta\gamma}$ with respect to particle as well as space indices. The procedure for a monatomic lattice is simply equivalent to suppressing all indices but cell indices.)

Because of the periodicity of the lattice, the eigenvectors will be of Bloch form:

$$\boldsymbol{\varepsilon}_i = \mathbf{y}_\mathbf{p}\exp(i\mathbf{p}\cdot\mathbf{r}_i). \tag{4.2}$$

Substitution of (4.2) into (4.1) yields the eigenvalue

$$\boldsymbol{\lambda}(\mathbf{p},t) = \sum_j \mathbf{G}_{ij}\exp[i\mathbf{p}\cdot(\mathbf{r}_j-\mathbf{r}_i)] = -t\mathbf{1}+\boldsymbol{\lambda}(\mathbf{p},0). \tag{4.3}$$

The sum over j is independent of i because $\mathbf{G}_{ij}$ depends only on $\mathbf{r}_{ji}=\mathbf{r}_j-\mathbf{r}_i$ and all cell positions are equivalent. The number of permissible values of $\mathbf{p}$ is equal to N the number of cells, and because of the cyclic boundary conditions these values of $\mathbf{p}$ are uniformly spaced over one cell in the reciprocal lattice space.

Since $\mathbf{G}_{ij}$ is a real even function of $\mathbf{r}_{ij}$, the eigenvalues (4.3) are real and degenerate in the pairs $\mathbf{p}$, $-\mathbf{p}$. The transformation to normal coordinates can be written in the form

$$\boldsymbol{\varepsilon}_j = N^{-\frac{1}{2}}\sum_\mathbf{p}\mathbf{y}_\mathbf{p}\exp(i\mathbf{p}\cdot\mathbf{r}_j), \tag{4.4}$$

$$\mathbf{y}_\mathbf{p} = N^{-\frac{1}{2}}\sum_j\boldsymbol{\varepsilon}_j\exp(-i\mathbf{p}\cdot\mathbf{r}_j), \tag{4.5}$$

where

$$\mathbf{y}_{-\mathbf{p}} = \mathbf{y}_\mathbf{p}{}^*, \tag{4.6}$$

preserves the reality of $\boldsymbol{\varepsilon}_j$. The interaction energy (2.1) can be written in terms of the normal coordinates:

$$-U = \mu N^{\frac{1}{2}}\mathbf{y}_0\cdot\mathbf{E}_0+\tfrac{1}{2}n\mu^2\sum_\mathbf{p}\mathbf{y}_\mathbf{p}\cdot\boldsymbol{\lambda}(\mathbf{p},t)\cdot\mathbf{y}_\mathbf{p}{}^*. \tag{4.7}$$

The terms in $\mathbf{y}_0$ are to be treated by completing the square. The term in $\mathbf{y}_\mathbf{p}$ can be diagonalized with respect to space. The integral (3.6) for the partition function breaks up into a product of Gaussian integrals. If we write $\boldsymbol{\lambda}(\mathbf{p},t)=\boldsymbol{\lambda}(\mathbf{p},0)-t\mathbf{1}=\boldsymbol{\lambda}(\mathbf{p})-t\mathbf{1}$ and designate the three space eigenvalues of $\boldsymbol{\lambda}(\mathbf{p})$ by $\lambda_a(\mathbf{p})$, $a=1,2,3$, the partition function aside from normalization constants is given by

$$Q(t) = K^{-(3N/2)}\exp[-\tfrac{1}{2}V\mathbf{E}_0\cdot\lambda^{-1}(0,t)\cdot\mathbf{E}_0/kT] \times\Big[\prod_{p=1}^{N}\prod_{a=1}^{3}(t-\lambda_a(\mathbf{p}))\Big]^{-\frac{1}{2}}, \tag{4.8}$$

where V is the volume of the specimen.

The partition function per dipole $Z(t)$ can according to (3.7) be given by

$$\ln Z(t) = -\mathbf{E}_0\cdot\boldsymbol{\lambda}^{-1}(0,t)\cdot\mathbf{E}_0/(2nkT)-(3/2)\ln K - (2N)^{-1}\sum_{a=1}^{3}\sum_{p=1}^{N}\ln[t-\lambda_a(\mathbf{p})]. \tag{4.9}$$

With the help of (2.10) we find then that the polarization is given by[16]

$$P=-[\lambda(0,t)]^{-1}\cdot E_0=[t\mathbf{1}-\lambda(0)]^{-1}\cdot E_0. \quad (4.10)$$

Since the field within the specimen is given by $\mathbf{E}=\mathbf{E}_0-4\pi\mathbf{L}\cdot\mathbf{P}$ where $\mathbf{L}$ is the depolarization tensor, the susceptibility tensor defined by $\mathbf{P}=\chi\cdot\mathbf{E}$ has the value

$$\chi=n\alpha\{1-n\alpha[\lambda(0)+4\pi\mathbf{L}]\}^{-1}, \quad (4.11)$$

where the replacement $t=(n\alpha)^{-1}$ has been made. But the eigenvalue $\lambda(0)$ is a sum whose distance terms can be replaced by an integral in the manner described by Lorentz.[2] And that integral yields a surface contribution $-4\pi\mathbf{L}$. Thus, $4\pi\mathbf{L}'=\lambda(0)+4\pi\mathbf{L}$ is a tensor independent of specimen shape that depends on the short-range forces as well as the crystal structure. The susceptibility tensor (4.11) thus has the form (3.13) anticipated—independent of specimen shape. For permanent dipole lattices, (3.10) implies that $n\alpha_s$ should be replaced by $1/t_s$.

5. DETERMINATION OF THE SADDLE POINT

Aside from a factor 3/2, the last term in (4.9) is an average of the values of $\ln(t-\lambda_a(\mathbf{p}))$ over the $3N$ possible eigenvalues. It is convenient, therefore, to introduce the notation

$$\langle\ln(t-\lambda)\rangle=\lim_{N\to\infty}(3N)^{-1}\sum_{a=1}^{3}\sum_{p=1}^{N}\ln[t-\lambda_a(\mathbf{p})]$$

$$=\tfrac{1}{3}\sum_{a=1}^{3}\int\ln[t-\lambda_a(p)]d\mathbf{p}\Big/\int d\mathbf{p}, \quad (5.1)$$

where the integrations are carried out over one cell of reciprocal lattice space since the possible values of $\mathbf{p}$ are uniformly distributed over such a cell. The partition function per dipole $Z(t)$ can therefore be determined from

$$Kt+\ln Z(t)=E_0\cdot[t\mathbf{1}-\lambda(0)]^{-1}\cdot E_0/(2nkT)-(3/2)\ln K+f(t,K), \quad (5.2)$$

$$f(t,K)=Kt-(3/2)\langle\ln(t-\lambda)\rangle. \quad (5.3)$$

A word of caution must be added here. It appears that any single term in the sum (5.1) makes a contribution of order $1/N$ and may be neglected in the limit as $N\to\infty$. In fact, the *individual* contribution of this term is lost in the passage to the integral. If, however, a transition should occur into a single state corresponding to the eigenvalue λ_m, the contribution of the term $\ln(t-\lambda_m)$ must be separately considered and will yield a finite contribution even as $N\to\infty$. This single term multiplies the partition function $Z(t)$ of (5.2) by a factor $(t-\lambda_m)^{-\frac{1}{3}}$. Such a factor will not affect the existence or location of a saddle point but may make a finite contribution by adding a new singularity or pole to the integrals (3.5) and (3.9).

The removal of a single term or any finite number of terms from the sum will not affect the convergence to the integral $\langle\ln(t-\lambda)\rangle$. Thus, we can make the important assertion $\langle\ln(t-\lambda)\rangle$ is independent of the shape of the specimen. This follows from the fact that only a small number of modes $\mathbf{p}$, whose wavelengths are comparable to the specimen dimensions, have eigenvalues $\lambda(\mathbf{p})$ that are shape dependent.

The saddle point may be located using the condition

$$(d/dt)[Kt+\ln Z(t)]_{t=t_s}=0. \quad (5.4)$$

By inserting (5.2), the saddle point condition can be written in either of the two forms:

$$\begin{aligned}(2K/3)[1-(E_e/n\mu t_s)^2]&=\langle(t_s-\lambda)^{-1}\rangle\\ (n\mu^2/3kT)[1-(\alpha_s E_e/\mu)^2]&=n\alpha_s\langle(1-n\alpha_s\lambda)^{-1}\rangle,\end{aligned} \quad (5.5)$$

$$\mathbf{E}_e=t_s[t_s\mathbf{1}-\lambda(0)]^{-1}\cdot\mathbf{E}_0=\mathbf{E}+4\pi\mathbf{L}'\cdot\mathbf{P}. \quad (5.6)$$

Note that the saddle point $t_s=(n\alpha_s)^{-1}$ is independent of specimen shape although $\mathbf{E}_0$ and $\lambda(0)$ separately depend on specimen shape.

6. THE CURIE TEMPERATURE AND THE CRITICAL FIELD CURVE

The validity of the previous work rests on the assumption that the partition function $Q(t)$ is obtained from a convergent multiple integral, i.e., that the energy $U(t)$ is a positive definite quadratic form[13] or that $\mathbf{G}_{ij}$ (with $\mathbf{G}_{ii}=-t\mathbf{1}$) is a negative definite matrix. The latter statement is equivalent to the requirement (see Eq. 4.7) that all eigenvalues of $\mathbf{G}_{ij}$ be negative: $\lambda_a(\mathbf{p})-t<0$. The requirement that t be larger than each of the eigenvalues $\lambda_a(\mathbf{p})$ may be satisfied[13] in the original integral representation (3.2) by requiring that the path of integration over t pass to the right of the maximum eigenvalue λ_m. Thus, a saddle point will exist in the allowed region of integration only if the saddle point equation (5.5) has a root for which $t_s>\lambda_m$, or $n\alpha_s<\lambda_m^{-1}$.

Let us consider, first, the saddle point equation (5.5) in the absence of an applied field. At high temperatures $K\to 0$ and t_s approaches the large value $(3/2K)$, i.e., α_s approaches the conventional value $(\mu^2/3kT)$. As the temperature is decreased, K increases, and t must decrease until finally, when $t\to\lambda_m$, a critical temperature is reached:

$$2K_c/3=n\mu^2/(3kT_c)=\langle(\lambda_m-\lambda)^{-1}\rangle. \quad (6.1)$$

At this temperature the effective polarizability has reached its maximum value $\alpha_s\to\alpha_m=(n\lambda_m)^{-1}$.

The reason for the importance of the eigenvalue λ_m in the above analysis is that the energy of any eigenstate of the system is $-1/2n\mu^2\lambda_a(\mathbf{p})$, so that $-1/2n\mu^2\lambda_m$ is the energy of the state of lowest energy of the dipole lattice. Thus, we might expect that at sufficiently low temperatures the system would "condense" into its lowest state. However, as Luttinger and Tisza have pre-

[16] The possibility that t may be field dependent is neglected here. This possibility can occur for the permanent dipole case, but the results stated here will nevertheless be correct (cf. Sec. VII).

viously remarked,[11] a knowledge of the energies alone does not determine the existence of a transition temperature. In particular, if $\langle(t-\lambda)^{-1}\rangle$ diverges as $t\to\lambda_m$, then a root t_s of (5.5) exists no matter how large K is or how small T is. In this case no sharp transition will take place. On the other hand, if $\langle(\lambda_m-\lambda)^{-1}\rangle$ is finite, a critical temperature T_c exists, as determined by (6.1).

If λ_m is a relative maximum, as well as an absolute maximum, i.e., if

$$\partial\lambda/\partial p_x=\partial\lambda/\partial p_y=\partial\lambda/\partial p_z=0, \tag{6.2}$$

at the eigenstate p_m, and $\partial^2\lambda/\partial p_x\partial p_y$ is a negative definite quadratic form, it is easy to verify that $\int(\lambda_m-\lambda)^{-1}d\mathbf{p}$ diverges if $d\mathbf{p}$ is a one-dimensional or two-dimensional volume element but converges if $d\mathbf{p}$ is a three-dimensional volume element. For the usual cases, then we expect to find transitions only in the three-dimensional crystalline case. (If the quadratic form $\partial^2\lambda/\partial p_x\partial p_y$ is not negative definite, even the three-dimensional integral will diverge so that no transition will occur.)

In some unusual cases $\lambda(\mathbf{p})$ will not be analytic at the eigenstate $\mathbf{p}_m$ (e.g., the behavior may be cusp-like), so that the Taylor expansion used above is not applicable. In such cases it may be useful to make the transformation

$$\int(\lambda_m-\lambda)^{-1}d\mathbf{p}=\int(\lambda_m-\lambda)^{-1}N(\lambda)d\lambda,$$

where

$$N(\lambda)=\int\delta[\lambda-\lambda(\mathbf{p})]d\mathbf{p} \tag{6.3}$$

is the density of states in the energy interval $d\lambda$. Convergence of the integral (i.e., the existence of a transition) then requires that the density of states vanish at $\lambda=\lambda_m$ as some finite positive power $(\lambda-\lambda_m)^\delta$, $\delta>0$.

The density of states in the one-, two-, and three-dimensional cases when λ_m is a relative maximum are given, respectively, by $N(\lambda)\sim(\lambda_m-\lambda)^{-\frac{1}{2}}$, 1 and $(\lambda_m-\lambda)^{\frac{1}{2}}$. Thus, the two-dimensional case is seen to be borderline, and it may be possible to find a two-dimensional structure for which a transition exists.

The nature of the state into which a transition may occur may be deduced by finding the states of maximum eigenvalue λ_m. This problem has already been treated by Luttinger and Tisza.[11] For the simple cubic, body-centered cubic, and face-centered cubic cases, they find three lowest energy simple antiferroelectric arrays whose eigenvalues λ_m are given, respectively, by simple cubic 5.351, body-centered cubic, 3.972, face-centered cubic 3.615. On the other hand, the eigenvalue for the polarized array is $\lambda(0)=4\pi(1/3-L)=4.188-4\pi L$, where L is the depolarization constant. Thus the simple cubic lattice definitely has an antiferroelectric transition regardless of shape, and the body-centered cubic and face-centered cubic arrays may have antiferroelectric transitions for reasonable shapes. For a sufficiently elongated sample (axis ratio of 6:1 in the face-centered cubic case) the ferroelectric eigenvalue is larger in the face-centered cubic and body-centered cubic cases. However, the eigenvalues $\lambda(\mathbf{p})$ change rapidly from nonshape dependent values to shape dependent values as $\mathbf{p}\to0$, so that the existence of a ferroelectric transition requires further investigation. In any case, the existence of a metastable antiferroelectric state must be considered. (See Sec. 7.)

In the presence of an applied field E, the critical temperature T_c becomes field dependent (see Eq. 5.5). The critical temperature $T_c(E)$ may be obtained by finding the maximum value of $\langle(t_s-\lambda)^{-1}\rangle/[1-(E_c/n\mu t_s)^2]$. This maximum value is achieved when $t_s=\lambda_m$. Thus, we find in agreement with Berlin and Thomsen

$$T_c(E)=T_c[1-(E/E_c)^2], \tag{6.4}$$

where

$$E/E_c=\alpha_m E_e/\mu.$$

The only difference between our results and Berlin's is in the value of T_c and E_c. For any given temperature (less than T_c) a critical field exists:

$$E=E_c[1-(T/T_c)]^{\frac{3}{2}}, \tag{6.5}$$

thus describing a "critical field curve." For $E>E_c$, a saddle point always exists, and no transition can occur. (Similarly for $T>T_c$.) Thus, the critical field curve is the dividing line between the disordered and the ordered state. The critical field strength E_c has a simple interpretation. This is the field that, at the maximum polarizability α_m, would saturate the lattice. It is clear that in the presence of such a field an antiferroelectric state cannot exist.

7. BEHAVIOR BELOW THE CURIE POINT

Below the Curie point, the saddle point equation (5.5) no longer has a root $t_s\gtrsim\lambda_m$. The integration over t must be reconsidered. The factor $(t-\lambda_m)^{-\frac{1}{2}}$ must be explicitly considered, as was noted in Sec. 5. This factor may be represented by a branch cut extending from λ_m to minus infinity on the real axis. The integration over t must pass around (i.e., to the right of) this branch cut. Since Eq. (5.4) is not satisfied, the exponent must possess a term linear in $t-\lambda_m$:

$$Kt+\ln Z(t)\simeq K\lambda_m+\ln Z(\lambda_m)+(t-\lambda_m)\{K[1-(E/E_c)^2]-K_c\}+\cdots. \tag{7.1}$$

Further, the coefficient of $(t-\lambda_m)$ is positive below the Curie temperature $T_c(E)$. Thus, a path of steepest descent may be chosen running from minus infinity to λ_m below the branch cut and back to minus infinity above the cut. (See Fig. 1, of reference 13.) Thus we conclude in agreement with Berlin and Thomsen that although $t_s=\lambda_m$ is not a saddle point, the major contribution to the partition function comes from the neighborhood of the point λ_m. The mean value of any

observable $H(t)$ will therefore be given by $H(\lambda_m)$. For example, the electric susceptibility (4.11) has the value

$$\chi=n\alpha_s[1-4\pi n\alpha_s L']^{-1} \quad T>T_c(E), \tag{7.2}$$

$$\chi=n\alpha_m[1-4\pi n\alpha_m L']^{-1} \quad T<T_c(E), \tag{7.3}$$

where $4\pi L'=\lambda(0)+4\pi L$, α_s is a solution of the saddle point equation (5.5), and $n\alpha_m=\lambda_m^{-1}$. Thus, below the critical temperature $T_c(E)$, the electric susceptibility is a constant, whereas above this temperature (through α_s) it will be temperature dependent and, in strong fields, field dependent. As $T\to 0$, Eq. (7.2) is still valid for $E>E_c$ providing α_s is given the value (from 5.5) $\alpha_s=\mu/E_e$, i.e., the lattice is saturated. These results are in qualitative agreement with those obtained by Berlin and Thomsen.

The susceptibility at the Curie point will be finite if $n\alpha_m[\lambda(0)+4\pi L]<1$, i.e., if $\lambda_m>\lambda(0)+4\pi L$. This condition is satisfied in simple cubic lattices since $\lambda_m=5.351$ and $\lambda(0)+4\pi L=4\pi/3=4.188$. For body-centered cubic and face-centered cubic lattices, however, this condition is not satisfied, if we use for our maximum eigenvalues the results obtained by Luttinger and Tisza using simple antiferroelectric arrays. On the other hand, for a spherical sample the susceptibility for these arrays should be finite at the Curie temperature. This dilemma is resolved in the spherical model by noting that for $p\gg V^{-\frac{1}{3}}$, $\lambda(\mathbf{p})$ is independent of specimen shape and as $\mathbf{p}\to 0$, $\lambda(\mathbf{p})$ approaches $\lambda(0)+4\pi L=4\pi L'$. Thus, the maximum eigenvalue occurs for an array that is almost ferroelectric but has no net polarization. This state, however, will probably not be stable.[17] For a sufficiently oblong sample, the true ferroelectric state will have but a slightly higher energy, and the addition of a small electric field will cause the sample to enter the ferroelectric state. The absence of an applied field will cause a break-up into domains at the expense of the depolarization energy.

For simple cubic lattices, the state of lowest energy (largest λ) for purely dipole-dipole interactions is the state $\mathbf{y}_\mathbf{p}$ for $\mathbf{p}=(\pi,\pi,0)$ and $\mathbf{y}$ in the z direction, the same state found by Berlin and Thomsen. This state consists of a set of strings of parallel dipoles. The strings run in the z direction, and the orientation of the dipoles on a given string is in the plus z direction or in the minus z direction. This orientation reverses as we pass from one string to an adjacent string by a lattice displacement in the x or y direction. Berlin and Thomsen introduced the long-range order parameter:

$$S_z=\langle|\sum_{\substack{\text{even}\\\text{dipoles}}}\epsilon_{jz}-\sum_{\substack{\text{odd}\\\text{dipoles}}}\epsilon_{jz}|\rangle/N=N^{-\frac{1}{2}}\langle|y_{(\pi,\pi,0)z}|\rangle. \tag{7.4}$$

In general, if λ_m is the maximum eigenvalue and y_m is the corresponding "state," $S=N^{-\frac{1}{2}}\langle|y_m|\rangle$ is a suitable long-range order parameter. The mean value of S for an induced dipole lattice, $S(t)$, is given by

$$S(t)=N^{-\frac{1}{2}}\frac{\int|y_m|\exp[-Ky_m^2(t-\lambda_m)]dy_m}{\int\exp[-Ky_m^2(t-\lambda_m)]dy_m}=[\pi NK(t-\lambda_m)]^{-\frac{1}{2}}. \tag{7.5}$$

For $T>T_c(E)$ a saddle point exists, and S may be obtained from $S(t)$ be replacing t by t_s. Therefore, above the Curie point, S is of order $N^{-\frac{1}{2}}$ and vanishes in the limit as N approaches infinity. For $T<T_c(E)$,

$$S=\frac{\int S(t)(t-\lambda_m)^{-\frac{1}{2}}\exp[NKt+N\ln Z(t)]dt}{\int(t-\lambda_m)^{-\frac{1}{2}}\exp[NKt+N\ln Z(t)]dt}. \tag{7.6}$$

The numerator has a simple pole, and the denominator can be integrated exactly using the exponent (7.1). The long-range order is found to be

$$S=[1-(E/E_c)^2-(T/T_c)]^{\frac{1}{2}} \tag{7.7}$$

and is seen to go to zero at $T=T_c(E)$. Thus, the critical temperature denotes the onset of long-range order.

The partition function per particle Z of (2.7) may be obtained from (3.5) and (3.7):

$$\begin{aligned}\ln Z&=Kt_s+\ln Z(t_s) \quad T>T_c(E)\\ &=K\lambda_m+\ln Z(\lambda_m) \quad T<T_c(E),\\ \ln Z(t)&=\mathbf{E}_0\cdot[t\mathbf{1}-\boldsymbol{\lambda}(0)]^{-1}\cdot\mathbf{E}_0/(2nkT)\\ &\quad-(3/2)\ln K-(3/2)\langle\ln(t-\lambda)\rangle,\end{aligned} \tag{7.8}$$

using (5.2). Note that the field dependent term in $\ln Z(t)$ can, using (4.10), be rewritten in the form $P\cdot E_0/(2nkT)$. The field dependent contribution to the free energy per unit volume, $n\psi$, is according to (2.7), given by the usual formula $-\mathbf{P}\cdot\mathbf{E}_0/2$. Above the critical temperature, t_s is also field dependent. However,

$$d(\ln Z)/dE_0=\partial\ln Z(t_s)/\partial E_0, \tag{7.9}$$

since the terms arising from differentiating with respect to t_s vanish because t_s obeys the saddle point condition (5.4). This justifies our previous procedure[16] in neglecting the field dependence of t_s when calculating the polarization.

The internal energy per dipole u can be calculated from the thermodynamic formula (2.8), again omitting derivatives with respect to t_s:

$$u=(3kT/2)[1-(2Kt_s/3)]-\mathbf{P}\cdot\mathbf{E}_0/(2n). \tag{7.10}$$

This result applies also for temperatures $T<T_c(E)$ if t_s is replaced by the constant value λ_m. Differentiation with respect to temperature yields the specific heat per

[17] This state may be perfectly stable in the spherical model, but it may not obey the strong conditions $\epsilon_j^2=1$ for all j.

dipole:

$$C=(3k/2) \qquad T<T_c(E),$$
$$C=(3k/2)+kK^2(dt_s/dK)[1-(E/E_c)^2] \qquad T>T_c(E). \quad (7.11)$$

These results are in qualitative agreement with those of Berlin and Thomsen. As the temperature is increased from absolute zero, the specific heat is constant up to the critical temperature and decreases monotonically for all higher temperatures. The specific heat is continuous at the critical temperature, but dC/dT changes abruptly from zero to a finite negative slope.

The term $3kT/2$ in the energy is simply the equipartition potential energy of an oscillator with three degrees of freedom and arises from the fact that the spherical model replaces $2N$ degrees of freedom by $3N-1$. At high temperatures, $t_s \to (3/2K)$ so that this term is nearly cancelled, and the high temperature energy and specific heat may have some validity. Below the Curie point, however, a more accurate classical treatment would probably yield a specific heat $C \simeq k$, and a quantum mechanical treatment would, in accord with Nernst's theorem, require C to vanish as the temperature approaches absolute zero.

8. SUMMARY OF DIELECTRIC PROPERTIES

Since the most important application of the present paper is the determination of the electric (or magnetic) susceptibility, we shall summarize here the most important dielectric properties as determined by the spherical model.

For three-dimensional lattices an ordered state is found at low temperatures, and it is separated from the disordered state by a critical field curve $E=E_c[1-(T/T_c)]^{\frac{1}{2}}$, where the critical field E_c and critical temperature T_c are given by

$$\mu E_c=(n\mu^2)(\lambda_m-4\pi L')/\lambda_m^2, \quad (8.1)$$

$$3kT_c=n\mu^2\langle(\lambda_m-\lambda)^{-1}\rangle^{-1}. \quad (8.2)$$

Here λ_m is the maximum of the eigenvalues $\lambda_a(\mathbf{p})$, i.e., the one associated with the ordered state. The value $4\pi L'=\lambda(0)+4\pi L$ is shape independent, structure dependent, and modified by the presence of any short range forces $\mathbf{J}_{ij}$. In the absence of these forces, $4\pi L'$ is the factor that enters into the effective field $E+4\pi L'\mathbf{P}$ for the corresponding induced dipole lattice. Thus, $L'=1/3$ for cubic lattices. (In this section it is assumed that the applied field is in the direction of one principal axis of the tensor $\mathbf{L}'$.)

Below the Curie temperature $T_c(E)$, the susceptibility is independent of temperature and field and has the constant value

$$\chi=(\lambda_m-4\pi L')^{-1} \quad T<T_c(E). \quad (8.3)$$

Above the Curie temperature $T_c(E)$, the susceptibility is given by

$$\chi=n\alpha_s(1-4\pi L'n\alpha_s)^{-1} \quad T>T_c(E), \quad (8.4)$$

where α_s is the "effective polarizability" determined for small fields by

$$(n\mu^2/3kT)=n\alpha_s\langle(1-n\alpha_s\lambda)^{-1}\rangle, \quad (8.5)$$

$$(n\mu^2/3kT)=n\alpha_s\sum_{r=0}^{\infty}(n\alpha_s)^r\langle\lambda^r\rangle. \quad (8.6)$$

From (8.5) *it follows that* α_s *decreases monontonically with increasing temperature.*

The critical field (8.1) and the susceptibility below the Curie point (8.3) depend only on the maximum eigenvalue λ_m and the eigenvalue $4\pi L'=\lambda(0)+4\pi L$ of a polarized needle; thus, they are easily determined. The critical temperature (8.2) and the susceptibility above the Curie point depend, however, on a detailed knowledge of the three-branched eigenvalue spectrum $\lambda_a(\mathbf{p})$. The eigenvalue dyadic $\boldsymbol{\lambda}(\mathbf{p})$ (whose three-space eigenvalues are $\lambda_a(\mathbf{p})$, $a=1, 2, 3$) is given by the poorly convergent series:

$$\lambda(\mathbf{p})=\sum_{j\neq i}G_{ij}\exp[i\mathbf{p}\cdot(\mathbf{r}_j-\mathbf{r}_i)]. \quad (8.7)$$

The short-range force contribution to $\boldsymbol{\lambda}(\mathbf{p})$ may be computed by direct summation. The poorly converging dipole-dipole series can be written in a rapidly convergent series form, owing to Ewald.[18] The Ewald series permit the rapid calculation of any specified eigenvalue $\lambda(p)$. Unfortunately, the susceptibility requires the calculation of integrals of the form $\int[t-\lambda_a(\mathbf{p})]^{-1}d\mathbf{p}$, and the author has not succeeded in effecting a closed form integration. It would seem, therefore, that final values for the susceptibility above the Curie temperature require numerical evaluation of Ewald's series plus a numerical integration. Before embarking on a long-range computational program, it seems worthwhile to investigate further the accuracy of the spherical method. For this purpose, we shall investigate the high temperature expansion of the electric susceptibility and compare the result with an exact calculation of the corresponding expansion coefficients (to be presented in a separate paper[19]).

The moments of the eigenvalue spectrum can be computed by taking space traces of the corresponding dyadics:

$$\langle\lambda^r\rangle=(1/3)\ \mathrm{tr}\langle\boldsymbol{\lambda}^r\rangle=(1/3)\ \mathrm{tr}[(1/N)\textstyle\sum_p\boldsymbol{\lambda}^r(p)]. \quad (8.8)$$

Using (8.7) with the understanding $\mathbf{G}_{ii}=0$ and the orthogonality relation

$$N^{-1}\textstyle\sum_p\exp[i\mathbf{p}\cdot(\mathbf{r}_j-\mathbf{r}_i)]=\delta_{ji}, \quad (8.9)$$

[18] P. P. Ewald, Ann. Physik **64**, 253 (1921). See also H. Mueller, Phys. Rev. **50**, 547 (1936); M. Born and H. Kornfeld, Physik. Z. **24**, 121 (1923); and H. Kornfeld, Z. Physik **22**, 27 (1924).

[19] R. Rosenberg and M. Lax, "High temperature susceptibility of permanent dipole lattice," J. Chem. Phys. (to be published).

the average moments of the dyadics are found to be

$$\langle\mathfrak{\lambda}\rangle=\mathbf{G}_{ii}=0, \tag{8.10}$$

$$\langle\mathfrak{\lambda}\cdot\mathfrak{\lambda}\rangle=\sum_j\mathbf{G}_{ij}\cdot\mathbf{G}_{ji}, \tag{8.11}$$

$$\langle\mathfrak{\lambda}\cdot\mathfrak{\lambda}\cdot\mathfrak{\lambda}\rangle=\sum_j\sum_k\mathbf{G}_{ij}\cdot\mathbf{G}_{jk}\cdot\mathbf{G}_{ki}. \tag{8.12}$$

In general, $\langle\lambda^r\rangle$ is expressed by a lattice "cluster" sum involving a closed chain of r points (with possible duplication of indices). The spherical model is, therefore, probably equivalent to a virial expansion procedure[19] in which more complicated types of cluster sums are neglected. Opechowski[20] has remarked that such simple chains become relatively more numerous for large r than clusters that are more multiply connected. The hope is that the behavior in the neighborhood of the critical temperature is determined primarily by the accumulated contributions of the long simple chains.

The effective polarizability α_s at high temperatures may be obtained by inverting the series (8.6) and using $\langle\lambda\rangle=0$:

$$n\alpha_s=x[1-\langle\lambda^2\rangle x^2-\langle\lambda^3\rangle x^3-(\langle\lambda^4\rangle-3\langle\lambda^2\rangle^2)x^4\cdots],$$
$$x=(n\mu^2/3kT). \tag{8.13}$$

All of the moments $\langle\lambda^r\rangle$ are independent of specimen shape. For purely dipole-dipole interactions

$$\langle\lambda^2\rangle=2\sum_j(r_{ij})^{-6}, \tag{8.14}$$

and takes the values 16.8, 14.4, and 14.5 for simple cubic, face-centered, and body-centeredar rays, respectively. Comparison of these results with Van Vleck[9] indicates that the expansion of α_s in inverse powers of T is exact to terms of order $1/T^3$. Furthermore, if (8.13) is converted to ordinary units of length and applied to the liquid case, $\langle\lambda^2\rangle$ takes the value

$$\langle\lambda^2\rangle=2n^{-2}\int_a^\infty r^{-6}(4\pi r^2n)dr=8\pi/(3na^2). \tag{8.15}$$

If we make Onsager's apparently unreasonable assumption[6] that the distance a of closest approach obeys $4\pi a^3/3=n^{-1}=$volume per molecule, then $\langle\lambda^2\rangle=2(4\pi/3)^2=35.1$. With this evaluation of $\langle\lambda^2\rangle$, the exact treatment and the spherical model agree with Onsager's phenomenological calculation[6] to terms of order $1/T^3$.

The exact treatment[19] of the term of order $1/T^4$ leads to a term of the form $\mathbf{G}_{ij}\cdot\mathbf{G}_{ji}\cdot\mathbf{G}_{ij}$, in addition to the triangle cluster (8.11). The results of the exact treatment of the $1/T^4$ term may be anticipated here by remarking that for the liquid case the spherical model is found to be more nearly correct than the Onsager treatment.

9. RELATED PROBLEMS

The methods and results of this paper are formally applicable to a number of related problems. For example, most of our equations remain valid in the presence of a classical exchange force $\mathbf{J}_{ij}$ that may be isotropic or may possess anisotropies related to the crystalline directions. Furthermore, this exchange force may act only between nearest neighbors, or it may involve second nearest neighbors, etc. The only assumption made is that $\mathbf{J}_{ij}$ is sufficiently short range so as not to produce surface effects, such as the depolarization produced by the dipole-dipole interaction. It is possible to interpret $\mathbf{J}_{ij}$ as any interaction that produces "bond-angle correlations," so that the influence of such correlations is automatically included in our analysis.

The reason for the generality of our results is that they have been expressed in terms of the eigenvalues $\mathfrak{\lambda}(\mathbf{p})$ rather than the interaction energies $\mathbf{G}_{ij}$. Thus, the shape of the critical field curve is independent of the detailed nature of the interactions $\mathbf{G}_{ij}$. In fact, the same shape will be obtained if interactions only between nearest neighbors is assumed. This explains why all of our general results when expressed in units of the critical temperature and field must be identical with those of Berlin and Thomsen.[13] On the other hand, without such an analysis as presented here, one would have no right to assume that the use of nearest neighbor interactions would yield the correct shape for say the critical field curve when long-range interactions are present. In fact, it is quite possible that for the original dipole lattice problem (not using the spherical model) there are qualitative differences between the results for nearest neighbor and long-range interactions.

Since our treatment has been purely classical, it is not possible to apply it directly to the ferromagnetic problem. However, our classical system behaves as if the effective field on a single dipole above the Curie temperature is

$$E_{\text{eff}}=(3\alpha_skT/\mu^2)[1-(\alpha_sE_e/\mu)^2]^{-1}E_e, \tag{9.1}$$

where

$$E_e=E+4\pi L'P.$$

(This point will be more fully justified elsewhere.) It is possible, now, to treat the single dipole quantum mechanically. $(P/n\mu)$ will be given by the Brillouin function[21] of $\mu E_{\text{eff}}/kT$. Of course, it is necessary to translate these results into magnetic notation and make the appropriate replacements $\mu=g\beta S$, $\mu^2=g^2\beta^2S(S+1)$, where S is the spin of the dipole in units of $\hbar$, β is the Bohr magneton, and g the gyromagnetic ratio.

Finally, we remark that this paper is also applicable to the Ising model problem including short- and long-range interactions. It is simply necessary to reinterpret the initial equations by regarding $\boldsymbol{\varepsilon}_i$ and $\mathbf{G}_{ij}$ as scalars. All of the final equations (when some factors of three that arise from counting degrees of freedom are removed) then remain valid.

[20] W. Opechowski, Physica **4**, 181 (1937); **6**, 112 (1938).

[21] See, for example, J. H. Van Vleck, *Electric and Magnetic Susceptibilities* (Oxford 1932), p. 257.

The Excluded Volume of Polymer Chains

J. J. HERMANS,* *Department of Chemistry, University of Groningen, Groningen, Netherlands*

AND

M. S. KLAMKIN† AND ROBERT ULLMAN,‡ *Department of Mathematics, Polytechnic Institute of Brooklyn*

(Received July 6, 1951)

The "random flight" distribution function for the relative positions of two segments of a linear polymer chain is based on the assumption that the space occupied by a single polymer segment is relatively small and may be neglected. In this paper, the space requirements of a real polymer chain are taken into account. A generalized Fokker-Planck equation is formulated, and the distribution function, the average square distance, and the average inverse distance between two chain segments are calculated.

I. INTRODUCTION

THE statistical treatment of polymer chains was first developed by Kuhn[1] on the basis of the so-called statistical chain elements. These elements have the property that their orientation is independent of any of the other elements of the chain, which reduces the problem to a simple random flight calculation. If there are N chain elements of length A, the distribution of the end-to-end distance is found to be Gaussian, and the average square of this distance is

$$\langle r_N^2\rangle_{Av}=NA^2. \tag{1}$$

The length of the statistical chain element is not equal to a monomer unit or a simple carbon-to-carbon bond, but it depends on such quantities as the carbon bond angle, the hindered rotation along the chain, and the solvent-polymer and polymer-polymer interactions. The length of the chain element is increased by hindered rotation and by the fixed carbon bond angle. This type of interference has been studied by several authors[2] and does not affect the form of relation (1). The present paper is not concerned with these problems but deals with what we have called long-range interferences, which arise because two elements cannot be in the same place at the same time. Theoretical studies of this volume effect have been presented by Flory,[3] Montroll,[4] Hermans,[5] Hadwiger,[6] and Frisch, Collins, and Friedman.[7]

Flory assumes that both the density distribution with respect to the center of gravity and the distribution of the end-to-end distance are still Gaussian, although the width of these Gaussian distributions is enlarged by the excluded volume effect. To find this enlargement, the influence of the long-range interference is treated as a swelling phenomenon to which the usual thermodynamic formula for polymer-solvent systems are applied. It is found that the ratio between $\langle r_N^2\rangle_{Av}$ and N is no longer a constant but increases with N. However, the precise physical significance of Flory's method remains somewhat obscure. It is difficult if not impossible to estimate the effect that the approximations introduced have on the final result.

Montroll studied the statistical properties of polymer chains on a plane square lattice and concluded that the average square of the end-to-end distance becomes proportional to the number of segments when this number becomes very large. For a completely random walk on this square lattice, taking into account the interferences between elements separated by not more than eleven steps on the lattice, his result is $\langle r_N^2\rangle_{Av}=3.3NA^2$. While Montroll's model of a polymer molecule is not as realistic as those chosen by other authors, his methods of calculation are more exact, and the effects of the approximations may be evaluated more accurately.

Frisch, Collins, and Friedman place the elements of the polymer chain on a lattice, using the plane square lattice, the hexagonal lattice, and the diamond lattice as models. They calculate the number of configurations permissible but do not come to any conclusions about the value of $\langle r_N^2\rangle_{Av}$.

The papers of Hermans[5] and Hadwiger[6] use the method explained in the following section and will be discussed there.

II. THE DISTANCE BETWEEN TWO ELEMENTS ON THE POLYMER CHAIN

Our model of the polymer molecule is a flexible chain of $N+1$ beads connected by links that have the properties of the statistical chain elements discussed above. Let A be the distance between successive beads and v be the volume excluded to the center of one bead by the presence of another. For irregularly shaped chain elements, v is very difficult to calculate and in fact depends upon the angle of approach of the elements. If the

* Part of this work was completed while J. J. H. held a Rockefeller fellowship at the Polytechnic Institute of Brooklyn.

† M. S. K. and R. U. gratefully acknowledge the support of the ONR under contract N6-onr26319

‡ Fulbright Fellow at the University of Groningen for the year 1951–52.

[1] (a) W. Kuhn, Kolloid Z. **68**, 2 (1934). (b) W. Kuhn and F. Grun, Kolloid Z. **101**, 248 (1942).

[2] (a) H. Eyring, Phys. Rev. **39**, Z46 (1932). (b) P. Debye, Rubber Reserve Report. (c) J. G. Kirkwood and J. Riseman, J. Chem. Phys. **16**, 565 (1948).

[3] P. J. Flory, J. Chem. Phys. **17**, 303 (1949).

[4] E. W. Montroll, J. Chem. Phys. **18**, 734 (1950).

[5] J. J. Hermans, Rec. trav. chim. **69**, 220 (1950).

[6] H. Hadwiger, Makromol. Chem. **5**, 148 (1951).

[7] Frisch, Collins, and Friedman, J. Chem. Phys. **19**, 1402 (1951).

beads are spheres of diameter a, v is equal to $4/3(\pi a^3)$, eight times the volume of the bead itself.

Let one of the elements of the chain (bead number p) be placed at the origin of a coordinate system, and let $f(\mathbf{r}, t-p)d\mathbf{r}$ be the probability that the center of bead number t is between $\mathbf{r}$ and $\mathbf{r}+d\mathbf{r}$. This distribution function f obeys the following equation:

$$f(\mathbf{r}, t-p+1)=\int \psi(\mathbf{s}, \mathbf{r}-\mathbf{s})f(\mathbf{r}-\mathbf{s}, t-p)d\mathbf{s}, \quad (2)$$

where $\psi(\mathbf{s}, \mathbf{r}-\mathbf{s})$ is the probability that the link connecting the t with the $(t+1)$ bead is given by $\mathbf{s}$ if bead t is at $\mathbf{r}-\mathbf{s}$. Both f and ψ may be functions of t, p, and N. The integration in Eq. (2) with respect to $\mathbf{s}$ is performed over the surface of a sphere of radius A.

If $t-p$ is large in comparison with unity, Eq. (2) may be changed to a differential equation[8] which is more easily treated. This leads to

$$\frac{\partial f}{\partial t}=-\sum_i \frac{\partial}{\partial x_i}(f\langle\xi_j\rangle_{Av})+\tfrac{1}{2}\sum_j\sum_k \frac{\partial^2}{\partial x_j \partial x_k}(f\langle\xi_j\xi_k\rangle_{Av})+ \quad (3)$$

terms of a smaller order of magnitude. ξ_1, ξ_2, and ξ_3 are the rectangular Cartesian components of $\mathbf{s}$, and x_1, x_2, and x_3 are the Cartesian components of $\mathbf{r}$. The average values of any function of the components of the vector $\mathbf{s}$ are given by

$$\langle\varphi(\xi_i, \xi_j, \xi_k)\rangle_{Av}=\int \varphi(\xi_i, \xi_j, \xi_k)\psi(\mathbf{s}, \mathbf{r})d\mathbf{s}. \quad (4)$$

The next logical step is the evaluation of the average quantities in Eq. (3), and it is at this point that Hadwiger's paper[6] differs from the treatment given here. Hadwiger assumes that the transition probability is given by

$$4\pi A^2\psi(\mathbf{s}, \mathbf{r}-\mathbf{s})=\beta(1-K|\mathbf{r}-\mathbf{s}|-|\mathbf{r}|), \quad (5)$$

where K is a constant. In other words, in the small interval between $\mathbf{r}$ and $\mathbf{r}-\mathbf{s}$, ψ is supposed to approximate a linear function of the distance r from the origin. However, since K is assumed to be independent of r, this implies that the effect of long-range interference in the core of the molecule is the same as in the periphery, although the density and the density gradient are different in different parts of the molecule. It seems to us that this is not in conformity with the physical situation, and accordingly Hadwiger's results are incorrect. We make, instead, the following assumption:

$$4\pi A^2\psi(\mathbf{s}, \mathbf{r})=\beta[1-vF(\mathbf{r}+\mathbf{s})], \quad (6)$$

where $F(\mathbf{r}+\mathbf{s})$ is the probability that any of the beads are at $\mathbf{r}+\mathbf{s}$. This probability depends on p, t, N, $\mathbf{r}$, and $\mathbf{s}$. Since $vF(\mathbf{r}+\mathbf{s})$ is the probable fraction of a volume element at $\mathbf{r}+\mathbf{s}$ that is occupied by other beads, Eq. (6) expresses the fact that the link connecting the t and the $(t+1)$ beads will most likely lie in a direction where the density of other beads is lowest. The factor β is a normalizing factor which will, in general, be a function of p, t, N, and $\mathbf{r}$ so as to make (see Eq. 4)

$$\int \psi(\mathbf{s}, \mathbf{r})d\mathbf{s}=1.\S \quad (7)$$

We consider the j bead at a position $\mathbf{R}$. It is the explicit dependence of F on $\mathbf{R}$ which is important when the t bead is fixed at $\mathbf{r}$. If $\mathbf{R}$ is equal to $\mathbf{r}$, the j bead is in a position where it interferes with the t bead, and the sum total of these interferences leads to the excluded volume effect.

Expanding $F(\mathbf{R}+\mathbf{s})$ about the point $\mathbf{R}$ yields

$$F(\mathbf{R}+\mathbf{s})=F(\mathbf{R})+\sum_i \xi_i\frac{\partial F}{\partial X_i}+\tfrac{1}{2}\sum_i\sum_j \xi_i\xi_j\frac{\partial^2 F}{\partial X_i \partial X_j}+0(\xi_i\xi_j\xi_k), \quad (8)$$

where X_1, X_2, and X_3 are the components of $\mathbf{R}$. Using Eqs. (4), (7), and (8) for computing the averages in (3) leads to the results‖

$$\beta\left[1-vF(\mathbf{R})-\frac{A^2}{6}\Delta_{\mathbf{R}}F(\mathbf{R})\right]_{\mathbf{R}=\mathbf{r}}=1,$$

$$\langle\xi_j\rangle_{Av}=-\frac{A^2}{3}\beta v\left(\frac{\partial F}{\partial X_j}\right)_{\mathbf{R}=\mathbf{r}}, \quad (9)$$

$$\langle\xi_j\xi_k\rangle_{Av}=\delta_{jk}\frac{A^2\beta}{3}(1-vF(\mathbf{R}))_{\mathbf{R}=\mathbf{r}}.$$

$\delta_{jk}=1$ when $j=k$ and 0 when $j\neq k$.

Substitution of β into the expressions for $\langle\xi_j\rangle_{Av}$ and $\langle\xi_j\xi_k\rangle_{Av}$ yields the results

$$\langle\xi_j\rangle_{Av}=-\frac{A^2 v}{3}\left(\frac{\partial F}{\partial X_j}\right)_{\mathbf{R}=\mathbf{r}},$$

$$\langle\xi_j\xi_k\rangle_{Av}=\delta_{jk}\frac{A^2}{3}. \quad (10)$$

[8] S. Chandrasekhar, Revs. Modern Phys. **15**, 31 (1943).

§ In order to clarify the procedure for those who are accustomed to dealing with numbers of configurations rather than normalized probabilities, we would like to make the following remarks.

If $Z(\mathbf{r}, t)d\mathbf{r}$ is *the number of configurations* of a chain of t beads such that the t bead is in the volume element $d\mathbf{r}$,

$$Z(\mathbf{r}, t+1)=\int d\mathbf{s}Z(\mathbf{r}-\mathbf{s}, t)\psi_t(\mathbf{s}, \mathbf{r}-\mathbf{s}),$$

where $\psi_t(\mathbf{s}, \mathbf{r}-\mathbf{s})$ is the number of ways in which the $t+1$ bead can be added when the t bead is at $\mathbf{r}-\mathbf{s}$. Thus formulated it is by no means obvious that $\int d\mathbf{s}\psi_t(\mathbf{s}, \mathbf{r}-\mathbf{s})=1$. However, we consider, from the very start, the whole chain of $N+1$ beads. We make a large number, say M, of snapshots and count the number $Mf(\mathbf{r}, t)d\mathbf{r}$ of snapshots in which bead number t is at $\mathbf{r}$; this function f depends on $\mathbf{r}$, t and also on N. Then we use Eq. 2, where ψ is a function of N as well. In this formulation the integral over ψ is bound to be equal to 1, because the $t+1$ bead must go *somewhere*.

‖ Whenever $\mathbf{R}=\mathbf{r}$ is used as a subscript, it has the following meaning. The operation indicated in the text is to be performed with respect to the variable $\mathbf{R}$, and the result obtained is to be evaluated at the point $\mathbf{R}=\mathbf{r}$.

In obtaining Eq. (10), it is assumed that terms of the order of $(vF)^2$ and of the order A^4 are omitted. This is equivalent to assuming that the fraction of the volume element occupied by the chain segments is small and that the length of a chain segment is small. The assumption of low polymer density will be discussed at greater length in Sec. IV of this paper. Substituting the results of Eq. (10) into Eq. (3) yields

$$\frac{\partial f}{\partial t}-\frac{A^2}{6}\Delta f=\frac{A^2 v}{3}\operatorname{div}(f[\operatorname{grad}_R F]_{R=r}), \tag{11}$$

where Δ and div are operations with respect to the coordinates of $\mathbf{r}$. In order to solve Eq. (11) it would be necessary to express $F(\mathbf{R})$ in terms of the variables of the equation. We have not been able to make any progress with the exact solution of the equation. It is important to notice that v, the volume excluded to one bead by the presence of another, appears only on the right-hand side. If v is set equal to zero, the answer is the well-known random flight result:

$$f^0(\mathbf{r}, t-p)=(\lambda/\pi(t-p))^{\frac{3}{2}}\exp[-\lambda r^2/t-p]; \quad \lambda=(3/2A^2). \tag{12}$$

This is the distribution function obtained without the excluded volume. In other words, if the effect of the volume of the statistical chain element becomes vanishingly small, the result reduces to that obtained when the excluded volume effect is neglected completely. This, of course, is to be expected, and it constitutes a partial check of the work done thus far.

It is clear that a perturbation procedure would lead to a good approximation for f if the term on the right-hand side of Eq. (11) is not too large. Setting $f=f^0$ and $F=F^0$ in the right side of Eq. (11) yields

$$\frac{\partial f}{\partial t}-\frac{A^2}{6}\Delta f=\frac{A^2 v}{3}\operatorname{div}(f^0[\operatorname{grad}_R F^0]_{R=r}), \tag{11a}$$

where f^0 is given in Eq. (12) and $F^0(\mathbf{R})$ is the probability that any one of the elements of the chain is at $\mathbf{R}$.

It is from this point onwards that our procedure differs from that followed in Hermans' previous paper[5] on the subject. This author assumed that $F^0(R)$ could be identified with the probability that any bead is at $\mathbf{R}$ when number p is at the origin, ignoring the knowledge that bead number t is at $\mathbf{r}$. It was pointed out to one of us by Alfrey[9] that this underestimates the excluded volume effect because the local density in the neighborhood of the point $\mathbf{r}$, on the assumption that bead number t is at $\mathbf{r}$, is much higher than the average density near this point. The very presence of bead t at $\mathbf{r}$ requires that other elements be near since these elements are linked in a chain.

The form of the function F^0 to be used here takes into account that beads number p and t are at 0 and $\mathbf{r}$, respectively, and has accordingly the form

$$F^0=\sum_{j=0}^{p-1} g_j+\sum_{p+1}^{t-1} h_j+\sum_{t+1}^{N+1} k_j. \tag{13}$$

The functions g_j, h_j, and k_j are the well-known random flight solutions for the probability that the j element is at $\mathbf{R}$. It is obvious that the form of these functions should change depending on whether $j<p$, $p<j<t$, or $j>t$. This is in fact so, and these functions can be written down by analogy with f^0 of Eq. (12). They are:

$$g_j(\mathbf{R})=a_j\exp\left[\frac{-\lambda R^2}{p-j}\right], \qquad a_j=\left(\frac{\lambda}{\pi(p-j)}\right)^{\frac{3}{2}}, \tag{14a}$$

$$h_j(\mathbf{R},\mathbf{r})=b_j\exp\left[\frac{-\lambda R^2}{j-p}-\frac{\lambda(\mathbf{R}-\mathbf{r})^2}{t-j}\right], \qquad b_j=\left(\frac{\lambda(t-p)}{\pi(t-j)(j-p)}\right)^{\frac{3}{2}}\exp\left[\frac{\lambda r^2}{t-p}\right], \tag{14b}$$

$$k_j(\mathbf{R},\mathbf{r})=c_j\exp\left[\frac{-\lambda(\mathbf{R}-\mathbf{r})^2}{j-t}\right], \qquad c_j=\left(\frac{\lambda}{\pi(j-t)}\right)^{\frac{3}{2}}. \tag{14c}$$

In Eq. (14b) the function h_j is obtained by considering the dependence of the probable distribution of the j element on its position relative to both the t and p elements.

The function f^0 in Eq. (12) is the Gaussian solution of the zero-order differential equation $\partial f/\partial t-(A^2/6)\Delta f=0$. It seems apparent that the solution of Eq. (11a) need no longer be Gaussian. This solution will be derived in a later section of the paper. However, the average square distance between the t and p chain elements will be derived directly, without using the distribution function itself.

From Eqs. (14a), (14b), and (14c) we find that

$$\operatorname{grad}_R g_j(\mathbf{R})_{R=r}=\frac{-2\lambda r a_j}{p-j}\exp\left[\frac{-\lambda r^2}{p-j}\right], \tag{15a}$$

$$\operatorname{grad}_R h_j(\mathbf{R})_{R=r}=\frac{-2\lambda r b_j}{j-p}\exp\left[\frac{-\lambda r^2}{j-p}\right], \tag{15b}$$

$$\operatorname{grad}_R k_j(\mathbf{R})_{R=r}=0. \tag{15c}$$

The last of these equations shows that the effect of the "tail," $j>t$ is zero. This is due to the fact that the distribution of chain elements with $j>t$ has spherical symmetry about the point $\mathbf{r}$, so that this tail can have no

[9] T. Alfrey, Midland, Michigan (private communication).

effect on the orientation of the t link in space. When Eqs. (12) through (15c) are used, the differential Eq. (11a) for f becomes

$$\frac{\partial f}{\partial t}-\frac{1}{4\lambda}\Delta f=-\left(\frac{\lambda}{\pi}\right)^{3}v\nabla \cdot\left\{(t-p)^{-\frac{1}{2}}\mathbf{r}\sum_{j=0}^{p-1}(p-j)^{-5/2}\exp\left[\frac{-\lambda r^{2}(t-j)}{(p-j)(t-p)}\right] +\mathbf{r}\sum_{j=p}^{t-1}(t-j)^{-\frac{1}{2}}(j-p)^{-5/2}\exp\left[\frac{-\lambda r^{2}}{j-p}\right]\right\}. \quad (16)$$

We multiply Eq. (16) by r^2 and integrate throughout space, and obtain

$$\frac{d}{dt}\langle r_{tp}^{2}\rangle_{Av}=A^{2}+\frac{8\lambda^{3}v}{\pi^{2}}[L(p,t)+M(p,t)],$$

$$L(p,t)=(t-p)^{-\frac{1}{2}}\sum_{j=0}^{p-1}(p-j)^{-5/2}\times\int_{0}^{\infty}r^{4}\exp\left[\frac{-\lambda r^{2}}{p-j}\right]dr, \quad (17)$$

$$M(p,t)=\sum_{j=p}^{t-1}(t-j)^{-\frac{1}{2}}(j-p)^{-5/2}\times\int_{0}^{\infty}r^{4}\exp\left[\frac{-\lambda r^{2}}{j-p}\right]dr.$$

Upon integration, Eq. (17) becomes

$$\frac{d}{dt}\langle r_{tp}^{2}\rangle_{Av}=A^{2}+3\left(\frac{\lambda}{\pi^{3}}\right)^{\frac{1}{2}}v\times[(t-p)\sum_{j=0}^{p-1}(t-j)^{-5/2}+\sum_{j=p}^{t-1}(t-j)^{-\frac{1}{2}}]. \quad (18)$$

For

$$t-p\geq 2,\quad \sum_{j=p}^{t-1}(t-j)^{-\frac{1}{2}}=2.61-2(t-p)^{-\frac{1}{2}}-\tfrac{1}{2}(t-p)^{-\frac{3}{2}}$$

to within better than one percent;

$$(t-p)\sum_{j=0}^{p-1}(t-j)^{-5/2},$$

a quantity of a lower order of magnitude, is estimated by converting the sum to an integral and is found to be equal to $\frac{2}{3}[(t-p)^{-\frac{1}{2}}-(t-p)^{-\frac{3}{2}}]$. The nature of our earlier approximations makes the significance of terms containing lower powers of $t-p$ doubtful. By retaining only the leading term, Eq. (18) becomes

$$(d/dt)\langle r_{tp}^{2}\rangle_{Av}=A^{2}[1+1.72v/A^{3}]+0(t-p)^{-\frac{1}{2}}. \quad (19)$$

Integrating between the p and t elements, we find

$$\langle r_{tp}^{2}\rangle_{Av}=(t-p)A^{2}[1+1.72v/A^{3}+0(t-p)^{-\frac{1}{2}}]. \quad (20)$$

The average square of the end-to-end distance is obtained by letting $t-p=N$:

$$\langle r_{N}^{2}\rangle_{Av}=NA^{2}[1+1.72v/A^{3}]. \quad (20a)$$

This shows that the average square of the end-to-end distance is proportional to the number of links, but that the ratio $\langle r_N^2\rangle_{Av}/N$ is larger than in Eq. (1). This result is in conformity with that obtained by Montroll.[4] Debye[10] using much the same method, has recently derived a result similar to Eq. (20a). A similar result was obtained by Sadron[11] who used a completely different method.

In Eq. (20a) the average squared distance between the t and p beads, $\langle r_{tp}^2\rangle_{Av}$ is a function of $t-p$ for $t>p$. The formula would be correct for both $t>p$ and $t<p$ if $t-p$ was replaced by $|t-p|$. This would arise naturally if the original statement of the problem did not specify that t was greater than p. This symmetry with respect to t and p is to be expected from physical considerations.

However, it should be mentioned that the "tails" of the molecule $j<p$ and $j>t$ do not contribute equally to the excluded volume formula. This may appear to be puzzling¶ at first sight, but is understandable in view of the particular way in which the problem is formulated.

The coordinate system in which positions of the segments of the polymer chain are specified is fixed so that the origin of coordinates moves with the p segment. Since this is so, the excluded volume is calculated by considering how the interactions of all the other segments interfere with some other segment (the t, in this case) relative to the p. In other words, the problem is formulated asymmetrically, and it is clear that the segments $j<p$ do not contribute to the interactions with the t segment in the same way as the segments $j>t$. In spite of this the final calculation leads to a formula for $\langle r_{tp}^2\rangle_{Av}$, which is symmetric with respect to t and p as it must be. It should be mentioned, though it is not exactly relevant to the above discussion, that the effects of the "tails" of the molecule ($j<p$ and $j>t$) are of a lower order of magnitude than the contribution of the elements $p<j<t$ and that the numerical coefficients of the terms of lower magnitude are without meaning (see Eq. (20)) because of the perturbation procedure used in the calculations.

Rough estimates may be made of the order of magnitude of the excluded volume if the shape of the chain element is specified. As given here, these shapes are highly idealized, and no exact significance is attributed to the actual number computed. Let us assume that the chain element is a spherical bead of diameter a. The quantity v is a sphere eight times the volume of the bead and is equal to $(4/3)\pi a^3$. Substituting this in Eq. (20a), one obtains

$$\langle r_{N}^{2}\rangle_{Av}=NA^{2}[1+7.16(a/A)^{3}]=KNA^{2}. \quad (21a)$$

[10] P. Debye, Ithaca, New York (private communication).
[11] Ch. Sadron, Strasbourg (private communication).
¶ The authors are indebted to H. M. James of Purdue University for raising this question.

The assumption that a chain element is a cylinder of length A is somewhat more realistic for some polymers than the spherical bead. Unfortunately, an exact calculation of v is dependent upon the angle of approach of two chain elements with the probability of a given angle of approach some sort of complicated function of the configuration of the chain itself. We therefore define $v=\pi d^2A$, where d is a quantity approximately equal to the diameter of the cylindrical element. Equation (20a) then becomes

$$\langle r_N^2\rangle_{Av}=NA^2[1+5.38(d/A)^2]. \tag{21b}$$

III. THE DISTRIBUTION FUNCTION

The purpose of this section is to solve Eq. (11a) for $f(\mathbf{r}, t-p)$, the probability that the t segment of the polymer chain is at $\mathbf{r}$ when the p segment is at the origin ($t>p$).

The nonhomogeneous part of Eq. (11a) may be divided into three parts (see Eq. (13)), $j<p$, $p<j<t$, and $j>t$. The last part is spherically symmetrical about the t element and contributes nothing to the problem (see Eq. (15c)).

The first and second parts are asymmetrically situated with respect to the t segment. It was shown in the calculation of $\langle r_{tp}^2\rangle_{Av}$ that the contribution of the "tail" $j<p$ is of the order $(t-p)^{-\frac{1}{2}}$ times that of the middle section $p\leqq j<t$. Since the contribution of the middle section is the only significant part, it is proper to look for a solution of Eq. (11a) which contains these terms alone. Rewriting Eq. (11a) and neglecting the terms arising from the "tails" of the molecule, we have

$$\frac{\partial f}{\partial t}-\frac{A^2}{6}\Delta f=\frac{A^2}{3}v\sum_{j=p}^{t-1}\operatorname{div}[f^0(\operatorname{grad}_R h_j)_{R=r}]. \tag{22}$$

If we assume that $f(\mathbf{r}, t-p)=f(r, t-p)$ (f is spherically symmetrical), Eq. (22) becomes

$$\frac{\partial(rf)}{\partial t}-\frac{1}{4\lambda}\frac{\partial^2(rf)}{\partial r^2}=-\frac{v}{r}\left(\frac{\lambda}{\pi}\right)^{\frac{3}{2}}\times\frac{\partial}{\partial r}\left\{r^3\sum_{j=p}^{t-1}(t-j)^{-\frac{1}{2}}(j-p)^{-5/2}\exp\left[\frac{-\lambda r^2}{j-p}\right]\right\}. \tag{23}$$

This equation is solved by using the Laplace transform. $F(r, p)$ is the Laplace transform** of $rf(r, t-p)$. The transform relationship will henceforth be written in the following manner: $F(r, p)\subset rf(r, t-p)$.

The transform of the inhomogeneous term in Eq. (23) is obtained by assuming that

$$\sum_{j=p}^{t-1}(t-j)^{-\frac{1}{2}}(j-p)^{-5/2}\exp\left[\frac{-\lambda r^2}{j-p}\right]\cong\int_0^{\kappa}(\kappa-u)^{-\frac{1}{2}}u^{-5/2}\Phi(\kappa-u)\exp\left[\frac{-\lambda r^2}{u}\right]du, \tag{24}$$

$$\kappa=t-p$$

$$\Phi(\kappa-u)=\begin{cases}0 & \text{if } \kappa-u<1,\\ 1 & \text{if } \kappa-u\geqq 1.\end{cases}$$

The integral in (24) is evaluated by convolution and Eq. (23) becomes

$$\frac{d^2F}{dr^2}-n^2F=A\exp[-nr],$$

$$n=2\lambda^{\frac{1}{2}}p^{\frac{1}{2}}, \tag{25}$$

$$A=8\lambda^{\frac{1}{2}}\pi^{-5/2}vp\Omega(p),$$

$$\Omega(p)=2\pi^{\frac{1}{2}}p^{\frac{1}{2}}\operatorname{erfc}p^{\frac{1}{2}}+2e^{-p}\subset\Phi(t)t^{-\frac{1}{2}}.$$

The solution of Eq. (25), subject to the requirement that $F(r, p)$ approach zero as r becomes very large, is

$$F=e^{-nr}(c_1+Br),$$

$$B=2\lambda^3\pi^{-5/2}p^{\frac{1}{2}}v\Omega(p), \tag{26}$$

$$c_1=\frac{\lambda}{\pi}-2\lambda^{5/2}\pi^{-5/2}v\Omega(p).$$

The constant c_1 is determined from the normalizing condition

$$\int_0^{\infty}4\pi rF\,dr=1/p.$$

Taking the inverse transform of F to find the distribution function

$$f(\mathbf{r}, t-p)=(\lambda/\pi(t-p))^{\frac{3}{2}}\exp\left[\frac{-\lambda r^2}{t-p}\right]-3M_0+2\lambda r^2M_1, \tag{27}$$

$$M_n=(\lambda/\pi)^{\frac{3}{2}}v\int_0^{\kappa-1}(\kappa-y)^{-\frac{1}{2}}y^{-(n+\frac{1}{2})}\times\exp[-\lambda r^2/y]dy.$$

Rewrite Eq. (27) with the integral replaced by a summation sign to obtain

$$f(\mathbf{r}, t-p)=(\lambda/\pi(t-p))^{\frac{3}{2}}\exp\left[\frac{-\lambda r^2}{t-p}\right]-(\lambda/\pi)^{\frac{3}{2}}(v/r^2)\times\frac{\partial}{\partial r}\left\{r^3\sum_{j=p}^{t-1}(t-j)^{-\frac{1}{2}}(j-p)^{-\frac{1}{2}}\exp\left[\frac{-\lambda r^2}{j-p}\right]\right\}. \tag{28}$$

** The Laplace transform used here does not contain the p before the integral,

$$F=\int_0^{\infty}e^{-pt}rf\,dt.$$

The distribution function of Eq. (28) satisfies Eq. (23) provided that the sum over j is treated as an integral when differentiating with respect to t.

The distribution function of Eq. (27) may be simplified by approximate evaluation of the integrals M_n.

Integrating by parts, we obtain

$$\int_0^{\kappa-1}(\kappa-y)^{-\frac{1}{2}}y^{-(n+\frac{1}{2})}\exp\left[\frac{-\lambda r^2}{y}\right]dy$$

$$=2(\kappa-1)^{-(n+\frac{1}{2})}\exp\left[\frac{-\lambda r^2}{\kappa-1}\right]$$

$$-2\int_0^{\kappa-1}(\kappa-y)^{-\frac{1}{2}}\frac{d}{dy}\left(y^{-(n+\frac{1}{2})}\exp\left[\frac{-\lambda r^2}{y}\right]\right)dy. \quad (29)$$

On the right-hand side of Eq. (29), the replacement of $\kappa-1$ by κ in the first term and in the upper limit of the integral does not appreciably affect the result if κ is large. Equation (29) may then be written equal to

$$2\kappa^{-(n+\frac{1}{2})}\exp[-\lambda r^2/\kappa]$$

$$-2\int_0^{\kappa}(\kappa-y)^{-\frac{1}{2}}\frac{d}{dy}\left(y^{-(n+\frac{1}{2})}\exp\left[\frac{-\lambda r^2}{y}\right]\right)dy.$$

The integral is easily evaluated by the Laplace transform convolution theorem.

It is obvious that the substitution of κ for $\kappa-1$ as the upper limit of the integral on the left-hand side of Eq. (29) would cause the integral to diverge.

After one substitutes the result of the approximation to M_n in Eq. (27), the distribution function may be written

$$f(\mathbf{r},t-p)=(\lambda/\pi(t-p))^{\frac{3}{2}}\exp\left[\frac{-\lambda r^2}{t-p}\right]$$

$$\times(1-6v(\lambda/\pi)^{\frac{1}{2}}+4v(\lambda/\pi)^{\frac{3}{2}}(\lambda r^2/t-p)). \quad (30)$$

This simple result has the required property of being somewhat smaller than f^0 when r is small, and somewhat larger than f^0 when r is large. The curves in Fig. 1 show how the distribution function for the excluded volume model (Eq. 30) differs from that for the random flight model (Eq. 12). From viscosity data it is possible to find $b^2=\langle r_N^2\rangle_{Av}/P$, where P is the degree of polymerization. For polystyrene in butanone Kirkwood and Riseman[2] found b to be 5.2A. Setting $Pb^2=NA^2$ and $NA=1.54P\cos(35\frac{1}{2}^\circ)$=fully extended length, reasonable values for N and A were calculated. Assuming that $v=200\text{A}^3$, we constructed the graphs in Fig. 1. It should be understood that no exact quantitative significance can be attributed to these graphs. The estimate for v is rough, and the estimate of b will have to be changed when the average quantities used in the viscosity theory[2] are revised in accordance with the excluded volume distribution function itself.

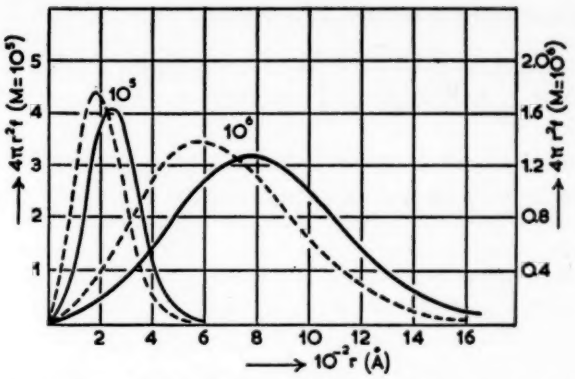

FIG. 1. A comparison between the distribution functions for the end-to-end distance of polystyrene molecules (molecular weights 10^5 and 10^6) as calculated from the random flight model (dashed line) and from the excluded volume theory (full line). Ordinates in arbitrary units.

The calculated average value of the square of the distance between the t and p element from Eq. (28) is given by

$$\langle r_{tp}^2\rangle_{Av}=\int r^2 f d\mathbf{r}=4\pi\int_0^\infty r^4 f dr$$

$$=(t-p)[1+1.72v/A^3]. \quad (31)$$

This is the same result derived earlier without the knowledge of the correct distribution function.

The theory of intrinsic viscosity of polymer solutions depends upon an estimate of the average value of the reciprocal of r_{tp}. Using Eq. (28), we obtain

$$\langle 1/r_{tp}\rangle_{Av}=\int(1/r)f d\mathbf{r}=[6/A^2(t-p)]^{\frac{1}{2}}$$

$$-(9/2\pi^2)(v/A^4)B_\kappa, \quad (32)$$

$$B_\kappa=\sum_1^{\kappa-1}(\kappa-y)^{-\frac{1}{2}}y^{-\frac{1}{2}}\cong 2.61/(t-p)^{\frac{1}{2}};\quad \kappa=t-p.$$

Rewriting Eq. (32), we have

$$\langle 1/r_{tp}\rangle_{Av}=(1/A(t-p)^{\frac{1}{2}})(1.38-1.19v/A^3). \quad (33)$$

The average squared distance and average reciprocal distance calculated from the distribution function of Eq. (30) are of the same form but contain slightly changed numerical factors than are given in Eqs. (31) and (33). This arises because it is assumed in deriving Eq. (30) that the sum of Eq. (28) may be replaced by an integral.

IV. THE BEAD DENSITY

The assumption that $vF^0\ll 1$ is used in the derivation of Eq. (11a). To estimate F_0 we replace the sums in

Eq. (13) by integrals. This yields

$$S_1=\sum_{j=0}^{p-1} g_j(\mathbf{R})\cong(\lambda/\pi)^{\frac{3}{2}}\int_0^p u^{-\frac{3}{2}}\exp\left[\frac{-\lambda R^2}{u}\right]du, \tag{34}$$

$$S_2=\sum_{j=p+1}^{t-1} h_j(\mathbf{R},\mathbf{r})\cong(\lambda(t-p)/\pi)\exp\left[\frac{\lambda r^2}{t-p}\right]\cdot J, \tag{35}$$

$$J=\int_0^{t-p} u^{-\frac{3}{2}}(t-p-u)^{-\frac{3}{2}}\times\exp\left[\frac{-\lambda r^2}{u}-\frac{\lambda|\mathbf{R}-\mathbf{r}|^2}{t-p-u}\right]du,$$

$$S_3=\sum_{j=t+1}^{N+1} k_j(\mathbf{R},\mathbf{r},t)=(\lambda/\pi)^{\frac{3}{2}}\times\int_t^N (u-t)^{-\frac{3}{2}}\exp\left[\frac{-\lambda|\mathbf{R}-\mathbf{r}|^2}{u-t}\right]du. \tag{36}$$

By a simple substitution, Eqs. (34) and (36) reduce to error integrals:

$$S_1=(3/2\pi A^2)R^{-1}\operatorname{erfc}[(3/2p)^{\frac{1}{2}}(R/A)], \tag{34a}$$

$$S_3=(3/2\pi A^2)|\mathbf{R}-\mathbf{r}|^{-1}\times\operatorname{erfc}[(3/2(N-t))^{\frac{1}{2}}(|\mathbf{R}-\mathbf{r}|/A)], \tag{36a}$$

$$\operatorname{erfc}x=(2/\pi)^{\frac{1}{2}}\int_x^\infty \exp(-y^2)dy.$$

Since $\mathbf{R}$ and $|\mathbf{R}-\mathbf{r}|$ are always larger than the diameter of the (cylindrical) chain element, the contribution of these terms to vF^0 is less than $3d/2A$, decreasing rapidly with increasing distance.

The integral J in Eq. (35) is evaluated by the use of the Laplace transform and the convolution theorem. The result is

$$S_2=(3/2\pi A^2)(R^{-1}+|\mathbf{R}+\mathbf{r}|^{-1})\times\exp[(3/2(t-p)(r^2-(R+|\mathbf{R}+\mathbf{r}|)^2/A^2]. \tag{35a}$$

Neither $\mathbf{R}$ nor $|\mathbf{R}-\mathbf{r}|$ can be smaller than d, so that here again the contribution to vF^0 is always less than $3d/2A$.

This analysis shows that for spherical beads of diameter A the condition $vF\ll 1$ is violated in the immediate vicinity of beads number t and p. This is restricted, however, to very small distances from these elements. For cylindrical elements the situation is the better the smaller the ratio of thickness to length. Moreover, it may be noted that replacing the sums in Eqs. (34) and (36) by integrals somewhat overestimates the density.

The above calculation for the bead density was required to determine the effect of the omission of certain terms in the modified Fokker-Planck equation, Eq. (11a). Specifically, in arriving at Eq. (10) from Eq. (9) terms of the order of $(vF)^2$ and $v^2F(\partial F/\partial X_j)_{\mathbf{R}=\mathbf{r}}$ were omitted. The results of this section lead to the conclusion that these terms are negligible in nearly all cases. The exceptions would refer to those polymer chains that are tightly coiled and have particularly bulky monomer units. Even in these cases the primary contribution comes from the terms considered, though the error might be appreciable.

In the discussion of the bead density thus far, we have been concerned primarily with the approximations earlier in the paper. Therefore, the calculations have not been of the bead density as a function of distance from the p element, but rather of the bead density having first assumed that the p and t elements are fixed in space with the t element at $\mathbf{r}$ relative to the p at zero.

However, the density of polymer segments as a function of the distance from the p element is a quantity of interest itself.[12] In the following paragraphs, the bead density will be calculated for both random flight polymer chains and for polymer chains with excluded volume. The results will be compared. The respective distribution functions are given by

$$f^0(\mathbf{r},t-p)=\left(\frac{\lambda}{\pi(t-p)}\right)^{\frac{3}{2}}\exp\left[\frac{-\lambda r^2}{t-p}\right], \tag{12}$$

$$f(\mathbf{r},t-p)=\left(\frac{\lambda}{\pi(t-p)}\right)^{\frac{3}{2}}\exp\left[\frac{-\lambda r^2}{t-p}\right]\times\left[1-6v\left(\frac{\lambda}{\pi}\right)^{\frac{3}{2}}+4v\left(\frac{\lambda}{\pi}\right)^{\frac{3}{2}}\left(\frac{\lambda r^2}{t-p}\right)\right]. \tag{30}$$

The probable density with respect to the p element is given by

$$G(\mathbf{r})=\sum_{\kappa=1}^{N-p} f(\mathbf{r},\kappa)+\sum_{\kappa=1}^{p-1} f(\mathbf{r},\kappa). \tag{37}$$

Replacing these sums by integrals yields

$$G^0(r)=\frac{\lambda}{\pi r}\left[\operatorname{erfc}\left(\frac{\lambda^{\frac{1}{2}}r}{N-p}\right)+\operatorname{erfc}\left(\frac{\lambda^{\frac{1}{2}}r}{p}\right)\right], \tag{38a}$$

$$G(r)=G^0(r)\left(1-4v\left(\frac{\lambda}{\pi}\right)^{\frac{3}{2}}\right)+4v\left(\frac{\lambda}{\pi}\right)^{3}\left[\exp\left(\frac{-\lambda r^2}{N-p}\right)+\exp\left(\frac{-\lambda r^2}{p}\right)\right], \tag{38b}$$

with Eqs. (38a) and (38b) referring to Eqs. (12) and (30), respectively.

The probable number of chain segments between r and $r+dr$ is given by $4\pi r^2NG(r)$. For both the random flight chain and the chain with excluded volume, $4\pi r^2NG(r)$ is proportional to r when r is very small. As r

[12] This calculation was suggested to one of us by H. Morawetz of the Polytechnic Institute of Brooklyn.

becomes large, $4\pi r^2 NG(r)$ becomes proportional[13] to $\exp[-\lambda r^2/N-p]+\exp[-\lambda r^2/p]$ for the random flight chain and proportional to $r^2(\exp[-\lambda r^2/N-p]+\exp[-\lambda r^2/p])$ for the chain with excluded volume. The concentration of polymer segments for large r is greater for real chains than for the idealized model without excluded volume as might have been expected in terms of a simple qualitative picture.

V. THE APPLICATION OF EXPERIMENTAL RESULTS

In the previous sections of this paper, we have shown that the square of the end-to-end distance of the linear polymer chain is proportional to the molecular weight. This result is similar to that obtained by some authors[4–6] who have conducted investigations on the excluded volume problem, but it differs appreciably from the theory proposed by Flory[3] who finds that the square of the end-to-end distance is proportional to the molecular weight to the α-power, where α is greater than one, and increases slowly with molecular weight.

It would be desirable to have experimental data that would enable one to compare $\langle r_N^2\rangle_{Av}$ directly with molecular weight. Investigations of the scattering of light by solutions of chain polymers are best for this purpose. Before such experiments are considered in detail, a discussion of some of the difficulties are in order.

The theory developed in the earlier sections of the paper attempted to account for long-range geometric effects only. The solutions to which this theory is applied are infinitely dilute, or practically speaking, are sufficiently dilute so that the interactions between different polymer molecules may be ignored. The dependence of the excluded volume on concentration has not yet been worked out. These difficulties and perhaps others not understood at this time complicate the problem of comparing theory with experiment.

Experiments comparing R^2 (the root-mean-square radius of the molecule)†† with molecular weight have been conducted by Outer, Carr, and Zimm,[14] and Kunst.[15] The results of Zimm and co-workers indicated that R^2 is proportional to M for linear chains of polystyrene. In Kunst's work, it was found that R^2 is proportional to M for polyisobutylene and that R^2 is proportional to M for polystyrene if the data are corrected to the same value of the second virial coefficient in light scattering. This correction minimizes the error arising from the variation of the "solvent effect" with molecular weight.

While the available light scattering data confirm the results of the theory (the value of $\langle r_N^2\rangle_{Av}$, not the distribution function), it is important to remember that this confirmation is not direct. The very application of light scattering data is based upon the presumed validity of the theories of light scattering. However, the theories of light scattering are dependent upon the use of the random flight polymer chain without excluded volume.[16] In addition, the use of real polymer solutions where there is a distribution of molecular weights could introduce discrepancies. It is the contention of the authors of this paper that while the experimental check of the theory by light scattering is satisfactory, it is nevertheless unwise to put too much emphasis on this sort of confirmation because the very application of such experimental data involves difficulties that are not easily removed.

A considerable mass of viscosity data is available for comparison with the excluded volume theory. The comparison is made by means of the theories of intrinsic viscosity,[2,17] and the difficulties in interpretation here are much greater than those encountered in using the results of light scattering experiments. However, the agreement between the excluded volume theory given here and intrinsic viscosity is not too good. The experiments of Kunst[15] on polyisobutylene and polystyrene indicate that the radius of the polymer coil squared is proportional to the molecular weight provided that the intrinsic viscosity is taken as proportional to molecular weight to the one-half power. According to the theories of intrinsic viscosity,[2,17] the intrinsic viscosity is proportional to molecular weight to the one-half power if the molecular weight is sufficiently high.

However, the viscosity experiments of Flory and co-workers[18] are not in agreement with the theoretical results given here; they indicate that R^2 varies with a power of molecular weight greater than one. What is more, Flory[19] has developed a theory of polymer configurations that leads to the conclusion that intrinsic viscosity varies with a power of molecular weight, which is somewhat greater than one-half. Because of the theoretical differences as to the dependence of molecular weight on viscosity and because of the different results obtained by different investigators[14,15,18] it is difficult to evaluate an excluded volume theory by consideration of the intrinsic viscosities of solutions.

VI. SUMMARY AND CONCLUSION

1. A theory of the excluded volume of linear unbranched polymer chains has been developed. The treatment is purely statistical, and the results are obtained by considering long-range interferences between

[13] Jahnke-Emde Tables of Functions (Dover Publications, New York, 1945), p. 24.

†† The theoretical calculation made in our paper is for the square of the end-to-end distance and not the root-mean-square radius, which is obtained by light scattering. For a random flight chain these are simply related ($\langle r_n^2\rangle_{Av}=(18/5)R^2$).[17] We have not been able to obtain a similar relation for the chain with excluded volume, but we will assume that $\langle r_N^2\rangle_{Av}$ is proportional to R^2 so that an experimental comparison may be made.

[14] Outer, Carr, and Zimm, J. Chem. Phys. **18**, 830 (1950).

[15] E. D. Kunst, Rec. trav. chim. **69**, 125 (1950).

[16] See for example B. H. Zimm, J. Chem. Phys. **16**, 1093 (1948), Eq. (3).

[17] P. Debye and A. M. Bueche, J. Chem. Phys. **16**, 573 (1948).

[18] P. J. Flory and T. G. Fox, Jr., J. Am. Chem. Soc. **73**, 1904, 1909, 1915 (1951); L. Mandelkern and P. J. Flory, International Chemical Congress, New York, September, 1951.

[19] P. J. Flory, J. Chem. Phys. **17**, 303 (1949).

polymer segments. The effects of bond angle and hindered rotation are taken into account in the definition of the statistical chain element. Concentration effects are neglected.

2. The differential equation for the distribution function is of a modified Fokker-Planck type. An important step in its derivation involves the definition of transition probability, $\psi(\mathbf{r}, \mathbf{s})$. It is assumed that the probability that a particular element of a chain is in a given direction is dependent on the concentration of all the other polymer elements in the immediate neighborhood and that the probability is greater when the density of interfering elements is least.

3. The distribution function, the average square of the distance between two segments of a chain, and the average reciprocal distance between two segments on a chain are derived. It is found that the average square distance $\langle r_{tp}^2 \rangle_{Av}$ is proportional to the molecular weight but that the constant of proportionality is larger than obtained for the "random flight" chain. The larger amount depends on the shape and length of the statistical chain element. The distribution function is a superposition of Gaussian and weighted Gaussian functions.

4. A number of mathematical approximations are made. The correctness of these assumptions is established if the average density of polymer segments is small in comparison with unity. A discussion of the density of polymer segments is given.

5. A comparison of the theoretical results with experiment is given. The agreement with available light scattering data is good, and the agreement with intrinsic viscosity data is good in some cases and bad in others. It is pointed out that comparison with experiment is not direct but depends upon the assumed correctness of present viscosity and light scattering theories.

THE JOURNAL OF CHEMICAL PHYSICS VOLUME 20, NUMBER 9 SEPTEMBER, 1952

Dipole-Dipole Interaction in Simple Lattices*

T. H. BERLIN AND J. S. THOMSEN
Department of Physics, The Johns Hopkins University, Baltimore, Maryland
(Received March 17, 1952)

A mathematical model, the spherical model, of electric dipole-dipole interaction in simple lattices is discussed. The partition function for the system, assuming just nearest neighbor interaction, is evaluated for one- and three-dimensional simple lattices. Only the three-dimensional lattice exhibits a phase transition. The transition is discussed. The transition behavior in the presence of an external field is also analyzed, and the electric susceptibility is computed.

INTRODUCTION

IN this paper the technique of sphericalization is applied to the problem of electric dipole-dipole interaction in simple lattices. This problem is analogous to the classical problem of antiferromagnetism. No attempt is made to discuss the results in connection with the behavior of real crystals. The model is regarded as a mathematical model, and the study is made with the aim of throwing possible light on transition phenomena.

A one-dimensional lattice of three-dimensional dipoles will first be discussed, simply for the purpose of elucidating the technique. Neither the one- nor the two-dimensional lattice shows a transition. Then a simple cubic lattice will be discussed. This lattice has a transition temperature, the transition being due to the onset of a long-range order. Finally, the lattice in an homogeneous electric field is discussed. It is found that the transition temperature is a function of the field strength and that the transition temperature reaches absolute zero for a finite value of the electric field. For field strengths greater than the critical field strength no transition exists. As is to be expected, the critical field is such that the energy of a dipole in this field is equal to the lowest energy of interaction of a dipole with its nearest neighbors, for nearest neighbor interaction only is assumed in the analysis.

* This work has been partly supported by the ONR.

THE SPHERICAL MODEL OF DIPOLE-DIPOLE INTERACTION

The thermodynamics of the system can be completely discussed if the evaluation of the partition function for the system can be carried through. We shall assume an electric dipole $\mu\boldsymbol{\varepsilon}_j$ situated at the jth lattice point, where μ is the strength of the dipole and $\boldsymbol{\varepsilon}_j$ is a unit vector free to point in any direction in space. The interaction energy between two dipoles is

$$U_{ij}=\mu^2(\boldsymbol{\varepsilon}_i\cdot\boldsymbol{\varepsilon}_j)/r_{ij}^3-3\mu^2(\boldsymbol{\varepsilon}_i\cdot\mathbf{r}_{ij})(\boldsymbol{\varepsilon}_j\cdot\mathbf{r}_{ij})/r_{ij}^5, \quad (1)$$

where $\mathbf{r}_{ij}$ the vector distance between the dipoles. We wish to consider nearest neighbor interaction only. Hence, the total interaction energy of the system of dipoles is

$$U=\tfrac{1}{2}\sum_{i,j}{}' U_{ij}, \quad (2)$$

where $\sum'$ indicates summation over nearest neighbors, and the sum is over all i and j.

The partition function is

$$Q=A\int\int\cdots\int e^{-U/kT}d\boldsymbol{\varepsilon}_1 d\boldsymbol{\varepsilon}_2\cdots d\boldsymbol{\varepsilon}_N, \tag{3}$$

where $d\boldsymbol{\varepsilon}_j=d\epsilon_{jx}d\epsilon_{jy}d\epsilon_{jz}$, A is a normalization constant, and the multiple integral is over all possible dipole configurations of the system. The integration is to be carried out subject to the restrictions

$$(\boldsymbol{\varepsilon}_j\cdot\boldsymbol{\varepsilon}_j)=1 \quad \text{for} \quad j=1, 2, \cdots, N. \tag{4}$$

This model is the classical model, except for the nearest neighbor restriction, and the evaluation of Q has not been carried through with the natural restrictions on $\boldsymbol{\varepsilon}_j$. The replacement of (4) by a much weaker restriction does, however, allow the exact computation of Q in closed form in the limit $N\to\infty$. The weaker restriction, "spherication," is

$$\sum_{j=1}^{N}(\boldsymbol{\varepsilon}_j\cdot\boldsymbol{\varepsilon}_j)=N. \tag{5}$$

It seems worth while to carry through the analysis with (4) replaced by (5). The reasons are that the restriction $\epsilon_j^2=1$ is retained in the average $\langle\epsilon_j^2\rangle=1$ by (5), and also the restriction (5) does not allow large fluctuations (this means that configurations in which $\epsilon_j^2\sim N$ contributes negligibly to Q). Therefore, we may expect that important features of the classical model are retained in the spherical model.

The problem then is the evaluation of

$$Q=A\int\cdots\int_{\sum_1^N\epsilon_j^2=N}d\boldsymbol{\varepsilon}_1\cdots d\boldsymbol{\varepsilon}_N e^{-U/kT}. \tag{6}$$

We are here only interested in the limit $N\to\infty$. Thus, we wish the limit free energy per "particle" which is

$$\psi=-kT\ln Z \quad \text{with} \quad Z=\lim_{N\to\infty}Q^{1/N}. \tag{7}$$

THE ONE-DIMENSIONAL LATTICE

We first consider a one-dimensional lattice, in the x direction, with spacing r and $n=N$ lattice points. The energy of interaction between nearest neighbors is

$$U_{ij}=\mu^2(\boldsymbol{\varepsilon}_i\cdot\boldsymbol{\varepsilon}_j)/r^3-3\mu^2\epsilon_{ix}\epsilon_{jx}/r^3. \tag{8}$$

The partition function is

$$Q=A\int\cdots\int_{\sum_1^N\epsilon_j^2=N}d\boldsymbol{\varepsilon}_1\cdots d\boldsymbol{\varepsilon}_N \times\exp[-K\sum_{i,j}{}'(\epsilon_{iy}\epsilon_{jy}+\epsilon_{iz}\epsilon_{jz}-2\epsilon_{ix}\epsilon_{jx})], \tag{9}$$

$K=\mu^2/2r^3kT$,

which is to be evaluated for N very large.

The restriction of the region of integration may be conveniently removed by means of the delta-function, so that

$$Q=A\int_{-\infty}^{+\infty}\cdots\int d\boldsymbol{\varepsilon}_1\cdot d\boldsymbol{\varepsilon}_N \times\exp[-K\sum_{i,j}{}'(\epsilon_{iy}\epsilon_{jy}+\epsilon_{iz}\epsilon_{jz}-2\epsilon_{iz}\epsilon_{jz})] \times\frac{1}{2\pi i}\int_{-i\infty}^{+i\infty}d\zeta\exp[+\zeta(N-\sum_1^N\epsilon_j^2)]. \tag{10}$$

The interaction energy is not a definite quadratic form. In order to interchange the order of the ζ- and $\boldsymbol{\varepsilon}$-integrations, we must write

$$Q=\frac{A}{2\pi i}\int_{\alpha-i\infty}^{\alpha+i\infty}d\zeta e^{N\zeta}\int_{-\infty}^{+\infty}\cdots\int d\boldsymbol{\varepsilon}_1\cdots d\boldsymbol{\varepsilon}_N \times\exp[-\zeta\sum_1^N\epsilon_j^2-K\sum_{i,j}{}'(\epsilon_{iy}\epsilon_{jy}+\epsilon_{iz}\epsilon_{jz}-2\epsilon_{iz}\epsilon_{jz})], \tag{11}$$

where α is real and positive and sufficiently large so that the line $\zeta=\alpha$ is to the right of all singularities of the integrand as a function of ζ. The integration over the variables $\boldsymbol{\varepsilon}$ is obviously a product of integrations over the components of $\boldsymbol{\varepsilon}$. Thus, we may write

$$Q=\frac{A}{2\pi i}\int_{\alpha-i\infty}^{\alpha+i\infty}d\zeta e^{N\zeta}\frac{\pi^{N/2}}{(D_x)^{\frac{1}{2}}}\cdot\frac{\pi^{N/2}}{(D_y)^{\frac{1}{2}}}\cdot\frac{\pi^{N/2}}{(D_z)^{\frac{1}{2}}}, \tag{12}$$

where D_x, D_y, and D_z are the determinants of the corresponding quadratic forms. Let us consider, for example, the quadratic form

$$\sum_{j=1}^{N}\zeta\epsilon_{jz}^2+\sum_{i,j}{}'a\epsilon_{ix}\epsilon_{jx}.$$

It is particularly convenient to take the matrix of the coefficients of the form to be cyclic. This is achieved in the one-dimensional lattice by closing the chain to form a ring. We, therefore, have eliminated the possibility of discussing "surface" effects. However, in the limit $N\to\infty$, the closing of the chain will have no effect on the "volume" behavior.

Let $V_1, \cdots, V_N$ denote the components of the characteristic vector of the interaction matrix corresponding to the characteristic value λ. (Note that the quadratic form is symmetric and can, therefore, be diagonalized by an orthogonal transformation.) Then we have

$$\begin{gathered}aV_{j-1}+\zeta V_j+aV_{j+1}=\lambda V_j, \quad j=2, \cdots, N.\\ V_1=V_{N+1}.\end{gathered} \tag{13}$$

The characteristic values are

$$\lambda_k=\zeta+2a\cos\frac{2\pi}{N}(k-1), \quad k=1, \cdots, N, \tag{14}$$

and the components of the characteristic vectors may be written

$$V_j^{(k)}=\frac{1}{N^{\frac{1}{2}}}\left[\cos\frac{2\pi}{N}(k-1)(j-1)+\sin\frac{2\pi}{N}(k-1)(j-1)\right], \tag{15}$$

where they have been normalized to unity.

The determinant D_x is simply the product of the characteristic values λ_k. Thus, the quantity a is $-2K$ for D_x, and $+K$ for both D_y and D_z. Furthermore, it is convenient to write

$$D=\exp(+\sum_1^N \ln\lambda_k).$$

We now have

$$Q=\frac{A\pi^{3N/2}}{2\pi i}\int_{\alpha-i\infty}^{\alpha+i\infty} d\zeta(\zeta-4K)^{-\frac{1}{2}} \times\exp\left\{N\zeta-\tfrac{1}{2}\sum_{k=2}^{N}\ln\left[\zeta-4K\cos\frac{2\pi}{N}(k-1)\right] -\sum_{k=1}^{N}\ln\left[\zeta+2K\cos\frac{2\pi}{N}(k-1)\right]\right\}. \tag{16}$$

As N becomes very large, the sum over k can be approximated by an integral. Hence,

$$Q=\frac{A\pi^{3N/2}}{2\pi i}\int_{\alpha-i\infty}^{\alpha+i\infty} d\zeta(\zeta-4K)^{-\frac{1}{2}}\exp[+Nf(\zeta,K)], \tag{17}$$

where

$$f(\zeta,K)=\zeta-\frac{1}{4\pi}\int_0^{2\pi} d\omega\ln(\zeta-4K\cos\omega) -\frac{1}{2\pi}\int_0^{2\pi} d\omega\ln(\zeta+2K\cos\omega).$$

The complex integral is completely defined by taking $\alpha>4K$.

Our next step is to evaluate the complex integral by the method of steepest descent. The result is that

$$Q=A\pi^{3N/2}\exp[+Nf(\zeta_s,K)]/[2\pi N(\partial^2 f/\partial\zeta^2)_{\zeta_s}(\zeta_s-4K)]^{\frac{1}{2}}, \tag{18}$$

where the saddle point ζ_s is determined by

$$\left(\frac{\partial f}{\partial\zeta}\right)_{\zeta_s}=1-\frac{1}{4\pi}\int_0^{2\pi}\frac{d\omega}{\zeta_s-4K\cos\omega} -\frac{1}{2\pi}\int_0^{2\pi}\frac{d\omega}{\zeta_s+2K\cos\omega}=0. \tag{19}$$

These integrals are readily evaluated and the equation for ζ_s is

$$1-\tfrac{1}{2}[\zeta_s^2-(4K)^2]^{-\frac{1}{2}}-[\zeta_s^2-(2K)^2]^{-\frac{1}{2}}=0. \tag{20}$$

It must be ascertained that $(\partial^2 f/\partial\zeta^2)_{\zeta_s}>0$, which is easily done.

We now have

$$\lim_{N\to\infty}Q^{1/N}=\exp[+f(\zeta_s,K)]\lim_{N\to\infty}[A\pi^{3N/2}]^{1/N},$$

and we may take

$$\ln Z=f(\zeta_s,K),$$

where the additive constant resulting from normalization has been omitted. Consequently, the free energy per dipole is given by

$$-\psi/kT=f(\zeta_s,K) \tag{21}$$

$$f(\zeta_s,K)=\zeta_s-\tfrac{1}{2}\ln\left\{\frac{\zeta_s+[\zeta_s^2-(4K)^2]^{\frac{1}{2}}}{2}\right\} -\ln\left\{\frac{\zeta_s+[\zeta_s^2-(2K)^2]^{\frac{1}{2}}}{2}\right\}.$$

The positive solution of (20) is needed to satisfy the requirements for a saddle point. We see also that ζ_s exists for every T in the range $0<T<\infty$. Then the free energy ψ behaves regularly as a function of T and no transition occurs.

The two-dimensional lattice is analyzed in a similar manner. No transition occurs. Therefore, we will continue with the three-dimensional analysis which does show a transition.

THE THREE-DIMENSIONAL LATTICE

We shall assume a simple cubic lattice with spacing r, and with n_1 sites in a row, n_2 rows in a plane, and n_3 planes, yielding $n_1n_2n_3=N$ lattice sites. The lattice points can be systematically numbered with the following scheme. Let the ith site be described by integers (k, l, m) and also by coordinates (x, y, z). Then we set $x=(k-l)r$; $y=lr$; $z=mr$; and $i=k+ln_1+mn_1n_2$ where $k=1, 2, \cdots, n_1$; $l=0, 1, \cdots, n_2-1$; $m=0, 1, \cdots, n_3-1$. The site (k, l, m) interacts with its six nearest neighbors specified by $(k\pm1, l, m)$, $(k, l\pm1, m)$, $(k, l, m\pm1)$. Furthermore,

$$U_{ij}=\mu^2(\boldsymbol{\epsilon}_i\cdot\boldsymbol{\epsilon}_j)/r^3-3\mu^2\epsilon_{i\eta}\epsilon_{j\eta}/r^3,$$

where $\eta=x$, y, or z depending on whether k, l, or m change by ±1.

The sphericalized partition function is

$$Q=\frac{A}{2\pi i}\int_{\alpha-i\infty}^{\alpha+i\infty}d\zeta e^{N\zeta}\int_{-\infty}^{+\infty}\cdots\int d\boldsymbol{\epsilon}_1\cdots d\boldsymbol{\epsilon}_N \times\exp\{-\zeta\sum_1^N\epsilon_j^2-K\sum_{i,j}'[(\boldsymbol{\epsilon}_i\cdot\boldsymbol{\epsilon}_j)-3\epsilon_{i\eta}\epsilon_{j\eta}]\}. \tag{22}$$

As before, we may write

$$Q=\frac{A}{2\pi i}\int_{\alpha-i\infty}^{\alpha+i\infty}d\zeta e^{N\zeta}\frac{\pi^{N/2}}{(D_x)^{\frac{1}{2}}}\cdot\frac{\pi^{N/2}}{(D_y)^{\frac{1}{2}}}\cdot\frac{\pi^{N/2}}{(D_z)^{\frac{1}{2}}}. \tag{23}$$

Use periodic boundary conditions to cyclize the interaction matrix and let $C_j^{(\eta)}$ $j=1, 2, \cdots, N$, correspond to the N elements of the cyclic matrix for each degree of freedom $\eta=x, y, z$. The conditions on the elements are

$$C_1^{(\eta)}=\zeta, \quad C_j^{(\eta)}=C_{N+j}^{(\eta)}=C_{N-j+2}^{(\eta)}. \tag{24}$$

We then have

$$\begin{aligned}
&C_2^{(x)}=-2K, \ C_{n_1+1}^{(x)}=K, \qquad C_{n_1n_2+1}^{(x)}=K;\\
&C_2^{(y)}=K, \qquad C_{n_1+1}^{(y)}=-2K, \ C_{n_1n_2+1}^{(y)}=K;\\
&C_2^{(z)}=K, \qquad C_{n_1+1}^{(z)}=K, \qquad C_{n_1n_2+1}^{(z)}=-2K;
\end{aligned} \tag{25}$$

and all elements not prescribed by (24) and (25) equal zero.

The characteristic values of the three matrices are

$$\begin{aligned}
\lambda_p^{(x)}&=\zeta-4K\cos\frac{2\pi}{N}(p-1)\\
&\quad+2K\cos\frac{2\pi}{N}(p-1)n_1+2K\cos\frac{2\pi}{N}(p-1)n_1n_2;\\
\lambda_p^{(y)}&=\zeta+2K\cos\frac{2\pi}{N}(p-1)\\
&\quad-4K\cos\frac{2\pi}{N}(p-1)n_1+2K\cos\frac{2\pi}{N}(p-1)n_1n_2;\\
\lambda_p^{(z)}&=\zeta+2K\cos\frac{2\pi}{N}(p-1)\\
&\quad+2K\cos\frac{2\pi}{N}(p-1)n_1-4K\cos\frac{2\pi}{N}(p-1)n_1n_2;\\
&\qquad p=1, 2, \cdots, N.
\end{aligned} \tag{26}$$

Then,

$$D_\eta=\prod_{p=1}^{N}\lambda_p^{(\eta)}=\exp\Big(\sum_{p=1}^{N}\ln\lambda_p^{(\eta)}\Big).$$

We must now find the largest positive finite value of ζ which is a singularity of the integrand in (23). Such a value of ζ will make one or more of the characteristic values equal to zero. Inspection of (26) makes it clear that this value of ζ is $8K$ at most. It is then found that $\lambda^{(z)}{}_{N/2+1}=0$ for $\zeta=8K$, and only this one characteristic value can be zero, with n_1 odd, n_2 even, and $p=1+N/2$. That one of the z characteristic values has a particular distinction is fundamentally due to the fact that we have made a particular arrangement of the Nth roots of unity with which to express the characteristic values of the cyclic matrices. This has shown up in the particular expressions in (26). One of the x or y characteristic values could have been given the particular distinction just as well. Convenient consequences of our choice will appear in the discussion of the nature of the transition and in the analysis of the effect of an applied external field.

For N very large, we may write

$$\begin{aligned}
D_x&=\exp\Big\{\frac{N}{(2\pi)^3}\int_0^{2\pi}\!\!\int\!\!\int d\omega_1d\omega_2d\omega_3\\
&\quad\times\ln(\zeta-4K\cos\omega_1+2K\cos\omega_2+2K\cos\omega_3)\Big\},\\
D_y&=\exp\Big\{\frac{N}{(2\pi)^3}\int_0^{2\pi}\!\!\int\!\!\int d\omega_1d\omega_2d\omega_3\\
&\quad\times\ln(\zeta+2K\cos\omega_1-4K\cos\omega_2+2K\cos\omega_3)\Big\},\\
D_z&=(\zeta-8K)^{\frac{1}{2}}\exp\Big\{\frac{N}{(2\pi)^3}\int_0^{2\pi}\!\!\int\!\!\int d\omega_1d\omega_2d\omega_3\\
&\quad\times\ln(\zeta+2K\cos\omega_1+2K\cos\omega_2-4K\cos\omega_3)\Big\}.
\end{aligned} \tag{27}$$

For further convenience let $\zeta=2Kt$. Then we have for the partition function

$$\begin{aligned}
Q&=A\pi^{3N/2}(2K)^{\frac{1}{2}}\exp(-3N/2\ln2K)\\
&\quad\times\frac{1}{2\pi i}\int_{\alpha'-i\infty}^{\alpha'+i\infty}dt(t-4)^{-\frac{1}{2}}e^{Nf(t,K)}
\end{aligned} \tag{28}$$

with

$$\begin{aligned}
f(t,K)&=2Kt-\frac{3}{2}\cdot\frac{1}{(2\pi)^3}\int_0^{2\pi}\!\!\int\!\!\int d\omega_1d\omega_2d\omega_3\\
&\quad\times\ln(t-2\cos\omega_1+\cos\omega_2+\cos\omega_3).
\end{aligned}$$

The integrand is singular for $t=4$, hence, we choose $\alpha'>4$.

Evaluating the complex integral by the method of steepest descent, the equation determining the saddle point t_s is $(\partial f/\partial t)_{t_s}=0$, which may be written as

$$\frac{4K}{3}=\frac{1}{(2\pi)^3}\int_0^{2\pi}\!\!\int\!\!\int\frac{d\omega_1d\omega_2d\omega_3}{t_s-2\cos\omega_1+\cos\omega_2+\cos\omega_3}. \tag{29}$$

This equation has a solution for t_s real and positive.

As T decreases from ∞, K increases from 0, and t_s decreases from ∞ monotonically. The integral in (29)

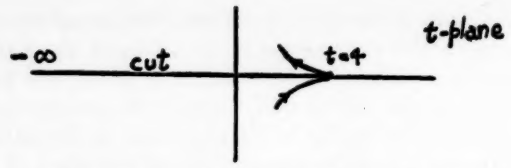

FIG. 1. The path of steepest descent for $T<T_c$.

has a maximum finite value for $t_s=4$. This defines a critical value K_c for K and T_c for T.

For $T<T_c$, $K>K_c$, we must reconsider the integrand since a saddle point in the sense of (29) no longer exists. If we let $t=4+\nu$, we find that in the neighborhood of $t=4$,

$$f(t, K)=f(4, K)+2(K-K_c)\nu+O(\nu^{\frac{3}{2}}). \tag{30}$$

The point $t=4$ is a branch point of order 1. We have a new path of steepest descent for negative ν which is fixed for all $K>K_c$. The path is qualitatively shown in Fig. 1. In the limit $N\to\infty$, we may take the path infinitesimally close to the real axis. Therefore, we find for Q,

$$Q=A\pi^{3N/2}\left[\frac{K}{\pi N(K-K_c)}\right]^{\frac{1}{2}} \times\exp[-3N/2\ \ln 2K+Nf(4, K)]. \tag{31}$$

The analysis has the following conclusions. Let

$$\frac{4K_c}{3}=\frac{1}{(2\pi)^3}\int_0^{2\pi}\int\int\frac{d\omega_1 d\omega_2 d\omega_3}{4-2\cos\omega_1+\cos\omega_2+\cos\omega_3}. \tag{32}$$

For $T>T_c$, $K<K_c$:

$$-\psi/kT=-(3/2)\ \ln 2K+f(t_s, K) \tag{33}$$

and $t_s(K)$ is given by (29).

For $T<T_c$, $K>K_c$:

$$-\psi/kT=-(3/2)\ \ln 2K+f(4, K). \tag{34}$$

We will now briefly describe some of the main thermodynamic properties of the system.

Since $\ln Z=-\psi/kT$, then if E is the average energy per dipole and C is the specific heat per dipole, we write

$$E=kT^2(d/dT)\ \ln Z, \qquad C=dE/dT. \tag{35}$$

Now

$$\ln Z=-3/2\ \ln 2K+f(t_s, K).$$

Therefore,

$$\frac{d}{dT}\ln Z=\left[-\frac{3}{2K}+\frac{\partial f}{\partial K}+\frac{\partial f}{\partial t_s}\frac{dt_s}{dK}\right]\frac{dK}{dT}.$$

For $T>T_c$, $\partial f/\partial t_s=0$, and for $T<T_c$, $t_s=4$. Consequently, $dt_s/dK\cdot\partial f/\partial t_s=0$ for all T and

$$\frac{d}{dT}\ln Z=-\frac{K}{T}\left[-\frac{3}{2K}+2t_s\right]. \tag{36}$$

Hence,

$$E=(3/2)kT\left[1-\frac{4K}{3}t_s\right], \quad T>T_c$$
$$E=(3/2)kT\left[1-\frac{16K}{3}\right], \quad T<T_c. \tag{37}$$

The energy is continuous at the critical temperature T_c.

We find that for the specific heat

$$C=(3k/2)\left[1+\frac{4K^2}{3}\frac{dt_s}{dK}\right], \quad T>T_c$$
$$C=3k/2 \qquad\qquad T<T_c. \tag{38}$$

Thus, there is a discontinuity in the slope of the specific heat at the critical temperature. The qualitative behavior is shown in Fig. 2. The slope, dC/dT, is negative and finite at $T=T_c$.

The nature of the transition is demonstrated by the following analysis. The nearest neighbor configuration of lowest energy is shown in Fig. 3. Suppose that the direction of orientation is the z direction. In the completely order configuration of the entire lattice, the dipoles in the planes of given z are alternately in the positive and negative z direction, and all planes are alike. Such an ordering can be made periodic if n_1, the number of dipoles in a row in the x direction, is odd and n_2, the number of rows in the y direction, is even. With the scheme of numbering the dipoles given above, the parameter of long-range order S_z can be defined by taking NS_z to be the average of the absolute value of the sum of the z components of all odd numbered dipoles minus the sum of the z components of all even numbered dipoles. The implication is that all odd numbered dipoles will form a ferroelectric lattice, and so will the even numbered dipoles but in the opposite direction. The absolute value is required because there is no preferential z direction in the field free case. Complete order gives $S_z=1$, complete disorder $S_z=0$.

To explicitly formulate S_z, we note that the interaction matrix is diagonalized by the transformations

$$y_{p\eta}=\sum_{j=1}^{N}V_j^{(p)}\epsilon_{j\eta}, \quad \eta=x, y, z. \tag{39}$$

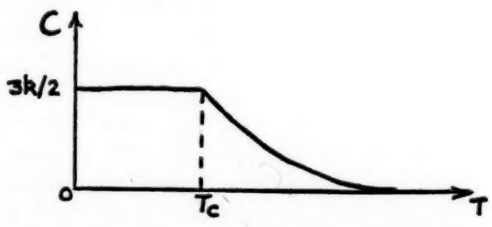

FIG. 2. The qualitative dependence of the specific heat on temperature.

The characteristic vectors and values are given by (15) and (26), respectively. We note further that $V_j^{(N/2+1)}=(-1)^{j-1}/N^{\frac{1}{2}}$, so that

$$y_{(N/2+1)z}=\frac{1}{N^{\frac{1}{2}}}\sum_{j=1}^{N}(-1)^{j-1}\epsilon_{jz}=\frac{1}{N^{\frac{1}{2}}}\{\sum_{j\,\text{odd}}\epsilon_{jz}-\sum_{j\,\text{even}}\epsilon_{jz}\}. \quad (40)$$

Consequently,

$$S_z=\left\langle\frac{|y_{(N/2+1)z}|}{N^{\frac{1}{2}}}\right\rangle. \quad (41)$$

We write

$$\langle|y_{pz}|\rangle=\frac{1}{Q}\frac{A}{2\pi i}\int_{\alpha-i\infty}^{\alpha+i\infty}d\zeta e^{N\zeta}\int_{-\infty}^{+\infty}\cdots\int d\varepsilon_1\cdots d\varepsilon_N|y_{pz}|$$

$$\times\exp\{-\zeta\sum_{1}^{N}\epsilon_j^2-K\sum_{i,j}{}'[(\varepsilon_i\cdot\varepsilon_j)-3\epsilon_{i\eta}\epsilon_{j\eta}]\}. \quad (42)$$

Integrating over the set of coordinates $\{\epsilon_{jz}\}$ and $\{\epsilon_{jy}\}$, and using (39),

$$\langle|y_{pz}|\rangle=\frac{1}{Q}\frac{A}{2\pi i}\int_{\alpha-i\infty}^{\alpha+i\infty}d\zeta e^{N\zeta}$$

$$\times\frac{\pi^{N/2}}{(D_x)^{\frac{1}{2}}}\cdot\frac{\pi^{N/2}}{(D_y)^{\frac{1}{2}}}\int_{-\infty}^{+\infty}\cdots\int dy_{1z}\cdots dy_{Nz}|y_{pz}|$$

$$\times\exp[-\sum_{j=1}^{N}\lambda_j^{(z)}y_{jz}{}^2] \quad (43)$$

and

$$\langle|y_{pz}|\rangle=\frac{1}{Q}\frac{A}{2\pi i}\int_{\alpha-i\infty}^{\alpha+i\infty}d\zeta e^{N\zeta}$$

$$\times\frac{\pi^{N/2}}{(D_x)^{\frac{1}{2}}}\cdot\frac{\pi^{N/2}}{(D_y)^{\frac{1}{2}}}\cdot\frac{\pi^{N/2}}{(D_z)^{\frac{1}{2}}}\frac{1}{(\pi\lambda_p{}^{(z)})^{\frac{1}{2}}}. \quad (44)$$

Therefore,

$$\langle|y_{(N/2+1)z}|\rangle=\frac{1}{(2\pi K)^{\frac{1}{2}}}\int_{\alpha'-i\infty}^{\alpha'+i\infty}dt(t-4)^{-1}e^{Nf(t,K)}\Big/$$

$$\int_{\alpha'-i\infty}^{\alpha'+i\infty}dt(t-4)^{-\frac{1}{2}}e^{Nf(t,K)}. \quad (45)$$

For $T>T_c$,

$$\langle|y_{(N/2+1)z}|\rangle=[2\pi K(t_s-4)]^{-\frac{1}{2}}. \quad (46)$$

For $T<T_c$, evaluation of the denominator in (45) yields

$$i[2\pi/N(K-K_c)]^{\frac{1}{2}}e^{Nf(4,K)}.$$

On evaluating the numerator, we get no contribution from the path of steepest descent, but we do get a contribution from the simple pole at $t=4$. This yields,

$$i[2\pi/K]^{\frac{1}{2}}e^{Nf(4,K)}.$$

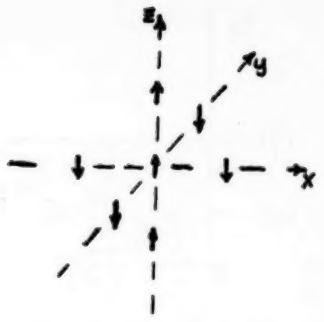

FIG. 3. Local dipole configuration of minimum energy.

Hence, for $T<T_c$,

$$\langle|y_{(N/2+1)z}|\rangle=\left[N\left(1-\frac{K_c}{K}\right)\right]^{\frac{1}{2}}=\left[N\left(1-\frac{T}{T_c}\right)\right]^{\frac{1}{2}}. \quad (47)$$

Therefore, in the limit $N\to\infty$, we find that

$$\begin{aligned}&S_z=0, \quad \text{for} \quad T>T_c;\\ &S_z=\left(1-\frac{T}{T_c}\right)^{\frac{1}{2}}, \quad \text{for} \quad T<T_c.\end{aligned} \quad (48)$$

The conclusion that the transition corresponds to the onset of long-range order is clear.

THE INFLUENCE OF AN APPLIED ELECTRIC FIELD

In the presence of an homogeneous applied electric field $\mathbf{E}$, there is the additional energy

$$-\sum_{j=1}^{N}(\mu\varepsilon_j\cdot\mathbf{E}).$$

The partition function can be readily computed because the additional energy is linear in ε_j and the interaction matrix is cyclic.

As before, the integration over the components $\{\epsilon_{jz}\}$, etc., can be expressed as a product of integrals for the three components separately. Consequently, we have to evaluate

$$\int_{-\infty}^{+\infty}\cdots\int d\epsilon_{1x}\cdots d\epsilon_{Nx}\exp\Big[-\zeta\sum_{i}^{N}\epsilon_{jx}{}^2$$

$$-K\sum_{i,j}{}'(\epsilon_{ix}\epsilon_{jx}-3\epsilon_{i\eta}\epsilon_{j\eta})+\frac{\mu E_x}{kT}\sum_{1}^{N}\epsilon_{jx}\Big]. \quad (49)$$

Using the transformation (39), we also note that $V_j^{(1)}=1/N^{\frac{1}{2}}$, so that

$$y_{1\eta}=\sum_{j=1}^{N}V_j{}^{(1)}\epsilon_{j\eta}=\frac{1}{N^{\frac{1}{2}}}\sum_{j=1}^{N}\epsilon_{j\eta}.$$

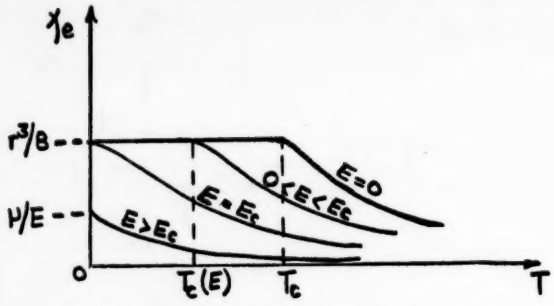

FIG. 4. The qualitative dependence of χ_e on temperature and applied field strength.

The integral (49) becomes

$$\int_{-\infty}^{+\infty}\cdots\int dy_{1x}\cdots dy_{Nx}\exp\left[-\sum_{j=1}^{N}\lambda_j^{(x)}y_{jx}^2+\frac{\mu E_x}{kT}N^{\frac{1}{2}}y_{1x}\right],$$

and on integration we have

$$\frac{\pi^{N/2}}{(D_x)^{\frac{1}{2}}}\exp\left[+\frac{N}{\lambda_1^{(x)}}\left(\frac{\mu E_x}{kT}\right)^2\right] \quad \text{with} \quad \lambda_1^{(x)}=\zeta.$$

Consequently, the partition function in the presence of an homogeneous electric field **E**, may be written as

$$Q(\mathbf{E})=A\pi^{3N/2}(2K)^{\frac{1}{2}}\times\exp(-3N/2\ln 2K)\frac{1}{2\pi i}\int_{\alpha'-i\infty}^{\alpha'+i\infty}dt(t-4)^{-\frac{1}{2}}\times\exp\left\{N\left[f(t,K)+\frac{1}{2Kt}\left(\frac{\mu E}{2kT}\right)^2\right]\right\} \quad (50)$$

$$E^2=E_x^2+E_y^2+E_z^2.$$

Again using the method of steepest descent to evaluate the complex integral, the equation for the saddle point is

$$\frac{4K}{3}\left[1-\left(\frac{Er^3}{2\mu t_s}\right)^2\right]=\frac{1}{(2\pi)^3}\int_0^{2\pi}\int\int\frac{d\omega_1 d\omega_2 d\omega_3}{t_s-2\cos\omega_1+\cos\omega_2+\cos\omega_3}. \quad (51)$$

This equation has significant properties. When $Er^3/2\mu \geq 4$, a saddle point t_s exists for all K, that is, for every temperature. This means that no transition occurs for field strengths $E\geq 8\mu/r^3$. On the other hand, if $E<8\mu/r^3$, then a critical temperature, $T_c(E)$, exists and occurs when $t_s=4$. In this case

$$T_c(E)=T_c[1-(E/E_c)^2], \quad E_c=8\mu/r^3. \quad (52)$$

Therefore, as E increases from zero, a transition occurs for every $E<E_c$. The transition temperature approaches absolute zero as E approaches E_c. Transitions no longer occur when $E>E_c$.

The critical field has a simple significance. The local dipole configuration with lowest energy is shown in Fig. 3. The energy of this configuration is $-8\mu^2/r^3$. The energy of the central dipole in the critical field is (assuming that the field is in the z-direction) $-\mu E_c=-8\mu^2/r^3$, which is precisely the lowest local configurational energy.

The electric susceptibility χ_e is given by[1]

$$\chi_e=\frac{kT}{E}\frac{\partial}{\partial E}\ln Z \quad (53)$$

and

$$\ln Z=-(3/2)\ln 2K+f(t_s,K)+(32K/t_s)(E/E_c)^2. \quad (54)$$

Although t_s is a function of E, $\partial/\partial t_s \ln Z=0$. Consequently,

$$\chi_e=r^3/2t_s. \quad (55)$$

The qualitative behavior of χ_e as a function of temperature and field strength is shown in Fig. 4.

For $E>E_c$, the value of χ_e at $T=0$ is

$$\chi_e=(r^3/8)(E_c/E)=\mu/E,$$

whereas for $E<E_c$, χ_e is constant with the value $r^3/8$.

[1] Since nearest neighbor interaction only has been considered, the depolarization arising from the *long-range* dipole interaction has also been neglected. Therefore, we make no distinction between the external field strength and the field strength in the lattice for the purpose of defining χ_e. This allows χ_e to be independent of the shape of the lattice, as χ_e would be in a more complete treatment including the long-range forces.

A Vibrational Analysis of the Fluorescence of Naphthalene Vapor*

O. SCHNEPP† AND D. S. MCCLURE
Department of Chemistry and Chemical Engineering, University of California, Berkeley, California
(Received January 24, 1952)

The fluorescence spectrum of naphthalene vapor has been photographed and found, under suitable conditions, to consist of a number of discrete bands. Thirty-nine bands were measured and a vibrational analysis was carried out making use of assignments of infrared and Raman fundamentals. The analysis indicates that the transition observed is forbidden by symmetry and made weakly allowed by a molecular vibration of frequency 478 cm^{-1} belonging to the representation $b2_u$. This indicates that the wave function of the lowest excited singlet state of naphthalene belongs to the irreducible representation A_g or $B1_g$ of the point group $D2_h$.

I. INTRODUCTION

THE near ultraviolet absorption spectrum of naphthalene consists of three main regions. The longest wavelength absorption is weak (absorption coefficient 200–300) and extends from 3200A to 2900A. A much stronger region of absorption (absorption coefficient 5000–6000) begins at 2900A and extends to about 2500A. This second region differs markedly from the first one inasmuch as it is much more diffuse in appearance. There is a third absorption region with an absorption coefficient of about 100,000 at 2200A. Studies on this spectrum have been made in the vapor phase by Henri and de Laszlo, in liquid solution by de Laszlo,[1,2] Morton and de Gouveia,[3] and Mayneord and Roe,[4] as well as others. The absorption in rigid glass has been described by Kasha and Nauman,[5] and that of the solid by Prikhotjko.[6,7] The fluorescence of naphthalene has, till now, been studied primarily in solid solution, by Kasha and Nauman,[5] and in liquid solutions.[8] The fluorescence spectrum of the vapor has been photographed by Pringsheim[9] and found to consist of a number of narrow bands superimposed on a continuous background. The effect of changing the wavelength of the excitation on the appearance of the emission spectrum of the vapor has been discussed by W. West,[10] who found that discrete bands were obtained when naphthalene was excited by light of wavelength between 3200A and 2900A whereas a continuous emission was observed when light of shorter wavelength was used. The fluorescence of the crystal at 20°K has been described by Obreimov and Shabaldas,[11] who found that they could interpret the whole spectrum in terms of progressions and combinations of known Raman frequencies of naphthalene starting with the first strong emission band.

Theoretical calculations have been made to determine the term scheme of the naphthalene molecule. The bond-orbital method, after refinements are added, gives consistently the result that the lowest level is totally symmetric, and therefore a transition from the ground state to this level is forbidden. This result has been reported by Blumenfeld[12] and by Craig.[13] On the other hand, the molecular orbital method has so far given the result that the lowest transition in naphthalene should be allowed by symmetry. Calculations have been made by German,[14] Coulson,[15] Davydov,[16] and Simpson.[17] Platt[18] proposed a one-dimensional free electron model which emphasizes the analogy between the spectra of cata-condensed aromatic hydrocarbon compounds. According to this picture, the lowest transition in naphthalene is the analog of the weak transition in benzene at 2600A. This would indicate that the transition is allowed in naphthalene, whereas it was forbidden in benzene, since naphthalene has a much lower symmetry. The most recent calculation has been carried out by Jacobs,[19] who treated the problem by the molecular orbital method and took into account configuration interaction. Her results again indicated that the lowest transition should be allowed. Sponer and Nordheim[20] have recently reviewed the experimental and theoretical data available and favored the possibility of the lowest transition being forbidden and representing a combination between the ground state and a totally symmetric excited state.

The allowed or forbidden character of an electronic transition is determined by the irreducible representa-

* This work was supported by the ONR under Contract N-6-ori-211, T.O. III.
† Now at Hebrew Institute of Technology, Haifa, Israel.
[1] Henri and de Laszlo, Proc. Roy. Soc. (London) **A105**, 662 (1924).
[2] de Laszlo, Z. Physik. Chem. **118**, 369 (1925).
[3] Morton and de Gouveia, J. Chem. Soc. **1934**, 911.
[4] Mayneord and Roe, Proc. Roy. Soc. (London) **A152**, 299 (1935).
[5] M. Kasha and R. V. Nauman, J. Chem. Phys. **17**, 516 (1949).
[6] Prikhotjko, J. Phys. U.S.S.R. **8**, 257 (1944).
[7] Prikhotjko, Izvest. Akad. Nauk SSSR, Ser. Fiz. **12**, 499 (1948).
[8] Pringsheim, *Fluorescence and Phosphorescence* (Interscience Publishers, Inc., New York, 1949), p. 408.
[9] Pringsheim, Ann. Acad. Sci. Varsovie **5**, 29 (1938).
[10] W. West, Ann. New York Acad. Sci. **XLI**, 203 (1941).
[11] Obreimov and Shabaldas, J. Phys. U.S.S.R. **7**, 168 (1943).
[12] Blumenfeld, J. Phys. Chem. U.S.S.R. **21**, 529 (1947).
[13] Craig, Proc. XIth Intern. Congr. Chem. (London) (July, 1947).
[14] German, J. Phys. U.S.S.R. **8**, 276 (1944).
[15] Coulson, Proc. Phys. Soc. (London) **60**, 257 (1948).
[16] Davydov, J. Exptl. Theoret. Phys. U.S.S.R. **17**, 1106 (1947).
[17] William T. Simpson, J. Chem. Phys. **16**, 1124 (1948).
[18] John R. Platt, J. Chem. Phys. **17**, 484 (1949).
[19] Jacobs, Proc. Phys. Soc. (London) **62A**, 710 (1949).
[20] Sponer and Nordheim, Disc. Faraday Soc. 19 (1950).

tions to which the two electronic states concerned belong. If the direct product of the representations of the two electronic states contains at least one of the representations of a vector x, y, or z, then the transition is allowed with a dipole induced along the direction given by this vector.

The naphthalene molecule belongs to the point group V_h. The molecule may, to a good approximation, be treated as a system of ten π-electrons. Because of the even number of orbitals, the electronic states found in this approximation can belong only to certain ones of the irreducible representations of the group V_h, namely, A_g, B_{1g}, B_{2u}, or B_{3u}. The ground state of the molecule belongs to the totally symmetric representation A_g. The vector x (long axis of the molecule) belongs to B_{3u} while the vector y (short axis) belongs to B_{2u}. Thus, transitions from the ground state to an electronic state belonging to B_{2u} are allowed with a dipole change along the short axis of the molecule, and a transition to a state of symmetry B_{3u} is allowed with a dipole change along the long axis. Transitions to states belonging to A_g or B_{1g} are forbidden, since the dipole moment integral will vanish in these cases.

A forbidden transition can be made weakly allowed by a combination of the electronic state with a vibrational mode of the proper symmetry.[21] If the excited state is of symmetry A_g, the transition $(A_g - A_g)$ will occur with a dipole change along the short molecular axis if a b_{2u} vibration combines with one of the electronic states and will occur with a dipole change along the long axis if a b_{3u} vibration combines. If, on the other hand, the upper state is of symmetry B_{1g}, the directions of dipole change will be reversed. In the case of A_{1g} the superposition of a vibration of symmetry b_{1u} on the pure electronic transition would also make the dipole moment integral nonvanishing, on symmetry grounds, for a dipole change perpendicular to the molecular plane. This possibility is unlikely for near ultraviolet transitions in the naphthalene molecule since its low-lying states are pure π-electron states according to present information.

The vibrational pattern accompanying an electronic transition, if properly understood, gives important clues as to the nature of the transition itself. The absence or presence of a comparatively intense band (0—0 band), on which totally symmetric vibrational modes are found superimposed, may often be taken to indicate that the electronic transition is symmetry forbidden or symmetry allowed.[21] The study of the long wavelength absorption of naphthalene is made difficult by the fact that a much stronger transition overlaps the weaker one. This difficulty is not encountered in the study of the emission spectrum, and therefore an analysis of the fluorescence spectrum was attempted in the hope that a clarification of the problem of the nature of the lowest excited state would be achieved.

[21] Herzberg and Teller, Z. physik. Chem. **B21**, 410 (1933).

II. EXPERIMENTAL

Apparatus

The plates of the fluorescence of naphthalene vapor were taken with a Hilger medium quartz spectrograph, E II. The exposure times varied from one to eight hours with a slit width of 50 microns. The plates used were 103-0 Eastman Kodak Spectrographic Plates. The apparatus was essentially a quartz Raman tube fitted with a quartz filter jacket, through which the filter solutions could be circulated. The solid sample of naphthalene was placed in a bulb at the rear end of the sample tube and the vapor was continuously renewed by pumping through a long, narrow tube. The sample tube was about 50 cm long and 4 cm in diameter. The exciting light was provided by a standard type of all-quartz mercury arc, which was nearly as long as the sample tube itself. The fluorescence from the vapor in the sample tube passed through a quartz window and directly entered the slit of the spectrograph.

Purity of Sample

The naphthalene used was Baker and Adamson resublimed naphthalene, which was recrystallized four times from redistilled 95 percent alcohol, then refluxed with an excess of sodium metal for 10 hours, distilled from the reaction mixture, vacuum distilled at about 4-cm pressure (B.P.=110°C), and finally recrystallized twice from distilled 95 percent alcohol. The refluxing step with sodium metal was undertaken to remove heterocyclic compounds containing sulfur, after Sponer and Nordheim.[20] The sulfur content was in this way reduced to less than 0.01 percent by weight, the limit of accuracy of the analysis undertaken. The vacuum distillation removes an impurity which seems to be formed during the refluxing and which is responsible for spurious fluorescence bands in the emission of the crystal.

Experimental Procedure

Before a plate of the fluorescence of the naphthalene vapor was taken, the whole system was evacuated to a pressure of less than 10^{-4} mm of mercury. The naphthalene was pumped through the sample tube in a continuous flow during the experiments. This procedure eliminated possible effects due to photodecomposition of the sample. The filter solution used for the actual plates was a solution of 0.6 g of potassium chromate in a liter of 0.05M sodium hydroxide. This filter solution isolates the 3126–3132A mercury lines with great efficiency, but its transmission of these lines was observed to decrease after exposure to the intense light of the source. The solution was therefore renewed at 1-hour intervals. Other filter solutions used in the course of this work were a phthalate filter, containing 7.5 g potassium acid-phthalate per liter water solution and a phthalate-cyanine filter containing 7.5 g potassium acid-phthalate and 0.2 g of the perchlorate of a simple

cyanine dye (described by Kasha[22]) per liter. Most of the plates were taken at room temperature, the vapor pressure being 0.07 mm of mercury. Some plates were, however, taken at a temperature of 40°C and a naphthalene pressure of 0.35 mm of mercury. Spectra were also taken at room temperature in the presence of nitrogen gas at one atmosphere.

III. APPEARANCE OF THE SPECTRUM

The fluorescence spectrum of naphthalene vapor has been photographed by P. Pringsheim[9] who described it as a more or less continuous emission with some band structure discernible between 3082A and 3341A. According to this author the 3022, 2967, and 2894A lines of the mercury spectrum served as principal exciting light.

If the whole of the mercury emission spectrum is allowed to excite naphthalene vapor in equilibrium with the solid at room temperature, the fluorescence is practically continuous. It begins at or near the band at 3083A and extends far towards the visible region to about 4000A. The only bands visible as such are the strongest at 3083, 3177, and 3182A. If, however, the mercury line group at 3126–3132A is selected by means of a filter of potassium chromate solution, a discrete band spectrum is obtained with little background. On a plate which is exposed for two hours with a slit width of 50 microns, about forty bands extending as far as 3500A can be measured with good accuracy. Figure 1 shows a contact print of a representative plate of this spectrum. When the temperature of the system is raised the spectrum becomes more intense, but the background increases appreciably so as to make the clear banded structure fade away into it somewhat beyond the 3341A mercury line.

The spectrum as obtained with different filter solutions was studied. The phthalate filter is a sharp cut-off filter, which allows all radiation to longer wavelength than 3126A to pass but reduces the intensities of the mercury lines to shorter wavelength very markedly. The spectrum observed with this filter was identical with that observed with K_2CrO_4. The phthalate-cyanine filter, on the other hand, caused the fluorescence spectrum to disappear entirely. The cyanine dye absorbs light strongly in the region of 3100A. The series of experiments described proves conclusively that the fluorescence spectrum, as observed at low pressure in this research, is excited by the mercury lines at 3126 and 3132A.

Plates were also taken with a low pressure of naphthalene in the sample tube being carried in a continuous flow of nitrogen gas at one atmosphere. In this case the general appearance of the spectrum and its extent were unchanged, but many bands were no longer sharp; and instead broad smears having ultraviolet edges where strong bands had been before appeared in their

[22] M. Kasha, J. Opt. Soc. Am. 38, 929 (1948).

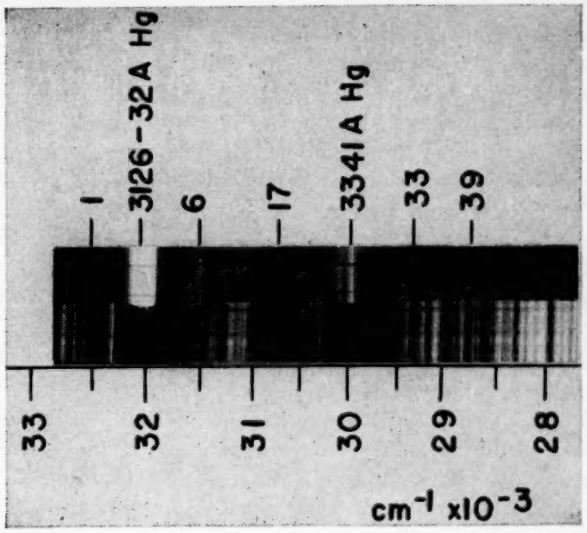

FIG. 1. Fluorescence of naphthalene vapor (upper strip) at 0.07 mm pressure, excited by the 3126–32A mercury line group. Iron arc (lower strip).

place. The intensities of bands also changed markedly and the relative intensities of many neighboring pairs of bands were inverted. Beyond the 3341A mercury line no band structure was to be discerned, and even to the shorter wavelength side of this line only comparatively few bands could be measured. The results of this experiment are significant in as much as they indicate that re-emission by the vapor molecules occurs before thermal equilibrium is established (in the absence of inert gas). This result is reasonable in view of the fact that the time between collisions at the prevailing pressure (0.07 mm) is of the same order of magnitude as the upper limit of the fluorescence lifetime (10^{-6} sec).[10]

For purposes of comparison the emission spectrum of naphthalene in two types of condensed phases was studied. The emission in solid solution at low temperature has been described by Kasha and Nauman[5] and that of the crystal at 20°K by Obreimov and Shabaldas.[11] These spectra were reinvestigated here and found to agree with those reported by the previous authors. The fluorescence of the crystal consists of very narrow lines at low temperatures, but the fluorescence in solid solution consists of broad bands which cannot be measured with the high degree of accuracy possible with the vapor spectrum. It may be said at this point that these spectra give additional information on the origin of bands since they can be taken at temperatures low enough that thermal energies are negligible in comparison with molecular vibrational energies.

IV. ANALYSIS OF THE FLUORESCENCE SPECTRUM OF THE VAPOR

A summary of the analysis of the fluorescence spectrum of naphthalene vapor described here is given in Table I. According to Pringsheim,[9] the fluorescence of naphthalene vapor begins with a weak band at 3082A

(32,446 cm^{-1}), which is followed by two more very weak bands, while the intense part of the spectrum begins with a band to which he ascribes the highest intensity at 3174A (31,506 cm^{-1}). According to Sponer and Nordheim[20] these two bands, whose wavelengths have been mentioned, represent the 0−1 (0 in the ground state and 1 in the excited electronic state) and 1−0 bands of the same vibrational mode, respectively. The argument is based on the intensities of these two bands in the absorption and emission spectra. The band at 32,446 cm^{-1} appears strongly in absorption and weakly in fluorescence, whereas the band at 31,506 cm^{-1} appears weakly in absorption and strongly in fluorescence. The interval between the 0−1 and 1−0 bands thus obtained is 940 cm^{-1}. This interval also agrees well with that obtained from the absorption and fluorescence spectra in rigid glass at low temperature.[5] Neither in absorption nor in emission is a prominent band found, which falls in between the two bands just mentioned and which could, therefore, be designated as the 0−0 band.

In the fluorescence spectrum obtained here these two bands appear with equal intensity, as far as can be judged. This discrepancy between the results obtained here and those of Pringsheim is to be expected, as we have shown that thermal equilibrium is not attained before emission occurs. It seems that the vibrationally excited upper electronic level is preferentially populated by the exciting light and, as a result, the emission from that level may well be more intense than that from the pure electronic upper state. It is indeed found that the intensity of the band at 31,506 cm^{-1} is much greater than that of the band at 32,446 cm^{-1} in the presence of inert gas at one atmosphere. This piece of evidence strongly supports the assignment of the bands as 1−0 and 0−1, respectively.

If we assume for the moment that the band at 32,443 cm^{-1} (according to our measurements) represents a transition from a vibronic upper state to the vibrationless ground state, then we should expect that transitions from this upper state to totally symmetric modes superimposed on the ground state would occur. It would be immaterial whether the transition were symmetry-allowed or symmetry-forbidden, since in either case the matrix element for such transitions would be nonvanishing. The only difference would be in the symmetry of the vibrational mode superimposed on the upper electronic state, and this frequency would not be observed in the differences between bands arising from the same upper state.

Known Raman frequencies of naphthalene, which have been observed to be well polarized and can therefore safely be ascribed to totally symmetric modes (A_g) include 512, 764, 1025, and 1380 cm^{-1} according to the vibrational assignment by Pimentel and McClellan,[23] published in a paper by Barrow and McClellan.[24] Now with these fundamentals and their combinations, taking the band at 32,443 cm^{-1} as origin, 19 out of the 39 bands measured are explained with remarkable accuracy. They can be represented by the formula $32{,}443 - 512p - 764q - 1025r - 1380s$ cm^{-1} and form our system A (see Table I).

In a similar manner it is to be expected that the band at 31,501 cm^{-1} (according to our measurements) will give rise to a similar system, if its assignment as 1−0 band is to hold. It is implied that this band involves the same vibrational mode superimposed on the ground state as the band at 32,443 cm^{-1} involves, superimposed on the excited electronic state. The system which results in this way will be referred to as system B and its bands may be represented by the formula $31{,}501 - 512p - 764q - 1025r - 1380s$ cm^{-1}. This system is weaker throughout than system A, in accordance with the fact that the intensity of the origin is smaller. This scheme accounts for ten more bands, in which the calculated frequencies agree very well with the measured values for the lines (see Table I).

The above statements concerning the agreement between measured and calculated frequencies of the bands in system B must be further qualified. Band No. 5, which forms the origin of this system, was originally found to have a frequency of 31,485 cm^{-1}. The centers of the fluorescence bands were measured, and the reproducibility of the frequency of band No. 5 was ± 5 cm^{-1}. Using this frequency, the agreement of the bands in system B was rather poor, all the deviations being positive and amounting to as much as 24 cm^{-1} in two cases. However, the same band was found to have a frequency of 30,501 cm^{-1} according to measurements of plates taken in the presence of inert gas at one atmosphere. Pringsheim[9] reports the same band at 31,506 cm^{-1}, and his measurements on other bands agree well with the intervals proposed here. An investigation indicated that the error in our measurements was due to the diffuseness of the bands and the presence of a stronger band about 60 cm^{-1} to longer wavelength. This band is much weaker on Pringsheim's plates as well as on plates taken here in the presence of inert gas. The presence of this strong band may well cause an error in judgment as to the position of the center of the weaker band. Measurements carried out subsequently in the course of which the ultraviolet edges of the bands were measured, gave again good agreement for the proposed and measured intervals. For this reason it is felt that the adoption of 31,501 cm^{-1} as the frequency of band No. 5 in the subsequent discussion is justified. It seems indicated at this point to present a comparison between systems A and B.

The comparison of system A with system B, given in Table II, shows that their patterns are practically

[23] George C. Pimentel and A. L. McClellan, J. Chem. Phys. **20**, 270 (1952).

[24] G. Barrow and A. L. McClellan, J. Am. Chem. Soc. **73**, 573 (1951).

TABLE I. The summary of the proposed analysis presented in this table assumes that the transition is forbidden by symmetry but made weakly allowed by vibrational interaction with the 478 cm^{-1} b_{2u} vibration. The 0—0 band therefore lies at a frequency of 31,979 cm^{-1}. The intensities are described as very weak, weak, medium, medium to strong, strong, and very strong. In the assignment column the vibrational interval in the ground state is given first and that in the upper state is given after the comma. The effect on the intensity of introducing inert gas is expressed by the symbols *i*, *d*, or ? as to whether the band's intensity is increased, decreased, or the effect cannot be determined. One assignment is given for most bands. A few bands can be assigned in more than one way. These assignments are:

Band No.	Alternative ass't.	Band No.	Alternative ass't.
12	1380+478,792(*D*)	31	2×764+512+478,0 (*B*) or 3001,478
15	512+747,0 (*C*)		
23	2×1025+478,792(*D*)	32	3058,478
30	2×1380+478,792(*D*)	35	2948,0

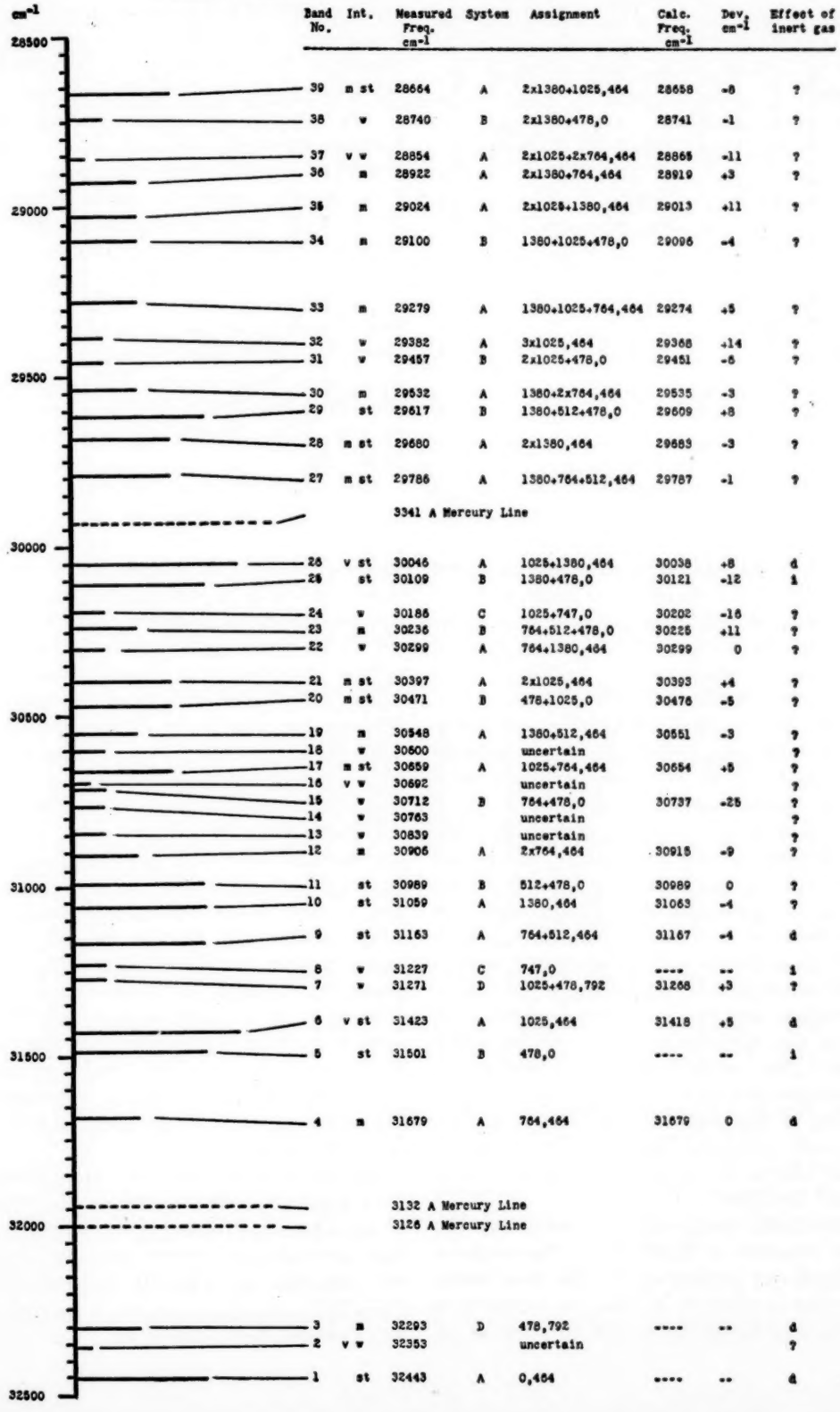

Band No.	Int.	Measured Freq. cm⁻¹	System	Assignment	Calc. Freq. cm⁻¹	Dev. cm⁻¹	Effect of inert gas
39	m st	28664	A	2x1380+1025,464	28658	+6	?
38	w	28740	B	2x1380+478,0	28741	-1	?
37	v w	28854	A	2x1025+2x764,464	28865	-11	?
36	m	28922	A	2x1380+764,464	28919	+3	?
35	m	29024	A	2x1025+1380,464	29013	+11	?
34	m	29100	B	1380+1025+478,0	29096	+4	?
33	m	29279	A	1380+1025+764,464	29274	+5	?
32	w	29382	A	3x1025,464	29368	+14	?
31	w	29457	B	2x1025+478,0	29451	+6	?
30	m	29632	A	1380+2x764,464	29635	-3	?
29	st	29617	B	1380+512+478,0	29609	+8	?
28	m st	29680	A	2x1380,464	29683	-3	?
27	m st	29786	A	1380+764+512,464	29787	-1	?
		3341 A Mercury Line					
26	v st	30046	A	1025+1380,464	30038	+8	*d*
25	st	30109	B	1380+478,0	30121	-12	*i*
24	w	30186	C	1025+747,0	30202	-16	?
23	m	30236	B	764+512+478,0	30225	+11	?
22	w	30299	A	764+1380,464	30299	0	?
21	m st	30397	A	2x1025,464	30393	+4	?
20	m st	30471	B	478+1025,0	30476	-5	?
19	m	30548	A	1380+512,464	30551	-3	?
18	w	30600		uncertain			?
17	m st	30659	A	1025+764,464	30654	+5	?
16	v w	30692		uncertain			?
15	w	30712	B	764+478,0	30737	-25	?
14	w	30763		uncertain			?
13	w	30839		uncertain			?
12	m	30906	A	2x764,464	30915	-9	?
11	st	30989	B	512+478,0	30989	0	?
10	st	31059	A	1380,464	31063	-4	?
9	st	31163	A	764+512,464	31167	-4	*d*
8	w	31227	C	747,0	----	--	*i*
7	w	31271	D	1025+478,792	31266	+3	?
6	v st	31423	A	1025,464	31418	+5	*d*
5	st	31501	B	478,0	----	--	*i*
4	m	31679	A	764,464	31679	0	*d*
		3132 A Mercury Line					
		3126 A Mercury Line					
3	m	32293	D	478,792	----	--	*d*
2	v w	32353		uncertain			?
1	st	32443	A	0,464	----	--	*d*

TABLE II. Vibrational quantum number assignments for band systems *A* and *B*.

System *A* (cm^{-1}) = 32,443 − 512*p* − 764*q* − 1025*r* − 1380*s*						System *B* (cm^{-1}) = 31,501 − 512*p'* − 764*q'* − 1025*r'* − 1380*s'*					
Band No.	Int.	*p*	*q*	*r*	*s*	Band No.	Int.	*p'*	*q'*	*r'*	*s'*
1	*st*	0	0	0	0	5	*st*	0	0	0	0
						11	*st*	1	0	0	0
4	*m*	0	1	0	0	15?	*w*	0	1	0	0
6	*v st*	0	0	1	0	20	*m st*	0	0	1	0
9	*st*	1	1	0	0	23	*m*	1	1	0	0
10	*st*	0	0	0	1	25	*s*	0	0	0	1
12	*m*	0	2	0	0						
17	*m st*	0	1	1	0						
19	*m*	1	0	0	1	29	*st*	1	0	0	1
21	*m st*	0	0	2	0	31	*w*	0	0	2	0
22	*w*	0	1	0	1						
26	*v st*	0	0	1	1	34	*m*	0	0	1	1
						36	*m*	1	0	2	0
27	*m st*	1	1	0	1						
28	*m st*	0	0	0	2	38	*w*	0	0	0	2
30	*m*	0	2	0	1						
32	*w*	0	0	3	0						
33	*m*	0	1	1	1						
35	*m*	0	0	2	1						
36	*m*	0	1	0	2						
37	*w*?	0	2	2	0						
39	*m st*	0	0	1	2						

identical. There are some comparatively weak bands in *A*, which would be expected to be even weaker in *B*, and were therefore not found there. There are also two bands in *B* which do not appear in *A* because they are obscured by scattered exciting light due to the mercury lines at 3341A and the 3126–3132A group. This parallelism again lends support to the assumption that bands Nos. 1 and 5 represent the 0−1 and 1−0 transitions involving the same vibrational mode.

Systems *A* and *B* have given a satisfying and simple interpretation to fully three-fourths of the total number of bands measured. There are, however, two more groups of bands which must be discussed. Band No. 8 is classified as weak from our plates at low pressure, but on the plates taken in the presence of inert gas at one atmosphere, it seems to gain remarkably in intensity. This is in agreement with Pringsheim[9] who ascribes it intensity seven out of a possible ten from his fluorescence experiments with far ultraviolet excitation. The band seems also to appear in the rigid glass at low temperature, and this is further evidence that it originates in the vibrationless state of the upper electronic level. Closer investigation does indeed reveal two possible combination bands superimposed on band 8 with separations of 512 and 1025 cm^{-1} from it. The combination band involving the 1380 cm^{-1} fundamental may be hidden by the mercury line at 3341A. This system will be called *C*.

The other remaining system (*D*) originates from the band, which is observed at 32,293 cm^{-1}. The intensity of the band is classed as medium in this work while Pringsheim marks it intensity 0. Also its intensity is observed to decrease markedly on the introduction of inert gas. It can be safely ascribed to a transition from a vibronic upper state. Two bands (7 and 12) are observed displaced by 1025 and 1380 cm^{-1} from band No. 3 at 32,293 cm^{-1} (see Table I).

It now remains to divide the 1−0 and 0−1 interval and to determine where the 0−0 band ought to be. Let us first examine the situation assuming that the electronic transition is symmetry-allowed but weak, owing to a chance cancellation of the matrix element of the transition. This possibility has been discussed in some detail by Sponer and Nordheim[25] and by Simpson.[17] If this assumption is made, the vibrational interval between the 0−0 band and the 1−0 band (1 in the ground state and 0 in the excited state) must correspond to a totally symmetric mode. Since the interval, (0−1, 1−0) to be divided is 942 cm^{-1} according to our measurements, the most probable vibrational frequency is 512 cm^{-1}. (This is the lowest totally symmetric frequency. The next higher one is 764 cm^{-1}.) This would make the same vibrational mode in the excited electronic state 430 cm^{-1}, a drop of less than 20 percent. This is roughly what would be expected of the vibrational frequency in the less strongly bonding excited state. The 0−0 band would then be at 32,013 cm^{-1}.

Serious difficulties are encountered when the scheme proposed in the preceding paragraph is examined further. For one, it would not be expected that a band, which is not the 0−0 band, would be the obvious origin of several totally symmetric progressions, if the transition were symmetry-allowed. Yet the band at 31,501 cm^{-1} is such an origin, and this band is known to arise from a transition from the vibrationless excited electronic state to some level in the ground state. The evidence for this is its increase in intensity in the fluorescence spectrum with increasing pressure, i.e., with an approach to equilibrium conditions. At the same time, it is also known that this band is not the 0−0 band from its small intensity in the absorption spectrum. It is possible, however, that the existence of system *B* is misleading due to the fact that naphthalene has a great many vibrational fundamentals which might accidentally fit the formula given. For this reason a more detailed investigation is in order. Progressions involving the fundamentals 512 cm^{-1} and 1025 cm^{-1} can of course be found superimposed on the possible 0−0 band at 32,013 cm^{-1} due to the choice of the interval between this band and band No. 5 at 31,501 cm^{-1}. But progressions or combinations involving the fundamentals of frequencies 764 and 1380 cm^{-1} are definitely absent.

Important information can, in addition, be obtained from published investigations of the vapor absorption of naphthalene. Prikhotjko[7] has recently reinvestigated this spectrum and reports that her plates agree well with the data published by de Laszlo.[2] She concludes

[25] H. Sponer and Gertrud Nordheim, ONR Contract N6ori-107, T.O. 1 (Annual Report, June 1948).

that vibrational intervals superimposed on the absorption band at 32,455 cm^{-1} are as follows: 473, 703, 1002, 1181, 1415 (703×2), 1449, and 1603 cm^{-1}. The paper referred to does not, however, give details of progressions and combinations found. Reference to the work of de Laszlo reveals resemblance in pattern to the emission spectrum discussed here. The principal bands may, for purposes of comparison, be represented by the equation $32{,}455+473p+703q+1002r+1181s$. The progression of the frequency 473 cm^{-1} suggests that this is very likely the upper state frequency of the 512 cm^{-1} ground-state vibration. This fact is of interest since the interval between a 0−1 and 1−0 band involving this mode would become $473+512=985$ cm^{-1}. If this interval were found, this would give support to the assumption that the transition is symmetry allowed. The spectrum of naphthalene in the vapor state contains two bands which, it has been shown, are 1−0 and 0−1 bands involving the same vibration. The interval between them is 940 cm^{-1} according to Pringsheim,[9] 949 cm^{-1} according to de Laszlo, 941 cm^{-1} according to Sponer and Nordheim and 942 cm^{-1} according to measurements carried out in the course of this work. It is therefore clear that these two bands do not involve the totally symmetric mode, and this supports the analysis of the lowest transition as symmetry-forbidden.

Further qualitative evidence may be obtained from the absorption and emission spectra of naphthalene in rigid glass solution. These two spectra at 77°K overlap in one weak band, which must be the 0−0 band, since thermal energies are small compared to vibrational energies at that temperature. The pattern of the emission spectrum is the same as in the vapor, if the 0−0 band is overlooked. The 0−0 band lies about 500 cm^{-1} to shorter wavelength from the first strong emission band, but the exact interval cannot be determined due to the breadth of these bands. The error in measurement is 30 cm^{-1} and the average of several measurements, carried out in the course of this work, was 470 cm^{-1} (the intrinsic inaccuracy for the interval is 60 cm^{-1}), whereas Kasha and Nauman[5] put it at 530 cm^{-1}. Support is thus obtained for the assumption that none of the strong bands represent the 0−0 transition. On the other hand, the exact mechanism, which gives rise to the first strong emission band, is not determined due to the inaccuracy of measurement of the interval between the first two bands of the solid solution fluorescence spectrum.

The difficulties encountered in the analysis of the fluorescence spectrum on the basis of an allowed transition are completely removed if we follow the suggestion of Sponer and Nordheim[20] and regard the electronic transition forbidden by symmetry. The totally symmetric progressions of vibrational frequencies are in this case superimposed on the 1−0 and 0−1 bands, which involve fundamentals belonging to the irreducible representations b_{2u} or b_{3u} of the point group V_h of the naphthalene molecule. It must then be determined which vibrational mode is instrumental in making the transition weakly allowed. The available facts, which are useful for this determination, may be summarized as follows. The bands at 32,443 and 31,501 cm^{-1} almost certainly represent the 0−1 and 1−0 bands involving the same vibrational mode. This gives us the sum of the vibrational frequencies of this mode in the upper and lower state as 942 cm^{-1}. Theory allows the prediction that the transition is between the ground state (A_g) and an excited electronic state of symmetry A_g or B_{1g}. In either case only vibrational modes belonging to the representations b_{2u} and b_{3u} need to be considered, as already anticipated above. These modes would be infrared active but would not be observed in the Raman spectrum of naphthalene. It is also known from the spectrum of naphthalene in rigid glass solution that the vibrational frequency in the ground state is within 100 cm^{-1} of 500 cm^{-1}.

According to Pimentel and McClellan[22,23] only a small number of modes need be considered. Sponer and Nordheim[20] consider the frequencies 620, 580, and 478 cm^{-1}. As these authors indicate, the 620 cm^{-1} fundamental is unlikely to be the one involved, since this would require a drop by almost 50 percent (to 322 cm^{-1}) in the excited state. This is not to be expected of a mode of the required symmetry. The 580 cm^{-1} fundamental has been assigned as a_u by Pimentel and McClellan. Their assignment was in this case based on a clear absence of the fundamental in the infrared spectrum of the vapor and its appearance in the spectrum of the crystal. This behavior is predicted only for this symmetry class. In addition, these authors have further evidence for their assignment from a normal coordinate analysis. They also have good evidence for their assignment of the 478 cm^{-1} fundamental as b_{2u}.‡ It seems from this, that the last of the three fundamentals considered is the most likely one to be instrumental in making the greater part of the lowest transition of naphthalene allowed. If we assume further that the excited electronic state is of symmetry A_g, which is indicated by theoretical calculations, rather than B_{1g}, the transition would have to be polarized along the short axis of the molecule.

Let us first assume that the 478 cm^{-1} fundamental makes the transition allowed and discuss the analysis on this basis. In this case the 0−0 band would be at a frequency of 31,979 cm^{-1} and the vibration in the upper electronic state would be about 14 cm^{-1} lower in energy than in the ground state. The position of band No. 8 must be explained in terms of another infrared fundamental. Its separation from the 0−0 band is 752 cm^{-1}. Pimentel and McClellan observed a fundamental at 747 cm^{-1} which they assign as belonging to b_{1u}. This would imply a perturbation by a state antisymmetric toward reflection in the molecular plane. The perturba-

‡ *Note added in proof:* In a recent private communication, G. C. Pimentel indicates that this assignment may change to b_{3u}.

tion should be relatively small, as such states are expected to lie in the far ultraviolet.

If we now examine the possibility of the transition occurring due to the superposition of the infrared-active fundamental of 580 cm^{-1} on the vibrationless electronic states, the 0—0 band must be fixed at 32,081 cm^{-1}. The upper state frequency of the vibration would be 36 cm^{-1}. Again the drop in frequency seems high. Band No. 8 differs from the 0—0 band in this case by 854 cm^{-1}, near which frequency Pimentel and McClellan report an infrared frequency of 841 cm^{-1}, which they assign, however, as a_u.

Finally, the 620 cm^{-1} fundamental needs to be considered more closely, although the resulting large drop in frequency in the upper state and the data from the fluorescence in rigid glass solution show that the presence of this mode is not likely. The upper state frequency, as already mentioned, would drop to 322 cm^{-1} and the 0—0 band would be at 32,121 cm^{-1}. The difference between this and the frequency of band No. 8 is 894 cm^{-1}, which is far from any fundamental, the nearest being at 915 cm^{-1}. This mode has been assigned by Pimentel and McClellan as b_{3u}.

Brief mention must be made of the mechanism of the excitation of the molecule. As has been stressed, the exciting light responsible for the fluorescence spectrum, as obtained here, is the 3126–3132A group of the mercury arc emission. The line at longer wavelength has a frequency of 31,933 cm^{-1}. It may then be assumed that the exciting light causes a transition from the thermally populated vibrational state, 512 cm^{-1} above the vibrationless ground state, to the vibronic level of the upper state, emission from which gives rise to system *A*. This mechanism would apply, whether the transition were allowed or forbidden by symmetry, since the 512 cm^{-1} fundamental represents a totally symmetric mode. The energy required for excitation would then be 512 cm^{-1} less than the 0—1 interval observed at 32,443 cm^{-1}, or 31,931 cm^{-1}. This agrees well with the frequency of one of the mercury lines.

Bands 3, 7, and 12, it has been suggested, belong to a distinct system, referred to as system *D*. It must then be possible to explain the origin of band No. 3 which gives rise to this sequence. This band is classed as of medium intensity but becomes appreciably weaker in the presence of nitrogen gas at one atmosphere. This would indicate that it originates from a vibrationally excited upper state, but it seems difficult to find a simple and satisfying explanation in terms of known intervals. It may arise from a transition from a vibrational level about 800 cm^{-1} above the electronic upper level to 478 cm^{-1} superimposed on the ground level. The totally symmetric mode of frequency 1025 or 940 cm^{-1} may have this energy in the excited electronic state.

As seen in the summary in Table I, an effort has been made to use as few vibrational modes as possible in explaining the main vibrational pattern of the spectrum. It appears, however, that a few bands can be explained in terms of the totally symmetric fundamentals 940 and 1460 cm^{-1}. The use of these modes has no advantage, however, but rather would serve to destroy the simplicity of the pattern. Those bands, which can be interpreted by means of these two fundamentals, are given here for reference:

940 cm^{-1}: bands Nos. 19, 23, 33, 39.
1460 cm^{-1}: bands Nos. 11, 29, 30.

V. SUMMARY AND CONCLUSIONS

We may summarize our position as follows. In the fluorescence spectrum of naphthalene vapor the great majority of the observed bands, including all the more intense ones, form two systems of progressions and combinations of totally symmetric vibrational modes superimposed on two bands. Assuming that there is only one electronic state in this region, neither one of these two bands can be interpreted as the 0—0 band, but the evidence agrees well with their assignment as 1—0 and 0—1 bands involving the same vibrational mode. Also the totally symmetric vibrations 1380 cm^{-1} and 764 cm^{-1} form prominent progressions and combinations in these two systems. However, no fundamental of either frequency is found to combine with the frequency which would have to represent the 0—0 frequency, were the transition allowed by symmetry. Qualitative evidence in support of this is obtained from the fluorescence of naphthalene in rigid glass, although there the bands are too broad to allow accurate measurements of the intervals involved. In this spectrum, however, a weak band appears approximately at the position where the 0—0 band would be expected. This transition can probably occur in this case due to perturbations by the solvent environment. Finally it may be concluded from the vapor absorption that the 1—0, 0—1 interval, in case of a symmetry allowed transition, would have to amount to 985 cm^{-1}, whereas the observed value is in the neighborhood or 940 cm^{-1}. It therefore seems necessary to conclude from the evidence presented here that the lowest electronic transition in naphthalene is forbidden by symmetry and made weakly allowed by the superposition of a nontotally symmetric vibrational mode on the pure electronic transition.

The actual symmetry of the excited electronic state cannot be uniquely determined from the evidence presented here. The state may belong to the representation A_g or B_{1g}, and it would only be possible to distinguish between these two symmetry classes, if the direction of the transition moment were known. If it is assumed that the analysis, presented here, is correct and the vibrational fundamental 478 cm^{-1} makes the transition allowed, and moreover, the assignment of this fundamental as belonging to b_{2u} (due to Pimentel and McClellan) is correct, a transition moment along the short axis would require the excited electronic state to

belong to A_g. A transition moment along the long molecular axis would require the symmetry to be B_{1g}. Work on the crystal is in progress which, it is hoped, will elucidate this point.[26]

Recently Platt[27] has presented arguments favoring an even-odd transition. This is of course directly contradictory to our conclusions. We believe that his general procedure is correct, but there remains the possibility that vibrational perturbations are being underestimated. In the symmetrically disubstituted naphthalenes the enhancement of the transition moment may be due to the greater vibrational-electronic interaction caused by nontotally symmetric vibrations. A decision can only be reached by studying the details of the vibrational pattern of the disubstituted naphthalenes. Sponer[28] has suggested examining the possibility of explaining the 0−1 and 1−0 bands of the naphthalene spectrum as 0−0 bands of two separate allowed electronic transitions. We have not been able to explain the fluorescence spectrum satisfactorily on this basis.

[26] O. Schnepp and D. S. McClure, to be published.
[27] John R. Platt, J. Chem. Phys. **19**, 1418 (1951).
[28] H. Sponer, private communication.

THE JOURNAL OF CHEMICAL PHYSICS VOLUME 20, NUMBER 9 SEPTEMBER, 1952

Kinetics of OH Radicals from Flame Emission Spectra V. A Study of the Acetylene-Oxygen Flame

K. E. SHULER
Applied Physics Laboratory, The Johns Hopkins University, Silver Spring, Maryland*

AND

H. P. BROIDA
National Bureau of Standards,† Washington, D. C.

(Received March 21, 1952)

The inner cone of the acetylene-oxygen flame burning lean (1:5), stoichiometric (2:5), and rich (4:5) at atmospheric pressure has been studied spectroscopically with the object of gaining some information about the elementary processes occurring in this flame. The rotational, vibrational, and electronic distributions of $OH(^2\Sigma^+)$ have been determined for each fuel mixture. The analysis of the data showed a rotational Maxwell-Boltzmann distribution with a rotational "temperature" several hundred degrees higher than the adiabatic flame temperature. The vibrational distribution of $OH(^2\Sigma^+)$ was distinctly nonequilibrium with an excess population in the level $v'=3$ analogous to that observed for the hydrogen-oxygen flame. This is attributed to the interaction of the $^2\Sigma^+$ and $^2\Sigma^-$ states of OH. The analysis of the electronic distribution of OH indicated that $OH(^2\Sigma^+)$ is present in its thermal equilibrium concentration in the flame at atmospheric pressure. The results of this study in conjunction with the work of Gaydon and Wolfhard on the low pressure acetylene-oxygen flame indicate that the radiation of $OH(^2\Sigma^+)$ is to a large extent chemiluminescence so that a considerable fraction of the excited hydroxyl radicals must have been formed in the $^2\Sigma^+$ state by a chemical reaction (or reactions).

1. INTRODUCTION

A SPECTROSCOPIC study of the hydrogen-oxygen flame at atmospheric pressure has shown[1] that the electronically excited $OH(^2\Sigma^+)$ radicals in the hot gases above the reaction zone are essentially in a thermal distribution with a rotational and vibrational temperature in good agreement with the calculated adiabatic flame temperature. The concentration of $OH(^2\Sigma^+)$ as indicated by its relative concentration compared to that of $O_2(^3\Sigma_u^-)$, was in good agreement with that calculated on the basis of complete thermal equilibrium. The observed vibrational nonequilibrium distribution in the inner cone was attributed to a predissociation involving $OH(^2\Sigma^+)$ and $OH(^2\Sigma^-)$.[2] This equilibrium distribution of $OH(^2\Sigma^+)$ in the atmospheric pressure hydrogen-oxygen flame agrees well with the findings of Gaydon[3] on the low pressure H_2-O_2 flame; the increased number of collisions at atmospheric pressure would, of course, tend to enhance the collisional equilibration.

In the acetylene-oxygen flame, however, the investigations of Gaydon and Wolfhard[4] have shown that there is a nonequilibrium distribution of $OH(^2\Sigma^+)$ at low pressure ($\leq$10 mm Hg) manifested both by a rotational "temperature" several thousand degrees higher than the

* Supported by the Bureau of Ordnance, U. S. Navy, under Contract NOrd-7386.
† NBS contribution sponsored by the ONR.
[1] H. P. Broida and K. E. Shuler, J. Chem. Phys. **20**, 168 (1952).
[2] A. G. Gaydon and H. G. Wolfhard, Proc. Roy. Soc. (London) **208A**, 63 (1951).
[3] A. G. Gaydon, *Spectroscopy and Combustion Theory* (Chapman and Hall, Ltd., London, 1948), second edition, Chap. III.
[4] A. G. Gaydon and H. G. Wolfhard, Proc. Roy. Soc. (London) **194A**, 169 (1948).

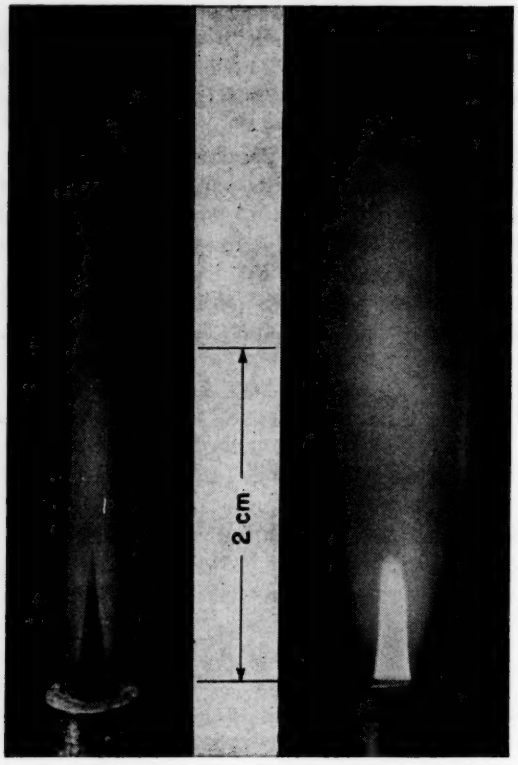

(A) (B)

FIG. 1. (A) Stoichiometric hydrogen-oxygen flame; (B) stoichiometric acetylene-oxygen flame. Both flames are burning above a torch having a 1.5-mm nozzle diameter. Unburned gas is flowing at a volume rate of 200 cm³/sec (NTP).

adiabatic flame temperature and by a large excess of $OH(^2\Sigma^+)$ above its thermal equilibrium value. It was therefore decided to study the acetylene-oxygen flame at atmospheric pressure to ascertain whether this non-equilibrium distribution of $OH(^2\Sigma^+)$ would persist at higher pressure.

2. EXPERIMENTAL

A detailed description of the experimental set-up and of the methods of analysis have been given in a previous paper.[1] An acetylene-oxygen welding torch with 1.5-mm nozzle diameter was used to form the flame and the radiation was focused on a direct-reading monochromator. The resulting spectra of the inner cone of rich ($C_2H_2/O_2=\frac{4}{5}$), stoichiometric ($C_2H_2/O_2=\frac{2}{5}$), and lean ($C_2H_2/O_2=\frac{1}{5}$) fuel mixtures were recorded by a photomultiplier tube connected to a pen recorder by a dc amplifier. These measurements were made in such a manner that the image of the inner cone completely filled the slit of the monochromator; the reported results therefore pertain to a vertical average over the inner cone.

Pictures of the stoichiometric acetylene-oxygen and hydrogen-oxygen flames are shown in Fig. 1. A detailed scanning study[5] on burner flames of this type has shown that any analysis with finite slit height can give only averaged results for "temperatures" and relative concentrations. This has already been emphasized in our previous paper on the hydrogen-oxygen flame,[1] and the terms "inner cone" and "temperature" as they are used below should be understood in that context. Since a flame involves both spatial and chemical rate processes, this problem can never be wholly avoided when the investigation has to be confined to some particular spatial region as is the case in a spectroscopic study.

As may be seen from Fig. 1(B), the outer cone of the acetylene-oxygen flame at about 2-cm distance from the nozzle of the burner is quite thick and the radiation reaching the spectrograph comes from a rather undefined source. This great thickness of the source with its concommitants of high self-absorption and a large temperature gradient gave rise to optical problems which obscured the analyses for the energy distribution and for the concentration of $OH(^2\Sigma^+)$. This problem did not arise in the outer cone of the hydrogen-oxygen flame (Fig. 1(A)) since this flame was a much thinner and a better defined source. It has been possible to overcome these difficulties in the acetylene-oxygen flame, at least for the rotational distribution, by focusing on the very edge of the outer cone where the flame thickness is only a few millimeters. Since such measurements are, however, not representative of the whole outer cone as such, they have not been studied in detail. As nearly as can be judged under these burning conditions, the rotational energy distributions of OH correspond to those expected for thermal equilibrium.

3. RESULTS

The results of this study for the inner cone of the acetylene-oxygen flame burning at atmospheric pressure with various fuel mixtures are presented in Table I. The rotational "temperatures" were determined by the modified iso-intensity method described elsewhere.[6]

TABLE I. "Temperatures" and energy distribution of $OH(^2\Sigma^+)$ in the inner cone of acetylene-oxygen flame.

	C_2H_2/O_2 =1/5 (Lean)	C_2H_2/O_2 =2/5 (Stoichio)	C_2H_2/O_2 =4/5 (Rich)
	[a] T_{adiab} =3080°K	T_{adiab} =3320°K	T_{adiab} =3400°K
T_{rot} (°K)	3500	3500	3500
T_{vibr} (°K)	Non-equilibrium	Non-equilibrium	Non-equilibrium
$V'=0-1$	2500	2500	2500
$V'=1-2$	3000	3000	3150
$V'=2-3$	5200	3650	4000
$I_{OH^*}/I_{O_2^*}$ (calc)	0.2	0.4	
$I_{OH^*}/I_{O_2^*}$ (exp)	0.4	1.3	[b]

[a] The adiabatic flame temperatures were taken from the compilation of Gaydon and Wolfhard, reference 4.

[b] The intensity of the Schumann-Runge bands at 3420A could not be determined under these rich burning conditions since the O_2 bands were badly overlapped in this region by some of the Deslandres-d'Azambuja bands of C_2.

[5] H. P. Broida and G. T. Lalos, J. Chem. Phys. (to be published).

[6] K. E. Shuler, J. Chem. Phys. 18, 1466 (1950).

Figure 2, which can serve as a representative example of the type of relationship obtained for all the fuel mixtures tested, shows the analysis for the inner cone of a lean ($C_2H_2/O_2=\frac{1}{5}$) acetylene-oxygen flame. In all cases, the good straight line relationship between $\log(A_{K'}/A_K)$ and $E_{K'}-E_K$ and the 0,0 intercept show that there is a rotational Maxwell-Boltzmann distribution of OH($^2\Sigma^+$).

The rotational "temperatures" determined from the slopes of these lines are, as shown in Table I, independent of the fuel-oxygen ratio and from 100 to 400°K higher than the corresponding adiabatic flame temperatures. These results are in accord with the vertical scan data on the acetylene-oxygen flame.[5] The rotational "temperatures" found for the inner cone in this study are about the average of the "base of the inner cone" and "tip of the inner cone" figures of the scanning study.

The analysis for the vibrational distribution of OH($^2\Sigma^+$) by the methods outlined in references 1 and 6 showed a distinct nonequilibrium distribution resembling very closely that found for the inner cone of the hydrogen-oxygen flames. Figure 3, which is a plot of E_v *vs* L for the lean ($C_2H_2/O_2=\frac{1}{5}$) acetylene-oxygen flame, is typical of the distribution found for the other fuel mixtures and shows this nonequilibrium distribution. An analysis of these distributions carried out by determining the vibrational "temperatures" from straight line segments drawn between $v'=0$ and 1, $v'=1$ and 2, and $v'=2$ and 3 show that the level $v'=3$ is overpopulated and $v'=1$ appears to be slightly underpopulated as compared to a Maxwell-Boltzmann distribution with $T_{equil}=T_{adiab}$. This is particularly true for the lean (1/5) fuel mixture and a calculation shows that the concentration of OH($^2\Sigma^+$) in $v'=3$ is about 2.5 times its equilibrium ($T_{equil}=T_{adiab}$) value. That this vibrational nonequilibrium distribution found for the inner cone of these flames is not due to incorrect vibrational transition probabilities is borne out by the fact that vibrational distribution studies on the outer cone (hot interconal gases) of the methane-oxygen[6] and hydrogen-oxygen[1] flame showed a vibrational equilibrium with $T_{rot}=T_{vibr}$.

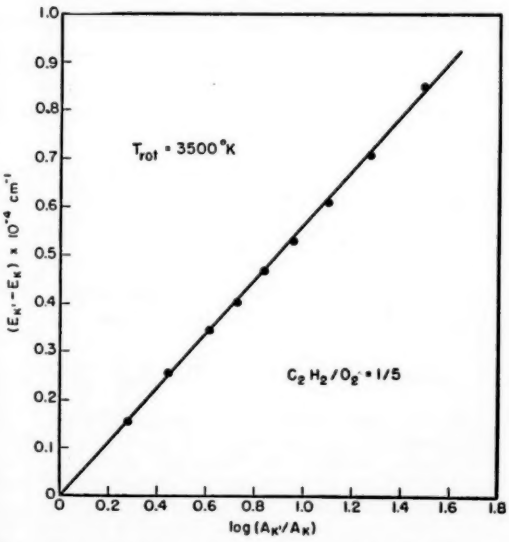

FIG. 2. A modified iso-intensity plot for the R_2 branch of the (0,0) band of OH($^2\Sigma^+\rightarrow{}^2\Pi$) in the inner cone of a lean ($C_2H_2/O_2=\frac{1}{5}$) acetylene-oxygen flame. The rotational "temperature" is obtained from the slope of the graph.

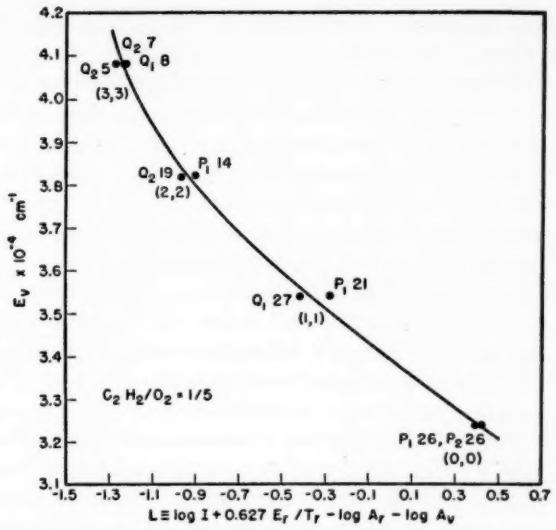

FIG. 3. The vibrational distribution of OH($^2\Sigma^+$) in the inner cone of a lean ($C_2H_2/O_2=\frac{1}{5}$) acetylene-oxygen flame for the levels $v'=0$, 1, 2, and 3. The curvature is indicative of the vibrational nonequilibrium distribution.

The relative concentrations of OH($^2\Sigma^+$) and $O_2(^3\Sigma_u^-)$ were determined by the method described earlier.[7] A comparison of the calculated equilibrium ratio of intensities of OH($^2\Sigma^+$) to $O_2(^3\Sigma_u^-)$ with the experimental intensity ratio showed good agreement (Table I), indicating an equilibrium amount of electronically excited OH in the inner cone of the atmospheric pressure acetylene-oxygen flame.[8]

4. INTERPRETATION OF RESULTS

4.1 Rotational Distribution

It is known from the work of Gaydon and Wolfhard[4] that, except for low K' values, there is a rotational Maxwell-Boltzmann distribution of OH($^2\Sigma^+$) in the low pressure acetylene-oxygen flame. The corresponding rotational "temperatures" are between 5700°K and 8750°K depending upon the pressure and the fuel to oxygen ratio, the temperatures increasing with decreasing pressure and for excess acetylene. These "temperatures" are considerably in excess of the adiabatic equilibrium flame temperatures (by about 3000 to 6000°K), and there is little question that in these low pressure flames there is chemiluminescence.

Similarly at atmospheric pressure the acetylene-

[7] K. E. Shuler, J. Chem. Phys. **19**, 888 (1951).

[8] These values should be compared with those of Table I of reference 1 and Table II of reference 7 for hydrogen-oxygen flames. In all cases, the calculated and experimental ratios differ by a factor of not more than 2 or 3.

oxygen flame gives a rotational Maxwell-Boltzmann distribution of $OH(^2\Sigma^+)$ with a rotational "temperature" in excess of the equilibrium adiabatic flame temperature. A possible reason for the reduction of the discrepancy between the rotational "temperature" and the adiabatic flame temperature from several thousand degrees for the low pressure flame to a few hundred degrees for the atmospheric pressure flame is the larger number of collisions at atmospheric pressure. It is to be noted that these equilibrating collisions help to maintain the rotational Maxwell-Boltzmann distribution at all times, the only quantity changing with collision frequency being the parameter which is identified with the temperature at thermal equilibrium.

The explanation for this persistence of a rotational equilibrium distribution with a nonequilibrium "temperature," i.e., an equilibrium nonequipartition distribution, may possibly be found in a very high efficiency of rotational-rotational energy interchange as compared to the exchange of rotational-vibrational or rotational-translational energy. It has been shown previously[6] that this type of specific energy transfer may lead to a Maxwell-Boltzmann distribution of rotational states with the rotational distribution modulus $\beta=1/RT_r$ independent of the translational, vibrational, and electronic distribution. A much higher efficiency of rotational-rotational energy transfer as compared to the slower energy exchange between *different* degrees of freedom could thus insure that the rotational distribution remains Maxwell-Boltzmann at all times while the distribution modulus (i.e., the "temperature") slowly approaches the equipartition value as the collision frequency increases with increasing pressure.

This hypothesis also has a bearing on the rather curious fact that in flames burning with air there is often a definite non-Maxwellian rotational distribution of $OH(^2\Sigma^+)$, whereas the corresponding flames burning in oxygen show a rotational equilibrium distribution. Some examples of this are the low pressure acetylene-air and acetylene-oxygen flames[4] and the atmospheric pressure methane-air and methane-oxygen flames.[9] This difference in behavior possibly may be explained on the basis that N_2 is much more efficient than O_2 in the transfer of rotational energy into other degrees of freedom so that equilibrating collisions with N_2 would bring about the equipartition of energy at the expense of the rotational Maxwell-Boltzmann distribution. This greater effectiveness of N_2 over O_2 in the interchange of rotational-translational energy has been indicated in some recent investigations.[10]

It may be noted from Table I that the rotational "temperature" of $OH(^2\Sigma^+)$ is independent of the acetylene-oxygen ratio, being about 3500°K for lean, stoichiometric, and rich mixtures. Measurements[5] made at the base of the inner cone where the thickness of the burned gas is comparatively small gave 4200°K for all mixtures. This again demonstrates the chemiluminescence of $OH(^2\Sigma^+)$ in the acetylene-oxygen flame. The data of Gaydon and Wolfhard[4] indicate that $OH(^2\Sigma^+)$ is formed with a rotational temperature of about 9000°K by some chemical reaction (or reactions). The observed rotational nonequipartition "temperature" and distribution in the reaction zone are characteristic of this chemical reaction, except for the modification of equilibrating collisions and the averaging with regions outside the reaction zone, and do not depend upon the equilibrium composition of the flame gases.

It may be of interest to speculate briefly on a possible mechanism by which $OH(^2\Sigma^+)$ may be produced in the acetylene-oxygen flame. It has been pointed out[11] that it is quite difficult in hydrocarbon combustion mechanisms to find elementary reactions which are sufficiently exothermic to produce the spectroscopically observed radicals in their electronically excited states. This difficulty may, however, be overcome by postulating an addition-type mechanism for the oxidation of acetylene.[12] One can then write

$$O_2+C_2H_2\rightarrow H-\underset{\displaystyle O-O}{\underset{|\quad|}{C=C}}-H\rightarrow 2HCO+55\text{ kcal}, \quad (1)$$

$$HCO+O_2\rightarrow HO_2+CO+40\text{ kcal}, \quad (2)$$

$$HCO\rightarrow H+CO-20\text{ kcal}, \quad (3)$$

$$HO_2+CO\rightarrow OH+CO_2+45\text{ kcal}. \quad (4)$$

Reactions (1) to (3) have been suggested by Herman *et al.*[12]; reaction (4) is proposed here as a plausible step for the formation of OH.[13] The above reactions would seem to be sufficiently exothermic for OH to be formed directly in the $^2\Sigma^+$ state during energetically favorable collisions.[14] It is also quite possible that reaction (4) produces $OH(^2\Sigma^+)$ with excess rotational energy since this type of process, i.e., simultaneous dissociation of a polyatomic molecule and electronic excitation of one of the fragments, is believed to lead to an abnormal distribution of rotational energy.[15]

It may be noted that it is not possible to write analogous exothermic reactions for the production of $OH(^2\Sigma^+)$ in the hydrogen-oxygen flame. This is in accord with the predominantly thermal radiation of $OH(^2\Sigma^+)$ observed for both the atmospheric pressure[1] and low pressure[16] hydrogen-oxygen flame.

[9] H. P. Broida, J. Chem. Phys. **19**, 1383 (1951).

[10] A. J. Zmuda, J. Acoust. Soc. Am. **23**, 472 (1951); W. J. Thaler, J. Acoust. Soc. Am. **24**, 15 (1952).

[11] K. J. Laidler and K. E. Shuler, Ind. Eng. Chem. **43**, 2758 (1951).

[12] Herman, Hornbeck, and Laidler, Science **112**, 497 (1950).

[13] This reaction has also been suggested by B. Lewis and G. von Elbe, *Combustion, Flames and Explosions of Gases* (Academic Press, Inc., New York, 1951), p. 85, in connection with the water catalysed reaction between carbon monoxide and oxygen.

[14] The bond dissocation energies for HO_2 used above were taken from A. D. Walsh, J. Chem. Soc., 331 (1948); the value for HCO (reaction 3) from M. Szwarc, Chem. Revs. **47**, 75 (1950).

[15] O. Oldenberg, Phys. Rev. **46**, 210 (1934).

[16] A. G. Gaydon, Rev. Inst. France, Petrole et Ann. Combustibles liquides **IV**, 405 (1949).

4.2 Vibrational Distribution

The results for the vibrational distribution are in agreement with the findings of Gaydon and Wolfhard.[2] The observed vibrational nonequilibrium distribution (see Table I and Fig. 3) of $OH(^2\Sigma^+)$ with the excess population in the $v'=3$ level is quite analogous to that found in the inner cone of the hydrogen-oxygen flame, and it thus seems likely that the same process is responsible for this particular distribution in the two flames. Since two entirely different fuels have been used, it seems evident that this vibrational nonequilibrium distribution cannot be attributed to some specific chemical reaction characteristic of the fuel, but that it is connected with some intrinsic properties of the OH radicals themselves. The suggestion[1,2] that there is a predissociation of $OH(^2\Sigma^+)$ and $OH(^2\Sigma^-)$ at about $v'=2$ or 3 fits the data thus far at hand, and the observed enhancement of the vibrational level $v'=3$ can plausibly be attributed to a preassociation reaction of the type

$$O(^3P)+H(^2S)\rightarrow OH(^2\Sigma^-)\rightarrow OH(^2\Sigma^+) \qquad (5)$$

involving O and/or H atoms in excess of their equilibrium concentration.

The smaller overpopulation of the $v'=3$ level in the acetylene-oxygen flame (2.5 times equilibrium) as compared to the hydrogen-oxygen flame (8.0 times equilibrium) might be caused by the increased collisional equilibration afforded by the presence of CO and CO_2 in the acetylene-oxygen flame. It is regrettable that no quantitative measurements of the vibrational distribution of $OH(^2\Sigma^+)$ are at hand for the low pressure acetylene-oxygen flame which would enable one to study the effect of pressure on the vibrational distribution and to check some of the above conclusions.

4.3 Electronic Distribution

The concentration of electronically excited OH is determined by comparing the calculated equilibrium intensity ratio of $OH(^2\Sigma^+)$ and $O_2(^3\Sigma_u^-)$ with the corresponding experimental intensity ratio.[7] This is a relative method in that an agreement between the equilibrium and the experimental intensity ratio shows only that $OH(^2\Sigma^+)$ is present in a thermal equilibrium concentration with respect to $O_2(^3\Sigma_u^-)$. However, this tends to establish that the concentration of $OH(^2\Sigma^+)$ is in equilibrium with the gas at the measured temperature. Firstly, it is highly improbable that both OH and O_2 are abnormally excited in just such a manner that they remain in an equilibrium distribution with respect to one another. Secondly, the appearance of electronically excited $O_2(^3\Sigma_u^-)$ in flames of such diverse fuels as NH_3,[17] H_2,[18] CO,[19] and C_2H_2 argues against the production of $O_2(^3\Sigma_u^-)$ by some specific chemical reaction characteristic of the fuel and leads to the belief that it is present in its thermal equilibrium concentration.[18,20] The observed equilibrium between $OH(^2\Sigma^+)$ and $O_2(^3\Sigma_u^-)$ (Table I) thus indicates that $OH(^2\Sigma^+)$ is present in a thermal equilibrium concentration (with $T_{\text{electronic}}\cong T_{\text{adiabatic}}$) in the atmospheric pressure acetylene-oxygen flame. This is in accord with the results of the scanning studies[5] which showed that the intensity of $OH(^2\Sigma^+)$ in the hydrogen-oxygen flame as compared to that for the acetylene-oxygen flame agrees with the calculated thermal intensity ratio after account has been taken of the somewhat different compositions and temperatures of the two flames.

These results may be compared with that of Gaydon and Wolfhard who found[16] that in the low pressure acetylene-oxygen flame the concentration of $OH(^2\Sigma^+)$ is about 500 times that of the low pressure hydrogen-oxygen flame. Since all evidence points to a thermal radiation of $OH(^2\Sigma^+)$ in the hydrogen-oxygen flame, their result indicates that the concentration of $OH(^2\Sigma^+)$ in the low pressure acetylene-oxygen flame is about 500 times its thermal equilibrium value. This difference between the low pressure and high pressure results may be attributed to the effect of the increased number of equilibrating collisions at higher pressure which serve to quench the chemiluminescence of $OH(^2\Sigma^+)$ and so tend to reduce the concentration of $OH(^2\Sigma^+)$ to its thermal value at atmospheric pressure. If a quantitative study of the concentration of $OH(^2\Sigma^+)$ were made over a range of pressure it should be possible to calculate the collisional lifetime of $OH(^2\Sigma^+)$ in the flame environment; the specific quenching efficiency of each of the various components of the flame mixture for $OH(^2\Sigma^+)$ could, however, be determined only with great difficulty in this manner.

Two reactions merit a brief mention as possible quenching reactions for $OH(^2\Sigma^+)$. The two components present in the largest concentration in the acetylene-oxygen flame are carbon-monoxide and oxygen, and it is therefore possible that they are important factors in the quenching of $OH(^2\Sigma^+)$. Two possible quenching reactions involving these components are

$$CO(^1\Sigma^+)+OH(^2\Sigma^+)\rightarrow O(^3P)+H(^2S)+CO(^1\Sigma^+) \qquad (6)$$

and

$$O_2(^3\Sigma_g^-)+OH(^2\Sigma^+)\rightarrow O_2(^3\Sigma_u^-)+OH(^2\Pi). \qquad (7)$$

Reaction (6), the dissociative quenching of chemiproduced $OH(^2\Sigma^+)$, could serve to account for the postulated excess of O and H atoms which are believed to be responsible for the vibrational nonequilibrium distribution of $OH(^2\Sigma^+)$ by the preassociation reaction (5). Reaction (6) is endothermic by only 6.8 kcal and could thus readily occur at these high flame temperatures. The energy transfer reaction (7) has been discussed

[17] G. A. Hornbeck (unpublished results).
[18] A. G. Gaydon, Nature **164**, 22 (1949).
[19] G. A. Hornbeck and H. S. Hopfield, J. Chem. Phys. **17**, 982 (1949).
[20] K. J. Laidler and K. E. Shuler, Chem. Revs. **48**, 193 (1951).

previously in connection with the formation of $O_2(^3\Sigma_u^-)$ in the hydrogen-oxygen flame.[7] Reaction (7) besides being a likely quenching process for $OH(^2\Sigma^+)$ would also contribute to the attainment of the observed equilibrium between $OH(^2\Sigma^+)$ and $O_2(^3\Sigma_u^-)$.[21]

5. SUMMARY

The results and conclusions of this study in conjunction with the work of Gaydon and Wolfhard on low pressure acetylene-oxygen flames may be summarized as follows: A large fraction of the electronically excited OH radicals in the reaction zone of the acetylene-oxygen flame are produced directly in the $^2\Sigma^+$ state by a chemical reaction or reactions. This chemiluminescence manifests itself by abnormally high rotational temperatures and by an excess concentration of $OH(^2\Sigma^+)$ in the low pressure flame. The higher collision frequency at higher pressure serves to quench the chemiluminescence so that $OH(^2\Sigma^+)$ is in its thermal equilibrium concentration at atmospheric pressure. The rotational "temperature" approaches the equilibrium adiabatic flame temperature under the influence of an increasing number of collisions in such a manner that the rotational Maxwell-Boltzmann distribution is maintained over the whole pressure range. This indicates that the interchange of rotational energy is much more effective than the exchange of rotational and translational or rotational and vibrational energies. The vibrational nonequilibrium distribution is analogous to that obtained for the hydrogen-oxygen flame and can be attributed to the interaction of the $OH(^2\Sigma^+)$ and $OH(^2\Sigma^-)$ states. The good correlation which it has been possible to establish between atmospheric pressure and the low pressure studies indicates that our knowledge of the physics and chemistry of flames may be greatly enhanced by conducting these flame studies over a wide range of pressures.

6. ACKNOWLEDGMENTS

We are greatly indebted to Miss Joan Beck of the Applied Physics Laboratory, the Johns Hopkins University, for performing many of the analyses and calculations, and to the Research Department of Leeds and Northrup Company who constructed the direct reading monochromator and loaned it to the National Bureau of Standards on a field trial basis.

[21] Reactions (6) and (7) would have to take place via nonlinear intermediate complexes since the electronic states of reactants and products do not correlate linearly. This will be discussed in more detail in a forthcoming paper by one of the authors.

High Frequency Dispersion in *n*-Propanol*

R. H. Cole and D. W. Davidson†
Metcalf Research Laboratory, Brown University, Providence, Rhode Island
(Received April 14, 1952)

Two dispersion regions in the liquid in addition to the primary dispersion have been measured at audio- and radiofrequencies below −120°C, which make small but significant contributions to the dielectric constant. Both move rapidly to lower frequencies with decreasing temperature and the relaxation times of the intermediate dispersion are 200 times smaller than for the primary one. The temperature and frequency dependences are those to be expected for orientation rather than induced polarization.

In a previous paper,[1] measurements of dielectric dispersion and loss in *n*-propanol at temperatures below −90°C were reported which showed, in addition to a Debye-type relaxation, evidence for a further dispersion at much higher frequencies. From the rather limited data then available, it was reasonable to infer that most of the difference between the extrapolated high frequency limit of the first dispersion and the optical refractive index value results from such a second absorption region which shifts rapidly to lower frequencies with decreasing temperature. Evidence for such a situation in this and higher normal alcohols at or near room temperature has been presented by Magat and co-workers[2] largely on the basis of necessarily rather limited ranges of frequencies in the microwave region. We have been able to obtain quite complete measurements of the further dispersion in *n*-propanol by taking advantage of the fact that it occurs at audio- and radiofrequencies for temperatures in the range −120 to −156°C. The results were obtained by the methods previously described.[1]

I. ANALYSIS OF THE DATA

The complex plane locus[3] of the dielectric constant ϵ^* is convenient for representation of the observed data, and to show the means employed to describe the composite dielectric constant in terms of overlapping additive dispersions. The sketch in Fig. 1 of the general form of the loci obtained for *n*-propanol is drawn with the high frequency portion of the curve at the left exaggerated in size for clarity. As discussed in I, the lower frequency data are quantitatively described by a Debye dispersion equation

$$\epsilon_1^*-\epsilon_1=(\epsilon_1'-\epsilon_1)-i\epsilon_1''=(\epsilon_0-\epsilon_1)/(1+if/f_1), \quad (1)$$

the locus of ϵ_1^* being the semicircle indicated in Fig. 1 with intercepts ϵ_0 and ϵ_1 and center frequency f_1.

The course and inflections of the locus at higher frequencies indicate the presence of not one, but two, further overlapping dispersion regions, as shown to scale in Fig. 2 for data at −132° and −151°. In order to separate these from the lower frequency dispersion, we have subtracted from the observed values of ϵ^* the values $\delta\epsilon_1^*=\epsilon_1^*-\epsilon_1$ calculated from Eq. (1) with the values of ϵ_0, ϵ_1, and f_1 fitting the low frequency data. For frequencies $f>10f_1$, the difference which we denote by $\epsilon_{hf}^*=\epsilon_{hf}'-i\epsilon_{hf}''$ is expressed with sufficient accuracy as

$$\epsilon_{hf}'=\epsilon'-(\epsilon_0-\epsilon_1)(f_1/f)^2,$$
$$\epsilon_{hf}''=\epsilon''-(\epsilon_0-\epsilon_1)(f_1/f). \quad (2)$$

This procedure gives the values of ϵ_{hf}^* indicated as crosses in Fig. 2. The values are fitted by a circular arc over a considerable range of frequencies about a central value f_2, as shown in Figs. 1 and 2. This form of dispersion has been found characteristic of a variety of dielectrics, and the analytic expression of the locus has been discussed elsewhere.[3] The departure of the experimental values from the circular arc at still higher frequencies indicates a third dispersion. Rough calculations suggest that a second subtraction of contributions $\delta\epsilon_2^*$ would give a circular arc locus for this also, but the data are sufficiently meager that a detailed analysis seems unjustified. Instead, estimates have been made of a center frequency f_3 of this dispersion for which ϵ' is midway between the intercepts ϵ_2 and ϵ_∞ of Fig. 1.

Values of the various parameters identified in Fig. 1 by which representative observed spectra in the range −120 to −156°C are described are listed in Table I. The depression angles of the circular arc loci, not listed in the table, show no systematic temperature depend-

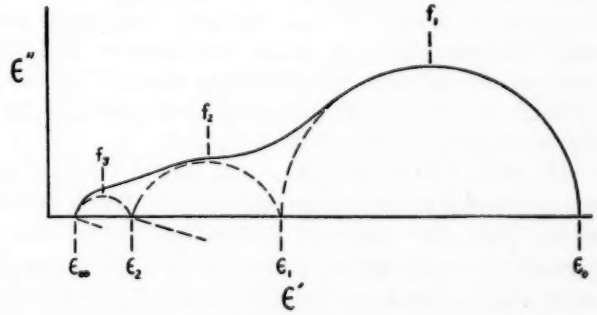

FIG. 1. Schematic dielectric constant locus for overlapping dispersions.

* This work was supported in part by the ONR.
† Now at the National Research Council of Canada, Ottawa.
[1] D. W. Davidson and R. H. Cole, J. Chem. Phys. **19**, 1484 (1951).
[2] Dalbert, Magat, and Surdut, Bull. Soc. Chim., France **16**, D345 (1949).
[3] K. S. and R. H. Cole, J. Chem. Phys. **9**, 341 (1941).

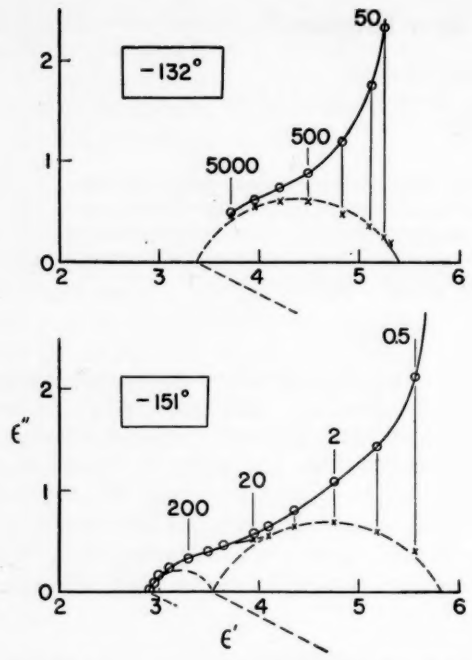

FIG. 2. High frequency portions of complex dielectric constant loci for *n*-propanol at −132° and −151°. Circles are measured values, crosses are values obtained by subtraction of contributions from the low frequency dispersion. Indicated frequencies are in kc/sec.

ence. The average value for the second dispersion is 24°, corresponding to a value $\alpha=0.27$ in the empirical arc dispersion function, and the value for the third is of the same order.

II. DISCUSSION

Because the measurements summarized in Table I give reasonably complete information about the high frequency dispersion only for the supercooled liquid at temperatures below the melting point of −126°C, the reasons for assurance that the observed values are not the result of solid formation or a glass transformation should be mentioned.

In the first place, the low frequency dispersion data are continuous smooth functions of temperature through the melting point, whereas solid formation when known to occur in this and other alcohols causes abrupt and pronounced decreases in dielectric constant. Second, the behavior is similar to that inferred both from less comprehensive data at room temperature and by extrapolation of measurements above the melting point. Finally, the lowest temperature investigated is 20° above the glass transformation region.[4]

The relaxation frequencies f_1 and f_2 have very similar temperature dependence, as illustrated by Fig. 3. In the upper plot, the observed values are plotted on a logarithmic scale against reciprocal absolute temperature, and in the lower against $1/(T-T_\infty)$, where as discussed in *I*, $T_\infty=73.5°$ is the empirical temperature found to give a linear dependence of $\log f_1$ and hence a rate equation of the form

$$f_1=A\exp[-B/(T-T_\infty)], \tag{3}$$

where A and B are constants. The straight line drawn through the points for $\log f_2$ *versus* $1/(T-73.5)$ with slope $-B$ is seen to fit them within their scatter, which is rather larger than for the values of f_1 primarily because of slight uncertainties and drifts in temperature to which the derived values of f_2 are very sensitive. The same Eq. (3), except for the value of the constant A, thus describes the temperature dependence of f_2, although the need for the parameter T_∞ is not as clearly demonstrated as it is for f_1.

Some interesting and suggestive correlations of the dielectric behavior with other properties of liquid alcohols exist. The empirical temperature $T=73.5°$K is the same as the Debye temperature θ calculated from the sound velocity c by the formula $k\theta=hc(3N/4\pi V)^{\frac{1}{3}}$ where V/N is the volume per molecule. Quite close agreement is also found between T_∞ and this Debye θ for propylene glycol and glycerol, but the fact that it is found for the value c computed on the basis of equal longitudinal and transverse sound velocities of the liquid must be noted. It is of interest also that the temperature T_∞ is just below the range in which the large specific heat and volume of the supercooled liquid falls quite abruptly to nearly the same value as for the solid and in which experimental equilibrium is much more slowly realized.[4]

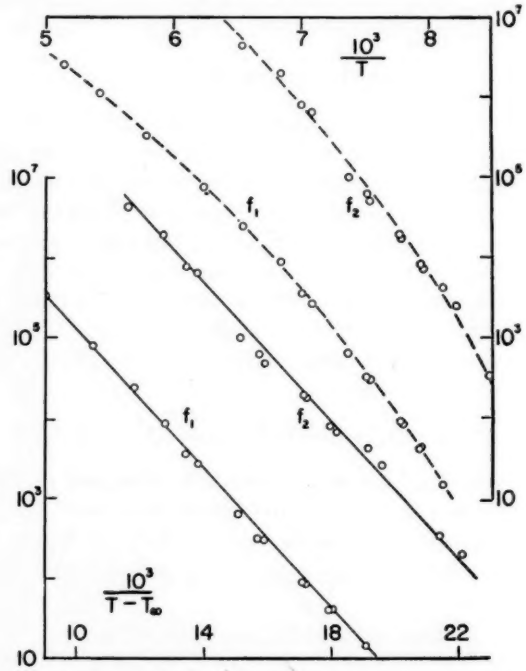

FIG. 3. Logarithmic plots of relaxation frequencies f_1 and f_2 for *n*-propanol. Dashed curves plotted against reciprocal temperature (scales above and to right); solid curves plotted against $10^3/(T-73.5)$ (scales below and to left).

[4] W. Kauzmann, Chem. Revs. 43, 219 (1948).

A literal interpretation of the quantity T_∞ as a temperature below which translational degrees of freedom are frozen in is probably an over-simplification, but a quite drastic change in properties of the supercooled liquid certainly occurs. Further measurements of the dielectric properties in this temperature range would be interesting if not made impractical by a prohibitively long time scale and lack of thermal equilibrium.

The variations with temperature of the dielectric constants ϵ_1, ϵ_2, and ϵ_∞ derived from the dispersion analysis are shown in Fig. 4. The low frequency limit ϵ_1 of the second dispersion is seen to increase appreciably at lower temperatures. Although the temperature coefficient of ϵ_1 is not determined accurately, it appears to be of the order one would expect for a dipole polarization superimposed on an induced polarization. The extrapolated values of the highest frequency intercept ϵ_∞ show no significant temperature dependence. If the value $\epsilon_\infty = 2.9$ is to be ascribed to induced polarization, the indicated slight temperature dependence of ϵ_2 is compatible with a temperature dependent dipole relaxation as the origin of the small difference $\epsilon_2 - \epsilon_\infty$.

The experimental evidence as to the high frequency dispersions evidently points to their explanation in terms of temperature dependent polarizations for which the approach to equilibrium is limited by thermal relaxation, even at frequencies as low as a few hundred cycles in the case of the second dispersion bounded by ϵ_1 and ϵ_2. It is thus quite definite that they must be classed in spectroscopic terminology as absorption regions of essentially zero proper frequency. This being the case, explanation of their origin would appear to involve rearrangements of the molecules in their local environment rather than distortion of their charge distribution by the effective electric field. That there can be more than one distinct "zero frequency" absorption process is reasonable for liquids of the complexity of *n*-propanol, even though the simplified bond moment model of the molecule ascribes its polarity to the C—OH group.

Attempts at a detailed molecular interpretation meet with the difficulty among others of properly accounting for intermolecular interactions, but comparisons with similar results for other alcohols should lead to useful conclusions. It is hoped that work in progress will provide sufficiently comprehensive measurements of this kind.

TABLE I. Parameters of dielectric dispersion in *n*-propanol. Values in parentheses are rough estimates by extrapolation; frequencies f_1, f_2, f_3 are in kilocycles/sec.

t°C	ϵ_0	ϵ_1	ϵ_2	ϵ_∞	f_1	f_2	f_3
−120	55.2	5.20	(3.50)	···	24.5	(4500)	···
−132	60.6	5.30	(3.40)	···	2.57	650	···
−140	64.0	5.58	3.56	···	0.32	63	···
−145	67.4	5.70	3.62	2.94	0.084	18	1000
−150	(71.6)	5.80	3.53	2.86	0.015	4.2	250
−156	···	6.35	3.55	2.80	···	0.20	35

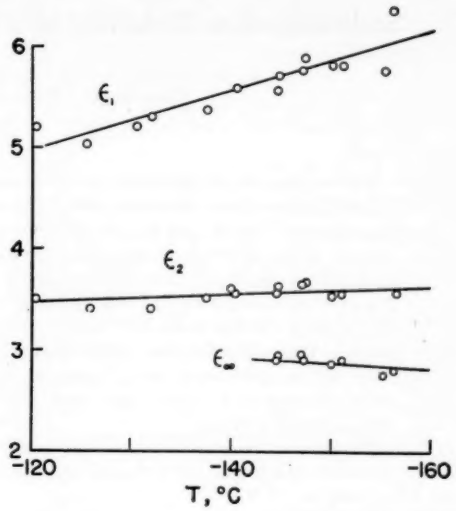

FIG. 4. Limiting dielectric constants of the dispersions as a function of temperature.

THE JOURNAL OF CHEMICAL PHYSICS VOLUME 20, NUMBER 9 SEPTEMBER, 1952

Sedimentation Behavior of Flexible Chain Molecules: Polyisobutylene*

L. MANDELKERN, W. R. KRIGBAUM, H. A. SCHERAGA, AND P. J. FLORY
Department of Chemistry, Cornell University, Ithaca, New York

(Received April 7, 1952)

The sedimentation constants s_0 at infinite dilution and the intrinsic viscosities $[\eta]$ of five fractions of polyisobutylene have been determined in cyclohexane, a good solvent. Their osmotic molecular weights ranged from 3.1×10^4 to 1.4×10^6. Under the assumption that the effective hydrodynamic radii vary as the average linear dimensions of the molecule, $f_0/\eta_0=P\langle r^2\rangle^{\frac{1}{2}}$ and $[\eta]=\Phi\langle r^2\rangle^{\frac{3}{2}}/M$, where f_0 is the frictional coefficient, η_0 is the viscosity of the solvent, $\langle r^2\rangle$ is the mean-square end-to-end distance of the molecule, and P and Φ are constants. In confirmation, $s_0[\eta]^{\frac{1}{3}}/M^{\frac{1}{3}}$ is constant throughout the molecular weight range investigated. Furthermore, $\Phi^{\frac{1}{3}}P^{-1}=2.5\times10^6$. The close agreement of this quantity with values for four other systems reported in the literature indicates that P, like Φ, is a universal constant for flexible chain molecules. It follows also that the observed proportionality of s_0 (or of M/f_0) to $M^{0.42}$ instead of to $M^{\frac{1}{2}}$ occurs because of intramolecular interactions which cause the molecule in solution to be expanded by a factor α which increases with molecular weight.

The above theory accounts for both the sedimentation and intrinsic viscosity behavior of flexible chain molecules in a satisfactory manner. Neither the Kirkwood-Riseman nor the Debye-Bueche theories succeeds in doing so.

INTRODUCTION

THE frictional coefficient f_0 for a flexible long chain molecule at infinite dilution may be expected, in first approximation, to increase as the square-root of the chain length. This follows from two elementary postulates: (1) that the configuration of such a molecule may be treated simply as a "random flight," hence, that an average linear dimension of the molecule, such as either the root-mean-square distance $\langle r^2\rangle^{\frac{1}{2}}$ from beginning to end of the chain, or the root-mean-square distance of the chain elements from the center of gravity (the radius of gyration), must vary as the square-root of the chain length Z, or as the square-root of the molecular weight M; and (2) that the radius of the "effective" hydrodynamic sphere should be approximately proportional to an average linear dimension such as $\langle r^2\rangle^{\frac{1}{2}}$. The notion of an effective hydrodynamic sphere is introduced, of course, in consideration of Stokes' law, although for a randomly coiled chain molecule the size of this sphere is not a clearly defined quantity. According to observation, f_0, as obtained from measurements of the sedimentation constant or of the diffusion constant, increases with a power of M slightly exceeding one-half.

Similarly, the viscosity increment due to a polymer molecule in dilute solution may be considered to be proportional to an effective hydrodynamic volume of the polymer molecule. The intrinsic viscosity $[\eta]$ will then be proportional to the ratio of this effective volume (which may not necessarily be identical with the one introduced above) to the molecular weight. Introducing postulate (1) and the analog of (2) applied to this case, we conclude that the intrinsic viscosity $[\eta]$ should be proportional to $M^{\frac{1}{2}}$. Experiments on linear polymers show that $[\eta]$ increases as a power of M generally exceeding one-half, though less than unity.

The above deviations from the first-order approximations are universally acknowledged to be related, but two different interpretations, each allegedly applicable to both phenomena, have been advanced in explanation. According to one of these,[1,2] postulate (1) is valid and the deviations are attributed to the error in (2); the hydrodynamically effective radius is assumed to increase more rapidly with molecular weight than the mean linear dimensions. According to the other interpretation[3,4] proportionality between the hydrodynamic radius and average linear dimensions (postulate (2)) is assumed to be a valid approximation over the range in molecular weight of interest, but postulate (1) is considered to be in error. Specifically, the osmotic forces of the surrounding solvent on the polymer molecule cause it to expand by a factor α beyond the domain calculated in the "random flight" approximation, and according to the theory of the interaction between the polymer molecule and its environment α should *increase with M* in a "good" solvent.

An abundance of experimental evidence supporting interpretation of intrinsic viscosities according to the latter view has been adduced recently.[5] Analysis of available results on the frictional coefficient as obtained from the velocity of sedimentation favored the second

* A portion of the work reported in this paper was carried out in connection with the Government Research Program on Synthetic Rubber at Cornell University under contract with the Synthetic Rubber Division of the Reconstruction Finance Corporation.

This paper was presented before the Division of Polymer Chemistry at the Meeting of the American Chemical Society, Buffalo, New York, March 25, 1952.

[1] J. G. Kirkwood and J. Riseman, J. Chem. Phys. **16**, 565 (1948).
[2] P. Debye and A. M. Bueche, J. Chem. Phys. **16**, 573 (1948).
[3] P. J. Flory, J. Chem. Phys. **17**, 303 (1949); P. J. Flory and T. G. Fox, Jr., J. Am. Chem. Soc. **73**, 1904 (1951).
[4] L. Mandelkern and P. J. Flory, J. Chem. Phys. **20**, 212 (1952).
[5] [a] T. G. Fox, Jr., and P. J. Flory, J. Phys. Colloid Chem. **53**, 197 (1949); J. Am. Chem. Soc. **73**, 1909, 1915 (1951); [b] H. L. Wagner and P. J. Flory, J. Am. Chem. Soc. **74**, 195 (1952); [c] L. Mandelkern and P. J. Flory, J. Am. Chem. Soc. **74**, 2517 (1952); [d] Flory, Mandelkern, Kinsinger, and Shultz; J. Am. Chem. Soc. (to be published).

interpretation also.[4] It became apparent in the course of this series of investigations that a most severe test of the various theoretical treatments could be realized from sedimentation constants and intrinsic viscosities determined for the same set of fractionated polymers using the same solvent. Such results are reported in this paper.

Polyisobutylene was chosen for the present investigation in view of the comparative abundance of information available concerning its behavior in dilute solutions.[5a,6] Cyclohexane, thermodynamically the best of the solvents which have been investigated for this polymer, was selected in order to accentuate as much as possible the deviations from the "ideal" relationships: $[\eta]\sim M^{\frac{1}{2}}$ and $f_0\sim M^{\frac{1}{2}}$.

EXPERIMENTAL

Five sharp fractions of polyisobutylene ranging in molecular weight from 30,000 to 1,400,000 were selected[7] from those obtained by a large-scale fractionation to be described in detail elsewhere.[6]

Intrinsic viscosities were measured in cyclohexane at 30° and in diisobutylene at 20°C. We have assigned values for the intrinsic viscosities in cyclohexane at 20° identical to those measured at 30°C, since for this solvent the temperature coefficient of the intrinsic viscosity has been shown to be negligible.[5]

Osmotic pressure measurements on some of these fractions in cyclohexane will be found in a paper to appear shortly.[6] The empirical viscosity-molecular weight relation reported therein for polyisobutylene in cyclohexane at 30°C is

$$[\eta]=2.76\times10^{-4}M^{0.69}, \tag{1}$$

and in diisobutylene at 20°C it is

$$[\eta]=3.63\times10^{-4}M^{0.64}. \tag{2}$$

The molecular weights reported here are averages obtained through use of Eqs. (1) and (2), appropriate corrections[8] for rate of shear having been applied where significant. The molecular weights calculated from intrinsic viscosities in the two solvents using Eqs. (1) and (2) agreed to within 2–3 percent in every case.

Sedimentation velocity measurements were carried out on these fractions in cyclohexane with a Spinco model *E* ultracentrifuge at 60,000 rpm, using a Philpot-Swensson optical system.

Heller and Thompson[9] have shown that the partial specific volume of polystyrene in several solvents is the same as the value of the bulk specific volume extrapolated linearly from above the glassy state transition. Accordingly, it was assumed that such an extrapolation would also hold for polyisobutylene in dilute solution, the equation for the specific volume of the bulk polymer being[10]

$$\bar{v}=1.077+6.8\times10^{-4}t+(32/M), \tag{3}$$

where t is the temperature in °C. From a consideration of similar substances, such as butyl rubber,[11] it was assumed that the compressibility of the polymer is negligible at the hydrostatic pressures obtaining in the ultracentrifuge runs.

The effect of pressure and temperature on the density[12] and viscosity[13] of cyclohexane, and the above temperature dependence of $\bar{v}$, were taken into consideration in correcting the observed sedimentation constants to 20°C and 1 atmos pressure. In addition, the polymer concentration was corrected for the dilution effect in the sector-shaped cell.[14]

RESULTS AND DISCUSSION

The sedimentation constant corrected as described above may be related to the frictional coefficient f by means of the Svedberg equation[15]

$$s=(M/N)(1-\bar{v}\rho)/f, \tag{4}$$

where N is Avogadro's number and ρ is the density of the solution. The frictional coefficient may then be expressed as follows:[16]

$$f=f_0(1+kc+k'c^2), \tag{5}$$

where k and k' characterize the concentration dependence of the frictional coefficient. According to Eqs. (4) and (5) the reciprocal of the corrected sedimentation constant is given, therefore, by

$$(1/s)=(1/s_0)(1+kc+k'c^2), \tag{6}$$

where s_0 is given by the analog of Eq. (4) written for infinite dilution. In Figs. 1–3 the reciprocals of the corrected sedimentation constants for all fractions appear plotted against the concentration expressed in g/100 cc. The values of s_0 and k given in Table I were obtained from the intercepts and slopes of the linear portions of these plots. Molecular weights and intrinsic viscosities also are included in Table I.

The results of investigations[5] on the intrinsic viscosities of a variety of linear polymers are in excellent

[6] W. R. Krigbaum and P. J. Flory (to be published).

[7] Each fraction had undergone a minimum of three precipitations. We estimate that the difference between $\bar{M}_w$ and $\bar{M}_n$ for these fractions is at most 10 percent, and probably considerably less for most fractions.

[8] Fox, Fox, and Flory, J. Am. Chem. Soc. **73**, 1901 (1951).

[9] W. Heller and A. C. Thompson, J. Colloid Sci. **6**, 57 (1951).

[10] T. G. Fox, Jr., and P. J. Flory, J. Phys. Colloid Chem. **55**, 221 (1951).

[11] P. W. Bridgman, Proc. Am. Acad. Arts Sci. **76**, 9 (1945).

[12] International Critical Tables **3**, 29, 33, 36.

[13] International Critical Tables **7**, 217, 223; Chavanne and van Resseghen, Bull. Soc. Chim. Belg. **31**, 87 (1922); J. Timmermans and F. Martin, J. Chim. phys. **23**, 747 (1926); J. N. Friend and W. D. Hargreaves, Phil. Mag. **35**, 57 (1944); P. W. Bridgman, Proc. Am. Acad. Arts Sci. **61**, 57 (1926); J. M. Geist and M. R. Cannon, Ind. Eng. Chem. Anal. Ed. **18**, 611 (1946).

[14] T. Svedberg and K. O. Pedersen, *The Ultracentrifuge* (Oxford University Press, London, 1940), p. 18.

[15] See reference 14, p. 10.

[16] See, for example, S. Newman and F. Eirich, J. Colloid Sci. **5**, 541 (1950).

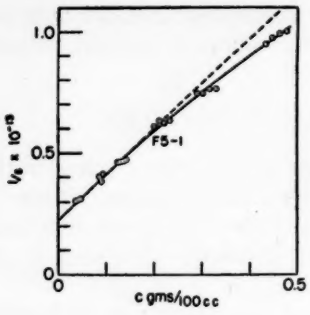

FIG. 1. Concentration dependence of corrected sedimentation constants plotted as $1/s$ *vs* c for fraction *F*5-1.

agreement with the simple relationship[3]

$$[\eta]=\Phi(\langle r^2\rangle)^{\frac{3}{2}}/M, \tag{7}$$

where $\langle r^2\rangle$ is the mean-square distance between the ends of the chain[17] and Φ is a constant which appears to be the same irrespective of the polymer or the solvent. Substituting $\langle r^2\rangle=\alpha^2\langle r_0^2\rangle$, where $\langle r_0^2\rangle$ represents the unperturbed mean-square end-to-end distance which is realized in an "ideal" solvent in which the osmotic forces acting on the molecule are zero and α, as mentioned earlier, is the linear distortion factor for the molecule in the nonideal solvent, we have alternatively

$$[\eta]=KM^{\frac{1}{2}}\alpha^3, \tag{8}$$

where $K=\Phi(\langle r_0^2\rangle/M)^{\frac{3}{2}}$ is a constant for a given polymer irrespective of the molecular weight and solvent. The factor α depends, as described elsewhere,[3] on the thermodynamic parameters which characterize the solvent-polymer interaction, and on the temperature and molecular weight.

By analogy we may write[4]

$$f_0/\eta_0=P(\langle r^2\rangle)^{\frac{1}{2}} \tag{9}$$

$$=P(\langle r_0^2\rangle/M)^{\frac{1}{2}}M^{\frac{1}{2}}\alpha, \tag{9'}$$

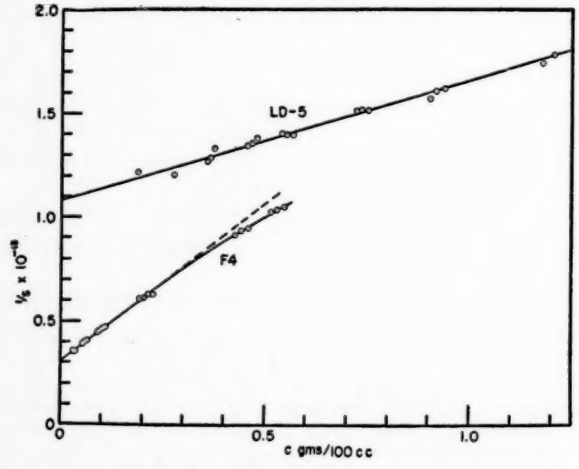

FIG. 2. Concentration dependence of corrected sedimentation constants plotted as $1/s$ *vs* c for fractions *F*4 and *LD*-5.

[17] For nonlinear polymers $\langle r^2\rangle$ should be replaced with $6\langle R^2\rangle$ where $\langle R^2\rangle$ represents the average of the square of the distances of the chain elements from the center of gravity of the molecule.

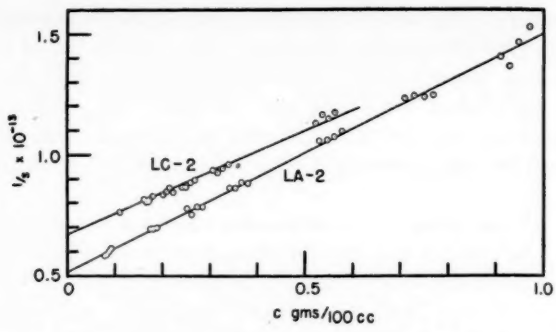

FIG. 3. Concentration dependence of corrected sedimentation constants plotted as $1/s$ *vs* c for fractions *LA*-2 and *LC*-2.

where η_0 is the viscosity of the medium and P is a universal constant analogous to Φ. Combining Eqs. (7) and (9), the frictional coefficient may be related to the molecular weight and intrinsic viscosity as follows:

$$f_0/\eta_0=P\Phi^{-\frac{1}{3}}(M[\eta])^{\frac{1}{3}}. \tag{10}$$

Substituting this expression in Eq. (4), written for infinite dilution,

$$s_0[\eta]^{\frac{1}{2}}/M^{\frac{1}{2}}=\Phi^{\frac{1}{3}}P^{-1}(1-\bar{v}\rho)/\eta_0 N. \tag{11}$$

Inasmuch as $\bar{v}\rho$ will be very nearly constant for a series of homologous polymer fractions in a given solvent, the left-hand member of Eq. (11) should be independent of M for a given solvent-polymer pair. The values of this quantity given in the last column of Table I are approximately constant; deviations from constancy for the two fractions of highest molecular weight probably are not significant. Similar constancy of $s_0[\eta]^{\frac{1}{2}}/M^{\frac{1}{2}}$ has been observed[4] for fractions of polystyrene in methyl ethyl ketone and in toluene,[18] and for cellulose acetate in acetone.[19] In the case of polyisobutylene this constancy is maintained even down to the comparatively low molecular weight of 30,000, indicating that proportionality between the effective hydrodynamic radius and the average chain-dimension persists at least to this range.

For polyisobutylene in cyclohexane the intrinsic viscosity may be taken to be proportional to $M^{0.69}$ as an empirical approximation [see Eq. (1)]. According to

TABLE I. Molecular weight, intrinsic viscosity and sedimentation data for polyisobutylene fractions.

Fraction[a]	M	$[\eta]_{20°}$	$(s_0\times10^{13})_{20°}$ sec.	k_{20}	$s_0[\eta]^{\frac{1}{2}}/M^{\frac{1}{2}}\times10^{17}$ [b]
*F*5-1	1,420,000±70,000	4.89	4.45 ±0.20	8.36	6.0±0.3
F-4	672,000±20,000	2.87	3.33 ±0.11	5.10	6.2±0.2
LA-2	172,000± 3500	1.12	1.94 ±0.04	1.91	6.5±0.2
LC-2	86,700± 1700	0.706	1.49 ±0.02	1.28	6.8±0.1
LD-5	30,900± 1500	0.342	0.925±0.013	0.54	6.6±0.2
					Av 6.4±0.3

[a] See reference 6.
[b] $[\eta]$ expressed in (g/100 cc)$^{-1}$ and M in molecular weight units.

[18] S. Newman and F. Eirich, J. Colloid Sci. **5**, 541 (1950).
[19] S. Singer, J. Chem. Phys. **15**, 341 (1947).

Eq. (11), therefore, s_0 should be proportional to $M^{0.44}$. When the logarithms of the s_0 values from Table I are plotted against $\log M$, as in Fig. 4, s_0 is found to be represented most satisfactorily by proportionality to the 0.42 power of M, in excellent agreement with the prediction based on the dependence of the intrinsic viscosity on M.

Perhaps the most far-reaching consequence of the interpretation of the frictional coefficient and related phenomena as set forth here and in an earlier paper[4] is the predicted universal constancy of the quantity $(s_0[\eta]^{\frac{1}{3}}/M^{\frac{2}{3}})/([1-\bar{v}\rho]/\eta_0 N)$, which according to Eq. (11) should have the same value, $\Phi^{\frac{1}{3}}P^{-1}$, for all flexible chain polymers irrespective of molecular weight, temperature, and solvent. Taking the average for $s_0[\eta]^{\frac{1}{3}}/M^{\frac{2}{3}}$ given in Table I and with $\bar{v}_{20}=1.091$ ml/g, $(\eta_0)_{20}=9.7\times10^{-3}$ poise, $\rho_{20}=0.779$ g/ml, $\Phi^{\frac{1}{3}}P^{-1}$ calculated from the sedimentation velocities for the polyisobutylene fractions in cyclohexane is 2.5×10^{6} employing the units indicated heretofore. This result is compared in Table II with values for $\Phi^{\frac{1}{3}}P^{-1}$ reported previously[4] based on sedimentation and viscosity data for polystyrene and

TABLE II. Values of $\Phi^{\frac{1}{3}}P^{-1}$ for several polymers.

Polymer	Solvent	$\Phi^{\frac{1}{3}}P^{-1}\times10^{-6}$
Polystyrene[a]	methyl ethyl ketone	2.6
Polystyrene[a]	toluene	2.3
Cellulose acetate[b]	acetone	2.7
Polysarcosine[c]	water	2.3
Polyisobutylene	cyclohexane	2.5
		Av 2.5±0.1

[a] See reference 18.
[b] See reference 19.
[c] See reference 20.

for cellulose acetate, and with that calculated from the recently published work of Fessler and Ogston[20] on the sedimentation of synthetic polysarcosine (sample VIII-75 with $M=16{,}100$) in water. Thus, the prediction that $\Phi^{\frac{1}{3}}P^{-1}$ should be a constant independent of the nature of the polymer or solvent appears to be well substantiated experimentally. We conclude, therefore, that the interpretation which assumes postulate (2) to be substantially correct and (1) to be in error, thereby yielding Eqs. (8) and (9′), allows an explanation of both the dependence of intrinsic viscosity on molecular weight and on temperature, and of the sedimentation constant on molecular weight in a consistent manner.

We now consider the alternative interpretation based on the assumption that postulate (1) is valid but that (2) is in error. The expression derived for the sedimentation constant by Kirkwood and Riseman[1] may be

[20] J. H. Fessler and A. G. Ogston, Trans. Faraday Soc. **47**, 667 (1951).

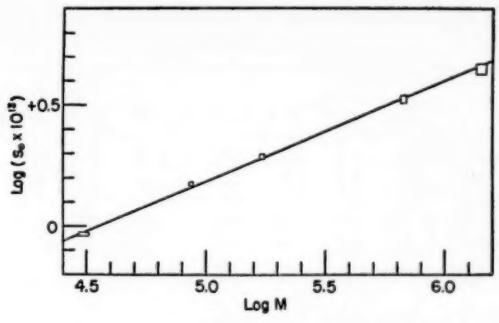

FIG. 4. Log-log plot of s_0 against M.

written

$$s_0=\left(\frac{1-\bar{v}\rho}{N}\right)\left[\frac{M_0}{\zeta}+\left(\frac{8}{3}\right)\left(\frac{1}{6\pi^3}\right)^{\frac{1}{3}}\times\left(\frac{1}{\eta_0}\right)\left(\frac{M}{\langle r^2\rangle}\right)^{\frac{1}{3}}M^{\frac{1}{3}}\right], \quad (12)$$

where N is Avogadro's number and ζ is a frictional constant for a chain unit, of molecular weight M_0, in the fluid medium. Postulate (1) having been accepted, $\langle r^2\rangle/M$ is considered constant, hence s_0 should increase linearly with the square-root of the molecular weight. The corrected sedimentation constants for polyisobutylene are plotted in this manner in Fig. 5, the experimental errors being indicated by the dimensions of each rectangle. Although the points suggest negative curvature, as should be expected if $\langle r^2\rangle/M$ actually increases with M, its reality should not be considered definitely established on the basis of this observation alone inasmuch as individual deviations from the straight line shown barely exceed the experimental errors. If, in conformity with the Kirkwood and Riseman treatment, $\langle r^2\rangle/M$ is assumed tentatively to remain constant with molecular weight, the value of this parameter and of the frictional coefficient ζ of a chain unit may be evaluated from the slope and intercept of this line. The values obtained are $\langle r^2\rangle/M=1.85\times10^{-16}$ in units of cm^2/M, and $\zeta=3.96\times10^{-10}$ (with $M_0=56$) in units of g/sec.

The Kirkwood and Riseman[1] expression for the in-

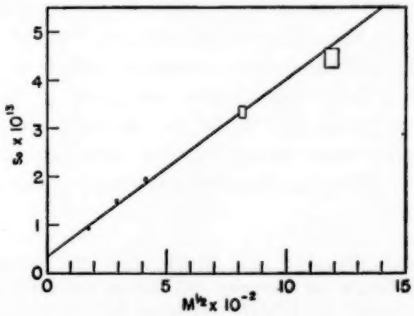

FIG. 5. Plot of s_0 against $M^{\frac{1}{3}}$.

TABLE III. Comparison of the calculated and observed values of $[\eta]$ and s_0.

M	$[\eta]$ Obs.	K-R	D-B	Eq. (11)	$s_0\times10^{13}$ Obs.	K-R	D-B	Eq. (11)
1,420,000	4.89	7.4	3.5	5.9	4.45	5.6	3.9	4.7
672,000	2.87	4.5	1.9	3.2	3.33	3.9	2.8	3.5
172,000	1.12	1.7	0.61	1.1	1.94	2.1	1.6	1.9
86,700	0.706	1.0	0.35	0.60	1.49	1.6	1.2	1.4
30,900	0.342	0.45	0.18	0.31	0.925	1.1	0.74	0.90

trinsic viscosity may be written

$$[\eta]=\frac{(6\pi^3)^{\frac{1}{2}}}{3600}N\left(\frac{\langle r^2\rangle}{M}\right)^{\frac{3}{2}}M^{\frac{1}{2}}xF(x), \tag{13}$$

where

$$x=\frac{\zeta}{(6\pi^3)^{\frac{1}{2}}\eta_0}\left(\frac{M}{\langle r^2\rangle}\right)^{\frac{1}{2}}\frac{M^{\frac{1}{2}}}{M_0}, \tag{14}$$

and $xF(x)$ is a function tabulated by Kirkwood and Riseman. Using the values of ζ and $\langle r^2\rangle/M$ determined from the sedimentation data, intrinsic viscosities have been calculated from Eq. (13) for the various polymer fractions. These values, appearing in Table III under the column heading "K-R," are seen to be consistently larger than the observed values. A corresponding discrepancy has been reported previously for polystyrene in toluene.[21]

The interpretation of the sedimentation and viscosity behavior given by Kirkwood and Riseman may be tested alternatively by comparing observed sedimentation constants with those calculated using parameters evaluated from the observed dependence of intrinsic viscosity on molecular weight. Intrinsic viscosities measured in good solvents, in general, and those for polyisobutylene in cyclohexane in particular, cannot be fitted accurately over wide ranges in molecular weight using Eqs. (13) and (14) with $\langle r^2\rangle/M$ constant. Disregarding the deviations which occur, one obtains $x=2.5$ from the exponent 0.69 of the intrinsic viscosity-molecular weight relation as given by Eq. (1). Choosing a molecular weight of 200,000 as the geometric mean of the range covered here, the value of the product $(\langle r^2\rangle/M)^{-\frac{1}{2}}\zeta$ of Eq. (14) is found to be 4.14×10^{-2}. According to Eq. (1), $[\eta]=1.26$ for a molecular weight of 200,000, which yields from Eq. (13) the values $(\langle r^2\rangle/M)=1.25\times10^{-16}$ and $\zeta=4.64\times10^{-10}$. These differ significantly from the values obtained from the sedimentation data. The sedimentation constants calculated from Eq. (12) using these parameters are given in the seventh column of Table III. While the agreement is somewhat better than that found for the intrinsic viscosity, a consistent deviation from the observed values is equally apparent.

[21] Newman, Riseman, and Eirich, Rec. Trav. chim. **68**, 921 (1949). Although the viscosity calculation was reported for only one fraction, $M=8\times10^6$, Dr. Newman has informed us that the calculated intrinsic viscosities were larger than those observed for all fractions studied.

Thus, although either the sedimentation or the intrinsic viscosity data may be fitted approximately (although not accurately) by the Kirkwood-Riseman theory, it is impossible to account for both using the same set of parameters.

Debye and Bueche take as their model of the flexible chain molecule a permeable sphere of radius R_s within which the density of segments is assumed to be uniform. A fundamental quantity in this analysis is the "shielding ratio," $\sigma=R_s/L$, where the "shielding length" L is the distance into the sphere at which the undisturbed velocity of the fluid has been decreased by a factor $1/e$. The intrinsic viscosity and sedimentation constant at infinite dilution may then be expressed as[2]

$$[\eta]=(4\pi R_s^3/3M)\varphi(\sigma), \tag{15}$$

$$s_0=\frac{(1-\bar{v}\rho)}{N}\left[\left(\frac{1}{6\pi\eta_0}\right)\left(\frac{M}{R_s}\right)\frac{1}{\psi(\sigma)}\right], \tag{16}$$

where R_s is assumed to be proportional to $M^{\frac{1}{2}}$, and the functions $\varphi(\sigma)$ and $\psi(\sigma)$ can be calculated from σ. Hence, according to the Debye-Bueche interpretation, the departure of the intrinsic viscosity from proportionality to $M^{\frac{1}{2}}$ is to be accounted for by $\varphi(\sigma)$, and the similar departure of s_0 from proportionality to $M^{\frac{1}{2}}$ by $1/\psi(\sigma)$. Conversely, σ may be evaluated from the dependence of either $[\eta]$ or s_0 on M; that is, from the deviation of these dependences from proportionality to $M^{\frac{1}{2}}$. The shielding ratio σ obtained from the former is 6.0 ± 0.6; that from the latter is 4.6 ± 0.2. The difference is greater than can be attributed to experimental uncertainties.

Intrinsic viscosities calculated according to the Debye-Bueche theory from the shielding ratio obtained from the sedimentation data are given in the fourth column of Table III. They are consistently lower than those observed, the disparity increasing with decrease in molecular weight. The sedimentation constants calculated from the σ-value obtained from the viscosity data, shown in the eighth column of the table, are likewise consistently low. Thus, as with the Kirkwood-Riseman treatment, agreement with both sets of data is unattainable from a single set of parameters.

For comparison, intrinsic viscosities and sedimentation constants are calculated from Eq. (11) using the average value $\Phi^{\frac{1}{2}}P^{-1}=2.5\times10^6$ taken from Table II, and s_0 or $[\eta]$ values, respectively, from Table I. From an inspection of these values appearing in Table III it is seen that the agreement between the calculated and observed sedimentation constants is very good. That obtained for the intrinsic viscosities, though less precise, is nonetheless satisfactory considering the fact that $[\eta]^{\frac{1}{2}}$ is the quantity calculated directly. Somewhat better agreement is obtained for the $[\eta]$ values calculated for the high molecular weight fractions if smoothed s_0 values from Fig. 4 are used instead of the observed values.

CONCLUSIONS

According to the above analysis of experimental data, including those for systems other than the one investigated here, a consistent account of the dependences of both the sedimentation constant and of the intrinsic viscosity for flexible chain molecules on molecular weight may be achieved on the basis of postulate (2) given at the beginning of the paper. Neither the equations derived by Kirkwood and Riseman nor those of Debye and Bueche provide a satisfactory account of experimental data when used in conjunction with postulate (1). If this postulate is rejected, however, their equations are not incompatible with the interpretation we have given. The Kirkwood-Riseman expression for the sedimentation constant, Eq. (12), may then be re-written

$$s_0=\left(\frac{1-\bar{v}\rho}{N}\right)\left[\frac{M_0}{\zeta}+\frac{8}{3}\left(\frac{1}{6\pi^3}\right)^{\frac{1}{2}}\times\left(\frac{1}{\eta_0}\right)\left(\frac{M}{\langle r_0^2\rangle}\right)^{\frac{1}{2}}M^{\frac{1}{2}}/\alpha\right], \quad (12')$$

where $\langle r_0^2\rangle/M$ is constant but α increases with M. Accordingly, s_0 should be plotted against $M^{\frac{1}{2}}/\alpha$ instead of $M^{\frac{1}{2}}$. The treatment we have set forth [i.e., that based on postulate (2)] is equivalent to the assertion that M_0/ζ is negligible in comparison with the second term in brackets, hence that s_0 is effectively *proportional* to $M^{\frac{1}{2}}/\alpha$. (Compare Eq. (9′) for the frictional coefficient.)

On the other hand, the first term in Eq. (12′) must assume dominance at sufficiently low molecular weights, for it is readily apparent that in the limit of very short chains s_0 should become independent of M. Thus, with the introduction of the molecular weight dependent expansion factor α, the Kirkwood-Riseman expression for the sedimentation constant offers satisfactory limiting forms for both long and short chains. It remains to establish the correct value of ζ. To this end we have plotted s_0 for the polyisobutylene fractions against $M^{\frac{1}{2}}/\alpha$, using values of α computed from the intrinsic viscosities.[5a] Although the data are not sufficiently accurate to allow the required extrapolation to $M^{\frac{1}{2}}/\alpha=0$ to be carried out with precision, a considerably smaller intercept (corresponding to a larger ζ) than that obtained from the s_0 *vs* $M^{\frac{1}{2}}$ plot is indicated. Measurements of the frictional coefficient at lower molecular weight appear to be required for a precise evaluation of ζ, and these probably may be obtained more readily from the diffusion constant.

Substituting Eq. (9′) for the frictional coefficient in Eq. (4) for the sedimentation constant and comparing the result with the rectified Kirkwood-Riseman equation (12′), with M_0/ζ set equal to zero, there is obtained[22]

$$P=3(6\pi^3)^{\frac{1}{2}}/8=5.13.$$

The experimental value for P, obtained by taking $\Phi^{\frac{1}{2}}P^{-1}=2.5\times10^6$ (Table II) and $\Phi=2.1\times10^{21}$ as established by intrinsic viscosity and light scattering dissymmetry measurements, is 5.1, in remarkable agreement with the above value deduced from the theory of Kirkwood and Riseman.

Finally attention should be directed to the possibilities afforded by Eq. (11) for determining molecular weights of flexible chain polymers from their sedimentation constants supplemented with intrinsic viscosities, but without the aid of diffusion measurements as in the classical method. The absolute accuracy of this procedure depends, of course, on the reliability with which the universal constant $\Phi^{\frac{1}{2}}P^{-1}$ is established. As is readily apparent, molecular weights could be deduced in an analogous way from the diffusion constant at infinite dilution and the intrinsic viscosity, without resort to sedimentation.

ACKNOWLEDGMENT

We are indebted to Dr. L. F. Nims of Brookhaven National Laboratory for making the ultracentrifuge available to us and for aid in the ultracentrifuge runs.

[22] The theoretical value of Φ deduced similarly (see reference 5a) from the correspondingly modified Kirkwood and Riseman expression for the intrinsic viscosity differs appreciably from the observed value.

An Electron Diffraction Study of Some Glasses

G. O. McCLURG
Physics Department, Illinois Institute of Technology, Chicago, Illinois
(Received February 7, 1952)

The interatomic spacings as obtained from the radial distribution method of analysis of electron diffraction patterns are given for vitreous silica, Vycor, and Pyrex glasses. The results are in general agreement with the x-ray diffraction results published by others.

INTRODUCTION

GLASS is pictured by Zachariasen[1] as an undercooled liquid in which the constituent atoms form an irregular network of oxygen polyhedra centered about the glass-forming cations. He also showed that for the vitreous oxides, the only possible polyhedra are tetrahedra. The network is not periodic and symmetrical as in crystals, yet is not entirely random since the internuclear distances do not sink below given minimum values.

Warren[2–9] and co-workers have presented evidence for this picture based on the analysis of x-ray diffraction patterns of glasses. Recently Milligan, Levy, and Peterson[10] have analyzed neutron diffraction patterns and have confirmed the spacings obtained by Warren. The diffraction pattern obtained from a glass sample consists of broad halos, such as are obtained from liquids or gases, rather than of sharp lines as are obtained from crystals.

RADIAL DISTRIBUTION FUNCTION

Pauling and Brockway[11] have computed a radial distribution function for the scattering of electrons by a sample. This distribution function when multiplied by r^2, represents the product of scattering powers in volume elements a distance r apart as a function of r. Since the electrons are scattered mainly by the atomic nuclei, a maximum in this function represents an internuclear distance in the sample. A similar distribution function was used by Warren in his analysis of the x-ray data. The function given by Pauling and Brockway is

$$D(r)=K\int_0^\infty s^6 I(s)[\sin sr/sr]ds.$$

In this equation, s is $4\pi\lambda^{-1}\sin(\theta/2)$, K is a constant, $I(s)$ is the experimental intensity distribution obtained from the diffraction pattern, θ is the angle between the direction of the incident beam and the direction of the diffracted beam, and $D(r)$ is the radial distribution function. For a given value of r, the integral can be evaluated graphically, and a curve giving $r^2D(r)$ as a function of r can be obtained. The maxima on this curve will then represent internuclear distances in the sample.

EXPERIMENTAL PROCEDURE

The major instrument used in this investigation was an RCA type B electron microscope with an electron diffraction unit. The instrument provides an electron gun complete with a regulated accelerating-voltage supply, magnetic lenses for collimating the beam, facilities for placing the specimen in the beam, and a photographic chamber for recording the diffraction pattern. The microphotometer tracings from which the intensity curves were obtained were made on a Leeds and Northrup Recording Microphotometer. Eastman Kodak lantern slide contrast plates were used to record the diffraction patterns.

Three different glasses were used in this investigation. One was vitreous silica, which is pure silicon dioxide. One was Vycor, a low expansion hard glass consisting of about ninety-six percent silicon dioxide. The third glass was Pyrex obtained from standard glass tubing. The average composition of Pyrex glass is 80.5 percent SiO_2, 12.9 percent B_2O_3, 3.8 percent Na_2O, 0.4 percent K_2O, and 2.2 percent Al_2O_3. Vycor and Pyrex are trade names belonging to the Corning Glass Works, Corning, New York.

Each glass was first washed in a saturated solution of sodium dichromate in concentrated sulfuric acid. Next it was pulverized by percussion using an agate mortar and pestle. Finally it was dusted dry on a $\frac{1}{8}$-inch diameter, 400-mesh, monel metal wire screen. The dusting was accomplished by dipping the wire disk into the powdered glass and tapping it gently to remove the surplus. Finally, the screen was mounted in a standard specimen holder and placed in the diffraction chamber in the microscope.

This method of sample preparation has several advantages. First, being a powder method, it yields a circular diffraction pattern with the attending convenience of circular symmetry. Second, it assures that the diffraction occurs at clean glass surfaces since the

[1] W. Zachariasen, J. Am. Chem. Soc. **54**, 3841 (1932).
[2] B. Warren, J. Appl. Phys. **13**, 602 (1942).
[3] B. Warren and J. Biscoe, J. Am. Ceram. Soc. **21**, 259 (1938).
[4] B. Warren, J. Appl. Phys. **8**, 645 (1937).
[5] Warren, Krutter, and Morningstar, J. Am. Ceram. Soc. **19**, 202 (1936).
[6] B. Warren and J. Biscoe, J. Am. Ceram. Soc. **21**, 49 (1938).
[7] B. Warren and J. Biscoe, J. Am. Ceram. Soc. **21**, 287 (1938).
[8] Biscoe, Pincus, Smith, and Warren, J. Am. Ceram. Soc. **24**, 116 (1941).
[9] B. Warren and A. Pincus, J. Am. Ceram. Soc. **23**, 301 (1940).
[10] Milligan, Levy, and Peterson, Phys. Rev. **83**, 226 (1951).
[11] L. Pauling and L. Brockway, J. Am. Chem. Soc. **57**, 2684 (1935).

powder particles having none of the original outside surfaces vastly outnumber those which do. Last, since this method does not use an amorphous supporting film, the scattering is all due to glass. This fact simplifies the interpretation of the diffraction pattern.

CALIBRATION

In order to interpret the diffraction pattern, it is necessary to make a geometry and wavelength calibration and an intensity calibration. These two calibrations were placed on the photographic plate with the diffraction pattern.

The geometry and wavelength calibration was obtained by utilizing the diffraction pattern of a thin gold foil. By means of Bragg's law and the known gold crystal spacings, the ratio of $\sin(\theta/2)$ to λ can be obtained as a function of the distance on the photographic plate measured radially from the center of the diffraction pattern. For a particular point on the plate, the value of the ratio multiplied by 4π gives the value of s corresponding to that point.

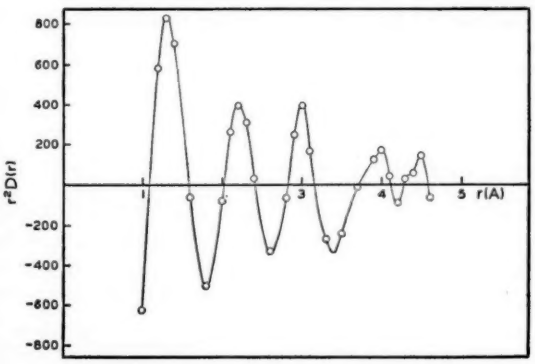

FIG. 1. Radial distribution curve for vitreous silica.

The intensity calibration was made using a constant beam-current and exposing successive strips of the photographic plate for one, two, three, etc. seconds, resulting in a series of strips having relative intensities of one, two, three, etc. The fact that the intensity calibration was on the same plate as the glass diffraction pattern insured equal development conditions and so insured the validity of the calibration.

A microphotometer trace of the diffraction pattern was made for each sample. Calibration curves were prepared giving the relative intensity in terms of the scale readings on the microphotometer trace and giving the ratio of $\sin(\theta/2)$ to λ in terms of the linear distance along the trace. Thus the relative intensity as a function of s can be taken directly from the microphotometer trace.

Hence, with $I(s)$ determined, the value of the radial distribution function $D(r)$ can be calculated by numerical integration for various values of r. The resulting curves are given in Figs. 1 and 2. The curve for Vycor differs so little from that of vitrous silica that it is not shown.

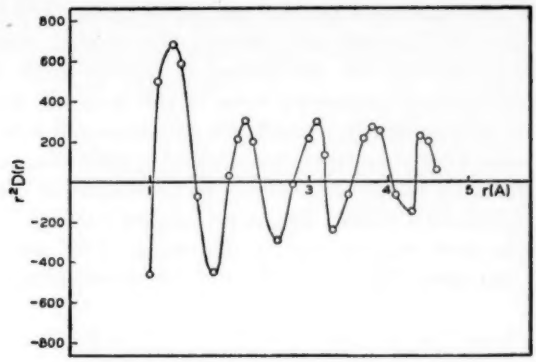

FIG. 2. Radial distribution curve for Pyrex.

RESULTS

The radial distribution function for vitreous silica shows five well-defined peaks. These peaks indicate interatomic distances of 1.3, 2.2, 3.0, 4.0, and 4.5 angstroms. Warren[5] has computed a radial distribution function for vitreous silica based on x-ray diffraction data. His curve has four distinct peaks and an inflection point which suggests a fifth. The four peaks indicate distances of 1.6, 3.2, 4.3, and 5.2 angstroms. The inflection point indicates a distance of 2.6 angstroms. In his analysis Warren concludes that the peak at 4.3 angstroms represents two interatomic distances that were unresolved by his method. These distances he chooses to be 4.0 and 4.5 angstroms. Thus, following Warren, the results of this investigation of vitreous silica give the distances to be silicon-oxygen, 1.3A; oxygen-oxygen, 2.2A; silicon-silicon, 3.0A; silicon-second oxygen, 4.0A; and oxygen-second oxygen, 4.5A. It will be noted that the last two distances confirm Warren's choice of 4.0A and 4.5A for the unresolved peaks. The three shorter distances, however, are consistently shorter than his. Since an electron diffraction pattern results from scattering centers located within a few atomic layers of the surface, whereas an x-ray pattern is a body effect, it is proposed that these differences are real differences arising out of the different structure of the surface layer.

The radial distribution function for Vycor shows five peaks in exactly the same positions as those for vitreous silica. Since Vycor is so nearly pure silicon dioxide, this result is to be expected. The internuclear spacings for Vycor then are identical with those of vitreous silica.

The distribution function for Pyrex has peaks at 1.3, 2.2, 3.1, 3.8, and 4.4 angstroms. According to Stevels,[12] both B_2O_3 and Al_2O_3 form oxygen tetrahedra in the presence of SiO_2. Thus, 95.6 percent of the composition of Pyrex is of the oxygen tetrahedron forming

[12] J. Stevels, *Progress in the Theory of the Physical Properties of Glass* (Elsevier Publishing Company, Inc., New York, 1948).

type. The other 4.4 percent are alkali oxides and impurities. In Zachariasen's theory, this means that a random network of tetrahedra is formed with the metallic cations occupying holes in the network. Since the oxygen tetrahedron bonds are very strong, it is to be expected that these distances should remain the same regardless of the presence of the metallic cations. Thus, the peaks at 1.3A and 2.2A can be assigned to the silicon-oxygen and oxygen-oxygen distances. The metallic ions can affect the orientations of the tetrahedra near them and, consequently, can cause changes in the distances from an atom in one tetrahedron to the atoms in the neighboring tetrahedra. Consequently, the silicon-silicon, silicon-second oxygen, and oxygen-second oxygen distances can be assigned at 3.1, 3.8, and 4.4 angstroms.

The author would like to take this opportunity to express his gratitude to Dr. P. L. Copeland for proposing the investigation and for many helpful discussions during its progress.

THE JOURNAL OF CHEMICAL PHYSICS VOLUME 20, NUMBER 9 SEPTEMBER, 1952

Equilibrium in the Exchange of Hydrogen between Phosphine and Water*

RALPH E. WESTON, JR., AND JACOB BIGELEISEN
Chemistry Department, Brookhaven National Laboratory, Upton, Long Island, New York

(Received April 14, 1952)

The exchange equilibrium $PH_2D(g)+H_2O(l)=PH_3(g)+HDO(l)$ has been measured at 25°C by the use of dilute sulfuric acid and buffer solutions as a catalyst. From this measurement and the ratio of the vapor pressures of H_2O and HDO the equilibrium constant for the exchange $PH_2D(g)+H_2O(g)=PH_3(g)+HDO(g)$ is calculated to be 1.52 at 25°C. The latter experimental value is combined with a theoretical computation of the temperature independent factor of the equilibrium constant to evaluate the difference in the zero point energies of PH_3 and PH_2D. This leads to the equation, which is valid up to about 500°K, $K_g=0.781e^{198/T}$. This equation is in good agreement with calculations based on the spectra of PH_3 and PD_3 and the rule of the geometric mean.

As part of a general program of studies on isotope exchange equilibria and isotope effects on reaction rates, the equilibrium in the exchange of hydrogen between phosphine and water has been investigated. The only previous work on hydrogen exchange involving phosphine was that by Melville and Bolland[1] on the exchange with hydrogen catalyzed by hydrogen atoms. Equilibrium was not attained, but they give an equilibrium constant for the reaction

$$PH_3+HD\rightleftharpoons PH_2D+H_2$$

calculated from theoretical considerations. However, the assignment of the doubly degenerate vibrational frequencies 992 and 730 cm^{-1} to phosphine and phosphine $-d_3$ instead of the correct values 2323 and 1630 cm^{-1} (see below) makes their value for the equilibrium constant too small by a factor of 2.2. We shall show that a value for the equilibrium constant for the exchange between phosphine and water, which is in good agreement with the experimental value, may be obtained from theoretical calculations.

EXPERIMENTAL

Phosphine was prepared by the alkaline decomposition of phosphonium iodide. The latter was prepared by the hydrolysis of a mixture of white phosphorus and diphosphorus tetraiodide,[2] and was sublimed in a stream of nitrogen. The crystals were then placed in a small bulb equipped with a dropping funnel and the bulb was then attached to a vacuum line for further manipulations. An excess of 40 percent sodium hydroxide solution was added dropwise, and the evolved phosphine allowed to pass through a trap at −78°, to remove water and hydrogen iodide. The phosphine was condensed in a trap at −196°, and the temperature of this trap was later raised to −78°, whereupon the gas distilled into storage bulbs held at −196°. Small amounts of noncondensable gas were then removed by pumping.

Isotopically enriched water was made up gravimetrically from 99.8 percent deuterium oxide and distilled water. In order for equilibrium between phosphine and water to be attained in a reasonable time, it was found necessary to acidify the solution slightly. Both dilute sulfuric acid and potassium sodium phthalate—potassium acid phthalate buffer solutions were used, and the atom-fraction of deuterium in the water was corrected for the protium added in acidifying the solution. A 10-ml portion of solution was pipetted into a 100-ml conical reaction vessel attached to the vacuum line through a stopcock and ground joint. The water was degassed by repeated cycles of freezing at −196°, pumping to high vacuum, and thawing. With the water frozen at −78°, phosphine was added at the desired

* Research carried out under the auspices of the U. S. AEC.

[1] H. W. Melville and J. L. Bolland, Proc. Roy. Soc. (London) **A160**, 384 (1937).

[2] *Inorganic Syntheses*, W. C. Fernelius, editor (McGraw-Hill Book Company, Inc., New York, 1946), Vol. 2, p. 141.

pressure and the reaction vessel removed to the thermostat, where it was placed in a shaking device. Samples were taken from the gas phase by removing the reaction vessel to the vacuum line, isolating 2–3 cc of gas in an evacuated bulb, and allowing this gas to pass through a trap at −78° to remove the small amount of water in the gas phase. The attainment of equilibrium was verified by taking gas samples at intervals until successive samples gave the same deuterium analyses. The kinetics of the exchange are currently under investigation and will be reported shortly.

These samples were quantitatively converted to hydrogen and uranium phosphide by passage over uranium turnings at 500–600°,[3] and the hydrogen was isotopically analyzed by mass spectrometric comparison with standards. The latter were prepared by decomposition over hot zinc of mixtures of deuterium oxide and distilled water which were made up gravimetrically. Samples were analyzed on a General Electric recording mass spectrometer and a Consolidated Nier isotope ratio mass spectrometer. The precision of the mass spectrometric analyses was about 1 percent, as shown by a typical calibration curve (Fig. 1).

EXPERIMENTAL RESULTS

Some preliminary experiments showed that aqueous solutions of phosphine are relatively stable, despite a previous statement[4] that such solutions decompose to form phosphorus, hydrogen, and lower phosphorus hydrides. We found no measurable amount of noncondensable gas produced by shaking solutions for 8 hours at 50°, and in equilibrium experiments, solutions were kept at room temperature for periods of days with no measurable formation of hydrogen.

TABLE I. Equilibrium constant for the exchange of hydrogen between phosphine and water.

Phosphine press., mm	pH[a]	t, °C	D_w	D_g	K_1
591	0.15[b]	27.0	0.0297	0.0120 0.0122	1.67
555	2.08[b]	27.0	0.0302	0.0121 0.0121 0.0133	1.64
554	1.13[b]	23	0.0302	0.0126 0.0123	1.65
520	2.08[b]	27.0	0.0301	0.0128 0.0126	1.61
507	4.03[c]	23	0.0289	0.0122 0.0122	1.61

Mean $K_1 = 1.63 \pm 0.02$

[a] Measured with glass electrode.
[b] Dilute sulfuric acid.
[c] Potassium sodium phthalate—potassium acid phthalate buffer.

[3] Bigeleisen, Perlman, and Prosser, *Analytical Chemistry* (to be published).
[4] D. M. Yost and H. R. Russell, Jr., *Systematic Inorganic Chemistry* (Prentice-Hall, Inc., New York, 1946), p. 245.

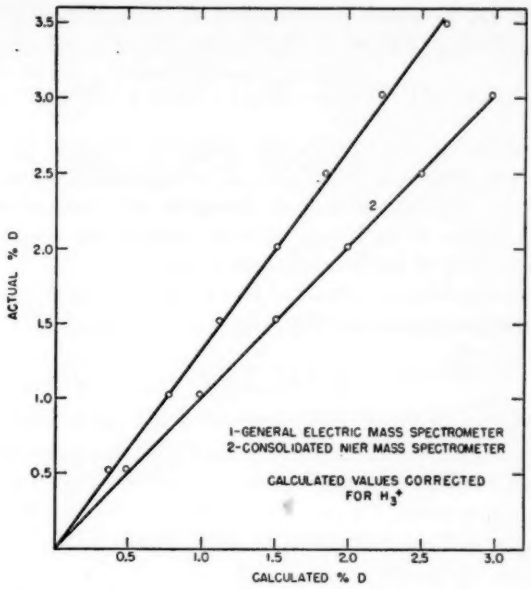

FIG. 1. Typical mass spectrometer calibration curves.

The equilibrium constant for the reaction

$$PH_2D(g)+H_2O(l)\rightleftharpoons PH_3(g)+HDO(l) \qquad (1)$$

is given by

$$K_1=(PH_3)(HDO)/(PH_2D)(H_2O)$$
$$=[(HDO)/(H_2O)]/[(PH_2D)/(PH_3)].$$

We shall express the ratios of concentrations in terms of atom-fractions of deuterium in the two components, since the latter were measured experimentally. If D_w is the atom-fraction of deuterium in water, then

$$D_w=[(HDO)+2(D_2O)]/2[(H_2O)+(D_2O)].$$

We can assume approximately statistical distribution for the equilibrium

$$2HDO\rightleftharpoons H_2O+D_2O;$$

hence

$$(HDO)^2/(H_2O)(D_2O)=4.$$

This leads to

$$(HDO)/(H_2O)=2D_w/(1-D_w).$$

Calculations show that the isotopic dilution of the water by equilibration with the amount of phosphine present is within the limits of experimental error, hence no correction has been made.

In the phosphine phase, the atom-fraction of deuterium is given by

$$D_g=[(PH_2D)+2(PHD_2)+3(PD_3)]/$$
$$3[(PH_3)+(PH_2D)+(PHD_2)+(PD_3)].$$

From statistical considerations, assuming random distribution of deuterium between the species PH_2D, PHD_2, and PD_3:

$$(PH_2D):(PHD_2):(PD_3)$$
$$=3(1-D_g)^2D_g:3(1-D_g)D_g^2:D_g^3.$$

Since D_g is small, the amount of PD_3 is negligible. Substituting $(PHD_2)/(PH_2D)=D_g/(1-D_g)$, we obtain

$$(PH_2D)/(PH_3)=3D_g(1-D_g)/(1-2D_g).$$

Values for the equilibrium constant obtained in this way are presented in Table I. The experimental error is greater than the effect of changing the temperature from 22° to 27°C, hence we shall assume the weighted mean value of the temperature to be 25°C.

The equilibrium constant K_1 can be converted to that for the gas phase reaction

$$PH_2D(g)+H_2O(g)\rightleftharpoons PH_3(g)+HDO(g), \qquad (2)$$

since $K_2=K_1P_{HDO}/P_{H_2O}$ where P is the vapor pressure. This ratio can be calculated by the use of the equation of Miles and Menzies[5] and the assumption of the rule of the geometric mean, $P^2_{HDO}=P_{H_2O}P_{D_2O}$. The value obtained for P_{HDO}/P_{H_2O} is 1/1.074 at 25°C, hence K_2 is 1.52 at 25°C. Interpolation in Table 1.14 of the book by Kirschenbaum[6] gives $P_{HDO}/P_{H_2O}=1/1.069$ at 25°C, which is apparently in error.

CALCULATION OF THE TEMPERATURE COEFFICIENT

From the paper of Bigeleisen and Mayer,[7] we have

$$\frac{s}{s'}f=\prod_i \frac{u_i}{u_i+\Delta u_i}e^{\Delta u_i/2}\frac{[1-e^{-(u_i+\Delta u_i)}]}{1-e^{-u_i}}$$

where f is the ratio of the partition functions for the isotopic molecules, s and s' are symmetry numbers, $u_i=hc\omega_i/kT$ where ω_i is the ith vibrational frequency, and $\Delta u_i=u_i'-u_i$. The prime refers to the lighter species. Then $K_2=f_{H_2O}/f_{PH_3}$. Using the vibrational assignments and anharmonic coefficients for the isotopic water molecules tabulated by Libby,[8] and the conversion factor $hc/k=1.43847$, we obtain $f_{H_2O}=1.2752\exp(886/T)$ in the vicinity of 25°C.

The term for the excitation of vibrations, $\Pi_i(1-e^{-u_i'})/(1-e^{-u_i})$, cannot be exactly evaluated because vibrational frequencies are not known for phosphine-d. In the case of phosphine-d_3, the calculated ratio is 1.054, hence we expect the correction for phosphine-d to be the same magnitude as the experimental error. Neglecting this term, we have

$$f_{PH_3}=s'/s\frac{\Pi_i\omega_i(PH_2D)}{\Pi_i\omega_i(PH_3)}\exp(\Delta u_i/2)=A\exp(B_{PH_3}/T).$$

From the Teller-Redlich[9] product rule, the product of the ratios of vibrational frequencies for the two isotopic species can be obtained in terms of atomic masses and molecular structure parameters. Using the method of Hirschfelder[10] to calculate products of moments of inertia from the molecular parameters of Loomis and Strandberg[11] and accepted values for the atomic masses, we obtain $A=3(0.544)$.

Using the experimental value of K_2 at 298°K, $K_2=1.52=f_{H_2O}/f_{PH_3}=(1.2752/1.632)\exp(886-B_{PH_3})/298$, from which $B_{PH_3}=688$, and $K_2=0.781\exp(198/T)$.

CALCULATION OF THE EQUILIBRIUM CONSTANT FROM SPECTROSCOPIC DATA

From the vibrational frequencies of phosphine and phosphine-d_3, an approximate calculation can be made for B_{PH_3} by assuming the law of the geometric mean. For phosphine, the vibrational frequencies and degeneracies used are 2328 (1), 2322.9 (2), 1121 (2), and 989.9–992.5 (1) cm^{-1}.[12] The corresponding frequencies for phosphine-d_3 are 1694 (1), 1630 (2), 806 (2), and 730 (1) cm^{-1}.[13] The necessary anharmonicity terms are not known for these molecules, but the neglect of this factor is estimated to introduce an error of only about 10 percent in the value of K_2. Assuming that the difference in zero-point energies between phosphine and phosphine-d is $\frac{1}{3}$ of that between phosphine and phosphine-d_3, we obtain $B_{PH_3}=699$, which leads to K_2 (theoretical) $=0.781\exp(187/T)$. At 298°K, K_2 (theoretical) $=1.46$, compared with the experimental value of 1.52. Hence the value obtained only from statistical thermodynamics and the appropriate spectroscopic data is an excellent approximation to the actual value.

ACKNOWLEDGMENT

We wish to thank Mr. H. C. Prosser for his diligent efforts in the preparation of the $HD-H_2$ standards from water, and Mr. A. P. Irsa for carrying out the mass spectrometric analyses.

[5] F. T. Miles and A. W. C. Menzies, J. Am. Chem. Soc. **58**, 1068 (1936).
[6] I. Kirschenbaum, *Physical Properties and Analysis of Heavy Water* (McGraw-Hill Book Company, Inc., New York, 1951), p. 25.
[7] J. Bigeleisen and M. G. Mayer, J. Chem. Phys. **15**, 261 (1947).
[8] W. F. Libby, J. Chem. Phys. **11**, 101 (1943).
[9] Cf., for example, G. Herzberg, *Molecular Spectra* (D. Van Nostrand and Company, New York, 1945), Vol. II, p. 231.
[10] J. Hirschfelder, J. Chem. Phys. **8**, 431 (1940).
[11] C. C. Loomis and M. W. P. Strandberg, Phys. Rev. **81**, 798 (1951), give $<HPH=93.5°$, and $P-H=1.419A$.
[12] V. M. McConaghie and H. H. Nielsen, Proc. Natl. Acad. Sci. **34**, 455 (1948).
[13] E. Lee and C. K. Wu, Trans. Faraday Soc. **35**, 1366 (1939), except 1630 cm^{-1} which is calculated from phosphine frequencies and the product rule.

Theoretical View on "Hot Atom Chemistry"

P. C. CAPRON AND Y. OSHIMA
Institut Interuniversitaire de Physique Nucléaire, University of Louvain, Louvain, Belgium
(Received March 10, 1952)

Considering only collisions of the "billiard ball" type the total retention is obtained as a sum of partial retentions for an infinite number of collisions. Expressions are derived which give the retention as a function of the initial energy of the recoil atom. The calculation shows that it is not possible to determine the initial recoil energy by the retention.

INTRODUCTION

EXPERIMENTS[1] performed on the formation of bromine isomers by thermal as well as resonance neutrons lead to the assumption of the existence of more than one capture level in the formation of the bromine isomers. Therefrom, it must be expected to find a difference in the recoil energy of the Br^{80} isomers following neutron capture.

This difference was made clear:

1. By experiments with electric fields.[2] The results show clearly that the isomers are not collected on the electrodes in the ratio of their formation.

2. By experiments on retention, which is defined as the fraction of the radioactivity resisting aqueous extraction. For C_6H_5Br irradiated in paraffin at a distance of two centimeters from the source with unfiltered neutrons, the retention was found:[3]

$$R_{Br^{80}(18\ min)}=0.50\pm0.06$$
$$R_{Br^{80}(4.4\ hr)}=0.65\pm0.03.$$

For $CHBr_3$ in the same condition, we find (unpublished results):

$$R_{Br^{80}(18\ min)}=0.53\pm0.024$$
$$R_{Br^{80}(4.4\ hr)}=0.69\pm0.036.$$

Originally, and according to the basic theory of Libby,[4] it was hoped to determine by the dilution effect the difference in the energy of the two isomeric atoms. In the meantime, Miller, Gryder, and Dodson[5] have considered the theory of the dilution effect in considerable detail and obtained results differing in some cases from those of Libby.

To explain our experimental results, we considered the theory again. Assuming a partial retention for every collision, the total retention is obtained by addition of all the partial retentions for infinite number of collisions.

The other assumptions are those of the "billiard ball" type of Libby[4] and Miller:[5]

E_0 is the initial kinetic energy of the recoil atoms.

ν is the minimum energy which the recoil atoms must have before the impact to break the bond by collision.

ϵ is the maximum energy which the recoil atoms must have after the impact to be trapped in a liquid cage and react with a radical trapped with it.

As Miller and others do, we neglect the fact that some collisions can occur which bring the recoil energy below ϵ but in which insufficient energy is transferred to cause bond rupture.

The recoil atom is incorporated into a stable compound whenever it falls to an energy below ϵ from an energy above ν in a collision. $r=[(M-m)/(M+m)]^2$ is the minimum fraction of the energy which can be retained after impact. M and m are the masses of the impact particles.

After an impact the recoil atoms are distributed between E and rE, if E is the energy before impact and rE the minimum energy after the impact. The probability to find the atoms between E_1 and E_1+dE_1 is given by $dE_1/[E(1-r)]$.

THEORY

Case I

Collisions with like Atoms[6] ($r=0$)

(1) First collision:

After the first collision, the probability for the atoms of E_0 to fall below ϵ is ϵ/E_0. In this collision the retention is ϵ/E_0.

(2) Second collision (Fig. 1):

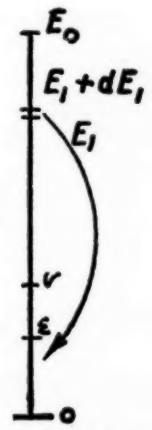

FIG. 1. Diagram representing the second collision of Case 1.

After the first collision, the atoms are uniformly distributed between E_0 and 0. The number of the atoms

[1] P. C. Capron and A. J. Verhoeve-Stokkink, Phys. Rev. **81**, 336 (1951).
[2] Capron, Crèvecoeur, and Faes, J. Chem. Phys. **17**, 349 (1949).
[3] P. C. Capron and E. Crèvecoeur, J. chim. phys. **49**, 29 (1952).
[4] W. F. Libby, J. Am. Chem. Soc. **69**, 2523 (1947).
[5] Miller, Gryder, and Dodson, J. Chem. Phys. **18**, 579 (1950).
[6] E. U. Condon and G. Breit, Phys. Rev. **49**, 229 (1936).

between E_1 and E_1+dE_1 is dE_1/E_0. Among these the ones which will fall below ϵ in the second collision are ϵ/E_1. The retention is given:

$$\int_{\nu}^{E_0} \frac{dE_1}{E_0}\frac{\epsilon}{E_1}=\frac{\epsilon}{E_0}(\ln E_0/\nu).$$

(3) Third collision (Fig. 2):

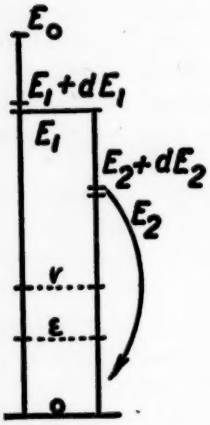

FIG. 2. Diagram representing the third collision of Case 1.

After the second collision, the number of the atoms between E_2 and E_2+dE_2 coming from dE_1 is:

$$\frac{dE_1}{E_0}\frac{dE_2}{E_1}.$$

Among these the ones which will fall below ϵ in the third collision are ϵ/E_2. The retention is given by

$$\int_{\nu}^{E_0}\int_{\nu}^{E_1} \frac{dE_1}{E_0}\frac{dE_2}{E_1}\frac{\epsilon}{E_2}=\frac{\epsilon}{E_0}\frac{1}{2}(\ln E_0/\nu)^2.$$

(4) Fourth collision:
The retention is given by

$$\int_{\nu}^{E_0}\int_{\nu}^{E_1}\int_{\nu}^{E_2} \frac{dE_1}{E_0}\frac{dE_2}{E_1}\frac{dE_3}{E_2}\frac{\epsilon}{E_3}=\frac{\epsilon}{E_0}\frac{1}{3!}(\ln E_0/\nu)^3.$$

The total retention for an infinite number of collisions is given by

$$R=\frac{\epsilon}{E_0}+\frac{\epsilon}{E_0}(\ln E_0/\nu)+\frac{\epsilon}{E_0}\frac{1}{2}(\ln E_{0/\nu})^2+\frac{\epsilon}{E_0}\frac{1}{3!}(\ln E_0/\nu)^3 + \frac{\epsilon}{E_0}\frac{1}{4!}(\ln E_0/\nu)^4+\cdots.$$

$$R=\frac{\epsilon}{\nu}. \qquad (1)$$

Case II

Collisions with Unlike Atoms ($r\neq 0$)

(A) $rE_0 \leqslant \epsilon < \nu$.

(1) First collision:
After the first collision the atoms are uniformly distributed between E_0 and rE_0. The probability to fall below ϵ is

$$\frac{\epsilon-rE_0}{E_0(1-r)}.$$

(2) Second collision:
The number of the atoms between E_1 and E_1+dE_1 is

$$\frac{dE_1}{E_0(1-r)}.$$

Among these the ones which will fall below ϵ in the second collision are

$$\frac{\epsilon-rE_1}{E_1(1-r)}.$$

The retention is given by

$$\int_{\nu}^{E_0}\frac{dE_1}{(1-r)E_0}\frac{\epsilon-rE_1}{(1-r)E_1}=\frac{1}{(1-r)^2E_0}(\epsilon\ln E_0/\nu-rE_0+r\nu).$$

(3) Third collision (Fig. 3):

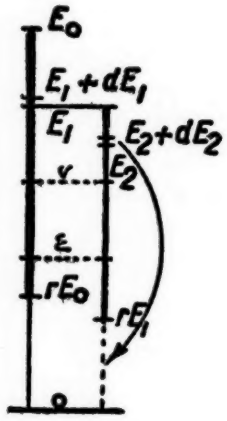

FIG. 3. Diagram representing the third collision of Case 2a.

After the second eollision, the number of the atoms between E_2 and E_2+dE_2 coming from dE_1 is

$$\frac{dE_1}{(1-r)E_0}\frac{dE_2}{(1-r)E_1}.$$

Among these the ones which will fall below ϵ in the third collision are

$$\frac{\epsilon-rE_2}{(1-r)E_2}.$$

The retention is given by

$$\int_{\nu}^{E_0}\int_{\nu}^{E_1}\frac{dE_1}{(1-r)E_0}\frac{dE_2}{(1-r)E_1}\frac{\epsilon-rE_2}{(1-r)E_2} =\frac{1}{(1-r)^3E_0}\{\epsilon^{\frac{1}{2}}(\ln E_0/\nu)^2-rE_0+r\nu+r\nu(\ln E_0/\nu)\}.$$

The total retention for an infinite number of collisions is given as follows:

$$R=\frac{\epsilon}{(1-r)E_0}\left\{1+\left(\frac{\ln E_0/\nu}{1-r}\right)+\frac{1}{2}\left(\frac{\ln E_0/\nu}{1-r}\right)^2+\frac{1}{3!}\left(\frac{\ln E_0/\nu}{1-r}\right)^3+\cdots\right\}$$

$$-\left[\frac{rE_0}{(1-r)E_0}+\frac{r}{(1-r)^2E_0}(E_0-\nu)+\frac{r}{(1-r)^3E_0}\{E_0-\nu-\nu(\ln E_0/\nu)\}+\frac{r}{(1-r)^4E_0}\times\{E_0-\nu-\nu(\ln E_0/\nu)-\nu\tfrac{1}{2}(\ln E_0)/\nu^2\}+\cdots\right],$$

$$R=\frac{\epsilon}{(1-r)E_0}\left(\frac{E_0}{\nu}\right)^{1/(1-r)}+1-\frac{\nu}{(1-r)E_0}\left(\frac{E_0}{\nu}\right)^{1/(1-r)},$$

$$R=1-\frac{(\nu-\epsilon)}{(1-r)\nu}\left(\frac{E_0}{\nu}\right)^{r/(1-r)}. \tag{2}$$

(B) $\epsilon\leqslant rE_0\leqslant\nu$:

(1) First collision:

After the first collision, the atoms are uniformly distributed between E_0 and rE_0. Since rE_0 is greater than ϵ, the retention is null in the first collision.

(2) Second collision (Fig. 4):

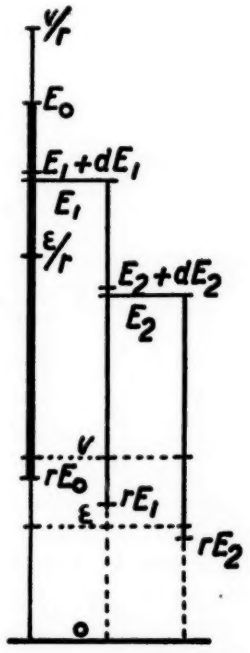

FIG. 4. Diagram representing the second and third collisions of Case 2b.

The number of atoms between E_1 and E_1+dE_1 is $dE_1/[(1-r)E_0]$. Among these atoms those which will fall below ϵ in the second collision are $(\epsilon-rE_1)/[(1-r)E_1]$. But the integration must be made between ν and ϵ/r, and the retention is given by

$$\int_\nu^{\epsilon/r}\frac{dE_1}{(1-r)E_0}\frac{\epsilon-rE_1}{(1-r)E_1}=\frac{1}{(1-r)^2E_0}[\epsilon\ln\epsilon/r\nu-r(\epsilon/r)+r\nu]. \tag{3}$$

(3) Third collision (Fig. 4):

The number of the atoms which will fall below ϵ in the third collision is given by

$$\int\int\frac{dE_1}{(1-r)E_0}\frac{dE_2}{(1-r)E_1}\frac{\epsilon-rE_2}{(1-r)E_2}.$$

This equation must be integrated from ν to ϵ/r for the part of E_1 greater than ϵ/r, and it must be integrated from ν to E_1, for the part of E_1 less than ϵ/r. The retention is given by

$$\int_\nu^{\epsilon/r}\int_\nu^{E_1}\frac{dE_1}{(1-r)E_0}\frac{dE_2}{(1-r)E_1}\frac{\epsilon-rE_2}{(1-r)E_2}+\int_{\epsilon/r}^{E_0}\int_\nu^{\epsilon/r}\frac{dE_1}{(1-r)E_0}\frac{dE_2}{(1-r)E_1}\frac{\epsilon-rE_2}{(1-r)E_2}$$

$$=\frac{1}{(1-r)^3E_0}\{\epsilon\tfrac{1}{2}(\ln\epsilon/r\nu)^2-r(\epsilon/r-\nu)+r\nu(\ln\epsilon/r\nu) \tag{4}$$

$$+\frac{1}{(1-r)^3E_0}(\ln rE_0/\epsilon)[\epsilon\ln\epsilon/r\nu-r(\epsilon/r)+r\nu]. \tag{4'}$$

(4) Fourth collision;

The retention in the fourth collision is given by:

$$\int_\nu^{\epsilon/r}\int_\nu^{E_1}\int_\nu^{E_2}\frac{dE_1}{(1-r)E_0}\frac{dE_2}{(1-r)E_1}\frac{dE_3}{(1-r)E_2}\frac{\epsilon-rE_3}{(1-r)E_3}+\int_{\epsilon/r}^{E_0}\int_\nu^{\epsilon/r}\int_\nu^{E_2}\frac{dE_1}{(1-r)E_0}\frac{dE_2}{(1-r)E_1}\frac{dE_3}{(1-r)E_2}\frac{\epsilon-rE_3}{(1-r)E_3}$$

$$+\int_{\epsilon/r}^{E_0}\int_{\epsilon/r}^{E_1}\int_\nu^{\epsilon/r}\frac{dE_1}{(1-r)E_0}\frac{dE_2}{(1-r)E_1}\frac{dE_3}{(1-r)E_2}\frac{\epsilon-rE_3}{(1-r)E_3}$$

$$=\frac{1}{(1-r)^4E_0}\left\{\epsilon\frac{1}{3!}(\ln\epsilon/r\nu)^3-r(\epsilon/r-\nu)+r\nu(\ln\epsilon/r\nu)+\tfrac{1}{2}r\nu(\ln\epsilon/r\nu)^2\right\} \tag{5}$$

$$+\frac{1}{(1-r)^4E_0}(\ln rE_0/\epsilon)\{\epsilon\tfrac{1}{2}(\ln\epsilon/r\nu)^2-r(\epsilon/r-\nu)+r\nu(\ln\epsilon/r\nu)\} \tag{5'}$$

$$+\frac{1}{(1-r)^4E_0}\tfrac{1}{2}(\ln rE_0/\epsilon)^2[\epsilon\ln\epsilon/r\nu-r(\epsilon/r)+r\nu]. \tag{5''}$$

The addition for an infinite number of collisions is as follows:

$$(3)+(4)+(5)+\cdots$$

$$=\frac{\epsilon}{(1-r)E_0}\left\{\left(\frac{\ln\epsilon/r\nu}{1-r}\right)+\frac{1}{2}\left(\frac{\ln\epsilon/r\nu}{1-r}\right)^2+\frac{1}{3!}\left(\frac{\ln\epsilon/r\nu}{1-r}\right)^3+\cdots\right\}$$

$$-\frac{1}{(1-r)E_0}\left[\frac{1}{(1-r)}(\epsilon-r\nu)+\frac{1}{(1-r)^2}\{\epsilon-r\nu-r\nu(\ln\epsilon/r\nu)\}+\frac{1}{(1-r)^3}\times\{\epsilon-r\nu-r\nu(\ln\epsilon/r\nu)+r\nu\tfrac{1}{2}(\ln\epsilon/r\nu)^2\}+\cdots\right]$$

$$=\frac{1}{(1-r)E_0}\left\{(\epsilon-\nu)\left(\frac{\epsilon}{r\nu}\right)^{1/(1-r)}-\epsilon+\frac{\epsilon}{r}\right\}. \tag{6}$$

$$(4')+(5')+\cdots$$

$$=\frac{1}{(1-r)^2E_0}(\ln rE_{0/\epsilon})\left\{(\epsilon-\nu)\left(\frac{\epsilon}{r\nu}\right)^{1/(1-r)}-\epsilon+\frac{\epsilon}{r}\right\}. \tag{7}$$

$$(5'')+\cdots$$

$$=\frac{1}{(1-r)^3E_0}\tfrac{1}{2}(\ln rE_0/\epsilon)^2\times\left\{(\epsilon-\nu)\left(\frac{\epsilon}{r\nu}\right)^{1/(1-r)}-\epsilon+\frac{\epsilon}{r}\right\}. \tag{8}$$

$$(6)+(7)+(8)+\cdots$$

$$=\frac{1}{(1-r)E_0}\left\{(\epsilon-\nu)\left(\frac{\epsilon}{r\nu}\right)^{1/(1-r)}-\epsilon+\frac{\epsilon}{r}\right\}\times\left\{1+\left(\frac{\ln rE_0/\epsilon}{1-r}\right)+\frac{1}{2}\left(\frac{\ln rE_0/\epsilon}{1-r}\right)^2+\frac{1}{3!}\left(\frac{\ln rE_0/\epsilon}{1-r}\right)^3+\cdots\right\}$$

$$=\frac{1}{(1-r)E_0}\left\{\epsilon\left(\frac{1}{r}-1\right)-(\nu-\epsilon)\left(\frac{\epsilon}{r\nu}\right)^{1/(1-r)}\right\}\times\left(\frac{rE_0}{\epsilon}\right)^{1/(1-r)},$$

$$R=\left\{1-\frac{(\nu-\epsilon)}{(1-r)\nu}\left(\frac{\epsilon}{r\nu}\right)^{r/(1-r)}\right\}\left(\frac{rE_0}{\epsilon}\right)^{r/(1-r)}. \tag{9}$$

(C) $r^2E_0\leqslant\epsilon<\nu$. (*Fig. 5*)

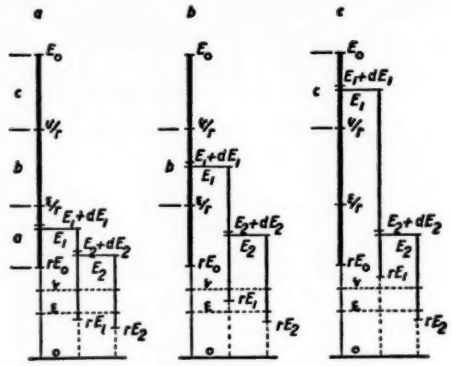

FIG. 5. Diagram representing the collision of Case 2c.

After the first collision all recoil atoms are distributed uniformly between E_0 and rE_0, in three energy ranges:

Range a:—Between rE_0 and ϵ/r. The retention starts from the second collision.

Range b:—Between ϵ/r and ν/r. The retention starts from the third collision.

Range c:—Between ν/r and E_0. The retention starts from the third collision.

(1) The retention of the atoms coming from the range a will be considered here. E_1 is between ϵ/r and rE_0. The number of the atoms between E_1 and E_1+dE_1 is $dE_1/(1-r)E_0$. Among these atoms those which will fall below ϵ in the second collision are $\epsilon-rE_1/(1-r)E_1$. The retention R_a after the second collision in the range a is

$$R_a=\int_{rE_0}^{\epsilon/r}\frac{dE_1}{(1-r)E_0}\frac{\epsilon-rE_1}{(1-r)E_1}. \tag{10}$$

The retention after the third collision in the range a is

$$R_{aa}=\int_{rE_0}^{\epsilon/r}\int_{\nu}^{E_1}\frac{dE_1}{(1-r)E_0}\frac{dE_2}{(1-r)E_1}\frac{\epsilon-rE_2}{(1-r)E_2}. \tag{11}$$

The retention after the fourth collision is

$$R_{aaa}=\int_{rE_0}^{\epsilon/r}\int_{\nu}^{E_1}\int_{\nu}^{E_2}\frac{dE_1}{(1-r)E_0}\frac{dE_2}{(1-r)E_1}\times\frac{dE_3}{(1-r)E_2}\frac{\epsilon-rE_3}{(1-r)E_3}. \tag{12}$$

(2) The retention of the atoms coming from the ranges b and c with only one collision in these ranges will be considered here. The retention after the third collision for the atoms from the range b is

$$R_{ba}=\int_{\epsilon/r}^{\nu/r}\int_{\nu}^{\epsilon/r}\frac{dE_1}{(1-r)E_0}\frac{dE_2}{(1-r)E_1}\frac{\epsilon-rE_2}{(1-r)E_2}. \tag{13}$$

The retention after the third collision for the atoms from

the range c is

$$R_{ca}=\int_{\nu/r}^{E_0}\int_{rE_1}^{\epsilon/r}\frac{dE_1}{(1-r)E_0}\frac{dE_2}{(1-r)E_1}\frac{\epsilon-rE_2}{(1-r)E_2}. \quad (13')$$

And the retention after the fourth collision is given by

$$R_{baa}=\int_{\epsilon/r}^{\nu/r}\int_{\nu}^{\epsilon/r}\int_{\nu}^{E_2}\frac{dE_1}{(1-r)E_0}\frac{dE_2}{(1-r)E_1}\times\frac{dE_3}{(1-r)E_2}\frac{\epsilon-rE_3}{(1-r)E_3}, \quad (14)$$

$$R_{caa}=\int_{\nu/r}^{E_0}\int_{rE_1}^{\epsilon/r}\int_{\nu}^{E_2}\frac{dE_1}{(1-r)E_0}\frac{dE_2}{(1-r)E_1}\times\frac{dE_3}{(1-r)E_2}\frac{\epsilon-rE_3}{(1-r)E_3}. \quad (14')$$

(3) The retention of the atoms coming from the ranges b and c doing more than one collision in these ranges will be considered here. The retention after the fourth collision is

$$R_{bba}=\int_{\epsilon/r}^{\nu/r}\int_{\epsilon/r}^{E_1}\int_{\nu}^{\epsilon/r}\frac{dE_1}{(1-r)E_0}\frac{dE_2}{(1-r)E_1}\times\frac{dE_3}{(1-r)E_2}\frac{\epsilon-rE_3}{(1-r)E_3}, \quad (15)$$

$$R_{cba}=\int_{\nu/r}^{E_0}\int_{\epsilon/r}^{\nu/r}\int_{\nu}^{\epsilon/r}\frac{dE_1}{(1-r)E_0}\frac{dE_2}{(1-r)E_1}\times\frac{dE_3}{(1-r)E_2}\frac{\epsilon-rE_3}{(1-r)E_3}, \quad (16')$$

$$R_{cca}=\int_{\nu/r}^{E_0}\int_{\nu/r}^{E_1}\int_{rE_2}^{\epsilon/r}\frac{dE_1}{(1-r)E_0}\frac{dE_2}{(1-r)E_1}\times\frac{dE_3}{(1-r)E_2}\frac{\epsilon-rE_3}{(1-r)E_3}. \quad (17'')$$

In the same manner, we obtain all the partial retentions. For an infinite number of collisions, the sum of these partial retentions will be calculated as follows (see Table I):

$$(A)=R_a+R_{aa}+R_{aaa}+\cdots$$
$$=\int_{rE_0}^{\epsilon/r}\frac{dE_1}{(1-r)E_0}\left\{1-\frac{(\nu-\epsilon)}{(1-r)E_1}\left(\frac{E_1}{\nu}\right)^{1/(1-r)}\right\}. \quad (18)$$

$$(B_1)=R_{ba}+R_{baa}+R_{baaa}+\cdots$$
$$=\int_{\epsilon/r}^{\nu/r}\int_{\nu}^{\epsilon/r}\frac{dE_1}{(1-r)E_0}\frac{dE_2}{(1-r)E_1}\times\left\{1-\frac{(\nu-\epsilon)}{(1-r)E_2}\left(\frac{E_2}{\nu}\right)^{1/(1-r)}\right\}. \quad (19_1)$$

$$(B_2)=R_{ca}+R_{caa}+R_{caaa}+\cdots$$
$$=\int_{\nu/r}^{E_0}\int_{rE_1}^{\epsilon/r}\frac{dE_1}{(1-r)E_0}\frac{dE_2}{(1-r)E_1}\times\left\{1-\frac{(\nu-\epsilon)}{(1-r)E_2}\left(\frac{E_2}{\nu}\right)^{1/(1-r)}\right\}. \quad (20_2)$$

$$(C_1)=R_{bba}+R_{bbaa}+R_{bbaaa}+\cdots$$
$$=\int_{\epsilon/r}^{\nu/r}\int_{\epsilon/r}^{E_1}\int_{\nu}^{\epsilon/r}\frac{dE_1}{(1-r)E_0}\frac{dE_2}{(1-r)E_1}\frac{dE_3}{(1-r)E_2}\times\left\{1-\frac{(\nu-\epsilon)}{(1-r)E_3}\left(\frac{E_3}{\nu}\right)^{1/(1-r)}\right\}. \quad (21a)$$

$$(C_2)=R_{cba}+R_{cbaa}+R_{cbaaa}+\cdots$$
$$=\int_{\nu/r}^{E_0}\int_{\epsilon/r}^{\nu/r}\int_{\nu}^{\epsilon/r}\frac{dE_1}{(1-r)E_0}\frac{dE_2}{(1-r)E_1}\frac{dE_3}{(1-r)E_2}\times\left\{1-\frac{(\nu-\epsilon)}{(1-r)E_3}\left(\frac{E_3}{\nu}\right)^{1/(1-r)}\right\}. \quad (21b)$$

$$(C_3)=R_{cca}+R_{ccaa}+R_{ccaaa}+\cdots$$
$$=\int_{\nu/r}^{E_0}\int_{\nu/r}^{E_1}\int_{rE_1}^{\epsilon/r}\frac{dE_1}{(1-r)E_0}\frac{dE_2}{(1-r)E_1}\frac{dE_3}{(1-r)E_2}\times\left\{1-\frac{(\nu-\epsilon)}{(1-r)E_3}\left(\frac{E_3}{\nu}\right)^{1/(1-r)}\right\}. \quad (21c)$$

In the same manner, we obtain (D_1), (D_2), (D_3), (D_4), and so on. The additions of (B_1), (C_1), (D_1), etc., (C_2), (D_2), (E_2), etc., and so on, are made easily, and the result is as follows (see Table I):

$$(B_1)+(C_1)+(D_1)+\cdots$$
$$=\frac{1}{(1-r)E_0}\left\{\epsilon\left(\frac{1}{r}-1\right)-(\nu-\epsilon)\left(\frac{\epsilon}{r\nu}\right)^{1/(1-r)}\right\}\times\left\{\left(\frac{\nu}{\epsilon}\right)^{1/(1-r)}-1\right\},$$

TABLE I.

1st collision									
2nd collision	$\int_{rE_0}^{\epsilon/r} R_a$								
3rd collision	$\int_{rE_0}^{\epsilon/r}\int_{\nu}^{E_1} R_{aa}$	$\int_{\epsilon/r}^{\nu/r}\int_{\nu}^{\epsilon/r} R_{ba}$					$\int_{\nu/r}^{E_0}\int_{rE_1}^{\epsilon/r} R_{ca}$		
4th collision	$\int_{rE_0}^{\epsilon/r}\int_{\nu}^{E_1}\int_{\nu}^{E_2} R_{aaa}$	$\int_{\epsilon/r}^{\nu/r}\int_{\nu}^{\epsilon/r}\int_{\nu}^{E_2} R_{baa}$	$\int_{\epsilon/r}^{\nu/r}\int_{\epsilon/r}^{E_1}\int_{\nu}^{\epsilon/r} R_{bba}$				$\int_{\nu/r}^{E_0}\int_{rE_1}^{\epsilon/r}\int_{\nu}^{E_2} R_{caa}$		
5th collision	$\int_{rE_0}^{\epsilon/r}\int_{\nu}^{E_1}\int_{\nu}^{E_2}\int_{\nu}^{E_3} R_{aaaa}$	$\int_{\epsilon/\nu}^{\nu/r}\int_{\nu}^{\epsilon/r}\int_{\nu}^{E_2}\int_{\nu}^{E_3} R_{baaa}$	$\int_{\epsilon/r}^{\nu/r}\int_{\epsilon/r}^{E_1}\int_{\nu}^{\epsilon/r}\int_{\nu}^{E_3} R_{bbaa}$	$\int_{\epsilon/r}^{\nu/r}\int_{\epsilon/r}^{E_1}\int_{\epsilon/r}^{E_2}\int_{\nu}^{\epsilon/r} R_{bbba}$			$\int_{\nu/r}^{E_0}\int_{rE_1}^{\epsilon/r}\int_{\nu}^{E_2}\int_{\nu}^{E_3} R_{caaa}$		
6th collision	R_{aaaaa}	R_{baaaa}	R_{bbaaa}	R_{bbbaa}	R_{bbbba}	R_{caaaa}			
7th collision									
⋮									
Sum	(A)	(B_1)	(C_1)	(D_1)	(E_1)	(B_2)			

$\int_{\nu/r}^{E_0}\int_{\epsilon/r}^{\nu/r}\int_{\nu}^{\epsilon/r} R_{cba}$	$\int_{\nu/r}^{E_0}\int_{\nu/r}^{E_1}\int_{rE_2}^{\epsilon/r} R_{cca}$							
$\int_{\nu/r}^{E_0}\int_{\epsilon/r}^{\nu/r}\int_{\nu}^{\epsilon/r}\int_{\nu}^{E_3} R_{cbaa}$	$\int_{\nu/r}^{E_0}\int_{\nu/r}^{E_1}\int_{rE_2}^{\epsilon/r}\int_{\nu}^{E_3} R_{ccaa}$	$\int_{\nu/r}^{E_0}\int_{\epsilon/r}^{\nu/r}\int_{\epsilon/r}^{E_2}\int_{\nu}^{\epsilon/r} R_{cbba}$	$\int_{\nu/r}^{E_0}\int_{\nu/r}^{E_1}\int_{/r}^{\nu/r}\int_{\nu}^{\epsilon/r} R_{ccba}$	$\int_{\nu/r}^{E_0}\int_{\nu/r}^{E_1}\int_{\nu/r}^{E_2}\int_{E_3}^{\epsilon/r} R_{ccca}$				
R_{cbaaa}	R_{ccaaa}	R_{cbbaa}	R_{ccbaa}	R_{cccaa}	R_{cbbba}	R_{ccbba}	R_{cccba}	R_{ccccc}

(C_2)	(C_3)	(D_2)	(D_3)	(D_4)	(E_2)	(E_3)	(E_4)	(E_5)

$$(C_2)+(D_2)+(E_2)+\cdots$$

$$=\frac{\ln rE_0/\nu}{1-r}\frac{1}{(1-r)E_0}\left\{\epsilon\left(\frac{1}{r}-1\right)-(\nu-\epsilon)\left(\frac{\epsilon}{r\nu}\right)^{1/(1-r)}\right\}$$

$$\times\left\{\left(\frac{\nu}{\epsilon}\right)^{1/(1-r)}-1\right\},$$

$$(D_3)+(E_3)+(F_3)+\cdots$$

$$=\frac{1}{2}\left(\frac{\ln rE_0/\nu}{1-r}\right)^2\frac{1}{(1-r)E_0}\left\{\epsilon\left(\frac{1}{r}-1\right)\right.$$

$$\left.-(\nu-\epsilon)\left(\frac{\epsilon}{r\nu}\right)^{1/(1-r)}\right\}\left\{\left(\frac{\nu}{\epsilon}\right)^{1/(1-r)}-1\right\}.$$

The sum of these terms is given by

$$\frac{1}{(1-r)E_0}\left(\frac{rE_0}{\nu}\right)^{1/(1-r)}\left\{\epsilon\left(\frac{1}{r}-1\right)-(\nu-\epsilon)\left(\frac{\epsilon}{r\nu}\right)^{1/(1-r)}\right\}\times\left\{\left(\frac{\nu}{\epsilon}\right)^{1/(1-r)}-1\right\}.$$

The sum of the rest terms, (A), (B_2), (C_3), etc. is given by

$$1-\frac{1}{(1-r)E_0}\left(\frac{rE_0}{\nu}\right)^{1/(1-r)}(\nu-\epsilon)\times\left\{\frac{1}{r}-1+\left(\frac{\epsilon}{r\nu}\right)^{1/(1-r)}-\frac{\ln rE_0/\nu}{1-r}\right\}.$$

Finally, we have obtained the next formula as the total retention.

$$R=1-\left\{1-\left(\frac{\nu}{\epsilon}\right)^{r/(1-r)}+\frac{(\nu-\epsilon)}{(1-r)\nu}\left(\frac{1}{r}\right)^{r/(1-r)}-\frac{(\nu-\epsilon)r}{(1-r)^2\nu}(\ln rE_0/\nu)\right\}\left(\frac{rE_0}{\nu}\right)^{r/(1-r)}. \quad (22)$$

(D) $\epsilon\leqslant r^2E_0\leqslant\nu$.

In this case, we have obtained the result by the same manner as in the case (C).

$$R=\left\{1+\left(\frac{1}{r}\right)^{r/(1-r)}-\left(\frac{\epsilon}{r\nu}\right)^{r/(1-r)}-\frac{(\nu-\epsilon)}{(1-r)\nu}\times\left(\frac{\epsilon}{r^2\nu}\right)^{r/(1-r)}+\frac{r(\nu-\epsilon)}{(1-r)^2\nu}\left(\frac{\epsilon}{r\nu}\right)^{r/(1-r)}(\ln\epsilon/r\nu)-\frac{r}{1-r}\left[1-\frac{(\nu-\epsilon)}{(1-r)\nu}\left(\frac{\epsilon}{r\nu}\right)^{r/(1-r)}\right]\times(\ln r^2E_0/\epsilon)\right\}\left(\frac{r^2E_0}{\epsilon}\right)^{r/(1-r)}. \quad (23)$$

DISCUSSION

Considering only collisions of the "billiard ball" type, we obtain the five following equations for the retention as a function of r and E_0.

(a) Collision with like atoms:

$$R=\epsilon/\nu. \quad (24)$$

(b) Collision with unlike atoms:

(1) $rE_0\leqslant\epsilon<\nu$

$$R=1-\frac{(\nu-\epsilon)}{(1-r)\nu}\left(\frac{E_0}{\nu}\right)^{r/(1-r)}. \quad (25)$$

(2) $\epsilon\leqslant rE_0\leqslant\nu$

$$R=\left\{1-\frac{(\nu-\epsilon)}{(1-r)\nu}\left(\frac{\epsilon}{r\nu}\right)^{r/(1-r)}\right\}\left(\frac{rE_0}{\nu}\right)^{r/(1-r)}. \quad (26)$$

(3) $r^2E_0\leqslant\epsilon<\nu$

$$R=1-\left\{1-\left(\frac{\nu}{\epsilon}\right)^{r/(1-r)}+\frac{(\nu-\epsilon)}{(1-r)\nu}\left(\frac{1}{r}\right)^{r/(1-r)}-\frac{r(\nu-\epsilon)}{(1-r)^2\nu}(\ln rE_0/\nu)\right\}\left(\frac{rE_0}{\nu}\right)^{r/(1-r)}. \quad (27)$$

(4) $\epsilon\leqslant r^2E_0\leqslant\nu$

$$R=\left[1+\left(\frac{1}{r}\right)^{r/(1-r)}-\left(\frac{\epsilon}{r\nu}\right)^{r/(1-r)}-\frac{(\nu-\epsilon)}{(1-r)\nu}\left(\frac{\epsilon}{r^2\nu}\right)^{r/(1-r)}+\frac{r(\nu-\epsilon)}{(1-r)^2\nu}\left(\frac{\epsilon}{r\nu}\right)^{r/(1-r)}(\ln\epsilon/r\nu)-\frac{r}{1-r}\times\left\{1-\frac{(\nu-\epsilon)}{(1-r)\nu}\left(\frac{\epsilon}{r\nu}\right)^{r/(1-r)}\right\}(\ln r^2E_0/\epsilon)\right]\times\left(\frac{r^2E_0}{\epsilon}\right)^{r/(1-r)}. \quad (28)$$

Remarks on the equations:

1. Putting $r=0$ in (25), (26), (27), and (28), they reduce to $R=\epsilon/\nu$.

2. There exists a continuity between (25), (26), (27), and (28).

3. Equations (25), (26), (27), and (28) have been controlled numerically by addition of the partial retentions calculated for every collisions. Example for $\epsilon=3$, $\nu=4$, $r=0.5$, $E_0=5$ (Eq. (25)):

Retention of first collision:	0.200000
Retention of second collision:	0.135536
Retention of third collision:	0.033544
Retention of fourth collision:	0.005184
Retention of fifth collision:	0.000525
Sum of these retentions:	0.374789
Retention calculated from the formula:	0.375

$\nu=4$ ev, $\epsilon=3$ ev, $r=0.5$, $E_0=5$ ev

4. For collisions with unlike atoms, it can be understood that the retention decreases with increasing E_0, when E_0 is near ν (Eq. (25)). After that, the retention will increase with increasing E_0 (Eq. (27)). For greater E_0, the retention will remain constant. For example, the retention for collision carbon-bromine and chlorine-

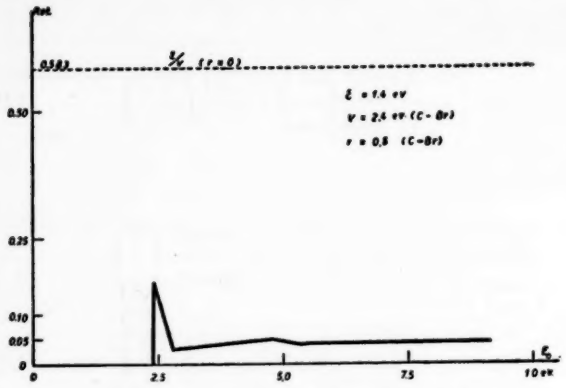

FIG. 6. Retention for carbon-bromine collisions.

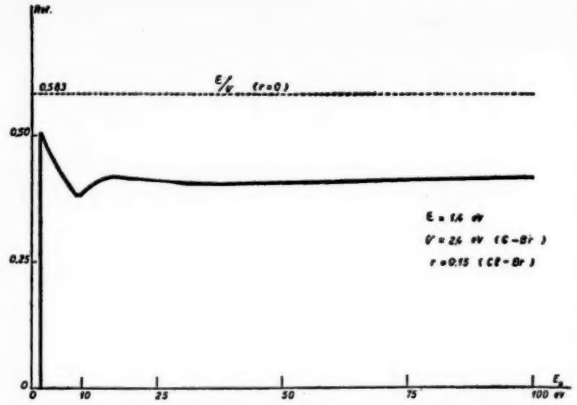

FIG. 7. Retention for chlorine-bromine collisions.

bromine have been calculated (Figs. 6 and 7):

ν is taken 2.4 ev (binding energy of C-Br),
ϵ is taken 1.4 ev in such a manner that $\epsilon/\nu \sim 0.6$,
$r=0.5$ (for C-Br collision), $r=0.15$ (for Cl-Br collision).

E_0	2.5	3.0	3.5	4.0	4.5	5.0	6.5	8.5
R	0.132	0.030	0.035	0.040	0.045	0.044	0.040	0.041

$\epsilon=1.4$ ev, $\nu=2.4$ ev, $r=0.5$ (C-Br collision) E_0 in ev unit.

E_0	4.0	6.0	10	20	40	60	80	100
R	0.464	0.424	0.381	0.411	0.405	0.405	0.414	0.414

$\epsilon=1.4$ ev, $\nu=2.4$ ev, $r=0.15$ (Cl-Br collision) E_0 in ev unit.

5. The retention is given by

$$R=\sum p_i R_i,$$

where p_i is the probability of the collision of type i, and R_i the retention for the collision of type i. This formula must be applied carefully. For example, the collision of recoil bromine atoms with the carbon in $CHBr_3$ may destroy the molecule and therefore no organic retention can be expected.

CONCLUSIONS

(a) The hope to measure the initial energies of the two recoil isomeric atoms of bromine by the difference of their retention must be abandoned. The calculation developed above shows the impossibility of determining the initial energy E_0 of the recoil atoms. Indeed, for collision with like atoms the retention is constant $R=\epsilon/\nu$, and for collision with unlike atoms there exist several values of the energy E_0 which have the same retention.

(b) For the two products C_6H_5Br and $CHBr_3$ the probability for collisions Br-Br is less in the first case than in the second. According to the calculation developed above the retention should be lower for C_6H_5Br than for $CHBr_3$, which is not in accordance with our experiments.

(c) According to Willard and others[7] the above calculations show that the difference in the retention of the two isomers and the retention itself must be explained by a process more complicated than the simple "billiard ball" type. In particular, the charge of the recoil atoms and the chemical nature of the organic products must play an important part.

[7] Goldhaber, Chiang, and Willard, J. Am. Chem. Soc. **73**, 2271 (1951).

Hydrogen Bonding and the Interactions of Water Molecules*

EDWIN S. CAMPBELL†
Department of Chemistry and Chemical Engineering, University of California, Berkeley, California
(Received December 17, 1951)

A study of proposed explanations for the forces governing the interaction of hydrogen-bonded molecules has been made by investigating various models for the intermolecular potential function for H_2O. Implications of the models concerning the known properties of H_2O have been examined.

1. After a survey of existing views and data on hydrogen bonding, the electrostatic model is chosen for further study. The criterion selected to winnow the proposed models is their ability to correlate second virial data and the energy of sublimation of ice.
2. The dipolar energy of ice is calculated after Ewald and Kornfeld. Although the dipole approximation fails to pass test No. 1, it is sufficient for interesting observations on some crystal properties of ice.
3. The consistency of the dipole model with Pauling's explanation of the entropy discrepancy is examined.
4. Point charge models are discussed and a multipole calculation made for the ice structure with the highest dipole-dipole energy.
5. Calculations made suggest that a properly chosen point charge model may suffice for the correlation of gas and crystal data.

I. INTRODUCTION

THE work of the forty years following the introduction of the hydrogen bond[1] has been largely of a qualitative nature, although vapor density and infrared measurements have been used to estimate a hydrogen bond energy and a few calculations have been made. Up to the present time, chemists have speculated concerning the origin and magnitude of forces which occur in those strongly associated substances traditionally considered as hydrogen-bonded. It is convenient to characterize the disagreement as one between two viewpoints. The first viewpoint maintains a rather ill-defined idea of a hydrogen bond, and, as proposed by some, seems to assume that the association must be considered in terms of a poorly specified quantum-mechanical interaction; the second viewpoint supposes that the forces involved in hydrogen bonding are of the same sort as those between any other electrically asymmetric molecules, and, to a first-order accuracy, are the classical forces arising from interaction of induced and permanent electric multipoles of the molecules, superimposed on the dispersion and repulsive forces exhibited by simpler nonpolar molecules.

The first interpretation was argued most recently by Lambert and Strong[2] in a report on their study of the virial coefficients of amines. A specious use of the Berthelot equation of state and the observed second virial coefficient for the calculation of energies of interaction led to the conclusion that the stronger association of primary and secondary amines would be considered best in terms of a "hydrogen bond."

Lambert and Strong differentiated between the interactions of primary and secondary and those of tertiary amines. Similarly, others who have treated the H_2O-H_2O interaction according to a classical electrostatic model have supposed that the HF—HF interaction should be viewed in terms of a "hydrogen bond." The contrast drawn between the behavior of H_2O and HF perhaps ignores the fact that at its boiling point (19.9°C) where saturated HF vapor has an average molecular weight of about 3.5,[3] water is a liquid in which all molecules are united in cooperative interaction. It may be that the difference in their properties arises not from the failure of the classical approximation for HF and its applicability to H_2O, but rather from the ability of H_2O with its approximately tetrahedral symmetry to form a three-dimensional packing, whereas HF with its cylindrical symmetry forms an essentially two-dimensional packing of chains and perhaps rings.[4] At 60°C and 1 atmos HF behaves as an approximately ideal gas.[4]

A distinction has been drawn at times between H_2O-H_2O interaction in the vapor and condensed phases on the basis that bands such as appear in HF spectra for both gaseous and condensed phases[5] occur in H_2O spectra only for the condensed phases. The foregoing observations coupled with the slightly larger dipole moment[6] and shorter distance of close approach[7] for HF would offer a possible explanation of this difference in behavior. Moreover, recently it has been shown that at higher temperatures at which water vapor can attain higher densities without condensing, it also exhibits an association band.[8]

* Excerpt from the dissertation submitted in partial fulfillment of the requirements for the Doctor of Philosophy in Chemistry at the University of California, Berkeley. This work was undertaken in part under a Du Pont Company Post-Graduate Fellowship in Chemistry, 1950–1951.

† Present address: Department of Chemistry, University of Southern California, Los Angeles 7, California.

[1] T. S. Moore and T. F. Winmill, J. Chem. Soc. **101**, 1635 (1912).

[2] J. D. Lambert and E. D. Strong, Proc. Roy. Soc. (London) **A200**, 566 (1950).

[3] K. Fredenhagen, Z. anorg u. allgem. Chem. **210**, 210 (1933). The average molecular weight quoted is the ideal gas value.

[4] R. A. Oriani and C. P. Smyth, J. Am. Chem. Soc. **70**, 125 (1948).

[5] Buswell, Maycock, and Rodebush, J. Chem. Phys. **8**, 362 (1940).

[6] R. A. Oriani and C. P. Smyth, J. Chem. Phys. **16**, 1167 (1948).

[7] Bauer, Beach and Simons, J. Am. Chem. Soc. **61**, 19 (1939).

[8] Gr. Landsberg, J. phys. et radium **6**, 305 (1945).

The second interpretation was presented in 1929 by Smyth and Engel,[9] who observed that the force field of a molecule carrying an electric doublet will depend not only on the dipole moment but also on the location of the doublet within the molecule. For example, ethyl bromide with a dipole moment of 1.86 *D* behaves rather normally since its large moment is shielded by large ethyl and bromide groups.

Smyth and collaborators[10] attempted to investigate the effect of the strong association of typically hydrogen-bonded molecules on their electronic systems by studying the electronic polarization of solutions of associated substances in nonpolar solvents as a function of concentration. They found that the variation with concentration of the Lorentz function for such molecules was no greater than for nonpolar molecules. Further, the change in the function upon vaporization was completely normal. These results were considered evidence that the disturbance of the electronic systems was not great and that the stronger association was produced by powerful dipolar forces. Pauling[11] has noted that these views are not essentially different from those he presents.[12]

In 1941 Stockmayer[13] developed a series expansion for the second virial coefficient[14] of a gas whose pair potential was that of a point dipole superimposed on the usual Lennard-Jones potential. Stockmayer's formula was applied by J. S. Rowlinson in a study of virial data on several polar gases.[15] When considering the data Rowlinson presents, it is necessary to keep the indeterminancy of results obtained from virial studies over the usual temperature ranges firmly in mind.[16] However, the data seem to be in qualitative agreement with Smyth's hypothesis that the strength of the association arises from dipole interactions when they can occur at relatively short distances.

The general agreement of Rowlinson's data with the predictions suggested by Smyth's view of the hydrogen bond encourages further more exacting inquiry. It is therefore interesting to find that Stockmayer,[13] using a dipole model, derived empirical values for the coefficients of the $1/r^6$ and $1/r^n$ terms for the potential function which enabled him to fit Keyes' precise virial data on H_2O from 400°K to 750°K to within an accuracy of one percent.

Since the definite molecular orientations within a crystal impose rather stringent requirements on the nature of the angular dependence of the potential function, the available x-ray and thermodynamic data on ice offer an opportunity to study the intermolecular interactions of one of the most common and important substances with hope for an eventual comment on the more general problem of the nature of the hydrogen bond. Here is an opportunity for an ultimate first-order quantitative check on the viewpoint first proposed by Smyth, that the association of substances which are considered to be hydrogen-bonded, arises primarily from interactions of electric doublets at short distances.

II. AVAILABLE DATA AND CALCULATIONS ON ICE

A. Previous Calculations

Bernal and Fowler,[17] Magat,[18] Bauer and Magat,[19] and Verwey[20] have made calculations on ice based on point charge models for the H_2O molecule. However, none of these calculations can be used to determine whether available data can distinguish between the point dipole model and other models which are *a priori* less objectionable.

Rowlinson's interesting paper[21] on the lattice energy of ice and the second virial coefficient of water assumes a point of view different from the one adopted here. His calculations are based on the assumption that Pauling's explanation[22] for the entropy discrepancy of ice requires a random orientation of the hydrogen positions. One of the objects of this research has been the study of the dependence of the energy of ice on the orientation of the hydrogens as a basis for comment upon Pauling's explanation.

In Sec. III near-neighbor calculations are shown to be inadequate. Therefore, the rather small difference between the near-neighbor and total energies as found by Bernal and Fowler, Verwey, and Rowlinson, although probably correct for the models they chose, is fortuitous.

Rowlinson made a simplifying assumption in assigning a quadrupole moment consistent with his point charge model.‡ Although the H_2O molecule may be

[9] C. P. Smyth and E. W. Engel, J. Am. Chem. Soc. **51**, 2669 (1929).

[10] Smyth, Engel, and Wilson, Jr., J. Am. Chem. Soc. **51**, 1736 (1929).

[11] L. Pauling, *The Nature of the Chemical Bond* (Cornell University Press, Ithaca, New York, 1945), p. 289.

[12] For further critical discussion of these two viewpoints see also: G. B. B. M. Sutherland, Trans. Faraday Soc. **36**, 894 (1940). General Discussion, Trans. Faraday Soc. **36**, 911 (1940). Reference 11, Chapter IX.

[13] W. H. Stockmayer, J. Chem. Phys. **9**, 398 (1941).

[14] For a lucid development of the virial expansion, see J. E. Mayer and M. G. Mayer, *Statistical Mechanics* (John Wiley and Sons, Inc., New York, 1940), Chapter XIII. The limitations on such a development are treated with excellence by R. Fowler and E. A. Guggenheim, *Statistical Thermodynamics* (Cambridge University Press, Cambridge, 1949), p. 255.

[15] J. S. Rowlinson, Trans. Faraday Soc. **47**, 120 (1951).

[16] J. Corner, Trans. Faraday Soc. **44**, 914 (1948).

[17] J. D. Bernal and R. H. Fowler, J. Chem. Phys. **1**, 515 (1933).

[18] M. Magat, Ann. phys. **6**, 183 (1936).

[19] E. Bauer and M. Magat, J. phys. et radium **9**, 319 (1938).

[20] E. J. W. Verwey, Rec. trav. chim. **60**, 887 (1941).

[21] J. S. Rowlinson, Trans. Faraday Soc. **47**, 120 (1951).

[22] L. Pauling, J. Am. Chem. Soc. **57**, 2580 (1935).

‡ Using a triangular model for H_2O with a negative charge of $-2q$ at the center of mass of the oxygen and of $+q$ at each hydrogen, Rowlinson assumed that (see Appendix I) $P_{YY}=P_{ZZ}=0$. This is only possible if the reference point for the Taylor series expansion is chosen as $(0, -(\frac{1}{3})^{\frac{1}{2}}/2r_0, 0)$ relative to the (XYZ) axis system. However, in his calculations, Rowlinson used the center of mass of the oxygen as the reference point. Although, for certain relative orientations, this simplification has only slight effect, in general its effect is non-negligible. For example, consider the $a_{000}c_{000}$ interaction of A_5 (see Appendix II) where the hydrogens on c_{000} have been shifted to give the principal axes $(X=X,$

treated in terms of a single quadrupole, if an axial quadrupole such as Rowlinson selected is used, then, relative to the center of mass of the oxygen as the reference point for the Taylor expansion, a second axial quadrupole with a moment one-half that of the first,§ directed alsong the bisector of the HOH angle, is required. This simplification in assigning the quadrupole to H_2O may partly account for his finding a dipole-quadrupole contribution 24 percent of the dipole-dipole contribution to the virial coefficient, whereas Margenau and Myers[23] found a ratio of 0.54. Rowlinson himself attributed the entire decrease in the ratio to Margenau and Myers' neglect of certain terms in their expansion of the integrand of the virial coefficient.

B. Crystal Structure of Ice

Barnes[24] concluded from his careful studies of the x-ray diffraction pattern of ice at 0°, −20°, −183°C, that ice undergoes no phase change within that temperature range. The extrapolation of crystal parameters gives 2.72 A° as the O−O distance at 0°K. If the x' and y' axes are separated by an angle of 120° and are each orthogonal to the z' axis, the four oxygen positions in the unit cell may be given in terms of unit translations along the (x', y', z') axes as follows: a: (1/3, 2/3, 1/16); b: (2/3, 1/3, −1/16); c: (1/3, 2/3, 7/16); d: (2/3, 1/3, 9/16).

The experimental ratio of the unit translations as found by x-ray diffraction agrees well with the theoretical value determined by the geometry of the ice structure: $(x':y':z')=1:1:(8/3)^{\frac{1}{2}}$. Each oxygen is surrounded by four other oxygens at the corners of a tetrahedron. The tetrahedra are joined apex to apex to give the ice structure the most open of the three space combinations of tetrahedra possible for a crystal.

Recently Wollan, Davidson, and Shull[25] made a study of the neutron-diffraction pattern of heavy ice at −90°C. Assuming the results of Barnes' investigations, they considered four models: (1) hydrogen atoms located midway between O−O positions, (2) an ordered crystal with respect to hydrogens as proposed by Bernal and Fowler,[17] (3) hydrogens rotating about oxygen positions, and (4) a random arrangement of the hydrogens as proposed by Pauling.[22] They concluded that only the random arrangement of the hydrogens was at all consistent with their observed intensities.

In private communication, R. H. Cole reported results of a new careful study of the relaxation process in ice. Dr. R. P. Auty, working with Professor Cole, found that the relaxation time could be accurately described from 0°C to −66°C by a rate formula with an activation energy of 13.2 kcal/mole and an activation entropy of 11.9 kcal/deg mole. For deuterium ice he obtained tentative values, which are now being verified, of 12.5 kcal/mole and 8.5 cal/deg mole, respectively. Professor Cole reported that only a very small conductance for ice was observed and that infrared work under Professor Hornig indicates a potential barrier for proton transfer of at least 26 kcal, and more probably, 75–100 kcal. He concludes that proton transfer is probably not the mechanism involved. Therefore, it would be interesting to obtain diffraction patterns at higher temperatures, where the relaxation time is rather small, to see what the diffraction data would then say about rotation of the hydrogens.

However, there is contradictory evidence on the orientation of the hydrogens based on crystal studies and work on the dielectric constant. Kauzman[26] has predicted that, because of its geometry, ice should probably show ferroelectric properties at sufficiently low temperatures. Latimer[27] reported that it was possible to freeze a permanent electric moment into ice. Although Barnes argued that the crystals he examined were not twinned, others[28] have presented rather cogent evidence that some ice crystals are twinned, some not. In his studies on the growth and decay of microcrystals of ice, Adams found that as he varied the vapor pressure of H_2O, some ice crystals developed pits on one end of the z' axis only, some at the center, and some at both ends of the z' axis. The asymmetry along the z' axis also had been observed by others in studies on natural snow flakes.

Recently Rossmann[28] reported that when sincle ice crystals which gave neither piezo- nor pyroelectric effects were split transverse to the z' axis, the two resulting crystals always exhibited both piezo- and pyroelectric activity along the z' axis. There was no activity perpendicular to the z' axis. He concluded that Barnes erred in his choice of space group and that ice did not belong to the holohedral class $D_{6h}{}^4$ since this space group does not allow piezoelectric activity.[28] He dismissed Barnes' second suggestion, the holohedral class $D_{3h}{}^4$, because of the apparent twinning, and suggested instead the hemihedral class C_{6v}. The various classes differ only in the symmetry assigned to the O positions. Finally, Jona and Scherrer,[28] in their paper on the elastic constants of ice give a summary of attempts to grow large single crystals which offers interesting comment on the polar character of ice.

$Y=-Y$). The actual dipole-quadrupole interaction is zero; neglect of the Y quadrupole gives a value of 0.82×10^{-13} erg. It should be noted that this relative orientation does not appear in the ice structure.

§ The figure ½ is exact only if the HOH angle is assumed to be tetrahedral.

[23] H. Margenau and V. W. Myers, Phys. Rev. **66**, 307 (1944).

[24] W. H. Barnes, Proc. Roy. Soc. (London), **A125**, 670 (1929). More recent studies over more limited temperature ranges have confirmed Barnes' analysis. See: H. D. Megaw, Nature **134**, 900 (1934); P. G. Owston and K. Lonsdale, J. Glaciol **1**, 118 (1948).

[25] Wollan, Davidson, and Shull, Phys. Rev. **75**, 1348 (1949).

[26] W. Kauzman, Revs. Modern Phys. **14**, 40 (1942).

[27] W. M. Latimer, Chem. Revs. **44**, 64 (1949).

[28] J. M. Adams, Proc. Roy. Soc. (London) **A128**, 588 (1930). F. Rossmann, Experientia **6**, 182 (1950). F. Jona and P. Scherrer, Helv. Phys. Acta **25**, 35 (1952). For a treatment of the appearance of piezoelectricity in crystals, see: W. A. Wooster, *Crystal Physics* (Cambridge University Press, Cambridge, 1938).

These observations imply that oriented domains with a net dipole moment may be found within the ice structure, but that in many cases the domains are twinned so that the net moment for the crystal may be approximately zero. The evidence for at least a locally ordered structure seems inconsistent with the results of investigation by neutron diffraction.

C. Energy of Sublimation of Ice at 0°K

Subject to the assumption that the potential energy U of two H_2O molecules is independent of the positions of other molecules:

$$\tfrac{1}{2}\sum_{\{\mathbf{r}\}} U(\mathbf{r}) = E^0 + E_{\text{vib}}{}^0.$$

$U(\mathbf{r})$ is the potential between any molecule in the lattice with another molecule at the lattice point defined by $\mathbf{r}$ and the sum is taken over the set of all $\mathbf{r}$; E^0 is the experimental energy of sublimation of ice and $E_{\text{vib}}{}^0$ is the zero point energy of ice. Various somewhat different values have been quoted, but the data given in references listed below[29] yield $E^0 = 11.3_6$ kcal/mole and $E_{\text{vib}}{}^0 = 0.4_3$ kcal/mole.

III. DIPOLE ENERGY OF ICE

A. General Problem

If it is assumed that two hydrogens are located near each oxygen, the dipole vector for a H_2O molecule may be directed along any of the six bisectors of the tetrahedral angle formed by an oxygen with two adjacent oxygens. The assumption that the same unit cell which Barnes[24] established for the oxygens is valid for the H_2O molecules already allows eighteen different orientations of the hydrogens. The striking fact is that each of these orientations yields a net dipole moment along the z' axis, which in Adams' and Rossmann's investigations appeared to be a polar axis! This suggests that further attempts to grow large crystals and to combine the study of their growth and decay with measurements of their axial dielectric properties might yield interesting information.

Unfortunately, therefore, comparative study of polar and nonpolar structures requires consideration of even larger unit cells. Since Barnes' assignment of symmetry was based on observations on the oxygens, there is no compelling guide for a choice of shape for a larger unit. As a compromise between the desirability of considering all possible orientations and the ability to consider but few, a unit cell composed of four of Barnes' units was chosen. If (l_1', l_2', l_3') are integers denoting l_1' unit translations along the x' axis, etc., then the four Barnes' units selected are: (0, 0, 0), (1, 0, 0), (0, 1, 0), (1, 1, 0). Any oxygen position in the crystal may now be defined by the symbol $xl_{1'}, l_{2'}, l_{3'}$ where $x = a, b, c, d$ specifies the type of position and (l_1', l_2', l_3') is the set of three integers which gives the unit translations along the (x', y', z') axes required to reach the unit cell in which the position lies.

The number of hydrogen orientations consistent with this unit cell and the requirement that one hydrogen is located along each O—O bond and two are near any one oxygen is now appalling. Nevertheless, all the orientations consistent with the assumption that the hydrogens near the a_{000} oxygen were located along the $a_{000}b_{000}$ and $a_{000}b_{-100}$ "bonds" were examined.|| The ratio of the largest to the smallest near-neighbor interaction energies found for those 65 orientations which gave no net moment to the ice structure was 1.86. However, the energies, including the next-nearest neighbor interactions, had such a narrow spread that it seemed impossible to guess which arrangements would be more stable, or, indeed, to predict which arrangements might have the same energy.

It was therefore necessary to use a precise method for calculating the energy of interaction of a dipole with a crystal of dipoles. Since the dipole-dipole energy varies as r^{-3} and the energy sum is taken over a three-dimensional lattice, the failure of a near-neighbor approximation is scarcely surprising.

B. Formulas for Energy of a Crystal of Dipoles

The necessary theory for this type of calculation has been developed by Ewald[30] and Kornfeld.[31] Ewald conceived of an elegant approach to the problem of determining the potential of a general ionic crystal. However, since the fundamental assumptions of the method are not completely clear in Ewald's article, they are set forth here.

The two following assumptions are equivalent: (1) the potential $U_F(\mathbf{r})$ produced by an ionic crystal F at the endpoint of a vector $\mathbf{r}$ (not a lattice point) is well defined by the conditions that the crystal have zero net charge and that the length of the crystal in any direction exceeds a certain minimum value. (2) There exists a function $U(\mathbf{r})$ to which the potential $U_F(\mathbf{r})$ of a finite uncharged lattice will converge as the length of each of the three axes becomes infinite. Thus the physical assumption (1) specifies a definite class of permissible orders of summation for the conditionally convergent series corresponding to the potential of an infinite lattice.

The direct calculation of $U(\mathbf{r})$ is laborious because of the slow convergence of the partial sums corresponding to finite uncharged lattices. Moreover, the conditional and non-uniform convergence in general prohibits the

[29] W. F. Giauque and J. W. Stout, J. Am. Chem. Soc. **58**, 1144 (1936). W. A. Roth, Z. physik chem. **A183**, 38 (1938). M. Trautz and H. Ader, Z. Physik **89**, 12 (1934). F. G. Keyes, Trans. Am. Soc. Mech. Engrs. **70**, 621 (1948).

|| 191 consistent orientations were found. Choices of positions were made until a consistent structure was obtained and then other possible choices were considered, stepwise. However, a few may well have been omitted by oversight.

[30] P. P. Ewald, Ann. Physik **64**, 253 (1921).

[31] H. Kornfeld, Z. Physik **22**, 27 (1924).

direct application of the methods of algebra or the calculus to obtain a more amenable form. These difficulties may be surmounted by introducing a suitable approximating function for the potential of a point charge which will define an absolutely and uniformly convergent series which can be transformed to yield functions which are easier to compute. Suppose:

(1) k_0 is a complex number and for each k_0, $\varphi(\mathbf{r}, k_0)$ is an analytic function in the domain $R_3 - \{(0, 0, 0)\}$. For each k_0, $(0, 0, 0)$ is a pole of $\varphi(r, k_0)$;

(2) $U_F(\mathbf{r}, k_0)$ is the potential arising from a finite lattice of singularities each of which is defined by the potential $\varphi(\mathbf{r}, k_0)$;

(3) For each finite lattice F

$$\lim_{|k_0| \to 0} U_F(\mathbf{r}, k_0) = U_F(\mathbf{r}),$$

and the convergence is uniform over $R_3 - \{C(i, \rho)\}$ where R_3 is the set of all (x', y', z') and $\{C(i, \rho)\}$ is the set of all open circles $C(i, \rho)$ of radius ρ centered at the ith point of the array and ρ is any positive number;

(4) $U_F(\mathbf{r}, k_0)$ converges absolutely and uniformly to $U(\mathbf{r}, k_0)$ in $R_3 - \{C(i, \rho)\}$ as the length of each of the independent axes for the array tends to infinity.

Then it is possible to carry through the operations of algebra and the calculus on $U(\mathbf{r}, k_0)$ with the assurance that after applying the operations to $U(\mathbf{r}, k_0)$, then

$$\lim_{|k_0| \to 0} U(\mathbf{r}, k_0) = U(\mathbf{r}).$$

The selection of $q \exp(ik_0 r)/r$ for an approximating function enabled Ewald to apply a transformation on a theta function of three variables to split the one series for $U(\mathbf{r}, k_0)$, which converges slowly, into two series: $U_1(\mathbf{r}, k_0, \epsilon)$ and $U_2(\mathbf{r}, k_0, \epsilon)$ such that $U(\mathbf{r}, k_0) = U_1 + U_2$. ϵ is an arbitrary parameter with the units of reciprocal distance whose selection governs the rapidity of convergence of U_1 and U_2. Suitable choice of ϵ renders both series tractable. The more difficult problem of determining the potential at a lattice point produced by all other points in the lattice was then solved by taking

$$\lim_{|k_0| \to 0} \left[\lim_{\mathbf{r} \to (0, 0, 0)} (U_i(\mathbf{r}, k_0) - \varphi_i(\mathbf{r}, k_0)) \right], \quad i = 1, 2.$$

In the preceding expression, $\varphi_i(\mathbf{r}, k_0)$ is the contribution to $U_i(\mathbf{r}, k_0)$ of a singularity with the potential $\varphi(\mathbf{r}, k_0)$ located at $\mathbf{r} = (0, 0, 0)$.

Since the potential of a dipole of moment p_1 and characteristic direction $\mathbf{s}$ is $p_1(\partial 1/r/\partial s)$, Kornfeld[31] was able to obtain the potential $U_D(\mathbf{r})$ of a crystal of dipoles by: (1) taking the directional derivative of $U(\mathbf{r}, k_0)$ along the dipole characteristic direction $\mathbf{s}$; (2) taking the limit as $|k_0| \to 0$.

In Ewald's development it is necessary to decompose the whole crystal lattice into sublattices of points each of which is obtained from any other point in the sublattice by a combination of an integral number of unit translations along three independent axes. The energy of a dipole with characteristic direction $\mathbf{s}_1 = (s_1^1, s_1^2, s_1^3)$ interacting with a sublattice of dipoles with characteristic direction $\mathbf{s}_2 = (s_2^1, s_2^2, s_2^3)$ may be written as

$$E(\mathbf{r}, \mathbf{s}_1, \mathbf{s}_2) = \sum_{i,j} a_{ij} s_1^i s_2^j, \quad i, j = 1, 2, 3.$$

$\mathbf{r}$ is a vector with its initial point at $\mathbf{s}_1$ and its end point at some point of the sublattice. The a_{ij} are constants determined solely by the geometry of the sublattice.

Kornfeld's general formulas[31] first were somewhat simplified by a consideration of the symmetry of the ice structure and then were used to compute the a_{ij} for each of the sixteen sublattices (corresponding to each of the four distinct oxygen positions: a, b, c, d).¶ The values of the a_{ij} were then used to construct a series of tables which permit the calculation of the dipole energy of any preassigned arrangement of the hydrogen positions.**

Finally, the tables were used to study eleven different arrangements $(A_1, \cdots, A_{11})$ of the hydrogens in the unit cell.†† The results are collected in Table I which also states whether the arrangement does or does not give a net moment to the crystal.

The arrangements were constructed by making

TABLE I. Dipole-dipole energy of ice as a function of hydrogen orientations.

Arrangement	Σs	U_D kcal/mole
A_1	$\neq 0$	4.447
A_2	$=0$	4.571
A_3	$\neq 0$	4.634
A_4	$\neq 0$	4.255
A_5	$=0$	5.062
A_6	$\neq 0$	4.683
A_7	$=0$	4.773
A_8	$\neq 0$	4.548
A_9	$\neq 0$	4.769
A_{10}	$\neq 0$	4.544
A_{11}	$=0$	4.657

U_D is the dipole energy of ice in kcal/mole at 0°K. μ is assumed to be 1.83D. See N. E. Dorsey, *Properties of Ordinary Water-Substance* (Rheinhold Publishing Corporation, New York, 1940), pp. 46–49. Since the contribution of the interactions of the permanent dipoles to the potential energy of the ice crystal is desired, the value of the dipole moment of the isolated molecule is used. The interaction energy of the induced with isolated and induced moments is crudely approximated in the semi-empirical $1/r^6$ term of the pair-potential. In any attempt to correlate gas and crystal data it would be inconsistent to consider induced moments apart from the $1/r^6$ term where they are roughly approximated in the pair-potential function used in treating the gas.

¶ The Ewald technique has the definite advantage of providing a possible independent check on the calculations by the expedient of selecting two different values of ϵ. However, it must be noted that approximate agreement using two different values of ϵ is meaningless. I obtained values for the series for a_{ij} in relative agreement within a few percent, but later found they were off in absolute value by a hundred percent. Separate sums for $\epsilon = 1/r_0$ and $\epsilon = (\frac{1}{2})^{\frac{1}{2}} r_0$ were made for E_1 and E_2. In each case the values checked to one part in the seventh digit.

** The tables, which are lengthy, are presented in the author's dissertation, "Hydrogen bonding and the interactions of water molecules."

†† The arrangements are defined in Appendix II.

choices of a hydrogen position and determining all consequences of each successive choice until the complete arrangement had been determined. If the possible arrangements resulting from any one choice are grouped together, in each case a structure with zero moment has the most negative energy. However, for the particular unit cell considered, there are approximately three times as many structures with, as without, net moments.

Considering only near and next-nearest neighbor interactions, the ice structures with zero net dipole moment had energies which fell within such a narrow range that it was impossible to predict which among them would be most stable.‡‡ The exact values for the dipole energies of arrangements $(A_1, \cdots, A_{11})$ all lie within the approximate range of 4.4 to 5.1 kcal. Since the dipole potential lacks symmetry that could account for the known ice structure, it would appear that the consideration of higher order multipoles (whose symmetry at least makes the ice structure more reasonable) might be expected to narrow this spread of energies as a function of hydrogen orientations.§§

Because of the apparently polar character of the z' axis,|| || somewhat different energies might be expected as the hydrogen orientations with respect to that axis are varied. In view of the absence of any recognized direction perpendicular to the z' axis, it would be interesting to see whether structures which differed only in hydrogen orientations with respect to the x' and y' axes might have energies which fall in a narrower range than those which differed in orientations with respect to the z' axis as well.

It is now possible to determine whether the empirical constants for the dispersion and repulsive forces required by a point dipole model for the water molecule will fit both gas and crystal data.

Mere comparison of the constants determined from the crystal by use of (1) the sum of the known energy of sublimation and the zero point energy; (2) the condition that $(\partial E/\partial r)_{0°K}=0$[32] with the constants which Stockmayer[13] obtained from virial studies indicates that this will be impossible. In fact, the virial coefficient at 600°K predicted by the crystal constants is more than two to three times too large.

It follows that available data are sufficiently sensitive to reject the point dipole model and that it is necessary to consider a point charge model. A possible explanation for the amazing success of the point dipole model for correlating gas data, and its utter failure to embrace both gas and crystal data will be considered in Sec. IV where various point charge models are examined.

IV. POINT CHARGE MODELS

A. Models Previously Considered; Selection of a Model for Subsequent Calculation

Bernal and Fowler,[17] Magat,[18] Bauer and Magat,[19] Verwey,[20] and Rowlinson[21] have considered various point charge models. Bernal and Fowler made an approximate calculation of the energy of vaporization of ice based on a point charge model with a center of negative charge 2ϵ located along the bisector of the HOH angle, removed 0.15 A° from the center of mass of the oxygen, and a charge of plus ϵ located on each hydrogen. ϵ was chosen to reproduce the known dipole moment.

As an independent check on the charge distribution assumed in their model, the authors compared the predicted moment of the OH bond along the HH line with the value calculated from the dipole moment of hydroquinone under the hypothesis that the OH groups were freely rotating. Although the agreement was excellent, such an argument is based on the rather dubious use of bond dipoles. Moreover, Lander and Svirbely[33] have since reported that a redetermination of the moment for hydroquinone gave 1.4D, whereas free rotation would predict 2.21D.

Magat considered two models in addition to the one proposed by Bernal and Fowler. In the first, the charge was placed on the oxygen and the hydrogens; in the second, a charge of plus one was placed on the hydrogens and the center of negative charge was displaced along the bisector of the HOH angle to the position required to reproduce the known dipole moment. Magat found that the energies predicted by the three models at a distance of 2.76 A° differed for some orientations by as much as a factor of ten.

Verwey objected that Bernal and Fowler's model considered only the effect of the hydrogens on two L electrons. He argued that the reduction of the dipole moment from that of two H embedded in a spherically symmetric $O^=$ resulted from (1) a screening of part of the H charge by a concentration of electronic charge around each hydrogen and (2) a shift in the center of gravity of the remaining electrons of the $O^=$.

In his treatment of the gas, Rowlinson[21] used a

‡‡ See Sec. II-A.

§§ The dipole potential has cylindrical symmetry about its characteristic direction and the energetically favored dipole-dipole orientation is head to tail. Therefore it seems reasonable to expect that a lattice of point dipoles should form a tetragonal crystal. The equipotential curves defined on any sphere about a H_2O molecule by

$$\sum_{n=1}^{N} \varphi(P_n).$$

$\varphi(P_n)$: the potential of the nth order multipoles (see IV-C) are complicated for $N \geqq 2$ and cannot easily be related to the ice structure. The point charge model (see IV-A), which determines the multipoles, possesses 4 charge centers on a triangle with an approximately tetrahedral angle and a potential symmetric with respect to the HOH plane and the perpendicular plane bisecting the HOH angle. Although such a symmetry does not lead in any obvious way to a tetrahedral structure, it is not in such marked dissonance with it.

|| || See Sec. II.

[32] J. Corner, Trans. Faraday Soc. **35**, 711 (1939), has derived equations for considering the effect of zero point energy on the equilibrium distance at 0°K. However, this correction would increase the magnitude of the error found here, since the zero point energy increases r_0.

[33] J. J. Lander and W. J. Svirbely, J. Am. Chem. Soc. **67**, 322 (1945).

model with no charge displacement, but in his discussion of the crystal, he considered one with a displacement of the negative charge on the oxygen perpendicular to the HOH plane.

If no reason can be adduced for favoring any one model, Magat's conclusion that widely different energies are obtained as empirical parameters are varied would certainly leave the significance of calculations based on a point charge model open to serious question. It is, therefore, imperative to consider carefully the choice of a model.

Verwey's criticism that the Bernal and Fowler model for H_2O failed to consider adequately the effect of the shift of center of gravity of the negative charge is well chosen. However, for calculations at short distances, it is an even worse approximation to consider the negative charge of the molecule (Verwey excepted the 2K electrons and the charge centered at the hydrogens) as consisting wholly of one point charge. Such a model seriously underestimates the effective screening of the nuclear charge and therefore seriously overestimates the higher multipole moments of water which the model is designed to approximate.¶¶ Now any spherically symmetric charge distribution contained within a sphere C defines a potential exterior to C which is the same as the potential of a point charge equal in magnitude to the net charge within C, placed at the center of symmetry of the distribution. Therefore, if the center of mass of the oxygen is selected as the reference point for the Taylor expansion (see Appendix I), then the position and magnitude of the point charges used to approximate the permanent multipole moments of the H_2O molecule are determined solely by the deviation of the charge distribution from spherical symmetry (relative to the center of mass of the oxygen). Since Verwey's model places at a single point all the negative charge of the molecule with the exception of the 2 K electrons and the negative charge centered at the hydrogens, it seriously overestimates this deviation.

It would seem better, in lieu of detailed information on the charge distribution, to assume, rather, a point charge model for which the difference between $2e^-$ and the charge centered near the H is located at the center of gravity of negative charge. Admittedly, this argument is some what less than compelling. Practically, Verwey's model has the disadvantage of an extreme sensitivity to a slight variation in parameters.

If there were zero dipole moment along the OH bond, then the center of gravity of negative charge would be 0.11A° from the oxygen nucleus.[34] The finite dipole implies that the center of gravity of the negative charge is less than 0.11A° from the oxygen nucleus. It would seem that Verwey's objection to the distance of 0.15A° along the bisector of the HOH angle for the displacement of negative charge from the oxygen nucleus in the Bernal-Fowler model is justified.

For calculations on ice, it is simpler to use a four charge model and to place the negative charge centers along the OH bonds. If a negative charge center is placed about 0.05A° from the oxygen nucleus on each OH bond, the maximum uncertainty in the placement is 5 percent for this type of model.

Some inquiry into the sensitivity of the model with respect to variation in parameters is essential. For this purpose, the interaction of an $a_{000}H_2O$ with a $b_{000}H_2O$ in the ice crystal was selected. The hydrogens on the a_{000} oxygen were assumed to have α, β orientations; those on the b_{000} oxygen to have β, γ orientations (see Appendix II).

At $r_0=2.72$A°, the energies of interaction for the three models: (1) negative charge of 3.313×10^{-10} esu undisplaced from the oxygen nucleus, (2) a negative charge of 1.756×10^{-10} esu $0.02r_0$ along each OH bond, (3) 1.869×10^{-10} esu $0.04r_0$ along each OH bond, give energies of interaction of 3.44×10^{-13}, 3.56×10^{-13}, 3.68×10^{-13} erg, respectively.*** Perhaps, therefore, the variation of this model within the aforementioned limits will not produce the overwhelming variation in energy of interaction which Magat found.

The four point charge model with 1.756×10^{-10} esu at $0.02r_0=0.054$A° along each OH bond is adopted for subsequent calculations.

B. The Point Charge Model and the Failure of the Point Dipole Model to Embrace Both Gas and Crystal Data

A point charge model suggests possible reasons for the failure of the point dipole model. For the particular $a_{000}b_{000}$ interaction described in the preceding section, the interaction energy for the point charge model was 3.56×10^{-13} erg per molecule pair; for the point dipole model, only 1.66×10^{-13} erg per molecule pair. This discrepancy arises because the ratio of (a) the distance of the charge center on each hydrogen from the reference point for the Taylor series expansion (the center of mass of the oxygen) to (b) the distance of separation of the two reference points is rather large, i.e., 0.35.

Whereas the most favorable orientation gives an angle factor of -2 in the formula for the dipole-dipole interaction energy, in the crystal the most negative factor is -1.5, and at most 1/4 of the near-neighbors possess that; the remaining 3/4 can have at most -1.

The excellent numerical accuracy of the calculated values for the second virial coefficient based on the dipole approximation would suggest that the value of the potential function which Stockmayer[13] constructed might not be too far in error after the average over angles is taken. However, the expected failure of the

¶¶ For discussion of multipoles see reference 35 and Appendix I.

[34] The OH distance in $H_2O(g)$ in the lowest vibrational level is 0.957A°. G. Herzberg, *Infrared and Raman Spectra* (D. Van Nostrand Company, Inc., New York, 1945), p. 489. The parameter of the isolated molecule is used, since, as explained in footnote to Table I, the induced effects are crudely approximated in the. $1/r^6$ term of the pair potential.

*** In each case the HOH angle was assumed to be tetrahedral.

TABLE II. Comparison of multipole approximation with a point charge calculation for the nearest neighbors in the arrangement of hydrogens A_5.

Interacting multipoles	Energy I	Energy II
First-order term		
Dipole-dipole	-2.219×10^{-13}	-1.664×10^{-13}
Second-order term		
Dipole-quadrupole	−0.412	−0.825
Third-order terms		
Quadrupole-quadrupole	−0.767	−0.511
Dipole-octupole	−0.065	−0.162
Fourth-order terms		
Quadrupole-octupole	−0.241	−0.361
Dipole-fourth order pole	−0.109	−0.284
Fifth-order terms		
Octupole-octupole	+0.448	+0.484
Quadrupole-fourth-order pole	−0.056	−0.148
Dipole-fifth-order pole	−0.088	−0.098
	−3.509	−3.569
Point charge energy	−3.823	−3.559
Percent error at fifth-order multipole term	8.2	0.28

Energy in ergs per molecule pair at 0°K. I: Energy for a–c type interactions. II: Energy for a–b type interactions.

point dipole model to reasonably approximate the angular dependence of the potential function makes it impossible for the model to embrace both the gas data, where a weighted average is taken over all orientations, and the crystal data which involves selected orientations.

C. Calculations on the Point Charge Model

In a calculation using a point charge model it is impossible to separate in a straightforward manner geometric factors which depend only on the space structure of oxygen positions from factors which involve the arrangement of the hydrogens. Such a separation is necessary if a study of various hydrogen orientations is to be at all practicable. Moreover, the use of a point charge model for gas calculations is not feasible since the expression for energy of interaction of point charges located at distinct points cannot be integrated in any simple fashion.

Fortunately, the introduction of the Taylor series expansion, i.e., the use of multipoles,[35] reduces the problem to the simpler one of angularly dependent forces arising from singularities at the same point.

The desired extension of this study to the consideration of point charge models using exact lattice sums for multipole interactions beyond the dipole approximation is a lengthy project which has not yet been undertaken. Preliminary to this extension, the arrangement of hydrogens A_5 was selected for further study.†††

As a check on the number of terms required for satisfactory multipole approximation, both point charge and multipole calculations were made for the nearest-neighbor positions in A_5. Fortunately, A_5 has such a high symmetry that there are only two fundamentally different interactions: those between a and c positions and those between a and b positions. The results of the calculations are given in Table II.

It appears that the multipole approximation including only dipole-quadrupole, quadrupole-quadrupole, and dipole-octupole interactions, which Rowlinson[21] used, still leaves a considerable error. Consideration of multipole interactions through at least terms of the fifth order and a determination of the discrepancy between the multipole approximation and the point charge model for nearest-neighbor interactions would seem to be required for any careful study of a point charge model.

TABLE III. Multipole energies for next-nearest neighbors in ice.

Interacting multipoles	Energy
Second-order term	
Dipole-quadrupole	-0.676×10^{-13}
Third-order terms	
Quadrupole-quadrupole	−0.362
Dipole-octupole	−0.195

Energy for the thirteen next-nearest neighbors in ergs per molecule pair at 0°K.

TABLE IV.

	c (erg cm^6)	λ (erg cm^n)	σ(A°)
Stockmayer			
$n=24$	7.04×10^{-59}	6.08×10^{-195}	2.76
Crystal constants			
$n=24$	3.6×10^{-59}	2.5×10^{-195}	2.73
$n=12$	9.4×10^{-59}	4.5×10^{-104}	2.80

To obtain a zeroth approximation to the higher order multipole energy of the ice structure A_5, the dipole-quadrupole, quadrupole-quadrupole, and dipole-octupole contributions were summed for the thirteen next-nearest neighbors. (The dipole energy was calculated for the entire crystal.) The results are presented in Table III.‡‡‡

Unfortunately, Table III demonstrates that, in general, terms of higher than third order are required for next-nearest neighbors and that even the next-nearest neighbor approximation is rather inadequate for second-and third-order terms in the Taylor series expansion.

Nevertheless, the data at hand should be adequate to obtain some indication of the possibility of correlating

[35] For a good discussion of multipoles, see: E. W. Hobson, *The Theory of Spherical and Ellipsoidal Harmonics* (Cambridge University Press, Cambridge, 1931); H. Margenau, Revs. Modern Phys. **11**, 5 (1939).

††† For definition of the symbol A_5 see Appendix II. A_5 was that one of the eleven arrangements of hydrogens studies in complete detail which gave the highest dipole-dipole energy.

‡‡‡ The dipole-dipole energy for the entire crystal, 3.516×10^{-13} erg/molecule (see Table I) may be compared with 3.606×10^{-13} erg/molecule for nearest neighbor interactions. The agreement between nearest neighbor and crystal energies for dipolar interactions in A_5 is fortuitous; for other structures the two energies differ by a factor of about 1.8.

TABLE V.

A	a_{000}	a_{100}	a_{010}	a_{110}	b_{000}	b_{100}	b_{010}	b_{110}	c_{000}	c_{100}	c_{010}	c_{110}	d_{000}	d_{100}	d_{010}	d_{110}
A_1	$\alpha\beta$	$\beta\gamma$	$\beta\delta$	$\beta\delta$	$\beta\gamma$	$\gamma\delta$	$\beta\gamma$	$\beta\delta$	$\gamma\delta$	$\alpha\delta$	$\beta\gamma$	$\beta\gamma$	$\alpha\delta$	$\alpha\beta$	$\beta\delta$	$\beta\gamma$
A_2	$\alpha\beta$	$\beta\gamma$	$\beta\delta$	$\beta\delta$	$\beta\gamma$	$\gamma\delta$	$\beta\gamma$	$\beta\delta$	$\gamma\delta$	$\alpha\delta$	$\alpha\gamma$	$\alpha\gamma$	$\alpha\delta$	$\alpha\beta$	$\alpha\delta$	$\alpha\gamma$
A_3	$\alpha\beta$	$\beta\delta$	$\alpha\beta$	$\beta\delta$	$\beta\gamma$	$\gamma\delta$	$\beta\gamma$	$\gamma\delta$	$\gamma\delta$	$\alpha\beta$	$\gamma\delta$	$\alpha\beta$	$\alpha\delta$	$\beta\gamma$	$\alpha\delta$	$\beta\gamma$
A_4	$\alpha\beta$	$\beta\delta$	$\beta\delta$	$\beta\delta$	$\beta\gamma$	$\gamma\delta$	$\beta\gamma$	$\beta\gamma$	$\gamma\delta$	$\alpha\beta$	$\alpha\gamma$	$\alpha\beta$	$\alpha\delta$	$\beta\gamma$	$\alpha\delta$	$\gamma\delta$
A_5	$\alpha\beta$	$\gamma\delta$	$\alpha\beta$	$\gamma\delta$	$\beta\gamma$	$\alpha\delta$	$\beta\gamma$	$\alpha\delta$	$\gamma\delta$	$\alpha\beta$	$\gamma\delta$	$\alpha\beta$	$\alpha\delta$	$\beta\gamma$	$\alpha\delta$	$\beta\gamma$
A_6	$\alpha\beta$	$\gamma\delta$	$\beta\delta$	$\gamma\delta$	$\beta\gamma$	$\alpha\delta$	$\beta\gamma$	$\alpha\beta$	$\gamma\delta$	$\alpha\beta$	$\alpha\gamma$	$\alpha\beta$	$\alpha\delta$	$\beta\gamma$	$\alpha\delta$	$\gamma\delta$
A_7	$\alpha\beta$	$\gamma\delta$	$\beta\delta$	$\beta\gamma$	$\beta\gamma$	$\alpha\delta$	$\beta\gamma$	$\beta\delta$	$\gamma\delta$	$\alpha\beta$	$\alpha\gamma$	$\alpha\delta$	$\alpha\delta$	$\beta\gamma$	$\alpha\delta$	$\alpha\gamma$
A_8	$\alpha\beta$	$\gamma\delta$	$\beta\delta$	$\beta\gamma$	$\beta\gamma$	$\alpha\delta$	$\beta\gamma$	$\beta\delta$	$\gamma\delta$	$\alpha\beta$	$\beta\gamma$	$\beta\delta$	$\alpha\delta$	$\beta\gamma$	$\beta\delta$	$\beta\gamma$
A_9	$\alpha\beta$	$\gamma\delta$	$\beta\delta$	$\beta\delta$	$\beta\gamma$	$\alpha\gamma$	$\beta\gamma$	$\beta\delta$	$\gamma\delta$	$\alpha\beta$	$\alpha\gamma$	$\alpha\gamma$	$\alpha\delta$	$\beta\delta$	$\alpha\delta$	$\alpha\gamma$
A_{10}	$\alpha\beta$	$\gamma\delta$	$\beta\delta$	$\beta\delta$	$\beta\gamma$	$\alpha\gamma$	$\beta\gamma$	$\beta\delta$	$\gamma\delta$	$\alpha\beta$	$\beta\gamma$	$\beta\gamma$	$\alpha\delta$	$\beta\delta$	$\beta\delta$	$\beta\gamma$
A_{11}	$\alpha\beta$	$\beta\delta$	$\alpha\beta$	$\beta\delta$	$\beta\gamma$	$\gamma\delta$	$\beta\gamma$	$\gamma\delta$	$\gamma\delta$	$\alpha\gamma$	$\gamma\delta$	$\alpha\gamma$	$\alpha\delta$	$\alpha\beta$	$\alpha\delta$	$\alpha\beta$

both gas and crystal data by means of a point charge model. For this purpose, the sum of the known energy of sublimation and the zero point energy is used in conjunction with the condition that $(\partial E/\partial r)_{0°K}=0$ and assumed values of the repulsive exponent to obtain empirical values for: (1) the coefficient c of the dispersion plus dipole-induced dipole forces (both of which have $1/r^6$ as the leading term), (2) the coefficient λ of the repulsive forces, and (3) $\sigma=(\lambda/c)^{1/n-6}$, the value of r at which the attractive and repulsive forces whose angular dependence is neglected are exactly balanced.§§§ $E^0+E_{\text{vib}}{}^0$ is assumed to be given by the expression:

$$E^0+E_{\text{vib}}{}^0=K_1c/r^6+K_2\lambda/r^n+M.$$

M is the energy arising from the interaction of the permanent multipoles of H_2O (obtained from Tables I, II, III); K_1 and K_2 are geometric structure factors. For the ice crystal, $K_1=2.559_8$; $K_2=2.0200$ if $n=12$, 2.0004 if $n=24$.

In Table IV the values of c, λ, and σ are compared with values Stockmayer[13] obtained from his study of the second virial coefficient of steam, using a point dipole model.

Using Stockmayer's values for c, the $1/r^6$ term in the expansion of the $\exp(-c/r^6kT)$ factor of $\exp(-U/kT)$ in the second virial coefficient is nearly the same as that for $\exp[-(p_1)^2g/r^3kT]$, after integrating the g-factor over angles.|| || || Using $n=24$, the introduction of higher order multipole interactions has decreased c by a factor slightly less than two and λ by a factor somewhat greater than two. However, for the selected orientations involved in A_5, the energy arising from angularly dependent forces has been increased by well over a factor of two.

These relative changes, which tend to cancel, suggest that a properly chosen point charge model may suffice for the correlation of both second virial and crystal data. The ultimate purpose of this study will require a careful investigation of this possibility.

Finally, the electrostatic energy of A_5, the ice structure with the highest dipole-dipole energy, was found to be: dipole-dipole energy 5.06 kcal/mole, dipole-quadrupole and higher order multipole energy, *ca* 6.15 kcal/mole; dispersion plus multipole-induced multipole minus repulsive energy, *ca* 0.59 kcal/mole.¶¶¶

§§§ See Margenau and Meyers, reference 23, for an excellent discussion of basic assumptions used here.

|| || || The integral of g^n vanishes for odd powers of n.

ACKNOWLEDGMENT

I have been fortunate in enjoying Dr. Bruno H. Zimms' critical comments and suggestions during the course of this reasearch. His incisive thought has been an inspiration.

APPENDIX I. MULTIPOLE MOMENTS OF H_2O[35]

It seems reasonable to suppose that the dispersion and repulsive forces exhibited by a water molecule have their highest symmetry relative to some point near the center of mass of the oxygen. Moreover, for crystal calculations, the center of mass of the oxygen is the only convenient reference point for the expansion of the Taylor series. With this choice of reference point, the principal axes which will diagonalize the second order term in the Taylor series expansion of the potential function for a water molecule is obvious.

Let the positive Y axis lie along the bisector of the HOH angle directed away from the hydrogens. Let the X axis lie in the HOH plane, directed so that in passing from the X to the Y axis a positive angle of 90° is traversed. Let $\mathbf{Z}=\mathbf{X}\times\mathbf{Y}$.

Consider the point charge model adopted in IV-A. Relative to the (X, Y, Z) axes, the coordinates of the charges are:

$$-q\text{: } 0.02r_0((2/3)^{\frac{1}{2}}, -(1/3)^{\frac{1}{2}}, 0);$$
$$-q\text{: } 0.02r_0(-(2/3)^{\frac{1}{2}}, -(1/3)^{\frac{1}{2}}, 0);$$
$$q\text{: } 0.3518r_0((2/3)^{\frac{1}{2}}, -(1/3)^{\frac{1}{2}}, 0);$$
$$q\text{: } 0.3518r_0(-(2/3)^{\frac{1}{2}}, -(1/3)^{\frac{1}{2}}, 0).$$

Let p_n be the moment of an nth order pole whose n characteristic directions are $X_1, \cdots, X_M, Y_1, \cdots, Y_N, Z_1, \cdots, Z_Q (M+N+Q=n)$. Then $P_n=0$ unless $Q=0$ and M is even. If M is even, $Q=0$, then:

$$p_n=2q(-1)^N[(0.3518)^n-(0.02)^n]\sin^M(A/2)\cos^N(A/2),$$

where A is the HOH angle.

If A is assumed to be the tetrahedral angle, then P_{XX} and P_{YY} together are equivalent to a single quadrupole of moment $-2P_{YY}$ whose characteristic directions in the (XYZ) system are $(-(1/2)^{\frac{1}{2}}, 0, (1/2)^{\frac{1}{2}})$ and $((1/2)^{\frac{1}{2}}, 0, (1/2)^{\frac{1}{2}})$.[36]

¶¶¶ The sum of the complete dipole energy of A_5 and the approximate values of the higher order multipole energy as determined from Tables II and III, was subtracted from the known energy of sublimation of ice to give an approximate value for the difference between the dispersion plus multipole induced multipole and repulsive energy terms.

[36] For a simple method for reducing the second-order term of the Taylor series to a single quadrupole, see: E. S. Campbell, J. Chem. Phys. (to be published, 1952).

APPENDIX II-A. DIPOLE DIRECTIONS IN THE ICE STRUCTURE

Let 0 be any oxygen position in the crystal. Let:

$x=(x'-y'/2)\cdot(8/3)^{\frac{1}{2}}\cdot r_0$; $y=y'(2)^{\frac{1}{2}}r_0$; $z=z'(8r_0/3)$.

(1) Consider the three positions closest to 0 which lie in a plane perpendicular to the z axis. Let:

α: the vector from 0 to that one of the aforementioned positions which will give α a negative x direction number

β: the vector from 0 to that one of the aforementioned positions which will give β a positive x direction number

γ: the vector from 0 to that one of the aforementioned positions which will give γ a zero x direction number

(2) δ: the vector to the fourth nearest position; δ has zero x and y direction numbers.

APPENDIX II-B. HYDROGEN POSITIONS FOR THE ELEVEN ARRANGEMENTS OF HYDROGENS STUDIED IN DETAIL

The first column in Table V, headed by A, gives the symbol which is used to designate the arrangement of the hydrogens defined in the same row of the table.

THE JOURNAL OF CHEMICAL PHYSICS VOLUME 20, NUMBER 9 SEPTEMBER, 1952

The Microwave Spectra, Structure, Dipole Moment, and Chlorine Nuclear Quadrupole Coupling Constants of Methylene Chloride*

ROLLIE J. MYERS† AND WILLIAM D. GWINN
Department of Chemistry and Chemical Engineering, University of California, Berkeley, California

(Received March 3, 1952)

The microwave spectra of $CH_2Cl_2^{35}$, $CH_2Cl^{35}Cl^{37}$, $CH_2Cl_2^{37}$, $CDHCl_2^{35}$, $CDHCl^{35}Cl^{37}$, $CD_2Cl_2^{35}$, and $CD_2Cl^{35}Cl^{37}$ have been examined and effective moments of inertia have been determined for these seven isotopic species. From these data the effective bond distances and angles were determined as C−Cl distance=1.7724±0.0005A, Cl−C−Cl angle=111°47′±1′, C−H distance=1.068±0.005A (average of all species), or 1.082A (extrapolated to infinite hydrogen mass), and H−C−H angle=112°0′±20′ (average of all species) or 112°58′ (extrapolated to infinite hydrogen mass). The best value for the dipole moment of methylene chloride was found from the Stark splitting to be $1.62\pm0.02\times10^{-18}$ esu. The chlorine nuclear quadrupole coupling constants were also determined and their relationship to the structure is discussed.

INTRODUCTION

PAST investigations have not established a complete structure for methylene chloride (CH_2Cl_2). The electron diffraction work[1] has provided values for the carbon-chlorine bond distance and the chlorine-carbon-chlorine bond angle, but it has not led to any information as to the placement of the hydrogen atoms in this molecule. Since the position of the hydrogen atoms is of considerable interest, we undertook this study of the microwave spectrum of methylene chloride. Our interest in this molecule was also enhanced by the problem of the quadrupole interaction of the two chlorine nuclei.

EXPERIMENTAL

The microwave spectrograph that was used for this investigation is very similar to that described previously.[2] As in those measurements, the frequencies of the absorptions were determined with the use of a crystal-controlled microwave frequency standard monitored continuously by comparison with radio station WWV. Frequencies listed with an accuracy of a few tenths of a mc/sec were determined by superimposing a frequency marker directly upon the absorption maxima. The apparent frequencies of the absorption maxima were determined by sweeping both from lower to higher frequencies and from higher to lower frequencies. The values recorded are the averages of these two values. This procedure eliminates the error due to different time delays in the frequency marker and microwave absorption circuits. Frequencies listed with an accuracy of a few mc/sec were determined by interpolating between frequency markers. These frequency markers occurred at least every 30 mc/sec on the absorption recordings.

The temperature coefficients of the absorptions were determined in a microwave cell which was cooled to solid carbon dioxide temperatures. It was found that at these temperatures methylene chloride was strongly adsorbed by the cell. For this reason we could only measure relative temperature coefficients.

In some cases it was found that the Stark components interfered with the observation of the quadrupole fine structure. In order to minimize this difficulty the conventional square wave modulation was replaced by a wave form of special shape. This wave form has a flat zero-based portion which is followed by a slowly rising exponential portion. This exponential rise has the effect of spreading the Stark components over a range of frequencies and decreasing their amplitude. This

* From the doctoral thesis of Rollie J. Myers (1951).
† U. S. Rubber Company Fellow 1950–51.
[1] L. O. Brockway, Revs. Modern Phys. 8, 231 (1936).
[2] Cunningham, Boyd, Myers, Gwinn, and LeVan, J. Chem. Phys. 19, 676 (1951).

special Stark modulation was used whenever quadrupole fine structure was being observed.

The dipole moment of methylene chloride was determined in a cell previously calibrated using the 1–2 line in $O^{16}C^{12}S^{32}$. It was the same cell and calibration as used previously.[2]

The ordinary methylene chloride was prepared by fractional distillation of a commercial grade. It boiled at 40.0°C corr. and had a $\eta_D^{25}=1.4212$. The deuterated and semideuterated samples were prepared by a method suggested by the technique of Bachrach.[3] Chloroform was allowed to react with acetic acid and zinc, and small quantities of methylene chloride were produced as a side product to the evolution of hydrogen gas. The methylene chloride was recovered by passing the evolved hydrogen gas through a trap cooled to solid carbon dioxide temperatures.

Semideuterated methylene chloride ($CDHCl_2$) was prepared using ordinary chloroform and deuterated acetic acid. Deuterated methylene chloride (CD_2Cl_2) was prepared using deuterated chloroform and deuterated acetic acid. Freshly distilled acetic anhydride and heavy water were utilized for the preparation of deuterated acetic acid, and the deuterated chloroform was obtained by the method of Earing and Cloke.[4]

The deuterated samples of methylene chloride were fractionated by a small Vigreux column. In the sample of CD_2Cl_2 no lines were found which were attributed to $CDHCl_2$. This indicates that the isotopic purity of the samples is very high.

SPECTRAL OBSERVATIONS AND ASSIGNMENT

The most striking aspect of the microwave spectrum of methylene chloride is the large number of absorptions that are observed. Previous investigators[5,6] have reported several absorptions in the region near 24,000 mc/sec. We found that there was an almost random distribution of absorptions from 17,000 to 36,000 mc/sec. Utilizing a nominal spectrograph sensitivity ($\sim 10^{-8}$ cm^{-1}) we observed about one distinct absorption every 50 mc/sec.

We were also impressed by the sharpness of many of the strongest lines and by the occurrence of closely spaced triplets. Only a few of the lines were observed to have complex fine structure.

From the quadrupole calculations which will be described later it was determined that high J valued transitions should appear only as closely spaced triplets or as single lines. It was also determined that the low J valued transitions should have complex fine structure.

A large number of observed lines would be expected for methylene chloride since its moments of inertia are large. Therefore, there will be many rotational energy levels with high relative populations. In addition, the selection rules are such as to allow many observable transitions between these levels.

Table I. Assigned $Q_{1\bar{1}}$ branch transitions for CH_2Cl_2.

Q_{11} transition	$CH_2Cl_2^{35}$ found mc/sec	$CH_2Cl_2^{35}$ cal[a] mc/sec	$CH_2Cl^{35}Cl^{37}$ found mc/sec	$CH_2Cl^{35}Cl^{37}$ cal[a] mc/sec	$CH_2Cl_2^{37}$ found mc/sec	$CH_2Cl_2^{37}$ cal[a] mc/sec
$1_{01}-1_{10}$	28,936.6[b]	28,936.6	28,890.0[b]	28,890.0		28,842
$2_{02}-2_{11}$	29,193.4[c]	29,193.5	29,135[d]	29,135		
$3_{03}-3_{12}$	29,582.0[c]	29,582.0	29,509	29,505		
$4_{04}-4_{13}$	30,105	30,106	30,005	30,004	29,905	29,902
$5_{05}-5_{14}$	30,769	30,770	30,635	30,636	30,502	30,502
$6_{06}-6_{15}$	31,577	31,582	31,405	31,407	31,225	31,235
$7_{07}-7_{16}$	32,546[d]	32,547	32,325	32,324	32,100	32,105
$8_{08}-8_{17}$	33,672[d]	33,676	33,393[d]	33,396	33,121	33,120
$9_{09}-9_{18}$	34,970	34,976	34,623	34,629	34,286	34,289
$10_{010}-10_{19}$	36,451.3[c]	36,459	36,026	36,036	35,614	35,621

[a] Calculated using the parameters in Table V.
[b] ±0.1 mc/sec, [c] ±0.3 mc/sec, [d] ±2 mc/sec; all others ±5 mc/sec.

Methylene chloride is a nearly prolate symmetric top with its dipole moment along the axis of intermediate moment of inertia. Most of the observed transitions correspond to the R_p and P_r ($\Delta J=\pm 1$, $\Delta K=\mp 1$) branches of the symmetric top spectrum. Lines of this type for methylene chloride may be expected to be observed with J as large as 100. For our purposes the lines of low J value are the more important, because centrifugal distortion makes the determination of rotational parameters uncertain when using high J valued assignments. Our lines of primary interest are then the low J valued transitions which appear as relatively weak lines with complex quadrupole fine structure.

The nature of the methylene chloride spectrum was calculated using the carbon-chlorine parameters determined by electron diffraction and an assumed position for the hydrogen atoms. The most prominent low J valued absorptions were those of a $Q_{1\bar{1}}$ branch. The $1_{01}-1_{10}$ transition should have a frequency, equal to $a-c$, somewhere from 24,000 to 34,000 mc/sec. The higher members ($2_{02}-2_{11}$, $3_{03}-3_{12}$ etc.) should form a series whose spacing depends on the asymmetry parameter κ (or δ). Except for a small amount of centrifugal distortion, the position of these $Q_{1\bar{1}}$ branch lines depends only on two parameters, κ and $a-c$.

Numerous attempts were made to make a $Q_{1\bar{1}}$ branch assignment in the region of 24,000 mc/sec. All of these attempts failed because these assignments were inconsistent with only two parameters. In addition, the lines or bands did not have the proper quadrupole pattern.

A series was eventually found which started in the 29,000 mc/sec region and fulfilled all the requirement. The lower members had a very complex quadrupole pattern and the higher members had a simple triplet structure. The temperature coefficients of their intensities indicated that they were of low J value and their frequencies could all be predicted on the basis of two rotational parameters. Three $Q_{1\bar{1}}$ branches were as-

[3] A. L. Bachrach, Masloboino-Zhirovoe Delo 9, No. 4, 42 (1934); see Chem. Abstracts 29, 3113 (1935).
[4] M. H. Earing and J. B. Cloke, J. Am. Chem. Soc. 73, 769 (1951).
[5] T. E. Turner, Ph.D. thesis, McGill University, 1948.
[6] P. Kisliuk and C. H. Townes, J. Research Natl. Bur. Standards 44, 611 (1950).

TABLE II. Other low J valued lines for CH_2Cl_2.

$0_{00}-1_{11}$ transition mc/sec	Relative strength	Temp.[a] coef.	Assignment
34,665.3±0.2	weak		$CH_2Cl_2^{37}$ $v=0$
34,866.5±0.2	medium		$CH_2Cl^{35}Cl^{37}$ $v=0$
35,067.0±0.2	strongest	+	$CH_2Cl_2^{35}$ $v=0$
35,258 ±2	medium	−	$CH_2Cl_2^{35}$ $v_4=1$(?)
35,451 ±5	weak		$CH_2Cl_2^{35}$ $v_4=2$(?)

$1_{01}-2_{12}$ transition mc/sec	Calculated[b] mc/sec	Assignment
41,197.8±0.2	41,197.4±0.5	$CH_2Cl_2^{35}$ $v=0$
40,842 ±1	40,843.0±0.5	$CH_2Cl^{35}Cl^{37}$ $v=0$

[a] A plus indicates relative increase in intensity with decreased temperature.
[b] Calculated using the parameters in Table V.

TABLE III. Other high J valued lines for CH_2Cl_2.

Transition	$CH_2Cl_2^{35}$ found mc/sec	$CH_2Cl_2^{35}$ cal[a] mc/sec	$CH_2Cl^{35}Cl^{37}$ found mc/sec	$CH_2Cl^{35}Cl^{37}$ cal[a] mc/sec
$6_{16}-7_{07}$	18,375	18,382		
$7_{17}-8_{08}$	25,533	25,540	24,100	24,114
$8_{18}-9_{09}$	32,769	32,776	31,140	31,152
$9_{18}-8_{27}$	23,312	23,301	24,947	24,933
$8_{17}-7_{26}$	30,812	30,805	32,229	32,221

[a] Calculated using the parameters in Table V.

signed correspondinging to $CH_2Cl_2^{35}$, $CH_2Cl^{35}Cl^{37}$, and $CH_2Cl_2^{37}$. These assignments are given in Table I.

An approximate quadrupole calculation indicated that the $0_{00}-1_{11}$ (freq.$=a+c$) transitions in methylene chloride might have very small quadrupole splitting. This fact was readily verified when several sharp lines were found near 35,000 mc/sec which had single positive Stark components. From the temperature coefficients of two of these lines and their intensities, the observed transitions were assigned to isotopic species and vibrational states. These $0_{00}-1_{11}$ assignments are given in Table II. As a further check of our assignments the frequencies of the $1_{01}-2_{12}$ (freq.$=a+3c$) transitions were measured and they are also given in Table II.

Some other frequencies for transitions which fell in the region of the spectrum that was examined were calculated using the moments of inertia determined from the above assignments. These transitions, which are given in Table III, represent a small portion of the transitions of the predominant type in methylene chloride's spectrum. In principle, this calculation could be carried on further so that the majority of the lines that were observed could be assigned. It was not felt that such a calculation was justified at this time. We have prepared a list of all of the lines observed for normal methylene chloride between 17,200 and 35,930 mc/sec. A copy of this list may be obtained from the authors by request.

It will be later shown that in addition to the consistency of the above spectral data our assignment is supported by the Stark effect on the $0_{00}-1_{11}$ transitions, the detailed quadrupole analysis of the $1_{01}-1_{10}$ and $10_{010}-10_{19}$ transitions, and by the structure of the molecule as determined by the assigned spectra of seven isotopic species.

In order to test the consistency of any structure for methylene chloride based on microwave data it was felt advisable to assign the spectra of as many isotopic species as possible. For this reason we prepared samples of both semideuterated methylene chloride ($CDHCl_2$) and deuterated methylene chloride (CD_2Cl_2). Assignments were easily made for the spectra of these samples when we utilized a tentative structure for these molecules. Attempts were made not to rely too much upon these structures to make the assignments and we feel all of the assignments have been independently confirmed. The assigned spectra of $CDHCl_2$ and CD_2Cl_2 are given in Table IV. In summary, the determined values of the rotational parameters and the moments of inertia for all of the isotopic species are given in Table V.

DIPOLE MOMENT MEASUREMENTS

A quantitative measurement of the Stark effect of assigned transitions serves both as a method of evaluat-

TABLE IV. Assigned transitions for $CDHCl_2$ and CD_2Cl_2.

Transition	$CDHCl_2^{35}$ found mc/sec	$CDHCl_2^{35}$ cal[a] mc/sec	$CDHCl^{35}Cl^{37}$ found mc/sec	$CDHCl^{35}Cl^{37}$ cal[a] mc/sec	$CD_2Cl_2^{35}$ found mc/sec	$CD_2Cl_2^{35}$ cal[a] mc/sec	$CD_2Cl^{35}Cl^{37}$ found mc/sec	$CD_2Cl^{35}Cl^{37}$ cal[a] mc/sec
$1_{01}-1_{10}$	24,171[c]	24,171	24,139	24.139		20,683		20,662
$2_{02}-2_{11}$	24,450	24,452	24,405	24,407	20,976.7[b]	20,976.6	20,942	20,942
$3_{03}-3_{12}$	24,878	24,877	24,820	24,813	21,425	21,423	21,370	21,369
$4_{04}-4_{13}$	25,453	25,454	25,365	25,362	22,030	22,029	21,948	21,946
$5_{05}-5_{14}$	26,183	26,188	26,063	26,061	22,805	22,803	22,687	22,684
$6_{06}-6_{15}$	27,090	27,088	26,920	26,917	23,761	23,757	23,590	23,593
$7_{07}-7_{16}$	28,167	28,165	27,943	27,942	24,908	24,906	24,687	24,685
$8_{08}-8_{17}$	29,434	29,433	29,143	29,140	26,268	26,263	25,974	25,974
$9_{09}-9_{18}$	30,900	30,903	30,535	30,539	27,850	27,847	27,473	27,476
$10_{010}-10_{19}$	32,583[c]	32,593	32,127	32,139	29,667.7[b]	29,677	29,196	29,210
$0_{00}-1_{11}$	30,224.7[b]	30,224.7	30,042.2[b]	30,042.2	26,670.2[b]	26,670.2	26,501.5[b]	26,501.5
$1_{01}-2_{12}$	36,283[c]	36,278	35,945[c]	35,945	32,656[c]	32,656		
$2_{02}-3_{13}$					38,502[c]	38,500	38,043[c]	38,043

[a] Calculated using the parameters in Table V.
[b] ±0.2 mc/sec, [c] ±2 mc/sec; all others ±5 mc/sec.

TABLE V. A summary of rotational parameters and moments of inertia.

	$CH_2Cl_2^{35}$	$CH_2Cl^{35}Cl^{37}$	$CH_2Cl_2^{37}$	$CDHCl_2^{35}$	$CDHCl^{35}Cl^{37}$	$CD_2Cl_2^{35}$	$CD_2Cl^{35}Cl^{37}$
a[a]	32,001.8	31,878.2_5	31,754	27,198	27,090.$_5$	23,676.$_5$	23,582
b[a]	3320.4	3231.5	3143	3305	3217.$_5$	3284	3197.$_5$
c[a]	3065.2	2988.2_5	2912	3027	2951.$_5$	2993.$_5$	2920
I_a[b]	15.7943	15.8555	15.918	18.584	18.65$7_5$	21.348	21.434
I_b[b]	152.22	156.41	160.80	152.92	157.10	153.90	158.08
I_c[b]	164.90	169.14_5	173.59	166.99	171.25	168.84	173.11

[a] In mc/sec.
[b] In (atomic mass units) (Angstrom units)^2. Calculated from a, b, and c using the constants of Dumond and Cohen (Revs. Modern Phys. **20**, 82 (1948)) which give $I_a = 505{,}446.5 \pm 905/a$. Moments of inertia in g (cm)^2 can be obtained from the above values by multiplying by $1.659723 \pm 0.00011 \times 10^{-40}$.

ing dipole moments and as a method of confirming the assignments. The quadrupole interactions found in the $0_{00}-1_{11}$ transitions for methylene chloride were found to be negligible. For this reason, the Stark effect could be calculated for these transitions without considering the quadrupole interactions. The dipole moments were calculated using the method of Golden and Wilson.[7] The measurements of the Stark coefficients for six isotopic species are given in Table VI.

It can be seen from Table VI that the dipole moments determined for the CH_2Cl_2 and $CDHCl_2$ species agree very well. In the case of CD_2Cl_2, the measurements were made more complicated by the interference of neighboring lines and it is not possible to state that the discrepancy shown here is definitely greater than the experimental error. We select $1.62 \pm 0.02 \times 10^{-18}$ esu as the best value for the dipole moment of methylene chloride. The best value, measured by the usual radio-frequency techniques, as selected by Barclay and Le Fevre[8] is 1.58×10^{-18} esu.

QUADRUPOLE INTERACTION

The first-order quadrupole Hamiltonian for two interacting nuclei has been established in two representations. The $(J, I_1, F_1, I_2, F, M_F)$ representation used by Bardeen and Townes[9] is the more convenient when the quadrupole interaction of one nucleus is much greater than the other, or when the rotational quantum number, J, is very large. The (J, I_1, I_2, I, F, M_F) representation used by Foley,[10] on the other hand, is the more convenient for two equivalent interacting nuclei. For example, in the case of methylene chloride which contains two equivalent chlorine nuclei with spins of 3/2, only second degree secular equations must be solved in Foley's representation.

It was found that the matrix elements given by Foley[10] contain some errors. Corrections for these errors and the matrix elements for the specific problem of two spin values of 3/2 are given in Appendix A.

The scale factor of the quadrupole interaction, $eQ\langle \partial^2 V/\partial z^2 \rangle_{Av}$, can be obtained from the molecular quadrupole interaction constants for a given J_τ level by the method of Bragg and Golden.[11]

The relative strengths of the quadrupole multiplets can be obtained by the method of Condon and Shortley.[12] Since only second-order secular equations are involved the diagonalizing transformations as well as the roots may be obtained very easily by the use of trigonometric functions and the matrix elements in Appendix A. Likewise, the choice of phase factors does not affect the calculations. Transitions are only allowed between levels specified by a common value of I. For all of the isotopic species of methylene chloride which retain the twofold axis, an additional restriction must be applied. Rotation of these molecules 180° about the twofold axis must either change the sign of the total wave function or leave it unchanged, depending upon the number of fundamental particles exchanged by the rotation. The degeneracy of the hydrogen spin

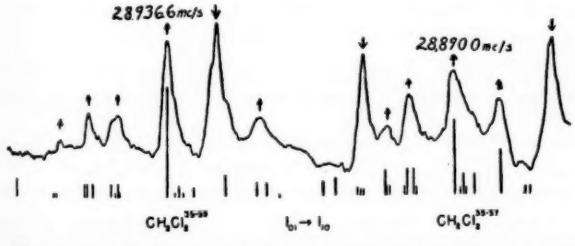

FIG. 1. A calculated and observed spectrum is given for the $1_{01}-1_{10}$ transitions of $CH_2Cl_2^{35}$ and $CH_2Cl^{35}Cl^{37}$. The small arrows indicate the effect of lowered temperature upon the intensities of the lines. Those absorptions marked with downward-pointing arrows are to be disregarded for they are presumably of high J or are of an upper vibrational state.

TABLE VI. The dipole moments of methylene chloride.

Isotopic species	$\Delta\nu/E^2$ mc/sec $\times$(Prac. volts/cm)$^{-2} \times 10^3$	esu $\times 10^{18}$
$CH_2Cl_2^{35}$	14.1_2	1.61_8
$CH_2Cl^{35}Cl^{37}$	14.2_1	1.62_3
$CDHCl_2^{35}$	16.9_1	1.61_6[a]
$CDHCl^{35}Cl^{37}$	17.0_8	1.62_5[a]
$CD_2Cl_2^{35}$	21.2_7	1.64_4
$CD_2Cl^{35}Cl^{37}$	21.0_3	1.64_0

[a] A correction of +0.008 unit has been applied to correct for the rotation of the principal axis from the symmetry axis.

[7] S. Golden and E. B. Wilson, J. Chem. Phys. **16**, 699 (1948).
[8] G. A. Barclay and R. J. W. Le Fevre, J. Chem. Soc. 556 (1950).
[9] J. Bardeen and C. H. Townes, Phys. Rev. **73**, 97 (1948).
[10] H. M. Foley, Phys. Rev. **71**, 751 (1947).
[11] J. K. Bragg and S. Golden, Phys. Rev. **75**, 735 (1949).
[12] E. U. Condon and G. H. Shortley, *The Theory of Atomic Spectra* (The Cambridge University Press, New York, 1935), p. 277.

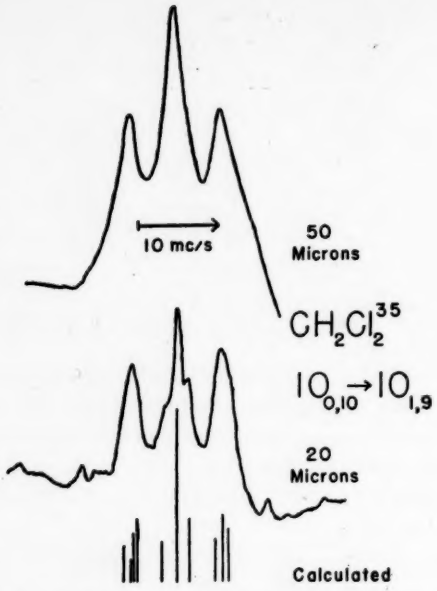

FIG. 2. A calculated and observed spectrum is given for the $10_{010}-10_{19}$ transition of $CH_2Cl_2^{35}$. The length of the arrow on the figure represents 10 mc/sec and its direction is that of increasing frequency.

energy levels gives an additional factor which must be used in the line strength calculations.

In Fig. 1 a comparison is given of the calculated and observed quadrupole multiplets for the $1_{01}-1_{10}$ transitions. The scale factors for the upper and lower levels were adjusted to give the best agreement between the calculated and observed spectra for $CH_2Cl_2^{35}$. The experimental curve contains some lines which were shown, by their temperature coefficients, to be transitions involving high J values or excited vibrational levels. These transitions are shown with downward pointing arrows which represent the effect upon their intensities of lowering the temperature. A comparison of the intensities of the $CH_2Cl_2^{35}$ transitions with those of the $CH_2Cl^{35}Cl^{37}$ shows the pronounced effect of the degeneracy of the hydrogen nuclear spin levels. The calculated spectrum for $CH_2Cl^{35}Cl^{37}$ was obtained by using the known ratio of the quadrupole moments of Cl^{35} and Cl^{37} and the scale factors determined from the $1_{01}-1_{10}$ transitions in $CH_2Cl_2^{35}$. All of the $CH_2Cl^{35}Cl^{37}$ levels were taken to have the same statistical weights.

As J increases the complexity of the $Q_{1\bar{1}}$ branch members first increases. For example, the $3_{03}-3_{12}$ transitions for $CH_2Cl_2^{35}$ were observed as a very complex pattern of lines grouped about 20 mc/sec on each side of a dominant center line. When J becomes larger than seven however, the $Q_{1\bar{1}}$ branch members begin to appear as symmetrical triplets. The hydrogen spin levels also play an important role in determining the qualitative appearance of the $Q_{1\bar{1}}$ branch members. For $CH_2Cl_2^{35}$ the low J valued transitions of odd J were observed to have a predominant line near the center of the pattern, while those of even J had only weak central lines. In the case of high J valued transitions the central line is always predominant but a similar systematic variation in its relative intensity has been observed. These statistical variations are reversed for even and odd J in $CD_2Cl_2^{35}$ and were not observed for $CDHCl_2$, $CH_2Cl^{35}Cl^{37}$, or $CD_2Cl^{35}Cl^{37}$. These observations are in accord with the symmetries of the energy levels and the statistical weights.

From the matrix elements in Appendix A it can be seen that for high J values the quadrupole energies all approach values of zero or $\pm\frac{1}{2}eQ\langle\partial^2V/\partial z^2\rangle_{Av}$. This is a consequence of the high J value spin uncoupling described by Foley.[10] High J valued transitions will appear as single lines if the scale factors for the upper and lower levels are nearly equal or as triplets if the scale factors are not equal.

In Fig. 2 a comparison is shown between a calculated and observed pattern for the $10_{010}-10_{19}$ transitions for $CH_2Cl_2^{35}$. For such a transition only the $\Delta F=0$ lines are important, and it was only necessary to select the scale factor difference which gave the best agreement between the calculated and observed spectra. This figure clearly illustrates the triplet-like appearance of the higher $Q_{1\bar{1}}$ branch members.

The scale factors of the quadrupole interactions depend upon the diadic, χ, whose elements are given by $\chi_{ij}=eQ(\partial^2V/\partial x_i\partial x_j)$, where x_i and x_j are usually identified with the principal axes (a, b, and c) of the inertial diadic. The diagonal elements of χ have a zero sum so that, $\chi_{aa}+\chi_{bb}+\chi_{cc}=0$. In the case of methylene chloride the Cl−C−Cl plane of molecular symmetry makes two of the off-diagonal elements, χ_{ac} and χ_{bc}, identically equal to zero. For the symmetrical species of methylene chloride there are, therefore, only three independent quadrupole interaction parameters.

The first-order quadrupole interaction depends upon the two independent diagonal elements of χ. An examination of the quadrupole interaction for several transitions has lead to the information and the quadrupole coupling parameters given in Table VII.

The second-order quadrupole interaction depends also upon the value of the off-diagonal element, χ_{ab}, and this element could be evaluated if there were near degeneracies between two rotational levels with the symmetries of A and B_c, or B_a and B_b. The ordinary prolate symmetric top degeneracy is not of this type so

TABLE VII. Quadrupole coupling constants for $CH_2Cl_2^{35}$ or $CD_2Cl_2^{35}$.

Transition	Molecule	Information
$0_{00}-1_{11}$	$CH_2Cl_2^{35}$	$\lvert\chi_{bb}\rvert \leq 5$ mc/sec
$1_{01}-1_{10}$	$CH_2Cl_2^{35}$	$\chi_{aa}-\chi_{cc}=-81.0\pm2$ mc/sec
$10_{010}-10_{19}$	$CH_2Cl_2^{35}$	$\lvert\chi_{aa}+2.094\chi_{cc}\rvert=39.8\pm1$ mc/sec
	$CD_2Cl_2^{35}$	$\lvert\chi_{aa}+2.084\chi_{cc}\rvert=40.5\pm1$ mc/sec

Calculated values

$\chi_{aa}=-41.8\pm1$ mc/sec
$\chi_{bb}=+\ 2.6\pm1$ mc/sec
$\chi_{cc}=+39.2\pm1$ mc/sec

that an accidental degeneracy would have to be found. We have not found such a degeneracy, and the first-order theory has been adequate in all the cases that we have examined.

Without a knowledge of χ_{ab} it is impossible to calculate the direction of the principal axes of χ in the Cl−C−Cl plane and the value of χ along these axes. However, if the electronic orbitals around the chlorine nuclei are assumed to be cylindrically symmetric, then the direction of this axis can be calculated together with the quadrupole coupling constant along this axis. This orbital coupling constant should be comparable to the similar constants found in linear and symmetric top molecules containing chlorine. Making this assumption of cylindrical symmetry one obtains

$$\chi_{\text{orbital}} = -2\chi_{cc} = -78.4 \pm 2 \text{ mc/sec}$$

and

$$\cos^2\theta/2 = (\chi_{cc} - \chi_{bb})/3\chi_{cc}$$

$$\theta = 112.0° \pm 1°.$$

This value for the chlorine-carbon orbital quadrupole coupling constant compares favorably with the value of −75.13 mc/sec[13] which has been found for the coupling constant in gaseous methyl chloride. In the solid state values of −68.40 and −72.47 mc/sec[14] have been measured at 20°K for CH_3Cl and CH_2Cl_2, respectively. In view of the recent evidence[15] which correlates the coupling constant and ionic character of a bond, the C−Cl bond in CH_2Cl_2 would seem to have a slightly smaller ionic character than that in CH_3Cl. This is in agreement with the decreased bond dipole moment calculated[16] for CH_2Cl_2.

The angle θ is the angle calculated as that between the two chlorine orbitals. In the next section we determine that the internuclear Cl−C−Cl angle is 111°47′±1′. The orbital angle, θ, is within experimental error of being equal to this internuclear angle. One can conclude from these data that if the chlorine orbitals are axially symmetric that they are with 0.5° of lying along the carbon-chlorine internuclear axis. This point will be discussed further in the next section.

STRUCTURE

Since methylene chloride has a tetrahedral structure there are four structural parameters to be determined. Two of these may be calculated directly from the three moments of inertia of a single isotopic species. The other two must be computed from the moments of inertia of two different isotopic species.

If we take the carbon atom as the center of a coordinate system with the x axis perpendicular to the H−C−H plane, the y axis perpendicular to the Cl−C−Cl plane, and the z axis along the intersection of these planes, then the projections, x_{Cl} and y_H, of the C−Cl and C−H bonds may be calculated for each isotopic species.

TABLE VIII. The projections of the C−Cl and C−H bonds perpendicular to the symmetry axis.

Molecule	x_{Cl}[a]	y_H[a]
	Angstrom units	
$CH_2Cl_2^{35}$	1.4675	0.8794
$CH_2Cl^{35}Cl^{37}$	1.4674	0.8801
$CH_2Cl_2^{37}$	1.4673	0.881
$CDHCl_2^{35}$	1.4675	0.888
$CDHCl^{35}Cl^{37}$	1.4673	0.887
$CD_2Cl_2^{35}$	1.4677	0.891
$CD_2Cl^{35}Cl^{37}$	1.4676	0.891

[a] Calculated using $m_H = 1.00813$; $m_D = 2.01471$; $m_C = 12.00382$; $m_{Cl} = 34.97867, 36.97750$.

For the symmetrical isotopic species such as $CH_2Cl_2^{35}$, $CD_2Cl_2^{35}$, etc. the moments which are determined from the microwave spectrum can be used directly to calculate x_{Cl} and y_H. For the less symmetrical species such as $CH_2Cl^{35}Cl^{37}$, $CDHCl_2^{35}$, etc. the principal axes are not parallel to our coordinate axes, and the x_{Cl} and y_H distances may be computed from the principal moments only after a translation and small rotation. The translational correction involves only masses while the rotational correction involves the use of an assumed structure. The rotational corrections are very small and are insensitive to the exact structure which is used. The results of these calculations are summarized in Table VIII.

It is apparent from Table VIII that the effective chlorine distance is very similar for all isotopic species, while the hydrogen distance seems to vary markedly when deuterium is substituted for the normal hydrogen atoms. The computation of these hydrogen projections involves the use of a small difference between large moments of inertia, and it would be expected that the small effects of vibration-rotation interaction would be more serious for the hydrogen distance than for the corresponding chlorine distance.

It is interesting to plot the hydrogen projection against the reciprocal of the total mass of the hydrogen atoms. Such a plot is shown in Fig. 3. It is seen from this figure that a value of 0.902A can be obtained if the curve is extrapolated to infinite hydrogen mass or 0.885A is obtained as an average of all values. Since the vibration-rotation interaction appreciably affects this distance, it is felt that the value determined by extrapolating to infinite hydrogen mass is perhaps a better approximation to the equilibrium distance. Even though these values differ by only 0.015A we shall make parallel calculations using both distances.

A quadratic expression in Z_{Cl} and Z_H can be established from the moments of inertia of a single isotopic species. Applying this relationship to each isotopic

[13] Gordy, Simmons, and Smith, Phys. Rev. **74**, 243 (1948).
[14] R. Livingston, J. Chem. Phys. **19**, 1434 (1951). This method does not determine the sign which we have presumed to be negative.
[15] C. H. Townes and B. P. Dailey, J. Chem. Phys. **17**, 782 (1949); W. Gordy, J. Chem. Phys. **19**, 792 (1951).
[16] See, for example, J. R. Thomas and W. D. Gwinn, J. Am. Chem. Soc. **71**, 2785 (1949).

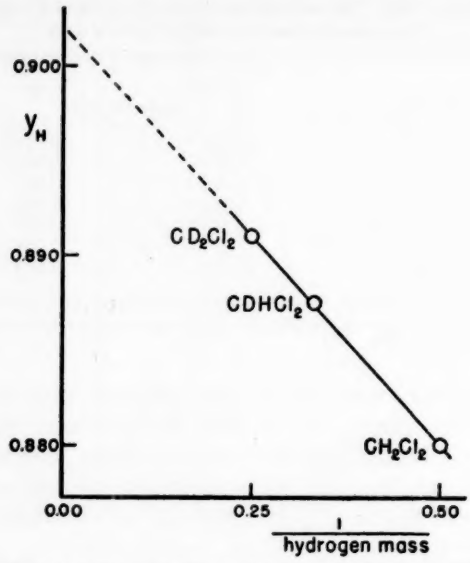

FIG. 3. A plot of the projections of the C—H bonds perpendicular to the symmetry axis found for different isotopic species.

species one obtains seven equations for two unknowns. These seven equations are solved graphically in Fig. 4. An intersection in this figure represents a simultaneous solution of z values for two isotopic species. In the absence of rotation-vibration interaction all of the curves should intersect at one point on the graph.

The curves in Fig. 4 for different chlorine isotopes are either superimposed or parallel. The different hydrogen isotopes, on the other hand, do yield satisfactory solutions. It is apparent that the z contribution of the hydrogen atoms to the moment of inertia is much greater than the y contribution. The center of mass of the molecule is moved toward the chlorine atoms in the z direction, and in this way the hydrogens have a greater effect.

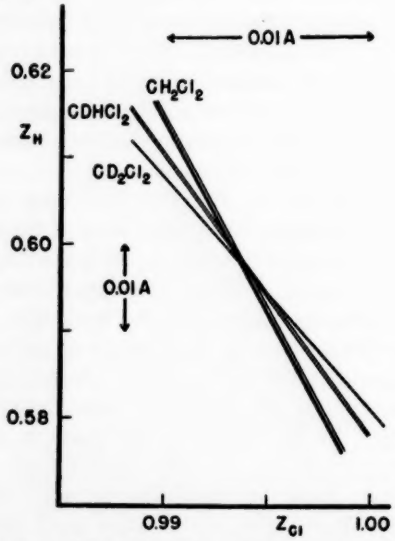

FIG. 4. A plot of Eq. (5) is given for seven isotopic species of methylene chloride. The curves for the isotopic species containing only different chlorine isotopes are superimposed on this plot for CD_2Cl_2 and closely parallel for $CDHCl_2$ and CH_2Cl_2.

All of the curves in Fig. 4 pass through a small area near the center of the graph. This area is a solution which simultaneously satisfies all of the equations. The center of this area is taken as the best solution and its limits of error are those necessary to include all of the curves. The best solution is

$$z_{Cl}=0.9939\pm0.0002\text{A}$$
$$z_H=0.5972\pm0.0007\text{A}.$$

All of the actual *intersections* shown in Fig. 4 are included within the area of this solution if the limits of error are increased by a factor of 4.5.

In Table IX the bond distances and angles are given which can be derived from the x, y, and z values. There is good agreement between these values and the previous electron diffraction results[1] for methylene chloride which are 1.77 ± 0.02A for the C—Cl distance and $112\pm2°$ for the Cl—C—Cl angle.

Both the Cl—C—Cl and H—C—H angles are noticeably greater than the tetrahedral angle. This could arise from chlorine-chlorine repulsion, hydrogen-hydrogen repulsion and chlorine-hydrogen attractions. In hybridization of s, p_x, p_y, and p_z carbon orbitals in methylene chloride it is found that when one orbital angle is greater than the tetrahedral angle that the other orbital angle must be smaller than the tetrahedral angle. To account for both angles being greater than the tetrahedral angle either the carbon orbitals must involve some d character or bent bonds must be introduced. Because of the high energy of the lowest d orbital in carbon we prefer bent bonds.

TABLE IX. Effective bond distances and angles.

C—Cl bond	1.7724 ± 0.0005A
Cl—C—Cl angle	$111°47'\pm1'$
C—H bond	1.068 ± 0.005A (average of all species) or 1.082A (extrapolated to infinite hydrogen mass)
H—C—H angle	$112°0'\pm20'$ (average of all species) or 112°58' (extrapolated to infinite hydrogen mass)

If bent bonds were present in methylene chloride we would expect to find that the angle between the two chlorine orbitals would be greater than the internuclear Cl—C—Cl angle. In the previous section we have shown that the nuclear quadrupole coupling constants lead to an approximate evaluation of the chlorine orbital angle. This angle was determined to be $112.0°\pm1°$. This value is within experimental error of being equal to the internuclear angle. However, the uncertainty in the chlorine orbital angle is sufficiently large so that these data are not inconsistent with a bent bond picture.

APPENDIX A. ELEMENTS OF THE FIRST-ORDER QUADRUPOLE HAMILTONIAN

If one uses the first-order quadrupole Hamiltonian as given by Bragg[17] for two equivalent nuclei and the

[17] J. K. Bragg, Phys. Rev. 74, 533 (1948).

matrix elements as given by Condon and Shortley,[18] the two nonvanishing elements in the JIF representation are

$$(JIF|H_Q|JIF)=\frac{eQ\langle\partial^2V/\partial z^2\rangle_{Av}}{2J(2J-1)I_1(2I_1-1)}$$

$$\times\Big\{3/8[F(F+1)-I(I+1)-J(J+1)]^2$$

$$+3/8\Big[\frac{(2I_1+1)^2-(I+1)^2}{(2I+1)(2I+3)}(F+I-J+1)(F+J-I)$$

$$\times(F+J+I+2)(I+J-F+1)\Big]$$

$$+3/8\Big[\frac{(2I_1+1)^2-I^2}{4I^2-1}(F+I-J)(F+J-I+1)$$

$$\times(F+J+I+1)(I+J-F)\Big]$$

$$+3/4[F(F+1)-I(I+1)-J(J+1)]$$

$$-2I_1(I_1+1)J(J+1)\Big\}$$

and

$$(JIF|H_Q|JI-2F)=\frac{3eQ\langle\partial^2V/\partial z^2\rangle_{Av}}{16J(2J-1)I_1(2I_1-1)}$$

$$\times\Big\{\frac{(2I_1+1)^2-I^2}{4I^2-1}(F+I-J)(F+J-I+1)$$

$$\times(F+J+I+1)(I+J-F)\Big\}^{\frac{1}{2}}$$

$$\times\Big\{\frac{(2I_1+1)^2-(I-1)^2}{(2I-3)(2I-1)}(F+I-J-1)$$

$$\times(F+J-I+2)(F+J+I)(I+J-F-1)\Big\}^{\frac{1}{2}}.$$

The diagonal element is consistent with that given by Foley,[10] but the off-diagonal elements given by Foley are incorrect for they are twice as large as those given here. Foley's $(I|I-2)$ element also omits a $+2$ in one of the terms.

The specific Hamiltonian elements for two nuclear spin values of 3/2 can be derived from the above equations. They are as follows:

First-Order Hamiltonian Elements for Two Spins of Three-Halves

Hamiltonian Elements Divided by $eQ\langle\partial^2V/\partial z^2\rangle_{Av}$

Diagonal elements

F	3	I 2	1	0
$J+3$	$1/2$			
$J+2$	$-\frac{3}{2J}$	0		
$J+1$	$\frac{-3(2J^2+9J-15)}{10J(2J-1)}$	0	$\frac{-(2J^2-1)}{5J(2J-1)}$	
J	$\frac{-(4J^2+4J-33)}{5J(2J-1)}$	0	$\frac{2J+3}{5J}$	0
$J-1$	$\frac{-3(2J^2-5J-22)}{10J(2J-1)}$	0	$-\frac{(J+1)(2J+3)}{5J(2J-1)}$	
$J-2$	$\frac{3(2J+3)}{2J(2J-1)}$	0		
$J-3$	$\frac{(2J+3)(J+1)}{2J(2J-1)}$			

Off-diagonal elements

F	$I=1,3$	$I=0,2$
$J+1$	$3/5\Big[\frac{(J+2)(2J+5)}{6J(2J-1)}\Big]^{\frac{1}{2}}$	
J	$\frac{3}{10J}\Big[\frac{(J+2)(J-1)(2J+3)}{(2J-1)}\Big]^{\frac{1}{2}}$	$\frac{1}{2}\Big[\frac{(J+1)(2J+3)}{J(2J-1)}\Big]^{\frac{1}{2}}$
$J-1$	$\frac{3}{5J(2J-1)}\Big[\frac{(J^2-1)(4J^2-9)}{6}\Big]^{\frac{1}{2}}$	

[18] E. U. Condon and G. H. Shortley, *The Theory of Atomic Spectra* (The Cambridge University Press, New York, 1935), p. 71.

Fluorescence Studies of Some Simple Benzene Derivatives in the Near Ultraviolet. III. Benzotrifluoride*†

MANTRALA L. N. SASTRI‡ AND H. SPONER
Department of Physics, Duke University, Durham, North Carolina
(Received April 22, 1952)

The fluorescence spectrum of benzotrifluoride has been studied using various sources of excitation. The spectrum consists of about 36 bands for which assignments are given according to the symmetry properties of the molecule. The analysis is in agreement with that of the absorption spectrum. In the region of overlap, fluorescence and absorption bands show close coincidence.

INTRODUCTION

THE present paper is an extension of the fluorescence studies, being carried out in the vapor phase in this laboratory, to benzotrifluoride ($C_6H_5CF_3$). The near ultraviolet absorption spectrum of this substance is known and has been analyzed by Sponer and Lowe.[1] An analysis by Cave and Thompson[2] confirmed these assignments. The Raman spectrum of benzotrifluoride was reported by Pendl and Radinger,[3] and the infrared spectrum by Thompson and Temple.[4] No fluorescence data have been found for benzotrifluoride vapor.

EXPERIMENTAL DETAILS

The experimental method adopted for obtaining the fluorescence spectrum of benzotrifluoride was essentially the same as that described in a previous paper[5] (called I hereafter). Excitation of the vapor was achieved by light from condensed sparks between Fe, Mn, and Sn electrodes, and also from a Hg arc lamp. These metals have at least one and more often several emission lines which coincide in wavelength with one or more of the strong absorption bands of benzotrifluoride. The optical arrangement used by Bass[5] was employed in the first experiments but was later somewhat modified in order to cut down the long exposure times. They are inevitable when a weak light source is used for producing an effect which is weak itself. The changes consisted in putting the fluorescence cell as close as possible to the light source and to the spectrograph slit by dispensing with the previous system of lenses. To approximate a fairly parallel beam and to avoid scattered light falling on the walls of the vessel, a porcelain tube was inserted between the spark and the front window of the cell. The inside of the tube was blackened to minimize internal reflections. Another tube, the inside of which was lined with reflecting aluminum, was placed between the exit window of the cell and the slit of the spectrograph. This arrangement, though somewhat crude, effectively reduced the long exposure times and also cut down considerably, almost to nothing, the intensity of scattered spark lines.

The fluorescence cell had to be refilled a few times since the quartz windows became fogged after long exposures to ultraviolet light though filters cutting off light shorter than 2350A were used. A red Purple Corex A filter No. 9863 was used throughout, alone and a few times in combination with organic cut-off filters in order to control the exciting wavelength region, as described in I.

The fluorescence spectra were taken at different vapor pressures, mostly at about 15 mm Hg, and were photographed with a Bausch and Lomb medium quartz spectrograph. The slit width was 50 microns. Exposure times, on Eastman II-O plates, were about 50 to 60 hours.

EXPERIMENTAL RESULTS

The fluorescence spectrum extends from about 2640 to about 2925A and consists of about 36 bands whose wavelengths and wavenumbers are listed in Table I along with intensity estimates and probable assignments. The intensity scale is: *vs*—very strong, *s*—strong, *m*—medium, *w*—weak, *vw*—very weak, *d*—diffuse. The bands are degraded to the red. The spectrum may be best described as a succession of rather narrow groups, each having a width of about 12A. The individual group, where resolved, consists of five bands. The groups are easily recognized in Table I as each begins with a wave number on the left side, and a zero on the right side of the comma under the assignment column. In this column numbers to the left of the comma indicate vibrational levels in the ground state, and the numbers to the right of the comma, with minus signs, belong to $v-v$ transitions.

The 0—0 band, known from the absorption spectrum,[1] did not appear in the fluorescence spectra taken with Hg, Sn, and Mn excitations. It is reabsorbed in

* Based on a portion of a thesis submitted by M. L. N. Sastri in partial fulfillment of the requirements for the degree of Doctor of Philosophy in the Graduate School of Arts and Sciences of Duke University, 1951.

† This investigation was assisted by the ONR under contract N6ori-107, T.O.I., with Duke University.

‡ Present address: National Physical Laboratory, New Delhi, India.

[1] H. Sponer and D. S. Lowe, J. Opt. Soc. Am. **39**, 840 (1949).
[2] W. T. Cave and H. W. Thompson, Disc. Faraday Soc. **9**, 35 (1950).
[3] E. Pendl and G. Radinger, Monatsh. f. Chem. **72**, 382 (1939).
[4] H. W. Thompson and R. B. Temple, J. Chem. Soc. 1432 (1948).
[5] A. M. Bass and H. Sponer, J. Opt. Soc. Am. **40**, 389 (1950).

TABLE I. Fluorescence bands of benzotrifluoride.

Wavelength[a]	Wave number cm^{-1}	Int.	Separation from 0, 0 37,819 cm^{-1}	Assignment
2643.4*	37,819	*w*		0, 0
2645.9*	37,783	*ew*	36	0, −36
2648.8*	37,743	*ew*	76	0, −75
Unresolved structure				
2653.1*	37,681	*m*	138	141, 0
2663.3*	37,536	*vwd*	283	2×141, 0
2667.0*	37,484	*m*	335	338, 0
Unresolved structure				
2677.4*	37,339	*mw*	480	338+141, 0
2687.8*	37,196	*mw*	623	623, 0
2690.8*	37,153	*mw*	666	662, 0; 623, −36
2692.7*	37,126	*ewd*	693	662, −36; 623, −75
2695.9*	37,082	*ewd*	737	662, −75; 623, −75−36
2699.1	37,038	*mw*	781	662, −75−36; 623+141, 0; 771, 0
2715.4*	36,816	*vs*	1003	1004, 0
2718.3*	36,777	*s*	1042	1004, −36
2721.1*	36,739	*w*	1080	1004, −75
2723.3*	36,709	*w*	1110	1004, −75−36
2726.2*	36,670	*m*	1149	1004+141, 0
2740.2*	36,483	*vs*	1336	1336, 0; 338+1004, 0
2743.0	36,446	*s*	1373	1336, −36; 338+1004, −36
2746.4	36,401	*md*	1418	1336, −75; 338+1004, −75
2749.4	36,361	*wd*	1458	1336, −75−36; 338+1004, −75−36
2751.4	36,334	*s*	1485	1336+141, 0; 338+1004+141, 0
2762.5	36,188	*ew*	1631	1004+623, 0
2765.5	36,149	*m*	1670	1004+662, 0
Unresolved structure				
2791.6	35,811	*s*	2008	2×1004, 0
2795.0	35,768	*md*	2051	2×1004, −36
2798.2	35,727	*md*	2092	2×1004, −75
Unresolved structure				
2802.7	35,670	*w*	2149	2×1004+141, 0
2817.5	35,482	*s*	2337	1336+1004, 0; 2×1004+338, 0
Unresolved structure				
2829.0	35,338	*wd*	2481	1336+1004+141, 0; 2×1004+338+141, 0
2843.6	35,156	*m*	2663	2×1336, 0; 2×1004+662, 0
Unresolved structure				
2856.3	35,000	*wd*	2819	2×1336+141, 0; 2×1004+662+141,0
2873.4	34,792	*mw*	3027	3×1004, 0
Unresolved structure				
2884.0	36,664	*wd*	3153	3×1004+141, 0
2899.4	34,480	*m*	3339	1336+2×1004, 0; 3×1004+338, 0
Unresolved structure				
2912.2	34,328	*w*	3491	1336+2×1004+141, 0; 3×1004+338+141, 0
2928.5	34,143	*w*	3676	3×1004+662, 0

[a] Bands marked with an asterisk coincide with observed absorption bands.

the quartz cell as evidenced by the appearance of two faint absorption bands at 2643.4 and 2645.9A on a plate taken with Hg arc excitation. The 0−0 band does, however, show up on a plate taken with Fe spark excitation. Figure 1 exhibits the fluorescence together with the absorption spectrum. Both enlargements have been adjusted to approximately the same dispersion.

DISCUSSION OF RESULTS

It is apparent from Table I that most bands are emitted from the vibrationless upper electronic state as indicated by the zero to the right of the comma (assignment column). The remaining bands, filling up the groups mentioned before, contain $v-v$ transitions of low vibrations superimposed on the first bands, as indicated by the small negative numbers to the right of the comma. No bands were found originating from higher vibrational levels of the upper electronic state, although excitation took place into the 0, 0 band and several higher absorption bands. These results—dissipation of the oscillatory energy of the upper state in collisions before radiation takes place—are in agreement with previous observations and have been discussed in I.

The bands originating from the vibrationless excited electronic state will be discussed first. They contain vibrational levels in the ground state in agreement with the selection rules operating according to the symmetry of the molecule. These selection rules were discussed by Sponer and Lowe who, in first approximation, assigned C_{2v} symmetry to the molecule and consequently regarded the electronic transition as A_1-B_1. It is allowed and the transition moment is in the plane of the molecule perpendicular to the C−CF_3 bond.

The analysis of the fluorescence spectrum follows the same rules as that of the absorption spectrum. The region of overlap between fluorescence and absorp-

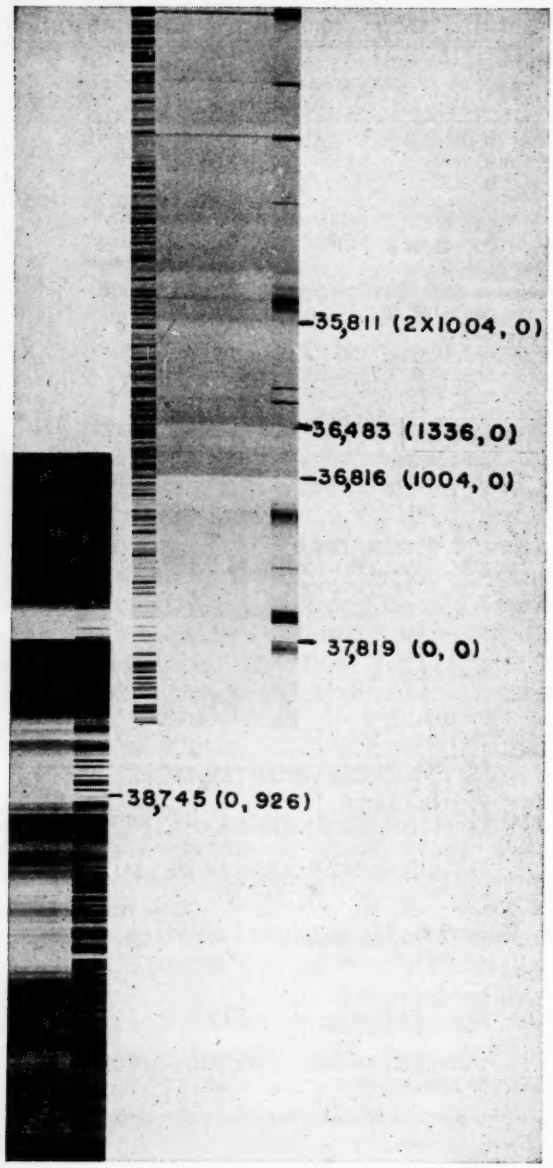

FIG. 1. Right: Fluorescence spectrum of benzotrifluoride vapor excited by Hg arc, vapor pressure 20 mm Hg. Left: Absorption spectrum of benzotrifluoride vapor taken with medium Hilger quartz spectrograph.

tion is proof that the same vibrations partake in the fluorescence bands as had been observed in absorption. They have the wave numbers 141, 338, 623, 662, 1004, and 1336 and, except for the last one, assignments to modes of vibration have been discussed for them.[1] The two strongest groups of the fluorescence spectrum, one beginning at 36,816 and the other at 36,483 cm^{-1}, are 1004 and 1336 cm^{-1} apart from the 0, 0 band and are repeated at intervals which are multiples of these frequencies. The 1336 cm^{-1} frequency may correspond to the 1324 cm^{-1} frequency observed weakly in the Raman and strongly in the infrared spectrum. Polarization measurements are missing. Since the 1336 cm^{-1} frequency occurs strongly, singly and doubly excited, and in combination with 1004, it probably represents a totally symmetric vibration. No corresponding upper state frequency was recorded in the absorption measurements. The weakness of the 1324 Raman line and its strong appearance in the infrared spectrum suggest rather a nonsymmetrical vibration as its origin. Now it seems probable that the 1336 is, at least partly, a combination of the two frequencies 1004 and 338 cm^{-1}. The latter frequency occurs singly excited and in combination with the 1004 cm^{-1} frequency (Table I). The intensity of the corresponding bands is high enough to suggest that the 338 vibration belongs to the α_1 type. Hence, one may conclude that the separation 1336, whether belonging to one or the sum of two vibrations, or both possibilities, represents mainly a totally symmetric vibrational mode.

The 1004 cm^{-1} belongs in all probability to a totally symmetric (α_1) carbon vibration in the ground electronic state.

The 662 cm^{-1} vibration occurs in the fluorescence spectrum in much the same fashion as the 338 cm^{-1} frequency, that is, singly excited and in combination with the carbon vibration of 1004 cm^{-1}. Sponer and Lowe have discussed this 662 frequency in detail. Since very little can be added to their discussion it will be mentioned only that it may be associated with the CF_3 group, but that its origin is not entirely certain. Symmetry α_1 had been suggested for this vibration.

The third group of the spectrum begins with a band at 37,196 separated by 623 from the 0, 0 band. The band at 36,188 has a distance of 1004+623 from the 0, 0 band. This 623 frequency which appears in weak bands only, has also been discussed previously and was interpreted as a β_1 vibration. It results from the splitting of the 606 cm^{-1} ϵ^+g vibration of benzene in substituted benzenes of lower symmetry. The 338 vibration, discussed earlier, may represent the α_1-component belonging to this splitting.

It is possible that the band 37,038 contains also the transition 771, 0. This transition was observed in absorption by Cave and Thompson.[2] It is to be expected since the corresponding vibrational frequency of 750 cm^{-1} in the upper electronic state, occurs in many absorption bands. Its identification in fluorescence is obscured by the overlapping of several different transitions.

We shall now discuss the pattern of an individual band group. Each group consists of five bands separated from the first on the violet side by 36, 75, 36+75, and 141 cm^{-1}. These numbers were discussed by Sponer and Lowe. Their conclusion that the 36 cm^{-1} represents the 1−1 transition of a very low vibration is in agreement with results from the fluorescence spectrum. On one of the plates the 0, 0 band and the band at 37,783 cm^{-1} which is 0, 0−36 appear as absorption bands. This is the result of reabsorption of these frequencies in the cell and indicates that the frequency difference of 36

cm^{-1} involves a low vibration. If the vibration giving rise to the strong Raman line of 139 cm^{-1} be taken as this low vibration, a simple calculation shows that at the temperature of the vapor (22°C) about one-fourth of the molecules are excited to one quantum of this vibration.§ The third and fourth bands in each group are separated by 75 and 36+75 cm^{-1}. They may, at least partly, involve transitions of frequency differences 2×36 and 3×36 cm^{-1}, that is, 2, 2 and 3, 3 transitions of the 139 cm^{-1} vibration. Symmetry type β_1 was suggested for this vibration.[1] This means that bands, in which it occurs singly excited, would belong to the forbidden part of the spectrum which arises from a transition moment lying in the direction of the C−CF$_3$ axis. The relative weakness of the band is compatible with this view, so is the weakness of the band at 37,536 which is interpreted as 2×141, 0 and which was reported by Cave and Thompson in absorption. Although for this band the vibrational eigenfunction is totally symmetric, the twofold excitation of a nonsymmetric vibration is, according to the Franck-Condon principle, less frequent than the onefold excitation.

The authors acknowledge the assistance of Dr. A. M. Bass in taking the spectrograms.

§ A microphotometer trace kindly taken by Dr. C. A. Beck and Dr. S. Silverman at the Applied Physics Laboratory (Johns Hopkins University) of one of Sponer and Lowe's absorption plates is in agreement with the calculation.

THE JOURNAL OF CHEMICAL PHYSICS VOLUME 20, NUMBER 9 SEPTEMBER, 1952

Elastic Scattering and Neutralization of Low Velocity Hydrogen Ions in Ethane and Propane

J. H. SIMONS*
School of Chemistry and Physics, The Pennsylvania State College, State College, Pennsylvania

AND

S. A. MCALLISTER†
College of Engineering, The University of Florida, Gainesville, Florida

(Received April 7, 1952)

The low velocity scattering of H^+, H_2^+, and H_3^+ in both ethane and propane have been measured at ion velocities of less than 150 volts. Ion neutralization was detected and measured for all three ions in both hydrocarbons and elastic scattering potential functions evaluated for all six interactions. The scattering of hydrogen ions in the first four members of the series of straight chain saturated hydrocarbons can now be compared, and it is shown that they change in a systematic manner.

PREVIOUS studies have reported the scattering of low velocity hydrogen ions in methane[1] and butane[2] and have evaluated potential laws of the form $V=-(K/r^n)$ for the interaction of hydrogen ions with the molecules of these substances. In the present study, ethane and propane are used as the scattering gases. This enables a comparison to be made of the first four members of the homologous series of the straight chain saturated hydrocarbons.

As was found with other hydrocarbons, collisions of the second kind were a major factor in the total inter-

TABLE I. Scattering of hydrogen ions in ethane.

H^+			H_2^+			H_3^+		
W volts	αT^0	αS^0	W volts	αT^0	αS^0	W volts	αT^0	αS^0
125.0	165.0	46.2	130.0	187.0	61.0	127.0	56.0	37.7
100.0	163.0	57.7	100.0	194.0	75.4	99.0	62.4	41.8
80.0	175.0	67.2	79.0	197.0	76.5	79.0	64.3	44.0
65.0	189.0	72.0	61.5	201.5	79.1	62.5	69.1	50.6
50.0	185.0	75.9	52.5	213.0	83.5	52.0	74.8	51.0
39.5	189.0	76.0	40.0	219.0	92.4	39.0	90.4	64.4
33.0	201.0	77.0	32.0	224.0	98.5	31.0	97.0	69.7
25.0	202.0	86.2	25.0	230.0	107.4	24.4	112.0	90.3
21.3	218.0	99.8	20.0	230.0	99.7	20.0	120.0	90.7
18.0	220.0	97.4	16.6	239.0	97.7	15.0	129.0	91.2
14.0	256.0	110.0	12.3	248.5	102.2	12.0	137.0	94.7
11.0	226.0	108.0	10.0	268.0	111.6	9.8	137.0	114.0
9.4	259.0	···	8.3	256.0	106.5	8.2	151.0	93.3
8.7	244.0	119.0	6.1	274.0	127.0	6.7	173.0	118.5
6.5	264.0	235.0	5.0	281.0	134.0	5.0	208.0	150.0

TABLE II. Scattering of hydrogen ions in propane.

H^+			H_2^+			H_3^+		
W volts	αT^0	αS^0	W volts	αT^0	αS^0	W volts	αT^0	αS^0
125.0	206.0	78.3	132.0	230.0	87.2	125.0	78.2	54.9
100.0	213.0	80.9	112.0	225.0	92.3	106.0	95.0	64.5
96.0	212.0	79.1	99.0	222.0	91.4	85.0	88.2	60.4
83.0	221.0	91.2	89.0	231.0	106.7	72.0	99.0	63.4
72.0	216.0	80.8	80.0	238.0	93.5	60.0	99.0	63.4
64.0	230.0	81.0	75.0	234.0	98.3	50.0	103.0	63.4
52.0	227.0	96.4	62.0	229.0	101.3	40.0	113.0	72.6
40.0	227.0	105.6	50.0	239.0	120.0	32.5	113.0	71.3
34.0	231.0	103.6	40.0	249.0	101.0	27.0	121.0	76.1
28.0	232.0	104.0	34.0	267.0	115.5	21.0	133.0	80.6
24.0	245.0	113.0	25.0	273.0	116.4	17.5	146.0	86.4
18.0	265.0	81.6	20.3	286.5	134.1	14.1	167.0	98.4
14.3	258.0	151.0	15.8	292.0	113.3	10.0	178.0	116.5
12.0	290.0	146.7	11.0	290.0	120.0	7.9	217.0	122.0
8.5	306.0	175.6	9.5	343.0	154.6	6.3	216.0	158.5
5.8	320.0	190.8	7.5	325.0	140.2	5.8	248.0	183.0
			5.6	510.0	144.5			

* Present location: College of Engineering, University of Florida, Gainesville, Florida.
† Present location: Photographic Products Dept., E. I. du Pont de Nemours, Inc., Parlin, New Jersey.

[1] J. H. Simons and G. C. Fryburg, J. Chem. Phys. **13**, 216 (1945).
[2] J. H. Simons and W. H. Cramer, J. Chem. Phys. **18**, 473 (1950).

TABLE III. Summary of scattering laws and potential functions.

Ion	Range	Potential function
	Ethane	
H^+	7–125 volts (3.47–3.18A)	$V=\frac{-951}{r^{6.55}}$
H_2^+	5–130 volts (3.47–2.42A)	$V=\frac{-16{,}250}{r^{9.46}}$
H_3^+	5–13.5 volts (3.68–2.99A)	$V=\frac{-794}{r^{6.54}}$
	13.5–127 volts (2.99–1.85A)	$V=\frac{-90.3}{r^{4.35}}$
	Propane	
H^+	6–41.4 volts (4.11–2.94A)	$V=\frac{-184}{r^{5.85}}$
	41.4–125 volts (2.94–2.65A)	$V=\frac{-95{,}071}{r^{10.66}}$
H_2^+	6–132 volts (3.71–2.80A)	$V=\frac{-310{,}000}{r^{11.23}}$
H_3^+	6–23.3 volts (3.83–2.65A)	$V=\frac{-51.7}{r^{3.76}}$
	23.3–125 volts (2.65–2.29A)	$V=\frac{-55{,}131}{r^{12.14}}$

action. Such collisions predominated in the interactions involving H^+ and H_2^+ but were not as important as collisions of the first kind in the interactions involving H_3^+.

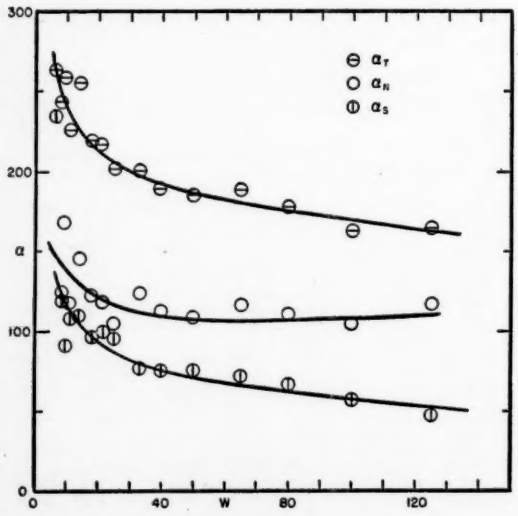

FIG. 1. The scattering of H^+ in ethane.

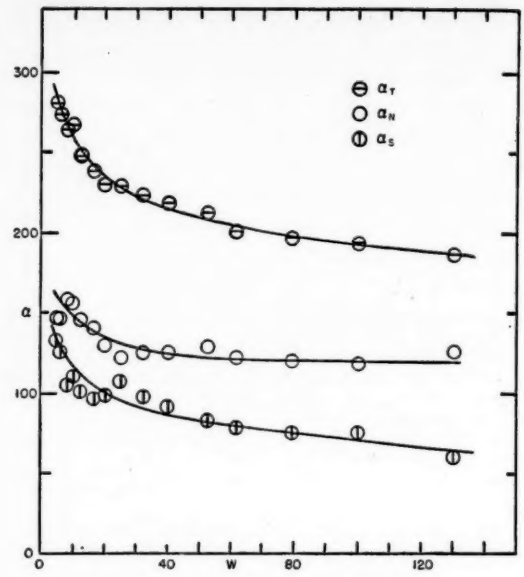

FIG. 2. The scattering of H_2^+ in ethane.

APPARATUS

The apparatus, except for minor modifications, was the same as previously described.[3,4] In the interval elapsed since the last measurements, a significant amount of mercury had diffused into the equipment. This produced sufficient vapor to contribute some scattering to the ion beam. This was reduced to an insignificant amount by lowering the temperature of scattering chamber to 7°C by passing a stream of cold water through a coil of copper tubing surrounding the chamber.

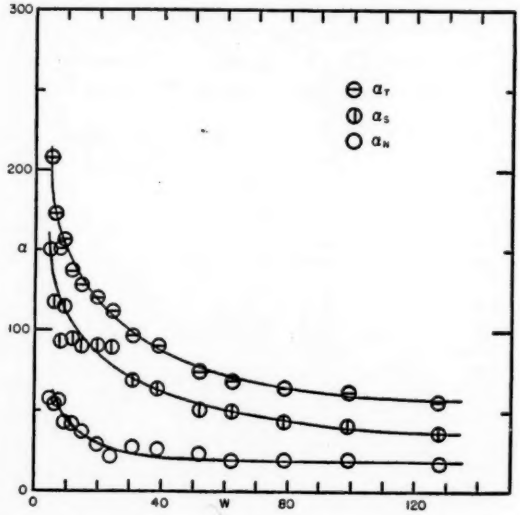

FIG. 3. The scattering of H_3^+ in ethane.

[3] Simons, Francis, Fontana, and Jackson, Rev. Sci. Instr. **13**, 419 (1942).

[4] G. C. Fryburg and J. H. Simons, Rev. Sci. Instr. **20**, 541 (1949).

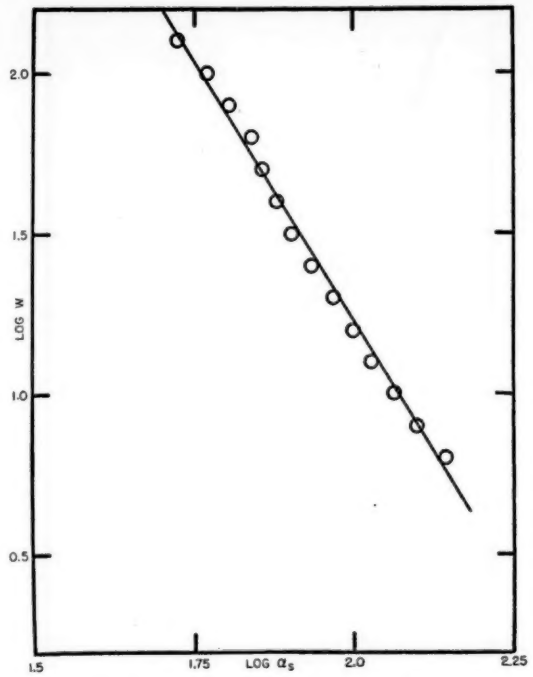

FIG. 4. The scattering of H^+ in ethane.

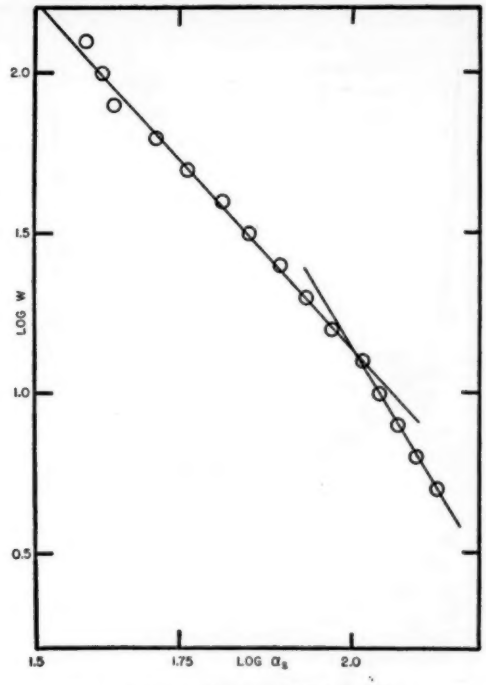

FIG. 6. The scattering of H_3^+ in ethane.

MATERIALS

The hydrocarbons were obtained from commercial cylinders. The propane, supplied as ninety-nine percent pure, was subjected to a simple distillation and the middle cut retained for use. The ethane was bubbled several times through solutions of pyrogallol and concentrated sulfuric acid to remove oxygen and olefins, respectively. It was then subjected to a simple distillation and the middle cut retained for use. Its determined boiling point was $-89°C$.

RESULTS

In Table I are given the results of the scattering of hydrogen ions in ethane. These results are also shown in Figs. 1, 2, and 3. Potential function graphs are shown in Figs. 4, 5, and 6. In Table II the results of the

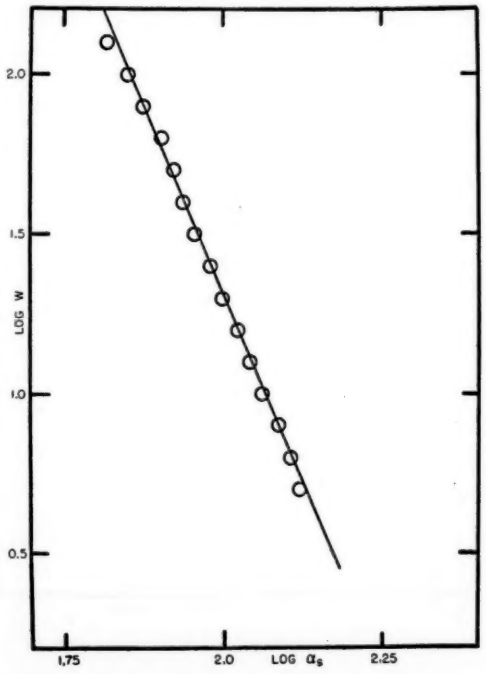

FIG. 5. The scattering of H_2^+ in ethane.

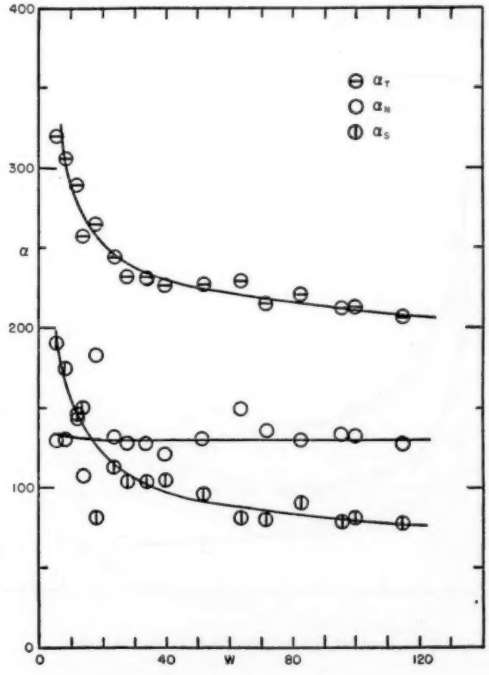

FIG. 7. The scattering of H^+ in propane.

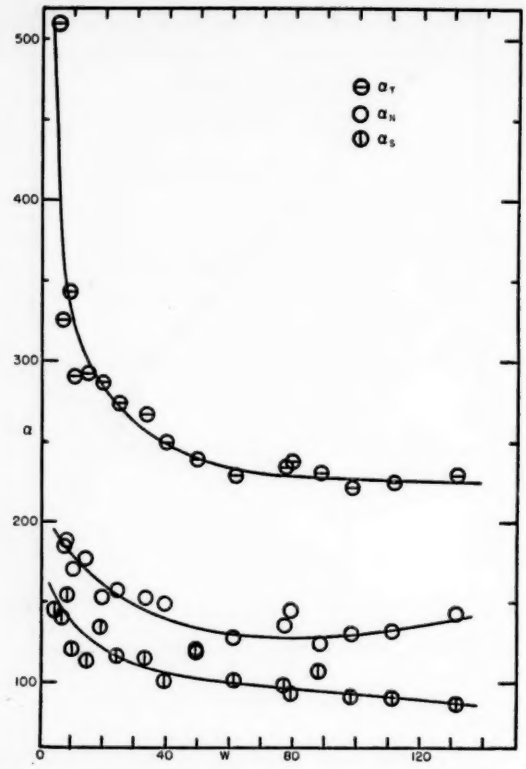

FIG. 8. The scattering of H_2^+ in propane.

scattering of hydrogen ions in propane are shown and also in Figs. 7, 8, and 9 with the potential function graphs in Figs. 10, 11, and 12. The potential laws as evaluated from the graphs are shown in Table III. In evaluating the potential functions, the approximate treatment suggested by Kells[5] was used as explained previously.[2]

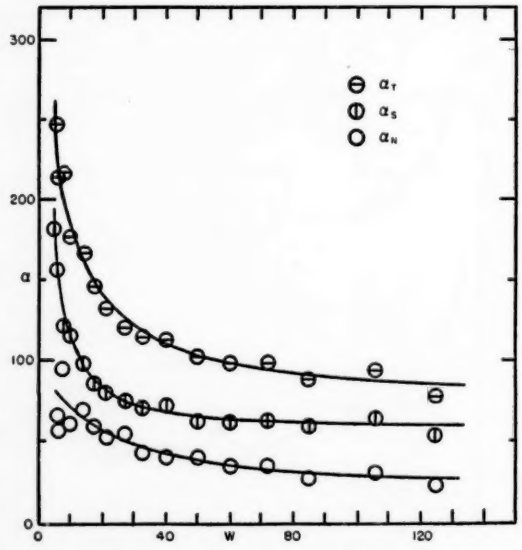

FIG. 9. The scattering of H_3^+ in propane.

[5] M. C. Kells, J. Chem. Phys. **16**, 1174 (1948).

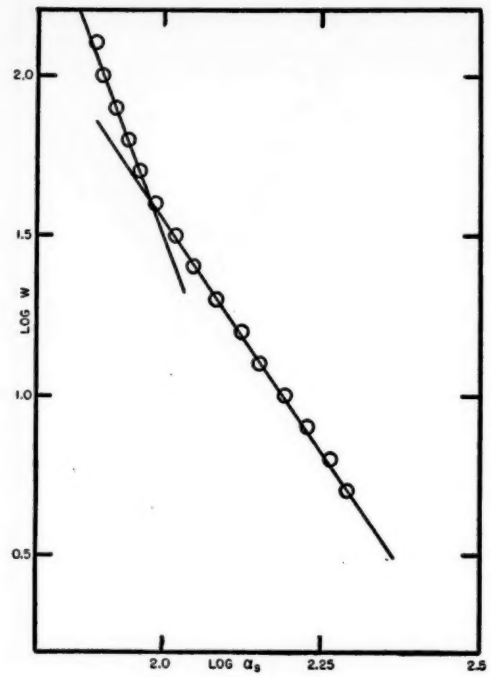

FIG. 10. The scattering of H^+ in propane.

DISCUSSION

In a given piece of apparatus with a definite geometry, the highest pressure usable to avoid the difficulties of multiple scattering decreases as the size of the molecules of the scattering gas increases. In some of our previous work with large molecules[2,6] it was found

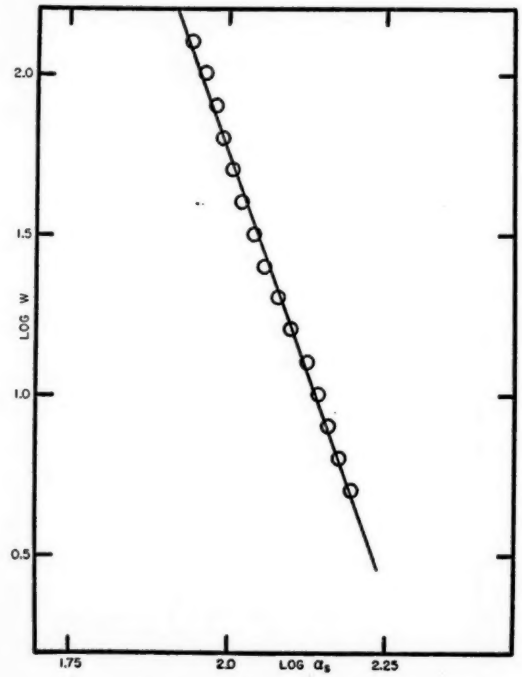

FIG. 11. The scattering of H_2^+ in propane.

[6] J. H. Simons and L. G. Unger, J. Chem. Phys. **13**, 221 (1945).

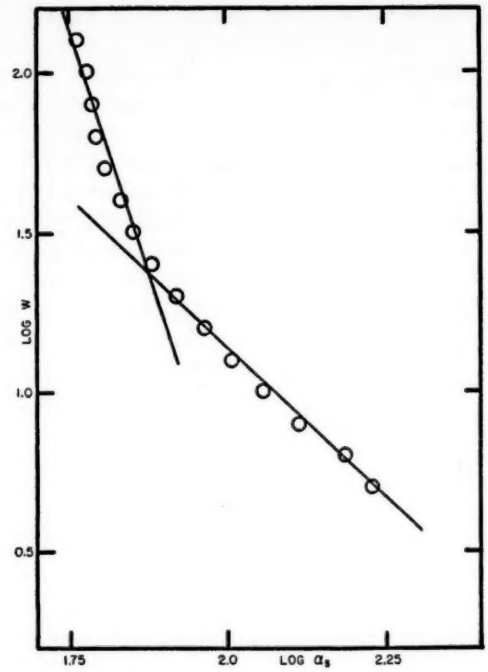

FIG. 12. The scattering of H_3^+ in propane.

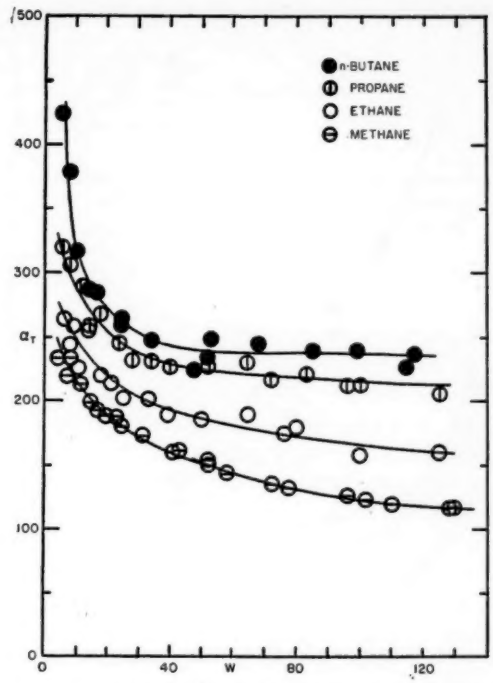

FIG. 14. The scattering of H^+ in the paraffins.

convenient to use higher pressures and to correct for multiple scattering by extrapolating α_T to zero pressure. In the present work, this was not necessary as demonstrated in Table III and Fig. 13 where it is seen that $\log 1/R$ *vs* P is a straight line for the experiment taken as an example. As α_T is dependent on the slope of this line, it is independent of pressure in the pressure range used. It has been shown previously[3] that α_S is a function of pressure and that it can be obtained by extrapolation to zero pressure without difficulty under conditions where α_T is independent of pressure. This is seen analytically in the following:

$$P=F(T)/\alpha_T \log\frac{1}{R_T}+\left[\frac{F(T)}{\alpha_T}\log R_T{}^0+P^0\right],$$

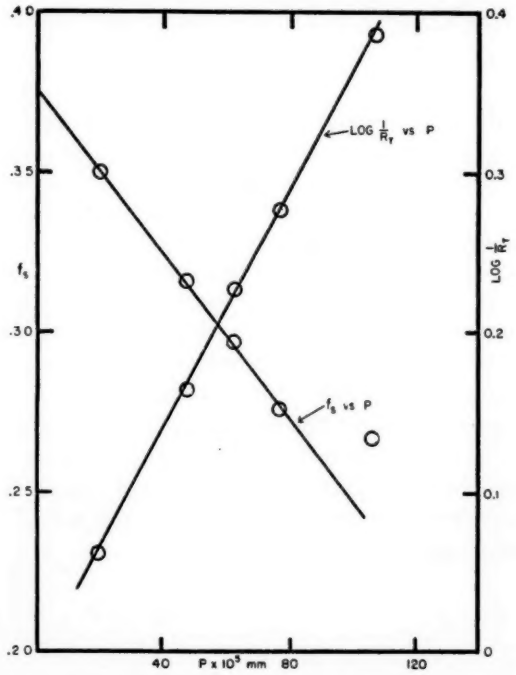

FIG. 13. The scattering of 100-volt H^+ in propane.

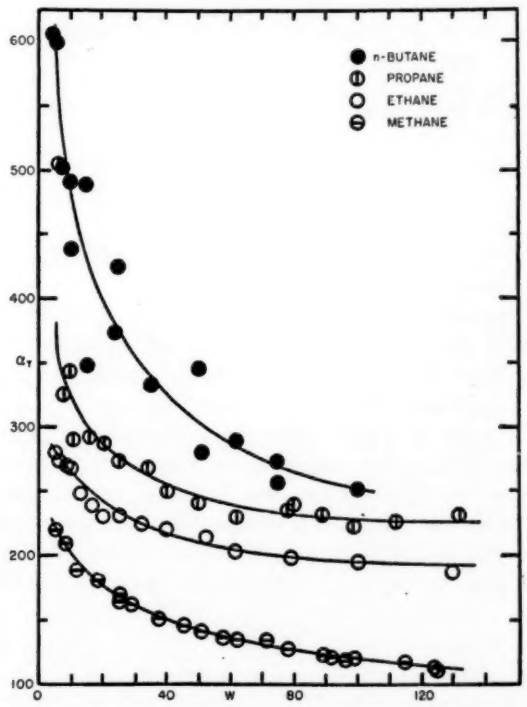

FIG. 15. The scattering of H_2^+ in the paraffins.

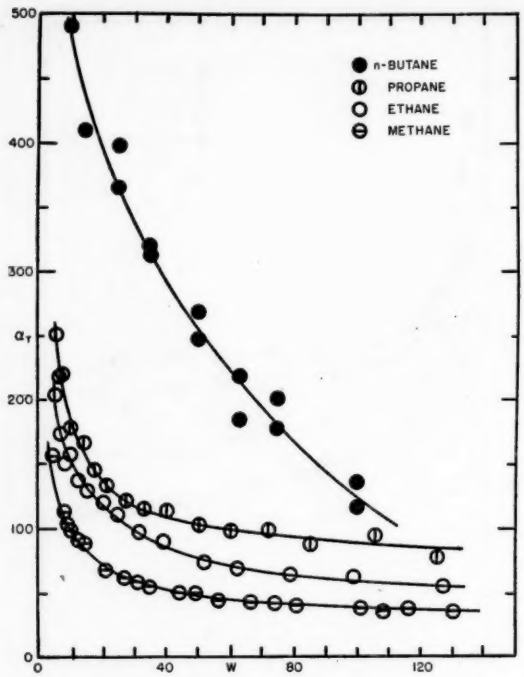

FIG. 16. The scattering of H_3^+ in the paraffins.

where

P = pressure,
$F(T)$ = temperature function = $2.303T/T^0l$,
α_T = total scattering cross section,
R_T = ratio of scattered to total ion current,
T = temperature,
T_0 = temperature, standard state,
l = length of scattering chamber, 4.176 cm, and
$R_T^0 = R_T$ at P^0 where P^0 is some low pressure such that α_T is independent of pressure.

If α_T is independent of pressure for R_T then the equation above is a straight line with a slope of $F(T)/\alpha_T$. This is seen in Fig. 13. Also if

$$f_s = \alpha_s/\alpha_T = [(1/R_s)-1]/[(1/R_T)-1],$$

then f_s is a linear function of P, and α_s is obtained by extrapolating f_s to zero P.

From plots of $\log\alpha_s$ *vs* $\log W$, Figs. 4–6 and 10–12, are obtained the values of K and n in the potential law $V = -K/r^n$. From the experimental data or smoothed out values taken from the scattering curves Figs. 1, 2, 3, 7, 8, and 9, these plots are sometimes relatively straight lines, but in many cases they are not. Where they are straight within the limits of experimental error, a simple potential law represents the interaction within the limits of the distances of approach of the interacting particles as covered by the experimental measurements. Where this plot is not a straight line, it can be treated approximately as two or more straight lines depending on its form, and the straight lines give an approximation of the interaction as a simple potential law valid only within the distances of approach of the interacting particles (or velocity of the ion beam) over which the straight line approximates the curved plot. In the physical picture of the interaction of an ion with a gas molecule, it is apparent that at great distances chiefly attractive forces will be operative. At closer distances which can be experienced at higher relative velocity, repulsive forces will operate. As these have a higher exponent in the potential law, the $\log\alpha_s$ *vs* $\log W$ plot will change slope at higher values of $\log W$. In cases where a combination of the particles of a chemical nature to produce a new species is possible, the value of the exponent may drop at high values of $\log W$ or at close distances of approach. This might give an S shaped form to the plot. If still higher values of $\log W$ were possible under experimental conditions, the exponent may again rise. The last portion may not be realizable experimentally as ionization would probably occur to confuse the interpretation at such high values of W.

TABLE IV. Cross sections for 100-ev protons.

Scattering gas	α_S^0	α_N^0	Ionization potential
He	3.3	<0.1	24.48
H_2	9.3	<0.5	15.43
H_2O	34	51	12.61
CH_4	47	77	13.04
C_2H_4	49	82	10.62
C_2H_6	58	112	11.78
C_3H_6	61	144	10.05
C_3H_8	80	130	11.30
n-C_4H_{10}	117	114	11.11
i-C_4H_{10}	203	71	11.06

It may be of interest to compare the total scattering of the four straight chain saturated hydrocarbons. This is done in Figs. 14–16. As neither α_s^0 nor α_n^0 vary greatly with V over small ranges in the vicinity of 100 volts, it is possible to compare these quantities for different substances in the vicinity of 100 volts. This is done in Table IV for H^+ ions. For the hydrocarbons it appears that α_s is consistent with an increase in the number of atoms in the molecule and is relatively additive. This gives an additional justification to a belief that there is some quantitative significance to α_N^0 as this is used in connection with the total scattering to evaluate α_s^0. As can be seen in Table IV, α_N^0 does not appear to be a simple function of the ionization potential of the scattering gas.

Some Molecular Constants of $HC^{13}N$†

R. E. KAGARISE, H. D. RIX, AND D. H. RANK
Department of Physics, The Pennsylvania State College, State College, Pennsylvania
(Received April 28, 1952)

The 003, 103, and 004 rotation-vibration bands of $HC^{13}N$ have been observed in the photographic infrared region of the spectrum. In addition, the Raman spectrum of the liquid was obtained with sufficient dispersion to measure the isotopic shift of ν_1. Values are given for B', B'', D', and D'' of the three infrared bands as well as for α_1 and α_3.

The average value of $B''=1.4400_6$ is in excellent agreement with $B''=1.44008$ calculated from microwave data and the velocity of light as $c=299{,}776$ km/sec.

THE use of multiple reflection absorption tubes makes possible the study of isotopic molecules in the photographic infrared region of the spectrum even though only modest amounts of material are available. We have constructed a two meter glass tube of the White[1] type having a volume of only 10 liters, with which we have been able to obtain optical paths up to 200 meters.

By making use of a small quantity of Eastman Kodak Company KCN which contained approximately 60 percent carbon 13, we have prepared about one liter of $HC^{13}N$ gas by the action of H_2SO_4 on the dry salt. We have photographed the 103 and 004 bands of the infrared rotation vibration system of this molecule under high dispersion in the first order of the 10-meter plane grating spectrograph previously described.[2] The 003 band was obtained in the first order of a 5-meter concave grating and the wavelength measurements were not as precise as those made on the other two bands. The wavelengths of the band lines were measured against second- and third-order iron standards and reduced to vacuum in the conventional manner. The wave numbers of the individual lines of the bands are listed in Table I.

DETERMINATION OF MOLECULAR CONSTANTS

The bands obtained were relatively weak and were not developed to quantum numbers higher than $J=21$. A small number of $HC^{13}N$ lines were blended with lines from the accompanying $HC^{12}N$ bands. These blends were not used to determine the molecular constants. We have determined the molecular constants by three different methods. The first of these was the conventional Δ_2F graphical method as described by Herzberg.[3] In addition, we have used the more precise least mean squares Δ_2F method previously described by one of us.[2] The third method employed was the $\nabla_+\tilde{\nu}$ and $\nabla_-\tilde{\nu}$ least mean squares method also described in reference 2. Since the maximum quantum number observed for the bands was $J=21$ and the precision of frequency measurements was only of the order of magnitude of ± 0.01 cm^{-1}, it was unnecessary to carry the fourth power term, i.e. $(D'-D'')m^4$, in the expression relating the frequencies of the band lines to the molecular constants and the m values for the band lines, in applying the last-mentioned method.

The values obtained for the molecular constants using the three different methods of evaluation are in satisfactory agreement so that we feel reasonably certain the errors in the B values are at most ± 0.0002 cm^{-1}. The average values obtained for the molecular constants in cm^{-1} are summarized in Table II.

RAMAN EFFECT

We have been able to obtain the Raman spectrum of $HC^{13}N$ vapor at a total pressure of the gas mixture of about 30 cm of Hg using an $f:2$ camera. The plates clearly showed the doublet ν_1 ($HC^{12}N$) and ν_1 ($HC^{13}N$). However, it was not possible to obtain photographs with sufficient dispersion to make a significant measurement of the isotopic shift for this mode of vibration in the vapor state.

We were able, however, to obtain the spectrum of the liquid with medium dispersion (14 A/mm) by using a

TABLE I. Wave numbers of the observed bands (ν_{vac} cm^{-1}) of $HC^{13}N$.

	003 $\nu_0=9571.73$ cm^{-1}		103 $\nu_0=11{,}591.42$ cm^{-1}		004 $\nu_0=12{,}561.84$ cm^{-1}	
J	R(J)	P(J)	R(J)	P(J)	R(J)	P(J)
0	9574.507	...	...	...	12,564.88	...
1	77.304	9568.866	11,596.97	...	567.32	12,558.99
2	79.976	65.906	599.62*	11,585.54	569.98	556.01
3	82.267*	62.906	602.17	582.56	572.53	552.93
4	85.259	59.872	604.64	579.44	575.01	549.81
5	87.752	56.775	607.05	576.23	577.39	546.61
6	90.216	53.532	609.38	572.96	579.69	543.33
7	92.587	50.307	611.68	569.63	581.95	539.97
8	94.958	47.005	613.83	566.22	584.10	536.52
9	97.238	43.662	615.91	562.71	586.15	533.00
10	99.477	40.244	617.98	559.12	588.14	529.41
11	9601.742	36.813	619.87	555.49	590.05	525.74
12	3.759	33.267	621.75	551.76	591.90	521.94
13	5.787	29.666	623.53	547.90	593.62	518.09
14	7.149*	26.022	625.25	544.05	595.30	514.23
15	9.684	22.291	626.83	540.08	596.88	510.16
16	11.605	18.538	628.43	536.03	598.37	506.10
17	13.340	14.761	629.87	531.91	599.81	501.95
18	14.973	10.859	631.27	527.72	12,601.11	12,497.70
19	16.715	6.883	632.60	523.48	...	493.34
20	18.331	2.887	11,633.80	519.13	12,603.54	488.96
21	9619.930	9498.814	...	514.69	...	484.51

* These lines were not used in the determination of the molecular constants.

† This research was carried out on Contract N6onr-269, Task V, ONR.

[1] J. U. White, J. Opt. Soc. Am. **32**, 285 (1942).

[2] Rank, Ruth, and Vander Sluis, J. Opt. Soc. Am. (to be published).

[3] G. Herzberg, *Infrared and Raman Spectra of Polyatomic Molecules* (D. Van Nostrand Company, Inc., New York, 1945), p. 390.

TABLE II. Molecular constants expressed in cm^{-1} for the 003, 103, and 004 bands of the infrared rotation vibration system of $HC^{13}N$.

	003	103	004
ν_0	9571.73	11,591.42	12,561.84
B'	1.4108	1.4012	1.3994
D'	3.0×10^{-6}	3.0×10^{-6}	2.5×10^{-6}
D''	3.10×10^{-6}	Average for three bands	
B''	1.4400_6	Average for three bands	
B''	1.4400_8	Calculated from microwave data[5] and $c=299{,}776$ km/sec[2]	
α_1	0.0096		
α_3	0.01016	From 004 band	

capillary sample tube having a volume of approximately 0.3 ml. The isotopic shift for $\Delta\nu_1$ in the liquid state was found to be $\Delta\nu_1=27.2$ cm^{-1}. Assuming that $\Delta\nu_1$ has the same value in the vapor phase as in the liquid and using Herzberg's[4] calculated value for $\nu_1=2092.4$ cm^{-1} for $HC^{12}N$, we obtain $\nu_1=2065.2$ cm^{-1} for $HC^{13}N$.

[4] See reference 3, p. 279.

CONCLUSION

In conclusion it can be stated that as soon as infrared measurements more extensive and precise than those of Richardson[5] are available for the fundamental vibrations and lower combination bands of $HC^{13}N$ it will be possible to calculate many of the anharmonicity constants with considerable precision. However, we feel that the frequencies of the fundamental vibrations are not known with sufficient accuracy at the present time to justify a calculation of these constants.

It should be noted that the value of B'' which we have obtained in this investigation is in excellent agreement with the recent microwave determination of B'' by Nethercot, Klein, and Townes[6] when combined with the value of the velocity of light determined from the $HC^{12}N$ bands.[2]

We are indebted to Dr. T. S. Oakwood of the Chemistry Department for the loan of the $KC^{13}N$ sample.

[5] W. S. Richardson, J. Chem. Phys. **19**, 1213 (1951).
[6] Nethercot, Klein, and Townes, Phys. Rev. (to be published).

THE JOURNAL OF CHEMICAL PHYSICS VOLUME 20, NUMBER 9 SEPTEMBER, 1952

The Properties of the Interstitial Compounds of Graphite. II. The Structure and Stability of Graphite Residue Compounds

GERHART HENNIG
Argonne National Laboratory, Chicago, Illinois
(Received March 27, 1952)

1. Controlled decomposition of lamellar compounds of graphite produces substances intermediate in composition between graphite and lamellar compounds. These intermediate compounds have been termed residue compounds. They are much more resistant to decomposition than the lamellar compounds.

2. The x-ray pattern of residue compounds shows a very slight increase in the c spacing of the graphite lattice. The increase is entirely insufficient to account for the trapped reactant. Consequently, the bulk of the trapped reactant is believed to be situated at crystal imperfections.

3. Quantitative studies of the composition of graphite bromide residue compounds have shown that their composition is strongly dependent on the type and subdivision of the graphite used and the temperature to which the compounds have been heated.

INTRODUCTION

GRAPHITE reacts with a large number of substances, such as bromine, ferric chloride, and potassium, to form compounds in which single layer planes of the reactant are wedged between the carbon layer planes of the graphite. These so-called lamellar compounds have been studied quite extensively.[1] Most of the reactant in the lamellar compounds can be removed by essentially reversing the procedure by which the lamellar compounds were formed. However, in all cases examined, it has been found that a considerable amount of reactant remains which cannot be removed without resorting to fairly drastic measures. The amount of reactant remaining is dependent on the amount of reactant present in the original lamellar compound. Compounds of this type, in which small amounts of reactant are held very strongly in the graphite, have been termed residue compounds. These residue compounds were described in the preceding paper of this series,[2] and in a preliminary report[3] from this laboratory on the diamagnetism of graphite bromide. Furthermore, it is likely that Ganguli[4] who reported the magnetic susceptibility of lamellar graphite bisulfate, was actually measuring residue compounds instead. He washed his bisulfate compounds for two

[1] See for example the review article by H. L. Riley, Fuel **24**, 1, 43 (1945).

[2] G. R. Hennig, ANL-4579 (February 15, 1951); J. Chem. Phys. **19**, 922 (1951).
[3] M. Goldsmith, J. Chem. Phys. **18**, 524 (1950).
[4] N. Ganguli, Phil. Mag. (7) **21**, 355 (1936).

days in water; this treatment is known to destroy the lamellar compound.

The purpose of the present paper is to describe experiments relating to the structure and stability of the residue compounds. It was pointed out in the preceding paper[2] that at least two different mechanisms can be postulated which will account for the ability of graphite to form residue compounds. The reactant may be trapped between the carbon planes as in the lamellar compounds, but in much lower concentrations. Alternately, the reactant may be trapped at imperfections of the crystal lattice. X-ray investigation of the residue compounds has been the most decisive method of distinguishing between these two mechanisms of trapping, as shall be shown. Molecules or ions trapped between the layer planes would cause a definite increase in the *c* axis of the graphite. Molecules trapped at imperfections would be unlikely to cause a change in the *c* axis of the graphite if the imperfections are randomly distributed. In fact, they would probably cause either no change in the diffraction pattern, or else only a line broadening if random imperfections are enlarged or new imperfections are formed.

The trapping centers have been characterized further by examining the residue compounds formed from various types of graphite which differ in the degree of perfection of the graphite crystallites.

The experiments to be described have been confined to the bromide and bisulfate residue compounds of graphite. The bromide is the easiest compound to prepare and is, therefore, best suited to quantitative studies. The bisulfate is of special interest for x-ray studies, since the bisulfate ion is particularly large.

EXPERIMENTAL

Materials

Six different types of graphite have been used. They will be identified by Roman numerals.

I. Pitch-bonded artificial graphite (Acheson). This material is very similar in properties to the National Carbon Company's Spectroscopic Electrodes. Similar material was used almost exclusively in the work reported in the previous paper of this series.

II. Kish. These large flakes of graphite which form on molten steel were washed repeatedly with hydrofluoric and hydrochloric acids.

III. Flakes of Madagascar natural graphite. The diameter of these particles was approximately ten times their thickness. The crystals were cleaned thoroughly before use.

IV. Microfyne graphite (Dixon Crucible Company, New Jersey). This is a finely powdered natural graphite which has a particle size of a few microns. The material was purified before use.

V. Crystals of Ogdensburg natural graphite. These crystals were kindly furnished by W. Primak of this laboratory. The crystals had been leached from limestone rock, purified first by an acid treatment and then by heating in helium to 3000°C. For this work, a particle size of 160 microns was isolated by screening.

VI. SP-1 spectroscopic graphite powder (National Carbon Company, Cleveland).

Preparation of the Graphite Bisulfate Residue Compounds

Samples of graphite were oxidized for one day in a 12*M* sulfuric acid solution 0.1 molar in nitric acid. The resulting lamellar-type compounds were converted slowly to residue compounds by washing with 8*M* sulfuric acid for one hour and then with distilled water for from two to four hours. The samples were dried at 100°C and their composition was determined by weighing before and after treatment.

Preparation of the Graphite Bromide Residue Compounds

Graphite bromide lamellar compounds were first prepared in either of two ways. Graphite was reacted with bromine either in a vacuum line which included a thermostated trap containing bromine at a known temperature and therefore vapor pressure, or in tightly stoppered bottles above solutions of bromine in carbon tetrachloride. At any pressure the bromination was initially rapid, but the reaction was allowed to proceed for at least a day to approach equilibrium. The brominated samples were weighed in tightly stoppered bottles, and their composition was calculated from the weight of the bromine taken up.

Graphite bromide residue compounds were prepared by debrominating these lamellar compounds in an air stream for 24 hours at room temperature. Their composition was again determined by weighing. It was noticed that pitch-bonded artificial graphite and finely powdered graphite specimens usually attained a constant weight within one day of debromination. Heavily brominated, coarse graphite powders sometimes lost small amounts of bromine for several additional days.

Preparation of Samples for X-Ray Measurement

The solid graphite samples were ground in a mortar, and the powder thus obtained was bonded with a small quantity of Duco cement for the diffraction measurements. The natural graphite samples were already in powder form and were not crushed further after the chemical treatment.

X-Ray Diffraction Measurements

The *a* and *c* spacings for thirteen different residue compounds, together with appropriate blanks, are given in Table I. It was found that the spacings of the residue compounds differed very little from those of graphite itself.

In addition to the measurements of Table I, it was noticed that the crystallite size of the residue compounds decreased with increasing concentration of impurity. Nevertheless the materials were still crystalline, of crystallite size 300A or larger.

Composition of the Residue Compounds

Four different factors were found to influence strongly the composition of residue compounds. These factors

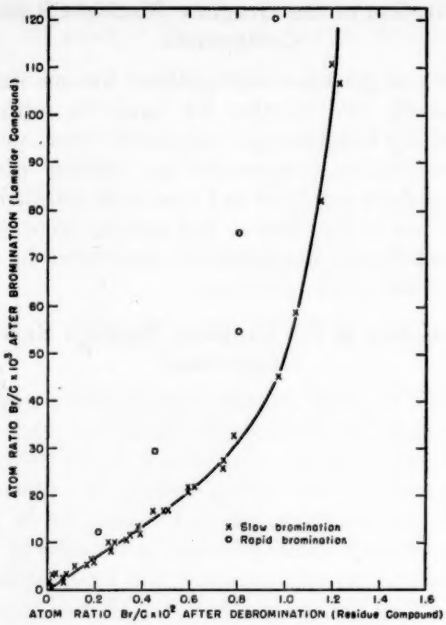
ATOM RATIO Br/C x10³ AFTER BROMINATION (Lamellar Compound)
ATOM RATIO Br/C x10² AFTER DEBROMINATION (Residue Compound)
x Slow bromination
o Rapid bromination

FIG. 1. Composition of the graphite bromide residue compound as a function of the composition of the parent lamellar compound (pitch-bonded graphite).

were the chemical composition of the parent lamellar compound, the type of graphite used, the subdivision of the graphite, and the temperature to which the residue compound had been heated.

The dependence of the composition of the residue compound on the composition of the parent lamellar compound was studied in some detail for pitch-bonded artificial graphite (Type 1). The atom ratio of bromine in the lamellar compound has been plotted in Fig. 1 against the atom ratio of bromine retained in the residue compound. It is apparent that the retention is an approximately linear function of the bromination for compounds whose atom ratio of retained bromine does not exceed *ca* 0.006. Also included in Fig. 1 are some data on rapid bromination in saturated bromine vapor followed after a few minutes by debromination. This method obviously reduced the retention in the residue compounds.

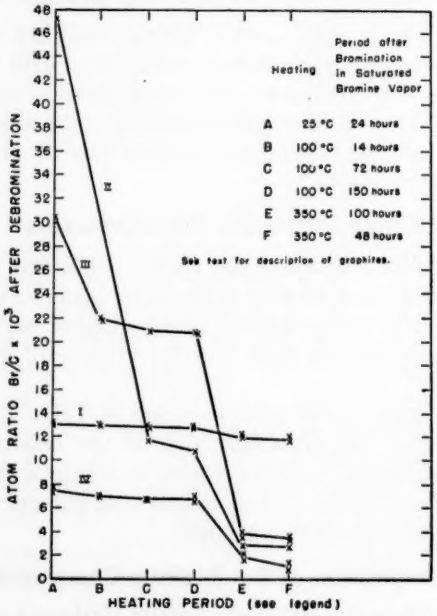
ATOM RATIO Br/C x 10³ AFTER DEBROMINATION
HEATING PERIOD (see legend)
Heating Period after Bromination in Saturated Bromine Vapor
A 25 °C 24 hours
B 100 °C 14 hours
C 100 °C 72 hours
D 100 °C 150 hours
E 350 °C 100 hours
F 350 °C 48 hours
See text for description of graphites.
II
III
I
III

FIG. 2. The effect of temperature on the stability of graphite bromide residue compounds for several types of graphite.

The effect of graphite type on the composition of the residue compounds was investigated by preparing the most concentrated lamellar compounds obtainable in saturated bromine vapor, and subsequently determining the amount of bromine remaining in the residue compound after debrominating these lamellar compounds in the usual manner. The concentration of bromine in the resultant residue compounds obtained from four types of graphite increased in the order

TABLE I. The x-ray spacings of graphite residue compounds.

Sample No.	Graphite type	Reactant	Concentration of reactant (moles/g atom $C \times 10^2$)	X-ray spacing (KX units) *a*-axis	*c*-axis
1	III	Blank		2.4562 ±0.0002	6.695 ±0.005
2	III	$H_2SO_4-HSO_4^-$	0.27	2.456 ±0.001	6.694 ±0.001
3			0.56	2.457 ±0.001	6.700 ±0.004
4			0.78	2.458 ±0.001	6.689 ±0.006
5			1.39	2.456 ±0.002	6.702 ±0.005
6			2.49	2.456 ±0.002	6.703 ±0.004
7			3.56	2.456 ±0.002	6.699 ±0.004
8[a]			1.06	2.457 ±0.002	6.701 ±0.006
9[a]			0	2.458 ±0.003	6.698 ±0.005
10[b]	III	Br_2	0.345	2.457 ±0.001	6.697 ±0.003
11	V	Blank		2.4560 ±0.0002	6.693 ±0.002
12	V	Br_2	0.335	2.456 ±0.001	6.692 ±0.007
13			1.33	2.456 ±0.001	6.748 ±0.008
14	I	Blank		2.457 ±0.001	6.696 ±0.007
15	I	$H_2SO_4-HSO_4^-$	0.59	2.457 ±0.001	6.68 ±0.01
16			0.70	2.457 ±0.003	6.70 ±0.01

[a] Prepared from residue compounds by heating. The mole ratio was 0.025 before heating to 230°C (Sample 8) and 0.029 before heating to 450°C (Sample 9).
[b] Prepared from a residue compound by heating to 100°C.

IV<I<III<II. This relationship is indicated on the left side of Fig. 2. At least part of the difference between various graphite types can be traced to the effect of particle size since the particle size of the materials used also increased in the above order. This effect of subdivision of the graphite on the composition of the residue compounds was studied on powders of natural (Type III) and artificial (Type VI) graphite. The results have been plotted in Fig. 3 as compositions of the parent lamellar compound against compositions of the residue compounds. It is apparent from Fig. 3 that finely divided graphite retained considerably less bromine than larger particles. On the other hand, there did not appear to be much difference between artificial and natural graphite powders of comparable particle size.

The composition of these residue compounds after heating to various temperatures is also shown in Fig 2.

It is evident that only Type I graphite forms residue compounds which remain reasonably stable at elevated temperatures. The composition of the residue compounds after heating at elevated temperatures was not particularly dependent on the subdivision of the samples. The retention of bromine at 310°C for numerous powders of natural and artificial graphite can be approximated by one curve (Curve *A*, Fig. 3) regardless of the particle size of the powder.

Chemical Reactions of Residue Compounds

Incidental to the measurements on the stability of residue compounds, some anomalous reactivities were observed. The graphite bromide residue compounds were found to show a higher chemical reactivity than graphite. Chlorine reacted quite rapidly with the residue compound although graphite itself reacts very slowly with chlorine. A few samples of standard artificial graphite were suspended in the saturated vapor above boiling liquid chlorine for 30 minutes, quickly transferred to potassium iodide solutions, and allowed to stand for at least 30 minutes. The amount of chlorine taken up was determined by titration with standard thiosulfate. It was found that the graphite had acquired only about 0.3 atom percent of chlorine. On the other hand, residue compounds containing about one atom percent of bromine gained between 3 and 4 atom percent of chlorine, or roughly ten times the amount acquired by pure graphite under similar conditions.

Aluminum trichloride does not normally react with graphite at room temperature. At 200°C in vacuum it did not cause any swelling of a graphite sample and the sample retained only 0.07 molecule of trichloride per 100 carbon atoms, probably because of surface contamination. A graphite bromide residue compound containing 1.44 bromine atoms per 100 carbon atoms reacted rapidly with aluminum trichloride, swelling first, and then falling apart. Its weight increase corresponded to 1.97 molecules of trichloride per 100 carbon atoms.

TABLE II. The fraction of reactant present in interlamellar positions in graphite residue compounds.

Sample No.	Reactant	Total concentration (moles/g atom $C\times10^5$)	Fractional change in c spacing ($\Delta c/c\times10^4$)	Concentration of interlamellar reactant from x-ray (moles/g atom $C\times10^5$)	Interlamellar fraction of reactant ($\times10^3$)
2	$H_2SO_4-HSO_4^-$	270	+ 1.5	1.4	5±30
3	$H_2SO_4-HSO_4^-$	560	+ 7.5	6.9	12±22
4	$H_2SO_4-HSO_4^-$	780	− 9.0	(− 8.3)	(−11±20)
5	$H_2SO_4-HSO_4^-$	1390	+10.4	9.6	7±10
6	$H_2SO_4-HSO_4^-$	2480	+12.0	11.1	4± 5
7	$H_2SO_4-HSO_4^-$	3560	+ 6.0	5.6	16±36
8	$H_2SO_4-HSO_4^-$	1060	+ 9.0	8.3	8± 8
9	$H_2SO_4-HSO_4^-$	0	+ 4.5	4.2	···
10	Br_2	345	+ 3.0	3.3	10±40
12	Br_2	335	− 1.5	(− 1.7)	(− 5±45)
13	Br_2	1330	+76.2	84	63±12
15	$H_2SO_4-HSO_4^-$	590	−23.9	(−22.1)	(−37±39)
16	$H_2SO_4-HSO_4^-$	700	+ 6.0	5.6	8±32

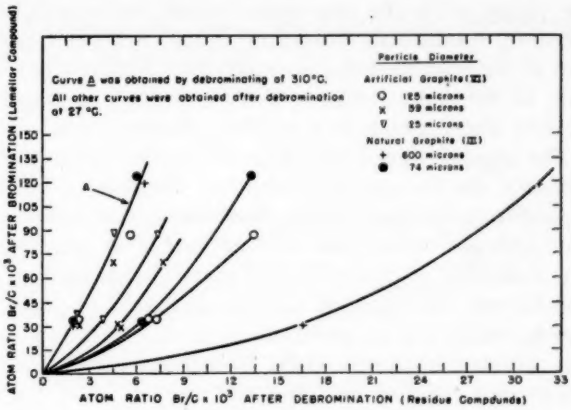
Curve A was obtained by debrominating at 310°C.
All other curves were obtained after debromination at 27 °C.
Particle Diameter
Artificial Graphite (II)
125 microns
59 microns
25 microns
Natural Graphite (III)
600 microns
74 microns
ATOM RATIO Br/C x 10³ AFTER BROMINATION (Lamellar Compound)
ATOM RATIO Br/C x 10³ AFTER DEBROMINATION (Residue Compounds)

FIG. 3. Effect of particle size on the relation between the composition of the parent graphite bromide lamellar compound and the corresponding residue compound.

Iodine and pure graphite did not react, but small amounts of residual bromine in the graphite induced an uptake of iodine which was measurable after an hour in saturated iodine vapor at 183°C. The reaction was very pronounced in samples reacted with iodine vapor at room temperature for 6 months. In these samples the presence of one atom percent of residual bromine induced enough iodine uptake to decrease the electrical resistance by more than 50 percent.

DISCUSSION

The conversion of graphite to residue compounds changed the *a* and *c* axes very little (Table I). Actually the change in the *a* axis never exceeded the limits of error of the measurements. The *c* axis, however, seemed to increase rather consistently. From this increase the quantity of interlamellar impurity was calculated by suitable assumptions regarding the size of bisulfate ions or bromine molecules between the planes. A volume of $95A^3$ was used for a bisulfate ion or a sulfuric acid molecule. The bromine atom was assumed to have an average volume of $40A^3$. These volumes are the average volumes occupied by the respective molecular species in their compounds with heavy cations. They are also in fair agreement with the molecular volumes calculated from the density of the corresponding liquid, and furthermore agree with the volumes deduced from the x-ray spacings[5,6] of the graphite bromide and bisulfate lamellar compounds. The concentration of interlamellar impurities in the residue compounds, calculated from the data of Table I, have been tabulated in column 5 of Table II. Column 3 shows the total concentration of impurities determined gravimetrically. The fraction of the impurities thus found to be interlamellar, i.e., accessible to x-ray measurement, has been tabulated in column 6, together with the probable error inherent in the x-ray measurements. It is apparent that only 1 percent or less of the impurities are trapped between

[5] W. Rüdorff, Z. anorg. u. allgem. Chem. **245**, 383 (1941).
[6] W. Rüdorff, Z. physik. Chem. **B45**, 42 (1940).

the planes with the one exception of compound 13, a heavily brominated compound in which about 6 percent of the bromine is still interlamellar. Apparently the bulk of the impurities are always trapped at imperfections where x-rays do not detect them.

The imperfections which trap the impurities are very probably the crystallite boundaries, because no other type of imperfection is known to be present in sufficient concentration to account for the extent of trapping. The definition of crystallite boundary should probably also include the edges of the mosaic blocks of perfect regions within the crystallites.

A number of observations have been made which allow some conclusions about the mechanism of trapping. It was found (Fig. 2) that small particles retained less bromine per mole of carbon than large particles. This makes it probable that the imperfections are quite large, at least along the average a direction of the crystallites composing the particles, so that an appreciable fraction of the imperfections communicate with the surface and, therefore, a fairly sizeable area at the periphery of the particle is able to expel its impurities to the surface. This area will be free of trapped bromine and, since it constitutes a larger fraction of the total volume in small particles than in large ones, will result in an effective decrease in the retention of bromine by small particles.

Actually, the width of the bromine-free area and therefore the average length of the imperfections can be estimated from the data in Fig. 2. Disregarding altogether the c direction of the crystallites, one can consider each particle as a disk of radius r. The imperfections which do not communicate with the surface are found in an area $a=(r-x)^2\pi$ where x is the average length of the imperfections. The retention of bromine is $R=ab/r^2\pi$ where b is a proportionality constant. Combining the values of the retention for large and medium sized spectroscopic crystals at high and at intermediate brominations, one calculates an approximate imperfection length of 10 microns. Actually the calculated length of the imperfections increased somewhat with the particle size. The dependence of the retention of bromine on the particle size of the graphite powders decreased after debromination at 310°C. It appears, then, that a much larger fraction of the imperfections becomes accessible to the outside, and that the remaining inaccessible imperfections are much smaller than the particle diameters, because for small x, the retention $((r-x)^2/r^2)b$ becomes nearly independent of r. Furthermore, the imperfections are probably much smaller, and more confined, in pitch-bonded graphite than in unbonded graphite, because bromine is retained much more tenaciously in the pitch-bonded material, as shown by reference to Fig. 2.

Another observation which requires explanation is the fact (Figs. 1 and 3) that the retention of bromine depends strongly on the composition of the parent lamellar compound. Two quite different explanations are possible. It may well be that the imperfections are quite short in the average c direction of the particles, so that an incompletely brominated lamellar compound contains a considerable number of imperfections which have simply not yet become accessible to bromine and which will only become accessible on complete bromination. In this connection it must be remembered that in all the lamellar compounds known,[1] incomplete reaction implies that layers of reactant and layers of unreacted graphite alternate with great regularity. Any imperfections in those unreacted carbon layers are also unlikely to contain reactant unless they are wide enough to communicate somewhere with a layer of reactant. The rather abrupt change in the slope of Fig. 1 would occur at the point where bromination has proceeded far enough to fill most of the imperfections.

The alternate explanation which would explain the composition of the residue compounds implies that the imperfections are long in all directions, but that the concentration of bromine in the imperfections is pressure dependent. On this model the change in the slopes of Figs. 1 and 2 could be attributed to a decrease in the volume of the imperfections caused by the swelling of the crystallites. The observation (Fig. 1) that rapid bromination resulted in abnormally low retention of bromine probably indicates that invasion of the imperfections by bromine is slower than the formation of lamellar bromine layers.

It is hoped that a detailed study of the residue compounds derived from lamellar compounds other than the bromide and bisulfate will elucidate further the structure of the residue compounds.

ACKNOWLEDGMENT

The author is particularly indebted to Professor W. H. Zachariasen, Dr. S. Siegel, and H. A. Plettinger for their invaluable help in taking the x-ray photographs and interpreting the patterns. Without this important assistance the interpretation of the nature of the residue compounds would have been impossible.

The Properties of the Interstitial Compounds of Graphite. III. The Electrical Properties of the Halogen Compounds of Graphite

GERHART HENNIG
Argonne National Laboratory, Chicago, Illinois
(Received March 27, 1952)

The presence of lamellar or of residual bromine in artificial graphite reduces the resistance, the absolute magnitude of its temperature coefficient near room temperature, and the magneto resistance. The Hall coefficient increases and eventually changes from negative to positive values. The changes resemble very closely those obtained in the oxidation of graphite in sulfuric acid. This similarity in properties suggests that the electron acceptors in these compounds are only weak scattering centers for conduction electrons.

Since the electrical properties of graphite bisulfate and of graphite bromide are very similar, it may be assumed that both compounds are of a similar type. Since the bisulfate compound is ionic in nature, the bromine in graphite bromide is also probably ionized. On this assumption the graphite bromides have the formulas $C_nBr \cdot 3\ Br_2$ for the lamellar and $C_nBr \cdot 2.25\ Br_2$ for the residue compounds.

Chlorine reacts with graphite at low temperatures only. The properties of the compounds of chlorine and graphite resemble in all respects those of the compounds of bromine and graphite. Attempts to react iodine and graphite have failed. Iodine chloride, however, reacts rapidly with graphite.

INTRODUCTION

THE oxidation of graphite to graphite bisulfate was shown in the first paper[1] of this series to change the electrical properties of graphite considerably. The bisulfate compounds exhibited the properties of a semiconductor which had lost electrons from its conduction band.

It is desirable to know whether the bisulfate ions exert any specific effects other than the removal of electrons from the conduction band or the production of holes in the nearly full band. These specific effects would include electron scattering and distortion of the band structure and would depend both on the charge and the radius of the electron acceptor. The magnitude of these specific effects can be estimated by measuring the properties of graphite compounds in which electron acceptors other than bisulfate ions are present. Compounds which satisfy this criterion were selected by a cursory examination of their Hall coefficients and include the compounds of graphite with halogens, with nitrogen oxides and acids, and with ferric chloride. Of these compounds, the halogen derivatives are considerably more convenient to study and have therefore been examined in some detail. As in the preceding papers,[1,2] the properties of the lamellar compounds were measured as well as the properties of the compounds which remain when the lamellar compounds are decomposed gently, the so-called residue compounds.[1,2]

In the course of this investigation, additional information has been obtained on the structure of the halogen compounds, and, in fact, the existence of two new graphite compounds, the chloride and the iodine monochloride, has been demonstrated.

Fluorine is known to react with graphite to form $(CF)_n$.[3] However, the resistance of this compound is extremely high. Therefore, the compound does not resemble graphite bisulfate at all, and its examination was deferred at least temporarily.

Bromine reacts with graphite to form typical lamellar compounds in which the amount of intercalated bromine increases with the external bromine pressure. Although Frenzel[4] has been quoted[5,6] as stating that the compound loses its bromine completely on standing in air, this is not strictly true. Instead, residue compounds of graphite bromide are formed[2] in which as much as one-third of the original bromine is retained. The present paper is devoted primarily to the study of these compounds.

Reactions of chlorine and iodine with graphite have not been described previously. In the present work the reactions of these two halogens with graphite were studied. Also studied were the reactions of graphite with iodine monochloride, a particularly interesting case since iodine monochloride resembles bromine in many respects.

As in the investigation of the graphite bisulfates, the halogen compounds of graphite were characterized mainly by the electrical resistance, its temperature dependence, and the Hall coefficient. It is not too difficult to correlate these properties with theory. The magneto resistance was also determined although its value from a theoretical point of view is somewhat dubious. The magnetic susceptibility is of theoretical interest but is difficult to determine routinely. However, a few isolated measurements of the susceptibility of graphite bromide have already been reported by M. Goldsmith[7] of this laboratory.

[1] G. Hennig, ANL-4579 (February 15, 1951); J. Chem. Phys. **19**, 922 (1951).
[2] G. Hennig, ANL-4645 (June 28, 1951); J. Chem. Phys. **20**, 1438 (1952).
[3] O. Ruff and O. Bretschneider, Z. anorg. u. allgem. Chem. **217**, 1 (1934).
[4] A. Frenzel, dissertation, Tech. Hochschule, Berlin, 1933.
[5] W. Rüdorff, Z. anorg. u. allgem. Chem. **245**, 383 (1941).
[6] H. L. Riley, Fuel **24**, 8 (1945).
[7] M. Goldsmith, J. Chem. Phys. **18**, 524 (1950).

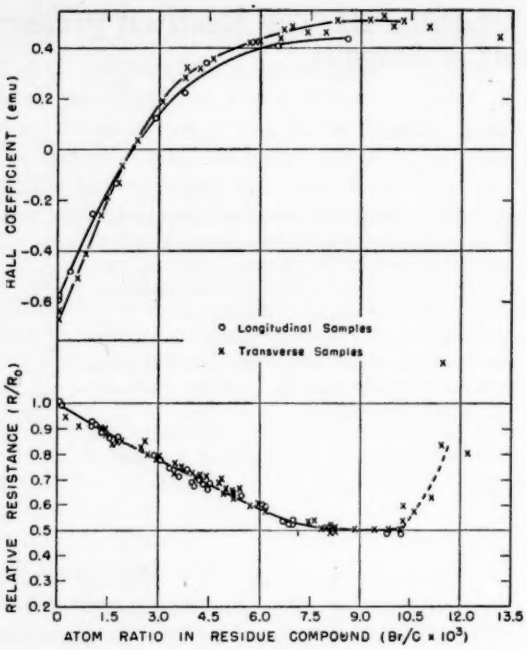
HALL COEFFICIENT (emu)
RELATIVE RESISTANCE (R/R0)
o Longitudinal Samples
x Transverse Samples
ATOM RATIO IN RESIDUE COMPOUND (Br/C x 10³)

FIG. 1. The electrical resistance and Hall coefficient of graphite bromide residue compounds.

EXPERIMENTAL PROCEDURE AND RESULTS

Graphite Bromide Compounds

As in all the experiments reported in this paper, the graphite used was a pitch-bonded artificial graphite.[1,2] Most of the resistance and Hall measurements were made on separate samples. The Hall samples were flat plates, usually 6×16×1 mm in size. They were clamped between current leads of amalgamated brass and potential probes of pointed tungsten. The resistance samples were either 2×2×40 mm or 1×1×30 mm rectangular prisms. These samples and their mounting have been described in a preceding paper.[1] Samples were brominated in carbon tetrachloride solutions of bromine, in the vapor above these solutions, or in the vapor above thermostated liquid bromine. These procedures, which have been described in the preceding paper,[2] all appeared to yield identical products. During the bromination, which was allowed to proceed for at least a day at room temperature, the resistance was measured periodically. When the resistance became constant, the bromine was removed by pumping or placing the samples in a fume hood. Again at least 24 hours were allowed for debromination. The debrominated samples, the so-called residue compounds,[2] were then weighed, and from the increase in weight the atom ratio of bromine to carbon was calculated. The resistances and Hall effects of these residue compounds have been plotted in Fig. 1 against this atom ratio. Both longitudinal samples, whose long dimension coincided with the axis of extrusion, and transverse samples were used. Although their initial resistances R_0 differed by an orientation factor of 2, and their initial Hall effects by a factor of 1.1, bromination left the orientation factors unchanged. Beyond an atom ratio (Br/C) of 0.01, the resistances rose abruptly and became unreproducible. This was caused by disintegration of the samples, which became bent and warped at the same time.

The Hall coefficients of lamellar graphite bromides were determined on combination resistance and Hall samples described previously.[1] These samples were all cut with their long axis at right angles to the axis of extrusion of the graphite bar. The samples were brominated in solutions of bromine in carbon tetrachloride and measured in these same solutions. The results have been represented in the upper part of Fig. 2. The lower curve of Fig. 2 represents the resistances of lamellar graphite bromides at various compositions. This curve was obtained indirectly. The resistance of a given lamellar compound was measured, and the compound was then converted to the residue compound. The composition of the residue compound was determined by weighing it. From this composition the atom ratio (Br/C) in the parent lamellar compound was obtained by referring to Fig. 1 of the previous paper,[2] in which compositions of residue compounds have been plotted against the composition of the parent lamellar compounds.

A few determinations were made of the magnetic field dependence of the resistance. All of these measurements were made on combination Hall and resistance samples. The field was always at right angles to the flow of the current. The resistances relative to the resistance of a sample at zero magnetic field at room temperature have been plotted in Fig. 3 against the square of the magnetic field for both lamellar and for residue compounds.

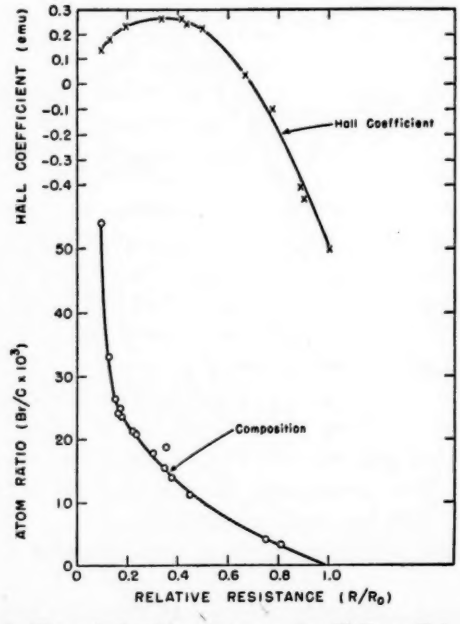

FIG. 2. The relationships between the Hall coefficient, electrical resistance, and composition of lamellar graphite bromide compounds.

The temperature dependence of the resistance was measured for residue compounds only and is shown in Fig. 4. The resistances have been calculated relative to the resistance R_0 of unreacted graphite at 25°C. The measurements in liquid nitrogen and at room temperature presented no difficulty. It was found, however, that dry ice-acetone baths could not be used because acetone slowly increased the resistance of the residue compounds. Petroleum ether and dry ice were found to have a smaller influence on the resistance; however, all samples were remeasured in petroleum ether at room temperature, and the results were corrected for any drift which had occurred. (Incidentally, the drift in acetone and other solvents reversed itself completely after evaporation of the solvent.)

The residue compounds of pitch-bonded graphite slowly lose bromine at temperatures above 1000°C. The mechanism of this debromination is probably complex since the rate is affected by unusual conditions. It

TABLE I. Effect of temperature on the properties of a typical graphite bromide residue compound.

Heat-treatment Time (min)	Heat-treatment Temp. (°C)	Relative resistance at 25°C (R/R_0)	Fractional weight increase ($100\ \Delta w/w$)	Hall coefficient (emu)	Average temp. coefficient of resistance between −196° and 25°C $\left(\frac{\Delta R \times 10_4}{(\Delta T)(R_{25})}\right)$
		1	0	−0.519	−31.7
		Graphite			
		Graphite bromide residue compound			
		0.478	6.38	+0.394	− 4.9
5	1000	0.610	5.15	+0.364	−10.7
5	1150	0.681	4.38	+0.342	−12.8
5	1400	0.829	3.27	+0.252	−16.9
5	1600	1.01	2.08	+0.122	−21.5
5	1800	1.18	1.12	−0.049	−24.6
5	1960	1.46	0	−0.359	−28.9
30	1960	1.38	−0.44	−0.466	−30.5
30	1965	1.32	−0.48	−0.480	−30.7

increased, for instance, whenever a sample remained for any length of time at room temperature between the heating periods. Furthermore, the decomposition produced not only bromine but also a substance which condensed on the cool parts of the furnace. This substance was red at first and turned dark later. The graphite samples swelled and became distorted during the debromination. Nevertheless, a set of resistance and Hall measurements was made on a bromide residue compound which was heated in gradual steps to 1965°C.

The data of Table I indicate that, as the heating progressed, the properties gradually approached those of bromine-free graphite. It is noteworthy that the total weight loss exceeded the weight of bromine in the sample. Thus, the bromine apparently carried some carbon with it on debromination. Also of interest is the fact that the resistance reached a maximum value after debromination of 1960°C and gradually decreased on further heating. This may indicate that the distortion

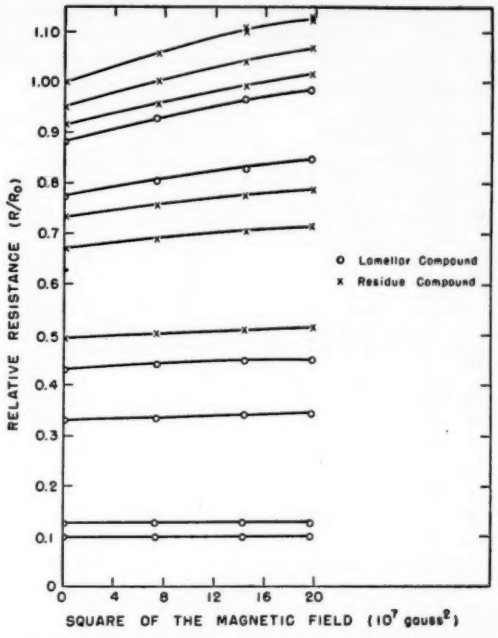

FIG. 3. The effect of magnetic field on the electrical resistance of graphite bromide compounds.

caused by the loss of bromine is relieved by plastic flow of the graphite and by diffusion.

Graphite Chloride Compounds

Resistance samples of graphite were suspended in liquid chlorine at −33°C. One of the samples was permanently mounted for resistance measurement and served as a monitor during chlorination. At intervals of approximately eight hours, samples were withdrawn and dechlorinated. During chlorination, the relative resistance decreased to 0.1 only after three days at −33°C. The slowness of this reaction is probably the

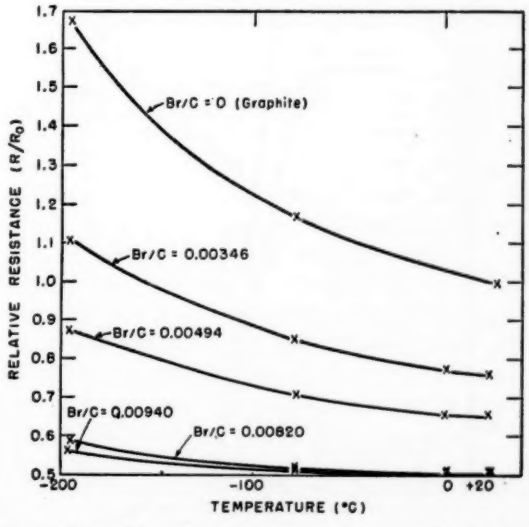

FIG. 4. The effect of temperature on the electrical resistance of graphite bromide residue compounds. (Relative to graphite at room temperature.)

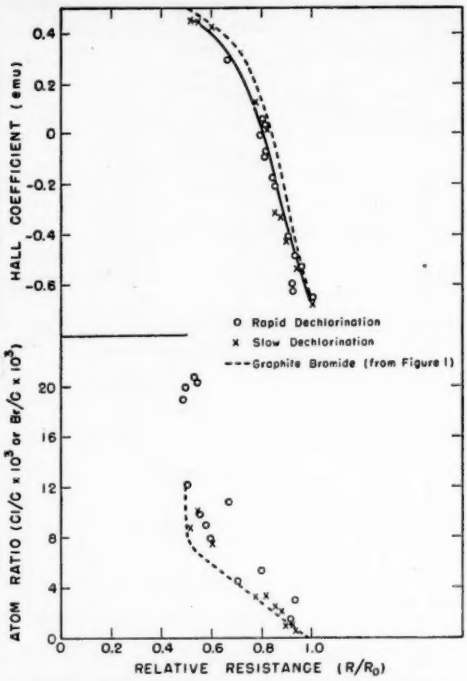
HALL COEFFICIENT (emu)
ATOM RATIO (Cl/C x 10³ or Br/C x 10³)
RELATIVE RESISTANCE (R/R₀)
O Rapid Dechlorination
x Slow Dechlorination
---Graphite Bromide (from Figure 1)

FIG. 5. The relationship between the Hall coefficient, electrical resistance and composition of graphite chloride residue compounds.

reason that the chlorine reaction on graphite had not been observed previously. In the vapor phase above liquid chlorine the reaction was even slower.

A set of combination Hall and resistance samples was reacted with liquid chlorine in either a steel bomb or in heavy-walled glass tubes at room temperature. The reaction under these conditions was faster but always ceased at an early stage of chlorination.

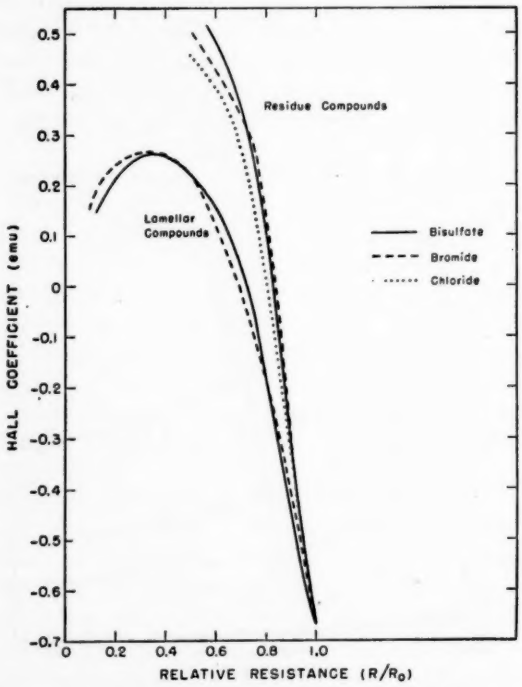

FIG. 6. Relationship between the Hall coefficients and the electrical resistances of graphite bisulfate, bromide, and chloride compounds.

A third set of chlorinations was carried out at temperatures between −78° and −30°C. The samples were not dechlorinated at room temperature, however, but were kept for several hours in a stream of dry helium at −78°C to remove the lamellar chlorine and thus form residue compounds. It was found that this technique of dechlorination gave the most reproducible retention of chlorine and, further, that the retention in atoms of halogen per atom of carbon agreed much better with that observed for graphite bromide residue compounds. The relationships between the properties of these graphite chloride residue compounds have been plotted in Fig. 5.

Graphite-Iodine Chloride Compounds

Iodine monochloride was prepared by passing chlorine gas over iodine crystals. No precautions were taken to obtain stoichiometric proportions of the reactants; thus excess iodine was probably dissolved in the iodine chloride.

When a graphite sample was suspended in iodine chloride vapor at room temperature, its relative resistance decreased within five minutes from unity to 0.135. Further exposure caused visible warping of the sample and a gradual increase in the resistance. The amount of iodine chloride taken up and the amount retained after pumping at room temperature were determined by weighing the sample. After 30 minutes of reaction, the weight increase was 16.2 percent, which dropped to 3.55 percent on dehalogenation. A longer reaction caused a gain of 73.5 percent; this decreased to 8.03 percent on pumping.

The results have purposely not been stated as atom ratios, because it appeared reasonable that there might be a slight excess of chlorine over iodine in the intercalated product. It must be remembered that a fraction of the halogen is probably ionic, and chlorine will most probably furnish most of the ions because of its larger electron affinity.

Attempted Preparation of Graphite Iodide Compounds

Iodine did not react with graphite under numerous conditions. Samples boiled for several hours in liquid iodine at 183°C did not gain weight significantly or become more conducting. Various solutions of iodine did not react. Exposure of graphite to iodine vapor at room temperature for several months did not produce any changes in electrical properties. A sample reacted for three days at −78°C with an iodine solution in petroleum ether did not become more conducting; this indicates that the interaction did not occur even at low temperatures.

DISCUSSION

The Electrical Properties

The Hall coefficients and electrical resistances of three classes of graphite compounds, the bisulfates, bromides, and chlorides, have been replotted in Fig. 6. At any given value of the relative resistance, the Hall coefficients of the bromide, chloride, and the bisulfate compounds are in very close agreement. The similarity in the properties of the halides and the bisulfates is believed to be evidence of a very similar structure for the compounds. The bisulfates are generally believed[6] to be partially ionic compounds, and thus it appears that graphite bromides and chlorides are also probably partially ionic. It must in fact further be concluded that the compounds are not only similar in structure, but that the negative ions in these compounds are only very weak scattering centers for conduction electrons. If the negative ions acted strongly as scattering centers, the effect of a bromide ion and a bisulfate ion on the resistance would be different because of their different sizes. This lack of scattering seems to support the assumption, made in the calculations at the end of a previous paper,[1] that the effects of the Coulomb field of the ions on the resistance are small. Actually the acceptors could be expected to be weak scattering centers. In the lamellar compounds they are presumably arranged in a periodic lattice, and electrons are not scattered by periodic potential functions.[8] In the residue compounds the acceptors are trapped at imperfections in the lattice.[2] These imperfections are presumably active scattering centers even in the absence of the acceptors, so that they mask the scattering by the acceptors.

Measurements of the magneto resistance have shown that the magnitude of this property decreases during bromination. Furthermore, the curves of Fig. 4 show no systematic differences between lamellar and residue compounds. Thus the magneto resistance depends only on the oxidation state of graphite and not on the distribution of the electron acceptors. In this respect, the magneto resistance resembles the resistance itself and differs from the Hall coefficient.

Further conclusions regarding the electrical properties will be deferred until the effects of donor impurities in graphite have been published. It should be noted that the electrical resistance and thermoelectric power of fully brominated graphite have been reported recently.[9] The electrical resistivity measurements agree qualitatively with the results of the present investigation, differing of course in detail, since powdered samples were used for the resistance measurements and since the present investigation has been limited to comparatively weakly brominated samples.

[8] A. H. Wilson, *The Theory of Metals* (Cambridge University Press, Cambridge, 1936), p. 21.

[9] McDonnell, Pink, and Ubbelohde, J. Chem. Soc. **1951**, 191 (January, 1951).

TABLE II. The degree of ionization of bromine in graphite bromide compounds.

Relative resistance	Acceptor concentration (per C atom $\times 10^4$)	Ratio of bromine atoms to bromine ions in Lamellar compounds	Ratio of bromine atoms to bromine ions in Residue compounds
1.0	0	...	...
0.95	1.17	6.4	4.4
0.90	2.3	6.2	4.4
0.85	3.6	5.9	4.4
0.80	4.8	6.1	4.7
0.75	6.2	6.2	4.6
0.70	7.7	6.0	4.6
0.65	9.2	6.1	4.5
0.60	10.9	6.0	4.3
0.55	12.8	6.0	4.2
0.50	14.8	6.0	
0.40	19.5	5.9	
0.30	25.7	5.8	
0.20	36.8	5.1	
0.15	48	4.5	

The Formula of Graphite Bromide

Since it has been concluded that the bisulfates and bromides probably have a similar structure, and since the chemical formulas for the bisulfate compounds are known,[10] it is possible to draw some conclusions as to the formulas of the bromides. For this purpose the acceptor concentration was determined at a few selected values of the resistance by referring to Fig. 1 of the paper dealing with graphite bisulfates.[1] At the same resistance values, the atom ratios (Br/C) were obtained from Figs. 1 and 2 of this paper. Since the acceptor concentration had been assumed equal to the bromide ions concentration, the concentration of un-ionized bromine could be calculated. The ratio of un-ionized to ionized bromine calculated from such data has been tabulated in Table II. This ratio is close to 6 for the lamellar compounds, indicating that the formula of lamellar graphite bromide is very probably $C_nBr \cdot 3Br_2$. The residue compounds are apparently best represented by the formula $C_nBr \cdot Br_{4.5}$ or presumably $C_nBr \cdot 2.2Br_2$.

It is quite surprising that the ionized fraction of bromine differs between lamellar and residue compounds and that it is also different from the fractional ionization of sulfuric acid in the bisulfate lamellar and residue compounds, $C_nHSO_4 \cdot 2H_2SO_4$ and $C_nHSO_4 \cdot 4H_2SO_4$.[1] The fact that only part of the molecules are ionized may probably be explained by the mutual electrostatic repulsion of the negative ions which requires uncharged molecules as "spacers" between them. It is however, not completely understood why the number of these "spacers" differs for different compounds.

[10] W. Rüdorff and U. Hofman, Z. anorg. u. allgem. Chem. **238**, 1 (1938).

The Potential Energy Curve of Mercury Hydride

GEORGE GLOCKLER AND SISTER HELENE VEN HORST*
Department of Chemistry and Chemical Engineering, State University of Iowa, Iowa City, Iowa
(Received March 10, 1952)

A potential energy curve for the mercury hydride molecule is constructed which takes into account the fact that the molecule can change from a structure bonded by exchange forces below about 2.65A, to a quasi-molecule held together by London dispersion forces at larger distances. The breaking off of certain bands can be understood on the basis of maxima in vibrational-rotational energy curves.

INTRODUCTION

THE well-known Morse curve[1] of the potential energy of diatomic molecules and radicals was corrected by Oldenberg[2] in order to make the proper area under any vibrational level (v) equal to $(v+\frac{1}{2})h$, as demanded by quantum theory considerations. This process yields a potential energy curve which should represent the actual molecule better than the simple Morse curve. Oldenberg also studied the possibility of the dissociation of a molecule by a sufficient increase of the rotational energy. As an example he used mercury hydride. However, Villars and Condon[3] pointed out that the instability of molecules in high rotational states is closely related to the tunnel effect.

There is another effect to be considered which may contribute to the ease of dissociation or the instability of a molecule such as mercury hydride. This molecule can also exist as a "quasi-molecule," where the two atoms are held together by "dispersion forces" according to London.[4] In most molecules it appears that the internuclear distance of the quasi-structure is considerably larger than the distance between the nuclei when they are held together by exchange forces of the usual valence type. However in mercury hydride the Van der Waals distance of the loosely bound structure and the internuclear distance of the "chemical molecule" are of the same order when the molecule is in its third quantum vibrational state. Hence under these conditions the molecule can switch over from the chemically bonded to the quasi-molecular state and reach dissociation sooner than expected. In terms of the potential energy curves it can be said that a radical change has taken place in the force field of the molecule at this internuclear distance.

Hulthén[5] has studied the band spectrum of mercury hydride and reports the average internuclear distances in the first five vibrational states of the electronic ground state ($X^2\Sigma^+$). As can be seen from Table I, the third and fourth vibrational levels of the ground state have relatively larger average internuclear distances than the zeroth, first, and second vibrational levels. This fact indicates that a serious change is taking place when the molecule reaches the third vibrational level and it is believed that the above-mentioned possibility of a change in force field to the quasi-molecule is responsible for this increase in average internuclear distance.

Another remarkable feature in the band spectrum of mercury hydride was discovered by Hulthén.[5] In the continuum between λ4552A (the convergence limit) and λ4917A there were found from eight to ten weak maxima which followed the bands before the continuum in a regular manner. No explanation could be given for the appearance of these maxima. The following interpretation of these higher intensity regions or bands seems plausible. It is supposed that the vibrational level system of the ground electronic state would continue as given by the vibrational states 0, 1, 2, and 3 were it not for the fact that the change of the force field causes the molecule to dissociate. In other words, in the continuum there are regions which the molecule can reach from the upper electronic states ($A^2\pi_{\frac{1}{2}}$ or $A^2\pi_{\frac{3}{2}}$) and from which it can either dissociate into atoms with kinetic energy *or* from which it can return to some lower energy level. The relative intensities of these two types of transitions depend on the respective transition probabilities

$$\int \psi(A^2\pi_{\frac{1}{2}};\, v'=0)\cdot ex\cdot \psi(\text{continuum})d\tau$$

and

$$\int \psi(A^2\pi_{\frac{1}{2}};\, v'=0)\cdot ex\cdot \psi(X^2\Sigma^+;\, v'')d\tau.$$

If the latter quantity is larger than the first, then the appearance of the intensity maxima observed by Hulthén[5] can be understood. Since Hulthén does not give wave numbers for the intensity maxima and since he states that they follow the bands before the continuum in the regular manner, it is assumed that these maxima coverage near the dissociation limit (D_0^*) of the valency-bonded mercury hydride molecule. Arbitrarily it is supposed that this dissociation limit occurs at 4917A and that it gives an indication of the heat of dissociation of a mercury hydride molecule with valency binding and not affected by a change in force field as is the case with the real molecule. A rough estimate of the minimum heat of dissociation (D_0^*) of

* In partial fulfillment of the requirements for the degree of Doctor of Philosophy at the State University of Iowa, Iowa City, Iowa.

[1] P. M. Morse, Phys. Rev. **34**, 57 (1929).
[2] O. Oldenberg, Z. Physik **56**, 563 (1929).
[3] D. S. Villars and E. U. Condon, Phys. Rev. **35**, 1028 (1930).
[4] F. London, Z. physik. Chem. **11B**, 222 (1930).
[5] E. Hulthén, Z. Physik **50**, 319 (1928).

this hypothetical molecule can therefore be obtained by subtracting the limit of the continuum (20339 cm^{-1}) from the ν_{00} band (24933 cm^{-1}) or $D_0^* \geq 4594$ cm^{-1} whereas $D_0 = 3034$ cm^{-1} for the real molecule. This procedure is of course quite arbitrary, but the actual value of D_0^* is not important. The main point is that there is some limit to which the levels of the hypothetical molecule converge and this limit must lie beyond the region of the intensity maxima or the observed continuum at λ4917A. The value of $D_0^* = 4594$ cm^{-1} is therefore a minimum. It is also assumed that the continuum expected to follow the intensity maxima and located beyond 4917A is too weak to be observed. When the position of the upper state ($A^2\pi_{\frac{1}{2}}$, $v'=0$) is considered in relation to the location of the ground state, as shown in Fig. 2, then it is seen that the observed transitions to the ground state ($v''=0, 1, 2, 3, 4$) can be reached in accordance with the Franck-Condon principle, and similarly the hypothetical levels ($v''^*=4^*-12^*$) are also located appropriately. The potential curves of the upper state and the ground state are also in proper relative position so that it can be understood that a continuum is observed in the region from 4552 to 4917A. This continuum could extend to about 5140A which is the limit expected from the Franck-Condon principle.

In order to draw the corrected potential energy curve, the average internuclear distances given by Hulthén were used (Table I). The minima of the internuclear distances were taken from the Morse curve since the corrected potential energy curve and the Morse curve do not differ very much in the left branch. The Oldenberg correction was applied yielding the maxima of the internuclear distances in the various vibrational states. Another correction suggested by Rydberg[6] was studied but it was found that it had little influence on the potential energy curve. The internuclear distance of the quasi-molecule was obtained from the Van der Waals radii as recorded by Stuart.[7]

THE CORRECTED POTENTIAL ENERGY CURVE

In order to apply the Oldenberg correction it is necessary to evaluate the integrals

$$\mu \int v_k dr = (v+\tfrac{1}{2})h$$

TABLE I. Internuclear distances (A) HgH ($X^2\Sigma^+$).

v''	R (min) (Fig. 2)	R (max) (Fig. 2)	R (average) (Fig. 2)	R (average) (Reference 5)
0	1.61	1.94	1.78	1.76
1	1.54	2.14	1.84	1.84
2	1.52	2.36	1.94	1.96
3	1.50	3.05	2.27	2.28
4	1.49	5.11	3.30	3.30
3*	1.50	2.55	2.03	···
4*	1.49	2.76	2.13	···

[6] R. Rydberg, Z. Physik **73**, 376 (1932).
[7] H. A. Stuart, *Molekülstruktur* (Julius Springer, Berlin, 1934).

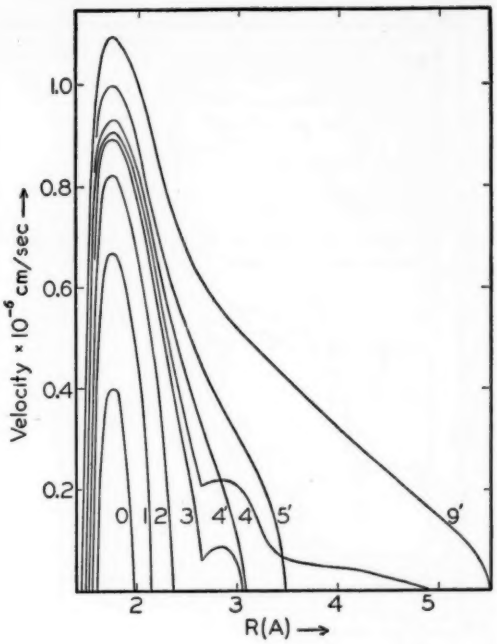

FIG. 1. The integrals $\mu \int v_k dr = (v+\frac{1}{2})h$.

where μ = reduced mass, v_k = velocity, r = coordinate, v = vibrational quantum number, and h = Planck's constant. These integrals are shown in Fig. 1 for the known vibration states 0 to 4 inclusive. The vibration states 4* to 12* assumed to exist in the region of the continuum are also indicated in this figure. In general these integrals obtained by graphical integration check the corresponding multiple of the Planck constant to better than one percent. It is well known that this correction does not give unequivocally the extreme values of the internuclear distance. However, the assumption that the minimum internuclear distance as given by the Morse curve is satisfactory for the present purpose and hence the maxima of the internuclear distances are known probably to within one-hundredth of one angstrom. The potential energy curves are shown in Fig. 2. The data given by Herzberg[8] have been used.

ASSUMED VIBRATION LEVELS

These vibration levels (4*−12*) of the ground electronic state were obtained by graphic extrapolation of the known levels ($v''=0, 1, 2, 3$) as a function of ($v''+\frac{1}{2}$) to the dissociation limit ($D_0^*=4594$ cm^{-1}). The corresponding term values are given in Table II and the "extended Morse curve" is shown in Fig. 2. The actual values of these terms are not significant. Since Hulthén does not report the wavelengths of these intensity maxima found in the continuum, these extrapolated values cannot be compared with experiment. The main point is that about ten levels are found by this extra-

[8] G. Herzberg, *Molecular Spectra and Molecular Structure. I. Spectra of Diatomic Molecules* (D. Van Nostrand Company Inc., New York, 1950).

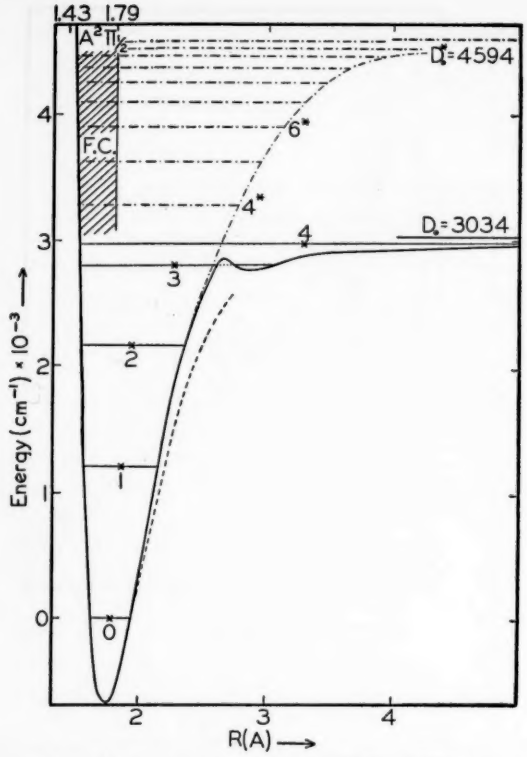

FIG. 2. Potential energy curves for HgH, $X^2\Sigma^+$. Corrected Morse curve including the quasi-molecule with $D_0=3034$ cm^{-1} (full line). The maximum is at 2.65A and the minimum is at 2.85A. Corrected Morse curve extended into the continuum with $D_0^*=4594$ cm^{-1} (dot dashes). Uncorrected Morse curve with $D_0=3034$ cm^{-1} (dashes). F. C., Franck-Condon region.

polated method. Hulthén[5] reported eight to ten intensity maxima.

On the basis of the present considerations it can be said that the third vibration level is actually lower than it would be, had the force field not changed from the pure valence binding to the quasi-structure. The maxima of the internuclear distance in the $v''^*=3$ and $v''=3$ levels are 2.55 and 3.05A, respectively. A corresponding energy change may be expected which is not known and is neglected as being relatively small, when comparison is made with the corresponding fourth levels. In this case the maxima are 2.76 and 5.11A for $v''^*=4$ and $v''=4$. The corresponding term values are 3267 and 2969 cm^{-1}. An eighty-five percent change in internuclear distance produced only a ten percent change in the energy. Hence the third level has not been affected greatly as mentioned above. The third level has to tunnel through a very small potential hill (60 cm^{-1}) at 2.65A. This potential hill shown in Fig. 2 arises from the combination of the corrected Morse curve of the valence state and the potential energy curve of the quasi-molecule.

THE QUASI-MOLECULE

London[9] uses 1.75A for the kinetic theory radius of the mercury atom. Stuart[10] estimates the corresponding radius of the hydrogen atom to be 1.1A. An extrapolation of the rare gas kinetic theory radii as a function of atomic number yields 1.12A.[11] The values used were: He (1.17), Ne (1.27), A (1.49), Kr (1.65), and Xe (1.81)A. Hence the internuclear distance of the quasi-molecule [Hg, H] is taken to be 2.85A. The polarizability of the hydrogen atom (α) is 0.66×10^{-24} cc[12] and other pertinent information was taken from London.[13] The energy given out when a mercury and a hydrogen atom form a Van der Waals or quasi-molecule is calculated to be 0.05 ev. Since similar calculations by London[13] for [Hg, Kr] and [Hg, A] yield about twice the experimental values, it is very likely that the present calculation also should be reduced and

$$\mathrm{Hg}+\mathrm{H}\rightarrow[\mathrm{Hg,\ H}];\quad \Delta E\doteq 0.03 \text{ ev.}$$

This value should give the minimum of the potential energy curve of the quasi-structure.

This minimum was incorporated into the potential energy curve, leading to a small maximum at 2.65A.

TABLE II. Assumed vibration levels in the continuum (4552→4917A).

v'' or v''^*	G (v'' or v''^*)	$A^2\Pi_{\frac{1}{2}}(0')-X^2\Sigma^+$ (v'' or v''^*)	$\lambda(A)$
0[a]	0.0	24932.8	4017
1	1203.8	23729.5	4219
2	2168.6	22764.2	4394
3	2801.4	22131.4	4520
4	2969.3	21963.5	4552
4*	(3267)	(21666)	(4616)
5*	(3620)	(21313)	(4692)
6*	(3895)	(21038)	(4753)
7*	(4092)	(20841)	(4798)
8*	(4247)	(20686)	(4834)
9*	(4363)	(20570)	(4861)
10*	(4455)	(20478)	(4883)
11*	(4524)	(20409)	(4900)
12*	(4588)	(20344)	(4915)

[a] Values for $v''=0-4$ from Table VIII, reference 5.

The height of the maximum was so adjusted that the rotational levels 8, 9, and 10 of $v''=3$ fitted best with the experimental term values given by Hulthén.[14]

POTENTIAL ENERGY CURVES WITH ROTATION

Villars and Condon[3] calculated potential energy curves for HgH ($X^2\Sigma^+$) and pointed out that the tunnel effect is very important in reference to the dissociation of the molecule in a given rotational-vibrational state. These curves have been redetermined with modern data.[8] The simple Morse curve is shown in Fig. 3 for those rotational states where breaking off of band lines has been found by Hulthén.[14] It is seen that 16 out of 24 term values behave as expected in the sense that these

[9] Reference 4, p. 249.
[10] Reference 7, p. 47.
[11] Reference 7, p. 36.
[12] J. H. Van Vleck, *The Theory of Electrical and Magnetic Susceptibilities* (The Clarendon Press, Oxford, 1932), p. 363.
[13] Reference 4, p. 248–9.
[14] E. Hulthén, Z. Physik **32**, 32 (1925).

term values lie below or above the maxima of the vibration-rotation potential curve as found by Hulthén. A somewhat better result can be obtained if the potential energy used by Villars and Condon[3]

$$U(r)=U_0(r)+[h/(8\pi^2c\mu r^2)]\times J(J+1)\ \text{cm}^{-1}$$

is expanded to include higher terms[8]:

$$U(r)=U_0(r)+[h/(8\pi^2c\mu r^2)]\times J(J+1)\ \text{cm}^{-1}$$
$$-[4B_e^3/\omega_e^2+\beta_e(v+\tfrac{1}{2})]\times J^2(J+1)^2\ \text{cm}^{-1}$$

where all symbols have their usual meaning. The added term allows for interaction of rotation and vibration. However, if β_e is calculated to be 0.59×10^{-4} (Eq. III-125 of reference 8 using $\alpha_e=0.312$) the results are not as satisfactory as when an empirical value of $\beta_e=4.5\times10^{-4}$ is used. Nor is another calculation, using $\alpha_e=0.312-0.07(v+\frac{1}{2})^2$ (reference 8, p. 539) as good as the empirical value of β_e just mentioned. This empirical value of β_e is, however, not small in reference to $D_e=4B_e^3/\omega_e^2=3.44\times10^{-4}$ as is expected. It is conceivable that higher powers in J should be used in the energy expression and that the proper relation between the magnitudes of β_e and D_e could then be satisfied. The vibration-rotation curves so obtained are shown in Fig. 4. Now 19 out of 24 term values are located satisfactorily in relation to the maxima of the potential curves. The main point is that evidently the presence of potential hills with the tunnel effect is responsible for the breaking-off of bands due to the dissociation of the molecule. The simple Morse curves are nearly as satisfactory as far as the main argument is concerned. However, the Oldenberg correction must be applied and then it is necessary to assume the maximum at 2.65A in order to have a satisfactory relation between the maxima of the potential hills and the known term values.

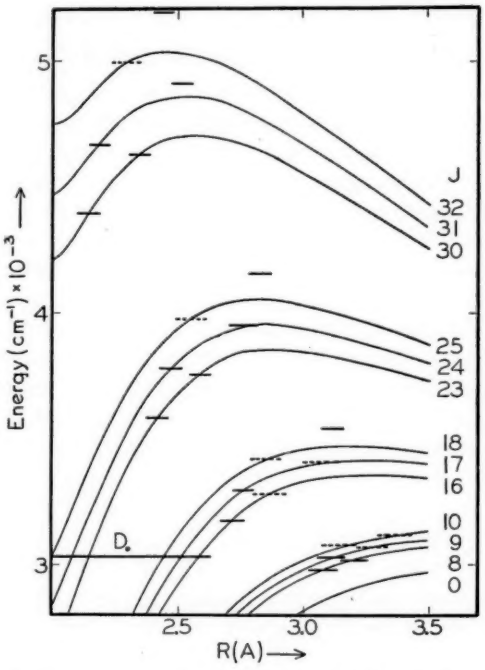

FIG. 3. Morse curves with rotation. Full lines indicate term values which are located below or above the maxima of the potential hills, as expected from the work of Hulthén (reference 14). Dotted lines indicate term values that are not so located.

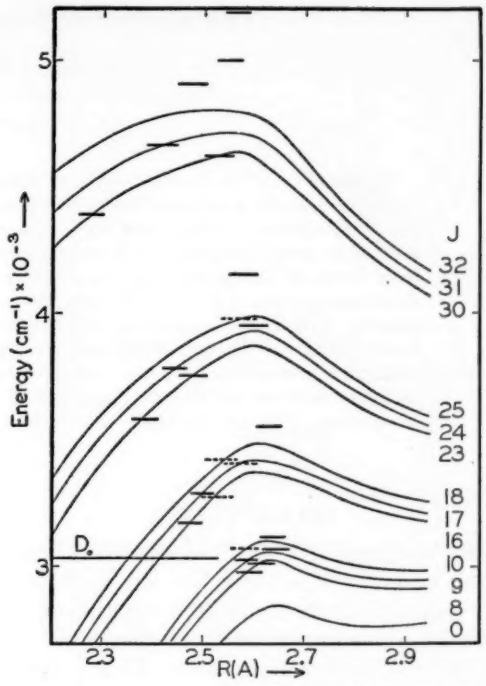

FIG. 4. Corrected Morse curves with rotation. Full lines indicate term values which are located below or above the maxima of the potential hills, as expected from the work of Hulthén (reference 14). Dotted lines indicate term values that are not so located.

The Dielectric Properties of Water in Solutions

G. H. Haggis, J. B. Hasted,* and T. J. Buchanan
The Middlesex Hospital Medical School, London, W. 1, England
(Received March 11, 1952)

Results of dielectric constant and loss measurements at $\lambda=9.22$, 3.175, and 1.264 cm are given for a wide variety of aqueous solutions of ions and organic molecules. The water relaxation time is shortened by positive ions and lengthened by hydrogen bond-forming molecules. The properties of water are treated by a statistical method in which the numbers of molecules in four, three, two, one, and zero-bonded states are estimated from dielectric and latent heat data. Fair agreement with experiment is obtained in calculating the static dielectric constant of ice at 0° and water from 0–370°C, using Kirkwood's dielectric theory and Verwey's calculation of the dipole moment of a four-bonded water molecule. The effects of temperature and solutes on the water relaxation time are discussed in terms of this statistical method. The effective number of water molecules "irrotationally bound," i.e., prevented from turning in the electric field by the ion or the organic molecule, is estimated from the depression of the low frequency dielectric constant, using a dielectric theory of mixtures. This number is zero for uncharged solute molecules but is finite for organic or inorganic ions.

INTRODUCTION

THE biochemical and physicochemical importance of water as a solvent has led during the last twenty years to an intensive study of the structure of water and of certain physical properties of solutions which are specifically related to it. Among these properties are the Raman[1] and infrared[2] spectra, the x-ray diffraction,[3,4] the thermodynamic properties,[5] and more recently the microwave dielectric dispersion.[6]

Previous descriptions of the structure of water and of the effect of solutes on it have been essentially qualitative. In the present work an attempt is made to formulate a quantitative statistical approach. This is extended to a discussion of the "bound" water or "hydration" around polar molecules and ions in the interpretation of dielectric dispersion measurements.

The frequency variation of the dielectric constant of an aqueous solution of polar molecules shows two dispersion regions, one due to the relaxation of the solute and one due to that of the water molecules. Microwave measurements in the wavelength region 1–10 cm cover the range of the water relaxation. Provided that the two dispersion regions are widely separated or that the solute makes only a negligible contribution to the dielectric constant in the microwave region, it is possible from microwave measurements to obtain information about the following:

1. The dielectric constant of the water between the two relaxation regions. This we shall interpret in terms of the water "irrotationally" bound to the solute, i.e., not free to rotate in the electric field.

2. The time of relaxation of the water molecules, which we shall relate directly to the water structure in the solution.

* At University College, London, W.C. 1, England.

[1] Cross, Burnham, and Leighton, J. Am. Chem. Soc. **59**, 1134 (1937).

[2] D. Williams and W. Millett, Phys. Rev. **66**, 6 (1944).

[3] G. W. Stewart, J. Chem. Phys. **7**, 869 (1939); **11**, 72 (1943).

[4] J. Morgan and B. E. Warren, J. Chem. Phys. **6**, 666 (1938).

[5] E. J. W. Verwey, Rec. trav. chim. **61**, 127 (1942).

[6] Hasted, Ritson, and Collie, J. Chem. Phys. **16**, 1 (1948).

METHOD OF MEASUREMENT

The methods of dielectric constant and loss measurement have been fully described elsewhere.

At $\lambda=9.22$-cm wavelength we have employed the two wave-guide absorption method developed by Collie, Hasted, and Ritson.[7] The absorption coefficient κ is measured in two H_{011} cylindrical wave guides filled with solution, the two diameters being selected so as to be just above and just below cutoff for the wave guide used. The wave guides are fed from the end of a rectangular guide, and a loop on the end of a concentric line is moved through the liquid to pick up the response, as in Fig. 1(B). The propagation constants p_1 and p_2 in the cylindrical guides are given by the relations,

$$p_1^2=(n_1-j\kappa_1)^2=\epsilon'-j\epsilon''-k_1\frac{c^2}{\omega^2}$$

$$p_2^2=(n_2-j\kappa_2)^2=\epsilon'-j\epsilon''-k_2\frac{c^2}{\omega^2},$$

where n_1, n_2 are the refractive indices and κ_1,κ_2 the absorption coefficients in the guides $k_1=1.831/r_1$ and $k_2=1.831/r_2$, r_1 and r_2 being the radii of the guides. We calculate the dielectric constant and loss from the absorption coefficients κ_1 and κ_2 in the two guides,

$$\epsilon'=\frac{\left(\frac{c^2}{\omega^2}\right)(k_1^2\kappa_1^2-k_2^2\kappa_2^2)}{\kappa_1^2-\kappa_2^2}-(\kappa_1^2+\kappa_2^2)$$

$$\epsilon''=2\kappa_1\left(\epsilon'-k_1\frac{c^2}{\omega^2}+\kappa_1^2\right)^{\frac{1}{2}}.$$

The latitude in the choice of r_1 and r_2 is sufficient to allow the two measurements of the attenuation in the guide to be approximately independent measurements of n and κ, the optical constants in free space. The minor

[7] Collie, Hasted, and Ritson, Proc. Phys. Soc. (London) **60**, 145 (1948).

improvements mentioned in a recent publication[8] were retained.

The measurements at 1.26 cm and 3.2 cm have been obtained by a null-balance method.[9]

A generator valve feeds energy along a wave guide directly into the liquid-cell—(A) in Fig. 2 and Fig. 1(A). The cells used are those described and used by Collie, Hasted, and Ritson,[7] but only a wide wave guide is used, and both amplitude and phase changes are determined in moving through the liquid.

The top end of the inner guide couples into the cable (*B*) in Fig. 2 which feeds energy to the line lengthener (*C*) and from there to the junction of the magic-tee (*D*). Another cable (*E*) picks up energy from the main wave guide at the probe (*F*), passes it through the cut-off attenuator (*G*) and along the "*E* arm" of the magic-tee to the junction (*D*). At the junction the energy either passes into the superheterodyne receiver or into the resistive load (*H*) in a ratio which depends on the relative phases and amplitudes of the incident vectors at the magic-tee junction. For any given position of the movable inner wave guide in the liquid-cell the amount of energy reaching the receiver can be nulled by adjustment of the cut-off attenuator and the line-lengthener. If the movable guide is now traversed back through the liquid-cell by one wavelength, the amplitude is decreased by the loss in the additional length of liquid and the phase is changed by 2π-radians. The cut-off attenuator can then be adjusted to make the receiver output again zero. The values of p_1 and κ_1 are calculated from the guide wavelength and the attenuator setting, and ϵ' and ϵ'' may then be calculated from the propagation constant equation given above.† The advantage of the method lies in the high accuracy with which the position of balance can be measured.

At 1.26-cm wavelength the intermediate frequency is stabilized by automatic frequency control with the generator klystron as standard.[10]

Measurements of the dc conductivity of the solutions have been carried out at controlled temperature using standard bridge techniques.

RESULTS

The experimental values of ϵ' and ϵ'' at $\lambda=9.22$ cm, 3.175 cm, and 1.264 cm and estimated accuracy are given in Table I. All results are at $T=25.0°\text{C}\pm0.2°\text{C}$.

Corrections for conductivity have been made according to the equation

$$\epsilon''_{\text{corrected}}=\epsilon''_{\text{observed}}+2\sigma/f,$$

where σ is the specific conductivity in esu and f the frequency. For the purpose of these corrections there is assumed to be no change in this conductivity with frequency, an assumption which has been discussed previously.[6]

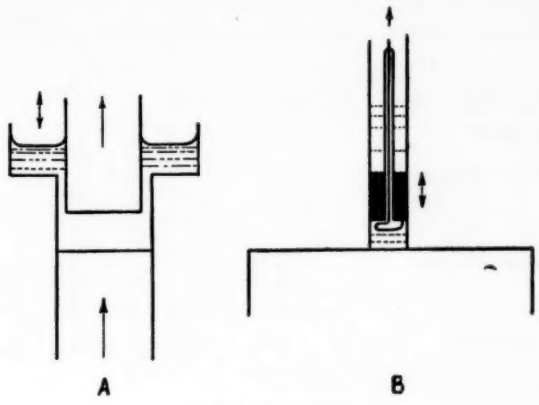

FIG. 1. Water cells.

It is possible to analyze the corrected results in terms of a low frequency dielectric constant ϵ_s,‡ falling to a high frequency dielectric constant ϵ_∞. If the solute molecule makes only small contributions to ϵ' and ϵ'' in the wavelength region $\lambda=1-10$ cm, then the single water relaxation time determines the frequency dependence of ϵ' and ϵ''. The following relations are generally true and not dependent on the dielectric model:

$$\epsilon'=n^2-\kappa^2=\frac{\epsilon_s-\epsilon_\infty}{1+\omega^2\tau^2}+\epsilon_\infty=\frac{\epsilon_s-\epsilon_\infty}{1+(\lambda_s/\lambda)^2}+\epsilon_\infty$$

$$\epsilon''=2n\kappa=\frac{(\epsilon_s-\epsilon_\infty)\omega\tau}{1+\omega^2\tau^2}=\frac{(\epsilon_s-\epsilon_\infty)(\lambda_s/\lambda)}{1+(\lambda_s/\lambda)^2},$$

where τ is a single relaxation time, corresponding to a wavelength λ_s, and ω and c have their usual significance. In Table I the experimental values of ϵ' and ϵ'' at each frequency are compared with the values calculated from the corresponding values given for ϵ_s and λ_s. These

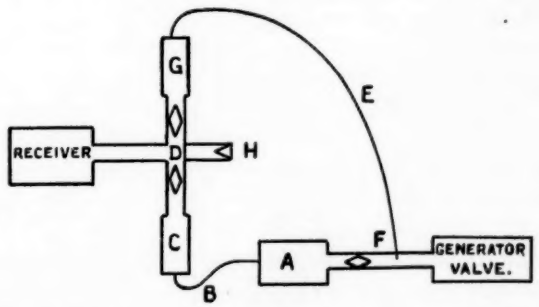

FIG. 2. Experimental arrangement for measurements at 3.2 and 1.26 cm.

[8] Hasted, Haggis, and Hutton, Trans. Faraday Soc. **47**, 577 (1951).

[9] T. J. Buchanan, Proc. Inst. Elec. Engrs. (London) Part III, **99**, 61 (1952).

† For rectangular H_{01} wave guide $k_1=\pi/b$, where b is the long dimension of the guide.

[10] G. H. Haggis, thesis for the Degree of Doctor of Philosophy, London, 1951.

‡ The symbol ϵ_s is used in the same way as in the previous work on ionic solutions. It should be noted that this is no longer equal to the static dielectric constant, as a result of the solute relaxation at lower frequencies.

TABLE I.

Solute at 25°C	Molarity	λ=1.264 cm ϵ'_{obs} ±1%	ϵ'_{calc}	ϵ''_{corr} ±2%	ϵ''_{calc}	λ=3.175 cm ϵ'_{obs} ±1%	ϵ'_{calc}	ϵ''_{corr} ±2%	ϵ''_{calc}	λ=9.22 cm ϵ'_{obs} ±1%	ϵ''_{calc}	ϵ''_{corr} ±1	ϵ''_{calc}	ϵ_s ±0.5	λ_s ±0.04
Pure water														78.2	1.56
n-Propyl alcohol	0.33 m	31.6	31.5	33.3	33.8	61.3	60.5	29.3	28.5	72.6	73.0	12.5	12.5	75.5	1.69
	0.66 m	29.5	29.5	32.0	32.4	58.2	59.0	30.2	28.9	70.7	70.5	13.0	13.0	73.9	1.81
	1 m	27.1	27.5	31.3	31.2	54.9	53.7	30.3	29.5	70.0	68.9	14.6	13.3	72.3	1.94
iso-Propyl alcohol	0.33 m	31.6	31.4	33.8	34.2	...	...	...	...	74.8	74.2	11.5	11.3	75.9	1.63
	0.66 m	28.9	28.6	32.3	32.5	...	...	...	...	72.3	71.6	11.0	10.7	73.4	1.73
	1 m	26.2	26.0	30.7	30.9	...	...	...	...	...	...	...	...	70.9	1.85
t-Butyl alcohol	0.33 m	31.6	31.2	33.3	34.0	59.9	59.7	29.6	29.5	73.7	73.4	12.9	12.6	75.9	1.74
	0.66 m	...	...	...	...	55.1	55.5	30.1	30.5	71.6	71.0	14.0	13.6	73.5	1.90
	1 m	...	...	...	...	50.4	50.8	30.2	31.2	69.9	68.7	15.3	14.8	71.5	2.06
Diethylketone	0.17 m	33.2	33.3	35.0	35.0	62.2	62.2	29.0	29.1	75.2	75.6	10.6	10.5	77.0	1.62
	0.33 m	31.6	31.6	34.1	34.2	61.1	61.0	29.3	29.1	74.6	74.5	10.8	10.6	76.5	1.67
Phenol	0.25 m	32.1	31.8	33.6	34.1	61.3	61.5	28.2	28.5	74.6	74.6	11.5	11.5	75.6	1.62
	0.5 m	29.1	28.7	31.2	32.0	58.4	58.2	27.9	27.2	71.3	70.7	12.1	12.0	73.0	1.67
Aniline	0.125 m	33.6	33.6	35.2	35.1	62.9	62.9	28.4	28.5	75.5	75.6	10.3	10.3	77.1	1.58
	0.25 m	32.5	32.5	34.2	34.0	61.9	61.7	28.3	28.2	74.1	74.2	10.4	10.4	76.0	1.61
Propionic acid	0.5 m	31.4	31.2	33.3	33.5	59.1	59.5	28.5	29.4	73.3	73.0	12.7	12.5	75.0	1.66
	1 m	28.9	28.7	31.4	31.6	55.4	55.6	28.5	28.6	69.4	69.4	13.4	13.3	71.5	1.77
	1.5 m	26.4	26.3	29.6	29.6	51.4	51.5	28.7	28.5	65.7	66.2	13.0	13.2	68.4	1.91
Ethylamine	0.6 m	30.1	30.0	33.1	33.4	57.6	57.7	30.0	30.2	72.4	72.6	12.9	13.0	75.0	1.77
	1.16 m	27.9	27.5	31.7	32.0	55.2	54.6	30.8	30.2	...	...	...	...	72.5	1.84
n-Propylamine	0.33 m	31.8		33.7		...	...	...	...	...	...	...	...		
	0.66 m	28.8		31.6		...	...	...	...	...	...	...	...		
Glutaric acid	0.33 m	32.5	32.2	33.1	34.0	60.6	60.6	28.4	28.5	73.6	73.0	13.1	12.8	74.9	1.63
	1 m	28.6	28.5	28.8	30.0	53.5	53.5	26.2	26.2	65.6	64.6	14.8	14.3	68.0	1.71
Ethylene diamine	0.525 m	31.3	31.1	33.0	34.0	59.7	59.7	29.2	29.6	74.3	73.7	12.0	12.0	75.5	1.71
	1.05 m	...	...	...	...	...	...	...	...	71.0	71.0	12.5	12.5	73.0	
	1.57 m	24.7	24.5	29.5	29.7	51.5	51.5	30.2	30.1	68.5	68.5	13.5	13.5	71.0	2.06
α-Alanine (*pH* 7)	0.5 m	31.5	31.5	32.9	32.9	...	...	...	...	70.9	71.0	11.7	11.7	72.5	1.57
	1 m	29.0	29.0	30.1	29.7	...	...	...	...	64.4	65.0	10.7	10.9	66.5	1.59
	1.5 m	26.7	26.7	27.4	26.9	...	...	...	...	57.7	59.3	8.1	8.5	60.2	1.60
β-Alanine (*pH* 7)	0.5 m	31.9	31.7	33.3	33.2	...	...	...	...	71.3	71.7	10.9	11.0	73.0	1.56
	1 m	29.9	29.9	30.5	30.3	...	...	...	...	64.8	65.3	10.0	10.2	67.0	1.55
	1.5 m	28.1	28.1	28.0	28.0	...	...	...	...	...	...	...	...	61.1	1.54
NaF	0.33 m	33.7	33.6	33.5	33.7	61.2	61.0	27.3	27.1	71.9	71.7	14.7	12.5	74.5	1.55
	0.66 m	32.8	32.9	31.8	32.5	59.0	58.6	26.3	25.7	69.2	69.2	14.3	11.0	71.3	1.54
	1 m	32.3	32.2	30.9	31.5	56.9	56.7	25.5	25.1	...	...	...	...	68.8	1.53
NaCl	0.33 m	33.8	33.6	32.9	33.5	59.5	60.4	25.9	26.9	72.4	71.5	14.3	12.0	71.8	1.49
	0.66 m	33.1	33.1	30.9	30.9	...	...	...	...	...	...	...	...	67.2	1.42
	1 m	32.4	32.3	28.7	29.2	54.6	54.6	21.7	21.7	...	...	...	...	63.0	1.37
NaBr	0.33 m	33.9	33.8	32.8	32.6	60.3	60.0	26.0	25.5	69.9	70.1	11.0	11.2	72.0	1.49
	0.66 m	33.4	33.4	30.7	30.6	57.0	57.3	22.7	23.0	...	...	...	...	66.8	1.40
	1 m	33.0	33.0	29.4	28.7	54.0	54.0	21.0	21.0	...	...	...	...	63.3	1.36
NaI	0.33 m	34.1	33.9	32.7	33.1	60.6	60.7	25.5	25.6	72.1	71.1	11.4	11.0	72.0	1.47
	0.66 m	33.7	33.7	30.6	31.0	57.4	57.6	22.7	23.0	...	...	...	...	67.0	1.39
	1 m	33.3	33.2	28.4	28.8	55.1	54.9	20.7	20.5					62.7	1.30
LiCl	0.31 m	33.4	33.3	33.0	33.5	60.4	60.6	26.5	26.6	71.6	71.4	12.7	12.4	73.2	1.55
	0.62 m	32.1	32.0	30.7	31.3	57.1	57.1	24.7	24.7	65.8	66.2	13.1	13.1	68.4	1.52
	0.93 m	30.9	30.8	28.6	28.9	53.7	53.7	22.7	22.7	...	...	...	...	64.0	1.48
KCl	0.5 m	33.5	33.5	32.5	32.6	59.7	59.7	25.1	25.1	...	...	...	...	71.3	1.47
	1 m	33.5	33.5	29.7	29.9	55.6	56.0	22.0	22.2	...	...	...	...	64.9	1.36
NH_4Cl	0.33 m	34.3	34.3	33.3	33.3	60.6	60.3	26.3	26.0	...	...	...	...	73.0	1.50
	0.66 m	33.4	33.3	31.7	32.1	58.5	58.5	24.6	24.6	...	...	...	...	69.4	1.46
	1 m	33.0	32.9	30.1	30.6	55.8	55.8	22.8	23.0	...	...	...	...	66.0	1.41

TABLE I.—*Continued.*

Solute at 25°C	Molarity	λ=1.264 cm ϵ'_{obs} ±1%	ϵ'_{calc}	ϵ''_{corr} ±2%	ϵ''_{calc}	λ=3.175 cm ϵ'_{obs} ±1%	ϵ'_{calc}	ϵ''_{corr} ±2%	ϵ''_{calc}	λ=9.22 cm ϵ'_{obs} ±1%	ϵ''_{calc}	ϵ''_{corr} ±1	ϵ''_{calc}	ϵ_s ±0.5	λ_s ±0.04
RbCl	0.33 m	34.1	33.8	32.9	33.9	60.5	61.0	27.1	27.6	72.6	72.5	15.3	12.5	74.0	1.54
	0.66 m	34.1	34.0	31.8	32.2	59.7	59.3	25.1	24.6	...	...	...	...	70.5	1.46
	1 m	33.7	33.6	29.5	30.0	56.3	56.1	22.2	22.2	...	...	...	...	65.2	1.38
KF	0.33 m	33.6	33.6	33.7	33.7	60.7	61.0	26.7	27.0	72.0	72.0	11.7	12.0	74.0	1.53
	0.66 m	32.4	32.4	32.0	32.0	58.0	58.1	25.3	25.5	...	...	...	...	70.1	1.52
	1 m	31.7	31.6	30.2	30.5	56.3	56.1	24.2	24.0	...	...	...	...	67.0	1.47
Na Propionate	0.5 m	30.0	29.7	31.3	32.0	55.7	56.2	27.5	28.5	71.6	70.0	14.1	12.0	71.0	1.67
	1 m	26.4	26.0	27.7	28.7	49.6	49.7	26.4	26.8	65.2	63.8	13.3	12.0	64.8	1.76
Na Butyrate	0.567 m	29.9	29.9	31.3	31.4	...	...	...	...	68.0	67.7	13.4	13.4	69.5	1.59
	1.14 m	25.7	25.5	27.1	27.6	...	...	...	...	...	...	...	...	61.2	1.66
Ethylamine HCl	0.5 m	31.2	31.1	32.6	33.1	56.7	57.3	28.0	29.0	70.6	70.6	14.3	13.5	72.4	1.67
	1.04 m	28.8	28.8	30.6	30.6	53.0	52.2	28.4	27.5	62.3	64.6	12.8	13.5	67.0	1.77
n-Propylamine HCl	0.33 m	31.9	31.6	32.9	33.2	59.1	59.5	27.0	27.6	72.4	71.5	13.9	13.2	73.0	1.60
	0.66 m	29.2	29.2	30.7	30.7	54.2	55.1	25.1	26.2	67.9	66.7	12.5	11.7	69.0	1.67
	1 m	27.1	27.1	28.6	29.0	...	...	...	...	64.2	63.0	13.0	12.2	64.5	1.70
Diethylamine HCl	0.33 m	30.6	30.6	32.0	32.4	...	...	...	...	70.5	70.5	11.0	11.0	71.8	1.60
	0.66 m	27.3	27.3	29.0	29.5	...	...	...	...	66.0	65.5	10.0	9.8	66.0	1.65
Tetraethylammonium Cl	0.2 m	31.5	31.4	32.5	33.0	...	...	...	...	71.9	71.7	11.7	11.7	73.6	1.61
	0.4 m	28.4	28.3	30.4	31.0	...	...	...	...	67.8	67.6	13.0	12.9	69.5	1.68
	0.6 m	25.7	25.6	28.1	28.7	50.3	50.3	26.3	26.3	...	...	...	...	65.6	1.75
Tetramethylammonium Br	0.33 m	31.5		32.4	...	...	...	...	...	...	...	...	...		
	0.66 m	29.0		30.0		...	...	...	...	...	...	...	...		
	1 m	26.4		27.8		...	...	...	...	...	...	...	...		
Tetramethylammonium I	0.125 m	33.5	33.2	33.9	34.6	62.0	62.2	27.9	28.2	74.7	74.2	12.3	12.2	75.8	1.58
	0.25 m	32.8	32.5	32.9	33.5	60.4	60.1	28.0	27.8	71.9	71.9	13.8	12.6	73.8	1.61
Guanidine Cl	0.36 m	33.4	33.2	32.5	33.3	60.0	60.0	26.8	26.8	71.6	71.6	10.8	10.8	73.2	1.55
	0.71 m	32.4	32.3	30.3	30.9	56.5	56.5	24.5	24.4	...	...	...	...	68.0	1.51
	1.07 m	31.2	31.2	28.5	28.8	52.4	52.5	21.9	22.3	...	...	...	...	62.5	1.47

values of ϵ_s and λ_s are chosen so as to give the best fit to the experimental data when the above equations are used. The agreement between theoretical and experimental values is illustrated in Figs. 3 and 4 which show a number of graphical plots of ϵ'' against ϵ'; for a single relaxation time these should, according to Cole and Cole,[11] fall on semicircles intercepting the horizontal axis normally at $\epsilon'=\epsilon_s, \epsilon_\infty$.

The estimated accuracies, are $\epsilon_s \pm 0.5$ and $\lambda_s \pm 0.04$. The value of ϵ_∞ is chosen to give the best fit to the results and is equal to 5.5 ± 1, as found for water.[7]

Solute molecules have been chosen to include a variety of hydrogen bond forming groups and, in particular, groups present in proteins. A discussion of protein hydration will be given in a forthcoming paper.[12]

THE STRUCTURE OF WATER

Following the classical work of Bernal and Fowler,[13] Morgan and Warren[4] conclude from the x-ray diffraction studies that "water is well described by the term 'broken down ice structure'—a structure in which each molecule is striving to bond itself tetrahedrally to four neighbouring molecules just as in ice, but in which bonds are continually breaking and reforming."

Pauling[14] has estimated that 15 percent of the hydrogen bonds are broken at 0°C. Assuming that further bonds are broken as the temperature is raised, Cross, Burnham, and Leighton[1] have considered the various ways in which the vibration of a free water molecule will be perturbed by the formation of 1, 2, 3, or 4 bonds. They have given a qualitative interpretation of the change in the main Raman absorption band in the temperature range 0–360°C.

Recently Lennard-Jones and Pople[15] have put forward the alternative viewpoint that there is very little breaking but considerable bending of bonds.

In discussing the dielectric properties of solutions and in particular the effect of solutes on the water relaxation time, the concept of the breaking of bonds and the extent to which they are broken are of some importance.

[11] K. S. Cole and R. H. Cole, J. Chem. Phys. **9**, 341 (1941).
[12] Buchanan, Hasted, Haggis, and Robinson, Proc. Roy. Soc. (London) A. (1952) (to be published).
[13] J. D. Bernal and R. H. Fowler, J. Chem. Phys. **1**, 515 (1933).
[14] L. Pauling, *Nature of the Chemical Bond* (Cornell University Press, Ithaca, New York, 1948).
[15] J. Lennard-Jones and J. A. Pople, Proc. Roy. Soc. (London) A. **205**, 155 (1951).

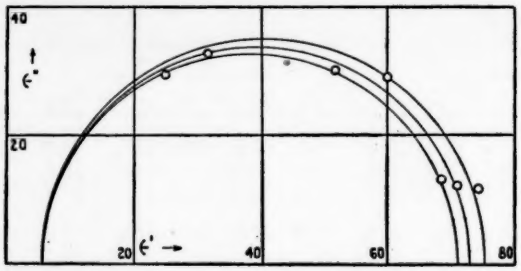

FIG. 3. Plots of ϵ''_{corr} against ϵ' for NaCl.

A qualitative picture of this relaxation process has been given by Hasted, Ritson, and Collie[7] in which liquid water is considered to be made up of ordered regions or microcrystalline domains whose boundaries are in continuous movement. When an electric field is applied, boundary movement results in orientation of water molecules in the field direction. Increasing temperature or inorganic ions in solution are considered to break up the structure to some extent, to increase the boundary area and shorten the relaxation time. An increase in structural temperature is shown also by the x-ray[3] and spectroscopic[2] data for ionic solutions.

Now it will be seen from Table I that solutions of organic molecules with polar groups have longer relaxation times than that of water. It is difficult to see how it is possible for these molecules to decrease the boundary area.

An attempt has, therefore, been made to develop a statistical approach to supersede the structural concept. It should be regarded only as a first approximation, since, for example, the bending of bonds is neglected. There is also, of course, some uncertainty in the use of the term "breaking of hydrogen bonds."

Let us assume that a certain percentage p of hydrogen bonds are broken at a given temperature T. There are five types of molecules present in the liquid; 4-bonded, 3-bonded, 2-bonded, 1-bonded, and 0-bonded. It is possible to treat water as a statistical assembly of molecules in these five states, molecules passing from one state to another by the "breaking" and "forming" of bonds. For a given value of p there will be an equilibrium percentage n_i of molecules forming i bonds ($i=0, 1, 2, 3, 4$). Let m_{ij} represent the number of bonds (per 100 molecules of water) of a type $i-j$ between two water molecules forming i and j bonds ($i, j=1, 2, 3, 4$). We assume that the probability of a bond being broken in a given time is independent of the type of bond.

For a given type of bond $(i-j)$, the probability of breaking is

$$m_{ij}f_1(T)e^{-\Delta H/RT},$$

where $f_1(T)$ is a function of temperature only and ΔH is the bond strength. The probability of a given bond $i-j$ being formed in the same time is

$$n_{i-1}\cdot n_{j-1}f_2(T, p),$$

$f_2(T, p)$ being a function both of the temperature and of the condition of the surrounding water molecules.§ Under equilibrium

$$m_{ij}f_1(T)e^{-\Delta H/RT}=n_{i-1}\cdot n_{j-1}f_2(T, p),$$

there being ten equations of this type for $i, j=1, 2, 3, 4$.‖ A further equation may be written

$$\sum_{i=0,1,2,3,4} n_i=100,$$

and since in ice there are 200 bonds per 100 molecules, we may write

$$\sum_{i,j=1,2,3,4} m_{ij}=2(100-p),$$

$m_{ij}\equiv m_{ji}$ being counted once.

The numbers of molecules and of bonds are further related by four equations of the type

$$in_i=m_{ii}+\sum_{j=1,2,3,4} m_{ij}$$

for $i=1, 2, 3, 4$. We thus have sixteen equations from which, for a given value of p, the sixteen unknowns m_{ij}, n_i and the ratio $f_1(T)e^{-\Delta H/RT}/f_2(T, p)$ may be determined. The basic assumption is that the free energy of breaking does not vary with i, j.

In order to calculate the values of n_i at a given temperature it is first necessary to make an estimate of p.

Pauling,[14] attributing approximately one-fourth of the heat of sublimation of ice to van der Waals forces, calculates ΔH to be 4.5 kcal/mole and p to be ~16 percent at 0°C.

There are, however, wide divergences between estimates of p given by different authors. Cross, Burnham, and Leighton[1] estimate that nearly 50 percent of the bonds are broken at 40°C, and Lennard-Jones and Pople[15] suggest that very few are broken.

Following Pauling we have assumed that the latent heat of vaporization (L) is made up of two parts, the heat necessary to overcome the van der Waals forces (W) and the heat required to break the remaining

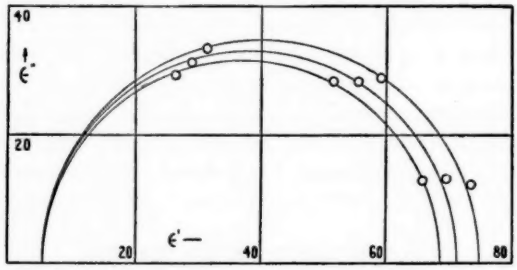

FIG. 4. Plots of ϵ''_{corr} against ϵ' for propionic acid.

§ As a refinement, some allowance should perhaps be made for the greater probability of less bonded molecules making a successful encounter.

‖ There will also be bond changes $i-j\rightarrow i-(j\pm1)$ as a result of breaking and forming of adjacent bonds. If the 10 equations given above are satisfied, bond changes of this type will take place as often in the reverse as in the forward direction.

hydrogen bonds (two per molecule). Thus,

$$p=100\left[1-\frac{L-W}{2\Delta H}\right].$$

We have taken a value of p at 0°C to give agreement with the dielectric data and calculated the temperature variation of p from the above equation, assuming the energy due to van der Waals forces to be temperature invariant and $\Delta H=4.5$ kcal/mole. This gives $p=9$ percent at 0°C and an apparent van der Waals energy for water of 2.5 kcal/mole.¶ In Table II we give our estimations of p and the corresponding values of n_i.

It is now possible to use these estimates in discussing the Kirkwood theory of the static dielectric constant, the dielectric relaxation process, and the behavior of the water when other molecules or ions are added.

THE DIELECTRIC PROPERTIES OF ICE AND WATER

Kirkwood has given a general formula for the dielectric constant of polar materials

$$\frac{(2\epsilon+1)(\epsilon-1)}{9\epsilon}=\frac{P_0}{v},$$

where v is the molar volume and the molecular polarization P_0 is given by

$$P_0=\frac{4\pi N}{3}\left[\alpha+\frac{\boldsymbol{\mu}\bar{\boldsymbol{\mu}}}{3kT}\right],$$

where N is Avogadro's number, α the optical polarizability, $\boldsymbol{\mu}$ the dipole moment of a molecule surrounded by its neighbours, and $\bar{\boldsymbol{\mu}}=g\boldsymbol{\mu}$ is the average dipole moment of a macroscopic sphere of the material immersed in a medium of the same dielectric constant, the central molecule being kept in the fixed orientation $\boldsymbol{\mu}$.

We will first calculate the dielectric constant of ice, assuming a random proton distribution. Ice consists almost entirely of four-bonded molecules. It has a high

TABLE II. Values of L, p, and n_i.

T	L kcal/mole	p %	n_4	n_3	n_2	n_1	n_0
Ice 0°C	12.2	0	~100.0	0	0	0	0
Water 0°C	10.7	9.0	72.4	20.0	6.0	1.5	0.1
25	10.5	11.3	67.0	23.2	7.6	2.0	0.2
60	10.1	15.8	58.5	25.8	11.0	3.8	0.9
100	9.7	20.2	49.8	28.3	15.0	6.0	1.5
200	8.4	34.1	28.8	29.1	24.4	14.1	4.9
300	6.0	61.3	5.0	14.7	26.3	33.0	21.0
370	1.9	~100.0	0	0	0	0	~100.0

¶ This "apparent" van der Waals energy may be lower than the value for ice as a result of bending of the bonds in water.

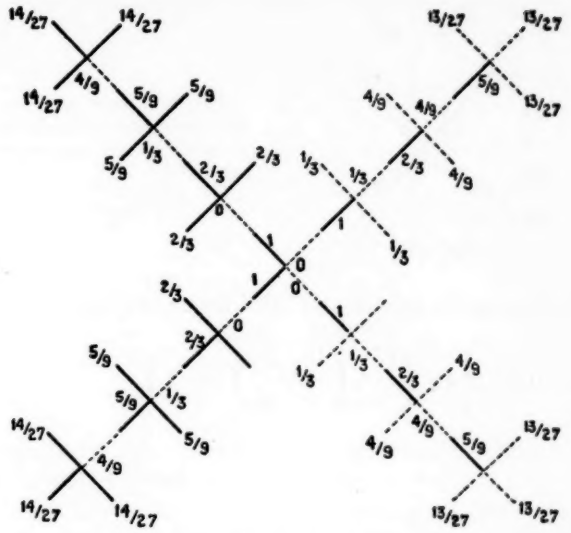

FIG. 5. Proton distribution about a fixed molecule in ice.

dielectric constant, so that Kirkwood's formula can be written as

$$\epsilon=n^2+\epsilon_{\text{vib}}+\frac{6\pi N}{v}\cdot\frac{g_4\mu_4^2}{3kT},$$

where n is the optical refractive index (1.33) and ϵ_{vib} is the contribution due to lattice vibrations at infrared frequencies. To give $\epsilon_\infty=3.2$,[16] ϵ_{vib} must be taken as equal to 1.4. g_4 and $\boldsymbol{\mu}_4$ refer to four-bonded H_2O molecules, the suffixes 3, 2, 1, 0 being reserved for 3-, 2-, 1-, 0-bonded molecules in liquid water.

The calculation of $\boldsymbol{\mu}_4$ is very sensitive to the charge distribution assumed for a water molecule. Verwey's[17] calculation seems more satisfactory than those based on dipole interaction, and we therefore use his value of 2.45-Debye units.

We calculate g_4 as follows: $\bar{\boldsymbol{\mu}}=g\boldsymbol{\mu}$ represents the average dipole moment of a macroscopic sphere, of which the central molecule remains in a fixed orientation $\boldsymbol{\mu}$. Let us consider the probabilities of protons occupying the various positions around a single water molecule held in a fixed orientation. We assume in ice a random distribution of protons such that two are attached to each oxygen and one proton lies along each 0—0 bond.[14] The probabilities will be as shown in Fig. 5. Taking the angle between bonds throughout as 109°, the vector $\boldsymbol{\mu}$ may be resolved into two vectors 0.862μ along the bonds. Resolving in the direction of $\boldsymbol{\mu}$, we find that the contribution of the central molecule and near neighbors to $\bar{\mu}$ is

$$0.862\mu\left[4\cos 54°30'+\frac{6}{3}\cos 71°\cdot\cos 54°\,30'\right].$$

[16] J. Lamb, Trans. Faraday Soc. **42A**, 238 (1946).
[17] E. J. W. Verwey, Rec. trav. chim. **60**, 887 (1941).

FIG. 6. Proton distribution for 4-bonded molecule at temperatures approaching 370°C.

Including the second and third layers, we have

$$\bar{\mu}=0.862\mu\left[4+\left(\frac{12}{3}+\left(\frac{18}{9}+\frac{72}{27}\right)\cos 71\right)\times\cos 71\right]\cos 54°\,30'$$

giving

$$g_4=\bar{\mu}/\mu=2.91.$$

The additional contribution from further bond layers and from closed rings is found to be negligible.

Inserting values for g_4, μ_4, v, etc., in the above equation for ice, we obtain a value of $\epsilon=92.7$ in good agreement with Cole's[18] recent value of 92.

We now proceed to the calculation of ϵ for water. Summing over the different types of molecules present, we have

$$\epsilon=n^2+\epsilon_{\text{vib}}+\frac{6\pi N}{v}\sum_{i=0,1,2,3,4}\frac{n_i}{100}\cdot g_i\mu_i^2.$$

Now the values of g_i will vary with the percentage of bonds broken. We first estimate values of g_4 at each temperature as follows. At 370° where nearly all the bonds are broken we should include only one layer of water molecules, since the few four-bonded molecules must be surrounded by molecules which form no other bonds. We have in this case (Fig. 6),

$$g_4=0.862\left(4+\frac{6}{3}\cos 71°\right)\cos 54°\,30'=2.34.$$

We assume that as p varies from 0 to 100, g_4 varies linearly from 2.91 to 2.34.

We make the further assumption that there is no correlation between the orientations of nonbonded neighbors and the central molecule, so that g_0 will be equal to 1, and values of g_3, g_2, and g_1 may be linearly interpolated between g_4 and g_0.

We consider now the calculation of values of μ_i, which will also vary with temperature, as a result of the increase in d, the interoxygen distance.

It is not permissible to estimate d from x-ray diffraction data, since molecules at intermediate distances cause broadening of the near neighbor peak in the radial distribution curve and a displacement of the maximum. We therefore calculate d from the temperature dependence of the density. Changes of density will be due partly to the variation of p, so that

$$\left[\frac{d_t}{d_{\text{ice}}}\right]^3-\frac{Kp}{100}=\frac{D_{\text{ice}}}{D_t},$$

where D_t, d_t, D_{ice}, d_{ice} are the densities and interoxygen distances in water at t°C and ice at 0°C; K is a constant chosen in such a way that there is no change in d on passing from ice at 0°C to water at 0°C. Values of d estimated in this way are shown in Table III.

Verwey's value of $\mu_4=2.45$ Debye units is not very different from the value calculated assuming dipole interaction,[19] for which we have an equation of the type $\mu_4=\mu_0/(1-k/d^3)$, where k is a constant. Values of μ_4 at different temperatures given in Table III are calculated from this equation, choosing k to give $\mu_4=2.45$ Debye units when $d=2.76$A. The final calculation is not very sensitive to small changes in d. The value of μ_0, the dipole moment of an unbonded water molecule, whatever its environment, is taken as 1.88 Debye units. Values of μ_3, μ_2, and μ_1 are interpolated linearly between μ_4 and μ_0.

Finally, we must include the contribution to the dielectric constant from processes occurring at higher frequencies than the orientation relaxation frequency. No data are available on the temperature variation of ϵ_{vib} for water, and since the contribution is small we shall take it to be the same as in ice. The high frequency dielectric constant $\epsilon_\infty=5.5\pm1$[7,20] is discussed below in terms of the rotation of zero- and one-bonded molecules; the contribution from which is included in the summation over the different states.

We tabulate values of d, μ_i, g_i, and ϵ in Table III.

The experimental measurements of ϵ are those of Akerlöf and Oshry.[21] These measurements were made under the equilibrium water vapor pressure at each temperature. We have therefore calculated molar volumes and interoxygen distances from densities at these pressures, and values of p from latent heats measured at these pressures.[22]

Our calculation of ϵ may be compared with those given by Oster and Kirkwood[19] and Lennard-Jones and Pople.[15] Oster and Kirkwood give a temperature variation in error by 10 percent per 60°C. As has been pointed out above, their estimations of coordination number and interoxygen distance are unsound and of g and α are inexact.

Lennard-Jones and Pople obtain very good agreement between theoretical and experimental temperature variation of ϵ in the range 0–80°C, but their absolute values

[18] R. H. Cole, unpublished communication to 1951 conference on dielectrics at Liverpool, England.

[19] G. Oster and J. G. Kirkwood, J. Chem. Phys. **11**, 175 (1943).

[20] E. Bauer and M. Magat, J. chim. phys. **45**, 93 (1948).

[21] G. C. Akerlöf and H. I. Oshry, J. Am. Chem. Soc. **72**, 2844 (1950).

[22] N. Dorsey, *Properties of the Ordinary Water Substance* (Reinhold Publishing Corporation, New York, 1940).

are 20 percent low. They consider the number of bonds broken to be very few but assume considerable bending of bonds. Although there must be some bending of bonds which our treatment neglects, it seems likely that Lennard-Jones and Pople exaggerate its extent in attributing the broadening of the peak in the x-ray radial distribution curve and the temperature variation of the dielectric constant, entirely to this effect. Morgan and Warren[4] have emphasized the difficulty of drawing unique conclusions from the x-ray data, and the agreement between Lennard-Jones and Pople's theoretical distribution curve and the experimental curve at 1.5°C is not exact. The experimental curve suggests rather more molecules at intermediate distances and rather less bending of bonds. Morgan and Warren's analysis of the x-ray data in terms of an average of three-bonded neighbors, with other neighbors at a continuous variety of distances, corresponds to a value of $p=25$ percent at 0°C. In so far as we take p equal to 10 percent at 0°C, we agree that bending of the bonds causes some broadening of the peaks in the radial distribution curve.

THE RELAXATION TIME OF WATER AND AQUEOUS SOLUTIONS

We can now extend these ideas to the dielectric relaxation process in water and aqueous solutions. We must first consider how orientation can take place in the various bonded states of the water molecule. Four-bonded and presumably also three-bonded molecules form part of the structure and cannot become reorientated without breaking bonds. Zero-bonded and one-bonded molecules can rotate without breaking a bond. Two-bonded molecules may also have to break a bond in order to rotate, but it seems probable[15] that in the unsymmetrically bonded case (Fig. 7) the rotational energy barrier will be considerably lower than the energy of rupture.

In the infrared region water shows two broad dispersion bands at approximately the same frequencies as the hindered rotation and translation bands in ice, but the dielectric constant of water in the far infrared ($\epsilon=4$)[20] is higher than the value for ice ($\epsilon=3.2$). We tentatively suggest that this is due to rotation of the zero- and one-bonded molecules. From the figures in Table III we calculate the contribution to ϵ for these processes at 25°C, to be 0.7, which is of the required order of magnitude.

Microwave measurements show a dielectric constant falling to 5.5 ± 1,[7] and extrapolation to the far infrared[20]

TABLE III.

T	d	μ_4	μ_3	μ_2	μ_1	g_4	g_3	g_2	g_1	ϵ_{calc}	ϵ_{exp}
Ice 0°C	2.76	2.45	···	···	···	2.91	···	···	···	92.7	92
Water 0°	2.76	2.45	2.30	2.18	2.03	2.81	2.36	1.90	1.45	89.0	88.2
25	2.78	2.44	2.29	2.17	2.03	2.80	2.35	1.90	1.45	78.3	78.2
60	2.82	2.42	2.27	2.17	2.02	2.79	2.34	1.89	1.45	65.8	66.6
100	2.84	2.39	2.25	2.16	2.02	2.76	2.28	1.86	1.43	53.7	55.4
200	3.01	2.29	2.21	2.10	2.00	2.69	2.24	1.83	1.42	31.6	34.6
300	3.29	2.18	2.10	2.03	1.96	2.55	2.17	1.77	1.39	15.2	17.7
370	···	···	···	···	···	···	···	···	···	7.4	9.7

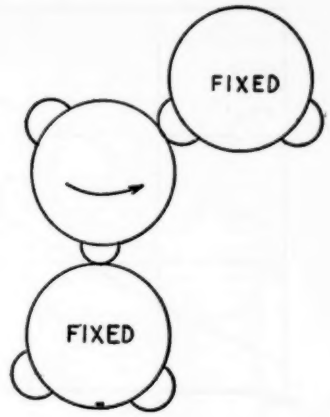

FIG. 7. Rotation of unsymmetrical 2-bonded water molecules.

suggests a further dispersion region. If we interpret the microwave dispersion as being due to the breaking of bonds, there is the possibility of the process illustrated in Fig. 7 occurring at slightly higher frequencies. Since only one-half of the two-bonded molecules are unsymmetrically bonded, we calculate that this process would contribute a further 1.6 at 25°C, thus accounting for the difference between $\epsilon=4$ and 5.5. The calculated temperature variation of this contribution is not outside the experimental limits of accuracy given by Collie, Hasted, and Ritson.[7]

The rapid increase of the dielectric constant in the microwave region suggests that the bonds are breaking and reforming. We must explain the following:

1. The temperature dependence of the relaxation time.
2. The effect of solutes in increasing or decreasing the relaxation time.

The bonded states will be in equilibrium with each other, and the factor governing the reorientation of four- and three-bonded molecules will be the rate of formation from these states of molecules in the unsymmetrical two-bonded state, which we assume free to rotate at higher frequencies than that at which they are formed. This rate will be dependent on the probability of breaking of a bond $f_1(T)e^{-\Delta H/RT}$ and on the number of bond types from which this state can be formed, i.e.,

$$1/\tau=(2m_{33}+m_{34}+m_{31}+m_{32})f_1(T)e^{-\Delta H/RT}$$
$$=2n_3f_1(T)e^{-\Delta H/RT}.$$

Collie, Hasted, and Ritson found that a logarithmic plot of relaxation time against reciprocal of temperature was slightly curved (Fig. 8) but gave an activation energy of approximately 5 kcal/mole. If we neglect the variation of $f_1(T)$ with temperature as compared with the exponential, we obtain an exactly linear plot of $\log n_3\tau$ against $1/T$ (Fig. 8), corresponding to an activation energy of about 3 kcal/mole for "breaking" and "reforming" of a bond. It is not surprising that this is lower than the bond energy (4.5 kcal/mole) for complete separation of the two water molecules.

When electrolytes or organic substances are dissolved

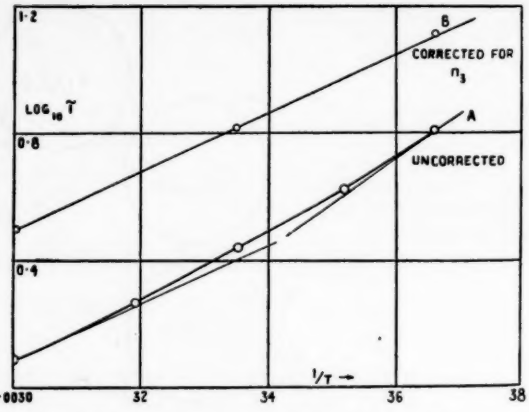

FIG. 8. Plots of logτ and log$n_3\tau$ against reciprocal of temperature.

in water up to 1-molar concentration, the single relaxation time of water is shortened or lengthened by an amount proportional to the concentration (Fig. 9). Writing $\lambda_{s\ (\text{solution})}=\lambda_{s\ (\text{water})}+c\cdot\delta\lambda_s$ where c is the molarity of the solution, we tabulate values of $\delta\lambda_s$ in Table IV.** It will be noticed that for ionic substances $\delta\lambda_s$ is negative and for substances likely to form hydrogen bonds $\delta\lambda_s$ is positive. We interpret this as an increase in the percentage of bonds broken when ions are added to water and a decrease when hydrogen bond forming groups are added; this will shift the equilibrium of bonded states and so change the value of n_3.

We shall try to explain the effect of solute molecules on p by considering the change in the number of bonds formed by the surrounding water molecules.

The water molecules round a positive ion are normally considered to be orientated as in Fig. 10(A).[13, 6, 23, 24] Verwey[5] has criticized this model and calculates heats of hydration for orientation round a positive ion as in Fig. 10(B). He considers that in this way a further bond can be formed to the next water sheath, making this position energetically more favorable. We feel, however, that the extra bond would be weak, as a result of the polarization of the water molecule in the ionic field; moreover, the orientation of two water molecules, as in Fig. 10(A), so that both form one bond less, is equivalent to the breaking of one water bond, so that this orientation is in any case energetically more favorable. This does not greatly affect Verwey's calculations of heats of hydration since the increased energy of orientation approximately balances the extra energy required to break a water bond. Neither the heats of hydration nor the entropy calculations[24] settle this point at all conclusively. Water molecules round negative ions are normally considered to be oriented as in Fig. 10(C).

A water molecule oriented as in Fig. 10(A) can form two bonds to neighboring water molecules, and a molecule oriented as in Fig. 10(C) can form three such bonds. A water molecule adjacent to the hydrogen bond forming group of an organic molecule can form four hydrogen bonds, and a molecule adjacent to a hydrocarbon chain can form three hydrogen bonds.

We assume that large negative ions or hydrocarbon chains, which interact little with the water, have only a small effect on p, i.e., as they are inserted into the "broken down" structure this becomes rearranged without breaking of bonds so that three or less bonded molecules are adjacent to the solute molecule or ion.

The reorientation of water molecules at a positive ion will result in breaking of bonds and increase in p, while the extra bonds formed to hydrogen bond forming groups will have the effect of decreasing p.

If we suppose positive ions six coordinated with water molecules oriented as in Fig. 10(A), approximately three bonds are broken per ion pair. Since in molar solution there are approximately 50 water molecules per ion pair and 100 bonds per 50 water molecules, this corresponds to $\Delta p\simeq+3$. Calculating the change in n_3 from the equilibrium distribution at 25°C, this gives $\delta\lambda_s=-0.15$, in fair agreement with the experimental value for NaCl.

The dielectric results show the same bond breaking effect for K^+, NH_4^+, and Rb^+ and a similar but smaller effect for Li^+.

If we suppose the $-$COOH group 4–6 coordinated with $\Delta p=-2$ to -3, this gives $\delta\lambda_s=+0.15$ to $+0.25$ also in fair agreement with experiment. $\delta\lambda_s$ values for alcohols and amines are rather higher than expected.

The negative $\delta\lambda_s$ values for NaF and KF are significantly less than those for NaCl and KCl. Fluorine is known to form hydrogen bonds, and it seems that the F^- ion makes a positive contribution to $\delta\lambda_s$.

We thus distinguish between the two types of water solute bond: bonds to hydrogen bond forming groups

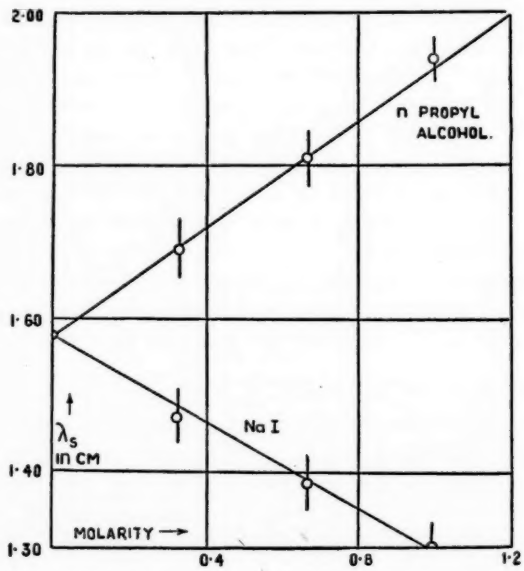

FIG. 9. Variation of relaxation time with concentration.

** $\delta\lambda_s$ so defined is twice the $\delta\lambda_s$ used by Hasted, Ritson, and Collie.

[23] D. H. Everett and C. A. Coulson, Trans. Faraday Soc. **36**, 633 (1940).

[24] D. D. Eley and M. G. Evans, Trans. Faraday Soc. **34**, 1093 (1938).

including the F^- ion and bonds to other ions. The former affect the relaxation time of the water, the latter do not.

The changes in relaxation time which we seek to explain are related to changes in the freedom of orientation of the water molecules in an electric field. A semi-quantitative interpretation of the results is possible only if we treat hydrogen bonds as comparatively rigid bonds but suppose that water molecules adjacent to the larger inorganic ions have considerable freedom of movement in the ionic field.†† This suggests that although hydrogen bonds are primarily electrostatic in nature,[15] the lone electron distribution, the localized proton charge, and the small covalent exchange considerably restrict the "bending" of the bond.

The dielectric results are in agreement with x-ray diffraction results,[3] which show structural changes equivalent to an increase in temperature for LiCl, NaCl, and NH_4Cl, and with spectroscopic evidence[2] for an ordering effect associated with the F^- ion. The spectroscopic evidence for an increase in order for Li^+ is not supported by our results or by the x-ray data.

NaI shows a negative value of $\delta\lambda_s$ slightly larger than NaBr and NaCl, in agreement with the spectroscopic and fluidity data.[25,26] Possibly the ion-water bonds which are quite directional in the case of F^-, still have a small positive effect on $\delta\lambda_s$ in the case of Cl^-, and this becomes less with increase in ion size.

Although effects due to individual ions seem to be additive in ionic solutions, this is not always true for molecules containing two active groups with the possibility of interaction between them. In dibasic acids such as glutaric acid the relaxation time change is much smaller than expected. For Dioxan[8] the change in relaxation time is not twice as great as for a single ketone, but for ethylene diamine it is greater than for a monoamine.

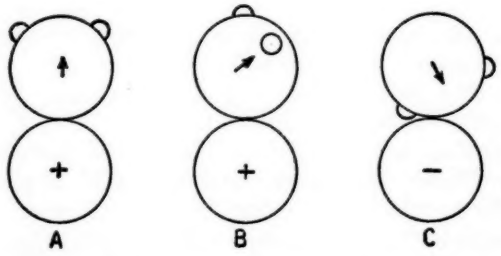

FIG. 10. Orientation of water molecules adjacent to positive ions (A and B) and negative ions (C).

†† Organic molecules have an "ordering" effect; large negative ions do not. It seems possible at first sight that this might be due to tetrahedral packing of water molecules round the organic group, i.e., to an ordering effect on water molecules outside the first surrounding layer. On more detailed consideration of the open "broken down" structure of water (if p is of the order of 10 percent) it seems unlikely that the number of bonds formed by water molecules adjacent to a given water molecule in the first layer will be affected by the position or orientation of other water molecules in the first layer.

[25] E. C. Bingham, J. Phys. Chem. **45**, 885 (1941).

[26] T. Watari, Bulletin of Tokyo Institute of Technology B, No. 2 (1950).

TABLE IV.

	$\delta\lambda_s \times 100$ (±4)
Dioxan[a]	+20
n-Propyl alcohol	+35
iso-Propyl alcohol	+30
t-Butyl alcohol	+40
Diethylketone	+30
Phenol	+20
Aniline	+15
Propionic acid	+20
Ethylamine	+20
n-Propylamine	+20
Glutaric acid	+15
Ethylene diamine	+30
α-Alanine	0
β-Alanine	0
NaF	−5
NaCl	−20
NaBr	−20
NaI	−25
LiCl	−10
KCl	−20
NH_4Cl	−15
RbCl	−20
KF	−10
Na Propionate	+15
Na Butyrate	+10
Ethylamine HCl	+15
n-Propylamine HCl	+15
Diethylamine HCl	+15
Triethylamine HCl	+20
Tetraethylammonium Cl	+30
Tetramethylammonium Br	+5
Tetramethylammonium I	+10
Guanidine Cl	−10

[a] See reference 8.

ELECTROSTRICTION

Since water becomes more close packed with increase in the percentage of bonds broken, we should expect an experimental correlation between relaxation time and volume changes.

Bernal and Fowler[13] calculated apparent ionic volumes from densities of salt solutions and volumes in the solid from crystal densities. They found apparent volumes equal to solid volumes for large monovalent ions, but for smaller ions apparent volumes were negative or, if positive, less than solid volumes.

Verwey[5] has pointed out that solid volumes depend on crystal packing and may not be equal to actual volumes in solution. He has also shown that it is energetically more favorable for a monovalent ion to be 6–8 coordinated, rather than 4 coordinated as Bernal and Fowler suppose. If we take the ionic coordination number in alkali halide solution as 6 and assume the radius in solution to be equal to the crystal radius, we have actual volume = (2×crystal radius)^3.

We calculate the apparent molar volume in solution in ccs/mole from densities in the usual way, and writing ΔV = (apparent volume in solution) − (actual volume), we tabulate a selection of values of ΔV, together with $\delta\lambda_s$ values, in Table V.

The partial molar volumes of the organic molecules in

solution are taken from the work of Traube[27] and Cohn and Edsall.[28,29] They found that these volumes were greater than the sum of the volumes attributed to the various atoms in the molecule by an "intermolecular space," which is approximately 13 cc/mole. This arises in part from the difference between covalent and van der Waals radii, but probably is due mainly to the open structure of hydrogen bonds round the COOH, OH, and NH_2 groups. For amino acids this effect is balanced by the electrostriction due to the charged groups,[29,30] and the volume difference $\Delta V=0$. For alanine we find $\delta\lambda_s=0$.

The lack of correlation between ΔV and $\delta\lambda_s$ in the case of NH_4Cl disappears if we suppose that the NH_4^+ ion is four coordinated to water molecules in solution, as a result of there being four center of positive charge. We have accordingly used the corrected value of the actual volume, 51 cc/mole, in the estimation of hydration given below, and this confirms that the number of water molecules bound to NH_4^+ is about 4.

TABLE V.

	Apparent volume (cc/mole)	Actual volume (cc/mole)	ΔV (cc/mole solute)[a]	$\delta\lambda_s$ cm (±0.05)
NaCl	17	33	−16	−0.20
NaBr	23	40	−17	−0.25
KCl	27	40	−13	−0.20
NH_4Cl	37[b]	43	−6	−0.15
$CH_3\cdot CH_2\cdot COOH$	67	54	+13	+0.20
$CH_3(CH_2)_2NH_2$	72	59	+13	+0.20
$NH_3^+(CH_2)_2COO^-$	59	59	0	0

[a] These volume changes are of the order of magnitude expected for $\Delta p \pm 3$, calculating from the equation relating density and p given above. They correspond very closely to the volume changes expected if water molecules were close packed on the side on which they form no hydrogen bonds.

[b] In Bernal and Fowler's tables NH_4^+ appears anomalous, but apparent volumes recalculated from density data in the International Critical Tables show no anomaly.

THE HYDRATION OF IONS

We define the hydration number n as the number of water molecules whose bonds with the solute molecule or ion are broken much less often than the water-water bonds and which are carried through the solution by the solute molecule or ion. This hydration number will only include the whole first sheath of water molecules if the strength of the solute-water bond is greater than the energy required (14 kcal/mole) to break the bonds to three other water molecules. If the solute-water bonds are weaker than 14 kcals/mole, the ion or molecule will be proportionately less hydrated, i.e., will not carry with it all the first sheath of water molecules.

We must first consider the strengths of the bonds between water molecules and organic groups or ions.

Butler[31] has calculated these bond strengths for a series of organic molecules from heats of hydration ($\Delta H_{\text{molecule}}$). He assumes that when an organic molecule is inserted into water, a cavity must be formed by removing water molecules from a tetrahedral structure and includes an energy term for the breaking of water-water bonds. In view of the considerations given above we do not believe this assumption to be justified, and we have, therefore, recalculated some of his results in the following way. We have assumed the heat of hydration of the hydrocarbon chain to be

$$\frac{\Delta H_{\text{ethane}}}{6}$$

per hydrogen. We assume that a cavity for the polar group is formed without breaking of hydrogen bonds and that van der Waals forces between the group and the water are not very different from those between water molecules. The average bond strength between the polar group and a water molecule is equal to

$$\frac{\Delta H_{\text{polar molecule}}-\Delta H_{\text{hydrocarbon}}}{\text{number of water molecules round polar group}}.$$

These bond strengths do not include the van der Waals energy and may, therefore, be compared directly with Pauling's[14] values but not with those of Butler.[31] We also extend the calculations to cover some inorganic and organic ions, taking the heats of hydration of Na^+ and Cl^- from Verwey and those of organic salts from Briegleb.[32] For positive ions we allow for breaking of water-water bonds, taking the ion-water bond strength as equal to

$$\frac{H_{\text{ion}}+\Delta p\times 4.5}{\text{coordination number}},$$

with Δp equal to half the coordination number. We tabulate bond strengths in Table VI.

It may be seen from this table that only ions are hydrated in the sense defined above.

We shall now consider the conclusions that may be drawn from the experimental values of ϵ_s given in Table I. Where our measurements indicate a single relaxation time, we assume that the solute molecule makes only a negligible contribution to ϵ, partly because of its low dipole moment and partly because of its longer relaxation time. Measurements on polar molecules smaller than propionic acid have not been discussed or included in Table I, as these show some solute contribution due to their relaxation falling within the wavelength range 1–10 cm. Alanine has a relaxation time in water corresponding to a wavelength $\lambda=12.5$ cm and gives appreciable solute contribution as a result of its high dipole moment. This case will be discussed below.

[27] J. Traube, Samml Chem. u Chem. Tech. Vorträge **4**, 255 (1899).

[28] Cohn, McMeekin, and Edsall, J. Am. Chem. Soc. **56**, 784 (1934).

[29] E. J. Cohn and J. T. Edsall, *Proteins, Amino-acids and Peptides* (Reinhold Publishing Corporation, New York, 1943).

[30] F. T. Gucker, Jr. and T. W. Allen, J. Am. Chem. Soc. **64**, 191 (1942).

[31] J. A. V. Butler, Trans. Faraday Soc. **33**, 229 (1937).

[32] G. Briegleb, Naturwiss. **30**, 436, 469 (1942).

It seems from the analysis of the results given below that there is no relaxation of polar groups, e.g., $-OH$, about the bond attaching them to the rest of the molecule, in the wavelength range 1–10 cm. This relaxation presumably occurs at longer wavelengths because of hindered rotation about this bond (energy barrier a few kcal/mole).[33]

ϵ_s therefore represents the low frequency dielectric constant of the water present in the solution and may be used to determine the extent to which water molecules round the ion or organic group are prevented by local fields from becoming oriented in the external field. Since these water molecules are restricted only in so far as the local field is stronger than the field due to neighboring water molecules, the dielectric effect should be closely related to hydration.[6] However, it is necessary to consider the water structure in detail as water molecules oriented as in Fig. 10(A) will contribute less to the dielectric constant than those oriented as in Fig. 10(B) or (C), where one proton or lone pair has freedom of movement. We shall define a number n_{irr}, the effective number of water molecules "irrotationally bound" to a solute molecule, i.e., unable to rotate in the electric field.

The estimation of irrotationally bound water from ϵ_s must depend on a dielectric theory of mixtures. The problem of a mixture of polar liquids in the region between their relaxations is equivalent to that of a mixture of polar and nonpolar liquids. This case has been investigated theoretically by Polder and van Santen,[34] and by Lewin;[35] also the case of electrical conduction, for which the equations are similar, has been investigated by Fricke.[36]

The dielectric constant (ϵ) of a mixture of randomly oriented spheroidal particles of low dielectric constant ($\epsilon_{solute}\sim 2$) in a medium of high dielectric constant ($\epsilon_{water}\sim 80$) is given by the equation

$$\epsilon-\epsilon_{water}=\frac{\beta\rho}{1-\rho}(\epsilon_{solute}-\epsilon).$$

This equation is derived directly from Fricke's equation by replacing conductivity symbols by ϵ, ϵ_{water} and ϵ_{solute}, and neglecting $\epsilon_{solute}/\epsilon_{water}$ in comparison with unity. ρ is the volume fraction of particles and β is a function of the particle axial ratio. A few β-values, taken from Fricke, are tabulated in Table VII.

For low solute concentrations we may write

$$\epsilon=\epsilon_{water}-\beta\rho(\epsilon_{water}-\epsilon_{solute})$$

to within an accuracy of $[(\rho^2/2)\times 100]$ percent in ϵ.

For solutions of small molecules and ions we have assumed that the solute molecule and associated water approximate to a sphere of low dielectric constant, and

[33] J. G. Aston, Chem. Revs. **27**, (1940).
[34] D. Polder and J. H. van Santen, Physica **12**, 257 (1946).
[35] L. Lewin, J. Inst. Elec. Engrs. (London) **94**, 65 (1947).
[36] H. Fricke, Phys. Rev. **24**, 575 (1924).

TABLE VI. Strengths of solute water bonds.

Group or ion	OH	NH_2	=O	$\diagdown\!\!\diagup$O	Na^+	Cl^-	NH_4^+	COO^-
Coordination No. assumed	3	3	2	2	6	6	4	6
Bond strength kcal/mole	3	3	3	3	18	15	19	22

we calculated n_{irr} from the equation

$$\epsilon=\epsilon_{water}-\delta c,\ddagger\ddagger$$

where c is the concentration in moles/liter, and

$$\delta=1.5\left[v\cdot\left(\frac{\epsilon_{water}-\epsilon_{\infty\ solute}}{1000}\right)+v_\omega\left(\frac{\epsilon_{water}-\epsilon_{\infty\ water}}{1000}\right)n_{irr}\right],$$

where v is the actual molar volume of the solute and v_ω is the molar volume of water ($v_\omega=18$)§§.

We find experimentally that up to 1.5-molar concentrations the value of δ is constant with ϵ_s varying linearly with concentration. Typical plots of low frequency dielectric constant against concentration are shown in Fig. 11.

We take $\epsilon_{\infty\ solute}$, the high frequency dielectric constant of the solute, as 2, and $\epsilon_{\infty\ water}$ as 5.5.[7] Values of n_{irr} calculated in this way are given in Table VIII together with the values of δ and the actual molar volumes in solution. These have been calculated from crystal radii and Traube's "group volumes," for the reasons given in the discussion on electrostriction above.

There will be two further effects which influence the dielectric constant of the solution, (1) a small effect due to the change in p (~1 percent) and (2), the electrostrictive effect (~2 percent). Since these effects are

TABLE VII.

Shape	$\beta\left(\frac{\epsilon_{solute}}{\epsilon_{water}}\ll 1\right)$
Spheres	1.5
Prolate spheroids axial ratio 4 to 1	1.6
Very long needles	1.67
Oblate spheroids, axial ratio 1 to 4	1.9
Very flat disks	Very large

‡‡ δ so defined is twice the δ used by Hasted, Ritson, and Collie.

§§ This treatment should not be confused with that of Oster [G. Oster, J. Am. Chem. Soc. **68**, 2036 (1946)], who is considering the static dielectric constant, which includes the low frequency solute contribution. It is possible that the single example of dioxan represents a nonpolar case and gives no solute contribution; this is precisely the case for which Oster's treatment does not give a value corresponding with experiment. He believes this is due to the hydrogen bond formation round this molecule; but if we treat this case as a mixture of polar and nonpolar molecules, the discrepancy disappears. We consider that there is hydrogen bond formation round many other molecules also but that because of the weak bond strength (Table VI), the water is not irrotationally bound.

TABLE VIII.

	δ (±0.5)	Actual volume (ccs/mole)	n_{irr}
Dioxan	8	69	0±0.5
n-Propyl alcohol	6	57	0±0.5
iso-Propyl alcohol	7	57	0±0.5
t-Butyl alcohol	7	73	0±0.5
Diethylketone	5±1	73	−1±1
Phenol	10±1	69	1±1
Aniline	8±1	71	0±1
Propionic acid	7	54	0±0.5
Ethylamine	6	43	0±0.5
n-Propylamine	9±1	59	1±1
Glutaric acid	11	86	0±0.5
Ethylene diamine	5	47	0±0.5
α-Alanine	12±1	60	2±1
β-Alanine	11±1	60	2±1
NaF	10	16	4±1
NaCl	16	33	6±1
NaBr	17	40	6±1
NaI	17	53	6±1
LiCl	15	30	6±1
KCl	14	40	5±1
NH_4Cl	14	51	4±1
RbCl	13	45	4±1
KF	12	24	5±1
Na Propionate	14	55	4±1
Na Butyrate	15	71	4±1
Ethylamine HCl	11	79	1±1
n-Propylamine HCl	14	95	1±1
Diethylamine HCl	19	111	3±2
Triethylamine HCl	20	144	2±1
Tetraethylammonium Cl	22	176	1±2
Tetramethylammonium Br	18±1	118	2±2
Tetramethylammonium I	17±1	130	1±2
Guanidine Cl	14	66	3±1

small and act in opposite directions, they have been neglected.

Our values of n_{irr} may be taken as a confirmation of the general correctness of this method of analyzing the experimental results, particular $n_{irr}=0$ for uncharged molecules. This also indicates that there is no relaxation of polar groups about the bond attaching them to the rest of the molecule.

It was shown in previous work[6] that the decrements of dielectric constant in solutions of monovalent ions were of such a size as to be accounted for on the assumption that only the first sheath of water molecules were affected by the ionic field.‖‖

The present analysis is an advance on these dielectric estimations of ionic hydration in that the volume of the ion is no longer neglected and the theory of mixtures is applied.

It will also be noticed that ionic solutions which were investigated up to concentrations of $2M$ in the previous work gave values of δ lower than those obtained in the present work. A detailed comparison of the values of ϵ_s at different concentrations will show that this is due not to the new figures being outside the limit of experimental error of the old, but to the dependence of ϵ_s on concentration having a slight curvature even below $c=1.5M$ (see Fig. 11).

In the cases of α- and β-alanine our experimental values of ϵ' and ϵ'' do not conform to a single relaxation time, since the high dipole moment results in some solute contribution. We have calculated this contribution at each frequency from low frequency decrements and solute relaxation times given by Cohn and Edsall.[29] For alanine there is close agreement between relaxation times given by Bateman and Potapenko[37] and by Conner and Smyth.[38] These contributions, which are of the order of 10 in ϵ' at $\lambda=10$ cm, have been subtracted to give the values of ϵ'_{corr} and ϵ''_{corr} in Table I; these fit equations for a single water relaxation time, as shown by the Cole and Cole diagram, given in Fig. 12.

In the case of small amides (unpublished data) divergences from the Cole and Cole plot were found. These molecules have dipole moments of about 4-Debye units as a result of resonance in the amide group, and their relaxation times in aqueous solution have not been

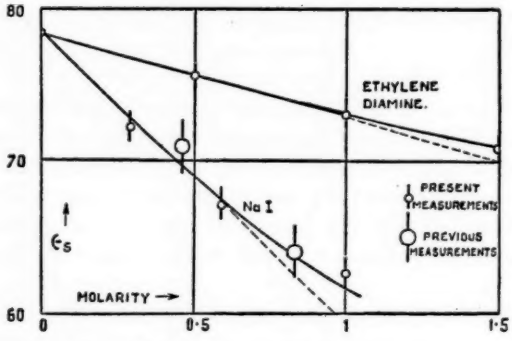

FIG. 11. Variation of ϵ_s with concentration.

studied. We have, therefore, been unable to estimate the hydration round these molecules.

The discussion given above of the orientation of water molecules round inorganic ions suggests that the positive ions make far the larger contribution to n_{irr}, but it is, of course, difficult to estimate the relative contributions quantitatively. On the basis of six coordination of both ions with water molecules oriented exactly as in Figs. 10 (A and C), supposing molecules oriented as in Fig. 10(C) to contribute approximately $\frac{1}{2}$, n_{irr} would be about 9 for NaCl. Although water molecules are predominantly oriented in this way, they will still have some freedom of movement, so that it is not surprising that the experimental values are rather lower than this. It seems from the results for inorganic ions and, for example, Na Propionate and Na Butyrate, that molecules oriented as in Fig. 10(C) make only a small contribution to n_{irr}.

‖‖ For divalent ions this is no longer true, and it would no longer be possible to discuss relaxation time and volume changes only in terms of the effect of the ion on p. It would be necessary to consider also the strength of bonds between first and second layer water molecules and the volume occupied by the first layer.

[37] J. B. Bateman and G. Potapenko, Phys. Rev. **57**, 1185 (1940).

[38] W. P. Conner and C. P. Smyth, J. Am. Chem. Soc. **64**, 1870 (1942).

In the case of NH_4^+ the negative $\delta\lambda_s$ and the value of $n_{irr}=4$ suggest that the water molecules are symmetrically bonded to the protons, as in Fig. 13(A). The positively charged amine groups, on the other hand, show a positive $\delta\lambda_s$ and small values of n_{irr} from which we conclude that the water molecules round these groups are tetrahedrally bound, as in Fig. 13(B). It is possible that owing to the flow of charge within the organic molecule the field round the N^+-H protons is no longer sufficient to make the symmetrical position energetically favorable.

The organic acid groups show positive $\delta\lambda_s$, suggesting that, even when dissociated, they form fairly directional hydrogen bonds to the water.

Since $\delta\lambda_s=0$ for alanine and the acid group should show a positive contribution, the contribution from the amine group must in this case be negative.¶¶ Guanidine also shows a negative $\delta\lambda_s$. Round these groups fields must be sufficiently strong to cause some reorientation of water molecules as round NH_4^+. This conclusion is confirmed by the n_{irr} values for these ions.

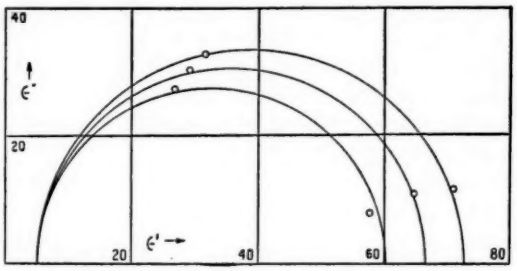

FIG. 12. Plots of ϵ''_{corr} against ϵ'_{corr} for alanine.

From dielectric decrements we estimate not true hydration but water "irrotationally bound." Only when water molecules are reorientated with their dipole aligned in the ionic field, as in Fig. 10(A) or Fig. 13(A), do they make an appreciable contribution to n_{irr}.

¶¶ See, however, discussion above of organic molecules containing more than one active group.

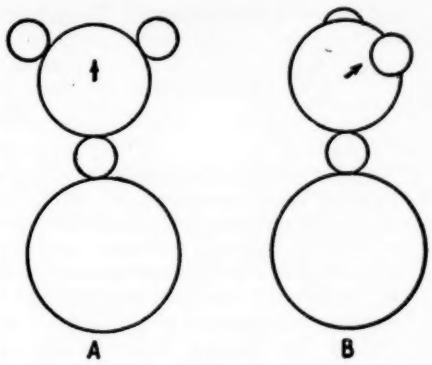

FIG. 13. Orientation of water molecules adjacent to positively charged basic groups.

An understanding of the nature and strength of bonds between water and hydrophilic groups is important in considerations of entropy and energy of hydration and also in the estimation of protein hydration from dielectric measurements[39] to be discussed in detail in a forthcoming paper.[12] We have tried in the present paper to relate the properties of water-water bonds and water-solute bonds to the dielectric properties of the bulk solution and to draw conclusions about the nature of the bonds from the dielectric measurements. Our statistical description of the water structure can be regarded only as semiquantatitive at the present time. A more detailed understanding of liquid water must depend on a more detailed understanding of the hydrogen bond between water molecules.

ACKNOWLEDGMENTS

We are indebted to the Telecommunications Research Establishment and to the Admiralty for the loan of klystron valves and to Dr. J. A. Saxton, of the National Physical Laboratory, for the temporary loan of a piston attenuator. One of us (J. B. H.) wishes to make acknowledgment to the Imperial Chemical Industries for a Research Fellowship at the University of London.

[39] Haggis, Buchanan, and Hasted, Nature **167**, 607 (1951).

Rotational Temperatures of OH in Several Flames*

H. P. Broida and G. T. Lalos
Division of Heat and Power, National Bureau of Standards, Washington 25, D. C.
(Received March 14, 1952)

The intensity of OH emission from various small regions of Bunsen-type flames of hydrogen, acetylene, methane, and propane, premixed with oxygen, has been observed spectroscopically and corresponding rotational temperatures have been determined by an iso-intensity method. An ultraviolet grating monochromator of high resolution was used; fuel to oxygen ratios were varied from about 0.5 to 2 times the stoichiometric value; and rotational temperatures were determined at several positions within each flame. The measured temperatures of the reaction zone varied little with mixture ratio for a given fuel and were greater than adiabatic, suggesting a lack of thermal equilibrium. In the hot gases beyond the reaction zone, however, evidence was found of both rotational and electronic equilibrium. The concentration of thermally produced OH in the burned gases was found to be so great that it tends to mask the emission from the reaction zone.

I. STATEMENT OF THE PROBLEM

SPECTROSCOPIC studies of emission from flames are of value in determining the intensity distributions of various intermediates and products of reaction and in evolving a mechanism of the combustion process. Estimates of flame temperatures from the relative intensity distributions of rotational lines emitted by excited free radicals in the hot gases are often made.[1–6] Interpretation of the observed intensities from the reaction zone is complicated by the effects of the burned gases which, in Bunsen-type flames, vary in thickness and possibly in composition over the area of the inner cone. Radiation from the inner cone must pass through this surrounding hot gas which influences the intensity of the observed radiation by both emission and absorption.

In an effort to obtain some insight into the effects of such a nonhomogeneous source on the measured intensity distributions from radicals and molecules in the hot gases, a systematic series of measurements was made in various parts of several flames. Oxygen premixed with different fuels was used without other diluent in all these flames. Intensities of the rotation lines of the R_2 branch of the 0, 0 vibrational transition of $^2\Sigma \rightarrow 2\Pi$-transition of OH were measured. From these intensities, temperatures of the rotational distributions of OH in the lowest vibrational state of the excited $^2\Sigma$ electronic state have been obtained as a function of position in the flame. Intensities of the $^2\Sigma^+ \rightarrow 2\Pi$ transition of CH were also measured in the hydrocarbon flames.

II. EXPERIMENTAL METHOD

A. Equipment

The apparatus used has been described in a previous publication.[4] Briefly, emission spectra were recorded by a high resolution grating monochromator[7] with a 1P28 photomultiplier as the detector. A resolving power, $\lambda/\Delta\lambda$, of 55,000 is readily attainable with this instrument. Using entrance and exit slits 0.006 mm wide (approximately 0.03A in the second order) in the OH spectrum from a flame it is possible to detect lines which are separated by 0.054A.

The portion of the flame to be studied was focused upon the entrance slit of the monochromator without magnification by a quartz lens. Vertical and horizontal positioning of the flame was accomplished with a rack and pinion device with which settings could be reproduced to 0.2 mm. The burner was a straightened oxy-acetylene torch having a port 1.5 mm in diameter. Tank gases having purities specified as follows by the supplier were used: oxygen, 99.7 percent; hydrogen, 99.8 percent; acetylene, 98 percent; methane, 99.6 percent; and propane, 98 percent. Pressure regulators reduced the tank pressures to five lb/in.^{2} gauge, and flow rates to the torch were measured to ± 5 percent with calibrated flowmeters of the floating ball type. Most measurements reported here were taken under the following conditions: flow rate of the combustible mixture, 200 cm^3/sec at atmospheric pressure; burner port, 1.5 mm diameter; slit, 0.010 mm wide and 1.0 mm long; and scanning rate, 5A/min. Two spectra were made at each position, one taken while scanning toward decreasing wavelengths and the other while scanning toward increasing wavelengths.

B. Effects of Experimental Operating Conditions on Measured Temperatures

Several operating parameters which might affect measured intensity distributions were varied separately

* This work was done under the sponsorship of the Navy Bureau of Aeronautics and the ONR.
[1] A. G. Gaydon and H. G. Wolfhard, Proc. Roy. Soc. (London) **A201**, 561 (1950).
[2] A. G. Gaydon and H. G. Wolfhard, Third Symposium on Combustion, Flame, and Explosion Phenomena (Williams and Wilkins, Baltimore, Maryland, 1949), p. 504.
[3] K. E. Shuler, J. Chem. Phys. **18**, 1466 (1950).
[4] H. P. Broida and K. E. Shuler, J. Chem. Phys. **20**, 168 (1952).
[5] W. S. Benedict and E. K. Plyler, Symposium on Energy Transfer in Hot Gases, Natl. Bur. Standards, Sept. 1951.
[6] H. P. Broida, J. Chem. Phys. **19**, 1383 (1951).
[7] This instrument was constructed by the Research Department of Leeds and Northrup Company and loaned to the Heat and Power Division at the National Bureau of Standards on a field trial basis.

to make certain that the measured values were independent of the apparatus. Table I lists these parameters and the ranges over which they were changed. Although the measured intensities differed by a factor of more than 250, it was found that the specified changes in operating conditions did not alter the calculated values of temperature by more than ±2.5 percent, which is considered to be within the experimental error of the measurements.

III. METHODS OF ANALYSIS

For rotational equilibrium, the intensity I_K, due to a transition from a rotational level K with an energy E_K, is given by

$$I_K = CA_K e^{-(E_K/kT)}, \quad (1)$$

in which A_K includes the transition probability of the particular transition, the frequency factor, and the statistical weight; k is the Boltzmann constant; T is the rotational temperature; and C depends upon the concentration of OH but is constant for a particular electronic and vibrational transition. Values of transition probabilities and energy levels were taken from the tables in reference 9. Usually temperatures are measured from slopes of plots of $\log(I_K/A_K)$ *vs* E_K. However, for intense sources this method is not satisfactory because self-absorption may cause serious error.[8]

The iso-intensity method, developed by Dieke and Crosswhite[9] can be used satisfactorily since to the first approximation lines of equal intensity are absorbed equally provided the temperature is uniform. It follows from Eq. (1) that for lines x and x' of equal intensity,

$$A_{x'}/A_x = e^{(E_{x'}-E_x)/kT} \quad (2)$$

and

$$T = \frac{E_{x'}-E_x}{k \log_e(A_{x'}/A_x)}. \quad (3)$$

In practice it is necessary only to match the intensity of a line from a lower rotational state ($x=1, 2, 3, 4,$ or 5) with the intensity of a line from a higher rotational state and to obtain the temperature from Eq. 3. An indication as to whether or not equilibrium exists is obtained by comparing temperatures obtained from two or more such pairs.

For more precise results, in this work the intensities of well-resolved lines were plotted against the K values and a smooth curve was drawn through the experimental points. Temperatures corresponding to at least 3 pairs of iso-intensity lines were determined and averaged. Three pairs giving the same temperature were considered to be evidence of a Boltzman distribution of rotational energy of the excited OH radicals.

An extension of this iso-intensity method, as developed by Shuler[8] probably gives a better indication of equilibrium. Values $E_{x'}-E_x$ for pairs of equal intensity are plotted against $\log_e(A_{x'}/A_x)$, and the rotational temperature is obtained from the slope of the curve. A straight line through the origin indicates a Boltzman distribution of intensities and departures from equilibrium appear as deviations from this straight line.

The procedure adopted here for determining temperatures was to find three iso-intensity pairs from each of two spectra obtained under the same conditions, to obtain the temperatures, and to average these six values arithmetically. The spread in such values varied between one and 10 percent. Measured temperatures were generally self-consistent and reproducible to better than ±2.5 percent. Spot checks of this were made by using the longer Shuler method on each type of flame in both inner and outer cones. No correction has been made for the contributions from the cooler surrounding gases since, without such a correction, a Boltzman distribution of rotational intensities was found in all flames.[10]

TABLE I. Experimental variation of the operating parameters.

Parameter	Range
Gas flow	14 to 200 cm³/sec (NTP)
Burner diameter	0.5 to 1.5 mm
Scanning rate	1.18 and 5.9 A/min
Slit width	0.008 to 0.020 mm
Slit height	0.3 to 6.0 mm

IV. RESULTS

Emission spectra of the R_2 branch of the 0, 0 vibrational transition of the $^2\Sigma \rightarrow {}^2\Pi$ electronic transition of OH (in the wavelength region near 3080A) were recorded from various regions of flames of hydrogen, acetylene, methane, and propane burning with oxygen. Rotational temperatures were computed from the measured intensities as described in Sec. III.

A. Vertical Scans

Flames were scanned vertically, using a slit one mm high and 0.010 mm wide, in steps of one mm over the inner cone and at somewhat larger intervals through the hot gases above this cone. The edge of the inner cone, characterized by peak intensity, was viewed from base to tip. Representative measurements on flames from stoichiometric mixtures of each fuel are presented in Figs. 1 through 4. The upper part of each figure is a plot of rotational temperatures of OH as a function of the distance above the base of the flame. Experimental points are not included since the large number of points tends to obscure the general trend. For a given fuel-oxygen mixture, the individually determined points usually fell within ±25°C of the curves and were reproducible under the various conditions listed in

[8] H. P. Broida, Symposium on Energy Transfer in Hot Gases, Natl. Bur. Standards, Sept. 1951.

[9] G. H. Dieke and H. M. Crosswhite, Bumblebee Series Report No. 87 (Nov. 1948) unclassified.

[10] Recently, more precise measurements have shown slight discrepancies in an acetylene flame; these will be discussed in a forthcoming paper by Shuler and Broida.

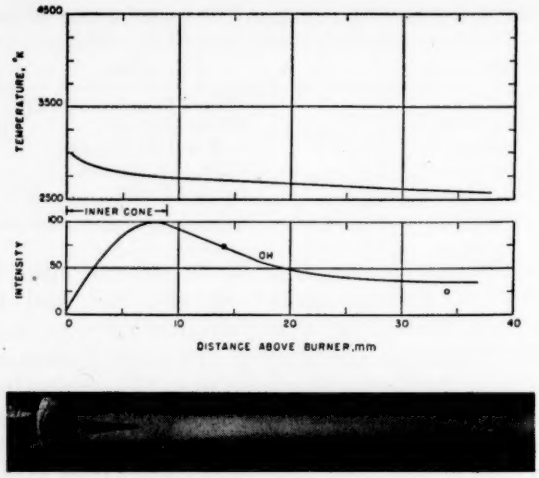

FIG. 1. Hydrogen-oxygen flame, stoichiometric mixture. The open circle is the OH intensity calculated using as reference the closed circle intensity.

Table I. The lower part of each figure is a photograph of the flame, enlarged so that horizontal positions on the photographs correspond to the respective points on the graphs.

The central strips of Figs. 1 through 4 show the relative intensities of the R_2 (1) line of OH as a function of distance above the base of the flame. For each fuel, the maximum intensity is taken arbitrarily as 100. This maximum always occurs near the tip of the inner cone above which the temperature drops at the rate of about 5°C/mm. This rate of cooling is much greater in flames from smaller ports. From the base to the tip of the inner cone the temperature decreases more rapidly, as is evident in the upper strip of each figure. As discussed in Sec. V, it appears that the gradual decrease of OH intensity above the tip is attributable almost entirely to the decrease in temperature. The drop in intensity from the tip to the base of the inner cone is due to the

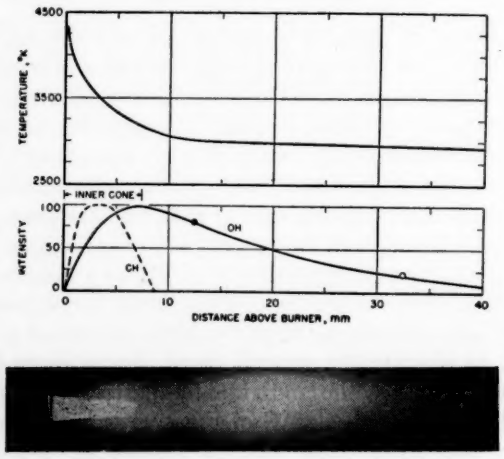

FIG. 2. Acetylene-oxygen flame, stoichiometric mixture. The open circle is the OH intensity calculated using as reference the closed circle intensity.

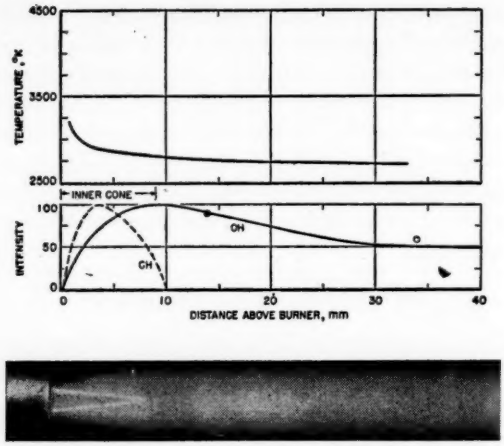

FIG. 3. Methane-oxygen flame, stoichiometric mixture. The open circle is the OH intensity calculated using as reference the closed circle intensity.

decreased thickness of hot gases surrounding the reaction zone.

Table II gives rotational temperatures of OH as determined for different flames near the base, at the tip, and at 5 mm and 25 mm above the tip of the inner cone. Values of flame temperatures appearing in the literature[11] on the sodium line-reversal method are given in the next to the last column. Also included are adiabatic flame temperatures calculated from chemical equilibria.

Figure 5 is a graph of measured intensities of the R_2 (1) line emitted from the flames with various fuels, as a function of the fraction of stoichiometric fuel in the mixtures. The ordinate is in arbitrary intensity units. It will be seen that maximum intensity for both hydrogen and acetylene occurs on the rich side of stoichiomet-

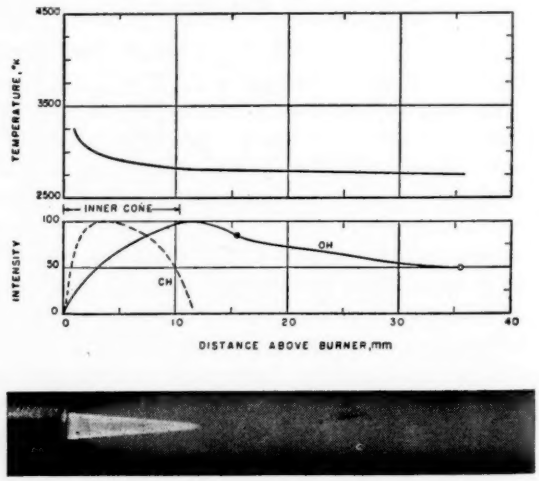

FIG. 4. Propane-oxygen flame, stoichiometric mixture. The open circle is the OH intensity calculated using as reference the closed circle intensity.

[11] H. H. Lurie and G. W. Sherman, Ind. Eng. Chem. **25**, 404 (1933).

TABLE II. Measured and calculated temperatures in various flames.

Fuel	Mixture $\frac{F/O_2}{(F/O_2)\text{ stoich.}}$	Measured OH rotational temp. (°K) base	tip	5 mm above tip	25 mm above tip	Na line Reversal[b] (°K)	Calculated Equil. temp. (°K)
H_2	1.0 (stoich.)	3000	2750	2700	2600	2750	3100[c]
	0.66 (lean)	2950	2625	2600	2575	2750	2825
	2.0 (rich)	2950	2775	2750	2600	2700	2925
C_2H_2	1.0 (stoich.)	4250	3175	3025	2950	3300	3325[d]
	0.5 (lean)	4100	2775	2750	2750	3200	3075
	2.0 (rich)	4100	3175	3050	2950	3400	3400
CH_4	1.0 (stoich.)	3200	2800	2750	2700	3150[a]	3050[e]
C_3H_8	1.0 (stoich.)	3300	2825	2800	2750		

[a] % Natural gas. [b] See reference 11. [c] See reference 4. [d] See reference 13. [e] F. Ruegg (private communication.)

ric mixture. This mixture ratio also gives the greatest measured rotational temperature.

Table III gives a comparison of the theoretically calculated and measured ratios of intensities of OH from several flames to the corresponding intensity from a flame of a stoichiometric hydrogen-oxygen mixture. The observations were made 5 mm above the tip of the inner cone using the R_2 (1) line. The calculated ratios were obtained from Eq. 1 by assuming purely thermal excitation and uniform temperature over the visible diameter in each flame. Measured OH rotational temperatures were used and OH concentrations were calculated from tables of equilibrium constants.[12] There was apparently no error in the measured ratios due to self-absorption since the relative intensities agreed with those obtained using the ${}^sR_{21}(2)$ line, which has a much lower transition probability.

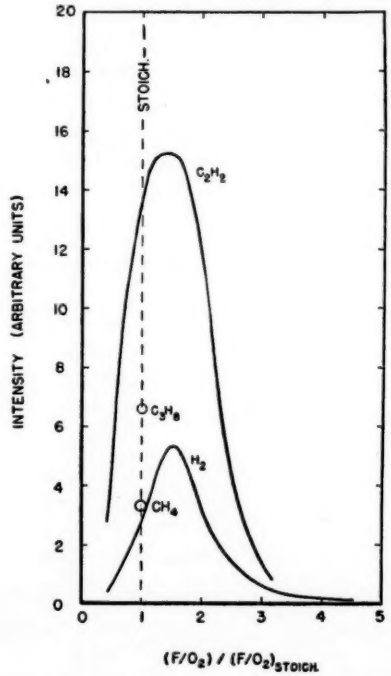

FIG. 5. Measured intensity of the $R_2(1)$ line as a function of the stoichiometric fuel.

[12] Hottel, Williams, and Satterfield, Thermodynamic Charts for Combustion Processes (John Wiley and Sons, Inc., New York, 1949).

In the reaction zone of hydrocarbon flames, emission from C_2 and CH is also very prominent. Some intensity measurements of CH, arbitrarily assigning 100 to the maximum, are plotted as the dashed curves of Figs. 2 through 4. Observed peak intensities of the Q head of the ${}^2\Sigma^+ \rightarrow {}^2\Pi$ (0, 0) transition of CH at 3143A were used for these measurements. The ${}^2\Sigma^- \rightarrow {}^2\Pi$ and ${}^2\Delta \rightarrow {}^2\Pi$ bands of CH at 3889A and 4315A, respectively, and the ${}^3\pi \rightarrow {}^3\Pi$ C_2 Swan bands (e.g., 0, 0 at 5461A), show similar intensity distributions in the inner cone.

It can be seen that the intensity of CH drops very rapidly near the tip of the inner cone. Careful observations with a monochromator slit height of 0.3 mm showed no observable CH emission (less than one percent of the maximum) 0.1 mm beyond the tip of the luminous inner cone. Since a slit height of one mm was used for the CH intensities in Figs. 2 through 4, the intensity appears to go beyond the tip.

B. Horizontal Scans

Typical variations of intensity and temperature with horizontal position at a distance 20 mm above the tip of the inner cone are shown in Figs. 6A and 7A for stoichiometric mixtures of hydrogen and acetylene with oxygen. Temperatures decreased very slowly from the center outward. Decrease in intensity is due to the combined effects of the decrease in temperature and to the decrease in the path-length of the emitting gas. The open circles on Figs. 6A and 7A are the calculated intensities relative to the intensities marked with the closed circles. The small contribution to the total

TABLE III. Measured and calculated intensities of various flames.

Fuel	Mixture $\frac{F/O_2}{(F/O_2)\text{ stoich.}}$	I/I_{H_2} Measured	I/I_{H_2} Calculated
H_2	1.0 (stoich.)	1.00	1.00
	0.66 (lean)	0.39	0.29
	2.0 (rich)	0.93	0.35
C_2H_2	1.0 (stoich.)	3.4	9.5
	0.5 (lean)	1.9	1.4
	2.0 (rich)	3.7	2.0
CH_4	1.0 (stoich.)	1.1	1.5
C_3H_8	1.0 (stoich.)	1.9	1.6

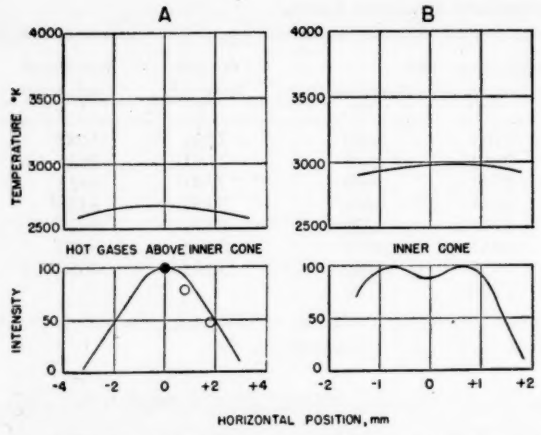

FIG. 6. Hydrogen-oxygen flame, stoichiometric mixture. The open circles are OH intensities calculated using as reference the closed circle intensity. (A) is measured 20 mm above tip of inner cone. (B) is measured 2 mm above base of inner cone.

intensity from the lower temperature regions indicates that the measured temperature through the center of the hot gases is close to that at the core.

In the acetylene flames a slightly different characteristic was noted, as indicated in Fig. 7A by the wings of the intensities at the edges of the hot gases. The photograph of Fig. 2 shows a similar flaring out in this region.

Typical variations of intensity and temperature with horizontal position near the base of the inner cone are shown in Figs. 6B and 7B for stoichiometric mixtures of hydrogen and acetylene. The latter figure clearly shows the reaction zone and the hot gases outside the inner cone. The positions of maximum intensity correspond to the edges of the inner cone and are of somewhat greater intensity than the center position due to the increased path of the reaction zone in the field of view.

V. DISCUSSION

It is apparent from Figs. 1–4 and Table II, that the measured temperature of a flame is without clear meaning unless the region of the flame observed and the mixture of fuel and oxygen are specified. In particular, there is a large difference between the OH rotational temperature measured at the base of the flame region and that measured in the outer cone.

The intensity of OH emission above the tip of the inner cone is so great that there is a large contribution to the measured intensity of the inner cone from the surrounding burned gas. Since the thickness of the surrounding gas is decreased toward the burner, the temperature measured near the base of the inner cone is considered most nearly characteristic of the rotational distribution of OH in the reaction zone.

Unexpectedly, with the method used, there was no indication of a departure from a Boltzman distribution of rotational intensities. Even in the case of acetylene for which a rotational temperature 1000°C greater than the adiabatic temperature was measured at the base of the inner cone, the various iso-intensity temperatures agree within ±25°C. It seems improbable that the superposition of intensities from the "hotter" reaction zone and the "cooler" surrounding hot gases should form an apparent Boltzman distribution from the base to the tip of the inner cone.

The measured OH rotational temperatures reported here are consistent with others in the literature. Measurements of Wolfhard quoted by Gaydon and Wolfhard[13] indicate that the measured temperature of the inner cone of the acetylene-oxygen flame is 4000°K; Dieke and Crosswhite[9] found that the temperature of the hot gases outside the reaction zone of this flame is 3000°K. Shuler[3] observed that 30 mm above the tip of the inner cone of a methane-oxygen flame the rotational OH temperature is 2600°K and that the temperature in the inner cone of hydrogen-oxygen is 2850°K. It is difficult to make accurate comparisons since the positions observed in the flame and the mixture ratios are seldom specified exactly.

As mentioned in the previous section, the apparent rate of decrease of temperature with increasing height is greater in the inner cone region than it is in the hot gases above the inner cone. It is difficult to explain the observation that, just above the reaction zone, the measured temperature is from 200 to 300°C below the adiabatic temperature. The rate of cooling (5°C per mm) above the inner cone is so low that cooling from the outer atmosphere is unlikely to be the cause. As was pointed out in Sec. IV, the effect of observing through the cooler outer layers cannot be the cause. It is possible that there may be sufficient mixing with the outside cold gases near the base of the flame to give this temperature difference.

Gaydon and Wolfhard[13] suggested that the increased intensity and the difference of the OH intensity distribution from that of equilibrium in the reaction zone

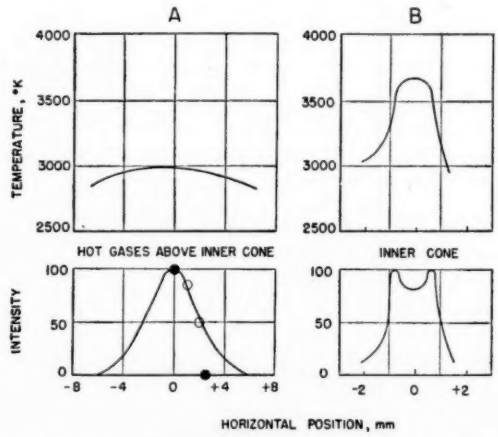

FIG. 7. Acetylene-oxygen flame, stoichiometric mixture. The open circles are OH intensities calculated using as reference the closed circle intensities. (A) is measured 20 mm above tip of inner cone. (B) is measured 2 mm above base of inner cone.

[13] A. G. Gaydon and A. G. Wolfard, Proc. Roy. Soc. (London) **A194**, 169 (1948).

of acetylene flames is due to chemiluminescence. This phenomenon would also explain the high rotational temperature found at the base of the flame and the fact that the same temperature is observed over a range of concentrations of acetylene in oxygen. This independence of mixture ratio was also observed at the base of hydrogen flames. However, the differences between the observed rotational temperatures and the adiabatic flame temperatures for hydrogen are too small to provide convincing evidence of chemiluminescence. Failure to find variations in rotational temperature with mixture ratio for both acetylene and hydrogen would seem to indicate that the excitation upon which the temperature measurement is based is characteristic of one or more of the intermediate chain reactions.

No explanation can be advanced for the fact that mixtures with less fuel than stoichiometric appear to cool less rapidly above the inner cone than mixtures having larger proportions of fuel.

The abnormal rotational distribution in the inner cone combined with the thermal distribution in the outer cone can be used to estimate the lifetime of excited OH. By extrapolation of the temperature trend in the hot gases above the tip, to the base of the flame, it is found that the measured temperature is higher than this extrapolated temperature from the base to about 2 mm beyond the tip. This excess temperature was found in all eight of the fuel-oxygen mixtures observed. Assuming that this gradual decrease of excess temperature is due to a loss of excited radicals by radiation alone, an estimate can be obtained for the lifetime of OH. The velocity of the gas just above the tip of the inner cone is given approximately by

$$V_g = \frac{\text{volume flow (NTP)}}{\text{cross section of burner port}} \times \frac{T_f}{T_g}$$

$$= \frac{(200)10^3(3000)}{(0.75^2)(300)} = (1.1)10^6 \text{ mm/sec.} \quad (4)$$

Since the excess temperature continues some 2 mm beyond the tip, a lifetime of $(1.8)10^{-6}$ sec. is indicated. This value is the same order of magnitude as the radiative lifetime of $(4)10^{-6}$ sec. measured by Oldenberg and Rieke.[14]

That CH does not extend beyond the tip of the inner cone can be used to set an upper limit on the lifetime of CH. Using the uncertainty in spatial resolution of 0.1 mm for the possible existence of CH intensity above the tip and making the same assumptions as used for obtaining the estimate of the excited OH lifetime, the lifetime of excited CH would be less than 10^{-7} sec.

The measured intensities in the various flames at atmospheric pressure show no large deviations from those expected at the corresponding rotational temperatures in the gases beyond the tips of the inner cones. Table III lists intensity ratios of the various flames relative to a stoichiometric hydrogen-oxygen mixture at a distance of 5 mm above the tips of the inner cones. The order-of-magnitude agreement between calculated and experimental ratios indicates that the electronic excitation temperature of OH is probably the same as the rotational temperature.

Other indications of equilibrium in electronic and rotational degrees of freedom above the inner cone are found in Figs. 1–4. Using the intensity and rotational temperature 5 mm above the tip (closed circle) as the reference point, the intensity 25 mm above the tip (open circle) was calculated from the measured temperature. The measured and computed intensities agree within the experimental error involved in the measurement of rotational temperature. Similarly intensities have been computed for the horizontal scans, with correction for path length. The agreement between calculated and measured intensities for the hot gases above the inner cone is shown by the open circles in Figs. 6A and 7A.

This evidence of thermal equilibrium in the hot gases above the inner cone supports a previous conclusion of Broida and Shuler,[4] based upon their measurements of rotational and vibrational temperatures of the excited state in the hot gases above the inner cone of similar hydrogen-oxygen flames. However, Benedict, Plyler, and Humphreys[15] found from infrared measurements that the rotational temperature in the ground state is 300 to 500°C less than in the excited state. They attribute this difference to the much longer lifetime of the infrared radiation and a weighting from the cool outer regions.

These studies of intensity distributions of OH in several different flames using an iso-intensity method have shown that measurements of OH rotational temperatures are quite reproducible under fixed conditions and that the values measured in the hot gases outside the reaction zone are consistent with equilibrium conditions at temperatures somewhat less than the calculated adiabatic temperatures. The abnormally large temperatures measured at the base of the inner cones of acetylene flames definitely shows that OH rotation in the $^2\Sigma^+$ state is not in equilibrium in the reaction zone of these flames.

[14] O. Oldenberg and F. F. Rieke, J. Chem. Phys. **6**, 439–447 (1938).

[15] Benedict, Plyler, and Humphreys, Phys. Rev. **82**, 337(A) (1951).

Nuclear Magnetic Resonance in Metals. I. Broadening of Absorption Lines by Spin-Lattice Interactions*†

H. S. GUTOWSKY AND B. R. MCGARVEY‡
Noyes Chemical Laboratory, University of Illinois, Urbana, Illinois
(Received March 21, 1952)

Magnetic resonance line shapes and widths, their temperature dependence, and the conduction electron shifts in resonance frequency are reported for the metals Li^7, Na^{23}, Al^{27}, Cu^{63}, Cu^{65}, Ga^{69}, Ga^{71}, Rb^{85}, Rb^{87}, and Cs^{133}. The absorption lines in most of these metals are broader than predicted for nuclear magnetic dipolar broadening alone. We propose that the mechanism responsible for most, if not all, of this additional broadening is the interaction between the nuclear spins and the conduction electrons, which also determines the spin-lattice relaxation time. Spin-lattice relaxation times T_1 are estimated from the nondipolar broadening of the experimental absorption lines. These T_1 values compare favorably with available directly measured values and with approximate T_1 values obtained by Korringa's theory from the measured resonance shifts. In the case of lithium, a dipolar line-width transition was observed at 255°K; this transition results from self-diffusion, for which we determine an activation energy of 9.8±1 kcal/mole.

INTRODUCTION

IT was noted in a preliminary letter[1] that nuclear magnetic resonance absorption lines in metals were broader than could be explained by Van Vleck's[2] theory of dipolar broadening. The experimental second moments for the absorption lines of Na^{23}, Al^{27}, Cu^{63}, and Cu^{65} were greater than predicted. Bloembergen[3] observed earlier that the line widths for Cu^{63} and Cu^{65} were rather large in the metals but made no detailed analysis and concluded the results were within experimental error of expectation. More recently, Knight[4] has reported that the line widths of V^{51} and Cb^{93} exceed the values estimated from the nuclear magnetic dipolar broadening alone. The resonance frequencies are known[5] to be higher in metals than in their compounds by up to several tenths of a percent, owing to[6] the contribution of the conduction electrons to the magnetic field at the nuclei in the metal. Anisotropy in these conduction electron shifts might lead to line broadening[1] in the metals; so could quadrupolar coupling in case the cubic symmetry of the electric field in the crystal lattice was disturbed in some manner.[1,4] The research described herein characterizes the major aspects of the line broadening effect and provides convincing evidence that it is a consequence of the strong interactions of the nuclear spins with the conduction electrons, which are responsible also for the very short spin-lattice relaxation time.

Heitler and Teller[7] first pointed out the importance of the conduction electrons in metals in determining the relaxation time for the transfer of energy between a nucleus and its surroundings. Korringa[8] has related the spin-lattice relaxation time T_1 to the conduction electron shift in resonance frequency, $\Delta H/H$. Korringa's final result[9] is

$$T_1(\Delta H/H)^2=\hbar/\pi kTg^2. \quad (1)$$

g is here the nuclear gyromagnetic ratio in Bohr magnetons. Typical values for T_1 in metals are the order of 10^{-4} sec compared to values of 10^{-2} to 10^4 sec for chemical compounds. The significance of this may be seen from the approximate equation[10] relating the inverse line-width parameter T_2 to the spin-spin interaction parameter T_2', and the spin-lattice relaxation time T_1,

$$(1/T_2)\cong(1/T_2')+(1/2T_1). \quad (2)$$

In most solids, T_1 is of such magnitude that the associated effect upon the shape and width of the resonance line is negligible, but in systems where the spin-lattice relaxation time is exceptionally short, the relaxation interaction can broaden the absorption line appreciably. This has been verified experimentally in solutions of paramagnetic salts.[10] The line broadening in the metals is interpreted in a similar fashion.

EXPERIMENTAL PROCEDURE

The particular apparatus and some of the methods have been described previously.[11,12] All experiments were at an applied magnetic field of 6365±2 gauss. Measurements included line shapes and widths, their temperature dependence, and the conduction electron shifts in resonance frequency.

A radiofrequency bridge system[10] was used with a signal generator, preamplifier, and receiver tuned at

* Supported in part by ONR.
† A report of this work was given at the Washington meeting of the American Physical Society, May, 1952; Phys. Rev. **87**, 226(A) (1952).
‡ AEC Predoctoral Fellow.
[1] H. S. Gutowsky, Phys. Rev. **83**, 1073 (1951).
[2] J. H. Van Vleck, Phys. Rev. **74**, 1168 (1948).
[3] N. Bloembergen, Physica **15**, 588 (1949).
[4] W. D. Knight, Phys. Rev. **85**, 762(A) (1952).
[5] W. D. Knight, Phys. Rev. **76**, 1259 (1949).
[6] Townes, Herring, and Knight, Phys. Rev. **77**, 852 (1950).
[7] W. Heitler and E. Teller, Proc. Roy. Soc. (London) **A155**, 637 (1936).
[8] J. Korringa, Physica **16**, 601 (1950).
[9] C. P. Slichter independently obtained the same equation by an approximate method in some unpublished research.
[10] Bloembergen, Purcell, and Pound, Phys. Rev. **73**, 679 (1948).
[11] H. S. Gutowsky and C. J. Hoffman, J. Chem. Phys. **19**, 1259 (1951).
[12] Gutowsky, McClure, and Hoffman, Phys. Rev. **81**, 635 (1951).

the resonance frequency. Null-T bridges[13] were found more convenient than the Purcell type[10] at lower frequencies. Line shapes were obtained by modulating the magnetic field at 30 cycles with an amplitude a small fraction of the line width. A plot of the output with a narrow band amplifier gave the derivative of the absorption line as the magnetic field applied to the sample was varied over the necessary range. Line widths δH are taken to be the separation of the two peaks on the derivative curves. A typical plot of the derivative curve for the Cu^{63} resonance is given in Fig. 1. Experimental second moments were obtained by integrating[14] the curves. The reported values are the averages of from five to nine separate plots. The maximum error in the second moments is approximately 6 to 8 percent. The estimated error in the line widths is about 3 percent for the broad lines and 6 percent for the much narrower lines of rubidium, cesium, and gallium. An additional error is present in the measurement of the narrow lines due to broadening by field inhomogeneities and modulation effects, which contribute between 0.05 and 0.10 gauss to the apparent line widths.

Metals investigated included lithium, sodium, aluminum, copper, gallium, rubidium, and cesium. The samples were obtained commercially and used without further purification. The resonance absorption occurs in the surface of the metal to the skin depth, so it is necessary to have very small particles to obtain maximum intensities. In the case of the alkali metals, the samples were dispersions of the metal in white mineral oil. The sodium dispersion is available commercially and has been described.[1] The others were made by heating a mixture of the metal and mineral oil above the melting point of the metal and agitating the mixture with a high speed stirrer. A dry nitrogen atmosphere was used to prevent oxidation. The stirring was continued as the dispersion was cooled until the metal particles solidified. This method gave a satisfactory particle size, and the dispersions showed no tendency to coagulate even when they were heated above the melting point of the metal. Aluminum and copper were fine powders; the oxide coating of the particles was sufficient insulation to permit their use without further treatment. The gallium was dispersed in mineral oil by shaking it by hand in a test tube; oleic acid was added as an anticoagulant.

TABLE I. Shifts in the nuclear magnetic resonance frequencies of metals compared to their compounds, at room temperature.

Nucleus	Compound[a]	$\Delta H/H$ This research	$\Delta H/H$ Knight
Li^7	$LiNO_3$[b]	$0.0261\pm0.0002\times10^{-2}$	$\sim0.02^{15}\times10^{-2}$
Na^{23}	NaOH	$0.112\ \pm0.001$	0.10^{5}
Al^{27}	$AlCl_3$	$0.161\ \pm0.001$	0.16^{5}
Cu^{63}	CuBr[c]	$0.237\ \pm0.001$	0.23^{5}
Cu^{65}	CuBr[c]	$0.235\ \pm0.002$	0.23^{5}
Ga^{71}	$GaCl_3$	$0.449\ \pm0.004$	0.44^{5}
Rb^{85}	RbOH	$0.650\ \pm0.005$	$\sim0.6^{15}$
Rb^{87}	RbOH	$0.653\ \pm0.002$	$\sim0.6^{15}$
Cs^{133}	CsCl	$1.49\ \pm0.01$	$\sim1.0^{15}$

[a] In aqueous solution unless specified otherwise.
[b] In liquid NH_3 solution.
[c] Solid.

[13] W. N. Tuttle, Proc. Inst. Radio Eng. **28**, 23 (1940); we are indebted to T. F. Wimett for suggesting their use.
[14] Gutowsky, Kistiakowsky, Pake, and Purcell, J. Chem. Phys. **17**, 972 (1949).

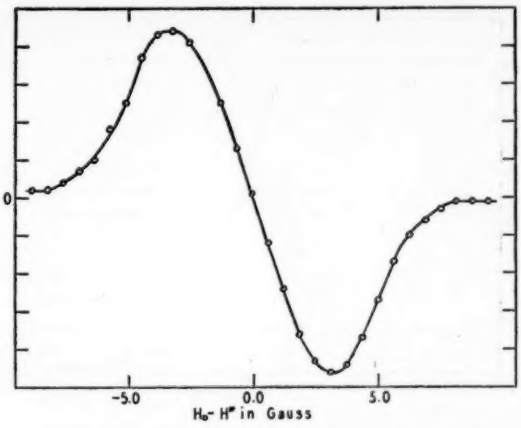

FIG. 1. The derivative of the Cu^{63} magnetic resonance absorption line at 298°K. The line width δH is 6.4 gauss, and the second moment ΔH_2^2 is 6.3 gauss^2.

An all-metal cryostat operating on the principle of a variable heat leak[11] was used for the experiments on the temperature dependence of line widths and second moments. The temperatures were measured with a copper-constantan thermocouple immersed directly in the sample. The resonance line shifts between the metals and their compounds were measured by two methods, depending on the magnitude of the shift. For aluminum, copper, lithium, and sodium, whose shifts are small, the shift was found by measuring the difference in applied magnetic field needed to center the resonance line of the metal and of the salt, alternately, when either was placed in the same coil, the frequency being kept constant.[11] For rubidium, cesium, and gallium, whose shifts are much larger, the applied field was kept constant and the frequency of the signal generator varied to center the resonance line for a given sample. The frequency of the signal generator was then measured by zero beating its signal with that of a BC-221 Signal Corps frequency meter set by reference to WWV. The errors in the observed resonance shifts are about ±1 percent of the measured values.

RESULTS AND DISCUSSION

Resonance Shift in the Metals

The resonance shifts observed for the metals at room temperature (298°K) are given in Table I along with the values reported by Knight.[5,6,15] The agreement between the two sets of data is quite good. The entries preceded by the sign $\sim$ are preliminary, approximate values.[15] All of the shifts measured by us were with respect to aqueous solutions of the salts except for

[15] D. F. Abell and W. D. Knight, Phys. Rev. **85**, 762(A) (1952).

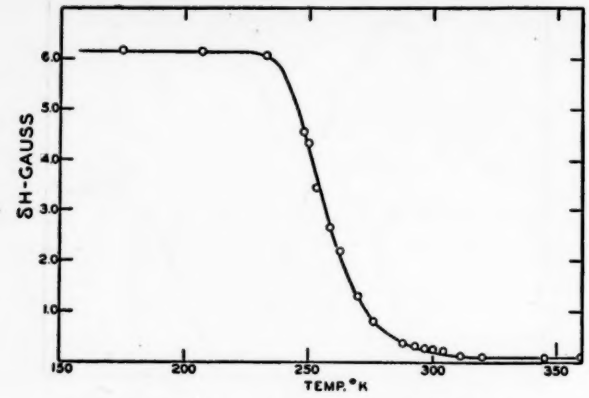

FIG. 2. The Li^7 magnetic resonance line-width transition in the metal.

CuBr, which was solid, and $LiNO_3$, which was dissolved in NH_3. Absorption intensities in the samples were adequate without the addition of paramagnetic salts,[10] which were not used since they introduce additional small shifts in resonance frequency.[16]

The resonance shifts in the metals are significant for comparison[6,17] with conduction electron theory. We defer discussion of this aspect of the data to a subsequent article in which our results on the temperature dependence of the resonance shifts[1] will be given. The present interest in the resonance shifts is their use in Eq. (1) for evaluation of T_1. It should be mentioned that there is some uncertainty in these shifts as a result of chemical shifts[1,11,16] among various compounds of a given element. Another source of uncertainty which we have discovered is the possibility that the resonance frequency for a salt in solution may depend on the concentration. We have observed such a dependence for CsCl and for various thallium salts. The concentration shifts are quite small for CsCl but are of the order of 0.05 percent for thallous salts in water solution. The reason for the dependence on concentration is not clear, and further work is being done in an attempt to learn its origin.

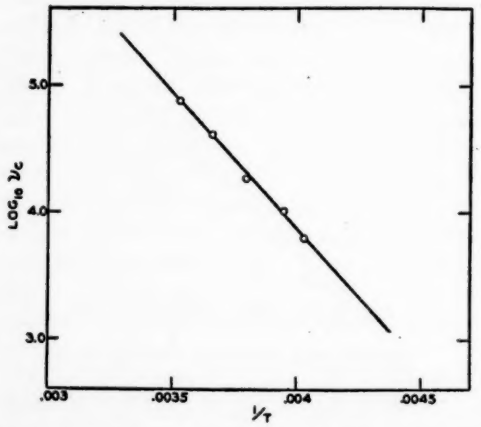

FIG. 3. The frequency ν of diffusional motion of lithium nuclei in the metal as a function of $1/T$, evaluated from the line-width data. The data are fitted by the equation $\nu=\nu_0 e^{-E_a/RT}$, with a ν_0 value of 2.9×10^{12} sec^{-1}, and E_a the activation energy for self-diffusion, 9.8 ± 1 kcal/mole.

[16] W. C. Dickinson, Phys. Rev. **81**, 717 (1951).
[17] W. Kohn and N. Bloembergen, Phys. Rev. **80**, 913 (1950); Phys. Rev. **82**, 283 (1951).

Temperature Dependence of Line Widths

The line width has been measured as a function of temperature for Li^7, Na^{23}, Rb^{87}, and Cs^{133}. The behavior of the line width of lithium is similar to that observed for sodium. The measurements on sodium were reported previously.[1] The results for lithium are given in Fig. 2. The line width narrows with increasing temperature over a range of 50°, from the rigid lattice value of 6.2 gauss to about 0.1 gauss, which is due apparently to field inhomogeneity and modulation effects. This transition is centered at 255°K, which is 200° below the melting point. Such line-width transitions to narrower lines at higher temperatures are typical of systems in which the line width is determined by dipolar broadening.[18] The narrowing results from the time averaging of the dipolar fields over any nuclear motion in the sample,[10] and the transition in lithium, as in the case of sodium, must be attributed to self-diffusion. The frequency of motion at a given temperature can be calculated from the line-width data.[18] The equation $\nu=\nu_0 e^{-E_a/RT}$ is then employed to find the activation energy E_a for the process. For lithium, $\log_{10}\nu$ is plotted against $1/T$ in Fig. 3, giving a value of 9.8 ± 1 kcal for the activation energy of self-diffusion and 2.9×10^{12} sec^{-1} for the frequency factor ν_0.

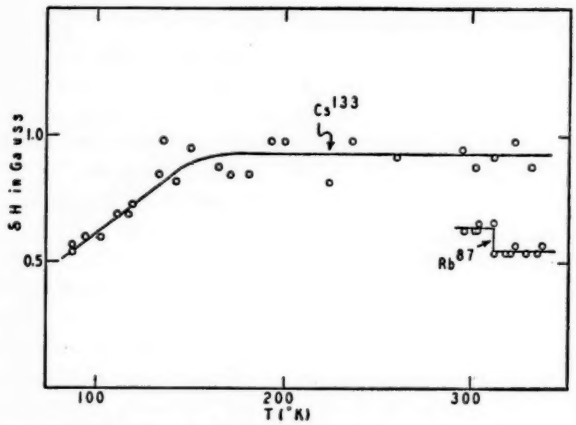

FIG. 4. The Cs^{133} and Rb^{87} magnetic resonance line widths as functions of temperature.

The behavior of the cesium line width with temperature is given in Fig. 4. In contrast to lithium and sodium, the cesium line is broadest at higher temperatures, with a constant value of about 0.9 gauss from 325° to 150°K, and *decreases* linearly with temperature below 150°K to 80°K, the lowest temperature observed.

[18] H. S. Gutowsky and G. E. Pake, J. Chem. Phys. **18**, 162 (1950).

Such a decrease in line width with temperature is inexplicable in terms of dipolar broadening. However, in Eq. (2), it is seen that the contribution of the spin-lattice interactions to the line width is proportional to $1/T_1$, while by Eq. (1) $1/T_1$ is proportional to T, so if the line width is determined largely by T_1, it should be linearly proportional to the temperature. This is the case for cesium below 150°K, but at higher temperatures the line width appears to be constant. The inflection point at 150°K could be explained by assuming that the part of the line width contributed by dipolar broadening undergoes a transition due to self-diffusion as observed for lithium and sodium, but this would not account for the continued constancy at higher temperatures. The contribution to the cesium line width by dipolar interactions should be approximately 0.5 gauss in a rigid lattice. The transition in the dipolar line width must occur somewhere below the melting point since the line width does not change at the melting point. It is reasonable, therefore, to ascribe the abrupt change at 150°K in the temperature dependence of the line width to the transition in the dipolar contribution. Also, it should be noted that the width of the line at liquid nitrogen temperatures is approximately the same as the width due to dipolar broadening. It would be of interest to extend the line-width measurements to even lower temperatures to see if the line width again becomes constant as it should.

TABLE II. Line widths and second moments of the resonance lines in metals.

Nucleus	Temperature	Line width δH	Second moment ΔH_2^2 (Expt.)	Second moment ΔH_2^2 (Theoret.)	Δ $\Delta H_2^2(E) - \Delta H_2^2(T)$
Li^7	77°K	6.2 gauss	4.1 gauss[a]	4.3 gauss[a]	−0.2 gauss[a]
Na^{23}	77	2.4	0.67	0.63	0.04
Al^{27}	298	8.5	10.5	7.5	3.0
Al^{27}	77	8.4	9.2	7.5	1.7
Cu^{63}	298	6.4	6.3	5.6[a]	0.7
Cu^{65}	298	5.3	5.0	4.4[a]	0.6
Ga^{69}	298	0.33	...	...	...
Ga^{71}	298	0.32	...	...	...
Rb^{85}	313	0.50	...	0.048	...
Rb^{87}	313	0.54	...	0.060	...
Cs^{133}	303	0.93	...	0.077	...

[a] Values in reference 1 are incorrect.

The line-width data for rubidium are given also in Fig. 4. The results are incomplete because it was not possible to measure the line width of Rb^{87} at low temperatures with the present equipment. The isotopic abundance of Rb^{87} is only 27 percent so that the signal obtained from it was rather weak. However, in the temperature range in which the line width was measured, its behavior was similar to that of cesium. The line width is essentially constant, except for a slight decrease upon warming at the melting point. Qualitatively, this decrease may be attributed to a slight increase in T_1. We have observed a small decrease in the resonance shift of Rb^{87} at its melting point and according to Korringa's theory[8] this should give a small increase in T_1.

TABLE III. Inverse sixth-power internuclear distance summations for calculation of second moments of resonance lines in powders of the simpler crystal types.[a]

Type of lattice	$\Sigma_j r_{0j}^{-6}$	$\Sigma_f r_{0f}^{-6}$
Simple cubic	$8.402a^{-6}$	...
Body centered cubic[b]	$29.03a^{-6}$	...
Face centered cubic[b]	$115.6a^{-6}$	...
NaCl type crystal[b]	$115.6a^{-6}$	$422.1a^{-6}$
CsCl type crystal[b]	$8.402a^{-6}$	$20.65a^{-6}$
CaF_2 type crystal (F)	$537.7a^{-6}$	$660.5a^{-6}$
CaF_2 type crystal (Ca)	$115.6a^{-6}$	$1322a^{-6}$
Hexagonal close packed	$14.45b^{-6}$	...

[a] a is the edge of the unit cube for the cubic types; b is the side of the hexagon in the hexagonal close packed case.
[b] Related summations have been computed by J. E. Mayer, J. Chem. Phys. 1, 270, 327 (1933).

Line Widths and Second Moments

The widths of the resonance lines in the metals, the experimental as well as theoretical second moments, ΔH_2^2, and their difference Δ are given in Table II. The theoretical second moments were calculated for nuclear magnetic dipolar broadening[2] from the equation for crystal powders,[14]

$$\Delta H_2^2 = (3/5)I(I+1)g^2\beta^2 \sum_j r_{0j}^{-6} + (4/15)\sum_f I_f(I_f+1)g_f^2\beta^2 r_{0f}^{-6}. \quad (3)$$

g is here the gyromagnetic ratio of the observed nucleus, in nuclear magnetons, β; I is the nuclear spin; r_{0j} the distance from a typical nucleus to its like neighbors; and the subscript f in the second term refers to unlike nuclei. The inverse sixth-power distance summations in terms of the lattice constants for the simpler crystal types are collected in Table III. The experimental lattice constants used for the various metals were taken from the Handbook of Chemistry and Physics.[19]

As can be seen from Table II, the experimental second moments of all the metals investigated, except lithium, are larger than the theoretical values. For lithium and sodium, the differences are within experimental error, but this is not so for Al^{27}, Cu^{63}, and Cu^{65}. Also, in the case of Al^{27}, the excess broadening Δ is found to be dependent on the temperature. The value for Δ at liquid nitrogen temperatures is about half of its value at room temperature. The second moments of lithium and sodium were evaluated at liquid nitrogen temperatures because of the narrowing by self-diffusion at higher temperatures. No second moments are reported for gallium because the absorption line could be picked up only in the liquid. Gallium crystallizes in a tetragonal lattice and the absorption line in the solid is presumed to be blotted out by quadrupolar effects. Experimental second moments are not reported for cesium and rubidium because the theoretical values in Table II show that the dipolar broadening should be very small for these metals. Most, if not all, of the

[19] *Handbook of Chemistry and Physics* (Chemical Rubber Publishing Company, Cleveland, 1948), 30th edition, p. 2015.

TABLE IV. The contribution of spin-lattice relaxation to the second moments of resonance lines in metals.

Nucleus	Temperature	T_1[a]	Z	Δ (Eq. (6))	Δ (Expt.)
Li^7	77°K	170[22] gauss^{-1}	6 gauss	0.0002 gauss^2	−0.2 gauss^2
Na^{23}	77	39[23]	2.7	0.004	0.04
Al^{27}	298	0.41[22]	11	1.3	3.0
Al^{27}	77	1.6[22]	9.5	0.3	1.7
Cu^{63}	298	1.3[3]	8	0.32	0.7
Cu^{65}	298	1.0[3]	7	0.35	0.6

[a] Extrapolated from measurements at other temperatures, assuming a linear $1/T$ dependence.

broadening in them and also in liquid gallium appears to be due to other causes. A separate detailed discussion in terms of the line widths of these three metals is given later on.

The normalized shape function $\mathbf{g}(H_0-H^*)$ for an absorption line broadened by both dipolar and spin-lattice interactions[20] may be written as

$$\mathbf{g}(H_0-H^*)=4T_1\int_{-\infty}^{+\infty}\frac{\mathbf{h}(H_0'-H^*)}{1+16\pi^2T_1^2(H_0-H_0')^2}dH_0', \quad (4)$$

where H_0 is the applied magnetic field, H^* is the magnetic field at the center of the line for a given frequency, T_1 is the spin-lattice relaxation time in units of gauss^{-1}, and $\mathbf{h}(H_0-H^*)$ is the normalized shape function determined by dipolar interactions alone. This equation is obtained by considering each energy level resulting from dipolar interactions to be broadened by the shape function

$$4T_1[1+16\pi^2T_1^2(H_0-H^*)^2]^{-1}, \quad (5)$$

which is just the resonance line broadened only by collisions or related phenomena.[21] An analysis of Eq. (4) reveals that a second moment does not exist for it even though one exists for the dipole-broadened line $\mathbf{h}(H_0-H^*)$. However, in practice, the integration is performed only over a small range of (H_0-H^*), so that the experimental second moments will correspond to dipolar broadening if T_1 is large, for then Eq. (4) approximates $\mathbf{h}(H_0-H^*)$ quite closely. For very small T_1, Eq. (4) approaches Eq. (5) as a limit, particularly if the dipolar broadening is small.

For the metals whose second moments were measured, T_1 is in the range where the shape function does not approximate too closely either limiting case. Although the second moment of the shape function does not actually exist for these metals, we may consider a pseudo second moment, wherein the integration is carried out only to a finite limit as is done experimentally. For the metals considered, this pseudo second moment is, to a good approximation, the sum of the dipolar second moment and the second moment of Eq. (5) with the integration cut off at Z, where Z is the distance in gauss from the line center to the point at which the experimental integration terminated. Therefore, a theoretical value for Δ, the excess broadening associated with T_1, is

$$\Delta=\left(8T_1Z-\frac{2}{\pi}\tan^{-1}4\pi T_1Z\right)\Big/16\pi^2T_1^2. \quad (6)$$

Values for Δ calculated in this way from experimental relaxation times are given in Table IV. Except for sodium, the T_1 values were themselves extrapolated from observations at liquid helium temperatures.[3,22] The sodium value was extrapolated from experimental results[23] at room temperature. The extrapolations were based on the $1/T$ dependence for T_1, predicted by Heitler and Teller[7] and by Korringa's theory[8] (Eq. (1)), which has been found to be approximately true for sodium[23] and aluminum.[22] However, at the field strengths we used, T_1T for lithium falls off markedly at higher temperatures.[22] Also, the line-width temperature dependence described above for cesium indicates that T_1T decreases for it at higher temperatures.

The calculated values of Δ are in qualitative agreement with the experimental values. The calculated values are smaller than the experimental values for aluminum and copper, but agree with the experimental values for lithium and sodium within the experimental error. The fact that the extra broadening in aluminum should be greater than in copper is predicted as is the negligible broadening in lithium and sodium. Also the observed temperature dependence of Δ for Al^{27} is what would be expected qualitatively from the $1/T$ dependence of T_1. The failure of the calculated values of Δ for aluminum and copper to agree with the experimental values is probably due to use of incorrect values of T_1. The very extensive temperature extrapolation can hardly be justified. Also, the behavior of lithium and cesium indicates that the true values of T_1 at room temperature for the other metals may be smaller than the extrapolated values. For aluminum and copper a decrease in the extrapolated value of T_1 by a factor of about ½ will give values of Δ in agreement with the experimental broadening. One can also estimate T_1 values from the resonance shifts in Table I. These T_1 values agree only approximately with the T_1 values obtained by the temperature extrapolation and result in Δ values in poorer agreement with experiment.

Further evidence that the broadening is due to the spin-lattice interaction is furnished by the absorption lines of rubidium, cesium, and gallium. The lines for these metals in the liquid state are considerably broader than the 0.05 to 0.1 gauss modulation and inhomogeneity broadening, and the widths do not change appreciably upon going between the liquid and solid states. Also, the lines in these metals are definitely Lorentzian in shape as can be seen in Fig. 5, where

[20] A brief discussion is given in reference 10; for a detailed analysis see N. Bloembergen, *Nuclear Magnetic Relaxation* (Martinus Nijhoff, The Hague, 1948), p. 42.

[21] J. H. Van Vleck and V. F. Weisskopf, Revs. Modern Phys. **17**, 227 (1945).

[22] N. J. Poulis, Physica **16**, 373 (1950).

[23] R. E. Norberg and C. P. Slichter, Phys. Rev. **83**, 1074 (1951).

the cesium derivative curve is plotted along with the derivative of a Lorentzian line with the same line width and passing through one point on the experimental curve. The fact that these absorption lines are Lorentzian in shape is experimental justification of our use of Eq. (5) as the broadening function and confirms our postulate that spin-lattice relaxation determines the width of the lines. Applying Eq. (5) to these three metals, we may compute T_1 from the experimental line widths by use of the subsequent equation,

$$T_1 = 1/2\pi\sqrt{3}\delta H, \tag{7}$$

where T_1 will be given in units of gauss^{-1} if δH is in gauss.

Values of T_1 computed by this equation from the experimental line widths are given in Table V. Aside from the assumption of the validity of Eq. (5), there is the error introduced by the 0.05 to 0.1 gauss contributed to the line widths by modulation effects and field inhomogeneity. An estimated average correction of 0.07 gauss has been subtracted from the experimental line widths, increasing the T_1 values by up to 25 percent.

TABLE V. A comparison of T_1 values from line widths with those from the resonance shifts.

Nucleus	Temperature	Corrected[a] δH	T_1 from δH (Eq. (7))	T_1 from $\Delta H/H$ (Eq. (1))
Ga^{69}	298°K	0.26 gauss	0.34×10^{-3} sec	0.75×10^{-3} sec
Ga^{71}	298	0.25	0.28	0.47
Rb^{85}	313	0.43	0.52	2.2
Rb^{87}	313	0.47	0.14	0.19
Cs^{133}	303	0.86	0.19	0.23

[a] Values from Table II less an estimated average 0.07 gauss broadening from field inhomogeneity and modulation effects.

Experimental spin-lattice relaxation times have not been reported so our values computed from the line widths by Eq. (7) can be compared only with those obtained with Eq. (1) from the resonance shifts. These values of T_1, computed from the experimental resonance shifts in Table I, are given in Table V for comparison. The agreement between the two sets of values is perhaps better than might be expected in view of the approximations in Korringa's theory.[8] The resonance

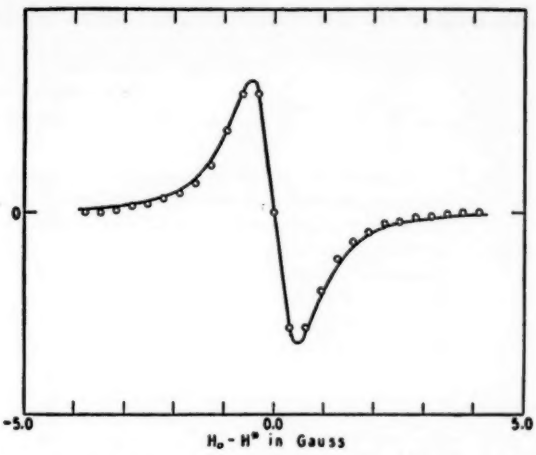

FIG. 5. The derivative of the Cs^{133} magnetic resonance line at room temperature compared to a Lorentzian line shape. The circles are experimental data; the line represents the derivative of a Lorentzian curve with the same line width and adjusted to pass through one of the experimental points.

shift T_1 values are consistently higher than those from line broadening, the factor being a maximum of two for Ga^{69}. One particular deviation is found in the T_1 values for different isotopes of the same metal. Equation (1) predicts that the ratio of relaxation times for two isotopes should equal the square of the inverse ratio of their g values. However, the line-width data on the isotopes of both rubidium and gallium give ratios of relaxation times equal to somewhat less than the second power of the inverse ratio of the g values.

ACKNOWLEDGMENT

We wish to express our deep appreciation and thanks to Mr. R. E. McClure, our electronics research assistant, for his very able assistance with some of the measurements, as well as for the design, construction, and maintenance of many of the electrical circuits. We would also like to thank D. W. McCall for his aid in the computation of the summations given in Table III. Equipment was provided mainly by a grant-in-aid from the Research Corporation.

Influence of the Solvent on Rates of Ionization, Entropies, and Heats of Activation

RALPH G. PEARSON
Northwestern University, Evanston, Illinois
(Received March 20, 1952)

A breakdown of the rates of reactions in which ions are formed from neutral molecules into heats and entropies of activation reveals the following regularities with change in solvent: the heats of activation do not change greatly and are more frequently larger in polar solvents than in nonpolar ones; the entropies of activation are always negative and become more negative as the polarity of the solvent decreases. An explanation is given in terms of solvent molecules "frozen" around the incipient ions of the activated complex. Nonpolar solvents suffer a greater loss in entropy in such "freezing" than polar solvents. An electrostatic calculation is given which is satisfactory for all solvents whose molecules contain a permanent dipole moment, but which must break down for nonpolar solvents.

THE influence of the properties of the medium on the rates of reaction in which ions are formed from neutral molecules is fairly well understood.[1] Thus, an increase in the dielectric constant, the solvating power, or the general polarity of the solvent leads to an increase in the rate of ionization. However, there seems to have been no systematic attempt made to separate the over-all effect of changing the medium into terms corresponding to changes in activation energy and frequency factor, respectively, in the rate constant. Indeed the general impression has been left that the variations in these kinetic factors are so random that no generalizations can be made.

However, a closer examination of a number of ionization reactions, which have been studied with sufficient accuracy so that changes in the activation energies and frequency factors may be considered significant, does in fact reveal certain regularities. Some selected reactions are shown in Table I. They include a number of reactions of organic halides including hydrolysis and solvolysis,

$$RX+H_2O\rightarrow ROH+H^++X^-, \quad (1)$$

and reactions with amines to form 'onium salts,

$$RX+B\rightarrow RB^++X^-. \quad (2)$$

Also two reactions involving proton transfer in the rate determining step are included:

$$HA+B\rightarrow BH^++A^-. \quad (3)$$

The data are presented in terms of heats of activation and entropies of activation according to the theory of absolute reaction rates, since this forms a much more satisfactory basis for an explanation of the results.

It is apparent that the following can be said of the data shown: First, heats of activation do not vary greatly with the solvent (a maximum of six kilocalories for any one reaction); they are, if anything, greater for the more polar or better solvating solvent.[2] Second the entropies of activation are always negative and vary considerably with the solvent, becoming more negative as the polarity of the solvent decreases.

An explanation of the entropy changes can be given in terms of orientation of solvent molecules around the incipient ions in the transition state. A useful analogy has been drawn between such oriented and tightly held solvent molecules and "frozen" molecules with their corresponding loss of freedom of motion.[3] Thus, an ionization is generally accompanied by a negative entropy change because of the loss in entropy of the solvent. Now in a strongly polar liquid such as water the molecules already exist in a partially frozen state because of strong intermolecular forces, hydrogen bonding, etc. Hence, while strongly bound to ions such molecules would suffer a relatively small loss in entropy by such binding. Nonpolar liquids, on the other hand, are quite free in the liquid state and on freezing, or being tightly bound to ions, would suffer a considerable entropy decrease. Thus, the entropy of freezing of most organic liquids is about -10 eu (unless the solid state has free rotation), whereas the entropy of freezing for water is -5.5 eu.

The explanation for the changes in the heats of activation with solvent is not so easy, but the same concept will help to explain why heats of activation can be greater in a more polar solvent. Thus, the heat of solvation of ions in a polar liquid is reduced by the amount of energy required to break the molecular bonds between solvent molecules. These bonds must also be broken, presumably before the solvent can solvate the incipient ions of the activated complex. The over-all activation energy, of course, depends upon a number of factors. Two of these factors are: (1) the strengths of the covalent bonds being made and broken in the reaction, and (2) the repulsive energies due to the

[1] (a) R. A. Ogg, Jr. and M. Polanyi, Trans. Faraday Soc. **31**, 604 (1935); (b) W. F. K. Wynne-Jones and H. Eyring, J. Chem. Phys. **3**, 492 (1935); (c) R. A. Ogg, Jr. and O. K. Rice, J. Chem. Phys. **5**, 140 (1937); (d) G. Scatchard, J. Chem. Phys. **7**, 657 (1939); (e) K. Laidler and H. Eyring, Ann. New York Acad. Sci. **39**, 303 (1940).

[2] Solvents are better classified in terms of their general polarity or solvating properties rather than of their dielectric constants. The latter property by itself is not a reliable criterion since a liquid like nitrobenzene or nitromethane, while having a high dielectric constant, is not a good solvating medium because it cannot effectively coordinate anions.

[3] Magee, Ri, and Eyring, J. Chem. Phys. **9**, 419(1941); W. F. K. Wynne-Jones and H. Eyring, see reference 1(b).

interaction of filled electron shells in the reactant molecules as they are brought close together. These factors are properties of the reactants and would depend only slightly on the solvent.

The final important factor in the activation energy is the interaction of the solvent in stabilizing the ion pair or strong dipole of the transition state (compared to the solvation energy of the reactants). This energy term is difficult to estimate, but intuitively one would feel that the more polar the solvent the greater the solvation energy. It is of interest to calculate on the basis of electrostatic theory what influence the dielectric constant, at least, has on the energy. The same calculations can also be used to evaluate the contribution of electrostatic effects to the entropy of activation.

The appropriate equation to use seems to be that of Kirkwood[4] for the free energy of an idealized dipole in a continuous dielectric of constant D compared to that in a similar medium (for nonelectrostatic forces) of unit dielectric constant,

$$\Delta F_{el}=-\frac{\mu^2}{r^3}\left(\frac{D-1}{2D+1}\right), \tag{4}$$

where μ is the dipole moment and r the radius of the molecule in which the dipole is embedded. Applying this to the transition state theory one obtains[1(e)]

$$\ln k=\ln k_0-\frac{N(D-1)}{RT(2D+1)}\left(\frac{\mu_A^2}{r_A^3}+\frac{\mu_B^2}{r_B^3}-\frac{\mu_\ddagger^2}{r_\ddagger^3}\right) \tag{5}$$

for a bimolecular reaction between molecules A and B. The important quantity is $\mu_\ddagger$, the dipole moment of the activated complex which is much greater than the dipole moments of A and B in an ionization. Thus k, the rate constant in a medium of dielectric constant D, exceeds k_0, the rate constant in a medium of constant unity. Remembering $k=RT/Nh\exp(-\Delta F^\ddagger/RT)$, the thermodynamic relationships

$$(\partial\Delta F/\partial T)_P=-\Delta S \quad \text{and} \quad \Delta H=\Delta F+T\Delta S \tag{6}$$

are used, giving

$$\Delta S_{el}^\ddagger=-\left(\frac{\mu_A^2}{r_A^3}+\frac{\mu_B^2}{r_B^3}-\frac{\mu_\ddagger^2}{r_\ddagger^3}\right)\frac{3D}{(2D+1)^2}\left(\frac{\partial \ln D}{\partial T}\right)_P. \tag{7}$$

The foregoing examples are typical of a number of similar reactions which have been studied in two or more solvents. Other references: Grimm, Ruf, and Wolff, Z. physik. Chem. **6**, 41 (1890); J. A. Hawkins, J. Chem. Soc. **121**, 1170 (1922); H. E. Cox, J. Chem. Soc. **119**, 142 (1921); J. W. Baker and W. S. Nathan, J. Chem. Soc. 519 (1935); J. K. Syrkin and A. T. Gladischew, Acta Physicochim. U.S.S.R. **2**, 291 (1935); S. Winstein and E. Grunwald, J. Am. Chem. Soc. **70**, 846 (1948); I. V. Potopov and V. A. Holtsschmidt, J. Phys. Chem. U.S.S.R. **15**, 1094 (1941); Evans, Watson, and Williams, J. Chem. Soc. 1345 (1939); H. C. Raine and C. N. Hinshelwood, J. Chem. Soc. 1378 (1939); N. K. Vorobev, J. Phys. Chem. U.S.S.R. **14**, 686 (1940).

[4] J. Kirkwood, J. Chem. Phys. **2**, 351 (1934).

TABLE I. Heats and entropies of activation for ionization reactions.

Solvent	Heat of activation	Entropy of activation
$C_6H_5COCl+H_2O\rightarrow C_6H_5COOH+H^++Cl^-$ [a]		
5% water-acetone	11 kcal	−41.3 eu
15% water-acetone	13.0	−29.3
25% water-acetone	14.3	−23.3
33.3% water-acetone	15.7	−17.1
40% water-acetone	16.3	−13.9
$p-NO_2C_6H_4CHBr+H_2O\rightarrow p-NO_2C_6H_4CH_2OH+H^++Br^-$ [b]		
10% water-dioxane	15.4	−44.2
30% water-dioxane	17.2	−36.8
50% water-dioxane	18.8	−30.1
$H_2NCH_2CH_2CH_2CH_2CH_2Cl\rightarrow CH_2CH_2CH_2CH_2-CH_2+Cl^-$ [c] (NH_2 + ring)		
benzene	14.6	−34.9
toluene	16.0	−32.1
ethylene dichloride	13.9	−30.8
nitrobenzene	16.4	−26.5
90% methanol-water	20.2	−11.4
water	20.3	− 6.6
$CH_3I+C_5H_5N\rightarrow C_5H_5NCH_3^++I^-$ [d]		
benzene	13.5	−33.4
toluene	13.9	−33.1
mesitylene	14.3	−32.6
i-propyl ether	13.2	−39.0
dioxane	13.0	−33.1
anisole	12.6	−33.2
chloroform	12.6	−34.5
chlorobenzene	13.3	−32.3
iodobenzene	13.2	−30.5
acetone	13.4	−28.8
50% ethanol-benzene	15.3	−26.6
nitrobenzene	13.1	−28.4
benzonitrile	13.1	−28.8
ethanol	17.4	−20.5
$p-ClC_6H_4CH=NCl+(C_2H_5)_3N\rightarrow p-ClC_6H_4C\equiv N+(C_2H_5)_3NH^++Cl^-$ [e]		
benzene	11.3	−44.5
methanol	17.0	−22.1
$CH_3CH_2NO_2+C_5H_5N\rightarrow CH_3CHNO_2^-+C_5H_5NH^+$ [f]		
70% ethanol-water	16.5	−29.7
30% ethanol-water	15.2	−28.3
water	16.0	−25.0

[a] B. L. Archer and R. F. Hudson, J. Chem. Soc. 3259 (1950), unimolecular rate constant.
[b] J. W. Hackett and H. C. Thomas, J. Am. Chem Soc. **72**, 4962 (1950), bimolecular rate constant
[c] G. Salomon, Helv. Chem. Acta, **16**, 1361 (1933).
[d] N. J. T. Pickles and C. N. Hinshelwood, J. Chem. Soc. 1353 (1936); R. A. Fairclough and C. N. Hinshelwood, J. Chem. Soc. 1573 (1937).
[e] Jordan, Dyas, and Hill, J. Am. Chem. Soc. **63**, 2383 (1941).
[f] F. V. Williams and R. G. Pearson (unpublished results).

Table II shows some calculated values of $\Delta F_{el}^\ddagger$, $\Delta S_{el}^\ddagger$ and $\Delta H_{el}^\ddagger$ for a number of solvents using a hypothetical reaction where the first term in parentheses in Eq. (7) has the reasonable value of 60 kcal. Experimental values of $(\partial \ln D/\partial T)_P$ have been used. The values of $\Delta F_{el}^\ddagger$ are reasonable for all solvents, predicting a continuously increasing rate with increasing dielec-

TABLE II. Calculated values of $\Delta F_{el}^{\ddagger}$, $\Delta H_{el}^{\ddagger}$ and $\Delta S_{el}^{\ddagger}$ for a reaction where $-[(\mu_A^2/r_A^3)+(\mu_A^2/r_A^3)-(\mu_{\ddagger}^2/r_{\ddagger}^3)]=60$ kcal.

Solvent	$D_{20}°$	$-(\partial \ln D/\partial T)_P$[a]	$-\Delta F_{el}^{\ddagger}$	$-\Delta H_{el}^{\ddagger}$	$-\Delta S_{el}^{\ddagger}$
Hexane	1.9	0.714×10^{-3}	11.2 kcal	14.4	10.6
Carbon tetrachloride	2.2	0.843	13.7	17.1	11.4
Benzene	2.3	0.876	13.8	17.2	11.5
Toluene	2.3	0.673	14.1	16.7	8.8
Anisole	4.4	5.2	20.9	33.5	42.2
Chloroform	4.5	3.33	21.0	29.1	27.0
Chlorobenzene	6.7	2.89	23.8	28.8	16.8
Ethyl bromide	9.4	4.91	26.6	32.9	21.2
Acetophenone	18.1	4.10	27.4	30.3	9.7
Acetone	20.0	4.63	27.8	30.8	9.9
Ethyl alcohol	25.0	6.02	28.2	31.3	10.4
Methyl alcohol	32.5	5.39	28.6	30.8	7.3
Nitrobenzene	35.8	5.21	28.8	30.7	6.3
Water	80.0	4.63	29.6	30.3	2.4

[a] Compare E. A. Moelwyn-Hughes, Proc. Roy. Soc. (London) **A155**, 308 (1936).

tric constant. That this is not completely in agreement with experiment is due, as previously indicated, to the lack of complete correlation between dielectric constant and solvating power.

The values of $\Delta H_{el}^{\ddagger}$ are a little surprising in that they do not show a large dependence of the activation energy on the dielectric constant. Thus, for all the solvents whose molecules have a permanent dipole moment of any consequence, the electrostatic energies are the same within five kilocalories (a large negative value of $\Delta H_{el}^{\ddagger}$ corresponds to a low activation energy). For the nonpolar molecules a greater activation energy difference is predicted of some fifteen kilocalories. This is not in agreement with the results indicated in Table I.

The values of $\Delta S_{el}^{\ddagger}$ are satisfactory for all the polar molecules again in that they are negative and become continuously more negative as the polarity diminishes. For the nonpolar solvents there is disagreement with experiment in that only small negative values are predicted. That there should be a correspondence for polar molecules between the electrostatic calculations and the type or reasoning based on "frozen" solvent molecules is not surprising.[5] Thus, the entropy term in Eq. (7) depends on the change in dielectric constant with temperature. This term is always negative since the effect of increased temperature is to reduce the alignment of polar molecules in the electric field and to reduce the number of dipoles per unit volume for all molecules. The first factor is the important one for polar molecules and is directly related to the susceptibility of the molecules towards orientation or "freezing."

For nonpolar molecules only the change in density is involved in the temperature coefficient of the dielectric constant. This does not seem to be related to the susceptibility towards orientation, and hence Eq. (7) will not correspond physically to the entropy loss of "frozen" solvent molecules. Also, it has been shown by Bell[6] that for solvents of low dielectric constant Eq. (4) is not apt to be valid, since a necessary condition is that the orientation energy be less than the thermal energy. This requires essentially that $\mu^2/r^3DkT<1$. In any event to get agreement with experiment it will be necessary to have a dielectric constant that is strongly dependent on the temperature. This can be done only by using the dielectric constant in the neighborhood of the dipole rather than the gross dielectric constant. The former quantity will be temperature dependent even for a nonpolar medium and will presumably correspond to a greater interaction than that calculated by Eq. (4).[7]

Another theory useful for estimating solvation energies is that based on internal pressures or cohesive energy density.[8] Applied to kinetics this leads to the equation[1(e)]

$$\ln k=\ln k_0+\frac{V_A}{RT}\left[\left(\frac{E_A}{V_A}\right)^{\frac{1}{2}}-\left(\frac{E_s}{V_s}\right)^{\frac{1}{2}}\right]^2+\frac{V_B}{RT}\left[\left(\frac{E_B}{V_B}\right)^{\frac{1}{2}}-\left(\frac{E_s}{V_s}\right)^{\frac{1}{2}}\right]^2-\frac{V_{\ddagger}}{RT}\left[\left(\frac{E_{\ddagger}}{V_{\ddagger}}\right)^{\frac{1}{2}}-\left(\frac{E_s}{V_s}\right)^{\frac{1}{2}}\right]^2. \quad (8)$$

Here k_0 is the rate constant in an ideal solution; E_A, etc. are the energies of vaporization of the reactants, solvent, and activated complex; and V_A, etc. are the corresponding molar volumes.

Equation (8) has frequently been invoked to explain why the formation of ions from neutral molecules goes more rapidly in polar solvents than in nonpolar media. However, the type of reasoning on which Eq. (8) is based will predict that the only effect of changing the solvent is on the heat of activation of the reaction. This is because the theory is based on the concept of a random molecular distribution in which deviations from ideality are due to energy differences only, i.e., regular solutions. It is clear that such a theory should not be applied to rates of ionization, since the chief feature of such reactions is the nonrandom distribution of solvent molecules around the activated complex and the associated large entropy changes.[9]

[5] R. P. Bell, J. Chem. Soc. **1943**, 629.

[6] R. P. Bell, Trans. Faraday Soc. **31**, 1557 (1935).

[7] See the discussion on hyperpolarizability by Sutton, Coulson, and Maccoll, Trans. Faraday Soc. **48**, 106 (1952).

[8] G. Scatchard, Chem. Rev. **8**, 321 (1931); J. H. Hildebrand and S. E. Wood, J. Chem. Phys. **1**, 817 (1933).

[9] See also Halpern, Brady, and Winkler, Can. J. Research **28B**, 140 (1950).

Photoconductivity of Violanthrone

HIDEO AKAMATU AND HIROO INOKUCHI
Department of Chemistry, Faculty of Science, Tokyo University, Tokyo, Japan
(Received April 17, 1952)

Photoconductivity of violanthrone, iso-violanthrone, and pyranthrone, the organic semiconductors, has been investigated. From the threshold of spectral response of photoelectric current, the energy gap between the full ground band and the empty excited band was estimated as 0.84 ev, 0.93 ev, and 1.14 ev, respectively. These results are in good agreement with that estimated from the temperature dependence of resistivity, and furthermore with the optical absorption of crystals.

INTRODUCTION

WE have found in the previous work that violanthrone, iso-violanthrone, and pyranthrone have electrical conductance to a certain degree.[1] Similar behavior was found for the other related compounds, that is the condensed polynuclear aromatic compounds.[2] Cyananthrone, for example, has the resistivity of 1.2×10^7 ohm-cm at 15°C and the activation energy of the conductance estimated from the temperature dependence is 0.20 ev. The whole feature shows that these organic compounds appear to be semiconductors. Furthermore, considering the absence of any ionic character nor impurities, they can be assumed to be intrinsic semiconductors. The similar result has found by Eley for phthalocyanine.[3] This property will be attributed to the structure of energy-bands common to the whole crystal, arising by intermolecular overlapping of the π-orbitals of the polynuclear condensed rings.

We have found then that some of these compounds show the photoconductivity. This offers another method to verify the origin of the conductivity being electronic and the energy gap in the band structure of these organic crystals.

EXPERIMENTAL PROCEDURE AND RESULTS

Violanthrone, iso-violanthrone, and pyranthrone have been purified chemically by the usual method, and then sublimed in vacuum more than twice until the conductivity being constant.

The photocell was made as follows. Two pieces of tin foil, 10 mm in width, were stuck on a quartz plate keeping the gap between them one mm. The film of violanthrone or iso-violanthrone was deposited by vacuum evaporation between the foils. Increases in conductivity produced by illumination, which was done perpendicular to the face of the plate, were measured in terms of current changes for a constant potential difference between the foils. The potential difference applied was 950 volts per cm or more; the current was amplified 1700 times by a direct-current amplifier. The observed dark-current was the order of 10^{-12} or 10^{-13} amp. The ratio of photoelectric current to dark-current was about 10 to 20 when a 500-watt tungsten lamp was placed at the distance of 10 cm from the cell.

In the case of pyranthrone, because of its high resistivity, the above cell could not be applied. The following method was used. Aluminum and pyranthrone films were deposited alternately by vacuum evaporation on a quartz plate, in consequence, pyranthrone film was sandwiched between two aluminum films. The upper film of aluminum was made to be so thin, about 500A in thickness, as to be transparent. The light was illuminated through this face. The potential difference was applied between these aluminum films.

The photoelectric current was produced by illumination of monochromatized light from a 500-watt tungsten lamp, operating at a constant voltage of 75 volts. The calibration of the intensity for wavelength was made by using a thermocouple, which was placed at the position of photocell. The sensitivity of the thermocouple is 0.68 microvolt per one microwatt. The illuminated light had the maximum intensity at 14300A, where the reading of the thermocouple was 5.86×10^3 microwatt. The observed value of the photoelectric current was calibrated to the equivalent value per one watt in intensity of the incident radiation in each case. The spectral response of photoelectric current is shown in Figs. 1–3.

The photoelectric current decreases as the wavelength of the incident radiation is increased in each case, and the threshold is found. The value of light quantum in ev at each threshold is shown in Table I. Assuming a crystal

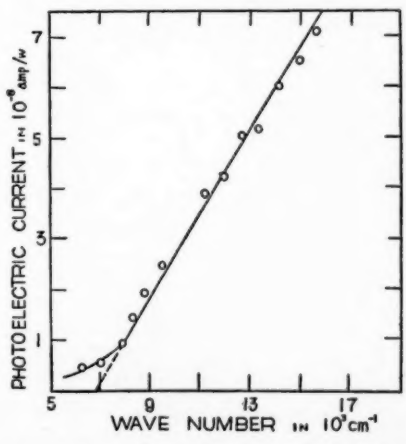

FIG. 1. Photoconductive response of violanthrone.

[1] H. Akamatu and H. Inokuchi, J. Chem. Phys. **18**, 810 (1950).
[2] H. Inokuchi, Bull. Chem. Soc. Japan **24**, 222 (1951); **25**, 28 (1952).
[3] D. D. Eley, Nature **162**, 819 (1948).

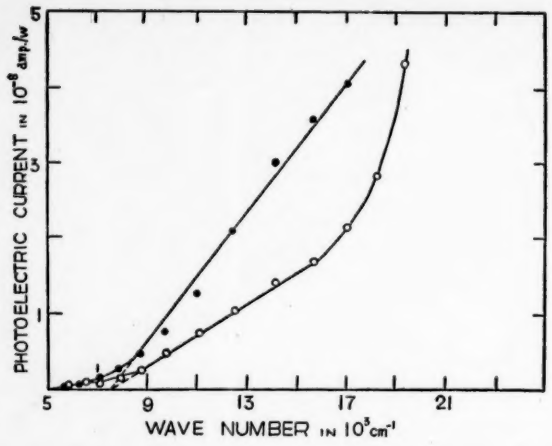

FIG. 2. Photoconductive response of iso-violanthrone. ○ 950 volts/cm in field strength, ● 1900 volts/cm in field strength.

band structure, this value must be the energy gap between the full ground band and the empty excited band. In comparing these values to that estimated from the temperature dependence of the resistivity,[1] the agreement is pretty good as shown in Table I.

It is frequently believed that, in the case of ionic crystals, the energy gap estimated from optical activation energy is much larger than that estimated from the thermal activation energy. The difference is often as large as twofold.[4] The cause of this discrepancy is usually interpreted by the Franck-Condon principle. In our results for molecular crystals, the values estimated from photoconductivity are also a little larger than that from the activation energy of the conductance. This may be partly due to the experimental error and partly due to the Franck-Condon principle. Nevertheless, it seems worthy to notice that the discrepancy is relatively small.

OPTICAL ABSORPTION

To find the band structure common to the whole crystal, the optical absorption of the crystal has been

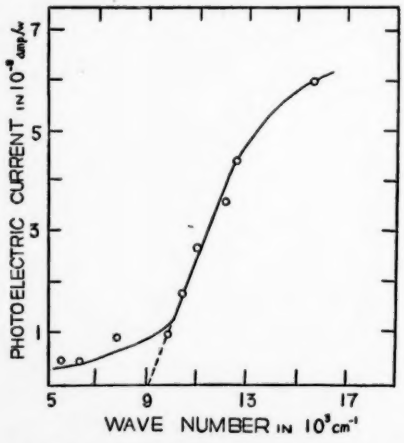

FIG. 3. Photoconductive response of pyranthrone.

[4] N. F. Mott and R. W. Gurney, *Electronic Processes in Ionic Crystals* (Oxford University Press, New York, 1940), p. 160.

TABLE I.

	Violanthrone	iso-Violanthrone	Pyranthrone
Threshold wave number	6.8×10^3 cm^{-1}	7.5×10^3 cm^{-1}	9.2×10^3 cm^{-1}
Energy gap from photoconductivity	0.84 ev	0.93 ev	1.14 ev
Energy gap from thermal activation energy	0.78 ev	0.75 ev	1.06 ev

examined. We hoped to find at least a correlation between the optical absorption and the photoconductivity.

Experiments were carried out for the film deposited by vacuum evaporation on a quartz plate in each case. The film thickness varied from transparent to opaque along the length of the quartz plate, and the portion of a suitable thickness was selected for the absorption measurement. For comparison with the crystal, the absorption of a solution in α-methyl naphthalene and in concentrated sulfuric acid were examined simultaneously. The concentration of the solution was the order of 10^{-5} mole/1 in each case. The absorption ratio *versus* wavelength curves were obtained for all specimens by means of Beckman spectrophotometer. Absorption ratio curves are shown in Figs. 4–6.

The absorption peaks of the solution shift to longer wavelength when sulfuric acid was used as solvent instead of α-methyl naphthalene. In the crystal, the absorption band becomes very broad, in consequence, it is difficult to find a direct connection with that of the solution. This may be partly due to the low resolving power of the experimental conditions. In all cases, however, the absorption decreases steadily toward the wavenumber range between 7000 and 9000 cm^{-1}. Beyond this range it increases again sharply. We suppose that the latter increasing of absorption is due to the vibration effect, perhaps C-H vibration, since it is observed in all cases similarly and also for the sulfuric acid solution.

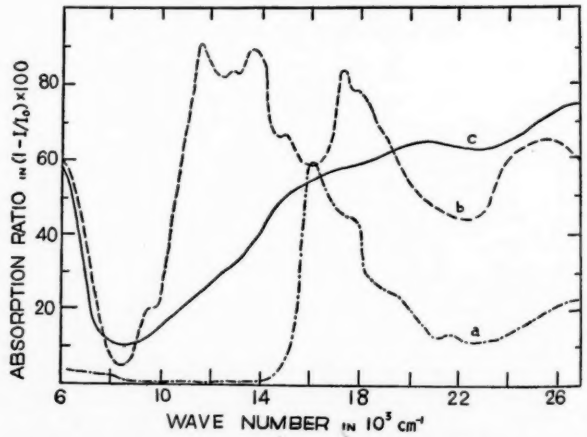

FIG. 4. Optical absorption of violanthrone in (a) α-methyl naphthalene solution, (b) conc. sulfuric acid solution, and (c) crystal state.

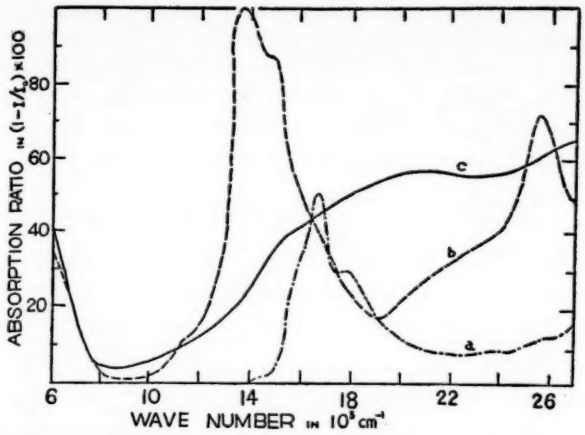

FIG. 5. Optical absorption of iso-violanthrone in (a) α-methyl naphthalene solution, (b) conc. sulfuric acid solution, and (c) crystal state.

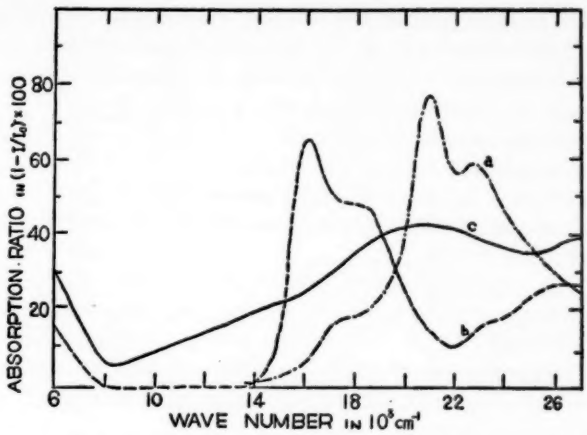

FIG. 6. Optical absorption of pyranthrone in (a) α-methyl naphthalene solution, (b) conc. sulfuric acid solution, and (c) crystal state.

Nevertheless, the cause of this absorption remains obscure at present. It may be supposed that the absorption edge due to the electron state of crystal lie in the range between 7000 and 9000 cm^{-1} in wave number. This is consistent with the result of photoconductivity.

In conclusion, results of photoconductivity, optical absorption, and temperature dependence of electrical conductance satisfactorily coincide with each other. Furthermore, the discrepancies between them are noticeably small in comparison with the case of usual semiconductors. This will be, perhaps, due to the fact that the organic compounds studied here are intrinsic semiconductors made of a molecular lattice, and have simple definite band structures.

ACKNOWLEDGMENT

We wish to thank Mr. T. Fukushima for his assistance in the absorption measurement. The cost of this research has been defrayed from the Scientific Research Encouragement Grant from the Ministry of Education, to which our thanks are due.

THE JOURNAL OF CHEMICAL PHYSICS VOLUME 20, NUMBER 9 SEPTEMBER, 1952

Electronic Barrier Layer Phenomena in Chemisorption and Catalysis

P. B. WEISZ
Socony-Vacuum Laboratories, Research and Development Department, Paulsboro, New Jersey
(Received June 23, 1952)

Chemisorption processes lead to interactions between electrons in the chemisorbed molecules and the electronic structure of the solid. Resulting electronic boundary layer phenomena are closely analogous to those studied in rectifier theory. Analysis by the methods of rectifier theory explains the variation of heat of adsorption with the amount adsorbed, gives the temperature dependence of chemisorption, and yields the increase of activation energy with frequency factor commonly observed in catalysis.

THE chemical behavior of molecules is determined by their electronic structure. Logical extension of this fact to chemical interaction between solids and molecules leads one to invoke the electronic structure of the solid in seeking an understanding for such interactions.[1]

Adsorbed molecules and solid contact each other at the surface of the solid, and electron energy levels will, in general, not be identical in the two partners. Therefore, any resulting donation or acceptance of electrons by the solid should lead to electronic boundary phenomena quite analogous to those occurring in metal semiconductor or other contacts between two electronically dissimilar materials, as have been studied in connection with the electrical rectification properties of such junctions.

As a result of electron transfers a potential energy barrier will be set up at the interface, extending several to many atomic distances below the surface. With the simplest theory for the barrier, the potential set up—in equilibrium—will at the interface be equal to the difference in the free energy of the electrons (Fermi energies) in the solid and in the adsorbate E_0 and will

[1] D. A. Dowden, J. Chem. Soc. **1950**, 242.

fall to zero towards the interior in a manner depending on the magnitude of E_0, the density and energetics of acceptors and donors in the solid, its dielectric constant, and temperature. For each case the shape of the potential barrier is calculable on the basis of equilibrium relationships among the charge carriers, donors, and acceptors in the solid, and Poisson's law in the manner developed by Schottky[2] and others, in connection with rectifier theory.

In applying this physical picture and associated theory to solid-molecule interaction, we obtain the following.

The number of molecules chemisorbable by electron transfer per unit surface will be obtainable from

$$n_s=(1/e)\int_0^\infty \rho dx=(K/4\pi e)\int_0^\infty (d^2E/dx^2)dx,$$

where ρ is the charge per unit volume and E the electrical potential, at a distance x from and within the solid surface, e the electronic charge, K the dielectric constant; the methods developed for the Schottky barrier layer are used to evaluate the integral. Problems concerning the number of chemisorbed molecules can then be reduced to considerations concerning this charge integral. For example, in the mathematically simplest case (nearly all donors or acceptors ionized, and $E_0 \gg kT$) the number of molecules chemisorbed is

$$n_s=[(K/2\pi e)E_0N]^{\frac{1}{2}},$$

where N is the volume density of donors for current carriers in the solid.

In the process of building up the equilibrium layer of n_s the surface potential E rises from zero to E_0. The heat of adsorption, equal to (E_0-E), will accordingly drop for successively adsorbed molecules from E_0 to zero. The potential energy rise due to charge transfers from already adsorbed molecules is imparted to the surface generally through the agency of mobile electrons (or holes) existing in the solid. The variation of heat of adsorption is explained without the necessity of invoking either heterogeneity of surface sites or interaction between adsorbed molecules.

Temperature dependence of chemisorption results for solid electronic structures in which changes in Fermi level occur over the temperature interval in question and also as a consequence of rate considerations concerning the rate of appearance of mobile carriers at the surface. (In metals, chemisorption would be expected to occur at even the lowest temperatures, since no activation energy for current carriers is needed. This does not exclude activation energies required by other steps of a chemisorptive mechanism such as U in

$$N_2 \rightarrow N_{2\text{ chemisorbed}} \xrightarrow{U} N_{\text{chemisorbed}}+N_{\text{chemisorbed}}.)$$

Otherwise, a limitation on the initial rate of sorption will be given by the rate of diffusion of carriers to the surface in the initial potential-free state, which is of the form

$$(dn/dl)_{\text{sorption}} \lessapprox 10^{16}N^{\frac{1}{2}}e^{-(Q/2kT)},$$

where Q is the energy of activation for current carriers, demonstrating strong dependence of observable rates on electronic structure and temperature.

When a chemisorptive process is a prerequisite for catalytic reaction, such rate limitations lead to the existence of induction periods when $Q/2kT$ is in the range which will affect practical measurements.

When the rate of catalytic conversion is related to the desorption of species, it will depend on the number of chemisorbed species n_s and on the rate of diffusion of carriers to the top of the potential barrier, dn_c/dt:

$$\text{rate} \sim n_s \times dn_c/dt,$$

where

$$dn_c/dt=-N_cbFe^{-(eE_0/kT)},$$

involving, therefore, N_c the density of mobile carriers within the solid (which for nonmetallic conductors will itself contain an exponential term $e^{-(Q/2kT)}$), the mobility b of carriers, and the electric field intensity F at the top of the barrier calculable from boundary layer theory. The number of adsorbed molecules n_s is in itself dependent on E_0 due to the considerations above, larger n_s always accompanying larger E_0. Therefore, higher activation energies would accompany higher frequency factors for the observed rates, a common observation in catalysis.

Common ground appears to exist between chemisorptive phenomena and contact rectification phenomena for the application of electronic boundary theory. Difficulties in knowledge and mathematical treatment, such as relate to polarization energies, and problems concerning "surface states" appear to be common to both fields. A more detailed discussion is in preparation.

[2] W. Schottky and E. Spenke, Wiss. Veroffentl. Siemens-Werken **18**, 1 (1939).

A Note on the Detection of Free Radicals by Means of Paramagnetic Resonance Absorption. Biradicals*

CLYDE A. HUTCHISON, JR., ARTHUR KOWALSKY, RICARDO C. PASTOR, AND G. W. WHELAND
Institute for Nuclear Studies and Department of Chemistry, University of Chicago, Chicago, Illinois
(Received July 8, 1952)

The application of paramagnetic resonance absorption to the detection of organic free radicals is discussed. The advantages of this method over conventional measurements of magnetic susceptibility are illustrated by the results of measurements on *p,p'*-biphenylene-*bis*-(diphenylmethyl).

SERIOUS difficulties are encountered in the application of conventional magnetic techniques (measurement of magnetic susceptibilities) to the study of various problems of chemical interest involving the occurrence of paramagnetic molecular species. Examples of such problems are: (a) the occurrence of free radicals as reaction intermediates; (b) the dissociation in solutions of organic molecules such as the hexaarylethanes; (c) the occurrence of organic molecules in magnetic states such as the biradical states of certain substances or the triplet states involved in phosphorescence. The difficulties are twofold: (1) relatively very large amounts of diamagnetic material are usually present, and this may largely obscure the paramagnetism; (2) the diamagnetism of the paramagnetic molecule itself must be known, and there is usually no reliable method of estimating or measuring its value. Difficulty (1) may frequently be eliminated by proper design of experiment, but difficulty (2) is more fundamental. It has, for example, been pointed out, first by Wheland[1] and then by Selwood and Dobres[2] that there are reasons for expecting the free radical dissociation products of the hexaarylethanes to have anomalously large diamagnetism, thus leading to serious errors in the degrees of dissociation as calculated by conventional methods of treating the magnetic susceptibility data.

The techniques of electronic paramagnetic resonance absorption afford the possibility of experimental study of problems such as those described above without the attending difficulties (1) and (2). The resonance phenomenon is peculiar to the unpaired electrons in the paramagnetic species, and thus one is able to observe or count unpaired electrons while ignoring the diamagnetism of the molecular species in question or of the medium in which it is contained.

An example of the application of such methods is afforded by our investigation of the absorption of microwave radiation at 23,500 mc in Chichibabin's hydrocarbon, *p,p'*-biphenylene-*bis*-(diphenylmethyl),

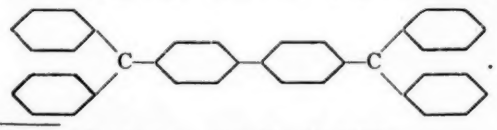

There has been much speculation[3] as to the relative abundance of the paramagnetic forms (triplet state) of this substance, such as

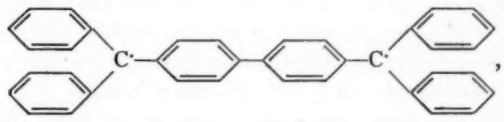

(A)

and the diamagnetic forms (singlet state), such as

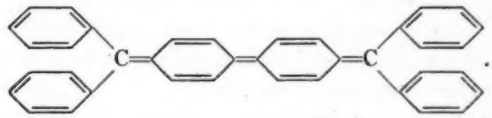

(B)

The compound is very deeply colored and extremely reactive suggesting, that it might be a free radical.

The magnetic susceptibilities of this compound and of its solution in benzene have been measured by Muller and Muller-Rodloff.[4] They found that it possessed, within the error of the experiment, the diamagnetic susceptibility estimated for the form (B) from measurements on similar compounds for which the biradical structure was not possible. They believed that they would have been able to detect 2 percent biradical. They hence concluded that the substance exists in the form (B). However, the difficulties (1) and (2) mentioned above are seen to be encountered in this experiment.

Subsequently, Schwab and Agliardi[5] investigated the *ortho-para* conversion of hydrogen by a solution of Chichibabin's hydrocarbon and concluded that 9.7 percent of the substance was in the biradical form. Muller[6] on the other hand using a larger conversion factor reinterpreted these data as being in agreement with his conclusion that not more than 2 percent of the molecules exist in a biradical state.

Calculations[7] of the energies of the singlet and triplet states have indicated that the triplet lies ~2.5 kcal higher than the singlet for a planar configuration of the

* This work has been supported by the ONR.

[1] Wheland, *Advanced Organic Chemistry* (John Wiley and Sons, Inc., New York, 1949).

[2] Selwood and Dobres, J. Am. Chem. Soc. **72**, 3860 (1950).

[3] Muller, Fort. d. Chem. Forschung **1**, 325 (1949); Muller, *Neuere Anschauungen der Orgnischen Chemie* (Julius Springer, Berlin, 1940), p. 295; Bent and Gould, J. Am. Chem. Soc. **57**, 1217 (1935); Eistert, Ber. deut. chem. Ges. **69**, 2393 (1936).

[4] Muller and Muller-Rodloff, Ann. Physik **517**, 134 (1935).

[5] Schwab and Agliardi, Ber. deut. chem. Ges. **73**, 95 (1940).

[6] Muller, Fort. d. Chem. Forschung **1**, 382 (1949).

[7] Huckel, Z. physik. Chem. **34**, 339 (1936); Huckel, Z. Elektrochem. **43**, 834 (1937); Diatkina and Syrkin, Acta Physicochim. U.R.S.S. **21**, 23 (1946).

molecule. This would result in ~4 percent of the molecules being in the triplet state at 300°K.

We have examined two solutions in benzene of Chichibabin's hydrocarbon each with a volume of 0.050 ml and with concentrations 0.0050 *M* and 0.0080 *M* corresponding to 2.5×10^{-7} mole and 4.0×10^{-7} mole, respectively. The solutions were prepared in a nitrogen atmosphere, sealed in Pyrex sample tubes in vacuum and kept in light-tight containers when not in use. The magnetic absorption was measured using a right circular cylindrical transmission cavity operated in the TE_{011} mode. The sample was located on the axis of the cavity. The static magnetic field was modulated sinusoidally at 60 cycles sec^{-1} with amplitude sufficient to sweep through the entire range of detectable resonance. The output of a crystal detector was amplified and observed on the vertical axis of an oscilloscope on whose horizontal axis was impressed the modulating voltage. The horizontal axis was calibrated in terms of field strength employing the proton resonance, and the vertical axis was calibrated against a known variable voltage. Areas under the absorption curves were calculated by numerical integration and normalized to the same radiation intensities assuming no saturation.

These solutions exhibited a magnetic resonance absorption which was very approximately 15 gauss wide at half-maximum absorption. The areas under the absorption curves produced by a series of four solutions in benzene of 2,2-diphenyl-1-picrylhydrazyl[8] containing from 1.62×10^{-6} to 9.04×10^{-8} mole of the free radical were plotted against the amount of solute. The resulting curve up to much larger absorptions than those produced by the Chichibabin's hydrocarbon was a straight line passing through the origin. The amounts of biradical were determined by comparison of its absorption areas with the values on the curve for the hydrazyl. It was assumed that a given number of biradical molecules would produce 8/3 the absorption area of the same number of hydrazyl (monoradical) molecules used as standard. It was assumed that all of the hydrazyl molecules were free radicals.

In this manner it was found that in the 0.005 *M* solution of Chichibabin's hydrocarbon, 4 percent of the molecules were in the biradical state and in the 0.008 *M* solution 5 percent. The difference between these two results is approximately the error of the determination. It was assumed throughout that there was no magnetic saturation, which has been shown to be justified in the case of the standard, 2,2-diphenyl-1-picrylhydrazyl, but is not known to be exactly the case for the biradical. The solid Chichibabin's hydrocarbon also showed magnetic resonance absorption.

These experiments serve to illustrate the superiority of the method of electronic paramagnetic resonance absorption over the conventional magnetic susceptibility measurement in a problem in which the difficulties (1) and (2) which are mentioned above are encountered in an acute form.

Other problems of the types discussed in the first paragraph are at present being studied in this laboratory by means of resonance techniques. Examination of the resonance in Chichibabin's hydrocarbon at various concentrations and temperatures is in progress. We have examined thiobenzophenone and $\Delta^{9,9'}$-bifluorene both in solutions and in the form of the pure solids and have found them to show no paramagnetic resonance absorption at room temperature in the absence of light. The first of these compounds is brightly colored and very reactive and has been suspected of being in a biradical state.[9] Measurements of the static magnetic susceptibility show it to be diamagnetic.[10] In the case of the second compound it has been claimed that steric hindrance may result in its being in a biradical state.[11] However, the analysis of x-ray diffraction by the crystalline compound does not support this view.[12] The study of *p,p'-bis*-(dimethylamino)-thiobenzophenone, rubrene, and other compounds when strongly illuminated is in progress. The compounds mentioned show no paramagnetic resonance in the absence of light.

We wish to thank Clarence Arnow for the development and construction of portions of the electronic equipment and Edward A. Bartal, Hans Riehm, and Jay S. Hitchcock for the construction of microwave components and other machine work employed in these experiments.

[8] Hutchison, Pastor, and Kowalsky, J. Chem. Phys. **20**, 534 (1952).

[9] Bergmann and Engel, Z. physik. Chem. **8**, 136 (1930); Bergmann, Magat, and Wagenberg, Ber. deut. chem. Ges. **63B**, 2576 (1930).

[10] Allen and Sugden, J. Chem. Soc. **1936**, 440.

[11] Van Dormael, Bull. Soc. Chim. Belges **58**, 412 (1949); Bergmann and Hirshberg, Bull. Soc. Chim. France **17**, 1091 (1950); Bergmann, Berthier, Pullman, and Pullman, Bull. Soc. Chim. France **17**, 1079 (1950); Wawzonek and Fan, J. Am. Chem. Soc. **68**, 2541 (1946).

[12] Fenimore, Acta Cryst. **1**, 295 (1948).

Letters to the Editor

THIS section will accept reports of new work, provided these are terse and contain few figures, and especially few half-tone cuts. The Editorial Board will not hold itself responsible for opinions expressed by the correspondents. Contributions to this section should not exceed 600 words in length and must reach the office of the Editor not later than the 15th of the second month preceding that of the issue in which the Letter is to appear. No proof will be sent to the authors. A publication charge of $10.00 per Letter is made which, when honored, will entitle the Institution to 100 free reprints.

O—H Stretching Frequencies in Very Short and Possibly Symmetrical Hydrogen Bonds

R. E. RUNDLE AND MATTHEW PARASOL
Department of Chemistry, Iowa State College, Ames, Iowa
(Received June 12, 1952)

DIFFICULTY in finding the O—H stretching frequency in nickel dimethylglyoxime, where the O—H—O distance is but 2.44A,[1] led us to examine crystals containing established O—H—O distances,[2] using both normal and deuterated compounds. The results shown in Fig. 1, show a more remarkable shift in frequency with distance than previously noted, presumably because of the sparcity of infrared data on crystalline mulls and because for short O—H—O distances O—H absorption bands become broad, indistinct, and displaced so far as to have gone unrecognized.

Typical O—H absorption is illustrated in Fig. 2 for weak, moderate, and very strong hydrogen bonds. For O—H—O distances below 2.7A, frequency is very sensitive to distance and should be useful for rapid determination of distances from the empirical curve (Fig. 1). There are indications that very broad bands, characteristic of strong hydrogen bonds, become sharper as the O—H—O bond becomes symmetric.

Evidence for symmetric hydrogen bonds in nickel dimethylglyoxime is as follows: Substitution of D for H in the above compound causes the O—H stretching frequency at 1775 to disappear. The sharp, single N—O stretching band at 1560 cm^{-1} is shifted to 1600 cm^{-1} (Fig. 2). No other changes are caused by the substitution. The shift in the NO frequency can be ascribed to the lower oxygen-hydrogen interaction upon substitution of D for H, in accordance with the Robertson-Ubbelohde effect[3] and establishes an observable influence of hydrogen bonding upon the NO frequency. In asymmetric hydrogen bonding the molecular configuration,

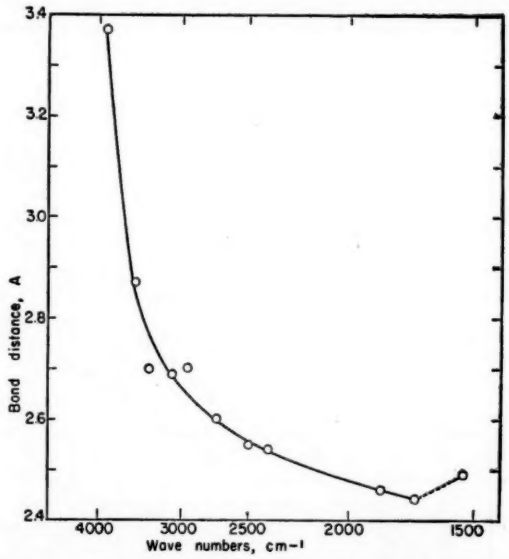

FIG. 1. Bond distance *versus* stretching frequency for O—H—O hydrogen bonds. Compounds, reading from left to right: calcium hydroxide, oxalic acid dihydrate, pentaerythritol, resorcinol, diaspore, ammonium trihydrogen periodate $[(NH_4)_2H_3IO_6]$, sodium bicarbonate, potassium dihydrogen phosphate, maleic acid, nickel dimethylglyoxime, and palladium dimethylglyoxime. The distance for maleic acid was obtained from Professor Kathleen Lonsdale, private communication.

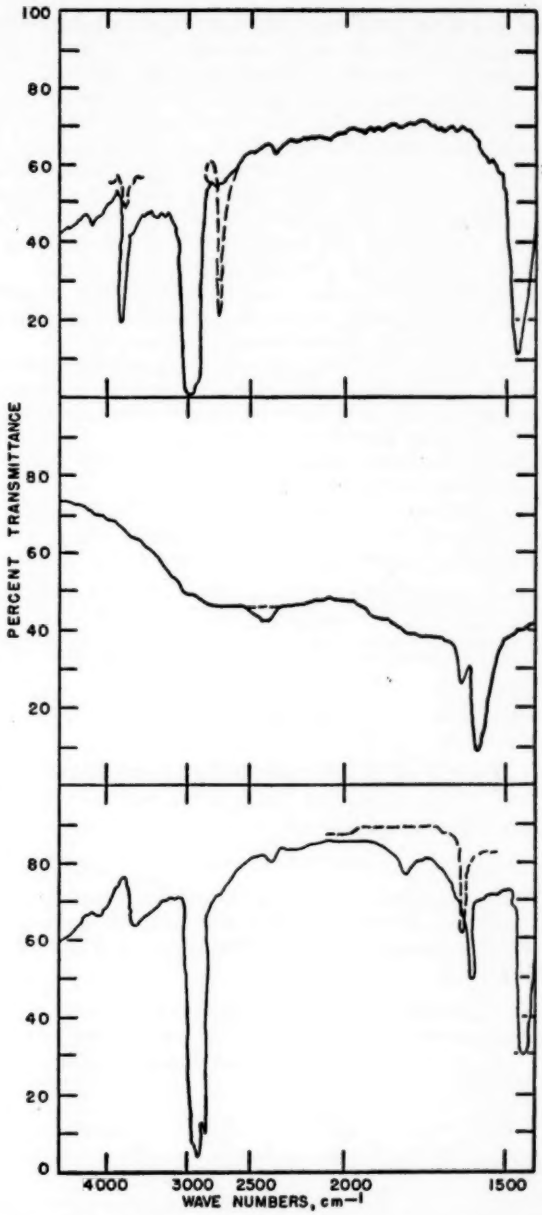

FIG. 2. Typical infrared spectra for negligible, medium, and very strong hydrogen bonding. Dotted lines show changes in spectra upon deuterating the compounds. Upper curve, calcium hydroxide; middle, potassium dihydrogen phosphate; lower, nickel dimethylglyoxime.

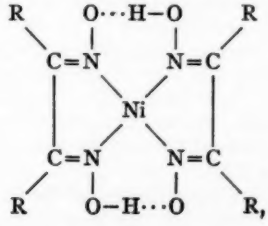

would lead to two NO frequencies, both subject to influence by D substitution. Since only one is observed, all NO bonds appear equivalent, and symmetric hydrogen bonds are indicated.

Noteworthy, too, is the fact that the O−H frequency is lower for the palladium than for the nickel complex (Fig. 2). The isomorphous palladium complex has larger lattice constants and almost surely has a larger O−H−O distance. For asymmetric O−H···O bonding this would lead to a shorter O−H distance and a higher O−H frequency, while for symmetrical O−H−O bonding, it would lead to a longer O−H bond and a lower O−H frequency, in agreement with experiment.

A large number of similar nickel and palladium complexes, such as nickel nioxime, nickel heptoxime, etc., show similar spectra and must also have symmetric hydrogen bonds.

It appears that for distances somewhat greater than 2.44A the O−H−O bond may be asymmetric (maleic acid) or symmetric (palladium dimethylglyoxime), with quite different frequencies (Fig. 1). Whether the bond is symmetric or not depends, presumably, on charge and resonance effects, both of which favor the symmetric bond in the palladium compound.

The authors are indebted to Mr. Marvin Margoshes for obtaining most of the spectra and to Margoshes and Dr. C. V. Banks and Dr. V. Fassel for helpful discussions.

[1] Godycki, Rundle, Voter, and Banks, J. Chem. Phys. **19**, 1205 (1951).
[2] For a review of O−H−O distances with references to the original literature see J. Donohue, J. Phys. Chem. **56**, 502 (1952).
[3] J. M. Robertson and A. R. Ubbelohde, Proc. Roy. Soc. (London) **170A**, 222 (1939); C. E. Nordman and W. N. Lipscomb, J. Phys. Chem. **19**, 1422 (1951).

Two D_2O Microwave Absorption Lines*

C. I. Beard and D. R. Bianco
The Applied Physics Laboratory of The Johns Hopkins University, Silver Spring, Maryland
(Received July 17, 1952)

TWO absorption lines in the microwave region have been observed in D_2O vapor, and their Stark spectra have been studied. The observed lines with their assignments are shown in Table I.

Table I. Observed D_2O rotational absorption lines.

Molecule	Transition	Frequency (Mc/sec)
D_2O	$2_{2,0;2}\rightarrow 3_{1,3;-2}$	10,919.8 ±0.1
D_2O	$5_{3,2;1}\rightarrow 4_{4,1;3}$	10,947.4 ±0.1

The lines were observed on a standard microwave spectrometer using square wave voltage modulation at 100 kc/sec. The detailed Stark structures were studied with an adjustable dc voltage modulated with a small sinusoidal ac voltage at 100 kc/sec. The frequency measurements were made using a secondary standard and crystal harmonic multiplication. The frequency standard was continuously monitored on an oscilloscope against WWV at 5 Mc/sec.

The Stark cell is a 10-foot section of *X*-band wave guide with a septum in the center. The constant used to find the electric field intensity from the measured voltage applied to the guide was determined by a study of the Stark splitting of $O^{16}C^{12}S^{32}$. The value of dipole moment taken for this transition was 0.7085 ±0.004 debye unit as determined by Shulman and Townes.[1]

The calculated Stark splittings were made using the expression developed by Golden and Wilson[2] for nondegenerate levels. The energy levels were taken from Fuson, Randall, and Dennison's work[3] on heavy water. The line strengths used in the perturbation calculations were secured from tables of line strengths given by Cross, Hainer, and King.[4]

In addition to the identification of the transitions by Stark splitting, further proof that the lines represented the isotopic species D_2O was found from a detailed study of the relative intensities of these two lines compared with the known H_2O and HDO lines in the microwave region as the concentration ratios were varied. The D_2O sample was secured from the Stuart Oxygen Company through the Isotopes Division of the AEC and was approximately 99.8 percent pure. To approach the maximum D_2O concentration point, break seal tubes in vacuum were used followed by flushing several grams of D_2O vapor through the wave guide with a flow system. With this process the intensity

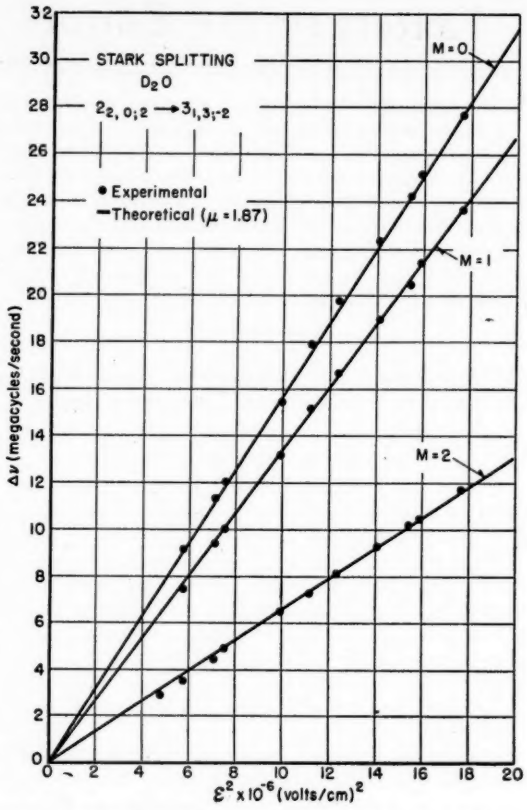

Fig. 1. Stark effect study of the 10,919.8 Mc/sec line of D_2O.

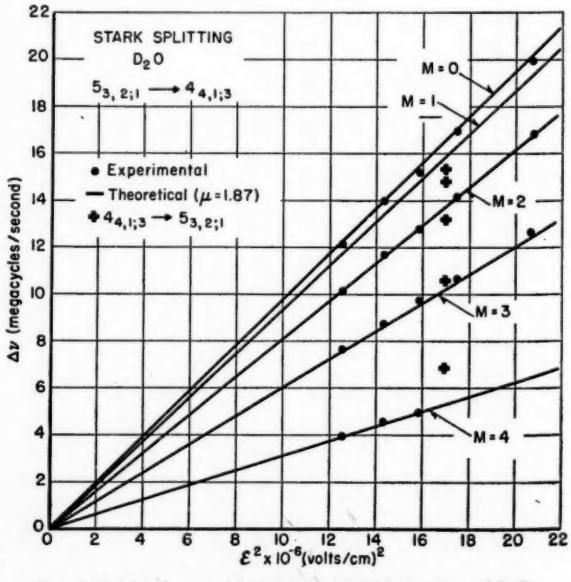

Fig. 2. Stark effect study of the 10,947.4 Mc/sec line of D_2O.

of the HDO lines decreased strikingly to noise level, whereas only these two D_2O lines increased.

The calculated splitting for the $2_{2,0;2}\rightarrow 3_{1,3;-2}$ line is given by the expression $\Delta\nu=(0.4490-0.06514M^2)\mu^2E^2\times 10^{-6}$ where $\Delta\nu$ is the Stark splitting in Mc/sec, $M=0, 1, 2$, μ is the electric dipole moment in debye units, and E is the electric field intensity in volts/cm.

The calculated splitting for the $5_{3,2;1}\rightarrow 4_{4,1;3}$ line is given by $\Delta\nu=(0.2790-0.01183M^2)\mu^2E^2\times 10^{-6}$, where in this case $M=0, 1, 2, 3, 4$.

For both of these lines a μ of 1.87 debye units in these expressions fits the experimental data as shown in Figs. 1 and 2. Although μ could be determined to ± 0.01 debye unit from the data, the final tolerance is ± 1 percent which is the accuracy of the electric field measurement. This compares with values of 1.78, 1.84, and 1.87 as determined by other methods and workers.[5]

The energy levels of D_2O as given by Fuson, Randall, and Dennison uncorrected for centrifugal distortion place the $5_{3,2;1}$ level above the $4_{4,1;3}$ level. The centrifugal distortion correction, however, reverses this order. Stark splitting calculations were carried out for both cases. The results at one value of E for the transition $4_{4,1;3}\rightarrow 5_{3,2;1}$ are shown in Fig. 2 by the crosses. These points do not fit the data. Our results, then, agree with the conclusions of Fuson, Randall, and Dennison on heavy water.

As seen in Fig. 2 the $M=0$ and $M=1$ components of the 10,947.4 Mc/sec line are not completely resolved. To secure the field intensity required for resolution would require a higher voltage than our equipment is designed for at present.

For the $M=4$ component of the 10,947.4 Mc/sec line, it was not desirable to secure additional points at high field values as the 10,919.8 Mc/sec line began to split into this line at high fields.

* The work described in this paper was supported by the Bureau of Ordnance, U. S. Navy, under Contract NOrd 7386.

[1] R. G. Shulman and C. H. Townes, Phys. Rev. **77**, 500 (1950).
[2] S. Golden and E. B. Wilson, Jr., J. Chem. Phys. **16**, 660 (1948).
[3] Fuson, Randall, and Dennison Phys. Rev. **56**, 982 (1939).
[4] Cross, Hainer, and King, J. Chem. Phys. **12**, 210 (1944).
[5] L. G. Wesson, *Tables of Electric Dipole Moments* (Technology Press, Massachusetts Institute of Technology, 1948).

Aromaticity of Conjugated Monocyclic Hydrocarbons

KURT MISLOW
Department of Chemistry, New York University, New York, New York
(Received July 14, 1952)

IT is interesting to speculate on the possible aromatic character of compounds of the type C_nH_n (n is even) with $n>8$. From the M.O. treatment, it appears[1] that benzene is unique, with the largest delocalization energy per π-electron, and further that only ring systems with $n=4m+2$ ($m=1, 2, \cdots$) lead to stable diamagnetic molecules, the aromatic electrons occupying nondegenerate levels and forming "abgeschlossene Elektronengruppen." Benzene is further unique in that the strain energy of the σ-framework is at a minimum for $n\sim 6$ in the series of planar regular polygons comprising the C_nH_n group.[2]

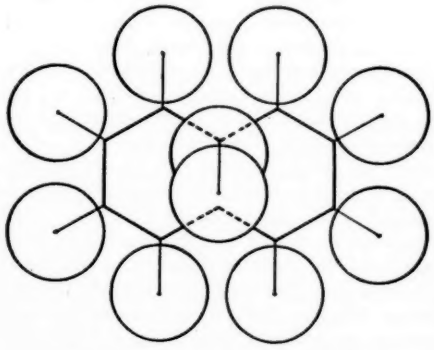

FIG. 1. Diagram of cyclodecapentaene.

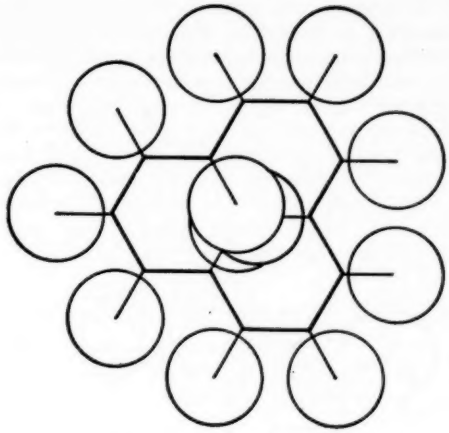

FIG. 2. Diagram of cyclododecahexaene.

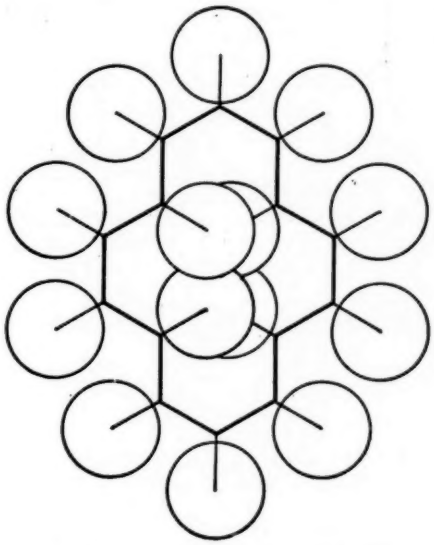

FIG. 3. Diagram of cyclotetradecaheptaene.

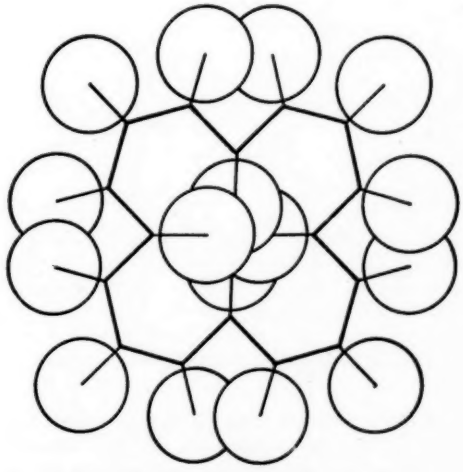

FIG. 4. Diagram of cyclohexadecaoctaene.

The suggestion is sometimes made[3] that hydrocarbons of this type with $n>8$ might exist in unstrained conformations and might

therefore be coplanar and aromatic. While this assumption is correct in so far as the carbon skeleton itself is concerned, it ignores the effect of hydrogen interference. An examination of such molecules which takes into account the pertinent atomic dimensions (C−C∼1.40A, C−H∼1.10A, Van der Waals radius of H∼1.0A) clearly reveals that appreciable repulsion must exist between the "central" hydrogens of coplanar cyclodecapentaene (Fig. 1), cyclododecahexaene (Fig. 2), cyclotetradecaheptaene (Fig. 3), cyclohexadecaoctaene (Fig. 4) (where, in addition, the carbon skeleton is distorted from the optimum angle of 120°, and the "peripheral" hydrogens interfere), and cycloöctadecanonaene (Fig. 5), quite aside from the consideration that the second and fourth molecules belong to the $4m$ class. In analogy with compounds like *o*-diphenylbenzene, *cis*-stilbene, 1,3,5-triphenylbenzene, and probably triphenylmethyl, where hydrogen interference may cause distortion from coplanarity,[4] one might expect these compounds to assume the buckled rather than the coplanar conformation. If the criterion of coplanarity (or only moderate divergence therefrom) is included in our definition of aromaticity, these compounds will very probably not be aromatic; it is difficult in these cases to estimate the precise decrease in stabilization energy resulting from noncoplanarity.

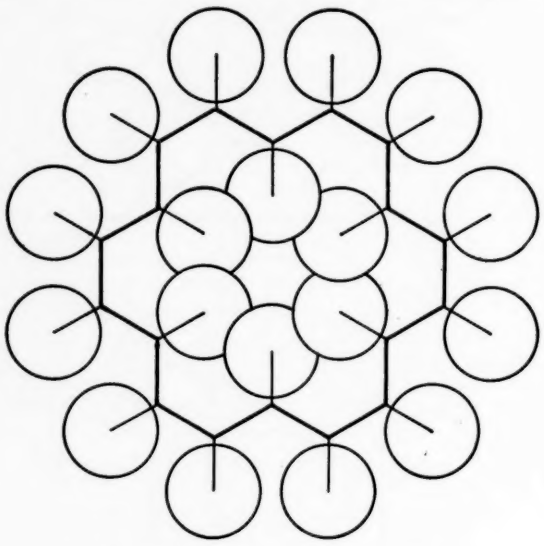

FIG. 5. Diagram of cycloöctadecanonaene.

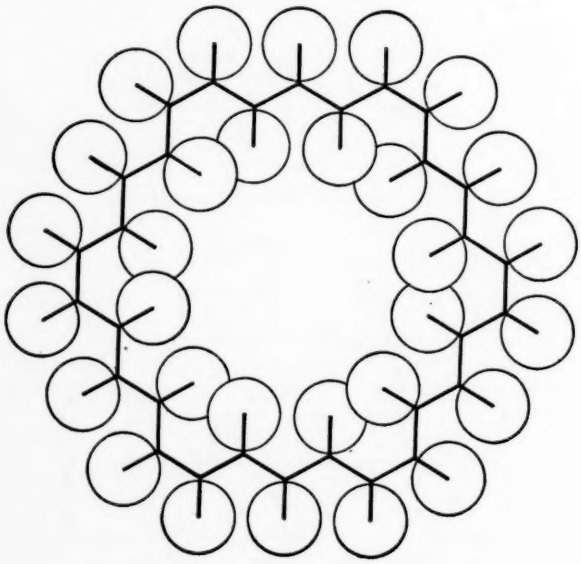

FIG. 6. Diagram of cyclotriacontapentadecaene.

More "open" molecules would be more likely to exist as planar species. Cyclotriacontapentadecaene, $C_{30}H_{30}$ (Fig. 6), where interference takes place only between alternate "central" hydrogens, and where the potential field of the hydrogens within the ring is not as prohibitive, may serve as an illustration. The interference here is comparable with that found in the *p*-polyphenyls, which are coplanar[4] despite *ortho*-hydrogen repulsion. It is worthy of note that the estimated delocalization energy of $C_{30}H_{30}$ is ∼140 kcal/mole, on the basis of a M.O. treatment in which overlap between noncontiguous π-electrons has been neglected.

From the above considerations it would appear that synthetic efforts made toward the preparation of coplanar benzenoid monocyclic hydrocarbons might conceivably be rewarded for $C_{30}H_{30}$ (or larger systems). Cyclodecapentaene was reported formed in the polymerization of acetylene,[5] but this substance is now known to be in actuality a mixture of vinylcycloöctatetraene and *cis*-1-phenyl-1,3-butadiene.[6]

These arguments do not apply, of course, to large-ring heterocycles, where the problem of "central" hydrogen interference does not arise, as, for example, in the porphyrin and phthalocyanine series.

[1] E. Hückel, Z. Physik **70**, 204 (1931); **76**, 628 (1932).
[2] W. G. Penny, Proc. Roy. Soc. (London) **146A**, 223 (1934).
[3] C. R. Noller, *Chemistry of Organic Compounds* (W. B. Saunders Company, Philadelphia, 1951), p. 769.
[4] G. W. Wheland, *The Theory of Resonance* (John Wiley and Sons, Inc., New York, 1944).
[5] Reppe, Schlichting, and Meister, Ann. Physik **560**, 93 (1948).
[6] A. C. Cope and S. W. Fenton, J. Am. Chem. Soc. **73**, 1195 (1952), D. S. Withey, J. Chem. Soc. **1930** (1952).

The Absorption Spectrum of Hydrated Americium Chloride*

BETSY J. STOVER† AND JOHN G. CONWAY
Radiation Laboratory, University of California, Berkeley, California
(Received July 14, 1952)

THE study of the absorption spectra of the lanthanide and actinide elements is an important step in the correlation of these two groups since the spectra arise from transitions within the $4f$ and $5f$ electronic shells. Previous work in this laboratory has shown a similarity in the solution absorption spectra of americium and europium.[1] Freed and Leitz observed 17 lines in the spectrum of hydrated americium chloride.[2] The data reported here are more complete since a large sample and a spectrograph of greater dispersion were used.

Approximately one mg of americium (separated and purified by Dr. B. B. Cunningham) was available for growing crystals. Slow evaporation, the first crystal growing method tried, proved unsatisfactory since the product was an opaque powder completely useless for spectroscopy. The failure to grow clear crystals undoubtedly resulted from the decomposition of water by the intense alpha-radiation (approximately 7×10^9 alphas min^{-1}). To minimize the radiation chemistry effect, the solutions were evaporated rapidly under a heat lamp. The products obtained were conglomerate rather than single crystals, but were sufficiently clear for optical work. These preparations gradually grew opaque as a result of alpha-decomposition of the water of crystallization, but they could be used for about two days.

The sample was mounted on a thin glass window which was then fastened to a brass container which had another window on the opposite side. This sample mounting was used for all measurements. Figure 1 shows the 77°K optical arrangement; the Dewar flask is removed for the room temperature measurements. A Baird three-meter grating spectrograph was used, and the spectrum was measured from 3600A to 8500A at both temperatures. The wavelengths, vacuum wave numbers, and relative intensities appear in Table I.

TABLE I. Wavelengths, intensities, and wave numbers for $AmCl_3 \cdot H_2O$ at room temperature and liquid nitrogen temperature.

	R.T.				N_2T		
No.	λ(A)	I	$\tilde{\nu}(cm^{-1})$	No.	λ(A)	I	$\tilde{\nu}(cm^{-1})$
1	8133	10	12,292	1	8180	10wh	12,222
				2	8159	10s	12,253
				3	8123	8h	12,307
				4	8108	8h	12,330
				5	8078	5	12,376
				6	8064	5	12,397
				7	8051	5	12,417
2	7993	8	12,508	8	8011	7	12,479
				9	7964	6	12,553
3	5168	10	19,346	10	5169	10	19,341
4	5163	10	19,364	11	5164	10	19,359
5	5154	7	19,397	12	5152	10	19,405
6	5139	5h	19,454	13	5137	10	19,461
				14	5131	4	19,484
				15	5119	8	19,529
				16	5110	8	19,564
7	5104	5h	19,587	17	5104	4	19,587
				18	5097	6	19,614
8	5084	8h	19,664	19	5090	5	19,641
				20	5074	5	19,703
				21	5067	8	19,730
9	5060	10h	19,757	22	5060	10	19,757
10	5047	10h	19,808	23	5051	10	19,793
				24	5045	10	19,816
				25	5038	10	19,844
				26	5010	5	19,955
11	4991	4	20,030	27	4996	4	20,010
				28	4988	4	20,043
12	4974	3	20,098	29	4972	3	20,107
13	4726	3	21,154				
14	4695	8s	21,293	30	4693	6	21,302
15	4646	6	21,517	31	4650	8	21,499
16	4639	6	21,550	32	4644	8	21,527
17	4596	5	21,752	33	4595	5	21,757
				34	4589	5	21,785
				35	4583	4	21,814
				36	4569	4	21,881
18	4555	10	21,948	37	4555	10	21,948
19	4434	5	22,547	38	4432	6	22,557
20	4315	5h	23,168	39	4318	7	23,152
21	4301	5h	23,244	40	4302	7	23,238
22	4285	5h	23,331	41	4292	5	23,293
				42	4283	7	23,342
				43	4270	5	23,413
23	4237	4	23,595	44	4239	4	23,534
24	4211	4	23,741				
25	4110	4	24,324				
26	4056	4	24.648				
27	4051	4	24,678				
				45	4032	5	24,795
				46	4027	5	24,825
28	4023	8	24,850	47	4025	5	24,838
29	4006	6	24,956				
30	3960	10s	25,245	48	3963	6	25,226
				49	3961	6	25,239
31	3952	5	25,297	50	3953	4	25,290
				51	3948	4	25,322
32	3811	5s	26,232	52	3813	4	26,219
				53	3811	6	26,232
	3801	5h	26,301	54	3801	10	26,301
				55	3797	10	26.329
				56	3787	7	26,399
34	3784	4	26,420	57	3784	9	26,420
35	3765	4	26,553	58	3767	5	26,539
				59	3764	5	26,560
				60	3751	4	26,652
				61	3733	5	26,780
36	3729	4	26,809	62	3728	4	26,816
				63	3722	5	26,860
				64	3704	4	26,990
37	3694	4	27,063				
				65	3667	4	27,262
38	3656	4	27,345	66	3662	4	27,300
				67	3644	4	27,435
				68	3631	5	27,533
39	3624	4	27,686	69	3626	6	27,571
				70	3619	6	27,624

s = sharp; w = wide; h = hazy.

The most striking effect observed at low temperature is the greatly increased resolution. No densitometer measurements were made, but visual comparisons of similar exposures at the two temperatures revealed no marked alteration of relative intensities. This fact indicates that the population of the levels is not changed appreciably by lowering the temperature to 77°K.

A study was made of the frequency distribution of wave-number differences in an attempt to determine the energy difference between the $^7F_0$ ground state and possible low-lying excited levels. A number of constant intervals were observed varying from 20 cm^{-1} to 140 cm^{-1}, which probably correspond to vibrational levels reported for hydrated europium chloride.[3] Others were observed at 176, 288, 322 or 353, and 450 cm^{-1}. Since we have no temperature dependence data, no assignments can be made, and no distinction can be made between electronic and vibrational levels.

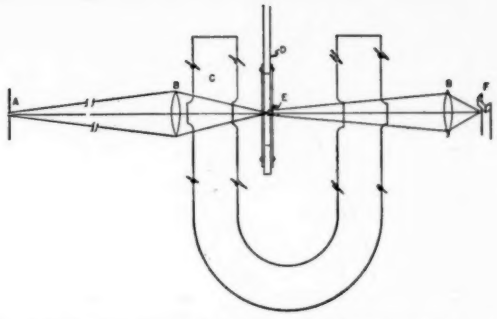

FIG. 1. Optical arrangement for obtaining the absorption spectra of $AmCl_3 \cdot H_2O$ at room temperature and liquid nitrogen temperature. A. Slit; B. Condensing lens; C. Dewar flask with optically flat windows; D. Sample holder; E. Position of sample; F. Tungsten filament lamp.

We wish to thank Dr. B. B. Cunningham for the loan of the americium.

* This research was done under the auspices of the AEC.

† Present address: Radiobiology Laboratory and Department of Chemistry, University of Utah, Salt Lake City, Utah.

[1] Stover, Conway, and Cunningham, J. Am. Chem. Soc. **73**, 491 (1951).
[2] S. Freed and F. J. Leitz, J. Chem. Phys. **17**, 540 (1949).
[3] Spedding, Moss, and Waller, J. Chem. Phys. **8**, 908 (1940).

Note on the Critical Temperature of Solids

BERNI J. ALDER AND GEORGE JURA
Department of Chemistry and Chemical Engineering, University of California, Berkeley, California

(Received July 7, 1952)

FROM the available solidification data of several gases, Simon[1] and Bridgman[2] have argued for and against the existence of a critical temperature for the solid state. We present computations which make it appear that solids do exhibit critical temperature phenomena. The calculated temperatures and pressures are much higher than those which have been experimentally studied.

It is convenient to define the critical temperature as that temperature at which the molar internal energy E and volume v of the two phases become equal. Our procedure is to determine the envelope under which these criteria are satisfied. Then we investigate the possible intersection of this envelope with the equations of state of the two phases.

For a solid at temperature T and volume v

$$E_S = W(r) + \int_0^T C_v dT, \tag{1}$$

where $W(r)$ is the potential energy of the solid at 0°K. This involves the use of the appropriate Madelung sum of the lattice and a knowledge of the potential function. If the temperatures of interest are high compared to the Debye temperature at this volume, and we assume that the motions can still be considered harmonic, Eq. (1) reduces to

$$E_S = W(r) + 3RT. \tag{2}$$

The energy of the gas can be written

$$E_G = 3RT/2 + 2\pi N^2/v \int_0^\infty V(r) g(r, T, v) r^2 dr, \tag{3}$$

where N is Avogadro's number, $V(r)$ the pair potential, and $g(r, T, v)$ the radial distribution function. Equating E_S and E_G one obtains

$$3RT/2 = -W(r) + 2\pi N^2/v \int_0^\infty V(r) g(r, T, v) r^2 dr. \tag{4}$$

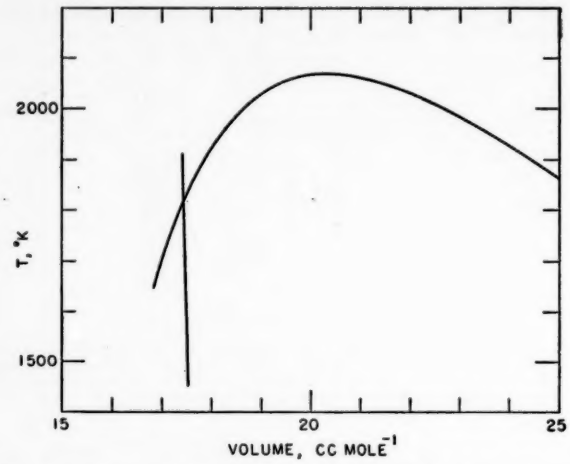

FIG. 1. Plot of volume *vs* temperature; the intersection of the two curves gives the computed critical point.

A number of approximations have been made in arriving at Eq. (4). The zero point energy has been neglected. Since the volumes of the two phases are nearly equal, this contribution will be approximately the same for the two phases. Further, this term will, in general, be small compared to the other terms. Secondly, possible electronic terms have been omitted. Since we deal only with the rare gases, the temperatures are low enough so that we need not consider these terms. The major approximation lies in the assumption that the motions in the solid can be considered harmonic regardless of the volume. The existence of a critical temperature for the solid state depends upon the behavior of C_v at temperatures where the atomic motions are possibly greatly anharmonic. From the previous equation it follows that sufficient conditions for the nonexistence of the singular point is that $Cv_s - \frac{3}{2}R \leqslant (\partial V_G/\partial T)$, where V_G is the potential energy of compression of the gas to volume v. The sufficient condition for the existence of a critical point is that $Cv_s - 3/2R > (\partial V_G/\partial T)$.

The evaluation of the terms on the right-hand side of Eq. (4) permits an explicit solution of the temperature at which $\Delta E, \Delta v = 0$. The radial distribution function that we have used is an extension of the hard sphere treatment of Kirkwood[3] and co-workers. The potential functions are the appropriate Lennard-Jones functions.[4] Though the evaluation of the potential energy term may be in error, the effect on the final results is relatively small. The nearly horizontal line in Fig. 1, is the T *vs* v curve for argon evaluated in this manner.

For the equations of state for the solid[5] and gas we have used

$$\log(p+a) = b \log T + c \tag{5}$$

and

$$p(v-b) = RT, \tag{6}$$

respectively. The empirical vapor pressure equation for the solid appears to be the best available at the present time. Its use involves a long extrapolation beyond its verified range. The hard sphere equation of state for the gas appears to be reasonable at the high temperatures. If these two equations are combined, we can see whether it intersects the envelope obtained from Eq. (4). The result for argon is the nearly vertical line in Fig. 1. The intersection of the two curves, is obviously the critical temperature. The critical constants for some of the rare gases are given in Table I. The values for argon and neon are approximate. The values for helium are even more approximate.

TABLE I. Computed critical constants for the solid rare gases.

Solid	T_c(°K)	V_c(cc/mole)	V(cc/mole) solid at 0°K	V_0(cc/mole) close packed volume of spheres	P_0(atmos)
He	90	8.0	...	...	29,000
Ne	540	9.1	13.95	8.76	150,000
A	1840	17.4	24.98	16.82	250,000

[1] Simon, Ruhemann, and Edwards, Z. physik. Chem. (B) **6**, 331 (1930).
[2] P. W. Bridgman, Phys. Rev. **46**, 930 (1934).
[3] Kirkwood, Mann, and Alder, J. Chem. Phys. **18**, 1040 (1950).
[4] Fowler and Guggenheim, *Statistical Thermodynamics* (Cambridge University Press, Cambridge, 1939), p. 285.
[5] M. Ruhemann and B. Ruhemann, *Low Temperature Physics* (Cambridge University Press, Cambridge, 1937), p. 97.

Directional Variation of Frequency in the Infrared Spectrum of Crystals

L. COUTURE-MATHIEU,* J. A. A. KETELAAR, W. VEDDER, AND J. FAHRENFORT
Laboratory for General and Inorganic Chemistry of the University of Amsterdam, Amsterdam, Netherlands
(Received July 1, 1952)

IT has been observed that in some piezoelectric crystals certain Raman frequencies exhibit a change in frequency with the orientation of the crystal with respect to the incident and diffused beams.[1,2]

This effect has been attributed to the change in the frequency of the elastic waves with the change of the angle φ between the moment **M** and their propagative vector **k**. When this angle is 90° the wave is called transversal, whereas for $\varphi = 0°$ it is purely

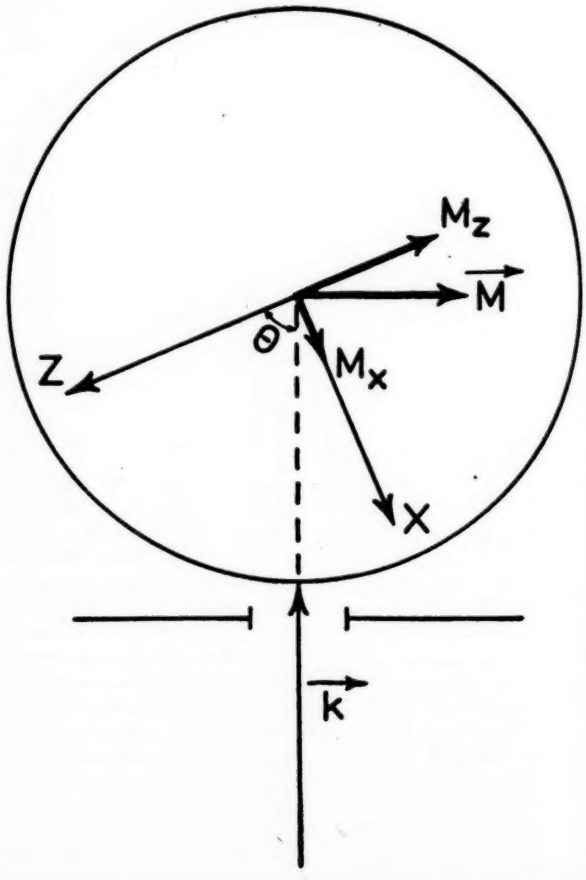

FIG. 1. Arrangement of the quartz cylinder with respect to incident light **k**.

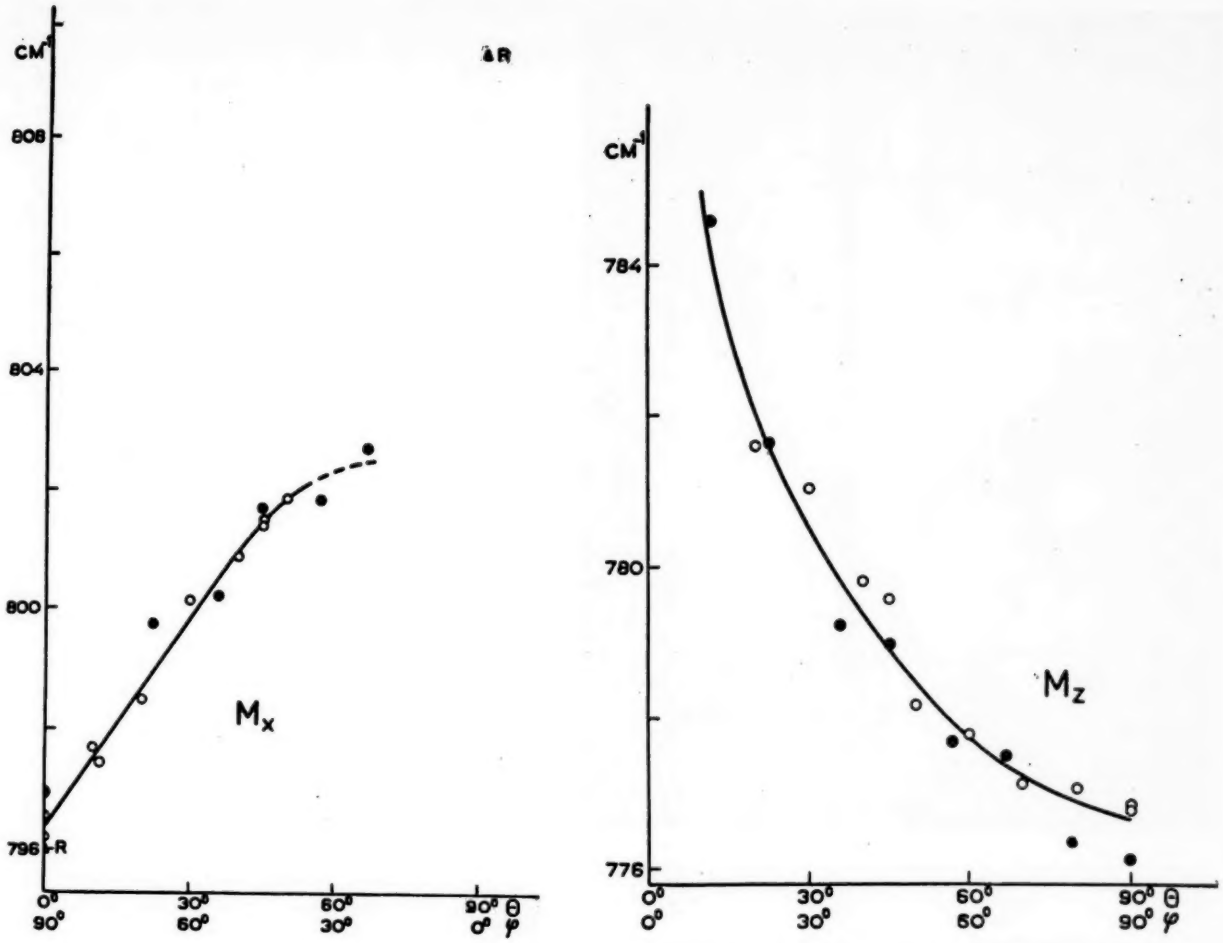

FIG. 2. Frequency of the two bands associated with M_x and M_z, respectively, as a function of the orientation. ○ = cylinder; ● = prism, ▲R = Raman effect (M_z is inactive).

longitudinal. In the Raman effect, e.g., in quartz, the frequency change was found to be from 796 cm^{-1} to 809.5 cm^{-1} for both extremes.[2]

We have now investigated the infrared reflection spectrum of a cylinder of quartz with the axis Y perpendicular to the hexagonal axis Z of the crystal and to the piezoelectric axis X and of an irregular eight-sided prism with the same orientation of the axis.

The reflection spectrum was observed for perpendicular incidence and with polarized light with the electric vector at right angles to the axis of the cylinder and of the prism, respectively. The orientation of the crystal is determined by the angle θ between the direction of the beam $\mathbf{k}$ and the axis Z (Fig. 1).

In the region of 780–800 cm^{-1} two bands were observed;[3] the lower frequency component was observed single at 776.5 cm^{-1} for $\theta=90°$ thus corresponding to an electric moment M_z, whereas the other was observed single at 796.5 cm^{-1} at $\theta=0°$ and thus has a moment parallel to the X axis. However, at intermediate values of θ both were observed but with increasing values of θ at decreasing frequencies for the first one and at increasing frequencies for the latter one (Fig. 2).

Naturally, the extreme of a pure longitudinal wave is inactive in the infrared at $\varphi=0°$.

Thus we deduce that in accordance with the results found in the Raman effect the frequency increases with increasing longitudinal character of the wave, that is, with decreasing value of $\varphi=(\mathbf{M}, \mathbf{k})$ (Fig. 2). This change was to be expected from calculations of Poulet.[4]

This effect can be expected in the infrared for all classes of non-cubic crystals irrespectively, whether piezoelectric or not, provided the electric moment is sufficiently large.

* Address: Lab. de Recherches Physiques de la Sorbonne, Paris.

[1] L. Couture-Mathieu and J. P. Mathieu, Compt. rend. **231**, 839 (1950); J. P. Mathieu and L. Couture-Mathieu, J. Phys. (U.S.S.R.), (to be published); C. Vassas-Dubuisson, Compt. rend. **233**, 374 (1951).
[2] J. P. Mathieu and L. Couture-Mathieu, Compt. rend. **234**, 1961 (1952).
[3] O. Reinkober, Ann. Physik **34**, 343 (1911).
[4] H. Poulet, Compt. rend. **234**, 2185 (1952).

An Experimental Investigation of Spinning Detonation

RUSSELL E. DUFF AND HERBERT T. KNIGHT
Los Alamos Scientific Laboratory, Los Alamos, New Mexico
(Received June 23, 1952)

SEVERAL fundamentally different theories of spinning detonation have been proposed by Becker[1] and Jost,[2] Shtsholkin[3] and Zeldovich,[4] and Manson[5] and Fay.[6] Unfortunately, the experimental facts as observed by Campbell, Woodhead and Finch[7–9] and by Bone, Fraser, and Wheeler[10–12] do not permit a clear choice to be made between these theories. For this reason further experiments have been conducted at this laboratory to increase our experimental understanding of this phenomenon in order to resolve the long-standing problem of its cause.

Most of the experimental work reported to date has been done with stoichiometric mixtures of carbon monoxide and oxygen. Table I shows the first determination of the pitch diameter ratio

FIG. 1. A 0.0002-in. Dural foil 5.4μ sec after being struck by the shock wave of a spinning detonation.

of the spinning detonation in a $\frac{1}{2}$-in. tube as a function of the percentage of carbon monoxide in the gaseous mixture. The theoretical dependence as predicted by the acoustic theories of Manson and Fay is also included in Table I. The values of the ratio of detonation velocity to the sound speed at the Chapman-Jouget plane needed in the acoustic theories were obtained from detailed equilibrium calculations of the detonation parameters. Note that the agreement between theory and experiment is quite good.

Some insight into the shape of the detonation shock wave is provided by Fig. 1. This picture shows the distortion of a 0.0002-in. Dural foil approximately 5.4μ sec after it was first struck by the shock wave of a spinning detonation in a 40 percent CO+60 percent O_2 mixture. The foil was originally stretched across the end of the 80-mm i.d. detonation tube perpendicular to the tube axis. The foil was illuminated by an intense light source and photographed at an angle of 45° to its surface. The deflection of the grid lines painted on the foil relative to the vertical reference line in front of the foil shows graphically the motion of the foil. A paper by Shreffler and Deal[13] describing the experimental techniques used to obtain pictures of this type will be published in the near future.

TABLE I. Pitch diameter ratio as predicted by the acoustic theories and the ratio observed.

% CO	p/d Predicted	p/d Observed
30	3.012	3.04
40	3.129	3.04
50	3.138	3.06
60	3.141	3.09
66.7	3.141	
70	3.140	3.04
80	3.129	3.08
90	2.982	3.03

A significant fact demonstrated by this photograph and others like it is that the shock wave is not a simple surface. It is made of at least two parts which meet in a line near a diameter. This type of shock wave is somewhat similar to that postulated by Shtsholkin and Zeldovich.

During the preparation for the experiment of Fig. 1, an interesting observation was made. It was necessary to obtain a simple spinning detonation in a large tube. It was impossible to obtain such a detonation in a glass tube; but when a Lucite tube was used, the desired detonation was obtained immediately. The glass tube shattered close behind the detonation front, while the Lucite tube did not break at all. This result suggests that wake confinement is essential for the propagation of a spinning detonation as would be predicted by the vibrational theories of Manson and Fay.

A smear photograph taken through a slit perpendicular to the axis of a tube will show the dependence of luminosity on time at a particular place in the tube, as well as the asymmetry of the luminous front of the spinning detonation. Figure 2 is an example of such a photograph. The roughly sinusoidal wave in the wake is particularly important since, when correlated with smear photographs taken through a longitudinal slit, it shows that a luminous zone, essentially parallel to the tube axis, moves around the tube with uniform angular velocity. The horizontal striations observed in the usual smear photographs are caused by this front passing the longitudinal slit on the tube. The striations do not appear to be the loci of intersections of luminous particle paths and retonation waves as suggested by Bone, Fraser, and Wheeler.

The existence of a luminous zone in the wake of a spinning detonation is predicted by Fay. It corresponds to the pressure peak of a transverse acoustic vibration in the wake. Further support for the acoustic theory is provided by the fact that the

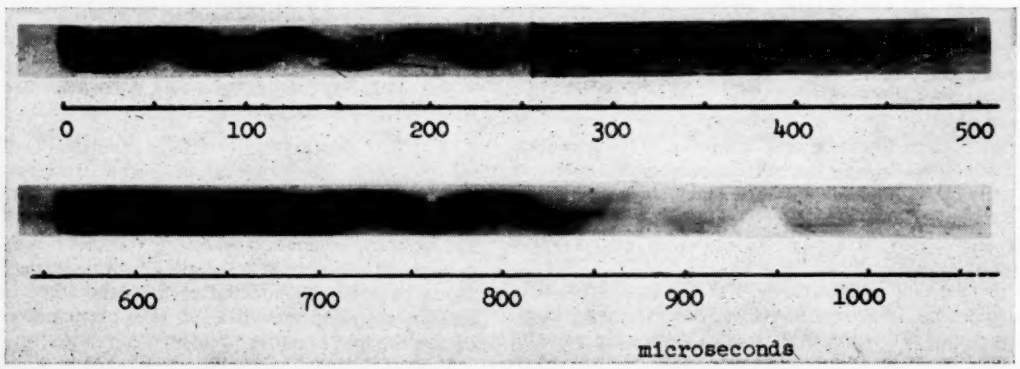

FIG. 2. A spinning detonation as viewed with a smear camera through a slit perpendicular to the tube axis. The lower trace was obtained after the reflected shock passed the slit.

frequency of the sinusoidal wave observed in Fig. 2 increases slightly when the reflected shock returns from the closed end of the tube as would be expected since the speed of sound in the burned gases is increased by the reflection.

Further results will be published from time to time as they become available.

[1] R. Becker, Z. Elektrochem. **42**, 457 (1936).
[2] W. Jost, *Explosion and Combustion Processes in Gases* (1946).
[3] K. I. Shtsholkin, Compt. rend. (Doklady) **47**, 482 (1945).
[4] J. B. Zeldovich, Compt. rend. (Doklady) **52**, 147 (1946).
[5] N. Manson, Compt. rend. **222**, 46 (1946).
[6] J. A. Fay, *A Mechanical Theory of Spinning Detonation* (to be published).
[7] C. Campbell and D. W. Woodhead, J. Chem. Soc. **129**, 3010 (1926).
[8] C. Campbell and D. W. Woodhead, J. Chem. Soc. **130**, 1572 (1927).
[9] C. Campbell and A. C. Finch, J. Chem. Soc. **1928–2**, 2094.
[10] W. A. Bone and R. P. Fraser, Trans. Roy. Soc. (London) **A228**, 197 (1929).
[11] W. A. Bone and R. P. Fraser, Trans. Roy. Soc. (London) **A230**, 371 (1933).
[12] Bone, Fraser, and Wheeler, Trans. Roy. Soc. (London) **A235**, 29 (1936).
[13] R. G. Shreffler and W. E. Deal, *Free Surface Properties of Explosive Driven Metal Plates* (to be published).

Calculation of the Concentration of Atomic Hydrogen at a Cathode

HUGH W. SALZBERG AND SIGMUND SCHULDINER
Chemistry Division, Naval Research Laboratory, Washington, D. C.

(Received July 18, 1952)

IN three papers by Parsons and Bockris,[1] Bockris and Azzam,[2] and Bockris and Potter[3] the concentration of hydrogen atoms on the surface of a cathode is calculated by the use of the formula

$$i=2F(kT/h)10^{-18}x^2\exp(-\Delta G_0^*/RT), \tag{1}$$

where i is the current density, F is the faraday, kT/h is the frequency factor, x is the fraction of surface covered by hydrogen atoms, and 10^{-9} is the number of gram atoms of hydrogen per square centimeter when the surface is fully covered.

Using this equation, the current at which the surface is completely covered is calculated to be 1 amp/cm².

On the basis of this calculation it is stated that above these critical current densities, removal of atomic hydrogen from the surface must proceed by an electrochemical mechanism, namely,

$$MH+H_3O^++e\rightarrow M+H_2O+H_2. \tag{2}$$

Equation (1), however, is incorrect, both in concept and in detail.

First, it is dimensionally incorrect. The rate of a molecular combination, according to the absolute rate theory of Glasstone, Laidler, and Eyring[4,†] is given by

$$r=(kT/h)C_A^2(F^*/F_a^2)\exp(-\Delta G_0^*/RT), \tag{3}$$

where C_A is the concentration of reacting material, F^* is the partition function of the activated complex, and F_A is the partition function of A. Here, both the concentration of A and its partition functions are expressed in terms of molecular concentrations either as molecules per cubic centimeter or as molecules per square centimeter. Since the C^2 and F^2 terms cancel out, this is dimensionally correct, and the rate is finally expressed in terms of molecules per cm² or cm³ per second.

If C_A^2 is expressed in terms of gram equivalents per cm² the partition functions must also be expressed in the same units. This is equivalent to dividing the right-hand term by N, Avogadro's number. In references 1–3, the authors, while using gram equivalents as their units of concentration, neglect to divide their rate by N, thus being in error by a factor of 6×10^{23}.

In addition to this, these authors have neglected the probability factor. In essence, they assume that any pair of molecules on the surface with the requisite energy will combine in 10^{-12} second, regardless of the distance between them. This is manifestly incorrect.

For combination to occur, the atoms must be on adjacent sites. That is, they must be in pairs. The number of such pairs on a surface is given by $sH^2/2L$, where L is the total number of sites, s is the number of sites immediately adjacent to any given site (usually either 4 or 6), and the factor 2 comes in because there are two atoms to every pair. H is the number of atoms/centimeter.[2]

If s is taken as 4, the correct form of the rate equation for a combination on a surface is given by

$$r=(kT/h)H^2(2/L)F^*/F_H^2\exp(-\Delta G_0^*/RT). \tag{4}$$

Assuming an activation energy of zero and a ratio of partition functions of unity, as is done in references 1–3, this equation becomes

$$r=H^2(2/L)(kT/h), \tag{5}$$

where the rate is in terms of molecules per cm² per second. To convert this to current, it must be multiplied by $2F/N$, the number of coulombs per molecule. This gives

$$i=(2F/N)H^2(2/L)(kT/h). \tag{6}$$

This equation differs from (1) in that it includes a probability factor and a conversion factor.

When i is 1 amp/cm², since L is 10^{15}, $F=10^5$, $N=6\times10^{23}$, and $kT/h=6\times10^{12}$, H becomes approximately 1.1×10^{10} atoms/cm². Therefore, instead of the surface being saturated at 1 amp/cm², the fraction of surface covered by atomic hydrogen is only 10^{-5}. For the surface to be saturated, the current must therefore be about 10^{10} amp.

This clearly negates the argument of Bockris *et al.* that the electrochemical mechanism must be operative at currents of an amp/cm² and up. It is, as a matter of fact, difficult to see on the basis of the above calculation how the electrochemical mechanism could be rate determining. Even at a hundred amp/cm², the fraction of the surface covered is only about 10^{-4}. The odds, even at this very high current density, are therefore 10,000 to 1 against a hydronium ion striking an adsorbed hydrogen atom instead of the surface of the metal.

In addition, the experimental data of Schuldiner[5] on bright platinum indicate that the electrochemical mechanism is not operative on platinum in acids at high current densities, where the slope of the overvoltage—log current density curve is 0.12.

We wish to thank Professor K. J. Laidler for his assistance on this problem.

[1] Parsons and Bockris, Trans. Faraday Soc. **47**, 920 (1951).
[2] Bockris and Azzam, Trans. Faraday Soc. **48**, 155 (1952).
[3] Bockris and Potter, J. Electrochem. **99**, 169 (1952).
[4] Glasstone, Laidler, and Eyring, *Theory of Rate Processes* (McGraw-Hill Book Company, Inc., New York, 1941).
† A simplified kinetic approach based on collision theory was used by Goodeve and Jack (Disc. Faraday Soc. **4**, 89 (1948)). From their equation almost the same numerical result is obtained as by Eq. (6) in this letter. Parsons and Bockris (see reference 1) in a comparison of their derivation with that of Goodeve and Jack, showed that the concentration of atomic hydrogen calculated by these two methods differed by a factor of $10^{4.5}$.
[5] Schuldiner, J. Electrochem. (to be published).

Disproportionation in Deuterated Ammonia*

JACOB BIGELEISEN
Chemistry Department, Brookhaven National Laboratory, Upton, Long Island, New York

(Received June 23, 1952)

IN a paper under the above title, Stedman[1] has reported the quantitative determination of the species NH_3, NH_2D, NHD_2, and ND_3 in a sample of ammonia gas containing fifty atom percent deuterium. The sample presumably was in equilibrium with respect to isotopic exchange at room temperature. The analysis was carried out by direct density measurements of the ν_2 vibration in the infrared absorption spectrum of the mixture. Quantitative extinction measurements made on the NH_3 and ND_3 bands gave the amount of these species. The amounts of NH_2D and NHD_2 were calculated from the total amount of nitrogen in the sample, the protium content, and the observed amounts of NH_3 and ND_3.

The results obtained from this analysis indicate that there is a marked deviation from statistical distribution of the protium and deuterium among the different isotopic species. In most isotopic disproportionation equilibria at and above room temperature statistical distribution of the isotopes is found, and in all approxi-

mate calculations the rule of the geometric mean is used. Stedman's results would imply a marked deviation in the case of ammonia.

One may utilize the data in Table IV of Stedman's paper to calculate the equilibrium constants for the reactions

$$2NH_3+ND_3=3NH_2D, \quad (1)$$

$$NH_3+2ND_3=3NHD_2, \quad (2)$$

with the results $K_1=27(0.01856)$ and $K_2=27(0.03925)$.

The structure of the ammonia molecule is well known.[2] The zero-order fundamental frequencies for the isotopic ammonia molecules are uncertain by an amount attributable to the anharmonicity. An approximate calculation of the anharmonic coefficients has been made by Dennison,[3] who has also evaluated the potential constants. From these data Kimball and Stockmayer[4] have calculated the partition function ratios for the various deutero-ammonia molecules. Their partition function ratios lead to the values $K_1=27(0.916)$ and $K_2=27(0.897)$ in accord with expectations from the rule of the geometric mean. The only uncertainties in these calculations are those which arise from the approximate treatment of the anharmonic corrections to the zero point energies. These cannot explain the large discrepancies between the calculated and observed values for K_1 and K_2.

Additional confirmation to the calculations of Kimball and Stockmayer are afforded by the recent experiments of Kemball,[5] who finds close to statistical distribution at 250° and 385°C, and by some experiments in this laboratory. Perlman, Bigeleisen, and Elliott[6] have measured the exchange equilibrium of deuterium between $NH_{3(g)}$ and $(H_2)_g$ in the range 210°–298°K. Their data are in good agreement with the previous ones of Herrick and Sabi,[7] who studied the same equilibrium between 298° and 455°K. These equilibrium data, when combined with the known structural parameters of NH_3 and H_2 and the well-known vibrational states of the H_2 molecule, lead to a difference in zero point energies between NH_3 and NH_2D of 635.0 ± 3 cm^{-1}. The value calculated from Dennison's potential function is 652 cm^{-1}. The calculations of Kimball and Stockmayer, as well as the confirmatory experimental evidence mentioned above, suffice to show that the disproportionation equilibria in deutero-ammonia reported by Stedman are subject to large errors. His data cannot be accepted as an exception to the rule of the geometric mean.

* Research carried out under the auspices of the AEC.

[1] D. F. Stedman, J. Chem. Phys. **20**, 718 (1952).

[2] G. Herzberg, *Infrared and Raman Spectra of Polyatomic Molecules* (D. Van Nostrand Company, Inc., New York, 1945), pp. 294, 437.

[3] D. M. Dennison, Revs. Modern Phys. **12**, 175 (1940).

[4] G. E. Kimball and W. H. Stockmayer, SAM Report 100 XR-1657, October 14, 1942, quoted in I. Kirshenbaum, *Physical Properties and Analysis of Heavy Water* (McGraw-Hill Book Company, Inc., New York, 1951), p. 55.

[5] C. Kemball, Trans. Faraday Soc. **48**, 254 (1952).

[6] Perlman, Bigeleisen, and Elliott (to be published).

[7] See reference 4, p. 58.

Mechanism of Conductivity in Semiconducting Phosphors

JENNY E. ROSENTHAL AND ARTHUR BRAMLEY
Bramley Consultants, Long Branch, New Jersey
(Received June 23, 1952)

SINCE semiconducting phosphors appear slated for important applications in electronics, a closer investigation of the mechanism of their semiconductivity should be of interest. The experimental data are as follows.

Samples of $ZnBeSiO_4$:Mn made semiconducting by heating in an atmosphere of methane were subjected to the action of a gas glow discharge. (In its action of this type of fluorescent material the glow discharge acts merely as a convenient source of ultraviolet radiation.) The wavelength of the radiation emitted by the phosphor was roughly independent of the degree of conductivity, suitable allowance being made for the absorption of the fluorescent radiation by the conducting sample. This absorption varies directly as the conductivity. Further experiments on this type of semiconducting phosphor, this time under monochromatic ultraviolet excitation, have confirmed the earlier observations in the glow discharge.

However, when the semiconducting phosphors are excited by electron bombardment, the wavelength distribution of the fluorescent radiation is shifted toward the blue.

The most plausible explanation of semiconductivity in phosphors is that it arises from the presence of ions of deviating valency. For example, the addition of a fraction of 1 percent of Li_2S to MnS changes divalent manganese into trivalent manganese.

In the case of zinc oxide, whose conductivity depends on the mode of preparation and varies within very wide limits, Bevan and Anderson[1] have suggested that we are dealing with surface conductivity. The experiments mentioned above furnish a strong indication that the semiconductivity of $ZnBeSiO_4$:Mn is also a surface phenomenon. Thus electron bombardment, which is essentially limited to the surface of the crystal, shows a dependence of the wavelength distribution of the fluorescent radiation on conductivity, while ultraviolet radiation, which penetrates more deeply into the crystal, is unaffected by the conductivity of the sample.

Since the conductivity measurements were made on powdered samples, it should be pointed out that the results obtained may refer to the microcrystalline contacts between the individual particles rather than to the absolute value of the conductivity across any one particle, if the latter quantity is high as compared with the conductivity across the microcrystalline contacts.

The semiconducting phosphors used in these experiments were prepared by Mr. T. Palumbo of Ceramic Heaters, whom we should also like to thank for the opportunity to see his data confirming our results.

[1] Bevan and Anderson, Disc. Faraday Soc. **8**, 238 (1950).

The Dissociation Energy of the C—I Bond in Methyl Iodide from Electron Impact Measurements*

C. A. MCDOWELL AND B. G. COX†
Department of Inorganic and Physical Chemistry, University of Liverpool, Liverpool 3, England
(Received July 7, 1952)

THE appearance potential of the CH_3^+ ion from methyl iodide is given by the equation

$$V(CH_3^+) \geqslant D(CH_3I)+I(CH_3), \quad (1)$$

the uncertainty being due to the possibility that the CH_3^+ ion might be formed with excess kinetic energy. Recently[1] it has been shown that measurements of the beam half-widths can be used to decide whether or not an ion is produced with excess kinetic energy; and the application of an equivalent method with the CH_3^+ from methyl iodide indicates that this ion is produced without excess kinetic energy. Thus measurement of the appearance potential of the CH_3^+ ion from CH_3I will enable $D(CH_3-I)$ to be calculated since $I(CH_3)$ is known.[2] We have found $V(CH_3^+)$ from CH_3I to be 12.36 ± 0.02 ev using the method of extrapolated voltage differences to assess the appearance potential. Since $I(CH_3)=10.08\pm0.1$ ev; we thus obtain $D(CH_3-I)=52.6\pm2.3$ kcal/mole.

To check this method of estimating $D(CH_3-I)$ we have also determined the appearance potential of the CH_3^+ ion from methane under the same operating conditions as used in studying CH_3^+ ions from CH_3I. Since CH_3^+ is also formed from methane without excess kinetic energy[1] we may write

$$V(CH_3^+)_{CH_4}-V(CH_3^+)_{CH_3I}=D(CH_3-H)-D(CH_3-I). \quad (2)$$

Our measurements lead to the result that $D(CH_3-H)-D(CH_3-I)=48.5\pm0.5$ kcal/mole. If to this difference we add our value for $D(CH_3-I)$, namely, 52.6 ± 2.3 kcal/mole, we obtain the result

TABLE I. Dissociation energy of the C−I bond in CH_3I from thermal data.

$D(CH_3-I)$ kcal/mole	Authors
52.8 ±1.4	Mackle and Ubbelohde[a]
54.65 ±1.7	Nicol and Ubbelohde[b]
54.00 ±0.5	Carson, Hartley, and Skinner[c]
53.6 ±2.2	Mortimer, Prichard, and Skinner[d]
57.6 ±3.2	Mackle, Maniece, and Ubbelohde[e]

[a] H. Mackle and A. R. Ubbelohde, J. Chem. Soc. 1161 (1948). The value given in Table I is the corrected one given by Nichol and Ubbelohde, see reference b.
[b] R. J. Nichol and A. R. Ubbelohde, J. Chem. Soc. 415 (1952).
[c] Carson, Hartley, and Skinner, Proc. Roy. Soc. (London) **A195**, 500. The value quoted in Table I is the corrected one given by Nichol and Ubbelohde, see reference b.
[d] Mortimer, Prichard, and Skinner, Trans. Faraday Soc. **48**, 220 (1952).
[e] Mackle, Maniece, and Ubbelohde, unpublished work quoted by Nichol and Ubbelohde, see reference b.

that $D(CH_3-H)$ equals 101.3±2.4 kcal/mole. This latter result is in very good agreement with the value for $D(CH_3-H)$ given by Kistiakowsky and Van Artsdalen.[3]

Several workers have recently given values for $D(CH_3-I)$ but all the data have been obtained by thermochemical measurement. It is of interest, therefore, to compare our electron impact value with those other results derived from thermal data. We have collected those more recently estimated in Table I, and it will be seen that our value of 52.6±2.3 kcal/mole is in good agreement with the lowest value.

Recently[4] it has been reported that measurements of the appearance potentials of I^+ and CH_3^+ from CH_3I lead to a value of 9.5 ev for the ionization potential of the CH_3 radical which is low by about 0.6 ev. This discrepancy is probably due to the I^+ ion being formed with some kinetic energy, for though the dissociation of CH_3I under the influence of electron impact produces CH_3^+ ions which do not possess excess kinetic energy, it does not follow that when the dissociation process

$$CH_3I+e=CH_3+I^++2e \qquad (3)$$

occurs, the I^+ ion is also produced without excess kinetic energy. If dissociation process (3) does give rise to I^+ ions which possess excess kinetic energy, then the value for $D(CH_3-I)$, deduced from $V(I^+)$, will be too large and this in turn will give a low value for $I(CH_3)$ when this datum is computed from the equation

$$V(CH_3^+)_{CH_3I}=D(CH_3-I)+I(CH_3). \qquad (4)$$

A full account of this work with similar data for other alkyl halides will be published soon.

* This work was assisted in part by a grant from the Hydrocarbons Research Group of the Institute of Petroleum.
† In receipt of a maintenance grant from the Department of Scientific and Industrial Research.
[1] C. A. McDowell and J. W. Warren, Disc. Faraday Soc. **10**, 53 (1951).
[2] J. A. Hipple and D. P. Stevenson, Phys. Rev. **63**, 621 (1943).
[3] G. B. Kistiakowsky and A. Van Artsdalen, J. Chem. Phys. **12**, 462 (1944).
[4] Dibeler, Riese, and Mohler, J. Chem. Phys. **20**, 761 (1952).

Thermodynamic Properties of Chlorine Trifluoride*

ALFONS WEBER AND SALVADOR M. FERIGLE
Spectroscopy Laboratory, Department of Physics, Illinois Institute of Technology, Chicago 16, Illinois
(Received June 27, 1952)

IN a recent letter M. D. Scheer[1] has calculated the thermodynamic properties of chlorine trifluoride, using the moments of inertia obtained from a study of the microwave spectrum[2] which favors an undistorted, planar, "T" structure, and the assignments given by Schäfer and Wicke[3] from a study of the Raman spectrum. The value of the entropy thus calculated for the ideal gas at 1 atmos pressure and at a temperature corresponding to the boiling point of the compound (284.91°K) is strikingly close to the value given by Grisard *et al.*[4] from thermal measurements. The corresponding values are 66.90 and 66.87±0.10 cal mole^{-1} deg^{-1}. However, the calculations of Scheer involve a clear inconsistency. For the microwave data rule out the pyramidal structure proposed by Schäfer and Wicke; consequently, their vibrational assignment must also be ruled out. If the planar structure is accepted, then the molecule belongs to the C_{2v} point group and hence the six fundamental frequencies are all nondegenerate, while in the C_{3v} pyramidal model there would be two nondegenerate and two doubly degenerate fundamental frequencies. The six frequencies for the planar model can be described in an approximate manner as two Cl−F symmetric stretchings; one Cl−F antisymmetric stretching; two planar bendings, symmetric and antisymmetric, respectively; and one out-of-plane vibration. It does not seem possible to give a definite assignment of the fundamental frequencies since only the small amount of data given by Schäfer and Wicke[3] seem to be available. However, a reasonable assignment of the fundamental frequencies in terms of these data might be the following:

Cl−F stretchings, 508, 644, and 750 cm^{-1};
Planar bendings, 316 and 428 cm^{-1};
Out-of-plane bending, 395 cm^{-1};

which, incidentally, are the same values of the fundamentals proposed by Schäfer and Wicke on the basis of a possible asymmetric pyramidal structure.

Using these frequencies and the structural data from the microwave work of Smith,[2] the entropy for the ideal gas at 1 atmos pressure and at a temperature of 284.91°K, is calculated as 66.64 cal mole^{-1} deg^{-1}. In this calculation, the moments of inertia given by Smith[2] (weighted according to isotopic abundance) and Birge's 1941 values for the physical constants have been used. By using these, the value given by Scheer as 66.90 has been obtained as 66.87 cal mole^{-1} deg^{-1}; this small difference is most likely due to slight discrepancies in the values used for the different constants.

The assignment proposed above and, therefore, the value for the entropy calculated here, are only tentative, because of the uncertainties in the spectral data previously mentioned. The values for some of the frequencies given by Schäfer and Wicke differ by as much as 25 cm^{-1} on different plates; also, the association existing in the compound[3] may produce a considerable shift in some of the frequencies. Hence, definite conclusions regarding the values of the thermodynamic properties of chlorine trifluoride from spectral data cannot be reached at present, but it seems interesting to point out the fact that the agreement claimed by Scheer[1] is completely fortuitous.

A paper published by Jones, Parkinson, and Murray (J. Chem. Phys. **17**, 501 (1949)) shortly after the paper of Schäfer and Wicke gives some more data for ClF_3 although no attempt was made by the authors to assign the observed data to fundamentals or combination bands. These data do not seem to be enough as to make a definite assignment possible.

* Supported in part by a grant from the Research Corporation and by contract DA-11-022-ORD-464 with the Office of Ordnance Research.
[1] M. D. Scheer, J. Chem. Phys. **20**, 924 (1952).
[2] D. F. Smith, Phys. Rev. **86**, 608 (1952).
[3] K. Schäfer and E. Wicke, Z. Electrochem. **52**, 205 (1948).
[4] Grisard, Bernhardt, and Oliver, J. Am. Chem. Soc. **73**, 5725 (1951).

Flame Propagation in Carbon Monoxide

G. MCDONALD
Lewis Flight Propulsion Laboratory, National Advisory Committee for Aeronautics, Cleveland, Ohio
(Received June 3, 1952)

PEASE and Tanford[1] have proposed that the flame speed of carbon monoxide and air mixtures with added water is controlled by the diffusion of hydrogen atoms from the flame zone into the preflame gas where, it is assumed, they initiate combustion reactions. These authors have developed an equation which relates the thermal equilibrium hydrogen atom concentration to the flame speed. The equation predicts that a dry mixture of carbon monoxide and oxygen will have the same flame speed as a dry mixture of carbon monoxide and air.

I have measured the flame speed of dry mixtures of carbon monoxide and oxygen and also of carbon monoxide and air. These had equivalent carbon monoxide—oxygen ratios. The flame speeds were determined by measuring the shadowgraph of a Bunsen cone which was burning the premixed gases. The flame speed was calculated by the total area method. The gases were dried before mixing by passage through anhydrous magnesium perchlorate. After mixing and immediately before burning, the gases were dried by passage through either anhydrous magnesium perchlorate or phosphorus pentoxide.

In these experiments measurements were made of the flame speed of four separately prepared mixtures of carbon monoxide and oxygen and of eight separately prepared mixtures of carbon monoxide and air. A dry carbon monoxide—oxygen mixture has a larger flame speed than a dry carbon monoxide—air mixture. The average flame speed of an 80 percent carbon monoxide—20 percent oxygen mixture is 27.0 cm/sec. The average deviation in measurement is 0.7 cm/sec. The average flame speed of a 47 percent carbon monoxide—53 percent air mixture is 14.9 cm/sec. The average deviation in measurement is 0.6 cm/sec.

Incorporation of this burning velocity of the oxygen enriched dry mixture into the equations of Tanford and Pease instead of their 17 cm/sec would increase the difference between their predicted values of flame speed and experimental observations by approximately 10 percent for flames of low nitrogen content.

These different flame speeds for zero hydrogen atom concentrations also indicate that separate curves exist at each nitrogen concentration for flame speed *vs* hydrogen atom concentration. Tanford and Pease, by combining into one curve both large flame speeds of oxygen enriched flames and small flame speeds of carbon monoxide—air flames, imply that all carbon monoxide mixtures which have an equal carbon monoxide—oxygen ratio will be on the same curve for plot of flame speed *vs* hydrogen atom concentration.

[1] C. Tanford and R. N. Pease, J. Chem. Phys. **15**, 861 (1947).

Erratum: Force Constants and Calculated Thermodynamic Properties for SiF_4*

[J. Chem. Phys. **19**, 1084–5 (1951)]

FRED. L. VOELZ, ARNOLD G. MEISTER, AND FORREST F. CLEVELAND
Spectroscopy Laboratory, Department of Physics, Illinois Institute of Technology, Chicago 16, Illinois

IN re-examining some of the XF_4 type of molecules, the thermodynamic properties of SiF_4 were recalculated and the moment of inertia was found to be too large by 27.01 awu A^2. This causes a 0.467 cal deg^{-1} $mole^{-1}$ decrease in each of the free energy and entropy values given previously. However, the heat content and heat capacity remain unchanged since they do not involve the moments of inertia. Besides this, the thermodynamic properties have now been calculated for 273.16°K. They are $(H^0-H_0^0)/T=11.82$, $-(F^0-H_0^0)/T=54.23$, $S^0=66.05$, and $C_p^0=16.88$ cal deg^{-1} $mole^{-1}$.

* Part of a research program which is supported in part by the Office of Ordnance Research, Contract No. DA-11-022-ORD-464.

Influence of σ-Electrons on the Lower Excited Electronic Levels of Benzene*

KAZUO NIIRA
Physics Department, Tokyo Institute of Technology, Oh-okayama, Tokyo, Japan

(Received June 27, 1952)

RECENTLY, Altman[1] discussed the effect of σ-electrons in the molecules such as benzene and ethylene. In connection with this paper we should like to report our calculation on the influence of σ-electrons on the lower excited electronic levels of benzene.

Since the earlier work of G. Mayer and Sklar[2] many workers have engaged in the calculation of the lower excited electronic levels of benzene by the ASMO method (in LCAO approximation) including only six $2p\pi$-electrons. Especially, Parr, Craig, and Ross[3] made an elaborate calculation including configuration interaction and all of the many-center integrals, and gave a satisfactory agreement with experiment. But in such close approximation as this the exchange interaction between π- and σ-electrons of benzene may not be ignored.

We label C atoms of benzene from 1 to 6 counterclockwise and assume for π-electrons Hückel's functions:

$$\phi_l(\nu)=1/(6N_l)^{\frac{1}{2}}\cdot\sum_{k=1}^{6}\exp(2\pi ilk/6)Z_k(\nu),\quad (l=0,\pm1,\pm2,3) \tag{1}$$

where N_l is a normalization factor, Z_k the AO for $2pz$ of the k-th C atom. The z_k axis is perpendicular to the molecular plane and the y_k axis joins the C and H atoms. For σ-electrons we choose sp^2 hybridized orbitals:

$$\begin{aligned}\chi_k^{(1)}&=\frac{1}{\sqrt{3}}S_k-\frac{1}{\sqrt{2}}X_k-\frac{1}{6^{\frac{1}{2}}}Y_k,\\ \chi_k^{(2)}&=\frac{1}{\sqrt{3}}S_k+\frac{1}{\sqrt{2}}X_k-\frac{1}{6^{\frac{1}{2}}}Y_k,\\ \chi_k^{(3)}&=\frac{1}{\sqrt{3}}S_k+(\tfrac{2}{3})^{\frac{1}{2}}Y_k,\end{aligned} \tag{2}$$

where S_k, X_k, and Y_k are $2s$, $2px$, and $2py$ AO's of the k-th C atom, respectively. Further, we assume electron pair bonds between $\chi_k^{(3)}$ and h_k ($1s$ of the H_k atom) (CH bond) and between $\chi_k^{(1)}$ and $\chi_{k+1}^{(2)}$ (σ-bond). Neglecting overlapping among $\chi_k^{(1)}$, $\chi_{k+1}^{(2)}$, $\chi_k^{(3)}$ and h_k electrons we obtain the whole exchange energies W' as a sum of these between π-electrons and σ-bonds ($W(\sigma,\pi)$) and between π and CH bonds ($W(\mathrm{CH},\pi)$):

$$\left.\begin{aligned}W'&=W(\sigma,\pi)+W(CH,\pi)\\&=-\tfrac{1}{2}\sum_l\frac{1}{6N_l}\sum_{k,k'=1}^{6}\exp(2\pi il(k-k')/6)M_{|k-k'|},\\ M_{|k-k'|}&=\sum_{\nu=1}^{3}J_{|k-k'|}{}^{(\nu)}+L_{|k-k'|},\\ J_{|k-k'|}{}^{(\nu)}&=\sum_{i=1}^{6}\int\!\!\int\chi_i{}^{(\nu)}(1)Z_{k'}(1)\frac{e^2}{r_{12}}\chi_i{}^{(\nu)}(2)Z_k(2)d\tau_1d\tau_2,\\ L_{|k-k'|}&=\sum_{i=1}^{6}\int\!\!\int h_i(1)Z_{k'}(1)\frac{e^2}{r_{12}}h_i(2)Z_k(2)d\tau_1d\tau_2.\end{aligned}\right\} \tag{3}$$

Here the summation over l extends over all occupied π-orbitals in the electronic state involved. As a consequence of the assumption of electron pair bonds, W' is determined uniquely by the number of electrons occupying each π-orbital and is independent of spin multiplicity and spatial symmetry type of the electronic state. The Coulombic energies which are beyond our scope were already taken into account in the Mayer-Sklar method (except those involving h orbitals). We neglect integrals between non-neighbor AO's (M_2 and M_3) and three- and four-center integrals ($J_2^{(\nu)}$ and $J_3^{(\nu)}$), which are presumably small in our case, and adopt Zener-type functions for S_k, X_k, Y_k, and Z_k with effective charge of 3.18 and $1s$ function of H atom for h_k. Then

$$\left.\begin{aligned}J_0^{(1)}+J_0^{(2)}&=\tfrac{2}{3}G_1+4F_2+(4/3)C_{s\pi\pi s}\\&\qquad+C_{\pi'\pi\pi\pi'}+(5/3)C_{\sigma\pi\pi\sigma},\\ J_0^{(3)}+L_0&=\tfrac{1}{3}G_1+2F_2+\tfrac{2}{3}C_{s\pi\pi s}+C_{\pi'\pi\pi\pi'}+\tfrac{1}{3}C_{\sigma\pi\pi\sigma}+N_{\pi\pi},\end{aligned}\right\} \tag{4}$$

$$\left.\begin{aligned}J_1^{(1)}+J_1^{(2)}&=(4/3)L_{ss\pi\bar{\pi}}+L_{\pi\pi\pi\bar{\pi}}+(5/3)L_{\pi\sigma\sigma\pi},\\ J_1^{(3)}&=\tfrac{2}{3}L_{ss\pi\bar{\pi}}+L_{\pi\pi\pi\bar{\pi}}+\tfrac{1}{3}L_{\pi\sigma\sigma\pi},\end{aligned}\right\} \tag{5}$$

where G_1 and F_2 are Slater terms for atomic integrals and $C_{\alpha\beta\beta\alpha}$ (the exchange integral) and $L_{\alpha\beta\gamma\delta}$ (the hybrid-exchange one) are the notations according to Kotani, Amemiya, and Simose.[4] Equation (4) corresponds to K given by Penney.[5] Their values for equilibrium CC and CH distances in benzene are tabulated in Table I. For N_l's we take the values given by Parr, Craig, and Ross.[3] Then for the ground state $^1A_{1g}$: $0^2 1^2(-1)^2$,

$$W'=-20.41 \text{ ev}.$$

TABLE I. Integrals over atomic orbitals (ev).

G_1	2.18[a]
F_2	0.188[a]
$C_{\pi'\pi\pi\pi'}\equiv(ab_s;\,ab_s)$ [b]	0.0519[c]
$C_{\sigma\pi\pi\sigma}\equiv(ab_r;\,ab_r)$ [b]	0.562[c]
$C_{s\pi\pi s}$	0.3191[d]
$L_{ss\pi\bar{\pi}}$	0.8053[d]
$L_{\pi\pi'\pi'\bar{\pi}}$	0.1219[d]
$L_{\pi\sigma\sigma\bar{\pi}}$	0.2679[d]
$N_{\pi\pi}$	0.7370[e]

[a] Semiempirical values according to Van Vleck (J. H. Van Vleck, J. Chem. Phys. **2**, 297 (1934)).
[b] Notations by Parr and Crawford (R. G. Parr and B. L. Crawford, J. Chem. Phys. **18**, 1049 (1948)).
[c] Interpolated values from tables in reference b.
[d] Values derived from Kotani, Amemiya, and Simose, Table IV, reference 4.
[e] Interpolated value from M. Kotani and A. Amemiya, Table IV, reference 4.

TABLE II. Electronic levels of benzene (ev).

Level	ASMO[a]	ASMO+W'	ASMO +configuration interaction[b]	Observed
Singlets				
A_{1g}	0.0	0.0	0.0	0.0
A_{2g}	11.1	13.1	12.5	···
B_{1u}	7.3	8.3	9.0	6.2[c]
B_{2u}	5.9	6.9	4.4	4.9
E_{1u}	9.8	10.8	9.9	7.0
E_{2g}	10.9	13.3	7.7	6.2[d]
Triplets				
A_{1g}	13.6	15.6	14.9	···
A_{2g}	11.1	13.1	11.8	···
B_{1u}	3.1	4.1	4.1	3.8
B_{2u}	5.8	6.8	8.2	···
E_{1u}	4.4	5.4	4.7	···
E_{2g}	8.3	10.7	6.4	···

[a] C. C. J. Roothaan and R. G. Parr, J. Chem. Phys. **17**, 1001 (1949).
[b] Parr, Craig, and Ross (see reference 3).
[c] Interpretation before Craig.
[d] Interpretation by D. P. Craig, Proc. Roy. Soc. (London) **A200**, 401 (1950).

Relative to this value W's for excited states are computed, and Table II shows electronic energies of excited states corrected by W's. The corresponding correction to the calculated values of Parr, Craig, and Ross[3] are not given but it may be inferred that their assignment of 6.2 ev band as the $^1A_{1g}-{}^1E_{2g}$ transition is not conclusive.

The author wishes to thank Professor M. Kotani and Mr. E. Ishiguro of the University of Tokyo for helpful discussions.

* The paper is translated from Japanese, Busseiron Kenkyu **40**, 55 (1951).
[1] S. L. Altman, Proc. Roy. Soc. (London) **A210**, 343, 354 (1952).
[2] M. G. Mayer and A. L. Sklar, J. Chem. Phys. **6**, 645 (1938).
[3] Parr, Craig, and Ross, J. Chem. Phys. **18**, 1561 (1950).
[4] Kotani, Amemiya, and Simose, Proc. Phys.-Math. Soc. Japan **20**, Extra No. (1938); M. Kotani and A. Amemiya, Proc. Phys.-Math. Soc. Japan **22**, Extra No. (1940).
[5] W. G. Penney, Proc. Roy. Soc. (London) **A146**, 223 (1934).

A Method for Estimating Electronic Repulsion Integrals Over LCAO MO'S in Complex Unsaturated Molecules

ROBERT G. PARR
Department of Chemistry, Carnegie Institute of Technology, Pittsburgh, Pennsylvania
(Received July 1, 1952)

SUPPOSE that by some means one has obtained molecular orbitals ϕ_i as linear combinations of Slater $2p\pi$ atomic orbitals χ_p:

$$\phi_i=\sum_p C_{ip}\chi_p \tag{1}$$

and that one requires values for integrals over molecular orbitals of the form

$$(\phi_i\phi_j|\phi_k\phi_l)=\int\phi_i^*(1)\phi_j(1)(e^2/r_{12})\phi_k^*(2)\phi_l(2)d\tau. \tag{2}$$

Exact evaluation of these integrals is a tedious matter which requires prior knowledge of the numerical values of a large number of integrals over atomic orbitals.

To obtain approximate values for these integrals, one may first assume that

$$\chi_p\chi_q\equiv 0 \quad \text{for} \quad p\neq q \tag{3}$$

and renormalize the ϕ_i accordingly. One then obtains

$$(\phi_i\phi_j|\phi_k\phi_l)=\text{linear combination of integrals over atomic orbitals of the form } (\chi_p\chi_p|\chi_q\chi_q)\equiv(pp|qq). \tag{4}$$

The problem is thus formally reduced to the evaluation of a small number of integrals over atomic orbitals, all Coulomb integrals.

To obtain the integrals $(pp|qq)$, one may merely replace each $|\chi_p|^2e$ by a pair of tangent uniformly charged nonconducting spheres of *diameter*

$$R_p=(4.597/Z_p)\times 10^{-8}\text{ cm}, \tag{5}$$

where Z_p is the effective charge of the $2p\pi$ atomic orbital χ_p, and compute the Coulomb repulsive potential between $|\chi_p|^2e$ and $|\chi_q|^2e$ by classical electrostatic theory. This gives for the integral $(pp|pp)$ the correct value for $2p\pi$ Slater orbitals, namely,

$$(pp|pp)=5.3238\text{ ev}; \tag{6}$$

while for $(pp|qq)$ the result is

$$(pp|qq)=(14.395/r)\{(1/2)+(1/2)[1+(R/r)^2]^{-\frac{1}{2}}\}\text{ ev}, \tag{7}$$

where r is the distance between atoms p and q in A, provided that $R_p=R_q=R\leq r$. When $R_p\neq R_q$, the result for $(pp|qq)$ is slightly more complicated.

For benzene, if one takes $Z=3.18$ one obtains from Eq. (5) $R=1.45$A, which is greater than the distance between nearest neighbors, 1.39A. For simplicity one therefore takes $Z=3.307$, which gives $R=1.39$A. Application of Eqs. (6) and (7) then yields (atomic orbitals numbered consecutively around the ring): $(11|11)=17.61$, $(11|22)=8.84$, $(11|33)=5.58$, and $(11|44)=4.90$ ev. "True" values for these integrals, as given by Parr, Craig, and Ross,[1] are 16.93, 9.03, 5.67, and 4.97 ev, respectively.

Under the assumption of Eq. (3), there are only four distinct electronic repulsion integrals over molecular orbitals in benzene. Expanding these according to Eq. (4), one finds, in the notation of Parr, Craig, and Ross,

$$\left.\begin{aligned}
6\gamma_{00}=6\gamma_{01}=\text{etc.}&=(11|11)+2(11|22)+2(11|33)+(11|44)\\
6\delta_{01}=6\delta_{12}=\text{etc.}&=(11|11)+(11|22)-(11|33)-(11|44)\\
6\delta_{02}=6\delta_{13}=\text{etc.}&=(11|11)-(11|22)-(11|33)+(11|44)\\
6\delta_{03}=6\delta_{1-2}=\text{etc.}&=(11|11)-2(11|22)\\
&\quad+2(11|33)-(11|44)
\end{aligned}\right\}. \tag{8}$$

Using the numerical values above, one then obtains $\gamma_{00}=8.56$, $\delta_{01}=2.66$, $\delta_{02}=1.35$, and $\delta_{03}=1.03$ ev.

Parr, Craig, and Ross computed thirty different electronic repulsion integrals over molecular orbitals in benzene but found the values clustering in four distinct groups, average values within groups being 8.61, 2.69, 1.35, and 1.00 ev. The agreement between these average values and the values computed by the much shorter approximate method is very encouraging. The approximate method can be applied with some confidence to complex molecules containing heteroatoms, and the possibility of exact computation of electronic repulsion integrals through expansions of atomic orbitals in terms of step functions seems worth examining.

[1] Parr, Craig, and Ross, J. Chem. Phys. **18**, 1561 (1950).

On the Assignment of the Naphthalene Bands at 3200−2900A

D. P. CRAIG AND L. E. LYONS
Chemistry Department, University College, London, England
(Received July 8, 1952)

THE weak absorption bands in this region have been variously assigned. The main suggestions have been (electronic species) $^1A_g-{}^1A_g$ [1-4] and $^1A_g-{}^1B_{3u}$ [5] the former being symmetry

forbidden and the latter formally allowed but having a small, or even zero, transition moment. One might expect to choose between these from the vibrational structure, and indeed Sponer and Nordheim[4] provisionally interpreted their vibrational analysis in favor of the first assignment.

To assist in assigning this and the other ultraviolet band systems we have measured the absorption of thin crystals and sublimation flakes of naphthalene in polarized light in the spectral region 3300–2300A, including the weak system, the stronger system 2900–2500A, and the beginning (to $\epsilon\sim10^4$) of the intense system at 2200A. In each case measurements have been made of the ratio of the extinction coefficients for light polarized parallel and perpendicular to the b crystal axis. In the weak system the results qualitatively confirm those already known[6-9] *viz.*, that absorption is stronger when the electric vector is parallel to the b crystal axis than when parallel to the a axis, the light being incident normal to the ab plane. Further, measurement of the extinction coefficient ratio in the two directions gives values in the range 4.5−5.0 to 1, which is somewhat less than that calculated for the oriented-gas model of the crystal, but nevertheless confirms that the transition moment lies predominantly in the molecular plane and along the shorter molecular axis. Consistently, there is an intense system at 2200A from which the weak one, presumably, steals its intensity, which is polarized in the same sense and may therefore be assigned to the electronically allowed ${}^1A_g-{}^1B_{2u}$ transition.

For the weak system these results, taken with the Raman frequencies of naphthalene, appear to exclude the assignment A_g-B_{3u}; and taken with the infrared frequencies and the approximate location of the 0−0 band they give support to the assignment A_g-A_g along lines already indicated.[10] We consider first the assignment A_g-B_{3u}. To appear in absorption with short axis polarization, i.e., to a final state of *vibronic* species B_{2u}, perturbing vibrations of class b_{1g} must be active; such vibrations are Raman active and might therefore be expected in the Raman spectrum. There is, however, no known Raman frequency compatible with the 1−0 to 0−1 gap of 941 cm^{-1} observed by Sponer and Nordheim[4] with the exception of 512 cm^{-1}; this, however, is a polarized line and so of species a_g and not b_{1g}. This, in our view, makes the assignment A_g-B_{3u} untenable.

On the other hand, as was shown by Sponer and Nordheim, the 1−0 to 0−1 gap is compatible with several infrared frequencies, the choice among which depends upon locating the 0−0 band and finding the perturbing frequency measured, in the ground state, as equal to the 1−0 to 0−0 separation. The 0−0 band is not definitely seen in the vapor but appears weakly in solution; the following values of the perturbing frequency are to be found in solution spectra: 470 cm^{-1},[11] 456,[12] 536,[3] 460,[13] all ±60 cm^{-1}. In the crystal each molecule is in a local field which has a center of symmetry (site group C_i) and the $g-g$ prohibition is not broken down; consistently, the 0−0 band does not appear in the spectrum except with accompanying crystal vibrations. Its location may be found approximately as the mean of the absorption and fluorescence values 31,636 cm^{-1} [9] and 31,463 cm^{-1};[14] this leads to a separation 488 cm^{-1} from the 1−0 line at 31,062 cm^{-1}. These values for the perturbing frequency fit best the infrared 476 cm^{-1}. The species of this vibration has to be b_{2u} to effect the necessary mixing of electronic wave functions, and this is the species which Pimentel and McClellan[15] have assigned it on entirely independent grounds, *viz.*, polarized infrared studies.

This scheme meets with two objections. First, it is difficult to reconcile it to the figure 910 cm^{-1} for the somewhat diffuse 1−0 to 0−1 gap in fully deuterated naphthalene mentioned in a preliminary way by Sponer and Nordheim; and second, as Platt[5] has remarked, the intensity changes upon substitution suggest a $g-u$ and not a $g-g$ system. The latter argument, however, assumes that the vibrational contribution to the intensity remains fixed, which is very doubtful in view, for example, of the well-known two- or threefold intensity increase in the long wave absorption system of hexamethylbenzene over that of benzene. In spite of these unsettled points we believe that the weight of evidence supports 476 cm^{-1} for the perturbing frequency and so supports the assignment A_g-A_g.

We find also that in the region 2900–2500A there occurs absorption polarized along the short molecular axis. Here, too, the ratio of extinction coefficients for the two directions is less than that calculated for the oriented gas model. The presence of a band system of *vibronic* species A_g-B_{2u} seems probable; the question of electronic classification is left to a fuller report of this work.

[1] Craig, Proc. Int. Cong. Pure and Applied Chem. **11**, 411 (1947).
[2] Blumenfeld, Physic. Chem. Soc. U.S.S.R. **21**, 549 (1947).
[3] M. Kasha and R. V. Nauman, J. Chem. Phys. **16**, 516 (1949).
[4] Sponer and Nordheim, Disc. Faraday Soc. **9**, 19 (1950).
[5] John R. Platt, J. Chem. Phys. **17**, 484 (1949); **19**, 1418 (1951).
[6] Broderson, Compt. rend. **233**, 1094 (1951).
[7] Kastler, Disc. Faraday Soc. **9**, 69 (1950).
[8] Matsen *et al.*, ONR Report N8onr-70800.
[9] Prikhotjko, J. Phys. U.S.S.R. **8**, 257 (1944).
[10] Craig and Sponer, Disc. Faraday Soc. **9**, 69 (1950).
[11] Broderson and Langseth, Dan. Mat. Fys. Medd. No. **3**, 26 (1951)
[12] Mayneord and Roe, Proc. Roy. Soc. (London) **158A**, 634 (1937).
[13] Seshan, Proc. Indian Acad. Sci. **3A**, 148 (1936).
[14] Obreimov and Shabaldas, J. Phys. U.S.S.R. **7**, 168 (1943).
[15] George C. Pimentel and A. L. McClellan, J. Chem. Phys. **20**, 270 (1952).

Field Emission from Tantalum in the Normal and Superconducting State

ROBERT GOMER AND JOHN K. HULM
Institute for the Study of Metals, The University of Chicago, Chicago, Illinois

(Received July 3, 1952)

BY analogy with other phase transitions it is likely that energy changes of the order of kT_c per electron are involved in the transition from the normal to the superconducting state.[1] It was thought that a study of field emission from a superconductor might confirm this or show whether grosser effects exist.

A small projection microscope[2] with a tantalum cathode, (chosen for its convenient transition point 4.4K and suitable mechanical properties), was constructed so that the whole assembly fitted into the inner Dewar vessel of a liquid helium cryostat. Photographs could be taken through the unsilvered walls of the cryostat. The cathode was prepared by electrolytic etching in a 50:50 solution of concentrated H_2SO_4 and HF; the screen anode consisted of willemite deposited between layers of evaporated platinum. The microscope in the cryostat is shown in Fig. 1. Voltages could be measured to a few parts in 10^5 with a sensitive potentiometer operating across a small portion of the bleeder resistor of the power supply. Currents were measured with an accurate vacuum tube voltmeter using 9.4 megohm load in the cathode circuit. With this arrangement, currents could be read to 2 parts in 10^3 except at the lowest values where the accuracy was of the order of 1 percent.

Experimental procedure consisted of measuring field emission current as a function of voltage at He bath temperatures from 4.2° to 2.2°K, as determined from the He vapor pressure. With the bath still at these temperatures, the cathode was now heated electrically and the field emission current again measured over the entire voltage range. From the resistance of the cathode and the current at dullest red heat, the temperature rise of the cathode could be estimated, and a rough calculation based on the conductivity of the tungsten leads confirmed this estimate. The time constant of the system with regard to thermal equilibrium was estimated to be less than a minute for the highest temperature rise.

Table I shows that there was no difference in emission below and above the transition temperature within the experimental error, estimated at 0.2 percent. This fact was confirmed by measuring the emission current at a set voltage, which could be maintained steady to within one part in 10^5, with the bath at 2.5°K and the tip heated and cold. No change at all could be detected in the current at either 8400 or 9200 volts. No visible change in the pattern with temperature could be observed. Figure 2 shows a photograph of the pattern. It should be mentioned that no change in total emis-

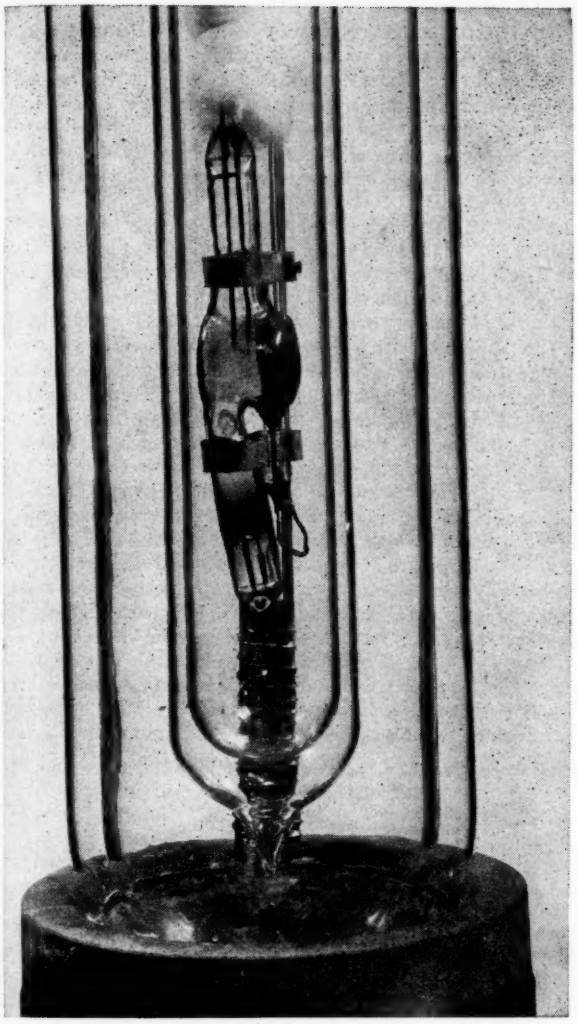

FIG. 1. Microscope assembly in the cryostat. The dark band on the lower arm is evaporated Ta from the getter. The tip is visible in front of the anode which appears as the dark region on the main body of the microscope.

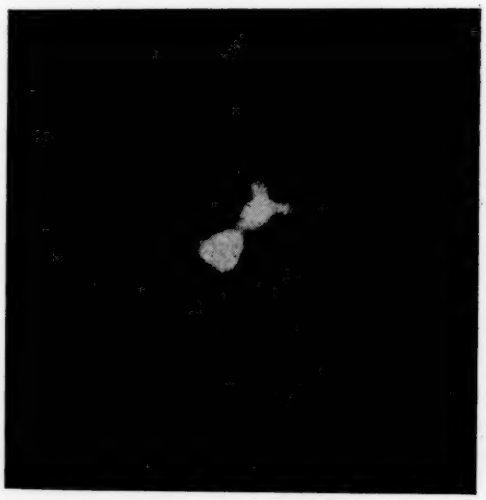

FIG. 2. Field emission pattern from tantalum. The triangular bright spot corresponds to the 111 direction, the small dark region at the upper right to the 100 and the two large dark regions to two (110) directions.

sion current with temperature from 30° to 300°K could be noticed. From theoretically obtained plots of the current distribution in field emission as a function of voltage,[3] it is estimated that this effect should amount to *ca* 0.3 percent of the current at the highest and very slightly more at lower voltages used.

Figure 3 shows some typical Fowler-Nordheim plots[2] ($\log I/V^2$ *vs* $1/V$) of the results. It is seen that excellent straight lines are

TABLE I. Field emission current from tantalum as function of voltage and temperature.

	Current	Voltage	
I	6.2×10^{-9} ampere	7976.1 volts	
	17.8	8362.4	
	47.1	8733.5	$T=4.2°K$
	133.0	9151.7	
	333.0	9554.6	
	658.0	9900.4	
II	1.4×10^{-9}	7504.3	
	4.9	7939.1	
	14.3	8302.2	
	42.3	8704.5	$T=3.8°K$
	138.0	9169.1	
	361.0	9591.6	
	908.0	10034.4	
III	1.5×10^{-9}	7550.7	
	5.1	7946.4	
	15.8	8337.8	
	53.4	8737.8	$T=3.5°K$
	127.0	9145.9	
	329.0	9575.7	
	703.0	9949.6	
IV	1.4×10^{-9}	7493.4	
	3.4	7823.9	
	13.2	8295.0	
	35.2	8666.8	$T=270°K$
	112.0	9119.1	
	295.0	9546.7	
	600.0	9891.7	
V	1.6×10^{-9}	7534.7	
	5.1	7934.1	
	16.0	8350.1	
	45.1	8745.1	$T=270°K$
	126.0	9148.8	
	323.0	9569.9	
	660.0	9921.1	
VI	1.8×10^{-9}	7586.9	
	5.2	7944.2	
	18.4	8375.4	
	47.6	8734.9	$T=2.5°K$
	144.0	9187.2	
	380.0	9613.3	
	899	10049.7	
VII	2.0×10^{-9}	7570.2	
	6.8	7989.9	
	18.3	8367.5	
	49.6	8750.1	$T=2.2°K$
	138.0	9161.1	
	363.0	9591.6	
	822.0	10001.8	
VIII	1.9×10^{-9}	7550.7	
	5.5	7971.0	
	15.5	8339.9	
	46.5	8756.7	$T=30°K$
	138.0	9184.3	
	343.0	9600.3	
	831.0	10038.8	

obtained. Assuming a mean work function of 5 volts for Ta, the tip radius is calculated[2] to be 5.7×10^{-5} cm. The current density at the highest voltages was therefore 80 amperes/cm². The highest surface magnetic field resulting from the field emission current is estimated to have been 2.5×10^{-3} gauss. This is quite insufficient to quench superconduction. It can be calculated from the estimated accuracy of the results that a change in work function of the order of 10^{-3} electron volt or a change of 5.10^{-2} ev in the effective band width of the conduction band could have been detected. The conclusion must therefore be reached that the potential barrier at the surface of a superconducting metal and the chemical potential of the conduction electrons are not affected to an extent much above kT_c if at all.

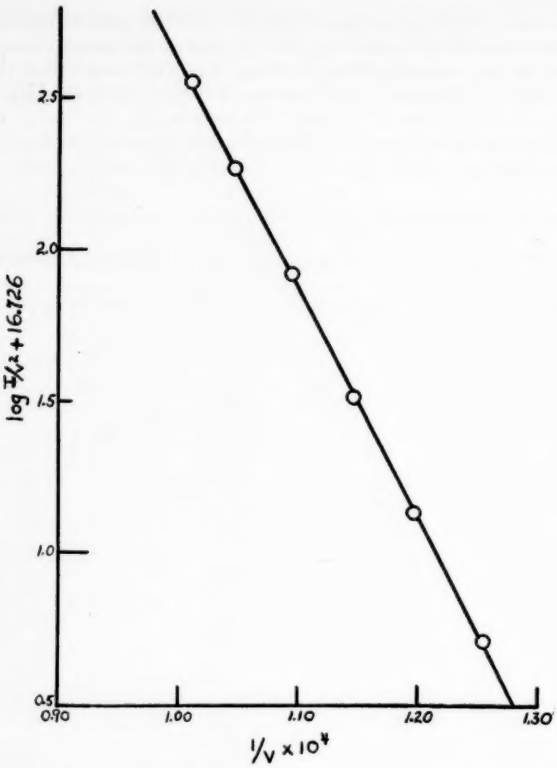

FIG. 3. Fowler-Nordheim plot for a representative run. The points obtained from other runs duplicate the ones shown, so that it is not possible to present them on the same graph.

This work was supported in part by Contract AF 33(038)-6534 with the United States Air Force. The authors wish to thank Dr. L. Guttman for a part of the liquid helium used in this work.

[1] D. Schoenberg, *Superconductivity* (Cambridge University Press, Cambridge, 1938).
[2] R. Gomer and D. Speer, "Molecular images with the projection microscope," J. Chem. Phys. (to be published).
[3] R. Gomer, "Velocity distribution of electrons in field emission," J. Chem. Phys. (to be published).

The Near Ultraviolet Spectrum of Formaldehyde

A. D. WALSH
Department of Chemistry, Leeds University, Leeds, England
(Received June 25, 1952)

THERE have been many attempts to interpret the near ultraviolet spectrum of formaldehyde.[1] The difficulty hinges upon the interpretation of two bands called α and A. α is weak and temperature-dependent in absorption, strong in fluorescence. The whole absorption is weak and has therefore been regarded as the result of a space symmetry-forbidden transition, A being interpreted as a $1\leftarrow 0$ and α as a $0\leftarrow 1$ transition, each involving one quantum of a nontotally symmetrical vibration. Since the lowest ground-state frequency is 1166 cm^{-1}, and the separation of A and α is only *ca* 1277 cm^{-1}, this interpretation is not without its difficulties. Brand[2] expressed the vibrational bands of the fluorescence spectrum by the formulas

$$\text{HCHO.}\quad \nu=(28312.7-113.2p)+[(1191.8-11.4p)n_2'-9.4n_2'^2]-(1165.9n_6''-2.3n_6''^2)-(1755.0n_2''-10.3n_2''^2)+6.5n_2''n_6'',$$

$$\text{DCDO.}\quad \nu=(28378-67p)+[(1173.5+4.1p)n_2'-8n_2'^2]-(937.8n_6''-3.1n_6''^2)-(1713.1n_2''-9.0n_2''^2)+7.0n_2''n_6''.$$

The agreement of ν_{obs} and ν_{calc} was so good that Brand's analysis must be substantially correct. It is not complete, however. The formulas contain a factor p, where $p=1$ if n_6'' is odd and 0 if n_6'' is even. Since ν_6 is not a totally symmetrical frequency, the total symmetry of the ground level differs according to whether n_6'' is even or odd. It therefore appeared that there were two principal fluorescing levels, one of which was able to combine with the ground state only when n_6'' was even and the other only when n_6'' was odd. The relation of these levels to each other was left unexplained.

An obvious possibility is to interpret the figure 113.2 cm^{-1} for HCHO as ν_6'. If then the upper state were $^{e1}A_2$ its total symmetry would be A_2 or B_2[3] accordingly as n_6' was 0 or 1. An A_2 level would combine with a B_1 lower level (n_6'' odd) but would not combine with an A_1 level (n_6'' even); whereas a B_2 level would combine with an A_1 but not with a B_1 lower level. This possibility has been adopted by Dyne.[4] It is not satisfactory for the following reasons. First, a reduction of ν_6 from 1165.9 cm^{-1} in the ground state to only 113.2 cm^{-1} in the excited state would be surprisingly large. So far as is known, there is no precedent for such an enormous reduction. Secondly, the interpretation completely neglects the fact that 113 cm^{-1} is just the separation of the $\nu_5''b_2$ and $\nu_6''b_1$ vibrations (1280–1166 cm^{-1}). Further, the corresponding figure for DCDO is 67 cm^{-1} which, within the accuracy with which the data are known, is equal to $\nu_5''-\nu_6''$ for DCDO (990–938 cm^{-1}). Put in another way, the separation of A and α is just equal to the ν_5'' frequency for both HCHO and DCDO. It is most unlikely that these agreements can be dismissed as mere coincidences.

These and other difficulties disappear if one accepts ν_5'' as involved in the fluorescence spectrum along with ν_2'' and ν_6''. The α-band is then to be interpreted as the $n_5''=1$ band, A being vibrationless. It becomes possible to alter Brand's formulas to

$$\text{HCHO.}\quad \nu=28312.7+(1190n_2'-12n_2'^2)-(1165.9n_6''-2.3n_6''^2)-(1755.0n_2''-10.3n_2''^2)+6.5n_2''n_6''-(1280n_5''-3n_5''^2)+4n_5''n_6''+7n_2''n_5'',$$

$$\text{DCDO.}\quad \nu=28378+(1183n_2'-8n_2'^2)-(937.8n_6''-3.1n_6''^2)-(1713.1n_2''-9.0n_2''^2)+7.0n_2''n_6''-(1000n_5'')+5.5n_5''n_6''+5n_2''n_5''.$$

The agreement of ν_{obs} and ν_{calc} is about as good as that given by Brand with the old assignments. The new assignments show that only lower state levels of total symmetry $^1A_1$ or $^1B_2$ occur. Bands to lower $^1A_2$ (e.g. $^{e1}A_1\times b_1\times b_2$) or $^1B_1$ (e.g., $^{e1}A_1\times b_1$) levels do not occur. n_5'' is never more than 1. n_6'' is always even. The lower levels of the A and α-bands are, respectively, $^1A_1$ and $^1B_2$. They have a common upper level. Yet it is known that both bands are perpendicular.[4,5] This is impossible if the upper level is singlet. One is thus driven to the conclusion that the upper level is triplet.

One has to inquire what would be the total symmetry of the upper level when this includes the effect of the triplet spin function on the space wave function. The product representations of spin and orbital wave functions for C_{2v} symmetry have been given by McClure[6] and by Weissman.[7] It is readily seen from these that the transition $^3A_2\rightarrow{}^1A_1$ may proceed by mixing with any of the allowed transitions $^1A_1\rightarrow{}^1A_1$, $^1B_1\rightarrow{}^1A_1$, or $^1B_2\rightarrow{}^1A_1$ provided these lie sufficiently near in energy. Similarly, the transition $^3A_2\rightarrow{}^1B_2$ may proceed by mixing with either of the two allowed transitions $^1A_1\rightarrow{}^1B_2$ or $^1B_2\rightarrow{}^1B_2$. On the other hand, the transition $^3A_2\rightarrow{}^1A_2$ can only occur by mixing with either of the two allowed transitions $^1B_1\rightarrow{}^1A_2$ or $^1B_2\rightarrow{}^1A_2$; while the transition $^3A_2\rightarrow{}^1B_1$ can only occur by mixing with one of the two allowed transitions $^1A_1\rightarrow{}^1B_1$ or $^1B_1\rightarrow{}^1B_1$. Now there are theoretical reasons why the only low-lying allowed electronic transitions is expected to be $^1B_2\leftrightarrow{}^1A_1$.[8] It follows that if the upper state of the fluorescence bands is $^3A_2$, transitions will only be observed to ground-state levels that have total symmetry $^1A_1$ or $^1B_2$; and that all the bands will be polarized parallel to the H−H line. It is practically certain that all the fluorescence and main long wavelength absorption bands have this polarization. Further, no other triplet upper state can be substituted for $^3A_2$ to explain the observed facts.

Thus (1) the vibrational structure and polarization data of the

fluorescence lead to the conclusion that the upper state is triplet and is in fact $^3A_2$, (2) the fluorescence and long wavelength absorption bands have the same electronic upper level; (3) the $^3A_2$ state gives rise to fluorescence bands that proceed only to $^1A_1$ or $^1B_2$ lower levels, (4) the $^3A_2$ upper level behaves as $^1B_2$ when it combines with $^1A_1$ lower levels and as $^1A_1$ when it combines with $^1B_2$ lower levels.

The key to an understanding of the vibrations that occur in the spectrum was the realization from theory[9] that in its first excited state, although sufficiently near to C_{2v} symmetry for the selection rules to hold, HCHO ought (a) to be nonplanar and (b) to have the O atom out of the mirror plane that bisects the HCH angle. (a) causes the $\nu_6 b_1$ vibration and (b) causes the $\nu_5 b_2$ vibration to occur. (b) is due essentially to the same reason as causes a certain excited state of CH_3I to have the I atom slightly off the trigonal axis of the CH_3 group.[1] A fuller account, both of the background theoretical work and of the HCHO spectrum analysis, will be submitted for publication elsewhere. It should in fairness, however, be said that though the analysis given here explains many points, it still leaves a number of important difficulties to be cleared up, notably in the rotational fine structure of the α-band.

The author would like to express his thanks to Dr. P. J. Dyne for several stimulating letters.

[1] See H. Sponer and E. Teller, Revs. Modern Phys. **13**, 75 (1941).
[2] J. C. D. Brand, J. Chem. Phys. **19**, 377 (1951).
[3] The symbols B_1 and B_2 are used as in reference 1. Other authors reverse the definitions of these symbols.
[4] P. J. Dyne, J. Chem. Phys. **20**, 811 (1952).
[5] G. H. Dieke and G. B. Kistiakowsky, Phys. Revs. **45**, 4 (1934).
[6] D. S. McClure, J. Chem. Phys. **17**, 665 (1949).
[7] S. I. Weissman, J. Chem. Phys. **18**, 232, 1258 (1950).
[8] H. L. McMurry and R. S. Mulliken, Proc. Natl. Acad. Sci. **26**, 312 (1940).
[9] A. D. Walsh (to be published).

Nuclear Magnetic Resonance Experiment on a Four-Proton System in a Single Crystal of $K_2HgCl_4 \cdot H_2O$

JUNKICHI ITOH, RIICHIRO KUSAKA, YUKIO YAMAGATA, RYÔITI KIRIYAMA, AND HIDEKO IBAMOTO
Department of Physics and Department of Chemistry, Osaka University, Osaka, Japan
(Received June 13, 1952)

PAKE[1] observed the nuclear magnetic resonance absorption by a two-proton system in a single crystal of gypsum. Since then, Andrew and Bersohn[2] calculated the energy levels and the transition probabilities in a three-proton system, which was investigated by Gutowsky *et al.*[3] using powders of some organic compounds. By using a single crystal of $K_2HgCl_4 \cdot H_2O$, we observed fine structures in each of the resonance lines separated by a two-proton interaction. As will be shown in this letter, it is ascribed to the resonance absorption in a four-proton system.[4]

The crystal of $K_2HgCl_4 \cdot H_2O$ has rhombic symmetry (space group, V_h^9-*Pbam*), and the unit cell contains four formula units.[5] Figure 1 shows the environment of two water molecules in the lattice. Considering from the crystal structure[5] and the dielectric behavior,[6] it is suggested that the dipole moments of these water molecules are oppositely directed along the c axis.

First, the crystal was rotated around the c axis which is kept always perpendicular to the static field. Generally, four well-separated peaks were observed on an oscilloscope screen, when a large modulation field was applied. The separation of the four peaks from their center of gravity was measured against the angle of rotation, which is shown in Fig. 2. This figure is very similar to the case of Pake's experiment on gypsum,[1] and it can be analyzed in the same way as due to two groups of two-proton systems. The best fit with the experimental plots is obtained by the assumption that each proton-proton direction is perpendicular to the c axis, and the angles between proton-proton lines and the a axis are $\pm 21°$, respectively. The proton-proton distance is 1.607A for both groups.

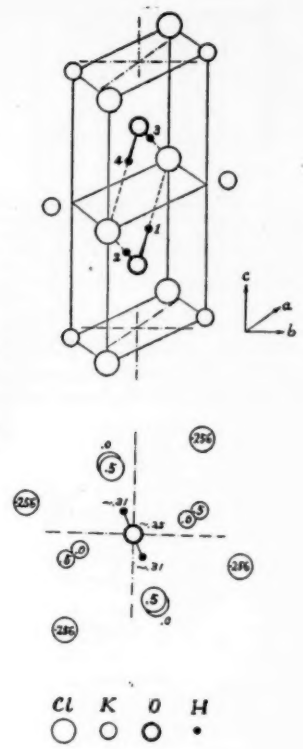

FIG. 1. Two water molecules and their environment in the lattice. The lower figure is the projection diagram on the c plane. The positions of the protons are determined by this experiment. The configuration of ions around the other two water molecules is just the mirror reflection of that shown in this figure with respect to the b plane.

Next, the shape of individual component lines was measured by a recording milliammeter using a very small modulation field. A typical result is shown in Fig. 3. This figure corresponds to the case when the static field is parallel to the c axis. In this case, since all proton-proton lines belonging to each water molecule are perpendicular to the static field, only two separated peaks are observed. The observed complex structure of each peak is ascribed to the interaction between proton 1 or 2 and 3 or 4 (see Fig. 1).

We calculated the energy levels in a four-proton system, extending the calculation of Andrew and Bersohn.[2] The secular equation cannot be solved analytically in the general case. But, since in our case, $P_{12}=P_{34}$, $P_{13}=P_{24}$, and moreover P_{12} is much larger than P_{13}, P_{14}, or P_{23}, the secular equation can be solved analytically to good approximation. The result is*

$$\Delta H = \pm \left[\tfrac{3}{2}P_{12} \begin{cases} +\tfrac{3}{4}(2P_{13}+P_{14}+P_{23}) & (1) \\ +\tfrac{3}{4}(2P_{13}-P_{14}-P_{23}) & (\tfrac{1}{2}) \\ -\tfrac{3}{4}(2P_{13}-P_{14}-P_{23}) & (\tfrac{1}{2}) \\ -\tfrac{1}{4}(2P_{13}+P_{14}+P_{23}) & (\tfrac{3}{2}) \\ -\tfrac{3}{4}(2P_{13}+P_{14}+P_{23}) & (\tfrac{1}{2}), \end{cases} \right.$$

where ΔH is the separation in gauss from the resonance field for a free proton and $P_{ij}=\mu r_{ij}^{-3}(3\cos^2\theta_{ij}-1)$. ($r_{ij}$ is the distance be-

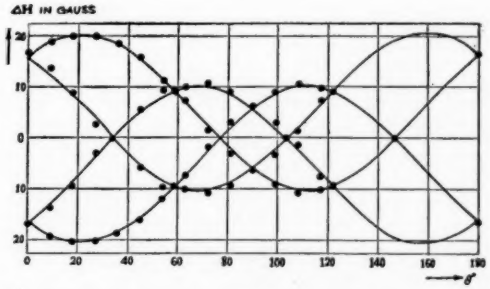

FIG. 2. Positions of resonance peaks measured on an oscilloscope screen. ΔH is the value of magnetic field strength measured from the resonance field for free proton. θ is the angle between the static field and a axis. ●'s are the experimental plots and the curves are the calculated ones. The static field is always in c plane.

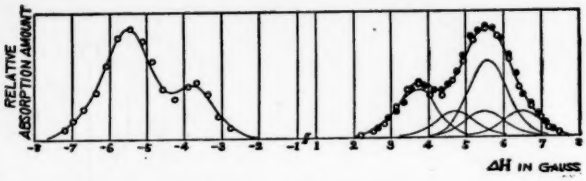

FIG. 3. Absorption line shape for the case when the static field is parallel to the c axis. Five Gaussian curves show the calculated component peaks. Also the summation curve of these five components is drawn. ○ and ● are the experimental plots for two different series. In the left half, only the summation curve is shown. ΔH is the value of the field strength measured from the resonance field for a free proton.

tween the proton i and j, θ_{ij} is the angle between the static field and the direction of the line joining the proton i and j, and μ is the proton moment.) The number in the last bracket is the intensity of the transition. For the best fit with the experimental plots, the value $r_{13}=3.60$A is to be taken. In Fig. 3 we showed five component peaks and their summation. Here the Gaussian distribution is assumed for each line, with the second moment calculated from the theory of Van Vleck.[7] The agreement is satisfactory. The absorption line shapes in various directions are also in agreement with the same assumption. The value $r_{13}=3.60$A coincides exactly with the assumption that the center of gravity of the water molecule lies at the position indicated by the x-ray analysis.

* For the discussion of this formula, we are indebted to Dr. K. Tomita.

[1] G. E. Pake, J. Chem. Phys. **16**, 327 (1948).
[2] E. R. Andrew and R. Bersohn; J. Chem. Phys. **18**, 159 (1950).
[3] Gutowsky, Kistiakowsky, Pake, and Purcell, J. Chem. Phys. **17**, 972 (1949); H. S. Gutowsky and G. E. Pake, J. Chem. Phys. **18**, 162 (1950).
[4] Some measurements were done with powders of a four-proton system by Gutowsky *et al.* (reference 3) without detailed analysis.
[5] MacGillavry, de Wilde, and Bijvoet, Z. Krist. **100**, 212 (1938).
[6] R. Kiriyama and H. Ibamoto, presented to the Second Congress of International Union of Crystallography, 1951 (to be published).
[7] J. H. Van Vleck, Phys. Rev. **74**, 1168 (1948).